UNIVERSITÉ DE GRENOBLE

THÈSE

Pour obtenir le grade de

DOCTEUR DE L'UNIVERSITÉ DE GRENOBLE

Spécialité : **Chimie et Biologie**

Arrêté ministériel : 7 août 2006

Présentée par

« Christiane Hanna Frederike WENK »

Thèse dirigée par **« Jean-Luc COLL »** et **« Pascal DUMY »**
codirigée par **« Didier BOTURYN »** et **« Véronique JOSSERAND »**

préparée au sein du **Laboratoire Institut Albert Bonniot INSERM/UJF U823 & Département Chimie Moléculaire UJF-CNRS UMR5250**
dans **l'École Doctorale Chimie et Science du Vivant**

CHIRURGIE GUIDEE PAR FLUORESCENCE DU FIBROSARCOME FELIN ET DEVELOPPEMENT ET CARACTERISATION D'UN VECTEUR BI-FONCTIONNEL POUR LE CIBLAGE DU CANCER

Thèse soutenue publiquement le **« 17 décembre 2012 »**,
devant le jury composé de :

M Jürgen, BORLAK
Professeur, Hanovre, Rapporteur
M Gilles, SUBRA
Professeur, Montpellier, Rapporteur
Mme Frédérique, PONCE
Professeur assitant, Lyon, Membre
Mme Anne, IMBERTY
Professeur, Grenoble, Membre
M Jean-Luc, COLL
Directeur de recherche, Grenoble, Membre
M Pascal, DUMY
Professeur, Montpellier, Membre

University of Grenoble
Ecole Doctorale Chimie et Sciences du Vivant

THESIS

For obtaining the degree

DOCTOR OF THE UNIVERSITY OF GRENOBLE

Specialty: PhD in Chemistry - Biology

Public defended by

Christiane Hanna Frederike WENK

The 17th of December 2012

Optical-guided surgery of the feline fibrosarcoma
&
Development and characterization of
a bi-functional vector for cancer targeting

Committee members:

Professor Jürgen BORLAK, Hannover	Reporter
Professor Giles SUBRA, Montpellier	Reporter
Doctor Frédérique PONCE, Lyon	Examiner
Professor Anne IMBERTY, Grenoble	Examiner
Doctor Jean-Luc COLL, Grenoble	Thesis director
Professor Pascal DUMY, Grenoble	Thesis co-director

A mes parents

REMERCIEMENTS

Au terme de ma thèse, je tiens à adresser mes remerciements à tous ceux qui ont contribué de près ou de loin à l'aboutissement de ce travail.

Je remercie,
Mes directeurs et co-directeurs de thèse, qui ont dirigé ces travaux et m'ont permise de découvrir le monde de la recherche. Un grand merci pour les critiques et corrections de ce manuscrit. Veuillez trouver ici l'assurance de mon profond respect.
Je remercie

Jean-Luc Coll pour m'avoir acceptée et accueillie dans son équipe, étant vétérinaire et débarquée d'Allemagne.
Merci pour ton encadrement, ta bonne humeur, ta patience, le soutien que tu m'as apporté, avec une humanité pareille…..
Le Professeur Pascal Dumy, pour m'avoir accueillie dans son laboratoire, d'avoir dirigé ces travaux et d'avoir rendu une thèse en cotutelle possible.
Didier Boturyn, pour m'avoir encadrée et fait découvrir les mystères de la synthèse peptidique, conseillée avec une grande disponibilité ainsi que pour sa confiance tout au long de mes travaux. Merci pour ta patience et pour toute l'aide que tu m'as apportée.
Véronique Josserand, pour sa disponibilité et le partage de son savoir, surtout en imagerie. Je te remercie pour ta compréhension et ton aide.

I thank Professor Jürgen Borlak and Professor Gilles Subra for giving me the honor of judging my work as reporters. Find within these words the expression of my truly gratefulness.

I thank Professor Anne Imberty and Frédérique Ponce for accepting to evaluate my work as members of my thesis committee. Therefore, I express my sincere thankfulness.

Je remercie Florence Ruggiero et Pierre Labbé pour leur temps et leurs conseils comme membres de mon comité de suivi de la thèse.

Je remercie Frédérique Ponce, encore une fois, et Claude Carozzo, pour leur collaboration dans les études « chat ». C'était un plaisir de faire avancer un tel projet avec vous. Cela m'a apporté beaucoup plus qu'une expérience scientifique.
Merci aux membres de leurs équipes pour leur participation fructueuse à ce projet, je tiens particulièrement à remercier Dorothée pour son aide et sa disponibilité.
Dans ce contexte je tiens à remercie Odile Allard et Phillipe Rizo de Fluoptics, pour leur collaboration, leurs réflexions et leur confiance tout au long cette étude. Particulièrement je remercie Stéphanie pour son soutien et sa présence dans ce projet. Je te remercie pour les discussions, les jours de « ouf » inoubliables et ta bonne humeur.

Merci à tous les membres des équipes 2 et 5 de l'Institut Albert Bonniot.
A mes collègues de bureau, Julien V, Julien G, Maxime, Mélanie, Jonathan, Daphné et Victor, Sandrine et Anastassia, Benoit et Lucie, et à ceux des bureaux voisins, Amandine, Claire, Michelle, Morgane, Laetitia,

Sylvie, Béatrice, Asma, Delphine, Céline, Pascal, Sana, Gabriele, Ihab, Blaise, Floriane, Sophie, Tudor et Maxime. Merci à vous tous pour votre gentillesse, votre bonne humeur, votre « follitude », vos conseils et votre aide…. Entre autre j'ai appris les mots les plus importants en français grâce à vous, en tombant dans tous les pièges de cette langue vive. C'était un plaisir d'être membre de « cette équipe » magnifique !
Egalement un grand merci à Christian, Mylène et Alexeï pour les heures passées ensemble à faire marcher les appareils fluos!
Je ne saurais pas oublier les gens indispensables, Denise, Dalenda, Michaelis, Jamila et Johanna !

Et puis un grand merci à Coco, au CHU maintenant, pour son travail et sa gentillesse tout au long de ces travaux.

*Tous les membres de **l'équipe « Ingénierie et Interactions Biomoléculaires »** pour leur serviabilité, leur bonne humeur et tout spécialement aux étudiants et techniciennes qui ont participées de manière très active à rendre tous les jours au DCM agréables. Merci à mes collègues et amis Corinne, Audrey, Isabelle et Abdel, et à Emilie, Romaric, Pierre, Mathieu, Julien, Nathalie, Julien G, Rémy et Cédric. Mais également à Régine et Véronique.*

*Plus particulièrement je remercie **Sandrine** et **Anastassia**, qui représentent beaucoup plus « que » des collègues, mais des amies formidables. Merci pour les moments passés ensembles, pour votre soutien, vos sacrifices, votre présence, vos « services de taxi » dans les pires moments,… votre partage de savoir-faire mais surtout des bons et mauvaises moments, nos rigolades, nos galopades….merci pour tout ! Et je ne pourrai pas oublier mon amie **Asma**, avec qui j'ai découvert le monde arabo-andalou. Merci pour tes écoutes, les discussions et le temps des « h's » et beaucoup plus…. !*

*J'adresse également mes remerciements aux personnes que j'ai rencontrées au cours de ma thèse et qui l'ont rendue par leurs présences, discussions et sourires, très plaisante. Plus particulièrement je m'adresse à **Sebastian** A et **Agnès** qui ont assuré aux derniers moments, **Monsef, Ester, Houda, Thanh, Vietnam** et **Noël**. Merci pour votre amitiè.*

*Danke an **Aliki** und **Christina**, die mir seit Jahren teure Freundinnen sind.*

*L'**Université Joseph Fourier**, pour avoir financé mes travaux de recherche durant trois ans.*

Un dernier grand merci aux personnes qui m'ont encouragée et soutenue dans mon parcours, espérant de n'avoir pas oublié quelqu'un. Qu'il me pardonne.

*Ein großes Dankeschön an meine **Familie**, für Ihre Unterstützung in jeder Hinsicht.*
*Danke an meine **Eltern**, die immer für mich da sind, immer ein offenes Ohr haben und mir ermöglicht haben, meinen Weg trotz aller Obstakel zu meistern. Danke für all die Erfahrung, Ratschläge, Taten und vor allem Liebe, die ihr mir gegeben habt.*
*Danke an meine Brüder, **Florian** und **Bastian,** ohne die meine Familie nie komplett wäre und natürlich an **Sonja**, die kleine **Sophia** und den süßen **Felix**, Onkel **Charly** und **Karla**.*

Enfin, j'aimerais bien laisser une pensée en mémoire de Sandrine, une amie rayonnante, avec qui j'adorais rêver de projets futurs et avec qui j'ai partagé ma passion : le cheval. Tu me manques.

PREFACE

This work has been accomplished in co-tutelle during the last three years of my PhD studies in team 5 "Cancer Targets and Experimental Therapeutics" of the research center INSERM/UJF U823 in the Institute Albert Bonniot, and in the team "Engineering and Interactions of BioMolecules (I2BM)" of the research unity UMR CNRS-UJF 5250 in the facilities of the Department of Molecular Chemistry at Grenoble. It was realized under the supervision of Jean-Luc Coll and Pascal Dumy, and co-supervised by Didier Boturyn and Véronique Josserand.

The studies on cats have been realized in collaboration with the Veterinarian University of Lyon (VetAgro-SUP) at Marcy l'Etoille.

This work gave reason for the following publications and presentations:

PUBLICATIONS

❖ articles

Keramidas, M; Josserand, V.; Righini, C.; Wenk, C.H.F.; Faure, C; Coll, J.L. 2010. "Intraperoperative near-infrared image-guided surgery for peritoneal carcinomatosis in a preclinical experimental model." *British Journal of Surgery*, Vol 97; ISSUE 5; pages 737-743.
[Presented in: APPENDICES]

Christiane H F Wenk & A. Briat, Mitra Ahmadi, Michael Claron, Didier Boturyn, Véronique Josserand, Pascal Dumy, Daniel Fagret, Jean-Luc Coll, Catherine Ghezzi, Lucie Sancey, Jean-Philippe Vuillez. 2012. "Reduction of renal uptake of 111In-DOTA-labeled and A700-labeled RAFT-RGD during integrin $\alpha v\beta 3$ targeting using single photon emission computed tomography and optical imaging". *Cancer science*, 103, Nr. 6: 1105–1110.
[Presented in: RESULTS & CONCLUSIONS, chapter II]

Pascal Dumy, Christiane Wenk, Michael Claron, Jean-Luc Coll, Bénédicte Allard, Didier Boturyn 2012. « Des molécules fluorescentes au service de la chirurgie. » *L'Actualité Chimique*, N°366 Pagination : 23-28
[Presented in: APPENDICES]

Christiane H. F. Wenk, Véronique Josserand, Stéphanie Guillermet, Corinne Tenaud, Didier Boturyn, Pascal Dumy, Dorothée Watrelot-Virieux, Claude Carozzo, Frédérique Ponce and Jean-Luc Coll 2012. "Near-infrared optical guided surgery of highly infiltrative fibrosarcomas in cats using an anti-alpha v ß3 integrin molecular probe." *Cancer letters - doi:10.1016/j.canlet.2012.10.041*
[Presented in: RESULTS & CONCLUSIONS, chapter I]

Christiane H. F. Wenk, Pascal Dumy, Véronique Josserand, Jean-Luc Coll and Didier Boturyn 2012. "Integrin and Matrix Metalloprotease Dual-Targeting with MMP substrate-RGD conjugate." *Organic & Biomolecular Chemistry* 11, pages 448–452

[Presented in: RESULTS & CONCLUSIONS, chapter III]

❖ review

Dufort, S.; Sancey, L.; Wenk, C.; Josserand, V., Coll, J.L. 2010. "Optical Small Animal Imaging in the Drug Discovery Process" *Biochim. Biophys. Acta Biomembrans*, 8. doi:10.1016/j.bbamem.2010.03.016
[Presented in: APPENDICES]

POSTER COMMUNICATION

NEAR-INFRARED GUIDED SURGERY OF CANCER: FROM MODELS TO CLINICAL CASES
Wenk C; Keramidas M; Josserand V.; Righini C. A.; Faure C.; Boturyn D.; Rizo P; Dumy P and Coll JL.
442. WE-Heraeus-Seminar "Molecular Imaging", October **2009**, Bad Honnef, **Germany**

NEAR-INFRARED GUIDED SURGERY OF CATS AND DOGS
Wenk C; Keramidas M.; Josserand V.; Righini C. A.; Faure C; Boturyn D.; Rizo P.; Dumy P. and Coll JL
5èmes Journées Scientifiques du CLARA ; March **2010**, Villeurbanne, **France**

IMPROVING TUMOR SURGERY AND DEVELOPING CANCER-TARGETED THERAPY BY MEANS OF REAL TIME FLUORESCENCE IMAGING
Wenk C and Keramidas M, Josserand V, Righini C, Boturyn D, Dumy P and Coll JL
Journée pour la Recherche Respiratoir (J2R), Nantes **2010, France**

SYNTHESES ET EVALUATIONS DE VECTEURS PEPTIDIQUES ACTIVABLES POUR L'IMAGERIE TUMORALE
Wenk C H F, Josserand V, Coll JL, Dumy P, Boturyn D
17ième congrès du groupe français des peptides et des protéins (GFPP); February **2011**, Aussois, **France**

NEAR-INFRARED IMAGING OF CANCER: OPTICAL GUIDED SURGERY AND SMART PROBES DEVELOPMENT
Wenk C H F, Josserand V, Guillermet S, Ponce F, Dumy P, Boturyn D, Coll JL
1er Journée Scientifique du médicament ; June **2011**, Grenoble, **France**

ACTIVATABLE-TARGETING-PROBES FOR NEAR-INFRARED IMAGING OF CANCER
Wenk C H F, Josserand V, Dumy P, Boturyn D, Coll JL
Cancer Microenvironment - XIth Topic Day Institut Albert Bonniot; October **2011**, Grenoble, **France**

SMART-PROBES FOR NEAR-INFRARED IMAGING OF CANCER
Wenk C H F, Josserand V, Dumy P, Boturyn D, Coll JL
Journées Thématiques GDR « Imageries in vivo » (IMAGIV) - Des nouveaux concepts en imagerie àl'application clinique; December **2011**, Paris, **France**

SMARGETING PROBES FOR OPTICAL IMAGING OF CANCER
    Wenk C H F, Josserand V, Dumy P, Boturyn D, Coll JL
    7th Cancer Scientific Forum of the Canéropôle CLARA, March **2012**, Lyon, **France**

OPTICAL-GUIDED SURGERY OF FIBROSARCOMA ON CAT PATIENTS. A VETERINARY CLINICAL STUDY
    Wenk C H F, Josserand V, Guillermet S, Tenaud C, Watrelot-Virieux D, Boturyn D, Carozzo C, Ponce F, Coll JL
    World Molecular Imaging Congress (WMIC), September **2012,** Dublin, **Ireland**

SMART PROBES FOR OPTICAL IMAGING OF CANCER
    Wenk CH. F.,Josserand V, Dumy P, Boturyn D, Coll JL
    World Molecular Imaging Congress (WMIC), September **2012,** Dublin, **Ireland**

ORAL COMMUNICATION

Near-infrared guided surgery of cancer: from models to clinical cases
    Wenk C H F; Keramidas M; Josserand V.; Righini C. A; Boturyn D.; Rizo P.; Dumy P. and Coll JL
    Hot Topics in Molecular Imaging (TOPIM) – ESMI winter conference "Emerging imaging methods in medicine" - January **2011**, Les Houches, **France**

Smartprobes for near-infrared imaging of cancer
    Wenk CH. F.,Josserand V, Dumy P, Boturyn D, Coll JL
    Comité de these, Institut Albert Bonniot, December **2010**, Grenoble, **France**

Smart-probes for optical imaging of cancer and optical guided surgery of cats
    Wenk CH. F.,Josserand V, Dumy P, Boturyn D, Coll JL
    Comité de these, Institut Albert Bonniot, October **2011**, Grenoble, **France**

Optical guided-surgery of the feline fibrosarcoma & design of SMARgetting probes
    Wenk CH. F.,Josserand V, Dumy P, Boturyn D, Coll JL
    Comité de these, Institut Albert Bonniot, June **2012**, Grenoble, **France**

HONOURS AND AWARDS

    Best communication/poster award:

    Wenk C; Journée pour la Recherche Respiratoir (J2R), Nantes **2010, France**

    Wenk C H F; Cancer Microenvironment **-** XIth Topic Day Institut Albert Bonniot; October **2011**, Grenoble, **France**

    Wenk C H F; World Molecular Imaging Congress (WMIC), September **2012,** Dublin, **Ireland**

T<small>ABLE</small> O<small>F</small> C<small>ONTENTS</small>

INDEX OF FIGURES

RESULTS & CONCLUSIONS

DISCUSSION & PERSPECTIVES

MATERIALS & METHODS

INDEX OF TABLES

LIST OF ABBREVIATIONS

AcOH   acetic acid

Alloc   Allyloxycarbonyl

AP-1   activator protein-1

Boc   Tertio-butyloxycarbonyl

CT   Computed Tomography

Cy5   Cyanine 5

Cy3   Cyanine 3

DiPEA   N,N-Diisopropylethylamine

DMF   N,N-Dimethylformamide

Dns   Dansyl

DNP   dinitrophenyl

ECM   extracellular matrix

equiv.   molar equivalent

EtOH   Ethanol

EPR   enhanced penetration and retention

ERK   extracellular signal-regulated kinase

F_{50} 50 %Fluorescence (time of reducing the maximal fluorescence intensity by half)

FACS   Fluorescence-Activated Cell Sorting

FAK   focal adhesion kinase

FGF-2   fibroblast growth factor-2

FITC   fluorescein isothiocyanate

Fmoc   9-Fluorenylmethyloxycarbonyl

FN   fibronectine

h   hour/-s

HAS   human serum albumin

HCC   hepatocellular carcinoma

Her2/neu   human epidermal growth factor receptor 2

ICG   indocyanine green

IL-8   Interleukin-8

JNK   c-Jun N-terminal Kinases

LUT   Lookup table (for transforming measured values (input data) in a visible grayscale image (output format))

mAb   monoclonal antibody

Mca   7-methoxycumarin

MeOH   Methanol

MFI   mean fluorescence intensity

min   minute/-s

MMP   Matrixmetalloprotease

MRI   Magnetic Resonance Imaging

MS   Mass Spectrometry

ms   millisecond

NF-κB   nuclear factor kappa-light chain-enhancer of activated B cells

NHS   N-hydroxysuccinimide

NIR   Near Infrared

NSCLC   Non small cell lung cancer

Pbf   2,2,4,6,7-Pentamethyl-dihydrobenzofurane-5-sulfonyl

PDGF   Platelet-derived growth factor

p.d.u.   procedure defined unit

PET   Positron Emission Tomography

PI3K   Phosphoinositole 3-Kinase

PyBop   (Benzotriazol-1-yloxy)tris(pyrrolidino)phosphonium hexauorophosphate

QSY   Quencher

RAFT   Regioselectively Addressable Functionalized Template

RFA   radiofrequency ablation

RGD   cyclic R-G-D-f-K

RT-HPLC   Reverse Phase High Performance Liquid Chromatography

RT   Retention Time

SASRIN   Super Acid Sensitive Resin

SBR   signal-to-background ratio

SLN   sentinel lymph node

SPECT   single photon emission computed tomography

SPPS   Solid Phase Peptide Synthesis

TFA   Triuoracetic acid

TIS   Triisopropylsilane

TNBS   Trinitrobenzensulfonic acid

TNF-α   tumor necrosis factor alpha

Trt   trityl / triphenylmethyl

US   ultrasound imaging

VEGF   vascular endothelial growth factor

„Ich kann freilich nicht sagen, ob es besser werden wird, wenn es anders wird; aber soviel kann ich sagen: es muss anders werden, wenn es gut werden soll.“

Georg Christoph Lichtenberg 1742–1799

[Certainly, I cannot tell if it will be better, when it changes; but what I can say so far: it will have to be different to be good.]

INTRODUCTION

PREAMBLE

In most cancers, tumor resection is the first therapeutic indication before chemotherapy or radiotherapy assuming that the tumor is removable. Since the patient survival strongly depends on the exhaustiveness of the tumor resection, innovative methods improving the quality of cancer surgery are needed to lower the risks of postoperative local recurrence.

Actually, several approaches for image-guided surgery are in development for clinical application, thereunder the design of optical imaging devices. This technology, working in an optical window with improved information out-come, the near-infrared (NIR), showed an improvement in the quality of the surgery in preclinical studies. First studies in clinics have been done by different research groups, but the translation from preclinics into clinics needs the adaptation of the imaging device for the operation block to warrant correct surgery.
Nevertheless, for a real clinical employment these systems are restricted to one imaging probe being the only one approved for use in human (FDA; ANSM) with the imaging properties needed. This is a critical point for the development and translation of NIR-optical imaging systems in clinical application, especially as the tracer used is non-specific and thus limited in its application.

Relating to this, a portable clinical imaging device (Fluobeam^{TM}) for optical guided surgery has been developed, working with a tumor targeting probe (AngioStamp™) in the NIR window. The combination of imaging device and specific tracer allowed speeding up high quality surgery in preclinical studies.

One part of my work was the transfer of this technology into a clinical veterinary phase, that is to say the clinical surgery of spontaneous tumors in cats, in order to evaluate this system regarding clinical surgery in humans.

In parallel, cancer diagnosis and therapy lack of specificity towards the tumor cells, limiting a precocious detection and safe treatment. Conventional cytostatic and cytotoxic treatments lead to adverse effects, which limit the dose of administration.
Consequently, clinical cancer research claim the development of new sensitive and performing diagnostic methods and of efficient therapeutics with reduced adverse effects.

Therefore, cancer research is pushed towards the development of targeting strategies. This corresponds to the use of new molecules emerging from biological knowledge of cancer and reacting specifically with the cancer cell.

Among the specific physiopathological phenomenon of cancer, targeting of tumor angiogenesis represents a promising strategy to limit tumorigenesis. Tumor neo-vessels differ from quiescent vessels concerning their structure but also in their functioning by overexpressing membrane receptors and other specific recognition elements on the surface of endothelial cells. At the same time these receptors are over-expressed by certain tumor cells themselves, which allows a targeting of the tumor directly. In order to efficiently target these receptors synthetic ligands have been developed with very high specificity and selectivity.
Other potential targets are enzymes over-expressed in the tumoral tissue. A group of these enzymes are amongst others in correlation with the receptors of angiogenesis and necessary for tumor cell invasion and spreading. Due to their cleavage activity they incorporate a target for activatable molecules in the sense of pro-drugs or quenched imaging agents.

In this context my laboratories have developed the vector "RAFT-(cRGD)$_4$", in the following simply called RAFT-RGD. This molecule is based on decapeptide scaffold with two independent domains, allowing the combination of two different functions. One domain presents a ligand in a multivalent fashion, whereas the other domain carries the vectorization agent: therapeutics or imaging agents.
The RAFT-RGD showed its capacity of targeting tumor and endothelial cells expressing the receptor integrin $\alpha_v\beta_3$ *in vitro* and *in vivo*, which allowed the fluorescence imaging *in vivo* of integrin $\alpha_v\beta_3$ positive tumors and serves also as the already mentioned tracer AngioStamp™.

My second project was the design of an innovative fluorescent molecule for cancer diagnosis and therapy, thus a pharmacodiagnosticum (or theranostic). The molecule constructed is a derivative of the RAFT-RGD combined with a cassette, cleavable by enzymes overexpressed in tumors. A fluorophore, quenched by another molecule in the cassette, is set free, when the peptide sequence connecting these molecules, is cleaved. The result is an increase in the fluorescence signal. The molecule, afterwards called RAFT-RGD-MMP, was synthesized and tested in first studies *in vitro* and *in vivo* using different tumor cell lines in order to study the capacity of dual-targeting compared to a mono-target approach.

I.   Tumorigenesis

I.1.   *Characteristics of tumorigenesis*

Cancer can be considered as a general term covering a plethora of different malignancies. These pathogenic conditions are characterized by changes in certain physical properties normally preserving cell homeostasis.

Cell homeostasis consists in the maintenance of a balance between the loss and repair of cells. In the case of tumors, an imbalance occurs between reduced cell loss and excessive cell growth.

Hanahan and Weinberg[1,2] described eight biological capabilities acquired by cancer cells called hallmarks of cancer. Mentioned are the sustaining of proliferative signaling, evading growth suppressors, resisting cell death, enabling replicative immortality, inducing angiogenesis, activating invasion and metastasis, reprogramming of energy metabolism, and evading immune destruction.

These mechanisms are needed for and lead to the multistep development called tumorigenesis. The term tumorigenesis describes the process of initiating and promoting the development of a tumor. In general it consists of three consecutive steps: 1) initiation of cell changes to be able to form tumors, 2) promotion, which is the growth of existing tumors and 3) progression, which is characterized by increased growth speed and invasiveness of the tumor cells (Figure I-1).

---

[1] Hanahan, D., und R. A. Weinberg. „The hallmarks of cancer". *Cell* 100 (2000): 57–70.
[2] Hanahan, Douglas, und Robert A. Weinberg. „Hallmarks of Cancer: The Next Generation". *Cell* 144, Nr. 5 (March 4,
[2] Hanahan, Douglas, und Robert A. Weinberg. „Hallmarks of Cancer: The Next Generation". *Cell* 144, Nr. 5 (March 4,
      2011): 646–674.
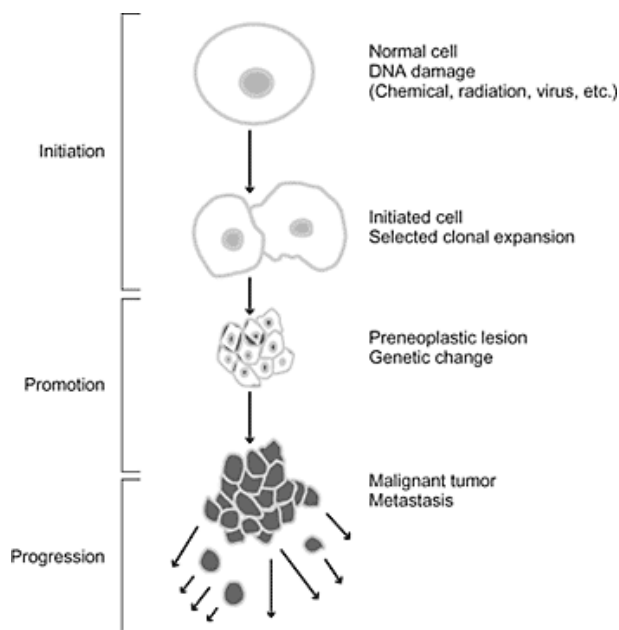
Figure I-1: Stages of tumorigenesis.
-After: H. Cortés-Funes "Antiangiogenesis Agents"*Drugs Today* 2002, 38(Suppl. A): 11-

Due to genomic instability and the inflammatory state of premalignant and malignant lesions, generation of the listed characteristics occurs. This is due to exposition to a carcinogen, either of chemical, physical or viral origin. Leading to activation of certain oncogenes and/or the inhibition of tumor suppressor genes, initiation and progression of cancer takes place.

After all, normal cells transform into "immortal" cells with higher activity in cell growth and cell-division. They possess means of modifying their environment and deregulating the physiological fine-tuned balance in order to support their development and spreading.
This is reflected for example by defect negative-feedback loops, like the oncoprotein Ras or the kinase mTOR, whose inhibition leads to enhanced proliferation. Other differences, compared to normal cells, is the evasion of growth suppressors, like retinoblastoma-associated and TP53 proteins, the enhancement of proliferation signaling and the resisting to physiological cell death, as well as inducing angiogenesis.

Hanahan *et al*. describe also that necrotic cells can recruit inflammatory cells of the immune system. In the context of neoplasia, this can actively promote tumor progression,

because such cells are capable of enhancing angiogenesis, cancer cell proliferation, and invasiveness[3].

Necrotic cells can release bioactiveregulatory factors, which can directly stimulate neighboring viable cells to proliferate, with the potential, to facilitate neoplastic progression.

It is known that some tumors are densely infiltrated by cells of the immune system and thereby mirror inflammatory conditions arising in non-neoplastic tissues.

Inflammation is in some cases evident at the earliest stages of neoplastic progression and is demonstrably capable of facilitating the development of neoplasias into cancers.

Additionally, inflammatory cells can release chemicals, notably reactive oxygen species that are actively mutagenic for nearby cancer cells, accelerating their genetic evolution towards states of heightened malignancy.

Apart from dysregulation of physiological mechanisms, cancer cells have certain morphological properties which make them histologically identifiable. The dedifferentiated cells are presenting rounded cytoskeleton, with reduced cell-to-cell and cell-to-extracellular matrix adhesion. The nucleolus is characterized by hypertrophy, macro- and microsegregation[4] and the neoplastic cell population is highly genotypically and phenotypically heterogeneous.

Besides, tumor cells are more or less organized in a supporting tissue. This so called tumor stroma consists of fibroblasts, smooth muscle cells, blood and lymphatic vessels and infiltrated immune cells, such as macrophages, mastocytes and lymphocytes, which are all embedded in an extracellular matrix (ECM)[5] (Figure I-2). Furthermore the tumor microenvironment consists of soluble factors such as cytokines and growth factors.

The vascularization and sprouting of new blood vessels in the tumor stroma is important for tumor growth and invasion of the surrounding tissue and metastasis. It represents not only the supplying system for nutrients, oxygen and the elimination pathway of waste but also a transport system for metastatic cells to reach the organs of metastasis manifestation. Thus, it is also an access point for molecules, either diagnostic or therapeutic ones.

---

[3] Hanahan, Douglas, und Robert A. Weinberg. „Hallmarks of Cancer: The Next Generation". *Cell* 144, Nr. 5 (March 4, 2011): 646–674.

[4] Baba, Alecsandru Ioan A I, und Cornel C Câtoi. *Comparative Oncology*. Bucharest: The Publishing House of the Romanian Academy, 2007.

[5] Li, Zhi-Wei, und William S Dalton. „Tumor microenvironment and drug resistance in hematologic malignancies". *Blood reviews* 20, Nr. 6 (November 2006): 333–342.

I am going now to give a brief description of the process of angiogenesis in order to introduce
the interest in targeting certain structures or enzymes for specific tumor imaging and therapy.
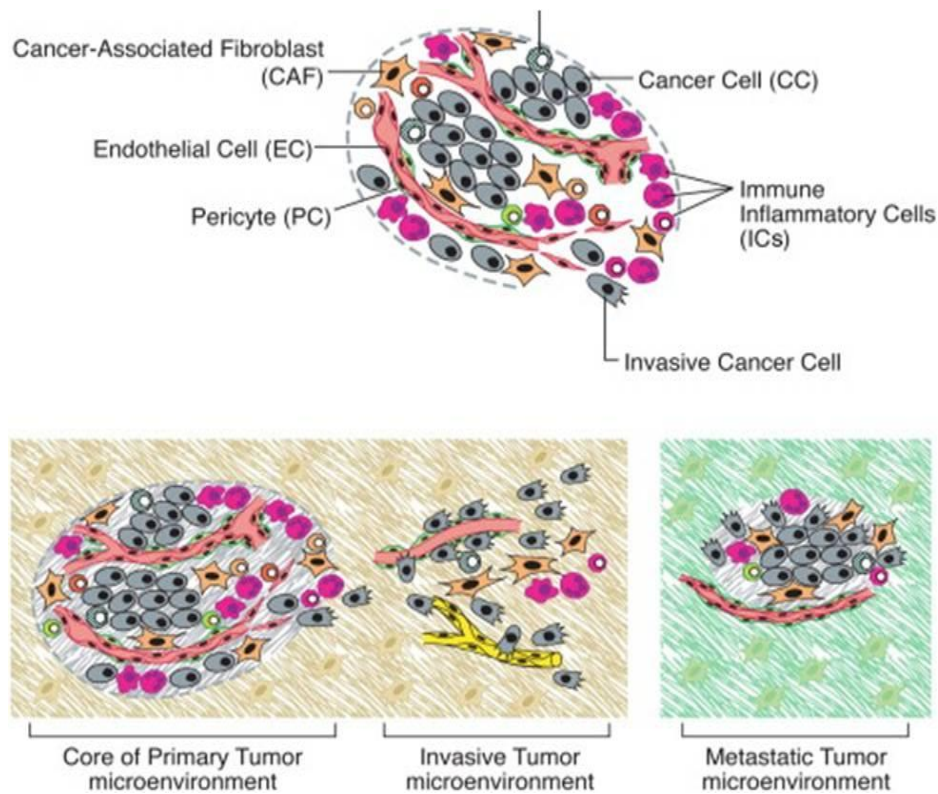
Figure I-2: The Cells of the Tumor Microenvironment.

(Upper) An assemblage of distinct cell types constitutes most solid tumors. Both the parenchyma and stroma of tumors
contain distinct cell types and subtypes that collectively enable tumor growth and progression. (Lower) The distinctive
microenvironment of tumors.

(hatched background represents the extracellular matrix)

-Adapted after Hanahan & Weinberg, *Hallmarks of Cancer: The Next Generation,* Cell Volume 144, Issue 5 2011 646 – 674.-

II. Angiogenesis

The formation of blood vessels is an important physiological process during embryogenesis and development.

Angiogenesis itself is the process of forming new blood vessels from existing ones. Therefore vascular basement membrane degradation is needed and remodeling of the ECM for migration of endothelial cells invasion of surrounding tissue and lumen formation is necessary.

Establishment of an arterial network requires vascular remodeling by perivascular mural cells including pericytes and vascular smooth muscle cells (Figure II-1).
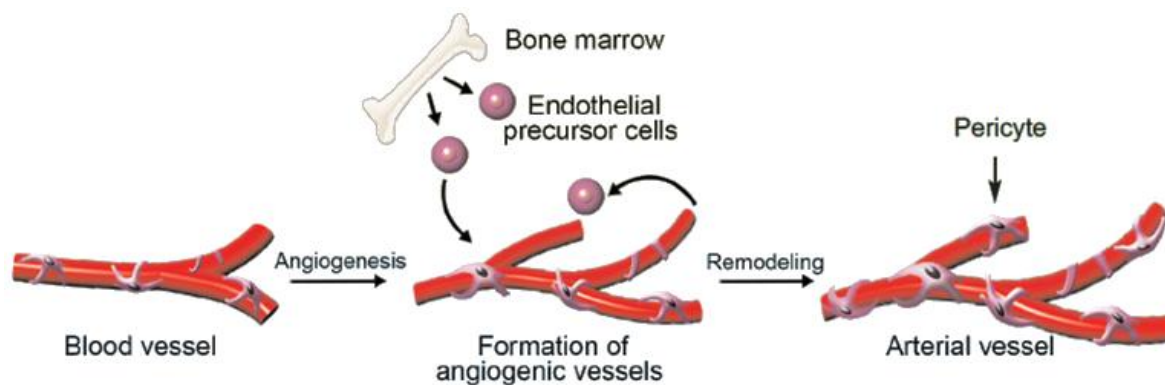
Figure II-1: Blood vessel formation.

- Cao, Yihai. "Therapeutic Angiogenesis for Ischemic Disorders: What Is Missing for Clinical Benefits?" *Discovery Medicine* 9, Nr. 46 (March 3, 2010): 179–184.-

Bone marrow-derived stem cells have been reported to play a critical role in contribution to growing vessels by the mechanism of differentiation into vascular endothelial cells[6].

Physiological angiogenesis in adults does only occur in certain cases like wound healing or during the menstrual cycle of a woman. Therefore it is a symptom of pathology like rheumatoid arthritis, retinopathy, psoriasis, arteriosclerosis or cancer[7].

While the tumor does not exceed 1-2 mm^3, the tumor cells do get enough oxygen and nutrition by simple diffusion[8]. Exceeding this size, the inhibitors of the angiogenesis are

---

[6] Lyden, D, K Hattori, S Dias, C Costa, P Blaikie, L Butros, A Chadburn, u. a. „Impaired recruitment of bone-marrow-derived endothelial and hematopoietic precursor cells blocks tumor angiogenesis and growth". *Nature medicine* 7, Nr. 11 (November 2001): 1194–1201.

[7] Carmeliet, Peter. „Angiogenesis in health and disease". *Nature medicine* 9, Nr. 6 (Juni 2003): 653–660.

oppressed and the pro-angiogenetic factors, like vascular endothelial growth factor (VEGF), platelet-derived growth factor (PDGF) and tumor necrosis factor-α (TNF-α), are secreted by the tumor cells, the tumor stroma, inflammatory cells or the ECM[9]. This is a process, which takes normally place due to stress (metabolic like hypoxia, hypoglycemia, low pH; mechanic, inflammation and/or gene dysregulation), and is called "angiogenic switch". This implies the shift of the balance to more pro- than anti-angiogenic signals and often occurs at an early, premalignant stage[10].

The endothelial cells that form existing blood vessels, respond to angiogenic signals in their vicinity by proliferating and secreting proteases. These proteases break open the blood-vessel wall to enable migration towards the site of the angiogenic stimuli. Then proliferating endothelial cells organize themselves into new capillary tubes by altering the arrangement of their adherence-membrane proteins. Finally, through the process of anastomosis, the capillaries, emanating from the arterioles and the venules, join to provide a continuous blood flow. This sustains tumor cell metabolism and sets up escaping avenues for metastatic tumor cells (Figure II-2).

Thus the tumor induces its proper vascularization, which allows its development and spreading[11,12].

---

[8] Folkman, J. „Endothelial cells and angiogenic growth factors in cancer growth and metastasis. Introduction". *Cancer metastasis reviews* 9, Nr. 3 (November 1990): 171–174.

[9] Carmeliet, P, und R K Jain. „Angiogenesis in cancer and other diseases". *Nature* 407, Nr. 6801 (September 14, 2000): 249–257.

[10] Rundhaug, Joyce E. „Matrix Metalloproteinases and Angiogenesis". *Journal of Cellular and Molecular Medicine* 9, Nr. 2 (2005): 267–285.

[11] Gimbrone, M A, Jr, S B Leapman, R S Cotran, und J Folkman. „Tumor dormancy in vivo by prevention of neovascularization". *The Journal of experimental medicine* 136, Nr. 2 (August 1, 1972): 261–276.

[12] Folkman, J, und D Hanahan. „Switch to the angiogenic phenotype during tumorigenesis". *Princess Takamatsu symposia* 22 (1991): 339–347.
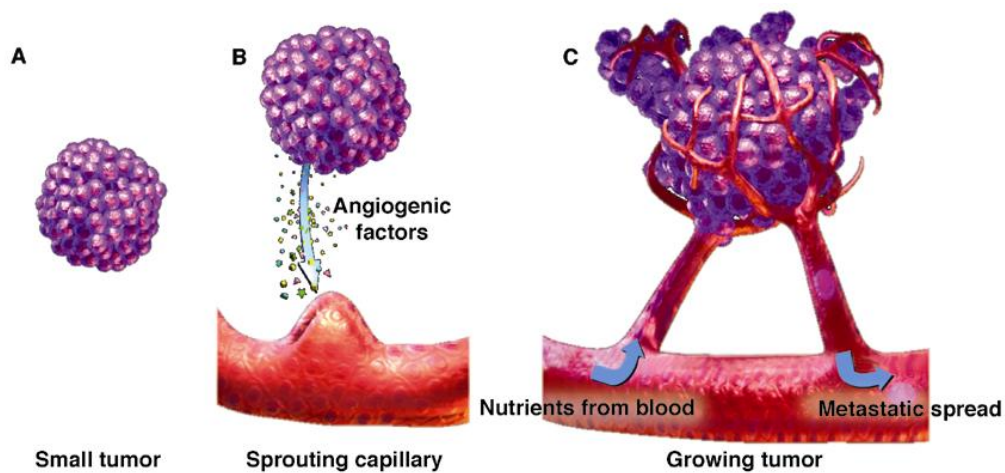
Figure II-2: Tumor development and angiogenesis.
- Siemann DW., Vascular targeting agents. Horizons in Cancer Therapeutics: From Bench to Bedside. 2002;3(2):4-15.-

Compared to normal blood vessels, tumor blood vessels have a chaotic vasculature and are tortuous, leaky, and dilated or uneven in diameter, with reduced attachment of pericytes[13].

Various classes of adhesion molecules are involved in tumor angiogenesis, such as members of the integrin, cadherin, selectin and immunoglobulin families.

Here I will focus on the integrins, as the $\alpha_v\beta_3$ integrin, represents our target.

---

[13] Rundhaug, Joyce E. „Matrix Metalloproteinases and Angiogenesis". *Journal of Cellular and Molecular Medicine* 9, Nr. 2 (2005): 267–285.

II.1.   *Integrins*

The integrins modulate physical processes like migration and invasion of the cell as well as intracellular pathways leading to cell survival and proliferation as well as cell death by anoïkis when cells loose contact with the ECM. The function of these receptors ranges from cell-substrate-attachment mediation to intracellular signal transduction. The signalization in all its complexity is accentuated by the capacity of the integrin to modulate the mediated signals of other membrane receptors and the other way round[14].

As integrins do not have an intrinsic enzymatic activity, they recruit different enzyme partners for signal transmission.

II.1.1.   *Integrin composition*

Integrins are heterodimeric cell surface receptors composed of noncovalently associated transmembrane glycoproteins, α and β, which connect adhesive proteins in the ECM to the cytoskeleton. There are at least 18 different α subunits and eight different β subunits identified, which represent - in an associated form - over 24 receptors for different spectra of extracellular ligands (Figure II-3)[15].

The α and β subunits consist of a large extracellular domain (700-1100 amino acids) and a short cytoplasmic domain of 30 to 50 amino acids. The N-terminal extremities, next to the extracellular domain of the α subunit, contain regions, which are capable to bind divalent cations (Mg^{2+}, Ca^{2+}). The β subunit has cystein-rich regions in its extracellular domain and a folded N-terminal, forming a large loop (Figure II-4)[16].

---

[14] Porter, J C, and N Hogg. "Integrins Take Partners: Cross-talk Between Integrins and Other Membrane Receptors." *Trends in Cell Biology* 8, no. 10 (October 1998): 390–396.

[15] *van den Steen et al., 2006, Journal of biol. Chem.. 281, 18626-18637.*

[16] Humphries, M.J. (2000) "Integrin structure" Biochem Soc Trans 28(4): 311-39
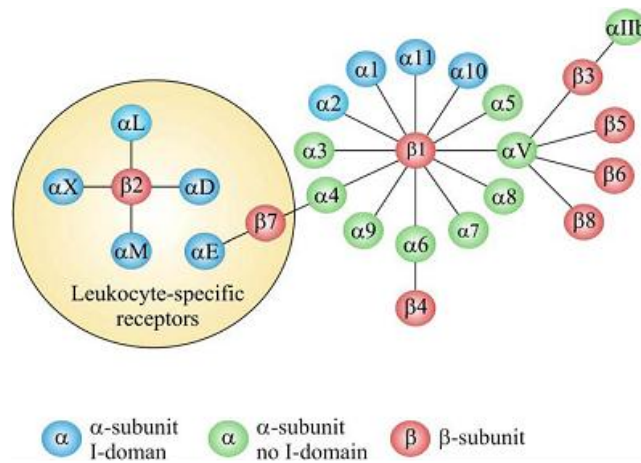
Figure II-3: The members of the human integrin superfamily and how they combine to form heterodimeric integrins.

At least 18 α subunits and eight β subunits have been identified in humans, which are able to generate 24 different integrins. Integrin subunits that bind to each other to form a heterodimer are connected by solid lines. Each integrin has distinct ligand-binding specificity and tissue and cell distribution.

- Niu G, Chen X. Why Integrin as a Primary Target for Imaging and Therapy. *Theranostics* 2011; 1:30-47.-
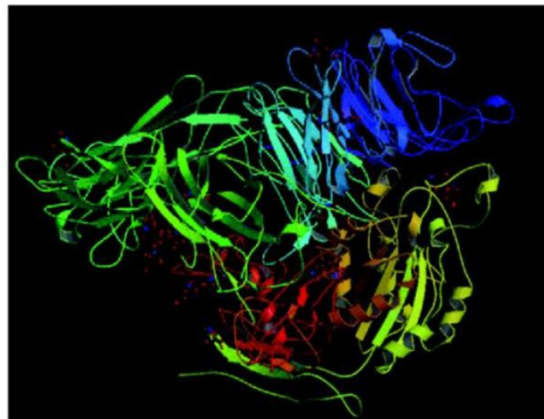
Figure II-4: The extracellular region of a human integrin.

The crystal structure represents a net form of integrin αVβ3 with no bound RGD

-Takada, et al. "The Integrins." Genome Biology 8, no. 5 (2007): 215.-

II.1.2.   *Integrin conformation & substrate recognition*

The association αβ determines the specificity of the integrin for its substrate. The interaction ligand-integrin is modulated by the avidity and the affinity and is strongly influenced by the ligand's conformation and the possible multimeric formation. The transmission of the signal in the cell is guaranteed by the "key-lock-principle". Nevertheless, as one ligand can be recognized by more than one integrin, cooperative and competitive effects between integrins lead to complex signaling. Thus precise analysis of its environment by the cell is more than a simple physical interaction of cell and ECM.

Being a dimer, different conformations of integrins can be observed, which modifies their affinity towards their ligand and their state of activation (Figure II-5). Integrin-ligand affinity is modulated by chemical allostery, mechanical allostery and integrin clustering. Several integrins are basically not active (Figure II-5, B), but expressed on the cell surface in an inactive form (Figure II-5, A). This results in a lack of ligand-receptor interaction and consequently no signal is emitted[17]. The cell glycocalyx is also of importance, as it occupies the cell-substrate space and thus influences the diffusion of reactants, limiting the attachment of both integrin and ligand to surfaces[18].
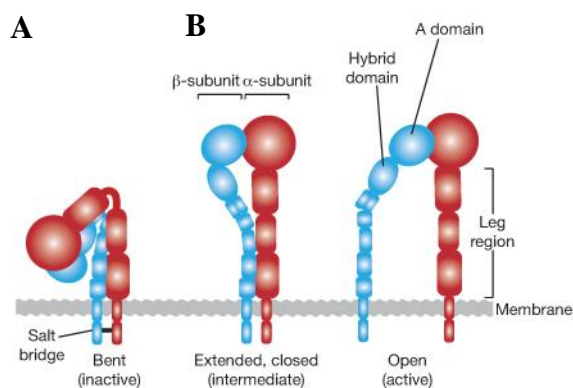
Figure II-5: Intergin formation: A) inactive, bend form; B) active form
-After: Bass, Mark D. „SHARPINing integrin inhibition". *Nature Cell Biology* 13, Nr. 11 (November 2, 2011): 1292–1293.-

---

[17] Takagi, Junichi, and Timothy A Springer. "Integrin Activation and Structural Rearrangement." *Immunological Reviews* 186 (August 2002): 141–163.
[18] Boettiger, David. „Mechanical control of integrin-mediated adhesion and signaling". *Current opinion in cell biology* (August 1, 2012).

Concerning their specificity for their ligands, integrins can be classified in different groups: laminin integrins, collagen integrins, leucocytes integrins, and integrins recognizing the short peptide sequence Arg-Gly-Asp (RGD)[19].

Upon engagement, integrins cluster at the attachment site and recruit multiple intracellular cytoskeletal proteins, such as α-actinin, talin, and filamin, as well as signaling proteins, including focal adhesion kinase and integrin-linked kinase[20,21]. The formation of focal adhesion contacts is a prerequisite for adhesion, spreading, and migration through structures of the ECM.

II.1.3.   Integrin turn-over

An important aspect is also the possible internalization of integrins by endocytic routes, such as the formation of circular dorsal ruffles during macropinocytosis and clathrin-dependent or -independent endocytic pathways. This implicates the rapid trafficking of integrins to early endosomes. Nevertheless the majority of these internalized integrins are rapidly recycled back to the plasma membrane ($t_{1/2}$ of integrin recycling often in less than 15 min)[22].

II.1.4.   Roles of integrin

As playing a principal role in the maintenance of tissue-cohesion and cell migration, integrin dimers are also implicated in the progression of several pathologies, making them a potential therapeutic target[16]. Integrins control also diverse other cellular processes, including proliferation, apoptosis and differentiation, thus are implicated in development, immune responses and progression of diseases.

Concerning cancer, the transformation of cancer cells is inter alia characterized by the disorganization of the cytoskeleton and the loss of adherence. Analyzing the modifications of expressed integrins in healthy tissues and tumor tissue, it has been observed that the integrins

---

[19] Takeda, Ikuko, Shin-Ichiro Maruya, Takashi Shirasaki, Hiroki Mizukami, Takenori Takahata, Jeffrey N Myers, Seiji Kakehata, Soroku Yagihashi, and Hideichi Shinkawa. "Simvastatin Inactivates Beta1-integrin and Extracellular Signal-related Kinase Signaling and Inhibits Cell Proliferation in Head and Neck Squamous Cell Carcinoma Cells." *Cancer Science* 98, no. 6 (June 2007): 890–899.

[20] R.E. Seftor, E.A. Seftor, M.J. Hendrix, Molecular role(s) for integrins in human melanoma invasion, Cancer Metastasis Rev. 18 (1999) 359–375.

[21] R.O. Hynes, Integrins: versatility, modulation, and signaling in cell adhesion, Cell 69 (1992) 11–25.

[22] Bridgewater, Rebecca E, Jim C Norman, und Patrick T Caswell. „Integrin trafficking at a glance". *Journal of cell science* 125, Nr. Pt 16 (August 15, 2012): 3695–3701.

do either positively either negatively participate in the phenotype of tumor transformation[23] (Table II-1).

Tumour type	Integrins expressed	Associated phenotypes
Melanoma	$\alpha v\beta 3$ and $\alpha 5\beta 1$	Vertical growth phase [35,172-174] and lymph node metastasis[173,175]
Breast	$\alpha 6\beta 4$ and $\alpha v\beta 3$	Increased tumour size and grade[176], and decreased survival[177] ($\alpha 6\beta 4$). Increased bone metastasis[36-38,64] ($\alpha v\beta 3$)
Prostate	$\alpha v\beta 3$	Increased bone metastasis[39]
Pancreatic	$\alpha v\beta 3$	Lymph node metastasis[40]
Ovarian	$\alpha 4\beta 1$ and $\alpha v\beta 3$	Increased peritoneal metastasis[178] ($\alpha 4\beta 1$) and tumour proliferation[179] ($\alpha v\beta 3$)
Cervical	$\alpha v\beta 3$ and $\alpha v\beta 6$	Decreased patient survival[41,180]
Glioblastoma	$\alpha v\beta 3$ and $\alpha v\beta 5$	Both are expressed at the tumour–normal tissue margin and have a possible role in invasion[181]
Non-small-cell lung carcinoma	$\alpha 5\beta 1$	Decreased survival in patients with lymph node-negative tumours[182]
Colon	$\alpha v\beta 6$	Reduced patient survival[109]

Table II-1: Role of integrins in the tumor progression.
-After: Desgrosellier, Jay S, und David A Cheresh. „Integrins in cancer: biological implications and therapeutic opportunities". *Nature reviews. Cancer* 10, Nr. 1 (January 2010): 9–22.-

---

[23] Mizejewski, G J. „Role of integrins in cancer: survey of expression patterns". *Proceedings of the Society for Experimental Biology and Medicine. Society for Experimental Biology and Medicine (New York, N.Y.)* 222, Nr. 2 (November 1999): 124–138.

II.2.   The integrin αvβ3

For example α_v integrins are highly expressed in tumor vasculature, where they can be accessed with peptides containing the RGD integrin recognition motif[24,25,26]. This approach will be discussed later on in the section "imaging probes for NIR imaging" on page - 40 -.

The expression of β_3 integrins is mostly associated with the ability of tumors to metastasize[27], as integrin α_vβ_3 has been linked to enhance transendothelial migration and production of MMP-2.

Concerning internalization processes α_vβ_3 integrins recycle through a "short-loop" pathway which returns these heterodimers from the early endosomes back to the plasma membrane without transiting through the perinuclear recycling compartment. This is said to be the control key to directionally persistent migration and branching morphogenesis of endothelial vessels[28]. Bridgewater *et al*. report also that inhibition of this receptor *via* small molecules (e.g. Cilengitide) in endothelial cells enhances the recycling of VEGF receptor 2. Thus, it is protected from degradation and increases its presence on the cell surface. This in turn promotes cell migration, aortic sprouting and tumor angiogenesis *in vivo*.

The integrin α_vβ_3 is probably the integrin the most strongly involved in the regulation of angiogenesis (Figure II-6) and up-regulated in endothelial tumors, wounds and inflammation. This was demonstrated as it is widely expressed on blood vessels of tumor biopsy samples but not on vessels in normal tissue[27]. Up-regulated not only in angiogenic endothelial cells but also in several tumor cells[29], it represents an attractive target for cancer targeting.

---

[24] Eliceiri, B P, und D A Cheresh. „Adhesion events in angiogenesis". *Current opinion in cell biology* 13, Nr. 5 (Oktober 2001): 563–568.

[25] Pierschbacher, M D, und E Ruoslahti. „Variants of the cell recognition site of fibronectin that retain attachment-promoting activity". *Proceedings of the National Academy of Sciences of the United States of America* 81, Nr. 19 (Oktober 1984): 5985–5988.

[26] Ruoslahti, Erkki. „Antiangiogenics meet nanotechnology". *Cancer cell* 2, Nr. 2 (August 2002): 97–98.

[27] Danhier, Fabienne, Aude Le Breton, und Veronique Preat. „RGD -based strategies to target alpha(v) beta(3) integrin in cancer therapy and diagnosis". *Molecular pharmaceutics* (September 11, 2012).

[28] Bridgewater, Rebecca E, Jim C Norman, und Patrick T Caswell. „Integrin trafficking at a glance". *Journal of cell science* 125, Nr. Pt 16 (August 15, 2012): 3695–3701.

[29] Weis, Sara M, und David A Cheresh. „αv Integrins in Angiogenesis and Cancer". *Cold Spring Harbor perspectives in medicine* 1, Nr. 1 (September 2011): a006478.
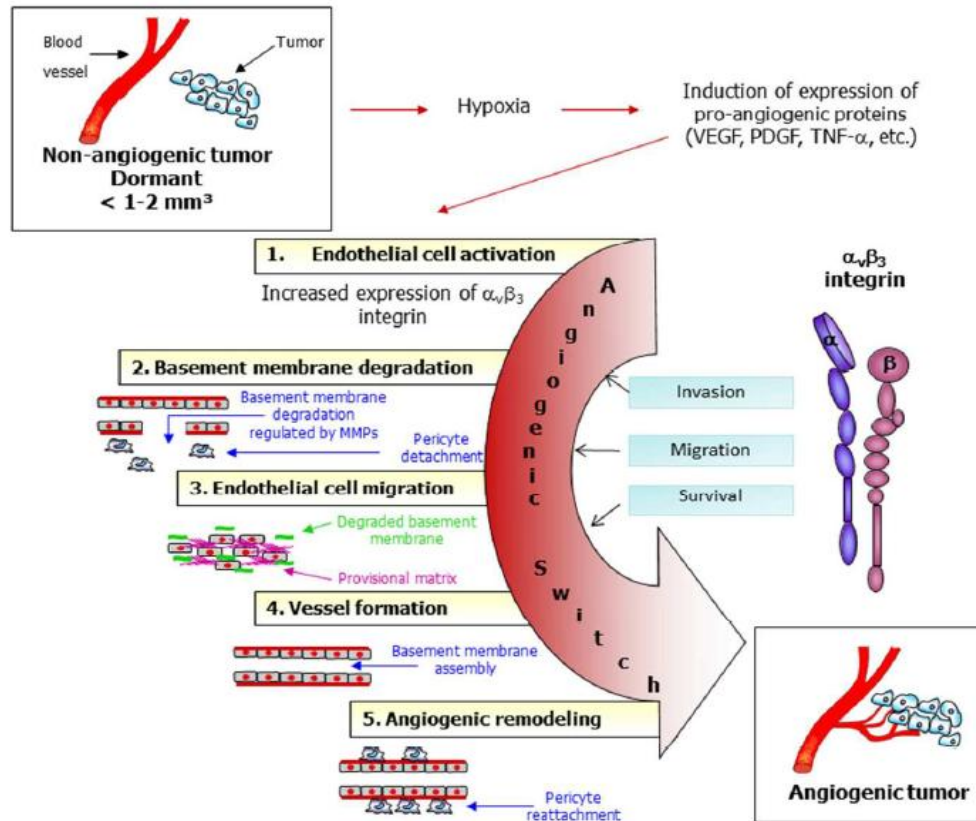
Figure II-6: Roles of the αvβ3 integrin in angiogenesis.
The integrin binds and activates MMP2 to help breaking down of the extracellular matrix. It regulates cell attachment, spreading and migration.
-After: Danhier, Fabienne, Aude Le Breton, und Veronique Preat. „RGD -based strategies to target alpha(v) beta(3) integrin in cancer therapy and diagnosis". *Molecular pharmaceutics* (September 11, 2012).-

III. Proteases and cancer

The interest in proteases, or proteolytic enzymes, in research is enormous. The mass of scientific articles represents a jungle of information and a broad spectrum of scientific domains is represented.

This is not astonishing as proteases play an important role in various physiological processes in all kinds of creatures. While catalyzing the breakdown of proteins by hydrolysis of peptide bonds, they are involved in the control of a large number of key physiological processes such as cell-cycle progression, cell proliferation and cell death, DNA replication, tissue remodeling, haemostasis in the sense of coagulation, wound healing and the immune response. And besides they are also involved in several pathological mechanisms.

To allude to some examples, there is inflammation, wound healing, infectious and degenerative diseases and cancer. After all they influence cell behavior, survival and death in their function as processing enzymes, characterized by a highly selective cleavage of specific substrates[30,31]. Thus, dysregulation of protease activity in general can lead to pathologies such as cardiovascular and inflammatory diseases, cancer, osteoporosis and neurological disorders[30].

For instance 679 known and putative human peptidases are listed by the MEROPS protease database[32] and additional 423 non-catalytic homologues in humans alone (as on August 2010). Of these proteases, at least 273 have been found in extracellular compartments or in the lumen of secretory compartments, 277 in intracellular compartments, and 16 in the cell membrane at the surface[33].

Rawlings *et al*. distributed the peptidases in 5 main mechanistic classes: Metalloproteases, Serine proteases, Cysteine proteases, Threonine proteases and Aspartic proteases (Figure III-1), plus proteases groups of unknown or unclassified catalytic mechanism[34].

MatrixMetalloproteases (MMPs) and Cathepsins have a special role as they are upregulated in cancer, but with a controversial role [31]. In general, molecular biology studies

---

[30] Turk, Boris. „Targeting proteases: successes, failures and future prospects". *Nature reviews. Drug discovery* 5, Nr. 9 (September 2006): 785–799.

[31] Drag, Marcin, und Guy S Salvesen. „Emerging principles in protease-based drug discovery". *Nature reviews. Drug discovery* 9, Nr. 9 (September 2010): 690–701.

[32] http://merops.sanger.ac.uk/

[33] Cudic, Mare, und Gregg B Fields. „Extracellular proteases as targets for drug development". *Current protein & peptide science* 10, Nr. 4 (August 2009): 297–307.

[34] Rawlings, Neil D, Alan J Barrett, und Alex Bateman. „MEROPS: the database of proteolytic enzymes, their substrates and inhibitors". *Nucleic acids research* 40, Nr. Database issue (January 2012): D343–350.

demonstrated the contribution of proteases to all stages of tumor progression. In the case of MMPs this includes an association in tumor growth, progression, metastasis and dysregulated angiogenesis.
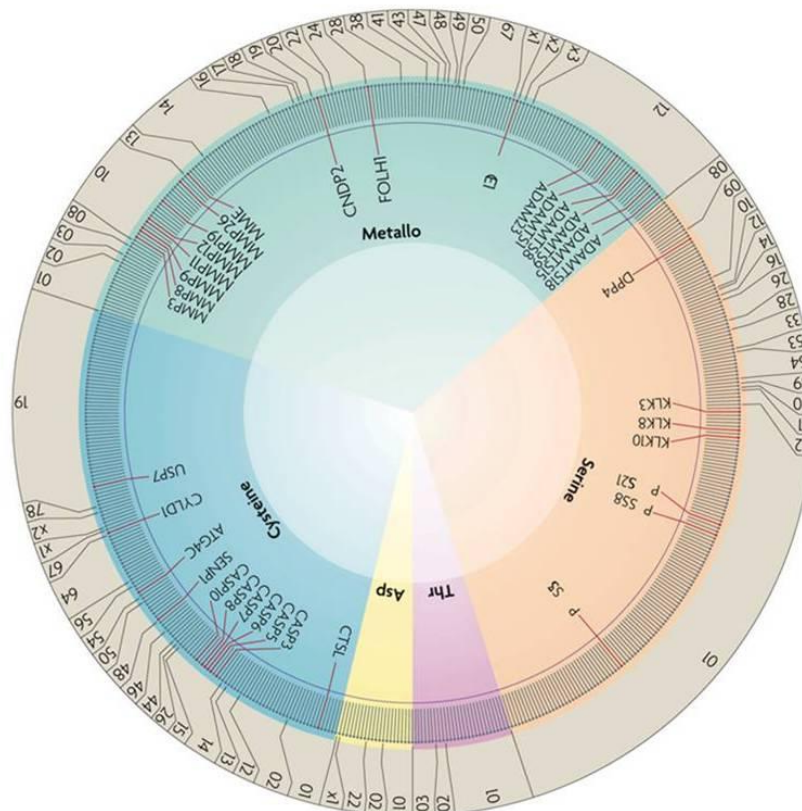
Figure III-1: Distribution of tumour-protective proteases in the human degradome.
Human proteases are distributed in 5 classes and 69 different families. Each individual enzyme is indicated by a grey line, and those with tumour-protective properties are shown in red. Numbers at the edge represent the different protease families of each catalytic class, according to the MEROPS database numbering.
-López-Otín, Carlos, und Lynn M. Matrisian. „Emerging Roles of Proteases in Tumour Suppression". *Nature Reviews Cancer* 7, Nr. 10 (Oktober 1, 2007): 800–808.-

III.1.   *Matrixmetalloproteases (MMPs)*

MMPs are a family of at least 23 zinc-dependent endopeptidases (they cleave protein substrates in the middle of the molecule) with hydrolytic activity for a diverse spectrum of extracellular proteins, especially components of the ECM. They can be divided in two structurally distinct groups: secreted MMPs and membrane-type MMPs (MT-MMPs). The secreted MMPs are then classified as collagenases, gelatinases, stromelysins and matrilysins due to their substrate specificity.

MT-MMPs (# 6)	Secreted MMPs			
Two: anchored mediated by glycosylphosphatidylinositol Four: transmembrane domain	Collagenases	Gelatinases	Stromelysins	Other MMPs
MMP-14 = MT1-MMP	MMP-1 = interstitial collagenases; MMP-8 = neutrophil collagenase; MMP-13 = rodent interstitial collagenase	MMP-2 = Gelatinase A MMP-9 = Gelatinase B	MMP-3 = stromelysin-1 MMP-10 = sroemysin-2 MMP-11 = stromelysin-3	MMP-7 = matrilysin MMP-12 = metalloelastase

Figure III-2: Table: Classes of the MMP family
-After:Pepper, M S. „Role of the matrix metalloproteinase and plasminogen activator-plasmin systems in angiogenesis".
Arteriosclerosis, thrombosis, and vascular biology 21, Nr. 7 (Juli 2001): 1104–1117.-

III.1.1.   *MMP structure*

MMPs consist of a catalytic domain with an active site cleft containing a catalytic zinc ion for substrate cleavage (Figure III-3). It is linked via the so called Hinge region to the C-terminal hemopexin-like domain (PEX). The hemopexin C domain is comprised of four hemopexin modules (I-IV), each representing a blade of beta-propeller structure. It allows MMPs to unwind/distort the triple helix of fibrillar collagens, so that the catalytic domain can cleave them[35]. The propeptide domain is at the N-terminal extremity. Gelatinases have additionally 3 type-II-fibronectin repeats for gelatin binding. MT-MMPs are membrane-

---

[35] Rundhaug, Joyce E. „Matrix Metalloproteinases and Angiogenesis". *Journal of Cellular and Molecular Medicine* 9, Nr. 2 (2005): 267–285.

bound enzymes. Therefore they have additionally a transmembrane α-helix, linking a cytoplasmic domain.
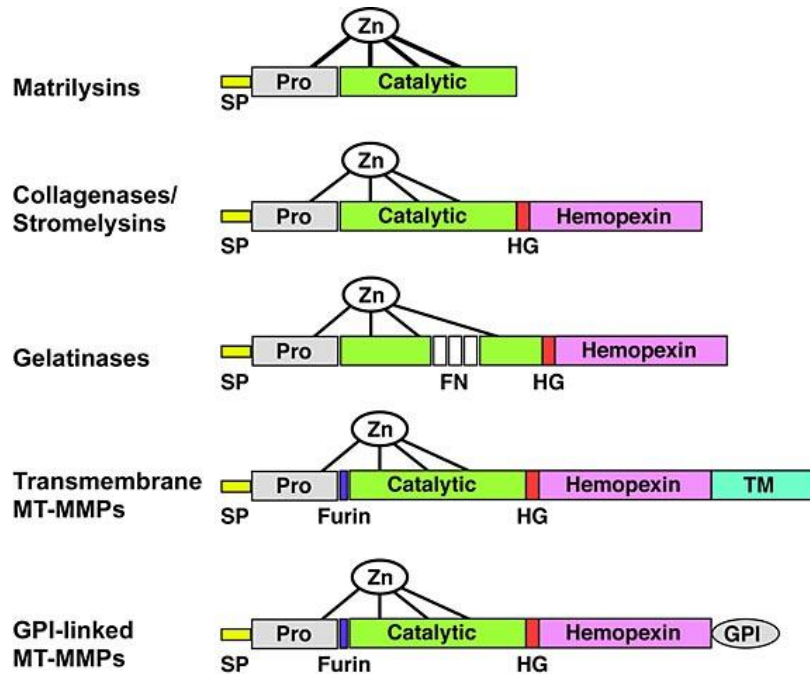
Figure III-3: Domain structure for the major classes of MMPs.

Major domains include the signal peptide (SP), prodomain (Pro), catalytic domain with the active sitezinc (Zn) bound to cysteine residues within this domain and "cysteine switch-residue" in the prodomain, the hinge domain (HG), the hemopexin domain, and in some cases either a transmembrane domain or GPI-anchor domain (GPI). A furin cleavage site between the prodomain and the catalytic domain is found in some MMPs. In the gelatinases, fibronectin-like type II repeats (FN) are also present.

-Brauer, Philip R. „MMPs--role in cardiovascular development and disease". *Frontiers in bioscience: a journal and virtual library* 11 (2006): 447–478.-

Secreted MMPs are first inactive pro-enzymes (Zymogens) until they are activated in the extracellular compartment[36,37]. Their activation is initiated by a specific multistep mechanism termed "cysteine switch", where the N-terminal propeptide domain is cleaved: A conserved unpaired cysteine residue in the pro-domain forms a coordinate bond with the zinc ion located in the active site. Cleavage of the pro-domain results in a disruption of the zinc-

---

[36] Pepper, M S. „Role of the matrix metalloproteinase and plasminogen activator-plasmin systems in angiogenesis". *Arteriosclerosis, thrombosis, and vascular biology* 21, Nr. 7 (Juli 2001): 1104–1117.

[37] Faust, Andreas, Bianca Waschkau, Jens Waldeck, Carsten Höltke, Hans-Jörg Breyholz, Stefan Wagner, Klaus Kopka, Walter Heindel, Michael Schäfers, und Christoph Bremer. „Synthesis and evaluation of a novel fluorescent photoprobe for imaging matrix metalloproteinases". *Bioconjugate chemistry* 19, Nr. 5 (Mai 2008): 1001–1008.

cysteine bond, followed by the loss of the amino-terminal pro-domain[38]. This enables the catalytic domain to degrade the specific substrate when it binds also to the active side cleft, containing the catalytic zinc ion, of the MMP.

Hydrolyzation by MMP-9 and -2 takes place at the Gly-Val bond, or Gly-Leu bond (also by MMP-1;-8;-13; -14)[39].

III.1.2.   MMP tuning

Normally, MMP expression is finely balanced at different levels and spatial restriction of extracellular proteolysis and matrix integrity is preserved by different mechanism.

First of all MMPs are secreted and may be stored in extracellular depots as precursor zymogens. They are susceptible to autolysis and the autolytically generated PEX domain of gelatinases binds to tissue inhibitors of MMPs (TIMPs) and substrates (see section VI, page - 54 -).

MMPs are subsequently tightly controlled by several endogenous inhibitors, such as the plasma inhibitor R2-macroglobulin and the four TIMPs[40]. In malignant tissues, MMPs and TIMPs are produced by both stromal cells of the tumor and by neoplastic cells as well as infiltrating inflammatory cells or endothelial cells themselves[41].

For example in inflammation, MMP-9 is predominantly expressed in neutrophils, macrophages, and mast cells[42].

Thus, a dyscontrol of this balance leads to a pathological over-expression.

As the tumor stroma turnover affects the growth of the tumor, the serum levels of MMPs and their inhibitors reflect this[43].

---

[38] H. Nagase, Activation mechanisms of matrix metalloproteinases, Biol. Chem. 378 (1997) 151–160.

[39] Selective Modulation of Matrix Metalloproteinase 9 Functions via Exosite Inhibition, Janelle Lauer-Fields et al, Journal of Biological Chemistry, Jluy 18,2008, Vol. 283, No. 29, PP. 20087-20095.

[40] Faust, Andreas, Bianca Waschkau, Jens Waldeck, Carsten Höltke, Hans-Jörg Breyholz, Stefan Wagner, Klaus Kopka, Walter Heindel, Michael Schäfers, und Christoph Bremer. „Synthesis and evaluation of a novel fluorescent photoprobe for imaging matrix metalloproteinases". *Bioconjugate chemistry* 19, Nr. 5 (Mai 2008): 1001–1008.

[41] Rundhaug, Joyce E. „Matrix Metalloproteinases and Angiogenesis". *Journal of Cellular and Molecular Medicine* 9, Nr. 2 (2005): 267–285.

[42] Hofmann, Uta B., Roland Houben, Eva-B. Bröcker, and Jürgen C. Becker. "Role of Matrix Metalloproteinases in Melanoma Cell Invasion." *Biochimie* 87, no. 3–4 (March 2005): 307–314.

[43] Turpeenniemi-Hujanen, T. „Gelatinases (MMP-2 and -9) and their natural inhibitors as prognostic indicators in solid cancers". *Biochimie* 87, Nr. 3–4 (April 2005): 287–297.

III.1.3.   Role of MMPs in angiogenesis

MMPs play an important role in the proteolysis of the ECM. This is important for some physiological process like angiogenesis, but also in pathological ones, especially in tumor progression.

MMP-2 and MMP-9, showing collagenolytic activity, enable endothelial cells to invade the basement membrane of vascular structures, where type IV collagen is the major component.

In studies, using knockout mice or MMP inhibitors, it has been demonstrated that MMP-2, MMP-9 and MT1-MMP are pro-angiogenic while MMP-3, MMP-7, MMP-9 and MMP-12 may inhibit tumor-inducing angiogenesis. A reason is their angiostatin production by plasminogen hydrolyzation in certain environments[44]. On the contrary Rundhaug *et al.* report an anti-angiogenic effect of soluble PEX domain of proMMP-2: Degradation of MMP-2 can result in the appearance of soluble PEX which binds to the integrin $\alpha_v\beta_3$ and inhibits consequently binding of the MMP-2 to this receptor[45]. This reflects the double-faced role of these enzymes in this process and the different possible interactions between receptor and enzyme.

In tumor angiogenesis, MMP-2 and MMP-9 are considered to play an important role for the angiogenic switch.

III.1.4.   Gelatinases and solid cancers

As already mentioned MMPs play a role in tumor formation, such as tumor invasion and angiogenesis (Figure III-4). In particularly, Gelatinases (MMP-2 and MMP-9) are associated in these processes in different manners, like tumor aggressiveness, metastatic potential[46] and poor clinical prognosis in malignant tissues, in which they are constantly detected[47,48,49]. MMP-9 was shown to contribute to the angiogenic switch during multistage

---

[44] Jin, Young-June, Iha Park, In-Kee Hong, Hee-Jung Byun, Jeongsuk Choi, Young-Myeong Kim, und Hansoo Lee. „Fibronectin and vitronectin induce AP-1-mediated matrix metalloproteinase-9 expression through integrin α(5)β(1)/α(v)β(3)-dependent Akt, ERK and JNK signaling pathways in human umbilical vein endothelial cells". *Cellular signalling* 23, Nr. 1 (Januar 2011): 125–134.

[45] Rundhaug, Joyce E. „Matrix Metalloproteinases and Angiogenesis". *Journal of Cellular and Molecular Medicine* 9, Nr. 2 (2005): 267–285.

[46] Yang, Jie, Zhihong Zhang, Juqiang Lin, Jinling Lu, Bi-feng Liu, Shaoqun Zeng, und Qingming Luo. „Detection of MMP activity in living cells by a genetically encoded surface-displayed FRET sensor". *Biochimica et biophysica acta* 1773, Nr. 3 (März 2007): 400–407.

[47] Faust, Andreas, Bianca Waschkau, Jens Waldeck, Carsten Höltke, Hans-Jörg Breyholz, Stefan Wagner, Klaus Kopka, u. a. „Synthesis and evaluation of a novel hydroxamate based fluorescent photoprobe for imaging of matrix metalloproteinases". *Bioconjugate chemistry* 20, Nr. 5 (Mai 20, 2009): 904–912.

carcinogenesis of skin and pancreas[50,51]. This might be because basement membrane degradation is required for intravasation and metastatic spread by cancerous cells.
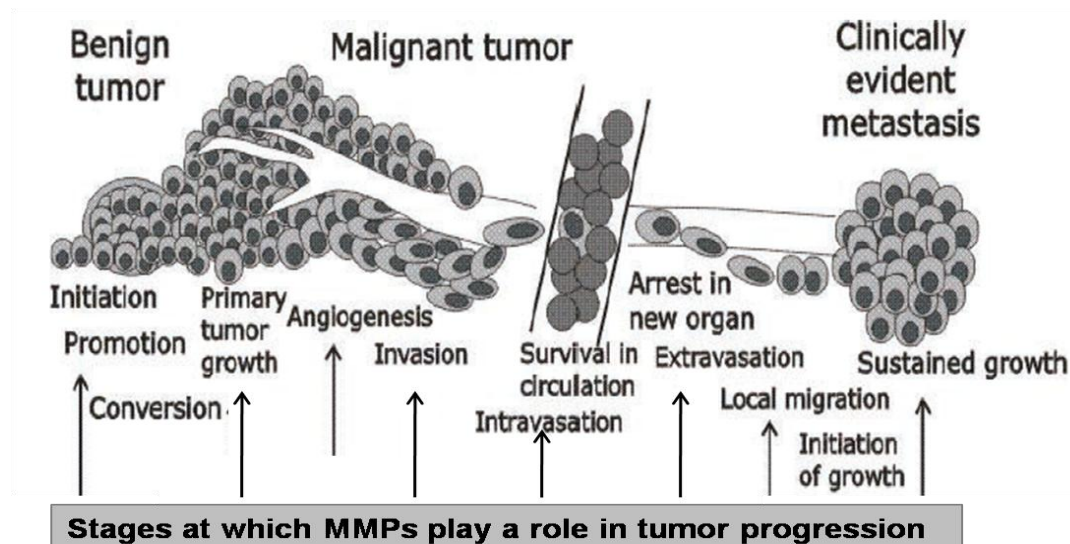
Figure III-4: MMPs in tumor progression.

-Modified from Vasala K., "Matrix Metalloprotease MMP-2 and MMP-9 in bladder Carcinoma", Academic Dissertation *University of Oulu*, 2008-

One important point for differentiation between benign and malignant cancer is the presence or the lack of the basal membrane. While in benign tumors the basal membrane is present, in malignant tissue the invasive growth leads to its fragmentation, reduplication or disappearance. The basal membrane in malignant cells changes its structure or/and ratios between various components, such as: type IV collagen, laminin, heparan sulfate proteoglycan and fibronectin.

Neoplastic cells secrete MMP-9 (also called gelatinase B, 92kDa gelatinase, 92kDa type IV collagenase) that destroys type IV collagen, which facilitates metastasizing through the lysis of basal membranes from blood and lymphatic vessels. Thus, malignant cells are

[48] Duncan, M E, J P Richardson, G I Murray, W T Melvin, und J E Fothergill. „Human matrix metalloproteinase-9: activation by limited trypsin treatment and generation of monoclonal antibodies specific for the activated form". *European journal of biochemistry / FEBS* 258, Nr. 1 (November 15, 1998): 37–43.

[49] Deryugina, Elena I, und James P Quigley. „Matrix metalloproteinases and tumor metastasis". *Cancer metastasis reviews* 25, Nr. 1 (März 2006): 9–34.

[50] Bergers, G, R Brekken, G McMahon, T H Vu, T Itoh, K Tamaki, K Tanzawa, u. a. „Matrix metalloproteinase-9 triggers the angiogenic switch during carcinogenesis". *Nature cell biology* 2, Nr. 10 (Oktober 2000): 737–744.

[51] Rundhaug, Joyce E. „Matrix Metalloproteinases and Angiogenesis". *Journal of Cellular and Molecular Medicine* 9, Nr. 2 (2005): 267–285.

disseminated, but they can also leave the vessels and implant in other tissues and organs, with the formation of metastases.

III.1.5.   The controversial role of gelatinases in tumorigenesis

MMP-2 correlates to local relapse in early stage breast carcinoma, cervical carcinoma (uterus) and so with poor survival, while its negativity is associated with a favorable prognosis. Concerning the prognosis this is also the case in bladder cancer and lung cancer (especially Non Small Cell Lung Cancer), colorectal and gastric carcinomas, melanomas and malignant brain tumors, where the MMP-2 protein expression correlates with the stage of carcinoma[52]. In prostate cancer the ratio of MMP-2 is also increased in high-grade or high-stage tumors, said to be playing a role in prostate cancer cell invasion and –induced angiogenesis.

At the same time MMP-2 and MMP-9 over-expression, concomitant with MMP-1 downregulation, is correlated with dramatic tumor escaping from antiangiogenic chemotherapy[53].

In tumor progression the MMP-9 activity is up-regulated during the switch from the pre-vascular to the vascular phase. Its activity causes a 2-fold increase in the extracellular VEGF mobilization from matrix stores for making it more available to VEGF receptors[54,55]. Hofmann *et al.*[56] reported that MMP-9 seems to be involved in the early steps of metastasis formation but not the later steps such as extravasation as in a melanoma cell invasion trial the majority of tumor cells expressed MMP-9, whereas experimental metastases did not express MMP-9 at all. Another instance of MMP-9 playing a multifaced role is its stimulating effect on proliferation of invasive squamous cell carcinoma in transgenic mouse models during early stages of cancer, but it restrictive impact on further malignant progression at later stages. Not astonishing the ideas of the significance of MMP-9 in cancer are controversial.

This controversial role of MMPs, MMP-9 respectively, as tumor-promoter and tumor-suppressor is also shown in clinical studies. Over-expression of MMP-9 is associated with

---

[52] Turpeenniemi-Hujanen, T. „Gelatinases (MMP-2 and -9) and their natural inhibitors as prognostic indicators in solid cancers". *Biochimie* 87, Nr. 3–4 (März 2005): 287–297.

[53] Moustoifa, El-Farouck, Mohamed-Anis Alouini, Arnaud Salaün, Thomas Berthelot, Aghleb Bartegi, Sandra Albenque-Rubio, und Gérard Déléris. „Novel cyclopeptides for the design of MMP directed delivery devices: a novel smart delivery paradigm". *Pharmaceutical research* 27, Nr. 8 (August 2010): 1713–1721.

[54] Pepper, M S. „Role of the matrix metalloproteinase and plasminogen activator-plasmin systems in angiogenesis". *Arteriosclerosis, thrombosis, and vascular biology* 21, Nr. 7 (Juli 2001): 1104–1117.

[55] Bergers, G, R Brekken, G McMahon, T H Vu, T Itoh, K Tamaki, K Tanzawa, u. a. „Matrix metalloproteinase-9 triggers the angiogenic switch during carcinogenesis". *Nature cell biology* 2, Nr. 10 (Oktober 2000): 737–744.

[56] Hofmann, Uta B., Roland Houben, Eva-B. Bröcker, und Jürgen C. Becker. „Role of matrix metalloproteinases in melanoma cell invasion". *Biochimie* 87, Nr. 3–4 (März 2005): 307–314.

favorable prognosis in patients with node-negative breast cancer and inversely correlates with liver metastasis in patients with colorectal cancer. Therefore, on the one hand a low level of MMP-9 in the early stage is correlated with an aggressive clinical course of mamma carcinoma, while on the other hand a high plasma MMP-9 activity is associated with worse overall survival. At the same time a hypothesis gives a favorable prognosis in association with MMP-9[57].

Finally, Turpeenniemi-Hujanen cites that gene expression profiles in breast carcinoma do have shown that MMP-9 is included in genes that are associated with aggressive disease, whilst these genes are involved in the control of cell cycle, signal transduction, angiogenesis, metastasis and cell invasion in general. MMP-9 in lung cancer, like lung adenocarcinoma and NSCLC (Non Small Cell Lung Cancer), is in correlation with the disease's prognosis and holds the role as a marker for aggressive behavior in NSCLC. In HNSCC (Head and neck squamous cell carcinomas) MMP-9 is suggested to play a great role in the impaired metabolism in cancer cells and the over-expression of the immunoreactive protein for MMP-9 has found to correlate with worse prognosis, and even with aggressive relapses. High MMP-9 expression in colorectal carcinoma and gastric carcinoma predicts early relapse and poor survival. It is also linked with tumor invasion and lymph node metastases in gastric carcinoma as well as in melanomas. Concerning malignant brain tumors, MMP-9 is suggested to be associated with neo-angiogenesis[57]. Also in hepatocellular carcinomas (HCCs), MMP-9 plays an important role in the tumor-stroma cross-talk which leads to tumor progression and metastasis and thus to a poor prognosis in human HCCs[58](Figure III-5).

---

[57] Turpeenniemi-Hujanen, T. „Gelatinases (MMP-2 and -9) and their natural inhibitors as prognostic indicators in solid cancers". *Biochimie* 87, Nr. 3–4 (März 2005): 287–297.

[58] Coulouarn, Cédric, Anne Corlu, Denise Glaise, Isabelle Guénon, Snorri S Thorgeirsson, und Bruno Clément. „Hepatocyte-stellate cell cross-talk in the liver engenders a permissive inflammatory microenvironment that drives progression in hepatocellular carcinoma". *Cancer research* 72, Nr. 10 (Mai 15, 2012): 2533–2542.
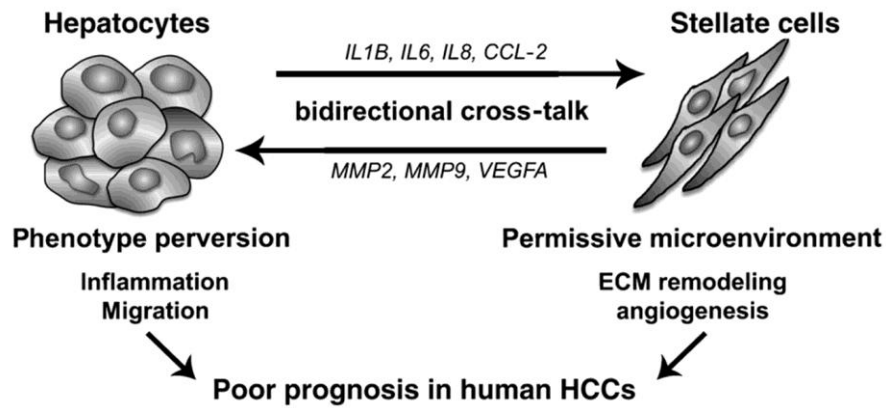
Figure III-5: Proposed model for molecular cross-talk between hepatocytesand activated HSCs in HCCs.

IV. Integrin $\alpha_v\beta_3$ and Gelatinases

Matrix Metalloproteases are known to be in correlation with certain integrins. Integrins are said to be regulating the activity of MMPs at the cell surface in inflammation, angiogenesis and tumor progression by mechanisms like gene expression, activation and localization[59].

IV.1.   Integrin-Gelatinases interactions

Respectively MMP-2 and MMP-9 are reported to be in a strong association with the integrin $\alpha v\beta 3$.

IV.1.1.   Integrin-Gelatinases interaction mediated through SIBLINGs

Fedarko et al.[60] describe, that SIBLINGs (Small, Integrin-Binding, LIgand, N-linked Glycoprotein) can specially bind ($K_d \sim$ nM) and activate MMPs. Binding of the SIBLING to their corresponding partner leads to structural changes resulting in activation of pro-MMPs. This happened without removal of the inhibitory propeptide and re-activation of TIMP bound MMPs. The known partners are bone sialoprotein (BSP) and proMMP-2, osteopontin (OPN) and proMMP-3 and dentin matrix protein-1(DMP-1) and proMMP-9. The SIBLINGs, overexpressed during tumor metastasis, contain the integrin binding tripeptide RGD. The RGD domain interacts with the integrin $\alpha_v\beta_3$ and due to this binding the SIBLINGs form complexes with their proMMP partners.

The expression of these SIBLINGs by tumor cells promotes the migration and adhesion of activated endothelial cells, which are crucial during angiogenesis (Figure IV-1). OPN acts as a chemotactic and adhesion molecule for macrophages and promotes their infiltration of the tumor. Chen *et al.*[61] showed that OPN also induces MMP-9 up-regulation in chondrosarcoma cells. As the receptor of OPN, amongst others, is the integrin $\alpha v\beta 3$, they conclude after investigation that this takes place by activation of a $\alpha v\beta 3$ integrin, FAK (focal

---

[59] Kim, Dong Seok, Ok-Hee Jeon, Hee Doo Lee, Kyung Ho Yoo, und Doo-Sik Kim. „Integrin alphavbeta3-mediated transcriptional regulation of TIMP-1 in a human ovarian cancer cell line". *Biochemical and biophysical research communications* 377, Nr. 2 (Dezember 12, 2008): 479–483.

[60] Fedarko, Neal S, Alka Jain, Abdullah Karadag, und Larry W Fisher. „Three small integrin binding ligand N-linked glycoproteins (SIBLINGs) bind and activate specific matrix metalloproteinases". *FASEB journal: official publication of the Federation of American Societies for Experimental Biology* 18, Nr. 6 (April 2004): 734–736.

[61] Chen, Ying-Ju, Ying-Ying Wei, Hsien-Te Chen, Yi-Chin Fong, Chin-Jung Hsu, Chun-Hao Tsai, Horng-Chaung Hsu, Shing-Hwa Liu, und Chih-Hsin Tang. „Osteopontin increases migration and MMP-9 up-regulation via alphavbeta3 integrin, FAK, ERK, and NF-kappaB-dependent pathway in human chondrosarcoma cells". *Journal of cellular physiology* 221, Nr. 1 (Oktober 2009): 98–108.

adhesion kinase), ERK (extracellular signal-regulated kinase), and NF-κB (nuclear factor kappa-light-chain-enhancer of activated B cells)-dependent pathway.
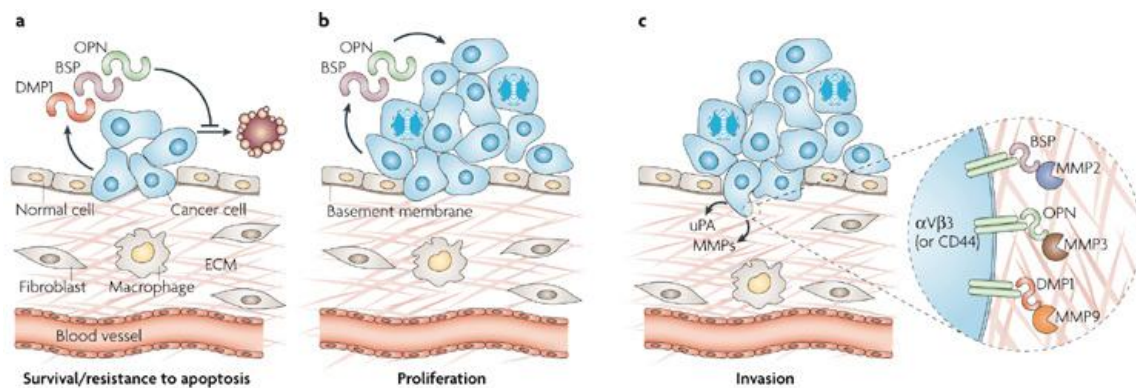
Figure IV-1: SIBLINGs

osteopontin (OPN), bone sialoprotein (BSP), dentin matrix protein 1 (DMP1), urokinase plasminogen activator (uPA).

-Adapted from Bellahcène, Akeila, Vincent Castronovo, Kalu U. E. Ogbureke, Larry W. Fisher, und Neal S. Fedarko. „Small integrin-binding ligand N-linked glycoproteins (SIBLINGs): multifunctional proteins in cancer". *Nature Reviews Cancer* 8, Nr. 3 (March 2008): 212–226.-

IV.1.2.   Integrin-Gelatinases interaction mediated through PEX binding

Brooks *et al.* also demonstrated that the Hemopexin-like domain (PEX) of MMPs represents a fragment with integrin binding activity. In the case of MMP-2 its PEX-fragment is forming a complex with the C-terminal of TIMP-2 (tissue inhibitor), which is need for cell-membrane-associated activation and thereby facilitating matrix degradation and cellular invasion[62,63].

IV.1.3.   Other interaction mechanisms of integrin and Gelatinases

Controversially to the PEX and SIBLING approach, Jiao *et al.* describe a direct binding of MMP-2 to the integrin $\alpha_v\beta_3$ *via* the C-terminus of active MMP-2 for regulation of

---

[62] P.C. Brooks, S. Strömblad, L.C. Sanders, T.L. von Schalscha, R.T. Aimes, W.G. Stetler Stevenson, et al., Localization of matrix metalloproteinase MMP-2 to the surface of invasive cells by interaction with integrin alpha v beta 3, Cell 85 (1996) 683–693.

[63] P.C. Brooks, S. Silletti, T.L. von Schalscha, M. Friedlander, D.A. Cheresh, Disruption of angiogenesis by PEX, a noncatalytic metalloproteinase fragment with integrin binding activity, Cell 92 (1998) 391–400.

MMP-2 activation during tumor cell migration and a possible implication of MMP-2 in the regulation of integrin $\alpha_v\beta_3$ recruitment[64].

In the cell-mediated collagen degradation and ECM re-arrangement MMP-2 is said to be bound and activated by integrin $\alpha_v\beta_3$[65].

Nevertheless Nisato *et al.* denied the binding of the PEX C domain of MMP-2 to integrin $\alpha_v\beta_3$, but show only binding of active MMP-2 to the integrin $\alpha_v\beta_3$ or the binding of pro-MMP-2, in the absence of carrier proteins, to integrin $\alpha_v\beta_3$ and $\alpha_v\beta_5$. They deemphasize the role of secreted MMPs in *in vitro* angiogenesis in favor to MT1-MMP[66], which is important for MMP-2 activation though.

Concerning MMP-9, Jin *et al.*[67] think of a FN- and VN-induced MMP-9 expression altering the structure of the ECM surrounding endothelial cells. This is due to the $\alpha_2\beta_1$ and $\alpha_v\beta_3$ integrin-mediated cell adhesion to FN or VN, which activate integrin-dependent intracellular signaling cascades that include PI3K (phosphoinositide 3-kinase), ERK and JNK (c-Jun N-terminal kinase), which subsequently leads to the stimulation of AP-1 (activator protein-1)-dependent MMP-9 expression in the cell line HUVEC.

Other scientists describe that MMP-2 substrate cleavage of fibronectin (FN) and vitronectin (VN) influences the integrin receptor $\alpha_v\beta_3$, which leads to a down regulation of MMPs.

In the study of Kim *et al.*[68] it is shown that saxatilin, a disintegrin, interferes in the balance between MMP-9 and its tissue inhibitor TIMP-1 at the transcriptional level.

---

[64] Jiao, Yang, Xue Feng, Yinpeng Zhan, Ruifei Wang, Sheng Zheng, Wenguang Liu, und Xianlu Zeng. „Matrix metalloproteinase-2 promotes $\alpha v\beta 3$ integrin-mediated adhesion and migration of human melanoma cells by cleaving fibronectin". *PloS one* 7, Nr. 7 (2012): e41591.

[65] Danhier, Fabienne, Aude Le Breton, und Veronique Preat. „RGD -based strategies to target alpha(v) beta(3) integrin in cancer therapy and diagnosis". *Molecular pharmaceutics* (September 11, 2012). http://www.ncbi.nlm.nih.gov/pubmed/22967287.

[66] Nisato, Riccardo E, Ghamartaj Hosseini, Christian Sirrenberg, Georgina S Butler, Thomas Crabbe, Andrew J P Docherty, Matthias Wiesner, u. a. „Dissecting the role of matrix metalloproteinases (MMP) and integrin alpha(v)beta3 in angiogenesis in vitro: absence of hemopexin C domain bioactivity, but membrane-Type 1-MMP and alpha(v)beta3 are critical". *Cancer research* 65, Nr. 20 (Oktober 15, 2005): 9377–9387.

[67] Jin, Young-June, Iha Park, In-Kee Hong, Hee-Jung Byun, Jeongsuk Choi, Young-Myeong Kim, und Hansoo Lee. „Fibronectin and vitronectin induce AP-1-mediated matrix metalloproteinase-9 expression through integrin $\alpha(5)\beta(1)/\alpha(v)\beta(3)$-dependent Akt, ERK and JNK signaling pathways in human umbilical vein endothelial cells". *Cellular signalling* 23, Nr. 1 (Januar 2011): 125–134.

[68] Dong Seok, Ok-Hee Jeon, Hee Doo Lee, Kyung Ho Yoo, und Doo-Sik Kim. „Integrin alphavbeta3-mediated transcriptional regulation of TIMP-1 in a human ovarian cancer cell line". *Biochemical and biophysical research communications* 377, Nr. 2 (Dezember 12, 2008): 479–483.

Disintegrins are a family of cysteine-rich proteins, gained from snake venom to serve as inhibitors of platelet aggregation during blood coagulation. They are competitive inhibitors of the integrin receptors.

They demonstrated that saxatilin reduces the MMP-9 expression in the human ovarian cancer cell line MDAH 2774 at the same time than it induces TIMP-1 expression. Finally, a decrease in the activity of MMP-9 can be observed.

Rolli *et al*. even describes the cooperation of activated integrin $\alpha_v\beta_3$ with MMP-9 in the regulation of migration of metastatic breast cancer cells. They showed that only breast cancer cell variants with active $\alpha_v\beta_3$ integrin produced mature MMP-9. And only mature MMP-9 enhanced $\alpha_v\beta_3$ integrin-dependent breast cancer cell migration[69].

This shows the close relationship between the integrin receptor $\alpha_v\beta_3$ and the ECM degrading gelatinases (MMP-2 & MMP-9) in cancer development, but also in inflammation. Thus, they both represent an attractive target for cancer research and clinics.

---

[69] Rolli, Melanie, Emilia Fransvea, Jan Pilch, Alan Saven, und Brunhilde Felding-Habermann. „Activated integrin alphavbeta3 cooperates with metalloproteinase MMP-9 in regulating migration of metastatic breast cancer cells". *Proceedings of the National Academy of Sciences of the United States of America* 100, Nr. 16 (August 5, 2003): 9482–9487.

V. Molecules for targeting and optical imaging of cancer

A variety of targeted and activatable imaging probes are massively being developed aiming at improving early cancers detection or other pathological situation such as inflammation. Different types of contrast agents can be attached to the targeting part of the molecules which can be detected by different physical means like X-ray and computed tomography (CT), magnetic resonance imaging (MRI), ultrasonography (US), positron emission tomography (PET) or single photon emission computed tomography (SPECT). When optical imaging is concerned, we must use biocompatible near-infrared fluorophores as contrast agent.

V.1.   *Choice of the Near-infrared window for in vivo optical imaging*

Fluorescence imaging is a technique using photons as information source. This technique is already well-known in *in vitro* applications, especially in the biomedical domain on the molecular (DNA, proteins) or cellular level (flow cytometry, histological labeling). *In vivo,* good preclinical results have been reported, but in the clinic it is little used because of lack of tracers. An important point to mention is the regulatory context of tracers used in human clinic concerning legal and safety aspects.

Optical fluorescence imaging represents a non invasive, fast, cheap and very sensitive method, with major limits concerning its weak spatial resolution and the limited detection in depth. It is complementary to other imaging techniques like MRI and PET or SPECT[70].

The principle of fluorescence optical imaging corresponds to the optical contrast gained by collection of altered irradiated light after exposure to certain light sources like laser, LED or Xenon.

In order to use this imaging technique for medical imaging in patients, certain constraints due to the tissue limiting its application *in vivo* had to be minimized.

These limits comprise light scattering during biological tissue penetration, which causes a strong loss in intensity and information for the exact localization of the fluorophore in the organism. Another loss in the fluorophore's intensity is the absorption of the light of

---

[70] De Grand, A.M., und JV Frangioni. „An operational near-infrared fluorescence imaging system proyotype for large animal surgery". *Technol Cancer Res Treat*. 2, 2003.

excitation and emission. Furthermore natural fluorescence (called auto-fluorescence) of substances in the tissue, like porphyrines, strongly decreases the contrast. The sensitivity is not only compromised by autofluorescence, but also from nonspecifically or unbound probes, referred to as reagent background or nonspecific signal.

Autofluorescence caused by cells, tissues and biological fluids signal distortion is minimized either by using selective filters or by using probes that can be excited at more than 500 nm.

Conventional fluorescent techniques, which use probes in the visible light spectrum (400-600 nm), thus have a spectrum associated with a relatively high level of nonspecific background light, resulting in a low SBR (signal-to-background-ratio). Light absorption by hemoglobin in the visible light spectrum (< 600 nm) and other components (e.g., water and lipids) in the infrared range (> 900 nm), offers an optical imaging window from approximately 650-900 nm. Hence at these wavelengths, in the near-infrared (NIR), the absorption coefficient of tissue is at a minimum (see Figure V-1).

At the same time, light scattering by dense media is also reduced in longer wavelengths, resulting in a greater penetration of the excitation light in the NIR. At the same time auto-fluorescence is minimal in the NIR window, improving the contrast (Figure V-2).
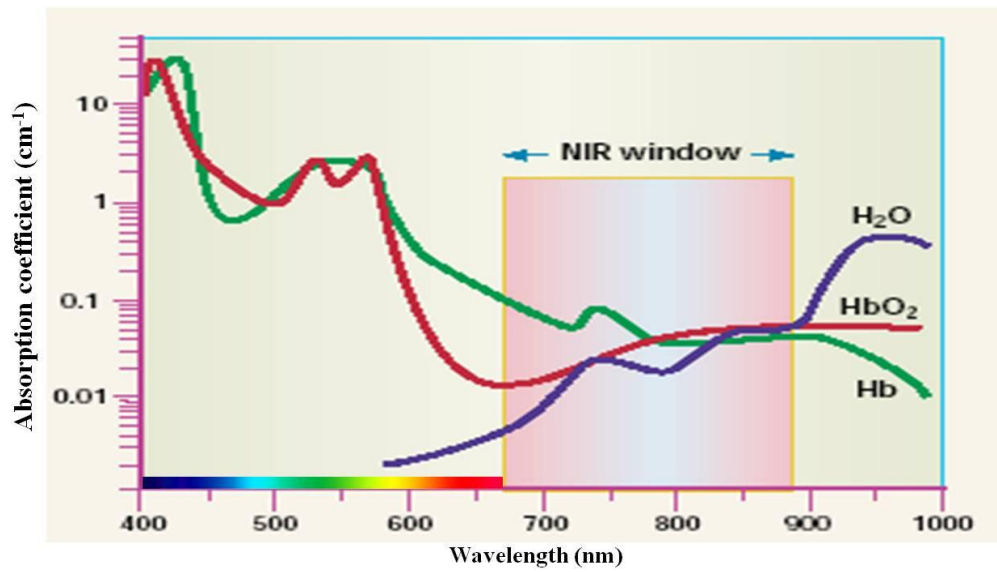
After Weissleder, Nat. Biotechnol. 2001; 19: 316-7

Figure V-1: Absorption in tissue.
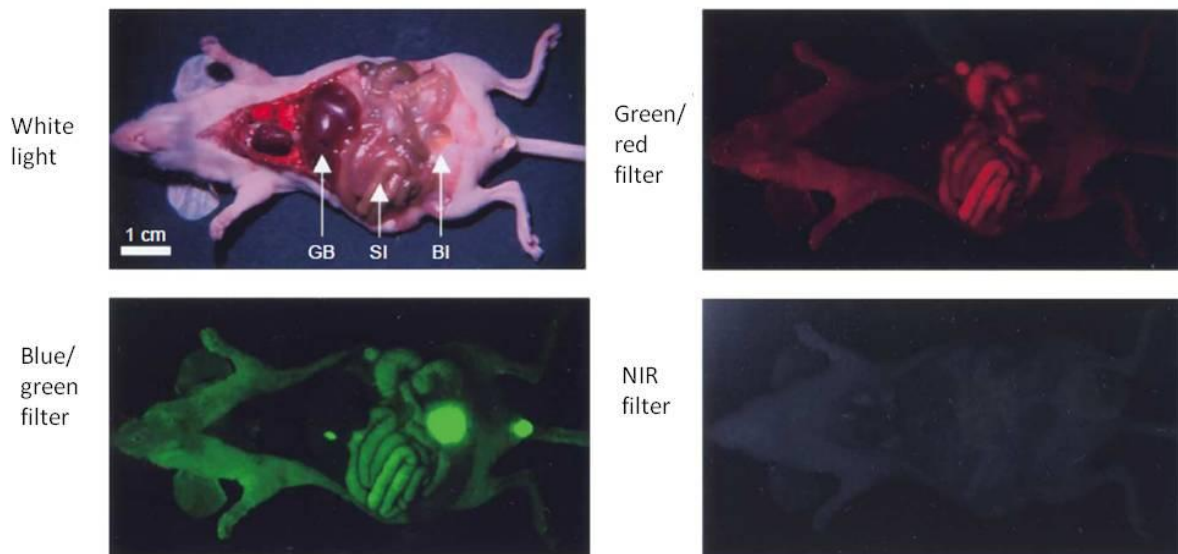
Figure V-2: Autofluoresence of mouse organs under different optical conditions.
The autofluoresence of the tissues has been imaged by using three different filter combinations (excitation/emission):
Blue/green (460-550 nm/505-560 nm), green/red (525-555 nm/590-650 nm) and near infra-red (725-775 nm/790-830 nm).
All images have been normalized the same way.
(GB: gall bladder, SI: intestines, Bl: Bladder)
-After Frangioni, 2003-

V.2.   *Basic principles of Fluorescence*

Fluorescence is the emission of light by a substance that absorbed light or other electromagnetic radiation[71,72].

The genesis of fluorescence is described by the Jablonski diagram (Figure V-3):
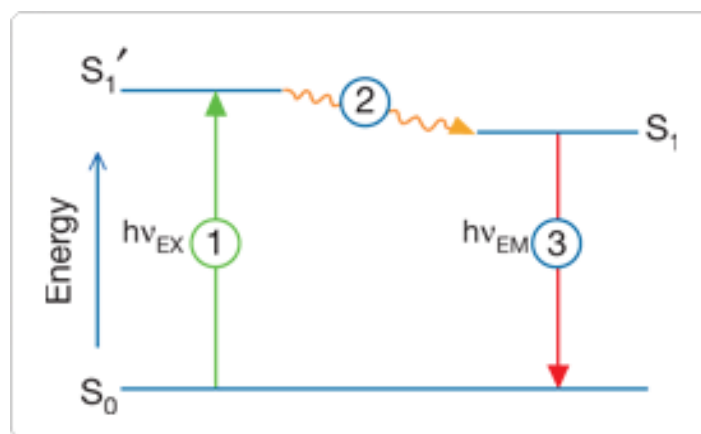
Figure V-3: The Jablonski diagram illustrates the processes of optical absorption and subsequent emission of fluorescence.

This diagram illustrates the electronic states of a molecule and the transitions between them. At first is the excitation (**1**) of an electron: A photon of energy $h\nu_{EX}$ is supplied by an external source such as an incandescent lamp or a laser. This energy is absorbed by the fluorophore, creating an excited electronic singlet state (S_1'). In the second stage, the so called excited-state lifetime (**2**), the excited state exists for a finite time (typically 1–10 nanoseconds). During this time, the fluorophore undergoes conformational changes and is also subject to a multitude of possible interactions with its molecular environment. These processes have two important consequences. First, the energy of S_1' is partially dissipated, yielding a relaxed singlet excited state (S_1) from which fluorescence emission originates. Second, not all the molecules initially excited by absorption (Stage 1) return to the ground state (S_0) by fluorescence emission. Other processes such as collisional quenching, Förster resonance energy transfer (FRET) and intersystem crossing may also depopulate S_1.

The fluorescence quantum yield, which is the ratio of the number of fluorescence photons emitted (Stage 3) to the number of photons absorbed (Stage 1), is a measure of the relative extent to which these processes occur.

---

[71] Brand, L and Johnson, M.L., Eds., *Fluorescence Spectroscopy (Methods in Enzymology, Volume 450)*, Academic Press (2008).
[72] Kobayashi, H., Ogawa, M., Alford, R., Choyke, P.L and Urano, Y., "New strategies for fluorescent probe design in medical diagnostic imaging," Chem Rev (2010) 110:2620–2640.

The third stage described the Fluorescence Emission (**3**): A photon of energy $h\nu_{EM}$ is emitted, returning the fluorophore to its ground state S_0. Due to energy dissipation during the excited-state lifetime (internal conversion and vibrational relaxation), the energy of this photon is lower, and therefore of longer wavelength than the excitation photon $h\nu_{EX}$. The difference in energy or wavelength represented by $(h\nu_{EX} - h\nu_{EM})$ is called the Stokes shift.

This explains why the energy of fluorescent photons is always less than that of the exciting photons

Fluorescence molecules or fluorophores have the property that one and the same can be excited and detected a couple of times unless it has not been destroyed irreversibly in the excited state (photobleaching).

V.2.1.   Extinction coefficient (EC) and quantum yield (QY)

While fluorophores are characterized by their proper wavelength range, Stokes shift and spectral bandwidth, fluorescence intensity per dye molecule is proportional to the product of extinction coefficient (EC) and quantum yield (QY) (Table V-1). The fluorescence output of a given dye depends on the efficiency with which it absorbs and emits photons, and its ability to undergo repeated excitation/emission cycles. Absorption and emission efficiencies can be quantified in terms of the molar EC for absorption and the QY for fluorescence. Both are constants under specific environmental conditions. The value of EC is specified at a single wavelength (usually the absorption maximum), whereas QY is a measure of the total photon emission over the entire fluorescence spectral profile. The range of these parameters among organic dye and autofluorescent protein fluorophores is approximately 5000 to

200,000 $cm^{-1}M^{-1}$ for EC and 0.05 to 1.0 for QY.

V.2.2.   Quenching and FRET

Fluorophore-Fluorophore interactions, also called fluorescence quenching, represents a biomolecular process reducing the fluorescence QY without changing the fluorescence emission spectrum. This occurs due to transient excited-state interactions (collisional quenching), or by so called self-quenching, which is the quenching of one fluorophore by another. This can happen in the case of high loading density of a polymer with numerous copies of a fluorescent molecule. This is very often used to generate the so called "smart-

probes" that contain fluorophores separated by a labile, cleavable function. These probes will be unpacked after they encounter a particular enzyme or physico-chemical conditions that will cut them in pieces thus releasing un-quenched fluorophores (Figure V-4). They can thus yield particularly high tumor/background signal ratios because of their non detectability in the native state.
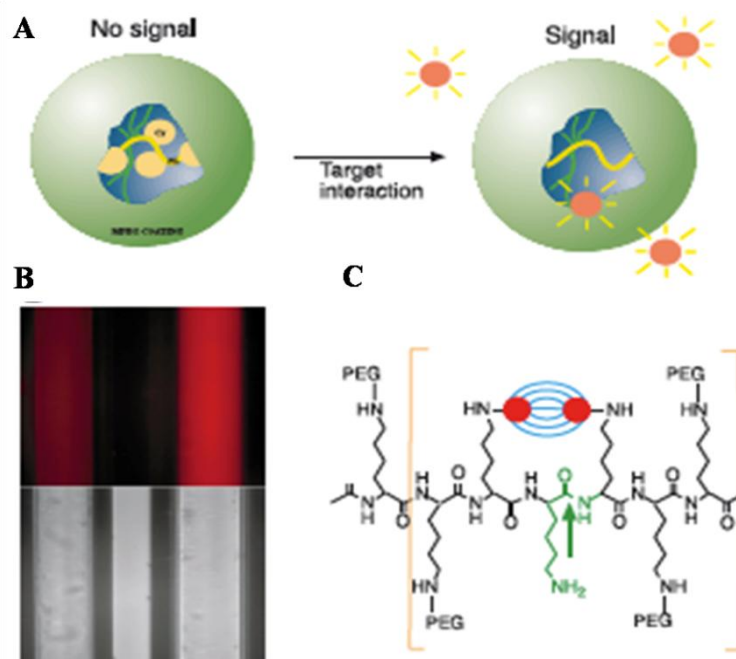
Figure V-4: Protease-activatable fluorescence imaging probe.
A)   Schematic diagram of probe activation. The initial proximity of fluorochrome molecules to each other results in signal quenching.
B)   NIRF image (top) and bright light image (bottom) with nonactivated (left) and activated (right) probe.
C)   Chemical structure of repeating garft copolymer segment indicating quenching of Cy and enzymatic degradation site (green arrow).
-After: Mahmood, Umar, Ching-Hsuan Tung, Alexei Bogdanov, und Ralph Weissleder. „Near-Infrared Optical Imaging of Protease Activity for Tumor Detection1". *Radiology* 213, Nr. 3 (Januar 12, 1999): 866–870.-

Förster (also called Fluorescence) resonance energy transfer (FRET) is based on the through-space dipolar transfer of excited-state energy to acceptor molecules up to 75 Å removed from the donor fluorophore[73,74](Figure V-5).

---

[73] Royer, C.A., "Approaches to teaching fluorescence spectroscopy," Biophys J (1995) 68:1191–1195.
[74] Lakowicz, J.R., *Principles of Fluorescence Spectroscopy, Third Edition*, Springer (2006).
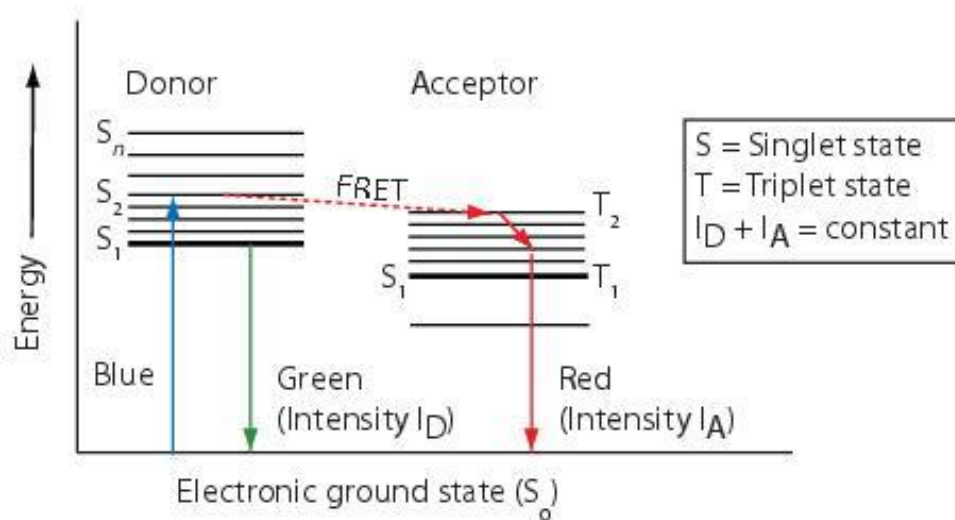
Figure V-5: Jablonski diagram - Principle of the Förster Resonance Energy Transfer (FRET).
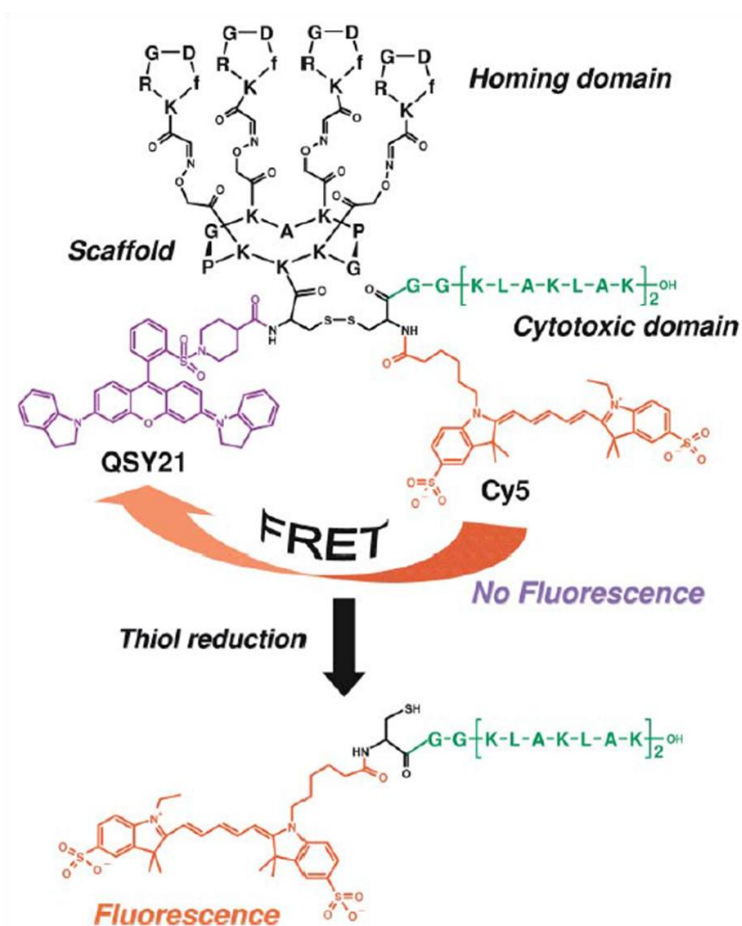
Figure V-6: Structure of activatable fluorescent KLA-containing conjugate.
-Foillard, Stéphanie, Lucie Sancey, Jean-Luc Coll, Didier Boturyn, und Pascal Dumy. „Targeted delivery of activatable fluorescent pro-apoptotic peptide into live cells". *Organic & biomolecular chemistry* 7, Nr. 2 (Januar 21, 2009): 221–224.-

Thus, FRET-based probes are providing additional information when compared to "self-quenched" ones, since we can follow the initial molecule as well as its two degradation products using spectral unmixing methods.

Amongst others, this was demonstrated by Foillard *et al.* using the FRET effect for validation of an integrin targeting molecule cleavable by enzymes and thus releasing a moiety of the compound, which could be follow up *in vitro*[75] (Figure V-6).

Other environmental factors with an impact on the fluorescent properties are the solvent polarity (solvent in this context includes interior regions of cells, proteins, membranes and other biomolecular structures), the proximity and concentration of quenching species and the pH of the aqueous medium.

These characteristics are important for the comprehension of fluorescence used (Table V-1).

---

[75] Foillard, Stéphanie, Zhao-hui Jin, Elisabeth Garanger, Didier Boturyn, Marie-Christine Favrot, Jean-Luc Coll, und Pascal Dumy. „Synthesis and biological characterisation of targeted pro-apoptotic peptide". *Chembiochem: a European journal of chemical biology* 9, Nr. 14 (September 22, 2008): 2326–2332.

Property	Definition	Significance
Fluorescence excitation spectrum	An X,Y plot of excitation wavelength versus number of fluorescence photons generated by a fluorophore.	Optimum instrument setup should deliver excitation light as close to the peak of the excitation spectrum of the fluorophore as possible.
Absorption spectrum	An X,Y plot of wavelength versus absorbance of a fluorophore.	To a first approximation, the absorption spectrum of a fluorophore is equivalent to the fluorescence excitation spectrum.* To the extent that this approximation holds, the absorption spectrum can be used as a surrogate for the fluorescence excitation spectrum.
Fluorescence emission spectrum	An X,Y plot of emission wavelength versus number of fluorescence photons generated by a fluorophore.	Fluorescence emission spectral discrimination is the most straightforward basis for multiplex detection ‡ and for resolving probe fluorescence from background autofluorescence.
Extinction coefficient (EC)	Capacity for light absorption at a specific wavelength.§	Fluorescence output per fluorophore ("brightness") is proportional to the product of the **extinction coefficient** (at the relevant excitation wavelength) and the **fluorescence quantum yield**.
Fluorescence quantum yield (QY = Φ)	Number of fluorescence photons emitted per excitation photon absorbed.	See "Extinction coefficient."
Quenching	Loss of fluorescence signal due to **short-range** interactions between the fluorophore and the local molecular environment, including other fluorophores (self-quenching).	Loss of fluorescence is reversible to the extent that the causative molecular interactions can be controlled.**
Photobleaching	Destruction of the excited fluorophore due to photosensitized generation of reactive oxygen species (ROS), particularly singlet oxygen ($^1O_2$).	Loss of fluorescence signal is **irreversible** if the bleached fluorophore population is not replenished (e.g., via diffusion). Extent of photobleaching is dependent on the duration and intensity of exposure to excitation light. The most effective remedy for photobleaching is to maximize detection sensitivity, which allows the excitation intensity to be reduced. Detection sensitivity is enhanced by low-light detection devices such as CCD cameras, as well as by high–numerical aperture objectives and the widest bandpass emission filters compatible with satisfactory signal isolation.

* Generally true for single fluorophore species in homogeneous solutions but not in more complex heterogeneous samples.
‡ Multiplex detection refers to the process of simultaneously labeling a specimen with two or more fluorescent probes to allow correlation of multiple structural or functional features. As well as specific association with their targets, the probes must have distinctive spectroscopic properties that can be discriminated by the detection instrument.
§ EC (units: cm^{-1} M^{-1}) is defined by the Beer-Lambert law A=EC•c•l, where A = absorbance, c = molar concentration, l = optical pathlength.
** In the case of self-quenching, this can be accomplished by disruption of fluorophore compartmentalization, denaturation or fragmentation of biopolymer conjugates, or functionalization of the fluorophore to produce increased electrostatic repulsion and water solubility.

Table V-1: Spectroscopic properties of fluorescent dyes.
-adapted after invitogen.com-

V.3.   *Imaging probes for NIR imaging of cancer*

Using fluorescence for imaging can be achieved either by the intrinsic properties of the tissue (label-free methods, not discussed here) or using exogenous optically active reporter molecules, targeting or not a defined biomarker[76].

So, analogous to radio-labeled agents, optical imaging probes can be non-specific or targeted.

V.3.1.   Non-specific agents

There are currently some non-specific agents available for research and clinical use, like fluorescein, indocyanine green (ICG), cresyl violet acetate, toluidine blue or Lugols's iodine.

Today only the two fluorescent markers, fluorescein and ICG, are available for injection in human.

Fluorescein can be functionalized but is easily bleached and emits light in the same wavelength as biological tissue's autofluorescence. Only ICG, with an emission peak at 830 nm, has optical properties that are suitable for NIR imaging, but cannot be functionalized because all the reactive chemical functions eventually accessible had been removed to generate this injectable form of ICG.

It has been used for imaging angiogenesis and identification of hepatic segments for facilitation of hepatic resection[77,78] and approaches have also been made in sentinel lymph node mapping (described in chapter IX, page - 78 -).

In view of the non-specificity towards tumors these agents cannot help to determine the tumor margins, although certain applications are described in particular for liver cancer due to the disordered biliary excretion of ICG in cancer tissues and noncancerous liver tissues compressed by the tumor[79].

V.3.2.   Specific agents

Several characteristics of cancer have been taken in consideration as probe targets, for example increased growth and growth factor signaling receptors, limitless replicative

---

[76] Rosenthal, E., and K.R. Zinn. In *Optical Imaging of Cancer: Clinical Applications*, Springer 2009.
[77] Pierce, M.C., D.J. Jvier, and R. Richards-Kortum. "Optical Contrast Agents and Imaging Systems for Detection and Diagnosis of Cancer." *Int J Cancer*. 123, 2008.1979-1990.
[78] Aoki, T., D. Yasuda, Y. Shimizu, et al. "Image-guided Liver Mapping Using Fluorescence Navigation System with Indocyanine Green for Anatomical Hepatic Resection." *World J Surg*. 32, n.d., sec. 2008.1763-1767.
[79] Ishizawa, T., N. Fukushima, J. Shibahara, et al. "Real-time Identification of Liver Cancers by Using Indocyanine Green Fluorescent Imaging." *Cancer*. 115, 2009.2491-2504.

potential, sustained angiogenesis, and increased proteolytic activity resulting in tissue invasion and metastasis (Figure V-7)[80].
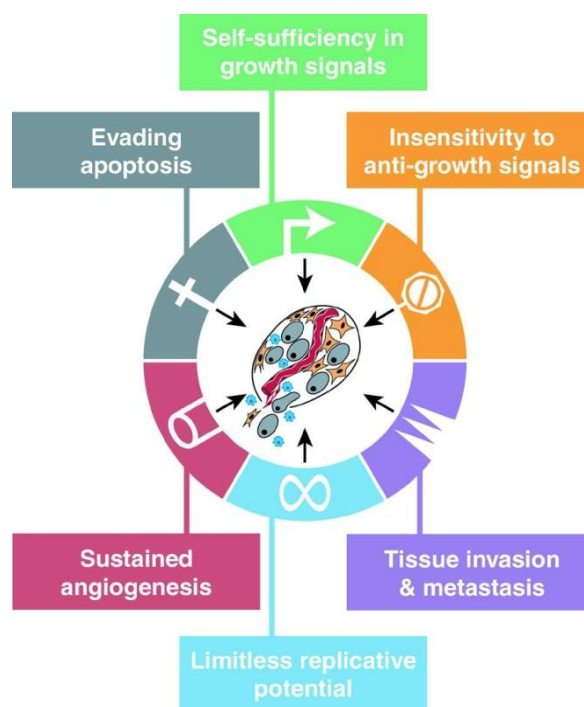
Figure V-7: Hallmarks of cancer and their targets for optical imaging.
EGF epidermal growth factor, cRGD cyclic arginine-glycineaspartate, VEGF vascular endothelial growth factor, NIRF near-infrared fluorescence.
-Hanahan, D., and RA Weinberg. "The Hallmarks of Cancer." Cell. 100, 2000. 57-70-

❖ Activatable or smart probes

Because of their differential expression in disease, proteases could be used to selectively deliver therapeutic or imaging agents. Proteases-activated prodrugs, nanotechnology – based drug delivery systems, hydrogels, gene delivery systems and imaging systems have been described for disease applications[81].

Concerning cancer another approach based on this knowledge is to exploit the characteristics of the tumor in using activatable "smart" probes, which are cleaved by overexpressed proteolytic enzymes. Combining target and function, these molecules could be

---

[80] Keereweer, S., J.D.F. Kerrebijn, P.B.A.A. van Driel, B. Xie, E.L. Kaijzel, T.J.A. Snoeks, I. Que, et al. "Optical Image-guided Surgery - Where Do We Stand?" *Mol Imaging Biol.* 13, 2011. 199-207.
[81] Cudic, Mare, und Gregg B Fields. „Extracellular proteases as targets for drug development". *Current protein & peptide science* 10, Nr. 4 (August 2009): 297–307.

used for the *in vivo* analysis of drug efficacy, pharmacodynamic properties and cancer detection.

The principle of activatable probes is a molecule showing little fluorescence at the time of administration (quenched or inactivated) and in presence of the targeted protease they are cleaved and thus gain in fluorescence intensity (Figure V-8)[82]. This allows the detection of proteases which can be associated with certain specific characteristics of the malignant tissue, e.g. invasive, aggressive or metastatic tendency of the tumor.

These probes lead to a higher SBR compared to nonspecific probes. For this reason such cleavable probes, activated by cathepsins and matrix metalloproteases (MMP) have been developed by Weissleder et al[83,84,85].This type of smart contrast agent was used in conjunction with endoscopic imaging, demonstrating identification of colonic adenocarcinoma in a murine model, using a probe cleavable by cathepsin-B[86].
Even though in general showing reduced background signal (higher SBR), some non specific cleavage or degradation can occur, showing residual background noise.

The developed smart-agents are currently commercially available (Visen Medical, Boston, MA, USA). Another quenching approach for MMP detection is described by Tsien et al[87], using activatable polyarginine-based cell-penetrating peptides made of negatively charged residues as inhibitory domain.
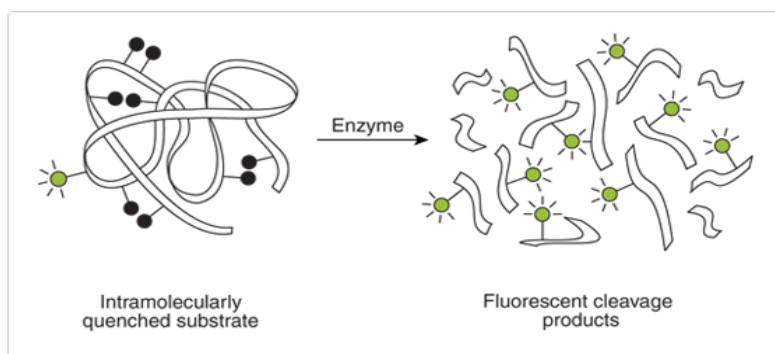
Figure V-8: Principle of enzyme detection via the disruption of intramolecular self-quenching.
Enzyme-catalyzed hydrolysis of the heavily labeled and almost totally quenched substrates relieves the intramolecular self-quenching, yielding brightly fluorescent reaction products.

---

[82] Ntziachristos, Vasilis. „Fluorescence molecular imaging". *Annual review of biomedical engineering* 8 (2006): 1–33.
[83] Mahmood, U., and R. Weissleder. "Near-infrared Optical Imaging of Proteases in Cancer." *Mol Cancer Ther*. 2, 2003.489-496.
[84] Wunderbaldinger, P., K. Turetschek, and C. Bremer. "Near-infrared Fluorescence Imaging of Lymph Nodes Using a New Enzyme Sensing Activatable Macromolecular Optical Probe." *Eur Radiol*. 13, 2003.2206-2211.
[85] Dufort, S, L Sancey, C Wenk, V Josserand, und J L Coll. „Optical small animal imaging in the drug discovery process". *Biochimica et biophysica acta* 1798, Nr. 12 (Dezember 2010): 2266–2273.
[86] Alencar H, Funovics MA, Figueiredo J, Sawaya H, Weissleder R, Mahmood U. Colonic adenocarcinomas: Near-infrared microcatheter imaging of smart probes for early detection – Study in mice. Radiology. 2007; 244:232–238.
[87] Jiang, T., E.S. Olson, Q.T. Nguyen, M. Roy, P.A. Jennings, and R.Y. Tsien. "Tumor Imaging by Means of Proteolytic Activation of Cell-penetrating Peptides." *Proc Natl Acad Sci USA*. 101, 2004.17867-17872.

Anyhow, these targeting molecules lack cancer specificity as in the case of cathepsins and MMPs, the enzymes aimed at are also products of macrophages and neutrophils, which represent hallmarks of inflammation[88] and cerebral ischemia[89].
The difficulties of MMP targeting and definition of MMP smart probes are described later on in detail.

Another approach is a quenched-probe system which has been used to detect specific nucleic acid sequences. It uses an oligonucleotide in a stem-loop hairpin configuration, with a fluorescent reporter and quencher conjugated to opposite ends (Figure V-9). When hybridized to the complementary target sequence, the hairpin opens, producing a fluorescent state[90].
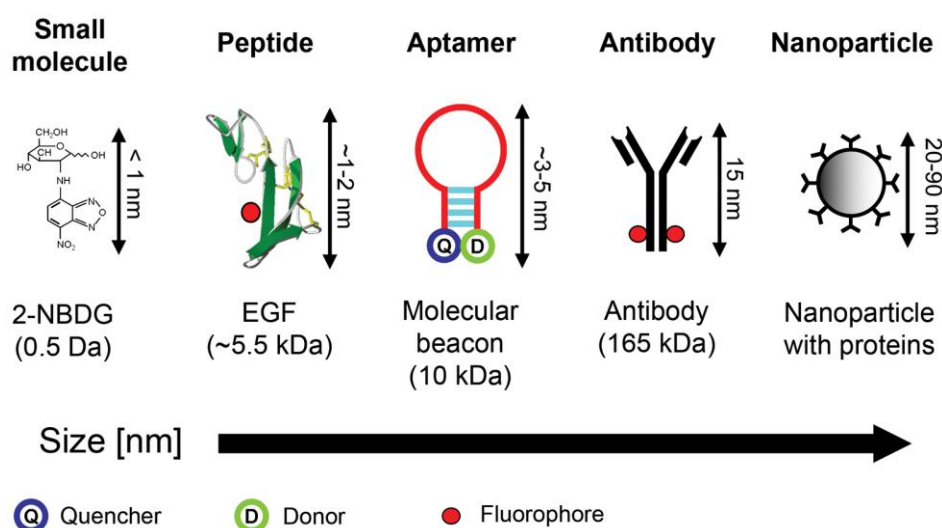
Figure V-9: Five classes of molecular-specific optical contrast agent.
From left to right in order of increasing size: Small molecules including glucose and peptides can be functionalized with fluorescent dyes. Aptamers can be designed to form activatable "smart probes", with fluorescence quenched until target binding. Antibody probes are generally functionalized with fluorescent dyes in the Fc domain. Targeting molecules can be coupled to nanoparticlebased optical reporters, including gold nanoparticles and quantum dots.
-Pierce et al. Int J Cancer. 2008 November 1; 123(9): 1979–1990.-

---

[88] Wunder, A., R.H. Straub, S. Gay, J. Funk, and U. Muller-Ladner. "Molecular Imaging: Novel Tools in Visualizing Rheumatoid Arthritis." *Rheumatology*. (Oxford) 44, 2009.1341-1349.

[89] Klohs, J., N. Baeva, J. Steinbrink, et al. "In Vivo Near-infrared Fluorescence Imaging of Matrix Metalloproteinase Activity After Cerebral Ischemia." *J Cereb Blood Flow Metab*, 2009.1284-1292.

[90] Optical contrast agents and imaging systems for detection anddiagnosis of cancer; Mark C. Pierce, David J. Javier, and Rebecca Richards-Kortum Int J Cancer. 2008 November 1; 123(9): 1979–1990.

❖ Targeting probes

Apart from targeting proteases overexpressed by tumor cells, the increased metabolism and the expression of growth signaling receptors as well as angiogenesis are features of tumor cells that are exploited for the design of targeting NIR probes (Figure V-10). Here a fluorophore is engrafted onto a specific ligand or monoclonal antibody. The advantage of such agents is their excellent SBR in whole animals and the longer period of image collection compared to the short-lived radiotracers labeled with fluorine-18 or carbon-11.

To mention some examples, several groups have described the use of various monoclonal antibodies coupled to fluorophores for the imaging of the epidermal growth factor (EGF) receptor, Her2/neu receptor or the VEGF receptor (all of them enforced expressed growth factor receptors) in all kinds of different tumors[91,92,93]. The same principle but with a quenched fluorophore has been described by Kobayashi et al.[94], which used avidin (targeting the d-galactose receptor) and trastuzumab (HER2 mAb) labeled with the TAMRA (fluorophore)-QSY7 (quencher) pair. Here, the probe is dequenched by cleavage after internalization into the cell, resulting in target-specific fluorescence imaging with high SBR. Another approach is mimicking ligands to target specific receptors. This is the case of the already described cyclic arginine-glycine-aspartate (cRGD) motif conjugated to fluorophores[95], which are used to detect their receptor ($\alpha_v\beta_3$) integrin.

One approach in this sense is the direct visual detection of the increases $\alpha_v\beta_3$ expression by binding of a small peptidomimetic antagonist coupled to a NIR fluorescent dye (VivoTag-S680), known as Integri-Sense (Visen Medical, Boston, MA, USA). It was shown to co-localize at the surface of both $\alpha_v\beta_3$ integrin positive endothelial and tumor cells. The signal is additionally enhanced by the internalization into αvβ3 integrin positive tumor cells, leading to a slower clearance of the probe from tumors compared to surrounding tissues[96]. This probe has been used to visualize liver metastasis from colon cancer in a rat model.

---

[91] Gleysteen, J.P., R.D. Duncan, J.S. Magnuson, J.B. Skipper, K.R. Zinn, and E. Rosenthal. "Fluorescently Labeled Cetuximab to Evaluate Head and Neck Cancer Response to Treatment." *Cancer Biol Ther*. 6, 2007.1181-1185.

[92] Lee, S.B., M. Hassan, R. Fisher, et al. "Affibody Molecules for in Vivo Characterization Oh HER2-positive Tumors by Near-infrared Imaging." *Clin Cancer Res*. 14, 2008.3840-3849.

[93] Withrow, K.P., J.R. Newman, J.B. Skipper, et al. "Assessment of Bevacizumab Conjugated to Cy5.5 for Detection of Head and Neck Cancer Xenografts." *Technol Cancer Res Treat*. 7, 2008.61-66.

[94] Ogawa, M., N. Kosaka, M.R. Longmire, Y. Urano, P.L. Choyke, and H. Kobayashi. "Fluorophore-quencher Based Activatable Targeted Optical Probes for Detecting in Vivo." *Mol Pharm*. 6(2), 2009.386-395.

[95] Chen, K., J. Xie, and X. Chen. "RGD-human Serum Albumin Conjugates as Efficient Tumor Targeting Probes." *Mol Imaging*. 8, 2009.65-73.

[96] Kossodo, S., M. Pickarski, S.A. Lin, et al. "Dual in Vivo Quantification of Integrin-targeted and Protease-activated Agents in Cancer Using Fluorescence Molecular Tomography (FMT)." *Mol Imaging Biol.*, 2009.

Mieog & Hutteman et al.[97] showed here that liver metastases could be delineated in spite of the normally high background signal in liver, kidneys, and bladder, which are the organs of clearance of the agent.

The use of the quenching technique has been described by our team in this respect as well, by means of the quenched cRGD molecule (RAFTc(-RGDfK-)(4)-Cy5-SS-Q), which becomes activated upon internalization into the cell[98].

Other ideas are based on the modification of tracers of other imaging technologies. Here, targeting probes of imaging technologies such as PET imaging are varied by conjugating them with a fluororophore for optical imaging. This is the case in a study of intracranial glioma, using glucose analog 2-deoxyglucose with IRDye800CW which targets the enforced expressed membrane glucose transporter protein GLUT[99].
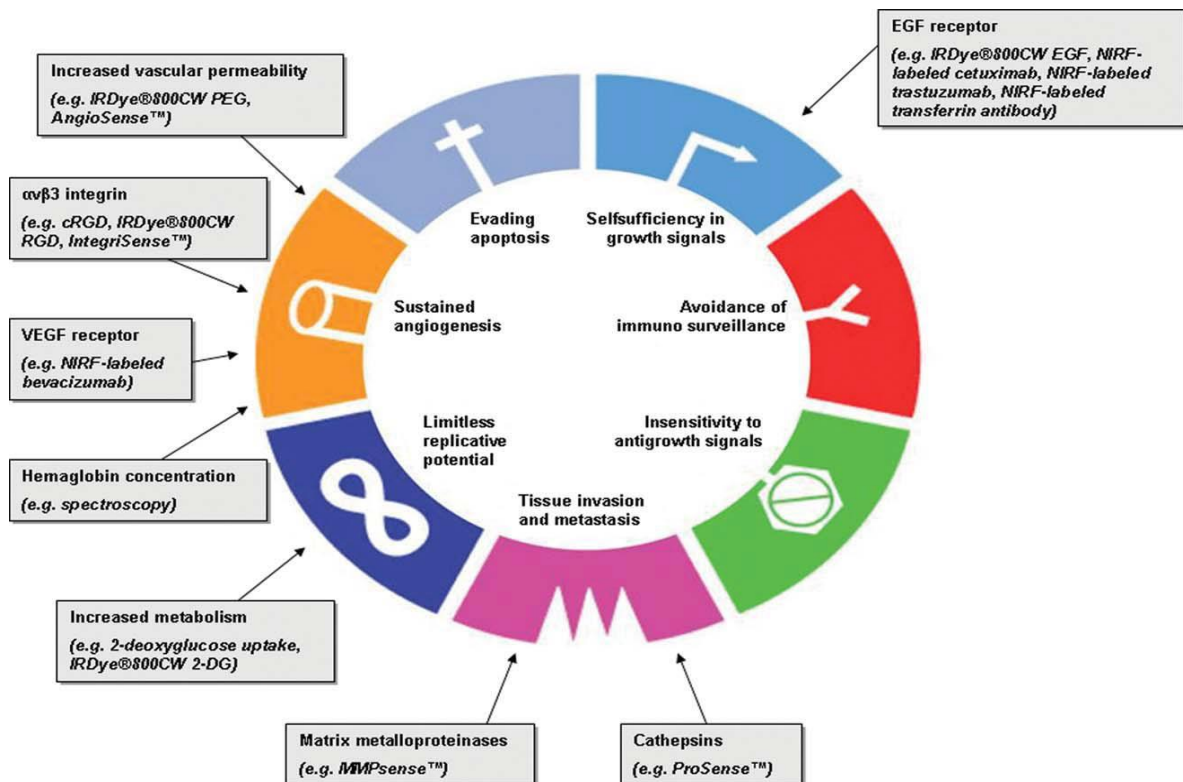
Figure V-10: Hallmarks of cancer and their targets for optical imaging.
-After Keereweer, S, H J C M Sterenborg, J D F Kerrebijn, P B A A Van Driel, R J Baatenburg de Jong, und C W G M Löwik. „Image-guided surgery in head and neck cancer: current practice and future directions of optical imaging". *Head & neck* 34, Nr. 1 (Januar 2012): 120–126.-

---

[97] Mieog, J. Sven D., Susan L. Troyan, Merlijn Hutteman, Kevin J. Donohoe, Joost R. van der Vorst, Alan Stockdale, Gerrit-Jan Liefers, u. a. „Toward Optimization of Imaging System and Lymphatic Tracer for Near-Infrared Fluorescent Sentinel Lymph Node Mapping in Breast Cancer". *Ann Surg Oncol*. 18, 2011.

[98] Jin, Z.H., J. Razkin, V. Josserand, et al. "In Vivo Noninvasive Optical Imaging of Receptor-mediated RGD Internalization Using Self-quenched Cy5-labeled RAFT-c(-RGDfK-)(4)." *Mol Imaging*. 6, 2007.43-55.

[99] Zhou, H., K. Luby-Phelps, B.E. Mickey, A.A. Habib, R.P. Mason, and D. Zhao. "Dynamic Near-infred Optical Imaging of 2-deoxyglucose Uptake by Intracranial Glioma of Athymic Mice." *PLoS ONE*. 4, 2009.e8051

Apart from ordinary molecules like peptides or glucoses, there exist nanoparticles. This subject will be presented at a short glance, as it is far too large for detailed explanation within my thesis.

❖ Nanoparticles

Quantum dot nanoparticles are small crystals (2–10 nm diameter), made of inorganic semiconductor materials. The high quantum yields result in high signal intensity, enabling detection at lower concentrations compared to organic fluorophores. In addition, the fluorescence emission spectra can be tuned, depending on their size, allowing for multiplexed imaging. Furthermore, quantum dot nanoparticles have proven to be photostable and have the possibility to target multiple biomarkers, due to their ability to contain multiple probe molecules. Finally, multimodal targeted quantum dot-based nanoparticles coated with paramagnetic micellar shells have been described, allowing for both optical and magnetic resonance detection of tumor angiogenesis[100]. However, the toxicity of quantum dot nanoparticles is a serious concern. The problem is that most quantum dots are based on heavy metal cores (e.g., Cd-Se, Cd-Te), which have been reported to be cytotoxic in their soluble form due to the release of toxic Cd2+ ions and their surface chemistry and stability towards aggregation[101]. These issues raise significant hazards concerning the feasibility of the clinical application of quantum dot nanoparticles.

Silica nanoparticles have been developed as an alternative to quantum dots that combine the versatility and functionality of organic dyes with the stability and biocompatibility of the silica surface[102]. The biodistribution, including long-term quantitative tissue distribution, subcellular distribution, and the toxicity of silica nanoparticles were assessed in a mouse model. The results show an accumulation of the agent in lungs, liver, and spleen, because the small size of the silica nanoparticles which results in high permeability, potentially causing liver injury when intravenously injected[103]. Size, surface area, surface

---

[100] Mulder, W.J., K. Castermans, J.R. van Beijnum, et al. "Molecular Imaging of Tumor Angiogenesis Using Alphavbeta3-integrin Targeted Multimodal Quantum Dots." *Angiogenesis*. 12, 2009.17-24.

[101] Kirchner, C., T. Liedl, S. Kudera, et al. "Cytotxicity of Colloidal CdSe and CdSe/ZnS Nanoparticles." *Nano Lett*. 5, 2005.331-338; Lewinski, N., V. Colvin, and R. Drezek. "Cytotoxicity of Nanoparticles." *Small*. 4, 2008.26-49.

[102] Choi, J., A.A. Burns, R.M. Williams, et al. "Core-shell Silica Nanoparticles as Fluorescent Labels for Nanomedicine." *J Biomed Opt*. 12, 2007.064007.

[103] Xie, G., J. Sun, G. Zhong, L. Shi, and D. Zhang. "Biodistribution and Toxicity of Intravenously Administered Silica Nanoparticles in Mice." *Arch Toxicol*. 84(3), 2009.183-190.

chemistry, solubility, and shape are probably all key features that play a role in determining the harmful potential for engineered nano-materials[104].

V.3.3.   *Double targeting*

Up to now NIR fluorogenic probes do have potential for *in vivo* imaging, but in regards to their pharmacokinetic profile, the molecule stability or the non-specific degradation, leading to a high background noise improvements for their application have to be made. Concerning activatable probes, there are only limited platforms available, which can clearly image proteases' activity *in vivo* after systemic administration, but most systems do show their proof-of-concept *in vitro* and *ex vivo*. The design of activatable probes needs also an increase in stability of the molecule as well as of the specificity of the molecule towards its target[105].

Chemical attempts of improving either the molecule stability or the targeting specificity were made by using polymeric nanoparticles[106]or using PEGylated poly(L-lysine)[107]. These are promising concepts, based mainly on the passive accumulation in the tumor tissue, the so called EPR (enhanced permeability retention) effect. Nevertheless, it is presumed that substrate sensitivity is decreased due to the high molecular weight polymer backbone, and the probably false fluorescence signals *in vivo* caused by the nonspecific EPR effect.

So another idea emerged: the combination of a relatively stable ligand with a second target or activatable sequence. This should lead to an increase in the specificity towards the cancer environment. The combination of two targets would also allow a design of molecules suitable for imaging and drug delivery. In the case of activatable sequences these molecules would offer the possibility to evaluate them by imaging methods and then serving as pro-drug vehicles.

---

[104] Oberdorster, G., E. Oberdorster, and J. Oberdorster. "Nanotoxicology: An Emerging Discipline Evolving from Studies of Ultrafine Particles." *Environ Health Perspect*. 113, 2005.823-839.

[105] Zhu, Lei, Jin Xie, Magdalena Swierczewska, Fan Zhang, Xin Lin, Xuexun Fang, Gang Niu, Seulki Lee, und Xiaoyuan Chen. „Dual-functional, receptor-targeted fluorogenic probe for in vivo imaging of extracellular protease expressions". *Bioconjugate chemistry* 22, Nr. 6 (Juni 15, 2011): 1001–1005.

[106] Lee, S., Cha, E. J., Park, K., Lee, S. Y., Hong, J. K., Sun, I. C., Kim, S. Y., Choi, K., Kwon, I. C., Kim, K., and Ahn, C. H. (2008) A nearinfrared-fluorescence-quenched gold-nanoparticle imaging probe for in vivo drug screening and protease activity determination. Angew. Chem., Int. Ed. Engl. 47, 2804–2807.

[107] Bremer, C., Tung, C. H., and Weissleder, R. (2001) In vivo molecular target assessment of matrix metalloproteinase inhibition. Nat. Med. 7, 743–748.

For example Choi et al. conjugated multiple c(RGDfK) peptides to HSA-TIMP2 (HAS = human serum albumin) to enhance the binding capacity of the protein (RGD-HSA-TIMP2) to tumors and their vasculatures. In form of ^{68}Ga-NOTA-RGD-HSA-TIMP2 they have been studied as potential PET probes for imaging $\alpha_v\beta_3$ integrin receptors in nude mice bearing human glioblastoma U87MG tumors[108].

Kratz et al. describes studies of pro-drugs based on Doxorubicin conjugated to a divalent integrin targeting peptide E-[c(RGDfK)$_2$], where a MMP-2/-9-cleavable octapeptide was introduced. The results show that the tumor inhibition capacity of the compound with MMP sequence was 6- to 10-fold higher compared to the control molecule *in vitro*[109].

The combination between the integrin $\alpha v\beta 3$ and the Gelatinases seems to be a good approach for double targeting with an improvement in specific targeting of tumor.

V.3.4.   *The integrin ligand RGD*

V.3.5.   Integrin $\alpha_v\beta_3$ and the RGD

As described earlier the integrin $\alpha_v\beta_3$ is known to play an important role in angiogenesis[110].

The repertoire of ligands of the receptor integrin $\alpha_v\beta_3$ comprises a numerous proteins bearing an exposed or cryptic RGD tripeptide. Amongst these there are vitronectin, fibronectin, fibrinogen, thrombospondin, ostepontin, von Willebrand factor, and others. The development of the angiogenesis inhibitor Cilengitide was based on these findings (Figure V-11).

RGD-based targeting has been successfully used to deliver drugs, biological[111], imaging agents[112], viruses[113], and nanoparticles[114] to tumor vasculature[115].

---

[108] Choi, Naeun, Sung-Min Kim, Kwan Soo Hong, Gyunggoo Cho, Jee-Hyun Cho, Chulhyun Lee, und Eun Kyoung Ryu. „The use of the fusion protein RGD-HSA-TIMP2 as a tumor targeting imaging probe for SPECT and PET". *Biomaterials* 32, Nr. 29 (Oktober 2011): 7151–7158.

[109] Ryppa, Claudia, Hagit Mann-Steinberg, Iduna Fichtner, Holger Weber, Ronit Satchi-Fainaro, Martin L Biniossek, und Felix Kratz. „In vitro and in vivo evaluation of doxorubicin conjugates with the divalent peptide E-[c(RGDfK)2] that targets integrin alphavbeta3". *Bioconjugate chemistry* 19, Nr. 7 (July 2008): 1414–1422.

[110] Malinin, Nikolay, Elzbieta Pluskota, and Tatiana Byzova. "Integrin Signaling in Vascular Function." *Current Opinion in Hematology May 2012* 19, no. 3 (2012): 206–211.

[111] Arap, W, R Pasqualini, und E Ruoslahti. „Cancer treatment by targeted drug delivery to tumor vasculature in a mouse model". *Science (New York, N.Y.)* 279, Nr. 5349 (Januar 16, 1998): 377–380.

[112] Sipkins, D A, D A Cheresh, M R Kazemi, L M Nevin, M D Bednarski, und K C Li. „Detection of tumor angiogenesis in vivo by alphaVbeta3-targeted magnetic resonance imaging". *Nature medicine* 4, Nr. 5 (Mai 1998): 623–626.

[113] McDonald, G A, G Zhu, Y Li, I Kovesdi, T J Wickham, und V P Sukhatme. „Efficient adenoviral gene transfer to kidney cortical vasculature utilizing a fiber modified vector". *The journal of gene medicine* 1, Nr. 2 (April 1999): 103–110.

[114] Larkin, Deirdre, Achim Treumann, Derek Murphy, Ciaran DeChaumont, Aoife Kiernan, und Niamh Moran. „Compartmentalization regulates the interaction between the platelet integrin alpha IIb beta 3 and ICln". *British journal of haematology* 144, Nr. 4 (Februar 2009): 580–590.

[115] Kazuki, N. et al; tissue-penetrating delivery of compounds and nanoparticles into tumors, *Cancer Cell* 2009

❖ *Ligands of the integrin αvβ3*

The motif –RGD- (Arginine – Glycine – Aspartic acid) is a tripeptide represented in most proteins of the extracellular matrix. Being recognized by and interacting with at least half of the integrins, the affinity of the receptor for the substrate differs. Here the substrate specificity depends on the RGD conformation in the protein, as well as on the residual sequences. The endogene ligand of the $\alpha_v\beta_3$ integrin is the vitronectin. Nevertheless a binding to other proteins via the RGD is possible, as in the case of fibronectine, fibrinogene, collagene, von Willebrand factor and thrombospondin.

Consequently, different approaches of RGD containing peptides with integrin $\alpha_v\beta_3$ specificity have been made (Figure V-11), ranging from linear RGD peptide sequences, cyclic RGD molecules, monomeric to multimeric RGD-based systems, RGD-based Semipeptides to nanoparticles, which are discussed in detail by Casiraghi et al[116].

Indeed cyclization is employed to improve the binding properties of RGD peptides conferring rigidity to the structure, providing a better presentation of the ligand (Figure V-12), and higher stability. Since the natural interactions between the $\alpha_v\beta_3$ integrin and RGD substrates may involve multivalent binding sites, the affinity is increased by multivalent cRGD presentation.

---

[116] Auzzas, L, F Zanardi, L Battistini, P Burreddu, P Carta, G Rassu, C Curti, and G Casiraghi. "Targeting Alphavbeta3 Integrin: Design and Applications of Mono- and Multifunctional RGD-based Peptides and Semipeptides." *Current Medicinal Chemistry* 17, no. 13 (2010): 1255–1299.
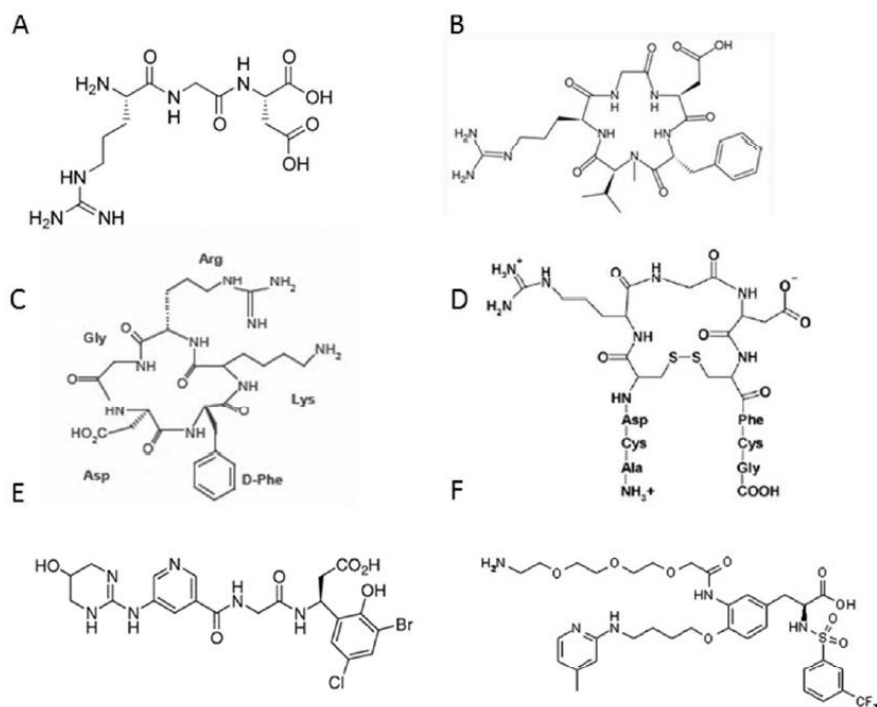
Figure V-11: Chemical structures based on the RGD motif.
A. The original RGD sequence; **B.** Cyclic RGD-peptide antagonist (c(RGDf[N-Me]V) or Cilengitide;
C.Cyclic peptide c(RGDfK); **D**. ACDCRGDCFCG (RGD4C); **E**. Example of
RGD peptidomimetic-containing the RGD sequence (S-247); **F**. Example of RGD-peptidomimetic;
-After: Danhier, Fabienne, Aude Le Breton, und Veronique Preat. „RGD -based strategies to target alpha(v) beta(3) integrin
in cancer therapy and diagnosis".*Molecular pharmaceutics* (September 11, 2012).-
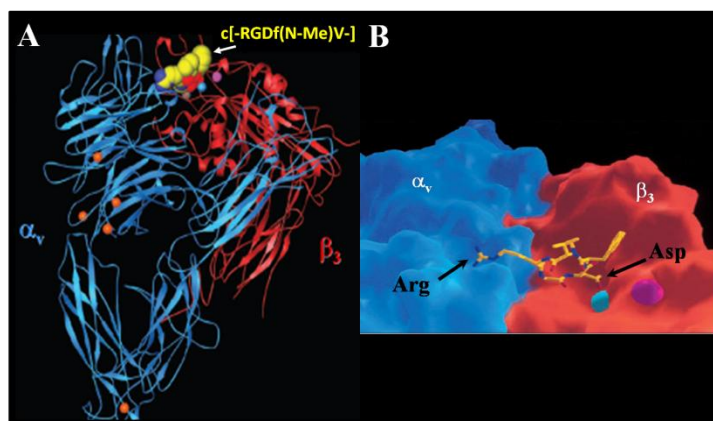
**Figure V-12: Representation of the extracellular domain structure of the integrin αvβ3, associated to the
ligand c[-RGDf(*N*-Me)V-] in presence of Mn²⁺.**
Different kinds of illustrting the crystal structure in A) and B)

-Modified after: Xiong, Jian-Ping, Thilo Stehle, Rongguang Zhang, Andrzej Joachimiak, Matthias Frech, Simon L Goodman,
und M Amin Arnaout. „Crystal structure of the extracellular segment of integrin alpha Vbeta3 in complex with an Arg-Gly-
Asp ligand". *Science (New York, N.Y.)* 296, Nr. 5565 (April 5, 2002): 151–155.-

❖ *cyclic RGD penta-peptides*

As linear RGD containing sequences did not show the expected accumulation in the tumor but in the liver in clinical studies[117] and are more sensitive to proteolytic degradation and changes in conformation, decreasing their integrin affinity, few cyclic peptides have been developed.

The first affinity and competition tests with the RGD moiety incorporated in cyclic penta- or hexapeptides have been started by the group of H. Kessler in the 1990s[118]. As a result the cyclopentapeptide c-[RGDfV] was recognized as selective ligand of the $\alpha_v\beta_3$ integrin. Its affinity for the purified free or immobilized $\alpha_v\beta_3$ integrin (IC_{50} = 50 nM (= peptide concentration needed to inhibit 50 % of the integrin − ligand binding) is comparable to the affinity of its endogen ligand, the vitronectin (IC_{50} = 25 nM)[119], but not as efficient in competition with fibrinogen or fibronectine and the immobilized $\alpha_{IIb}\beta_3$ (IC_{50} = 29 μM) and $\alpha_5\beta_1$ (IC_{50} = 6.4 μM). After all the methyl derivate (c-[-RGDf(*N*-Me)V]), also known as the anti-angiognetic agent cilengitide, shows a strong inhibition of the vitronectine fixation of the $\alpha_v\beta_3$ integrin (IC50 = 0.58 nM) as well as a weak competition in regards to the vitronectine - $\alpha_5\beta_1$ integrin − interaction[120].

Cilengitide effectively inhibits angiogenesis and is currently being tested in phase II trials in patients with lung and prostate cancer as well as glioblastoma. Paradoxically, it has been found that infusion of very low concentration of RGD-mimetic inhibitors stimulates tumor growth and angiogenesis by the already mentioned promoting VEGF-induced endothelial cell migration. Thus integrin inhibition maybe not sufficient to completely block tumor angiogenesis[121].

For optical imaging *in vivo*, the Chen's group introduced monomeric, dimeric, and tetrameric cyanine-ligand c(RGDfk) displays based on a glutamate backbone. It was shown

---

[117] Sutcliffe-Goulden, Julie L, Michael J O'Doherty, Paul K Marsden, Ian R Hart, John F Marshall, und Sukvinder S Bansal. „Rapid solid phase synthesis and biodistribution of 18F-labelled linear peptides". *European journal of nuclear medicine and molecular imaging* 29, Nr. 6 (Juni 2002): 754–759.

[118] Gurrath, M, G Müller, H Kessler, M Aumailley, und R Timpl. „Conformation/activity studies of rationally designed potent anti-adhesive RGD peptides". *European journal of biochemistry / FEBS* 210, Nr. 3 (Dezember 15, 1992): 911–921.

[119] Burgess, K, D Lim, und S A Mousa. „Synthesis and solution conformation of cyclo[RGDRGD]: a cyclic peptide with selectivity for the alpha V beta 3 receptor". *Journal of medicinal chemistry* 39, Nr. 22 (Oktober 25, 1996): 4520–4526.

[120] Xiong, Jian-Ping, Thilo Stehle, Rongguang Zhang, Andrzej Joachimiak, Matthias Frech, Simon L Goodman, und M Amin Arnaout. „Crystal structure of the extracellular segment of integrin alpha Vbeta3 in complex with an Arg-Gly-Asp ligand". *Science (New York, N.Y.)* 296, Nr. 5565 (April 5, 2002): 151–155.

[121] Danhier, Fabienne, Aude Le Breton, und Veronique Preat. „RGD -based strategies to target alpha(v) beta(3) integrin in cancer therapy and diagnosis". *Molecular pharmaceutics* (September 11, 2012). http://www.ncbi.nlm.nih.gov/pubmed/22967287.

that the binding affinity of RGD multipresentation in subcutaneous $\alpha_v\beta_3$ integrin positive U87MG glioblastoma xenograft models, moved from 42.9 nM for the monomer to 27.5 nM for the dimer, and 12.1 nM for the tetramer, in agreement with the multivalency phenomenon. The tetramer displayed the highest tumor uptake and tumor-to-normal tissue ratio[122].

Finally, the cyclopentapeptide –RGD- was strongly used for the vectorization of therapeutic agents and tumor detection[123]. The fact that using multiple ligands improves the targeting effect (Figure V-13), several approaches of designing multivalent composites containing cyclopentapeptides for tumor targeting have been made[124].
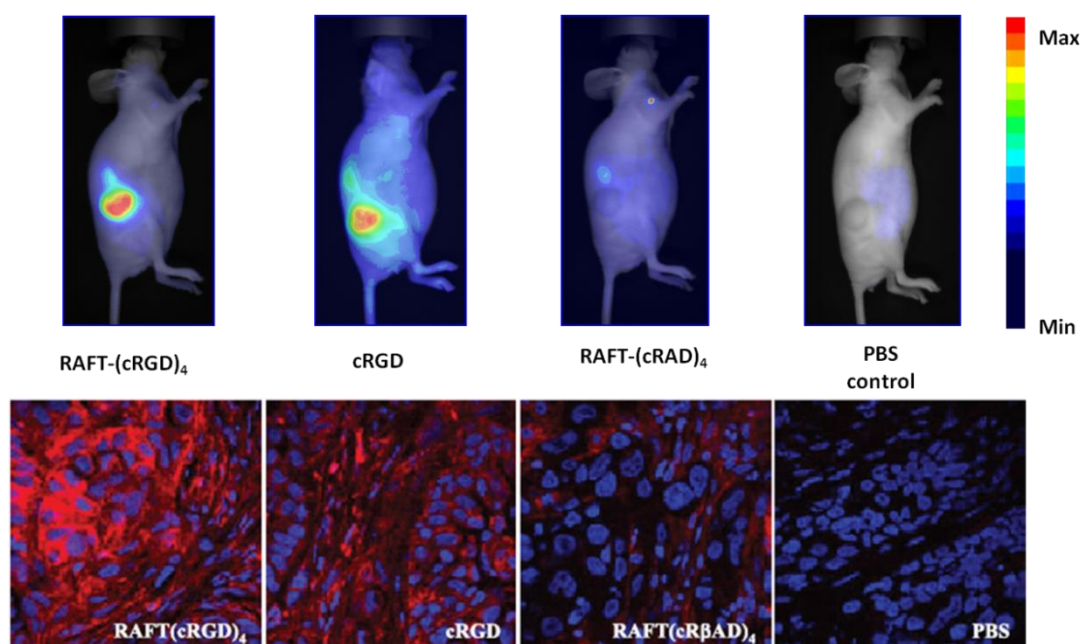
Figure V-13: Improved αvβ3 Integrin targeting.
The specificity is improved using four cRGD compared to mono cRGD. As controls served the non-specific sequence cRAD instead of RGD and PBS.
-After : Jin et al. „Noninvasive optical imaging of ovarian metastases using Cy5-labeled RAFT-c(-RGDfK-)4". *Molecular imaging* 5, Nr. 3 (Juli 2006): 188–197. &
Jin et al.„In vivo optical imaging of integrin alphaV-beta3 in mice using multivalent or monovalent cRGD targeting vectors". *Molecular cancer* 6 (2007): 41.-

---

[122] Auzzas, L, F Zanardi, L Battistini, P Burreddu, P Carta, G Rassu, C Curti, and G Casiraghi. "Targeting Alphavbeta3 Integrin: Design and Applications of Mono- and Multifunctional RGD-based Peptides and Semipeptides." *Current Medicinal Chemistry* 17, no. 13 (2010): 1255–1299.

[123] Garanger, Elisabeth, Didier Boturyn, und Pascal Dumy. „Tumor targeting with RGD peptide ligands-design of new molecular conjugates for imaging and therapy of cancers". *Anti-cancer agents in medicinal chemistry* 7, Nr. 5 (September 2007): 552–558.

[124] Jin, Zhao-Hui, Veronique Josserand, Jesus Razkin, Elisabeth Garanger, Didier Boturyn, Marie-Christine Favrot, Pascal Dumy, und Jean-Luc Coll. „Noninvasive optical imaging of ovarian metastases using Cy5-labeled RAFT-c(-RGDfK-)4". *Molecular imaging* 5, Nr. 3 (Juli 2006): 188–197.

❖   The RAFT- c(RGDfK)$_4$

In our laboratory we use the RAFT (Regioselectively Addressable Functionalized Template)[125], which is based on the in the 1980s developed template TASP (Template-Assembled Synthetic Protein) by Professor Manfred Mutter[126]. The RAFT allows the adequate steric organization on the template, representing an independent targeting and effecting moiety at the same time, due to the four to six lysine (K) residues and their orthogonal protection groups[127]. The cyclic decapeptide sequence of the RAFT is c[-Pro-Gly-Lys-Lys-Lys-]$_2$[128].

The sequence can be modified by introducing alanine residues instead of the lysine. Four c(RGDfK) moieties were anchored to four non contiguous lysine residues via oxime ligation chemistry (Figure V-14).

After leading to clustering of its receptor, the integrin $\alpha_v\beta_3$, by binding and creation of integrin dimers, the molecule is internalized *via* clathrin coated vesicles[129].
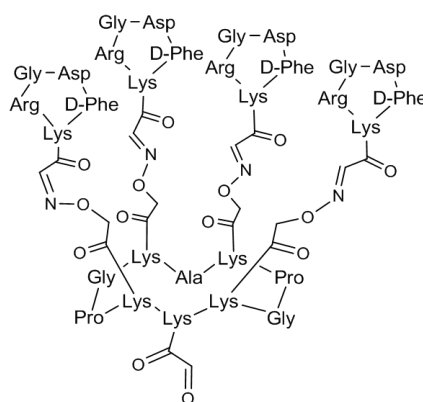
Figure V-14: The RAFT-c(RGD)4 scaffold.

[125] Dumy, P.; Favrot, M.-C.; Boturyn, D.; Coll, J.-L. Synthesis and characterization of novel systems for guidance and vectorization of compounds having a therapeutic activity. Brevet PCT/FR2003/002773 WO 2004/02894, 19 Septembre 2003.

[126] Carey, R I, K H Altmann, und M Mutter. „Protein design: template-assembled synthetic proteins". *Ciba Foundation symposium* 158 (1991): 187–199; discussion 199–203, 204–212.

[127] Dumy, P.; Eggleston, I. M.; Cervigni, S.; Sila, U.; Sun, X.; Mutter, M. A convenient synthesis of cyclic peptides as regioselectively addressable functionalized templates (RAFT). *Tetrahedron Lett* **1995**, *36*, 1255- 1258.

[128] Dumy, P.; Eggleston, I. M.; Cervigni, S.; Sila, U.; Sun, X.; Mutter, M. A convenient synthesis of cyclic peptides as regioselectively addressable functionalized templates (RAFT). *Tetrahedron Lett* **1995**, *36*, 1255-1258.

[129]Sancey, L., E. Garanger, S. Foillard, G. Schoehn, A. Hurbin, C. Albiges-Rizo, D. Boturyn, u. a. „Clustering and internalization of integrin alphavbeta3 with a tetrameric RGD-synthetic peptide". *Molecular Therapy*. 17(5), Mai 2009.

VI. Peptidic molecular probes for cancer targeting – the MMP smart approach

Targeting MMPs

VI.1.   MMP Inhibitors (MMPIs)

As inappropriate proteolysis has been found to have a major role in cancer as well as cardiovascular, inflammatory, neurodegenerative, bacterial, viral and parasitic diseases, the idea to target these proteases and blocking them is widely explored by pharmaceutical companies[130].

Inhibitors of MMPs include small molecules (like hydroxamates), blocking antibodies, natural inhibitors, including TIMP-1 to -4, prodomains, exosite domains and aptamers[131].

VI.1.1.   Natural inhibitors – TIMPs

TIMPs (tissue inhibitors of metalloproteases) control the activity of MMPs *in vivo* by forming complexes with the latent or activated enzymes. Experimental models show their ability to decrease angiogenesis, growth, migration and metastasis, but also their participation in the activation of MMPs. In some tumors the role of TIMPs is associated with aggressive behavior of the disease in others rather with tumor progression. At the same time increased expression of TIMPs can show an antimetastatic effect, but they are also indicative of poor prognosis as in human melanoma cells a growth-stimulating effect of TIMPs could be observed[132].

TIMPs have been described to form a 1:1 stoichiometric complex with all activated MMPs, with which they become covalently linked[133]. For example MT1-MMP functions as a cellular receptor and activator of Pro-MMP-2. They form a trimolecular complex on the cell surface with TIMP-2. While MMP-2, MT1-MMP, TIMP-2 and integrin αvβ3 are colocalized in caveolae in the basolateral compartment of human endothelial cells, MMP-9 and TIMP-1

---

[130] Turk, Boris. „Targeting proteases: successes, failures and future prospects". *Nature reviews. Drug discovery* 5, Nr. 9 (September 2006): 785–799.

[131] Overall, Christopher M, und Carl P Blobel. „In search of partners: linking extracellular proteases to substrates". *Nature reviews. Molecular cell biology* 8, Nr. 3 (März 2007): 245–257.

[132] Hofmann, Uta B., Roland Houben, Eva-B. Bröcker, and Jürgen C. Becker. "Role of Matrix Metalloproteinases in Melanoma Cell Invasion." *Biochimie* 87, no. 3–4 (March 2005): 307–314.

[133] Pepper, M S. „Role of the matrix metalloproteinase and plasminogen activator-plasmin systems in angiogenesis". *Arteriosclerosis, thrombosis, and vascular biology* 21, Nr. 7 (Juli 2001): 1104–1117.

are distributed on the cell surface and concentrated in the Golgi region[134]. The natural inhibitor for MMP-2 and MMP-9 are TIMP-1 and TIMP-2, respectively.

TIMP-1 is a 32 kDa protein that inhibits MMP-9 catalytic activity by forming an enzyme-inhibitor complex with high affinity[135]. Dufour et al.[136] demonstrated that the MMP-9 PEX domain binds specifically to TIMP-1, and in a 1:1 binding ratio to the catalytic core domain, it inhibits the proteolytic activity of secreted MMPs.

Concerning pro-MMP-2, its PEX-domain binds by interaction with blade IV to TIMP-2 (crystallography analysis) (Figure VI-1).

But also soluble PEX, a result of MMP-2 activation, can bind to TIMP-2 and thus inhibits MT1-MMP dependent MMP-2 activation[137].
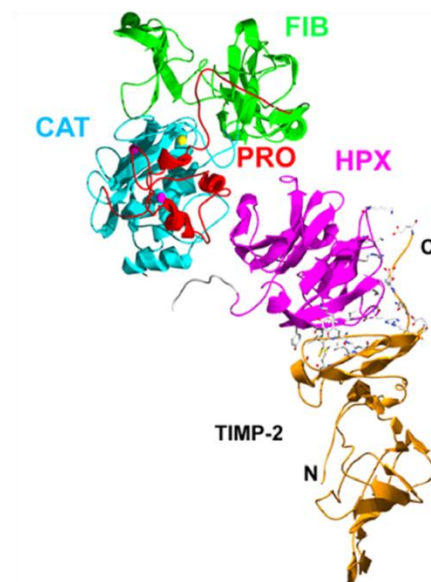
Figure VI-1: The complex of proMMP-2 and TIMP-2.
The pro-domain of proMMP-2 is shown in red, the catalytic domain in blue, the fibronectin type II repeats in green, the linker in grey and the hemopexin domain in purple. The TIMP-2 is shown in orange with the residues interacting with proMMP-2 as stick model in atom type. The important residues for this interaction on proMMP-2 are also represented as stick models.
-After: Maskos, Klaus. „Crystal structures of MMPs in complex with physiological and pharmacological inhibitors". *Biochimie* 87, Nr. 3–4 (März 2005): 249–263.-

---

[134] Pepper, M S. „Role of the matrix metalloproteinase and plasminogen activator-plasmin systems in angiogenesis". *Arteriosclerosis, thrombosis, and vascular biology* 21, Nr. 7 (Juli 2001): 1104–1117.

[135] Kim, Dong Seok, Ok-Hee Jeon, Hee Doo Lee, Kyung Ho Yoo, und Doo-Sik Kim. „Integrin alphavbeta3-mediated transcriptional regulation of TIMP-1 in a human ovarian cancer cell line". *Biochemical and biophysical research communications* 377, Nr. 2 (Dezember 12, 2008): 479–483.

[136] Dufour, Antoine, Stanley Zucker, Nicole S Sampson, Cem Kuscu, und Jian Cao. „Role of matrix metalloproteinase-9 dimers in cell migration: design of inhibitory peptides". *The Journal of biological chemistry* 285, Nr. 46 (November 12, 2010): 35944–35956.

[137] Nisato, Riccardo E, Ghamartaj Hosseini, Christian Sirrenberg, Georgina S Butler, Thomas Crabbe, Andrew J P Docherty, Matthias Wiesner, u. a. „Dissecting the role of matrix metalloproteinases (MMP) and integrin alpha(v)beta3 in angiogenesis in vitro: absence of hemopexin C domain bioactivity, but membrane-Type 1-MMP and alpha(v)beta3 are critical". *Cancer research* 65, Nr. 20 (Oktober 15, 2005): 9377–9387.

VI.1.2.   Synthetic inhibitors

In the 1950s, the idea to design drugs which suppress protease activity began. This was one approach thought to battle cancer, where MMPs were the first proteases targets seriously considered for combating cancer because of their role in extracellular matrix degradation[138].

Inhibitors are classified according to their mechanism (Table VI-1).

Canonical (lock-and-key)	Binding to target in a substrate-like manner (Michaelis-type complex); Ex.: serine protease inhibitors (serpins)	Mostly competitive
Exosite-binding inhibitors	Blocking the active site by contiguous binding and partial covering (substrate-like); Ex.: cystatins, cystein cathepsins	Mostly competitive
Quasi-substrate-like	Combination of canonical and exosite-binding mechanisms; Ex.: TIMPs	Mostly competitive
Allosteric	Prevention of dimerization by binding in the interdomain region away from the active site; Ex.: X-linked inhibitor of apoptosis protein, which inhibits caspase 9	Not competitive

Table VI-1: Classification of protease inhibitors according to their mechanism
-based on Turk, 2006-

Two major groups of MMPIs have been developed:

➢ Hydroxamates: Batimastat (BB94; British Biotech), Marimastat (BB2516; British Biotech); Prinomastat (AG-3340; Aguron);

➢ Non hydroxamates: Neovastat (AE-941; Aeterna ; extract of shark cartilage) ; Rebimastat (BMS-275291 ; Bristol-Myers Squibb) ; Tanomastat (Bay-12-9566 ; Bayer),Pyrimidine-2,4,6-triones (or barbiturates) (exhibition of specific activities for a subgroup of secreted MMPs comprising MMP-2,-8,-9,-14 and -16)

---

[138] Turk, Boris. „Targeting proteases: successes, failures and future prospects". *Nature reviews. Drug discovery* 5, Nr. 9 (September 2006): 785–799.

But all these MMP inhibitors have failed clinical trials because of severe side effects and/or no therapeutic benefit[138,139]. For instance only the tetracycline analog periostat (Colla-Genex) for the treatment of adult periodontitis is on the market. It inhibits the activity and the synthesis of MMPs.

These failures can be traced back to the fact that the compounds are mostly broad-spectrum MMP inhibitors arisen at a time of lack of knowledge of the various MMPs, their substrates and biology. So they lack of enzyme specificity and tent to cross-reactivity. Consequently MMP off-or anti-target activities reduce overall drug efficacy.

The unspecific MMP-inhibitor Batimastat for example induced liver metastases in mice and caused liver-specific over-expression of MMP-2 and -9 in tumor-free animals[140]. This paradoxical effect was not detectable after treatment with recently developed specific inhibitors of MMP-2 and -9.

It has also to be taken in consideration that while inhibiting the activity of a target the activation of downstream proteases or protease cofactor complexes might be blocked as well[139].

For example off-target effects on non-MMP metalloproteases result in musculoskeletal toxicity and other affections of physiological events.

Finally, many potent protease inhibitors have poor safety profiles. Also research with protease-knockout mice has shown that even the most simple protein-processing events often have complex consequences, and that protease signaling in its broadest sense is often only a small part of disease biology in the whole organism and not always the best aspect to target[141]. Nevertheless Turk proposed that the ideal inhibitor, in the view of the pharmaceutical industry, would be a non-covalent reversible inhibitor, as such an inhibitor would provide better selectivity with fewer side effects than covalent inhibitors. He also pointed out that competitive inhibitors can saturation of substrate competition, which results in substantially higher doses of the compounds and in narrowing the safety window.

Another approach has been done by identifying specific gelatinase-inhibitory peptides from phage display libraries. A potent and selective MMP-2 and MMP-9 inhibitory sequence

---

[139] Cudic, Mare, und Gregg B Fields. „Extracellular proteases as targets for drug development". *Current protein & peptide science* 10, Nr. 4 (August 2009): 297–307.

[140] A. Krüger, R. Soeltl, I. Sopov, C. Kopitz, M. Arlt,V. Magdolen, et al., Hydroxamate-type matrix metalloproteinase inhibitor batimastat promotes liver metastasis, Cancer Res. 61 (2001) 1272–1275.

[141] Turk, Boris. „Targeting proteases: successes, failures and future prospects". *Nature reviews. Drug discovery* 5, Nr. 9 (September 2006): 785–799.

was a cyclic peptide, containing the sequence His-Trp-Gly-Phe. It has been shown that they inhibit tumor and endothelial cell migration *in vitro* and tumor growth and invasion *in vivo*[142]. Also triple-helical phosphinate transition state analogs have been described to be highly selective for gelatinases. Another progress has been done in the development of MMP selective inhibitors based on novel zinc binding groups[143].

The discontinuation of a number of phase III trials and the limited success of the clinical application of clinical application of MMP inhibitors might also to be traced back to the fact that MMP inhibition may result in the stimulation rather than inhibition of angiogenesis, though they were presumed as molecules of antiangiogenic activity[142]. It is to take into notice that the inhibitor profile of an enzyme in cell-based assays and biochemical assays can differ, so both must be determined separately[144].

Another approach of inhibitory peptide design is the mimicking of the noncatalytic PEX-domain of MMP-9[145]. Here Dufour *et al.* demonstrated that their designed peptides block MMP-9 dimer formation and thus inhibit cell migration. This concept was a creation as response to the failure of broad-spectrum MMP inhibitors, evaluated in the 1990s. The idea is as catalytic sites of most MMPs are highly homologous, leading to difficulties of producing non-cross-reactive inhibitors, to target the PEX domain as they are less homologue.

Apart from targeting MMPs by blocking them, their properties of specific substrate cleavage gained interest for the development of either pro-drugs or smart imaging agents (see section activatable probes).

In regard to the appearance of MMPs in diseases they form an attractive therapeutic object. One approach is the inhibition of their activity another is taking the advantage of differential expression in different stages of disease to selectively deliver therapeutic or imaging agents.

---

[142] Pepper, M S. „Role of the matrix metalloproteinase and plasminogen activator-plasmin systems in angiogenesis". *Arteriosclerosis, thrombosis, and vascular biology* 21, Nr. 7 (Juli 2001): 1104–1117.

[143] Cudic, Mare, und Gregg B Fields. „Extracellular proteases as targets for drug development". *Current protein & peptide science* 10, Nr. 4 (August 2009): 297–307.

[144] Overall, Christopher M, und Carl P Blobel. „In search of partners: linking extracellular proteases to substrates". *Nature reviews. Molecular cell biology* 8, Nr. 3 (März 2007): 245–257.

[145] Dufour, Antoine, Stanley Zucker, Nicole S Sampson, Cem Kuscu, und Jian Cao. „Role of matrix metalloproteinase-9 dimers in cell migration: design of inhibitory peptides". *The Journal of biological chemistry* 285, Nr. 46 (November 12, 2010): 35944–35956.

VI.2.   MMP and "Smart" contrast agents and therapeutics

MMPs have been addressed with synthetic fluorogenic derivates as biochemical and pharmacological tool, as well as for targeted delivery systems. Most of these are FRET-based substrates designed from natural collagen-identified sequences, cleaved by MMPs.

As already mentioned, "Smart" probes or also known activatable molecules have been designed to ameliorate the contrast and SBR of imaging probes, using over-expressed enzymes.

Gelatinases cleavable sequences are used in imaging and as drug delivering compounds. Most of these are FRET-based substrates designed from natural collagen-identified sequences.

In particular, the substrate Mca-Pro-Leu-Gly-Leu-Dpa-Ala-Arg-NH$_2$, was extensively used for monitoring MMP activities and for screening inhibitors. Knight et al.[146] already showed with a MMP cleavable sequence and the quenching between dinitrophenyl (DNP) and 7-methoxycumarin (Mca) the use of quenched precursors.

Trying to approach the native substrates of the gelatinases and improving the drawbacks of the first collagen-based molecules well-defined triple helical molecules, mainly described by Gregg B. Fields group, have been developed[147,148,149]. The idea was to synthesize structures, which would be stable enough to remain in triplehelical conformation in the conditions of assays. Therefore different approaches have been described. *Fields et al.* developed first a solid-phase synthesis, featuring a C-terminal covalent branch and incorporating specific sequences between this branch and a N-terminal (Gly-Pro-Hyp)*n* domain[150](Figure VI-2).

Then "peptide-amphiphile" triple helices were designed, based on the non-covalent self-assembly of lipophilic molecules, N-terminally-linked to a peptide sequence. Finally,

[146] Knight, C G, F Willenbrock, und G Murphy. „A novel coumarin-labelled peptide for sensitive continuous assays of the matrix metalloproteinases". *FEBS letters* 296, Nr. 3 (Januar 27, 1992): 263–266.

[147] Akers, Walter J, Baogang Xu, Hyeran Lee, Gail P Sudlow, Gregg B Fields, Samuel Achilefu, and W Barry Edwards. "Detection of MMP-2 and MMP-9 Activity in Vivo with a Triple-helical Peptide Optical Probe." *Bioconjugate Chemistry* 23, no. 3 (March 21, 2012): 656–663.

[148] Akers, Walter J., Baogang Xu, Hyeran Lee, Gail P. Sudlow, Gregg B. Fields, Samuel Achilefu, and W. Barry Edwards. "Detection of MMP-2 and MMP-9 Activity in Vivo with a Triple-Helical Peptide Optical Probe." *Bioconjugate Chemistry* 23, no. 3 (2012): 656–663.

[149] Lauer-Fields, Janelle L, Thilaka Sritharan, M Sharon Stack, Hideaki Nagase, und Gregg B Fields. „Selective hydrolysis of triple-helical substrates by matrix metalloproteinase-2 and -9". *The Journal of biological chemistry* 278, Nr. 20 (Mai 16, 2003): 18140–18145.

[150] Lombard, Carine, Joëlle Saulnier, and Jean Wallach. "Assays of Matrix Metalloproteinases (MMPs) Activities: a Review." *Biochimie* 87, no. 3–4 (March 2005): 265–272.

triple-helical peptides containing fluorophores for continuous assay methods have been synthesized.
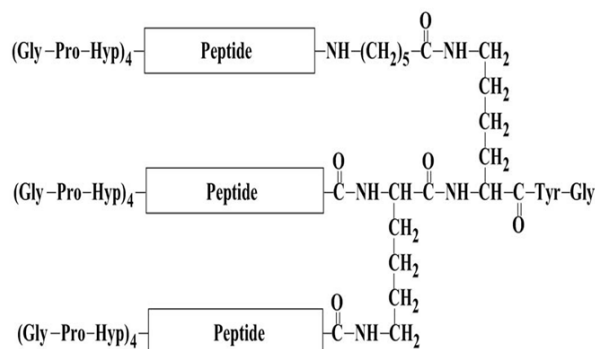
Figure VI-2: Schematic structure of branched triple-helical peptides.
-Fields et al. 2003-

The triple-helical peptide substrates were hydrolyzed in a similar manner to native collagens, cleavage occurring between Gly and Ile or Leu according to the chain type. The problem concerning these substrates is the difficulty in synthesis (not commercially available).

Besides a couple of linear sequences as quenched molecules are commercially available, like Cy5.5-Gly-Pro-Leu-Gly-Val-Arg-Gly-Cys-Ferritin-black hole quencher-3 nanocages[151].

Substrate sequences for Gelatinases and other proteases can be looked up the already mentioned MEROPS peptide database.

Moreover, several delivery devices have also been designed, using polymeric vehicles[152, 153], hydrogel matrix or liposomal devices functionalized with peptidic moieties embodying MMP cleavage sequences[154].

In order to obtain reasonable sized molecules, selectively cleaved by MMPs, with high plasma stability at the same time, Moustoifa et al. present a cyclopeptide approach for MMP directed delivery design. They argue that cyclization of linear peptides improves peptide stability in biological medium, preventing unspecific degradation. In order to allow a FRET

---

[151] *Molecular Imaging and Contrast Agent Database (MICAD)*. Bethesda (MD): National Center for Biotechnology Information (US), 2004. http://www.ncbi.nlm.nih.gov/pubmed/22649804.

[152] Vartak, Deepali G, und Richard A Gemeinhart. „Matrix metalloproteases: underutilized targets for drug delivery". *Journal of drug targeting* 15, Nr. 1 (Januar 2007): 1–20.

[153] Chau, Ying, Frederick E Tan, und Robert Langer. „Synthesis and characterization of dextran-peptide-methotrexate conjugates for tumor targeting via mediation by matrix metalloproteinase II and matrix metalloproteinase IX". *Bioconjugate chemistry* 15, Nr. 4 (August 2004): 931–941.

[154] Moustoifa, El-Farouck, Mohamed-Anis Alouini, Arnaud Salaün, Thomas Berthelot, Aghleb Bartegi, Sandra Albenque-Rubio, und Gérard Déléris. „Novel cyclopeptides for the design of MMP directed delivery devices: a novel smart delivery paradigm". *Pharmaceutical research* 27, Nr. 8 (August 2010): 1713–1721.

system to work they therefore introduced two hydrolysis sites in the cyclic peptide, resulting in cleavage by MMPs, especially MMP-9 and good plasma stability.

VI.2.1.   *Drug delivery*

In regard to the facts described earlier, the use of proteases, like MMPs in order to ameliorate drug delivery methods has been more and more considered during the last decade, especially in the case of cancer treatment.
Here is to say, that despite improvements and inventions in this field, no method has been developed which implies efficiency without causing severe side effects.

Up to now, surgical resection still remains the "tool" of choice in the battle against cancer. This therapy for primary tumors is though limited by tumor accessibility, tumor pathology and the eventual tumor spread or metastasis. Exploiting now the characteristics of enzymes which are over-expressed in cancer, the era of pro-drugs has begun.

Tumor-activated prodrugs rely on the facts that their activation occurs selectively in the tumor microenvironment. Therefore suitable characteristics of enzymes, serving in this manner, are:

- their significant over-expression in cancerous tissue
- a high affinity towards cleaving the pro-drug
- significantly elevated activity in the tumor environment
- no presence of the targeted enzyme in a pro-drug activating form in the patient serum
- the ability of the enzyme for selective and rapid activation of the pro-drug

❖ *Tumor-activated prodrugs*

As summed up by Atkinson et al.[155] several MMP-targeted "prodrugs" directed to the matrix metalloproteases have been developed.

The success of the "enzyme prodrug strategy" relies on the identification of suitable enzymes differentially active in the immediate environment of tumor cells[156]. MMP-2 and -9 substrate sequences have been used in prodrug strategies attempting to release doxorubicin, mephalan, camptothecin, vinblastine and a recombinant anthrax toxin[156,157].

Gelatinases represents thus enzymes with a sufficient activity and a high representation in the tumor tissue for possible pro-drug use.

The combination of imaging and therapeutic agent on one molecule, like a linear peptide sequence which is cleaved by these enzymes, is of high interest. Linear peptides are easier to synthesize compared to triple helical peptides and functionalization is simplified because of less synthesizing steps compared to cyclic ones. At the same time the close relation between the integrin $\alpha_v\beta_3$ and the Gelatinases open up new vistas for a possible gain in tumor specific targeting.

Thus, a linear substrate peptide sequence for Gelatinases would be of concern for testing the double targeting approach with the well studied RAFT-c(RGD)$_4$ for imaging and possible therapy.

---

[155] Atkinson, J M, C S Siller, und J H Gill. „Tumour endoproteases: the cutting edge of cancer drug delivery?" *British journal of pharmacology* 153, Nr. 7 (April 2008): 1344–1352.

[156] Kline, Toni, Michael Y Torgov, Brian A Mendelsohn, Charles G Cerveny, und Peter D Senter. „Novel antitumor prodrugs designed for activation by matrix metalloproteinases-2 and -9". *Molecular pharmaceutics* 1, Nr. 1 (Januar 12, 2004): 9–22.

[157] Ryppa, Claudia, Hagit Mann-Steinberg, Iduna Fichtner, Holger Weber, Ronit Satchi-Fainaro, Martin L Biniossek, und Felix Kratz. „In vitro and in vivo evaluation of doxorubicin conjugates with the divalent peptide E-[c(RGDfK)2] that targets integrin alphavbeta3". *Bioconjugate chemistry* 19, Nr. 7 (Juli 2008): 1414–1422.

VII.   Imaging and cancer

VII.1. General presentation of the methods used in Medical Imaging

Medical and biomedical imaging techniques are non-invasive imaging technologies, which do not harm the organism barriers apart from injection of certain tracers. The techniques are either based on electromagnetic rays, like gamma rays, x-rays or on radio-waves, ultrasounds and infrared rays (Figure VII-1).
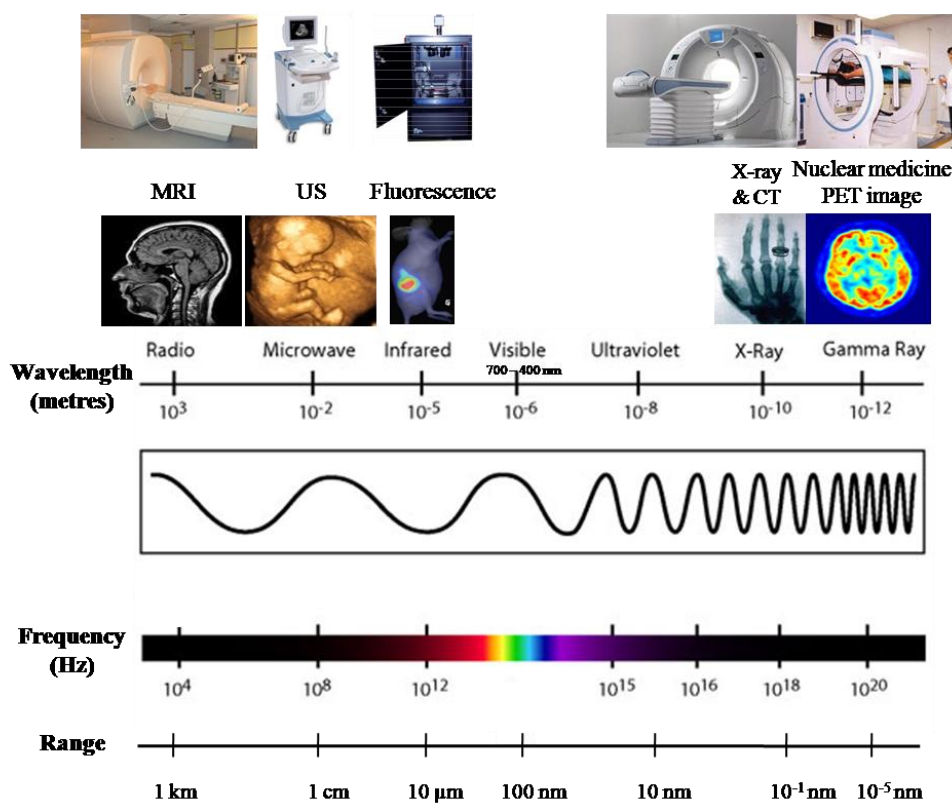
Figure VII-1: Representation of different medical imaging methods.

They imply diverse functional categories for different application:
- Structural imaging, giving information about the organs anatomy, like position, volume or lesions
- Functional imaging, giving information about the organism's function, like physiology and metabolism;

Due to their working principles, they fulfill certain characteristics concerning the spatial resolution and the sensibility.

VII.1.1. X-ray computed tomography (CT)

CT is very commonly used on human patients. Based on the oldest form of medical imaging, X-ray fluorimetry, the technology called X-ray scanner or X-ray computed tomography (CT) has been developed. After reconstruction, the scanner allows the view of slices or three dimensional views.

Biological tissues absorb at different degrees the X-rays, which is used for this technique. It measures the difference of absorption of the X-rays passing through the tissues.

X-ray imaging is an efficient and rapid method for anatomical imaging, with a good spatial resolution between 10 to 100 μm, not limited in depth.

The most used contrast agent is the x-ray absorbing iodine. It is mostly used for vascular imaging. Other contrast agents are for example metallic nanoparticles.

Representing weak contrast properties, strong quantities need to be injected, limiting the development of new targeting contrast agents.

As X-rays are radiation rays certain protective procedures have to be considered. Nevertheless the greatest risk for patients is contrast agent intolerance.

In cancer diagnostic this technique is used in several different cancer types, such as brain cancer, head-and-neck cancer, lung cancer and metastases, detection of enlarged lymph nodes and detection of abnormalities in abdominal organs (liver, spleen, kidney, pancreas, adrenal gland).

VII.1.2. *Magnetic resonance imaging (MRI)*

MRI is another standard method of clinical imaging for soft tissues, developed in the 1980s.

MRI is based on the fact that when a sample, lying within a magnetic field, is subjected to a radio-frequency pulse its protons absorb energy and generate a detectable signal during the relaxation phase. The signal strength is a function of the proton number. The relaxation process can be described by two fundamental rate constants: T1 (longitudinal relaxation) and T2 (transverse relaxation)[158]. The sensitivity of this method is low (mM concentrations) but its spatial resolution extremely good (μm). MRI is very useful for detecting tumors and measuring morphologic parameters. It is often used for diagnostics or staging of brain tumors, primary bone tumors, soft tissue sarcomas and tumors affecting the spinal cord. In some early cancers, such as cervix or bladder cancer, MRI is preferable to CT by better differentiating healthy tissue from the neoplastic one, indicating the growth depth.

Because there is no damaging radiation, multiple imaging sessions can be performed safely, allowing longitudinal follow-up of tumor growth. Finally, contrast agents, influencing either the T1 or T2 relaxation time constants, are developed to allow functional imaging[159,160,161,162].

---

[158] Cassidy, Paul J, and George K Radda. "Molecular Imaging Perspectives." *Journal of the Royal Society, Interface / the Royal Society* 2, no. 3 (June 22, 2005): 133–144.

[159] Louie, Angelique. "Design and Characterization of Magnetic Resonance Imaging Gene Reporters." *Methods in Molecular Medicine* 124 (2006): 401–417.

[160] Barrett, Tristan, Hisataka Kobayashi, Martin Brechbiel, and Peter L Choyke. "Macromolecular MRI Contrast Agents for Imaging Tumor Angiogenesis." *European Journal of Radiology* 60, no. 3 (December 2006): 353–366.

[161] Beaumont, Marine, Benjamin Lemasson, Régine Farion, Christoph Segebarth, Chantal Rémy, and Emmanuel L Barbier. "Characterization of Tumor Angiogenesis in Rat Brain Using Iron-based Vessel Size Index MRI in Combination with Gadolinium-based Dynamic Contrast-enhanced MRI." *Journal of Cerebral Blood Flow and Metabolism: Official Journal of the International Society of Cerebral Blood Flow and Metabolism* 29, no. 10 (October 2009): 1714–1726.

[162] Cuenod, C A, L Fournier, D Balvay, and J-M Guinebretière. "Tumor Angiogenesis: Pathophysiology and Implications for Contrast-enhanced MRI and CT Assessment." *Abdominal Imaging* 31, no. 2 (April 2006): 188–193.

VII.1.3. Ultrasonography (US)

In general, ultrasonography is one of the most popular imaging techniques for clinical use, because of its cheap, fast and easy use. It is a non irradiative method, based on the detection of ultra-sound reflections of the different tissues of the organism, on so of the detection of the smooth tissues. In principal it represents a structural imaging, but allows also functional imaging, like blood flow due to the Doppler echography. Apart from intra-surgical use, it is applied in the fast detection of pathologies, like cancer of the bladder[163]. Its resolution is quiet precise, ranging from 10 to 500 μm (depending on the transducer used), nevertheless decreasing rapidly with depth. Other obstacles are the bones, as the ultra-sound does not pass, the necessary direct contact of the transducer to the patient and experience of the operator.

Concerning image-guided surgery, this accurate, cost-effective and safe in application method, ultrasound is one the most employed methods. It is already used in breast biopsy or for revealing operative liver anatomy. In liver lesions, it guides the surgeon towards the lesion, enabling him to avoid vital structures as blood vessels and bile ducts.

VII.1.4. Nuclear imaging: PET and SPECT

Nuclear imaging is based on the detection of the disintegration of radioactive atoms, which are bound in the molecule structure of so called radio-pharmaceutics, given to the patient before imaging.

The images obtained give rather physiological than anatomical information, which is used due to administration of molecules with known biological behavior. The obtained images are mostly static but dynamic imaging is also possible (e.g. blood perfusion & circulation, glucose metabolism, level of ligand-receptor interaction).

Two technologies, based on the use of radio-elements are currently used: PET and SPECT.

---

[163] Rooks, V, W D Beecken, I Iordanescu, and G A Taylor. "Sonographic Evaluation of Orthotopic Bladder Tumors in Mice Treated with TNP-470, an Angiogenic Inhibitor." *Academic Radiology* 8, no. 2 (February 2001): 121–127.

PET requires the use of radioactive isotopes that emit positrons, such as ^{18}F, ^{15}O, ^{13}N, and ^{11}C with a short half-time life (< 2 hours)[164], while SPECT uses tracers that emit gamma ray or high-energy X-ray photons, such as ^{123}I, ^{125}I, ^{111c}In and ^{99m}Tc.

Positrons move a short distance through tissues, losing energy as they collide with other molecules, and eventually combine with electrons ("annihilation"), producing two high-energy gamma rays or photons traveling outward and in opposite directions.

In SPECT, a single photon per event is directly emitted, and this photon interacts with electrons and nuclei of nearby atoms within the tissue. Unlike positrons, these energetic photons do not "slow down" but are attenuated. Because there is only one photon per event, electronic collimation is not possible, and a physical collimator must be added.

Sensitivities are on the order of 10^{-14}–10^{-15} M for PET and 10^{-14} M for SPECT, and spatial resolution can reach 1.3 mm for PET and is sub-millimetric for SPECT[165].

PET is used to measure increased metabolism via the up-take by metabolically active cells and overexpression of glucose transporters (GLUTs) using Glucose-mimetic FDG (^{18}F-2-fluoro-2-deoxy-D-glucose)[166].

The problems are the limited administration time frame, because of short agents' half-life, and the restriction of these techniques into specialized centers (logistic, practice, finances).

For intra-operative evaluation of tumor localization and margin status in breast cancer surgery, a hand-held PET probe to detect the high-energy gamma rays during surgery has been developed[167,168]. SPECT is used for attempts in intra-operative lymph node-mapping[169].

---

[164] Levin, Craig S. "Primer on Molecular Imaging Technology." *European Journal of Nuclear Medicine and Molecular Imaging* 32 Suppl 2 (December 2005): S325–345.

[165] Chatziioannou, A F, S R Cherry, Y Shao, R W Silverman, K Meadors, T H Farquhar, M Pedarsani, and M E Phelps. "Performance Evaluation of microPET: a High-resolution Lutetium Oxyorthosilicate PET Scanner for Animal Imaging." *Journal of Nuclear Medicine: Official Publication, Society of Nuclear Medicine* 40, no. 7 (July 1999): 1164–1175).

[166] Keereweer, S., J.D.F. Kerrebijn, P.B.A.A. van Driel, B. Xie, E.L. Kaijzel, T.J.A. Snoeks, I. Que, et al. "Optical Image-guided Surgery - Where Do We Stand?" *Mol Imaging Biol.* 13, 2011. 199-207.

[167] Keereweer, S., J.D.F. Kerrebijn, P.B.A.A. van Driel, B. Xie, E.L. Kaijzel, T.J.A. Snoeks, I. Que, et al. "Optical Image-guided Surgery - Where Do We Stand?" *Mol Imaging Biol.* 13, 2011. 199-207.

[168] Strong, V.E., J. Humm, P. Russo, et al. "A Novel Method to Localize Antibody-targeted Cancer Deposits Intraoperatively Using Handheld PET Beta and Gamma Probes." *Surg Endosc.* 22, 2008. 386-391.

[169] Klar, M, M Bossart, E Stickeler, I Brink, M Orlowska-Volk, und D Denschlag. „Sentinel lymph node detection in patients with vulvar carcinoma; Feasibility of intra-operative mapping with technetium-99m-labeled nanocolloid". *European journal of surgical oncology: the journal of the European Society of Surgical Oncology and the British Association of Surgical Oncology* 37, Nr. 9 (September 2011): 818–823.

VII.2. *Optical Imaging*

Fluorescence Reflectance Imaging (FRI) is a very simple system using signal reflection, which allows two dimensional picture taking (Figure VII-2).
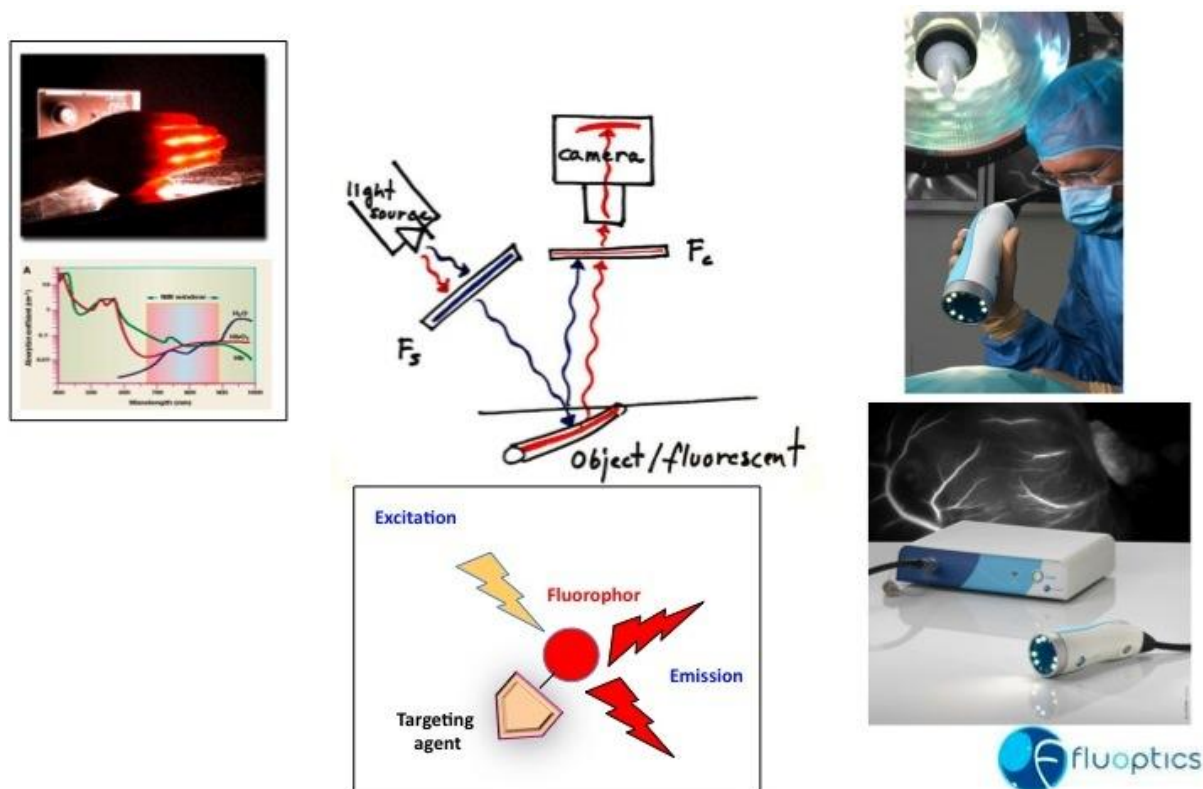
Figure VII-2: Principle of 2D-FRI and the Fluobeam™.

The imaging system consists of a NIR lamp (LED or laser) and a CCD camera, equipped with several filters in order to separate the scattered light and to eliminate the photons directly reflected by the object. The acquisition time is in the range of milliseconds to seconds. Several imaging systems based on 2D-FRI are now commercially available, such as the Photodynamic Eye (PDE; Hamamatsu Photonics, Hamamatsu City, Japan) and the Fluorescence-assisted Resection and Exploration (FLARE™) system[170] from the Fragioni laboratory (Brookline, MA, USA). Two smaller systems are the Mini-FLARE™, also from the Frangioni laboratory[171], and the Fluobeam™ from Fluoptics (Grenoble, France) (Figure VII-3).The group of Ntziachristos is also engaged in the development of NIR guided

---

[170] De Grand, A.M., and JV Frangioni. "An Operational Near-infrared Fluorescence Imaging System Proyotype for Large Animal Surgery." *Technol Cancer Res Treat*. 2, 2003.553-562.

[171] Stockdale, A., R. Oketokoun, S. Gioux, and JV Frangioni. "Mini-FLARE: a Compact and Ergonomic Dual-channel Near-infrared Fluorescence Image-guided Surgery System." *Abstract*, 2010

surgery[172,173,174]. Others are the ArteMIS™ handheld system, developed by O2view (Marken, The Netherlands), as well as the "da Vinci® Si" System (Intuitive Surgical, Sunnyvale, CA) and the SPY Intraoperative Imaging System (Novadaq Technologies, Mississauga, Ontario, Canada).
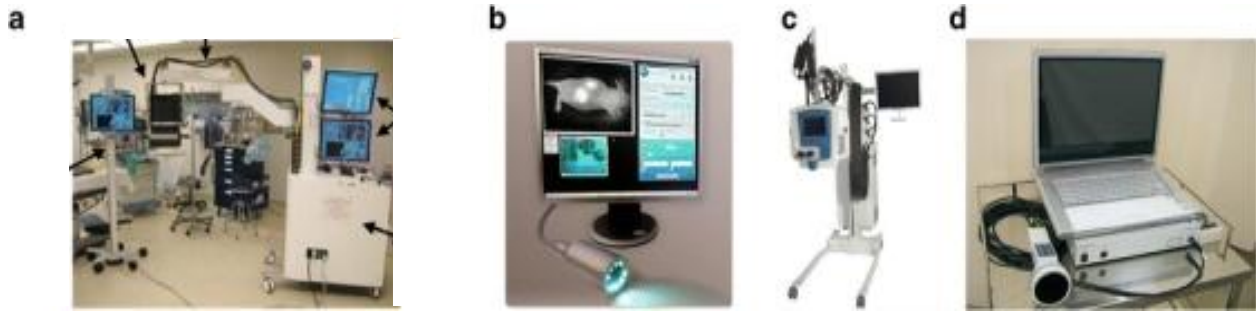
Figure VII-3: Near-infrared intra-operative camera systems.
a)   **FLARE™ camera system. b) Artist impression of Fluobeam™. c) ArteMIS™ camera system. d) The Photodynamic Eye.**
-Keereweer et al. 2011-

In the NIR optical window, tissue penetration is around 1 to 2 cm (compared to 1 to 2 mm in the visible light), showing a good sensitivity around 10^{-12} M and a spatial resolution of 2 mm. The information obtained is semi-quantitative.

Other optical-based imaging systems adapted to *in vivo* imaging are actively being developed. For example, NIR Spectroscopy can be used to detect and localize cancer[175] based on the intrinsic and differential absorption of photons of different NIR wavelengths by hemoglobin, deoxy-hemoglobin, water and lipids. Other techniques, like diffuse optical tomography[176]or time-domain optical mammography (Softscan®, Advanced Research Technologies[177]), are used to measure photon migration through the tissues in order to observe variations in the functional and structural NIR properties (e.g., scattering, oxy-, and

---

[172] Themelis, George, Jung Sun Yoo, Kwang-Sup Soh, Ralf Schulz, und Vasilis Ntziachristos. „Real-time intraoperative fluorescence imaging system using light-absorption correction". *Journal of Biomedical Optics* 14, Nr. 6 (November 1, 2009): 064012–064012.

[173] Themelis, George, Niels J Harlaar, Wendy Kelder, Joost Bart, Athanasios Sarantopoulos, Gooitzen M van Dam, und Vasilis Ntziachristos. „Enhancing surgical vision by using real-time imaging of αvβ3-integrin targeted near-infrared fluorescent agent". *Annals of surgical oncology* 18, Nr. 12 (November 2011): 3506–3513.

[174] Crane, Lucia M.A., George Themelis, K. Tim Buddingh, Niels J. Harlaar, Rick G. Pleijhuis, Athanasios Sarantopoulos, Ate G.J. van der Zee, Vasilis Ntziachristos, und Gooitzen M. van Dam. „Multispectral Real-time Fluorescence Imaging for Intraoperative Detection of the Sentinel Lymph Node in Gynecologic Oncology". *Journal of Visualized Experiments : JoVE*, Nr. 44 (Oktober 20, 2010). http://www.ncbi.nlm.nih.gov/pmc/articles/PMC3185642/.

[175] Nioka, S, and B Chance. "NIR Spectroscopic Detection of Breast Cancer." *Technol Cancer Res Treat*. 4, 2005.497-512

[176] Choe, R., S.D. Konecky, A. Corlu et al. "Differentiation of Benign and Malignant Breast Tumors by in Vivo Three-dimensional Parallel-plate Diffuse Optical Tomography." *J Biomed Opt*. 14, 024020

[177] Keereweer, S., et al. "NIR Spectroscopic Detection of Breast Cancer". Montreal, Canada, 2011

deoxy-hemoglobin concentrations), enabling differentiation between benign and malignant tumors[178]. Nevertheless, these techniques are not yet suitable for intra-operative use.

We used the Fluobeam™ (Fluoptics, Grenoble) in the current study, which I will mainly present here.

It is a portable 2D-FRI device for real-time NIR-imaging (Figure VII-4), able to work under NIR-filtered ambient light conditions[179]. It is composed of a control unit, with a laser source emitting at 785 nm and a power supply for light-emitting diodes (LEDs), next to an optical head, with a highly sensitive charge-coupled device camera and white LEDs for the illumination of the field of view[180,181]. It works with all NIR-probes and is on the market with a cancer targeting probe called AngioStamp™, the commercial name of RAFT-RGD, targeting integrin $\alpha_v\beta_3$.

[178] Intes X (2005) Time-domain optical mammography SoftScan: initial results. Acad Radiol 12: 934-947.

[179] Keramidas, M. *et al.* Intraoperative near-infrared image-guided surgery for peritoneal carcinomatosis in a preclinical experimental model. *Br J Surg* **97**, 737–743 (2010).

[180] E. Mery, E. Jouve, S. Guillermet, M. Bourgognon, M. Castells, M. Golzio, P. Rizo, J.P. Delord, D. Querleu, B. Couderc, Intraoperative fluorescence imaging of peritoneal dissemination of ovarian carcinomas. A preclinical study. Gynecologic oncology 122 (2011) 155-162.

[181] D.A. Heuveling, G.W. Visser, M. de Groot, J.F. de Boer, M. Baclayon, W.H. Roos, G.J. Wuite, C.R. Leemans, R. de Bree, G.A. van Dongen, Nanocolloidal albumin-IRDye 800CW: a near-infrared fluorescent tracer with optimal retention in the sentinel lymph node. European journal of nuclear medicine and molecular imaging 39 (2012) 1161-1168.
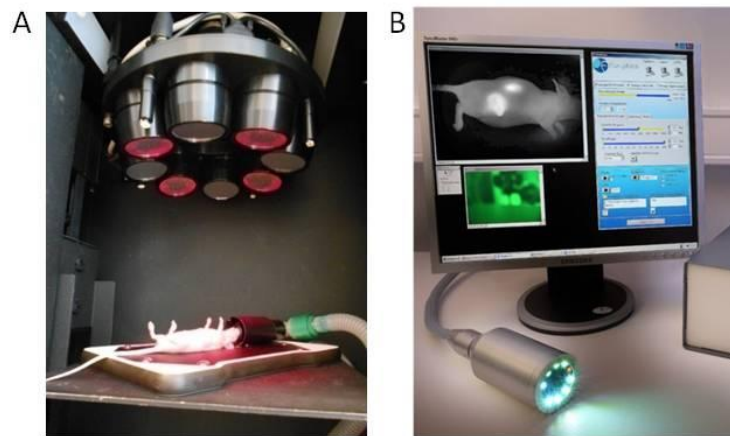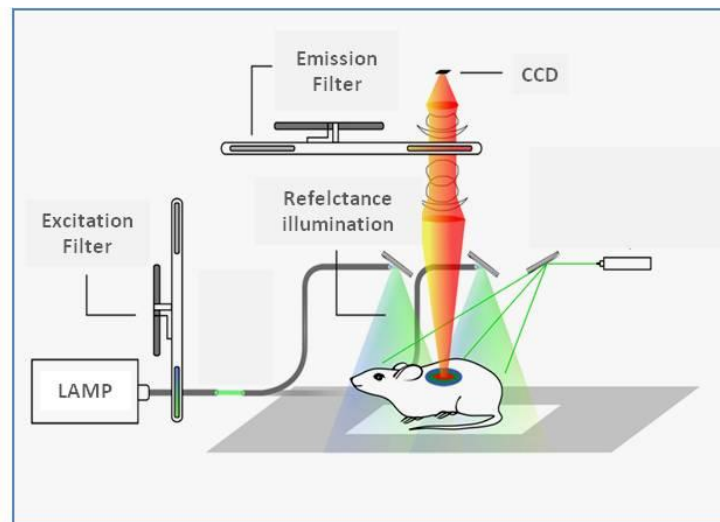
Figure VII-4: 2D-Fluoresence-reflectance imaging systems.
The injected fluorescent tracer is excited by a given wavelength. The emitted signal is collected by a CCD camera, equipped with filters for separation of the scattered excitation rays emitted by the fluorescent tracer.
A)   2D imaging system; B) Intra-operative imaging device (Fluobeam™, Fluoptics)
-Modified after Dufort, S. « Vectorisation de biomolécules pour l'imagerie et la thérapie des cancers », Thesis, 2010-

VIII.   Imaging and surgery

Cancer therapy depends on the nature, location and stage of the tumor.

Tumors are generally classified as either benign or malignant. To differentiate them, several characteristics have been evoked as listed in Table VIII-1.

In clinics, primary tumors are defined into T_0 to T_4, which is also used in staging of cancer:

T_0 – means a clinically undetectable tumor

T_1 – refers to a small, strictly circumscribed tumor, which does not reach the organ limits;

T_2 – in this case the tumor reaches the organ limits;

T_3 – the tumor is fixed to the neighboring organs;

T_4 – refers to a tumor that has invaded the neighboring organs.

CHARACTERISTICS/TUMORS	BENIGN	MALIGNANT
Growth type	Expansive	Infiltrating
Growth speed	Slow (in general)	Rapid (in general)
Stabilization	Frequent	Exceptional
Structure	Typical	Atypical (dedifferentiation – anaplasia)
Mitoses	Rare + Typical	Numerous + Atypical
Evolution	Local	Local + General
Metastasizing	No	Yes
Local consequences	Variable (compressions, …)	Severe (infiltration, destruction, necrosis, …)
General consequences	None (exceptions: secretory tumors or at particular sites)	Constant + severe (in the generalization phase)
Spontaneous evolution	Usually favorable	Always fatal
Evolution after removal	No recurrences	Common recurrences

Table VIII-1: Characteristics of benign and malignant tumors.
-Baba et al., 2007-

Surgical resection, if feasible, produces a survival benefit for patients with disease limited to organ-specific sites, as these patients are able to undergo surgical resection at the time of diagnosis or following conversion therapy with the appropriate integration of chemotherapy.

Unfortunately the long-term survival is directly linked to the exhaustive tumor removal with microscopic examination of margins showing no tumor cells (definition of « R0 » resection).

Pre-operative contrast CT and MRI as well as intra-operative ultrasonography are currently used for diagnosis and guidance of resection. The translation of these images to the operation field remains a major difficulty for the oncological surgeon. Visual appearance and palpation is the only way to discriminate between tumor and normal tissue and consequently determine an adequate tumor-free margin during surgery. Intra-operative ultrasounds can reveal not previously detected lesions, and thereby help with resection boundaries[182].

VIII.1. Surgical approaches in cancer

Surgery is the oldest form of cancer treatment but is also used in diagnosis (staging) or cancer prevention (*e.g.* colon cancer). Most cancer patients will have some type of surgery as it often offers the greatest chance for cure, especially when metastasis did not yet occur. Up to now operation techniques have evolved in order to save as much healthy and functional tissue as possible. The most common types of surgery reach from preventive, diagnostic and staging to curative or palliative surgery employing different kinds of techniques. Some of the techniques used, apart from the standard "scalpel" one, are Laser surgery, cryosurgery, electrosurgery, Mohs micrographic surgery, minimal invasive surgery and others (Table VIII-2), like cryoabaltion and radiofrequency ablation (RFA).

Surgery technique	Method / Instrument
Laser surgery	Photoablation; photocoagulation; less invasive surgery; vaporization of cancer tissue; alternative scalpel
Cryosurgery	Liquid nitrogen spray or LN-cooled object
Electrosurgery	High-frequency electrical current
Mohs micrographic surgery (microscopically controlled surgery)	
Minimal invasive / endoscopic surgery	Laparoscopy/Thorascopy
Others	High intensity focused ultrasound; microwaves/radio waves (radiofrequency ablation/ RFA); magnets; Gamma Knife & CyberKnife

Table VIII-2: Surgery Techniques.

-After information of the American Cancer Society, 2008 & 13 mastery of surgery 2007-

---

[182] Jarnagin, W R, A M Bach, C B Winston, L E Hann, N Heffernan, T Loumeau, R P DeMatteo, Y Fong, und L H Blumgart. „What is the yield of intraoperative ultrasonography during partial hepatectomy for malignant disease?" *Journal of the American College of Surgeons* 192, Nr. 5 (Mai 2001): 577–583.

Surgical resection represents the standard therapy in solid tumors like bone cancer (osteosarcoma, chondrosarcoma and ESFTs (Vertebral Ewing's Sarcoma Family of Tumors))[183], glioblastoma or other brain tumors[184], papillary thyroid carcinoma[185,186], squamous cell carcinomas or different sarcomas and represents common cancer treatment for hepatic cancer[187], breast cancer, prostate[188] cancer, colon cancer[189,190,191] and is still the most effective treatment of most tumors, e.g. for localized gastric lymphoma, for early, superficial disease within the oral cavity, for stage I and II oral cavity cancer, and as routine in the control of lymphatic disease in neck cancer[192]. Concerning microinvasive surgery, carcinomas should be excised with a security margin of at least 1- to 2-cm on the peripheral and deep aspects, whereas difficulties can be observed to discern margins. In some cases, a margin up to 4 to 6 cm is needed (*e.g.* gastric carcinoma)[193].

Sometimes a complete organ resection (-ectomy) is the only treatment, like for example thyroidectomy for all patients with a thyroid carcinoma, except in cases of anaplastic cancer[194], or complete operative resection in gastric adenocarcinoma, which remains the only potential curative modality[195].

Any local therapy for malignant hepatic tumors with curative intend, be it surgical resection, RFA (radiofrequency ablation), or some other tumor-ablative technique, has a significant proportion of patients subsequently developing clinically detectable hepatic or extrahepatic recurrence from coexistent micrometastatic disease. A big problem is the fact that a high percentage of lesions are undetected (about 28% in the case of hepacellular cancer)

---

[183] American Cancer Society, 2012

[184] Lu-Emerson, Christine, und April F Eichler. „Brain metastases". *Continuum (Minneapolis, Minn.)* 18, Nr. 2 (April 2012): 295–311.

[185] Abboud, Bassam, und Jenny Tannoury. „Surgical treatment of papillary thyroid carcinoma". *Le Journal médical libanais. The Lebanese medical journal* 59, Nr. 4 (Dezember 2011): 206–212.

[186] Bilimoria, Karl Y., David J. Bentrem, Clifford Y. Ko, Andrew K. Stewart, David P. Winchester, Mark S. Talamonti, und Cord Sturgeon. „Extent of Surgery Affects Survival for Papillary Thyroid Cancer". *Annals of Surgery* 246, Nr. 3 (September 2007): 375–384.

[187] Cirocchi, Roberto, Stefano Trastulli, Carlo Boselli, Alessandro Montedori, Davide Cavaliere, Amilcare Parisi, Giuseppe Noya, und Iosief Abraha. „Radiofrequency ablation in the treatment of liver metastases from colorectal cancer". *Cochrane database of systematic reviews (Online)* 6 (2012): CD006317.

[188] „Longer Survival Rates After Surgery For Prostate Cancer Patients". *Medical News Today*, o. J. http://www.medicalnewstoday.com/articles/84936.php.)

[189] American Cancer Society, 2012

[190] American Cancer Society, Intramural Research 2012

[191] „Treatment of non-localised, non-metastatic rectal cancer". *Prescrire international* 21, Nr. 128 (June 2012): 158–162.

[192] Fleming, et al. "Surgery in the Management of Gastric Lymphoma." *Cancer Vol 49*, March 1982.*;* Caroll, W.R. "25 - Surgery for Cancer of the Oral Cavity." In *Mastery of Surgery*, 1:305–318. 5th ed. Boston, Massachusetts: Fischer, Josef E., 2007.

[193] Brennan, M.F. "80 - Total Gastrectomy for Carcinoma." In *Mastery of Surgery*, 1:916–928. 5th ed. Boston, Massachusetts: Fischer, Josef E., 2007.

[194] Wells Jr., S.A. "35 - Total Thyroidectomy, Lymph Node Dissection for Cancer." In *Mastery of Surgery*, 1:411–433. 5th ed. Boston, Massachusetts: Fischer, Josef E., 2007.

[195] Brennan, M.F. "80 - Total Gastrectomy for Carcinoma." In *Mastery of Surgery*, 1:916–928. 5th ed. Boston, Massachusetts: Fischer, Josef E., 2007.

and in multicentric cancer, like hepatocellular carcinoma, a singular isolated attempt to eradicate it in closed fashion is ineffective[196].

Surgical tumor accessibility restrictions are dependent on the proximity to vital structures, the stage - in regards to metastases- and the individual health status of the patient - in regards to the general risks of surgery and anesthesia.

Eventually, the principle of tumor surgery is a complete fast and margin-negative resection, without unnecessary harm to vital and/or healthy tissues or structures and reduced risks of anesthesia or ischemia. Constrains are the tumor accessibility and visibility. Tumor margin delineation is crucial to avoid recurrence. Recurrences and patient's recovery are also influenced by missed metastases and drained lymph nodes, unnecessary damage to healthy tissue out of precaution or the iatrogenic spread of malignant cells.

In regards to all the restraints and in spite of all technical improvements, surgery still faces these challenges. This explains the interest in the development of (intra-operative) image guided surgery techniques.

As already mentioned current imaging modalities are CT and MRI (*e.g.* in neurosurgery[197]). CT, SPECT and US (and endoscopy) are used during surgery, for re-evaluation of the situation or as control during surgery in minimal invasive interventions or the placement of electrodes or other material (see Ablation techniques).

All these modalities have certain advantages and disadvantages, as seen in Table VIII-3.

Generally, there are limits concerning sensitivity, resolution, exposure to radioactivity and room needs. The facilities require substantial capital investment, safety precautions and the interpretation of the images can be challenging, requiring experience and understanding of artifacts that are common in the intra-operative setting[197].

Another problem is that in case of IRM, CT or SPECT, the surgery needs a break for image acquisition, whereas US needs direct tissue contact and is not feasible in open surgery.

Therefore optical imaging in the NIR window represents an easy-to-use real-time technique, which does not interfere into the visual appearance of the surgical field, and

---

[196] Curley, S.A., and J.S. Zager. "Cancer Radiofrequency Ablation and Other Tissue Ablative Techniques - Chapter 13." In *Mastery of Surgery*, 1:181–185. 5th ed. Boston, Massachusetts: Fischer, Josef E., 2007.

[197] Abernethy, L J, S Avula, G M Hughes, E J Wright, und C L Mallucci. „Intra-operative 3-T MRI for paediatric brain tumours: challenges and perspectives". *Pediatric radiology* 42, Nr. 2 (February 2012): 147–157.

without exposure to radioactivity, enabling a high spatial and temporal resolution. Moreover, it is possible to use targeting tracers.

Modality	Advantages	Disadvantages	Common Contrast agents/Readout	Example Clinical Applications
CT	• Unlimited depth penetration • High spatial resolution • Whole-body imaging possible • Short acquisition time (minutes) • Moderately expensive • Anatomical imaging	• Irradiation exposure • Poor soft tissue contrast • Probably not used for molecular imaging – currently only anatomical and functional imaging	• barium • iodine • krypton • xenon	• Tumor perfusion
PET	• Unlimited depth penetration • Whole-body imaging possible • Quantitative molecular imaging • Can be combined with CT or MRI for anatomical information	• Irradiation exposure • Expensive • Low spatial resolution (1–2 mm; 4–8 mm3) • Long acquisition times (minutes to hour)	• ^{11}C • ^{18}F • ^{64}Cu • ^{68}Ga	• ^{18}F-FDG-PET for cancer staging • Diagnosis of various diseases
SPECT	• Unlimited depth penetration • Whole-body imaging possible • Quantitative molecular imaging • Theranostic: Can combine imaging & radiotherapy • Can be combined with CT for anatomical information	• Irradiation exposure • Low spatial resolution (0.3–1 mm; 12–15mm3) • Long acquisition time	• ^{99m}Tc • ^{123}I • ^{111}In • ^{177}Lu	• Diagnosis of various diseases • Radiotherapy for NHL: ^{90}Y-Bexxar or ^{131}I-Zevalin • Radiotherapy of thyroid carcinoma with ^{131}I-iodide

MRI	• Unlimited depth penetration • Whole-body imaging possible • No ionizing irradiation • Excellent soft tissue contrast • High spatial resolution	• Expensive • Long acquisition time (min-hours) • Limited sensitivity for detection of molecular contrast agents	• Gadolinium (Gd^{3+}) • iron oxide particles (SPIO, USPIO) • manganese oxide • ^{19}F	• SPIOs for detection of lymph node metastases of prostate cancer • Characterization of focal hepatic lesions • Perfusion imaging of the heart
MRS	• Whole-body imaging possible • No ionizing irradiation	• Expensive • Long acquisition time (min - hours) • Low sensitivity	• choline • creatine • lactate • lipids • polyamines • N-acetyl-aspartate	• Metabolite levels in brain tumors • Treatment monitoring of Alzheimers
US	• No ionizing irradiation • Real-time imaging/short acquisition time (min) • High spatial resolution • Can be applied externally or internally (endoscopy) • Inexpensive • Highly sensitive	• Wholebody imaging not possible • Contrast agents currently limited to vasculature • Operator dependency	• Contrast Microbubbles	• Characterization of focal liver lesions • Echocardiography • Tumor perfusion of cancer
Optical	• No ionizing irradiation • Real-time imaging/short acquisition time (sec-min) • Relatively high spatial resolution • Can be applied externally or internally (endoscopy) • Inexpensive • Highly quantitative & sensitive • Multiplexing	• Limited depth penetration ($\leq$ 1 cm) • Wholebody imaging not possible	• Fluorescent molecules & dyes • Light absorbing nanoparticles	• OCT imaging of artherosclerosis • OCT imaging for colonoscopy screening • Raman imaging of skin cancer

Table VIII-3: Advantages and disadvantages of medical imaging modalities used with molecularly targeted or non-targeted contrast agents in a clinical setting.

-Adapted from Pysz et al. Clin Radiol. Clin Radiol. 2010 July; 65(7): 500–516.-
MRS = magnetic resonance spectroscopy

IX. NIR Fluorescence imaging for intra-operative guidance

One first attempt of translating optical techniques into clinic is the sentinel lymph node (SNL) mapping.

Being the first lymph node draining the lymphatic fluid coming from the tumor, the sentinel lymph node represents the first place of metastasis creation[198,199](Figure IX-1). It has been shown that detection of SNL using intraoperative fluorescence imaging in patients with cervical and vulvar cancer using indocyanin green (ICG) is feasible and results in a high SBR (around 8)[200]. SNL mapping using ICG has also successfully been used in breast cancer melanoma, and head and neck cancer[201,202,203] (Figure IX-2).
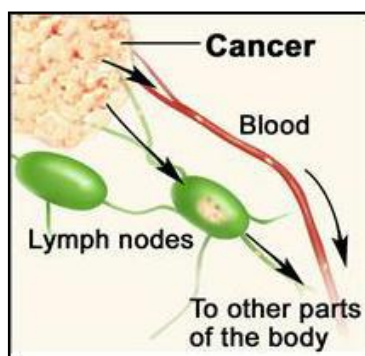
Figure IX-1: Metastatic cancer cells invade lymph vessels and blood vessels near a tumor and migrate to other parts of the body.
-National Cancer Institute 2012-

---

[198] Schaafsma, BE, JS Mieog, M. Hutteman, JR van der Vorst, PJ Kuppen, CW Löwik, JV Frangioni, CJ van de Velde, and A. L. Vahrmeijer. "The Clinical Use of Indocyanine Green as a Near-infrared Fluorescent Contrast Agent for Image-guided Oncologic Surgery." *J Surg Oncol.* 104(3), September 2011.

[199] Schaafsma, Boudewijn E, Joost R van der Vorst, Katja N Gaarenstroom, Alexander A W Peters, Floris P R Verbeek, Cornelis D de Kroon, J Baptist M Z Trimbos, u. a. „Randomized comparison of near-infrared fluorescence lymphatic tracers for sentinel lymph node mapping of cervical cancer". *Gynecologic oncology* (July 10, 2012).

[200] Crane, Lucia M.A., George Themelis, K. Tim Buddingh, Niels J. Harlaar, Rick G. Pleijhuis, Athanasios Sarantopoulos, Ate G.J. van der Zee, Vasilis Ntziachristos, und Gooitzen M. van Dam. „Multispectral Real-time Fluorescence Imaging for Intraoperative Detection of the Sentinel Lymph Node in Gynecologic Oncology". *Journal of Visualized Experiments : JoVE*, Nr. 44 (Oktober 20, 2010). http://www.ncbi.nlm.nih.gov/pmc/articles/PMC3185642/.

[201] Mieog, J. Sven D., Susan L. Troyan, Merlijn Hutteman, Kevin J. Donohoe, Joost R. van der Vorst, Alan Stockdale, Gerrit-Jan Liefers, u. a. „Toward Optimization of Imaging System and Lymphatic Tracer for Near-Infrared Fluorescent Sentinel Lymph Node Mapping in Breast Cancer". *Ann Surg Oncol.* 18, 2011.

[202] van der Vorst, Joost R., Boudewijn E. Schaafsma, Floris P.R. Verbeek, Stijn Keereweer, Jeroen C. Jansen, Lilly-Ann van der Velden, Antonius P.M. Langeveld, u. a. „Near-infrared fluorescence sentinel lymph node mapping of the oral cavity in head and neck cancer patients". *Oral Oncology* (o. J.). http://www.sciencedirect.com/science/article/pii/S136883751200245X.

[203] Troyan, Susan L, Vida Kianzad, Summer L Gibbs-Strauss, Sylvain Gioux, Aya Matsui, Rafiou Oketokoun, Long Ngo, Ali Khamene, Fred Azar, und John V Frangioni. „The FLARE intraoperative near-infrared fluorescence imaging system: a first-in-human clinical trial in breast cancer sentinel lymph node mapping". Annals of surgical oncology 16, Nr. 10 (Oktober 2009): 2943–2952.

Figure IX-2: NIR fluorescence labeling of lymphatic channels and SNL by ICG.

-Schaafsma, Boudewijn E., J.Sven D. Mieog, Merlijn Hutteman, Joost R. van der Vorst, Peter J.K. Kuppen, Clemens W.G.M. Löwik, John V. Frangioni, Cornelis J.H. van de Velde, und Alexander L. Vahrmeijer. „The clinical use of indocyanine green as a near-infrared fluorescent contrast agent for image-guided oncologic surgery". *Journal of surgical oncology* 104, Nr. 3 (September 1, 2011): 323–332.-

Another example of image- guided surgery, not comprising cancer, is the intra-operative fluorescent cholangiography, using ICG for robotic single site cholecystectomy[204], microscope integrated ICG videoangiography during microneurosurgical treatment of intracranial aneurysms or cerebrovascular surgery[205].

The previously mentioned SPY system was used in ICG guided open partial nephrectomy by Tobis et al.[206], demonstrating the safety of this kind of surgery and the improved discrimination of renal cortical tumors from normal tissue. At the same time it highlighted renal vasculature, which could enhance nephron sparing and decrease blood loss.

Also in determination of flap perfusion in reconstructive breast surgery after mastectomy intra-operative near-infrared fluorescence imaging for the evaluation of

---

[204] Buchs, Nicolas C, Monika E Hagen, François Pugin, Francesco Volonte, Pascal Bucher, Eduardo Schiffer, und Philippe Morel. „Intra-operative fluorescent cholangiography using indocyanin green during robotic single site cholecystectomy". *The international journal of medical robotics + computer assisted surgery: MRCAS* (Mai 31, 2012).

[205] Sevick-Muraca, E M. „Translation of near-infrared fluorescence imaging technologies: emerging clinical applications". *Annual review of medicine* 63 (2012): 217–231.

[206] Tobis, Scott, Joy K Knopf, Christopher R Silvers, Jonah Marshall, Allison Cardin, Ronald W Wood, Jay E Reeder, u. a. „Near infrared fluorescence imaging after intravenous indocyanine green: initial clinical experience with open partial nephrectomy for renal cortical tumors". *Urology* 79, Nr. 4 (April 2012): 958–964.

perforator location and flap perfusion was helpful[207]. Verbeek et al. tried the ICG-NIR fluorescence imaging for hepatic colorectal metastases with promising results[208].

Apart from ICG, Dam et al. lighted up ovarian cancer cells during surgery[209] in a small study of 10 patients by targeting the folate receptor-α. This technique allowed surgeons to spot a tumor 30 times smaller than the smallest they could detect using standard techniques (Figure IX-3).

Nevertheless they used fluorescein isothiocyanate (FITC) as dye. This functional fluorochrome fluoresces in the green light spectrum and thus does not fulfill the advantages of NIR dyes. Also the use of ALA-guided microsurgical resections in glioblastomas (5-aminolevulinic acid)[210,211] is a method lacking the described benefits of NIR fluorescence in real-time imaging for surgery.

Other studies showing the feasibility of NIR fluorescence guided surgery with specific tracers in cancer surgery or for the intra-surgical identification of vessels and tubes (like the ureter) identification but are still in preclinics, using rodent or swine models[212,213].
For example Keereweer et al. showed the interest of optical guided surgery of oral cancer and cervical lymh node metastases. Using the EGF receptor targeting NIR probe CW800 EGF and the glucose transporter system targeting NIR probe CW800 2-DG, they demonstrated efficient targeting of orthotopic cancer in mouse models[214]. A similar study was done in the laboratory of Ntziachristos at the TUM (Technische Universität München). His team showed the ability of an $\alpha_v\beta_3$ integrin-targeting molecule (IntegriSense-680) to detect breast-tumor xenografts in mice and to easier identify tumor negative margins with high specificity performing real-time

---

[207] Lee, Bernard T, Merlijn Hutteman, Sylvain Gioux, Alan Stockdale, Samuel J Lin, Long H Ngo, und John V Frangioni. „The FLARE intraoperative near-infrared fluorescence imaging system: a first-in-human clinical trial in perforator flap breast reconstruction". *Plastic and reconstructive surgery* 126, Nr. 5 (November 2010): 1472–1481.

[208] Verbeek, F. et al., WMIC, 2012: SS 168

[209] Dam, Gooitzen M. van, George Themelis, Lucia M. A. Crane, Niels J. Harlaar, Rick G. Pleijhuis, Wendy Kelder, Athanasios Sarantopoulos, et al. "Intraoperative Tumor-specific Fluorescence Imaging in Ovarian Cancer by Folate Receptor-α Targeting: First In-human Results". *Nature Medicine* 17, Nr. 10 (2011): 1315–1319.

[210] Cortnum, Søren, und René Johannes Laursen. „Fluorescence-guided resection of gliomas". *Danish medical journal* 59, Nr. 8 (August 2012): A4460.

[211] Gautschi, O.P., K. van Leyen, D. Cadosch, G. Hildebrandt, und J.-Y. Fournier. „Fluorescence Guided Resection ofMalignant Brain Tumors – Breakthrough in the Surgery of Brain Tumors". *Praxis* 98 (o. J.): 643–647.

[212] De Grand, A M, und J V Frangioni. „An operational near-infrared fluorescence imaging system prototype for large animal surgery". *Technology in cancer research & treatment* 2, Nr. 6 (December 2003): 553–562.

[213] Matsui, Aya, Eiichi Tanaka, Hak Soo Choi, Vida Kianzad, Sylvain Gioux, Stephen J Lomnes, und John V Frangioni. „Real-time, near-infrared, fluorescence-guided identification of the ureters using methylene blue". *Surgery* 148, Nr. 1 (Juli 2010): 78–86.

[214] Keereweer, Stijn, Jeroen D. F. Kerrebijn, Isabel M. Mol, J. Sven D. Mieog, Pieter B. A. A. Van Driel, Robert J. Baatenburg de Jong, Alexander L. Vahrmeijer, und Clemens W. G. M. Löwik. „Optical Imaging of Oral Squamous Cell Carcinoma and Cervical Lymph Node Metastasis". *Head & Neck* 34, Nr. 7 (2012): 1002–1008.

NIR imaging during surgery compared to visual inspection[215]. Similar results were obtained by our team demonstrating the improved resection of micrometastases in peritoneal carcinomatosis in mice due to NIR-guided real-time vision[216].
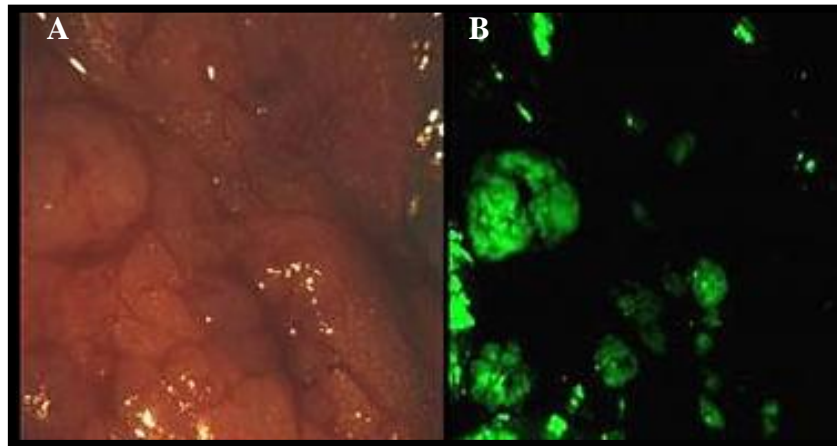
Figure IX-3: Tumor-specific fluorescence intra-operative imaging in ovarian cancer.
View of localized region in peritoneal cavity of an ovarian cancer patient as seen with A) the naked eye or B) with the aid of a tumor-targeted fluorescence dye.
-Dam, Gooitzen M. van, George Themelis, Lucia M. A. Crane, Niels J. Harlaar, Rick G. Pleijhuis, Wendy Kelder, Athanasios Sarantopoulos, et al. "Intraoperative Tumor-specific Fluorescence Imaging in Ovarian Cancer by Folate Receptor-α Targeting: First In-human Results". *Nature Medicine* 17, Nr. 10 (2011): 1315–1319.-

To conclude, up to now no clinically approved targeting NIR fluorescence contrast agents with corresponding imaging devices are available for clinical imaging of surgery.

As described, ICG is the only injectable agent with NIR properties. But ICG has comparatively poor fluorescent properties compared to emerging dyes, showing a low QY. In a complex with human serum albumin (HAS), it reaches a 3-fold higher QY, which improves SLN retention*[217]*. Nevertheless it stays unspecific and therefore limited to perfusion and non specific accumulation. Consequently, translation of the specific NIR fluorescence method into clinics is a combinational, investigational product of imaging device and imaging agent.

As shown, only few clinical pilot studies and several pre-clinical approaches in NIR-guided surgery took place with encouraging results.

---

[215] Themelis, George, Niels J Harlaar, Wendy Kelder, Joost Bart, Athanasios Sarantopoulos, Gooitzen M van Dam, und Vasilis Ntziachristos. „Enhancing surgical vision by using real-time imaging of αvβ3-integrin targeted near-infrared fluorescent agent". *Annals of surgical oncology* 18, Nr. 12 (November 2011): 3506–3513.

[216] Keramidas, M, V Josserand, C A Righini, C Wenk, C Faure, und J L Coll. „Intraoperative near-infrared image-guided surgery for peritoneal carcinomatosis in a preclinical experimental model". *The British journal of surgery* 97, Nr. 5 (Mai 2010): 737–743.

[217] Tanaka, Eiichi, Hak Soo Choi, Hirofumi Fujii, Moungi G Bawendi, und John V Frangioni. „Image-guided oncologic surgery using invisible light: completed pre-clinical development for sentinel lymph node mapping". *Annals of surgical oncology* 13, Nr. 12 (December 2006): 1671–1681.

This approach could improve and assure a complete and more secure tumor resection. Ergo, there is interest in pushing NIR-guided intra-operative surgery techniques further into clinics and evaluate them under clinical conditions in different cancer types.

One possibility to enhance clinical translation, concerning the feasibility and usefulness of targeted intra-operative NIR imaging, would be the implication of natural occurring tumors in domestic animals like cats and dogs. This implicates real disease circumstances and surgical conditions. Additionally, a possible direct analogy between human and animal exists with less legal constraints.

„Alle Ding' sind Gift und nichts ohn' Gift; allein die Dosis macht, dass ein Ding kein Gift ist."

(Omnia sunt venena, nihil est sine veneno. Sola dosis facit venenum.)

Paracelsus (1493-1541)

[Everything is a poison, nothing is without poison; the dose alone makes that it is not a poison.]

RESULTS AND CONCLUSIONS

I. OPTICAL GUIDED SURGERY OF FELINE FIBROSARCOMA

Introduction

The goal of any tumor resection is to obtain complete removal of the malignant lesion with adequate margins within surrounding healthy tissues taking into account both tumor control and functional reconstruction. To date, no intra-operative method is available and reliable enough to help the surgeon delineate precisely tumor extension in the adjacent normal tissues. Thus, surgeons rely on pre-operative imaging techniques to delineate tumor margins which may often be blurred by peritumoral edema or inflammation within surrounding normal tissues. Similarly, pre- and intra-operative detection of metastasis, especially lung metastases, is limited by the size of the tumor lesions and is often suboptimal with current imaging and operating techniques. Hence, there is a need for improved intra-operative methods to allow better tumor margin visualization and metastasis detection.

Our team has been involved for a long time in the development of the Fluobeam™ (Figure I-1), a NIR imaging device, nowadays in preclinical studies. As well, based on the initial work of Pr P Dumy (Departement Chimie Moléculaire, Grenoble, France), our 2 teams generated, evaluated and patented a RAFT-(cRGD)4-dye probe for NIR-optical imaging. This tracer is now licensed to Fluoptics™ and commercialized under the name of AngioStamp™.

Figure I-1: The imaging device: Fluobeam™

Using this targeted NIR probe, we previously demonstrated that optical guidance greatly improved the surgical quality by doubling the number of detected nodules and significantly reduced the duration of the surgery on mice bearing peritoneal carcinomatosis[218].

AngioStamp™ will be administered intravenously to patients prior to surgery. It is therefore considered as a drug by the French regulatory commission (ANSM, agence nationale de sécurité du medicament et des produits de santé). As such AngioStamp™ has to be produced in clinical grade quality (GMP) and must prove its absence of toxicity as well as its capacity to augment the quality of the patients' treatment.

The objective of the following study was to check, on spontaneous cancers arising in pets, that the intra-operative NIR-guided surgery is feasible.

This clinical veterinary phase is based on surgery of the feline fibrosarcoma, also known as fibroblastic sarcoma. It is a mesenchymal tumor representing 40 to 50% of all skin tumors in cats. This neoplasm is one of the most common tumors in cats and shows an asymmetrical and infiltrating growth pattern. In general, the tumor can occur anywhere in the body; nevertheless, there is a preference for the interscapular region. Infiltration into the surrounding subcutaneous soft tissue and sometimes the underlying skeletal muscle are

---

[218]Keramidas, M, V Josserand, C A Righini, C Wenk, C Faure, and J L Coll. "Intraoperative Near-infrared Image-guided Surgery for Peritoneal Carcinomatosis in a Preclinical Experimental Model." *The British Journal of Surgery* 97, no. 5 (May 2010): 737–743.

frequently observed. These characteristics account for the frequent local recurrence with rates ranging from 28% to 45% in different studies[219]. Wide or radical surgical excision currently represents the main therapeutic option[220]. It is generally accepted that complete resection improves the disease-free interval while incomplete resection increases the probability of treatment failure[221,222,223]. Because the extension of fibrosarcoma to surgical margins is important in predicting local recurrence, it is clear that quality of the surgery is crucially involved in the management of fibrosarcoma. Post-surgical therapeutic decisions are based on the status of surgical margins. These characteristics, added to the fact that this spontaneous soft tissue sarcoma mimics its human counterpart[224]sustain the possibility of easily transferring the system (Fluobeam™ & AngioStamp™) into human clinical studies for further evaluation in oncological surgery.

Since an agreement of the pet owners is needed, it was necessary to show them that the injection of AngioStamp™ will not harm the cat. We thus started a very light "toxicological study", or rather called short safety observation studies, on three laboratory cats. At the same time we wanted to use these experiments for the definition of the starting 1x dose that would sound adapted for detecting tumors.

---

[219] V.S. Bregazzi, S. M. LaRue, E. McNiel, D. W. Macy, W. S. Dernell, B. E. Powers, and S. J. Withrow. Treatment with a Combination of Doxorubicin, Surgery, and Radiation Versus Surgery and Radiation Alone for Cats with Vaccine-associated Sarcomas: 25 Cases (1995-2000). Journal of the American Veterinary Medical Association 218, no. 4 (2001) 547–550.; Kobayashi T, Hauck ML, Dodge R, et al. Preoperative radiotherapy for vaccine associated sarcoma in 92 cats. *Vet Radiol Ultrasound* 2002;43:473-479.

[220] A. E.Hershey, K. U. Sorenmo, M. J. Hendrick, F. S. Shofer, and D. M. Vail. Prognosis for Presumed Feline Vaccine-associated Sarcoma After Excision: 61 Cases (1986-1996). Journal of the American Veterinary Medical Association 216, no. 1 (January 1, 2000) 58–61.

[221] Kobayashi T, Hauck ML, Dodge R, et al. Preoperative radiotherapy for vaccine associated sarcoma in 92 cats. *Vet Radiol Ultrasound* 2002;43:473-479.

[222] A. E.Hershey, K. U. Sorenmo, M. J. Hendrick, F. S. Shofer, and D. M. Vail. Prognosis for Presumed Feline Vaccine-associated Sarcoma After Excision: 61 Cases (1986-1996). Journal of the American Veterinary Medical Association 216, no. 1 (January 1, 2000) 58–61.

[223] K. Cronin, R. L. Page, G. Spodnick, R. Dodge, E. N. Hardie, G. S. Price, D. Ruslander, and D. E. Thrall. Radiation Therapy and Surgery for Fibrosarcoma in 33 Cats. Veterinary Radiology & Ultrasound: The Official Journal of the American College of Veterinary Radiology and the International Veterinary Radiology Association 39, no. 1 (February 1998) 51–56.

[224]E.P. Spugnini, A. Baldi, B. Vincenzi, F. Bongiorni, C. Bellelli, G. Citro, A. Porrello, Intraoperative versus postoperative electrochemotherapy in high grade soft tissue sarcomas: a preliminary study in a spontaneous feline model. Cancer chemotherapy and pharmacology 59 (2007) 375-381.

I.1. Preliminary safety observation studies

I.1.1. Introduction

The first aim of this preliminary safety observation study in cats was the evaluation of potential acute effects related to the administration of a single intravenous dose of AngioStamp™.

Therefore increasing doses have been tested on three cats: 0.9 mg/kg, 2.4 mg/kg and 4.5 mg/kg, respectively, corresponding to doses 1X, 3X and 5X (Figure-I-2), estimated on the bases of previous injection performed in mice and rats (further information see in "Materials and Methods").

Cat 1 (1X) **Cat 2 (3X)** **Cat 3 (5X)**
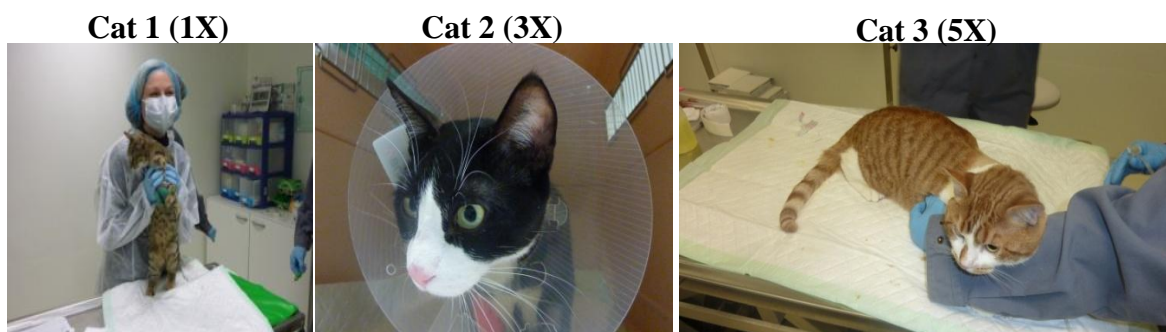
Figure-I-2: Laboratory cats used for preliminary experiments with doses 1X, 3X and 5X.

One hour before injection of the tracer, the animals were clinically examined and two catheters were placed, one in the bladder and one in the cephalic vein (see "Materials and Methods").

Before and after intravenous injection of AngioStamp™ the cats remained under medical control and the biochemical parameters were followed during 7 days post injection (Figure I-3).
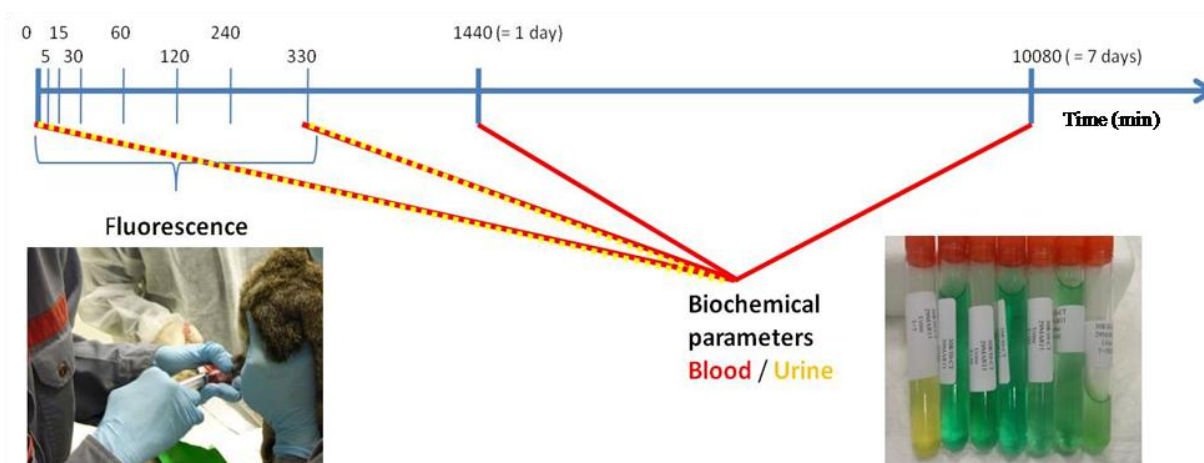
Figure I-3: Schedule of sampling and fluorescence imaging

I.1.2.   *Results*

We expected to evaluate on these 3 cats: i) the absence of acute immediate toxicity, ii) the kinetic of distribution of the injected molecule as well as the level of intensity of fluorescence each dose was providing in the normal skin (useful for the determination of the working dose) and iii) the absence of biochemical disorders in blood and urines.

❖ *Absence of toxicity*

No visible adverse effects due to the intravenous application of AngioStamp™ at the doses of 0.9, 2.4 and 4.5 mg/kg were observed.

The physical examination and follow-up of the blood and urine biochemical parameters confirmed that administration of AngioStamp™ at these 3 doses did not lead to any detectable toxicity (tables showing biochemical results in **"Appendices"**).

I.2.   *Fluorescecnce kinetic distribution of AngioStamp*

Using the same 3cats injected with 0.9, 2.4 and 4.5 mg/kg of AngioStamp™ we ran a small study in fluorescence (Em780/ Ex795) on the different fluids as well as on the body of the animals in order to follow its kinetic of elimination and also to evaluate the amount of fluorescence signal in the skin. This last value would provide information on the basal intensities of fluorescence in the normal tissues, and on the possible detection of the signal expected in tumor tissues (see protocol and scheme above). We can thus see if the calculated dose provides a sufficient level of detection for inter-operative imaging.

The fluorescence intensity was measured in chronological sequences of blood (200 µL), plasma (200 µL) and urine (10 µL) samples using the per-operative Fluobeam™. Images from T0 to 5 h 30 post injection of AngioStamp™ were also taken on the following shaved body regions: region of the right kidney and shoulder. The kidneys were chosen as the tracer has a renal elimination and the shoulder region, since it is the preferred localization the feline fibrosarcoma.

The unit p.d.u. (procedure defined unit) and the sampling are described in the Materials and Methods chapter.

The introduced term F_{50} describes the time needed for the fluorescent tracer signal to lose 50% of its maximal intensity.

I.2.1.   *Fluorescence in the plasma*

In all animals, the fluorescence in the plasma presents a peak at 5 min post injection followed by a rapid decrease (Figure I-4).The maximal signal is 5-times higher in cat 2 and nearly 11-times higher in cat 3 compared to cat 1.

In cat 1 the maximal signal is decreases by 50% at 10 min (F_{50} = 10 min), in cat 2 the F_{50} is at 25 min, thus 15 min more than in cat 1, and concerning cat 3 the F_{50} is reached at40 min post injection (p.i.) (Table I-1).

The fluorescence signal in cat 1 returns to the basal level after 4 h. as previously observed in mice, while at 5h30 (last measurement) the level of fluorescence in the plasma of cat 2 and 3 is still at 14% and 12% of their maximal peak value.

Plasma	Cat 1 Dose 1X (0.9 mg/kg)	Cat 2 Dose 3X (2.4 mg/kg)	Cat 3 Dose 5X (4.5 mg/kg)	Mouse
Peak (minutes)	5	5	5	5
p.d.u. max ($/10^3$)	4	18	38	0.9
Time F_{50} (min)	10	25	40	10 (40)
% of maximal fluorescence at 5h30	0	14	12	0
p.d.u. 5h30 ($/10^3$)	0	2.6	4.7	0

Table I-1: Compared fluorescence data of cat plasma.
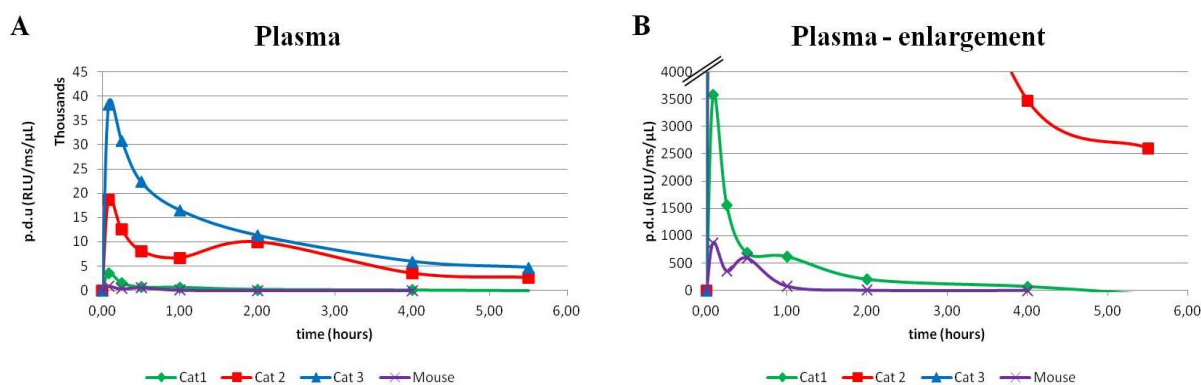
Figure I-4: Fluorescence kinetic of plasma samples (A & B, enlargement) and of the three cats, compared to mouse data.

I.2.2.   *Fluorescence in the blood*

The total blood shows a similar fluorescence kinetic profile than that of plasma. A peak appears at 5 min followed by a smooth and steady decrease of the signal intensity after a second faint peak at the third or fourth measurement (Table I-2; Figure I-5).

As expected, the intensities are lower in total blood compared to plasma measurements because blood is much more absorbing than plasma.

As compared to cat 1 at 5 min, the maximal signal measured in cat 2, cat 3 and mice are 17-times, 24-times and 1-time, higher respectively. The maximal signal in cat 1 decreases rapidly to reach the F_{50} at 10 min. In cat 2, cat 3 and mice, the F_{50} is reached after 27 min, 18 min or 8 min p.i., respectively. In cat 1 the signal rapidly decreases and is back to the background levels after 4 h, as previously described in mice. This is somewhat delayed in cats 2 and cat 3 and 5% or 4% of the max intensity of fluorescence are still present at 4 h.

Blood	Cat 1 Dose 1X (0.9 mg/kg)	Cat 2 Dose 3X (2.4 mg/kg)	Cat 3 Dose 5X (4.5 mg/kg)	Mouse
Peak (minutes)	5	5	5	5
p.d.u. max	438	7600	10300	399
Time F_{50} (min)	10	27	18	8
% of maximal fluorescence at 5h30	0	1	3	0
p.d.u. 5h30	0	92	340	0

Table I-2: Compared fluorescence data of cat blood.
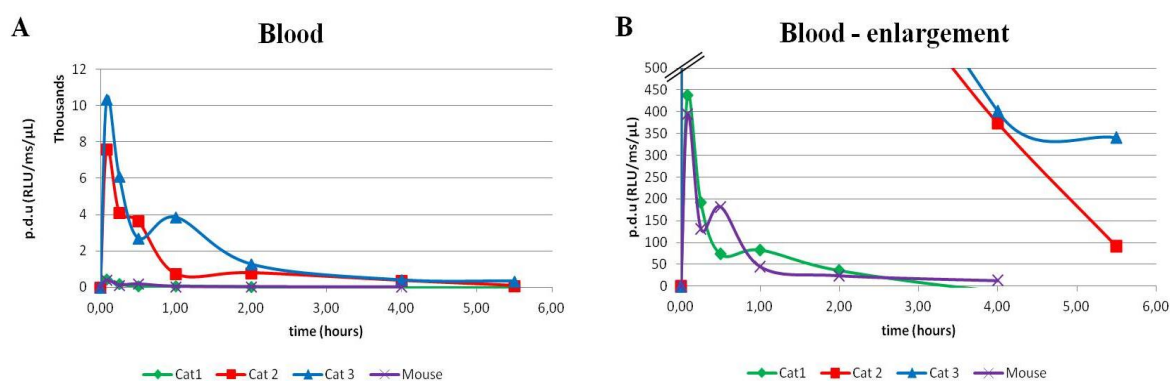
Figure I-5: Fluorescence kinetic of blood samples (A & B, enlargement) and of the three cats, compared to mouse data.

I.2.3.   *Fluorescence in the urine*

AngioStamp™ is known to be eliminated by renal excretion via the urine. In all three cats tested here, the urine was already showing a fluorescence peak as soon as 5 min post injection (Table I-3; Figure I-6).

In cat 2 and cat 3 the maximal signal is 4-times stronger compared to cat 1.
4 h after injection, the fluorescent signal in the samples of cat 1 is close to the basal level.
In cat 2 the fluorescent signal remains at 5h30 about 50% of the maximal measured signal.
In cat 3 no decrease in the signal during time is measured.

Urine	Cat 1 Dose 1X (0.9 mg/kg)	Cat 2 Dose 3X (2.4 mg/kg)	Cat 3 Dose 5X (4.5 mg/kg)
Peak (minutes)	5	5	5
p.d.u. max	$1.9*10^4$	$7.1*10^4$	$6.9*10^4$
% of maximal fluorescence at 5h30	0	50	100

Table I-3: Compared fluorescence data of cat urine.
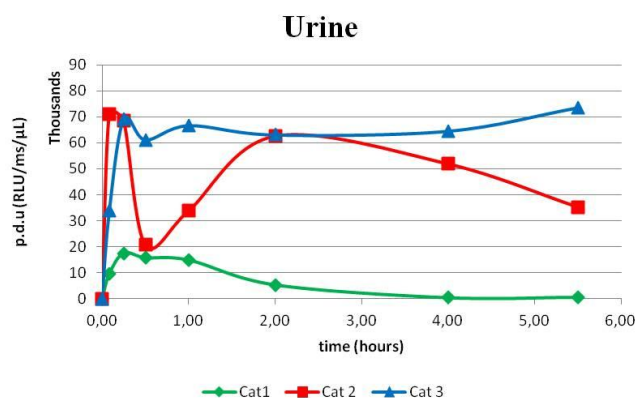
Figure I-6: Fluorescence kinetic of urine samples of cat 1 to 3.

I.2.4.   *Fluorescence in the kidney*

The fluorescent signal measured at kidney level increases directly after the injection of AngioStamp™ and reaches a peak at 1 h in cats 1 and 2 against 30 min in cat 3(Table I-4; Figure I-7). In mice the peak was already reached at 5 min. The signal then decreases smoothly but steadily, showing a similar profile to plasma and blood measurements.

When comparing the maximal signals of cats 2, 3 and mice to that of cat1, cat 2 shows a 6.5-times, cat 3 an 82-times and mice a 3-times higher signal. In cat 1 the F_{50} is reached after 3h30, in cat2 at 3h15 and in cat 3 at 2h30 p.i. In mice the F_{50} is at 2 h p.i. At 5h30 a residual fluorescence could be measured of 11 % of the maximal signal in cat 1, 18 % in cat 2, and 29 % in cat 3.

Thus the dose 1x is far more rapidly eliminated with an increasing ratio between cat 1 and cats 2 and 3, showing a difference at 5h30 of nearly 10-times (cat 1 & cat 2) and 193-times (cat 1 & cat3).

Kidney	Cat 1 Dose 1X (0.9 mg/kg)	Cat 2 Dose 3X (2.4 mg/kg)	Cat 3 Dose 5X (4.5 mg/kg)	Mouse
Peak (minutes)	60	60	30	5
p.d.u. max	16	105	1330	50
Time F_{50} (h)	3h30	3h15	2h30	2
% of maximal fluorescence at 5h30	11	18	29	n.d.
p.d.u. 5h30	2	19	385	n.d.

Table I-4: Compared fluorescence data of cat kidney.
n.d. = no data
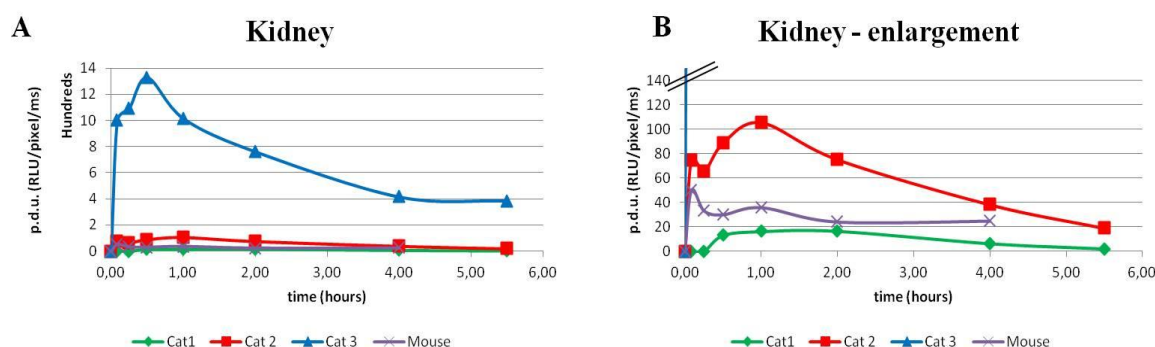
Figure I-7: A) Fluorescence kinetic of the kidney region (B enlargement) of the three cats, compared to mouse data.

I.2.5.   *Fluorescence in the shoulder*

The fluorescence measured at the level of the shoulder increased until reaching a maximal signal at 1 h p.i. in cat 1 and 2, and 30 min in cat 3 (Table I-5; Figure I-8). The maximal signal in cat 2 and cat 3 represents roughly 17- to 134 -times the one measured in cat 1.

The F_{50} in cat 1 corresponds to 1h45, in cat 2 to 4h and in cat 3 to 3h.

At 4h post injection the fluorescent signal was returned to basal level in cat 1. Cat 2 and cat 3 still presented elevated levels of fluorescence after 5h30, being at 34% and 44%, respectively of their maximal signal.

Shoulder	Cat 1 Dose 1X (0.9 mg/kg)	Cat 2 Dose 3X (2.4 mg/kg)	Cat 3 Dose 5X (4.5 mg/kg)
Peak (minutes)	60	60	30
p.d.u. max	7	122	938
Time F_{50} (h)	1h45	4	3
% of maximal fluorescence at 5h30	0	34	44
p.d.u. 5h30	0	41	408

Table I-5: Compared fluorescence data of cat shoulder.
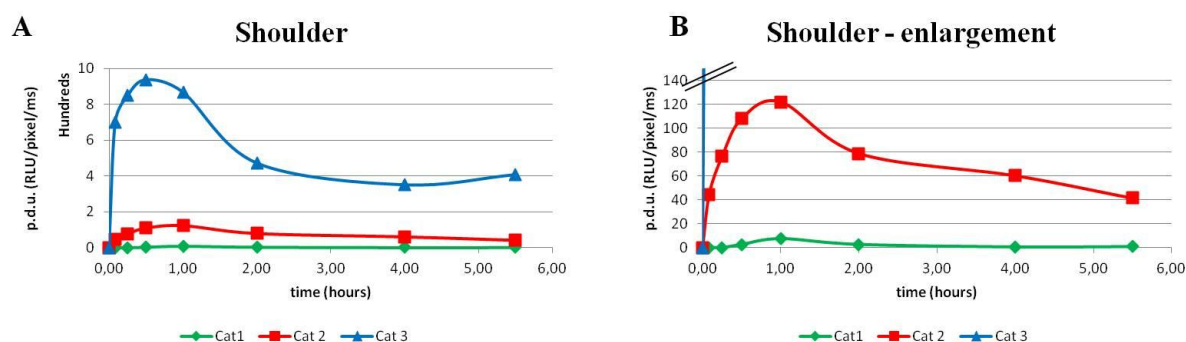
Figure I-8: A) Fluorescence kinetic of the shoulder region (B enlargement) of the three cats.

I.3.   *Conclusion and Discussion*

Based on the fluorescence kinetic data obtained in mice with best conditions already evaluated in former studies, the dose of 0.9 mg/kg was found to be sufficient for further surgical experiments in cats.

The difference in signal, measured in kidney and plasma or blood in cat 2 and cat 3 compared to cat 1 lead to the presumption that molecule elimination in the kidneys reaches a plateau due to saturation of the glomeruli in the kidneys after 5 min already. Thereafter a slow desaturation follows, depending on the residual tracer circulation in the organism. The higher the concentration, the slower the desaturation of this organ occurs. Consequently, a higher molecule concentration is circulating in the organism for a longer period of time. This reciprocal proportion is due a so-called first-order reaction, characterized by elimination of a constant proportion (%) per time interval, but not a constant amount.

This could explain the faster peaking of maximal signal in the shoulder of cat 3 than cat 1 and cat 2. The difference measured in the blood and plasma fluorescence intensities might reflect more certainly differences in the absorption coefficient of blood as described in the introduction chapter.

In conclusion we can claim, that despite minor differences, the biodistribution profile of AngioStamp™ in cats is comparable to the one previously described in mice.

I.4.   *Surgery of the feline fibrosarcoma*

Since the preliminary toxicological study did not show any sign of toxicity, we were authorized by the veterinary university and the animal owners to perform fluorescent-guided surgery on cat "patients". On spontaneous tumor bearing animals several questions still needed to be answered:

➢ How much AngioStamp™ should be injected?
➢ How long before surgery AngioStamp™ should be injected?
➢ Is the AngioStamp™ binding only to the tumor tissue?
➢ What is the sensibility of the method?
➢ What is the feeling of the surgeon regarding the technology?

In order to answer these questions, 14 cats were enrolled and classified in six different groups (Table I-6). Each animal was examined and controlled by means of X-ray scans before being referred to the surgical department (Figure I-9). All cats but one recorded in this study suffered of fibrosarcoma in the shoulder region. The last one presented a tumor on lumbar heights (Table I-7).

Group	AngioStamp™ (mg / kg)	Time of surgery after injection (h)	n (group size)
1	0.6	16	1
2	0.3	16	4
3	0.3	24	2
4	0.3	36	2
5	0.15	36	3
6	0.15	24	2

Table I-6: Conditions tested.

Figure I-9: X-ray scanner images of case #5.
A) shows the slice on the level of the primary tumor. In B) developed lung metastases
can be seen.

Patient & date of surgery	AngioStamp™ (mg/kg)	Surgery (h p.i.)	Tumor location & health status (before surgery)	Weight (kg)	age (years) & sex	Color/ race	Remarks follow-up
1) " Sally " June 2011	0.625	16	Right shoulder & axillar region (punction: blood); anaemic	3.9	10; ♀	Tri-color/ ESH	n.r. until August 2012
2) "Sunny " June 2011	0.3	16	Left shoulder; n.r.*	2.8	11 ; ♀	Grey striped / ESH	n.r. until August 2012
3) "Mousse " September 2011	0.3	16	right side of thorax; n.r.*	4.4	12; ♀ castrated	Tri-color/ ESH	n.r. until August 2012
4) " Lilou " October 2011	0.3	16	Left shoulder & axillar region until height of diaphragm n.r. *	6.5	7; ♀	white/ ESH	Recrudescence after 6 months – euthanasia 8 months after surgery
5) "Comette" October 2011	0.3	24	Right shoulder incl. scapula; Tumor necrotic; lung-metastases	3.6	13; ♀	black / ESH	6 months after surgery: Neoplasia (no metastasis) euthanasia after failure of treatment
6) "Toundra " Oktober 2011	0.3	16	right side of thorax; n.r.*	3.2	9 ; ♀	Tri-color / ESH	n.r. until August 2012
7) " Pepper " November 2011	0.3	24	Dorsal (column vertebral, thoracal) n.r. *	5.7	9; ♀	Tri-color / ESH	n.r. until August 2012
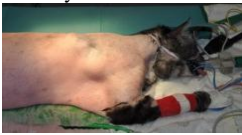
8) "Chouchou" February 2012	0.3	36	Dorso-lateral dexter (scapula & column vertebral); 3rd surgery (2nd relaps), no other remarks	8.2	8; ♂ castrated	Light-coloured grey-striped / ESH	n.r. until August 2012
9) "Aragorn" February 2012	0.3	36	Dorsal (column vertebral, thoracal) n.r. *	5.8	8; ♂	gray-white-black striped / ESH	n.r. until August 2012
10)" Kochka " March 2012	0.15	36	Left shoulder; Amputation of left front leg; n.r.*	4.9	11.5; ♀ castrated	Black / ESH	2 months after surgery: tumor of paw – euthanasia
11) "Nickdouille La Fripouille" March 2012	0.15	36	1) Left shoulder, necrotic; 2) right shoulder; n.r.*	3.8	10; ♂	Red-black striped / ESH	n.r. until August 2012
12) "Isis" March 2012	0.3	36	Rezidive, tumor left shoulder;	6.4	9; ♀	Red-black striped / ESH	† 3 days after surgery because of probable septicemia
13)"Pepere" June 2012	0.15	24	Left side inter-scapular	5.5	12; ♂	ESH	n.r. until August 2012
14) "Crackeurs" June 2012	0.15	24	Lumbale region, right dorsal	5.9	8; ♂ castrated	Red striped ESH	n.r. until August 2012

Table I-7: Patient data, showing dose and time of surgery after injection of AngioStamp™, region of the tumor, notable complications for surgery (health status, other than primary tumor), weight, age, sex, color and follow-up until august 2012.

(n.r. *= no remarks; ESH = European short hair)

Surgery was performed in the standard surgery facilities of the veterinary campus in Lyon (VetAgroSup, Marcy l'Etoille) in collaboration with the teams of Frédérique Ponce (Oncology of small animals department) and Claude Carozzo (Surgery of small animals department) and the pathological facilities.

The system for imaging, called Fluobeam™, was installed near the operation table so that the screen was visible for the surgeon's assistant(s) only. One assistant was holding the Fluobeam™ in his hands during image acquisition (Figure I-10). Surgery was performed as usual, *i.e.* without the help of fluorescence. The surgeon was interrupted from time to time for a few minutes in order to take images and to record video sequences of the operation scene.

We observed that the tumors of all patients were significantly labeled by AngioStamp™, showing the best tumor-to-healthy tissue ratio at a dose of 0.3 mg/kg injected at 36 h before surgery. We also demonstrated that the percentage of tumor tissue per sample correlated with its profile of fluorescence intensity.

The results of this study initially performed on 12 first cats (group 6 was not studied at the time we submitted these results for publication) are presented in the publication:

"**Near-infrared optical guided surgery of highly infiltrative fibrosarcoma in cats using an anti-$\alpha_v\beta_3$integrin molecular probe", Wenk et al.; Cancer Letters, 2012 submitted.**
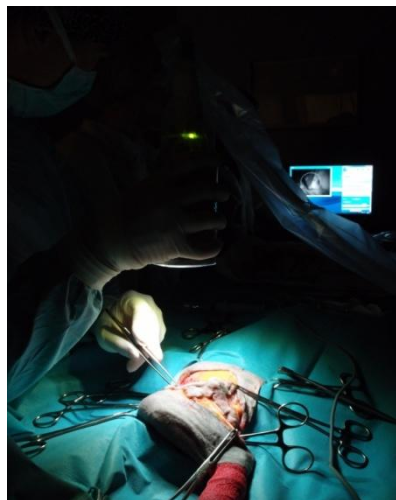
Figure I-10: Intra-operative imaging by using the Fluobeam™.

"Near-infrared optical guided surgery of highly infiltrative fibrosarcoma in cats using an anti-$\alpha_v\beta_3$integrin molecular probe",

Wenk et al.; Cancer Letters, 2012

Near-infrared optical guided surgery of highly infiltrative fibrosarcomas in cats using an anti-α_vß$_3$ integrin molecular probe

Christiane H. F. WENK[1,2,], **Véronique JOSSERAND**[1,2], **Stéphanie GUILLERMET**[4], **Corinne TENAUD**[1,2], **Didier BOTURYN**[5], **Pascal DUMY**[5], **Dorothée WATRELOT-VIRIEUX**[3], **Claude CAROZZO**[3], **Frédérique PONCE**[3] and **Jean-Luc COLL**[1,2,✉]

[1]Institut National de la Santé et de la Recherche Médicale (INSERM), Unité 823, Institut Albert Bonniot, Grenoble, France

[2] Université Joseph Fourier (UJF), Grenoble, France

[33]Unité ICE 2011-03-101, VetAgro Sup, Campus Vétérinaire de Lyon, Marcy l'Etoile, France

[4]Fluoptics®, Grenoble, France

[5]CNRS, UMR-5250, Département de Chimie Moléculaire, Grenoble, France

(✉) Corresponding author: Jean-Luc Coll

Telephone: +33 4 76 54 95 53
Fax: +33 4 76 54 94 13

Short Title: Optical-guided surgery of cat fibrosarcoma

ABSTRACT:

We investigated how near-infrared imaging could improve highly infiltrative spontaneous fibrosarcoma surgery in 12 cats in a clinical veterinary phase. We used an RGD-based nanoprobe at different doses and times before surgery and a portable clinical grade imaging system. All tumours were labelled by the tracer and had an overall tumour-to-healthy tissue during surgery ratio of 14 ± 1. No false negatives were found, and the percentage of tumour cells was linearly correlated with the fluorescence intensity. All cats recovered well and were submitted to long-term follow-up that is currently ongoing 1 year after the beginning of the study.

Introduction

To date, surgical tumour resection has been the therapeutic method of choice for most cancers. The limitations of surgical intervention include low tumour accessibility, difficult visual tumour delineation, micro-metastasis detection and damage to vital structures. Intra-operative guided surgery may help to overcome and/or improve these restraints.

Certain cancer surgery approaches are already being clinically evaluated for safe and complete tumour resection e.g., the 5-ALA-guided microsurgical resections in glioblastomas performed in Germany and Switzerland (5-aminolevulinic acid; [1]); however, these methods are limited by the low tissue penetration of UV, the protoporphyrin IX expression and the bleaching effect. Other clinical intra-operative imaging techniques are currently in use, such as magnetic resonance imaging (MRI), ultrasound (US), computed tomography (CT), and x-ray fluoroscopy. Nevertheless, all of these methods have certain limitations such as safety, costs, room problems or limited direct contact with the tissue through a matching medium, which is the case in the US [2]. Therefore, optical imaging represents a promising technology for overcoming some of these hindrances.

Fluorescence imaging in the near-infrared (NIR) wavelength (700 – 900 nm) is an optical modality that allows a real-time assessment of tumour borders while being easy to handle, safe for the clinicians (non irradiative method), and it can provide the simultaneous acquisition of surgical anatomy (white light and colour video) and NIR fluorescence signal [3]. Near-infrared probes present a number of advantages as the absorption coefficient of the tissue is minimal, resulting in high tissue penetration and sufficient contrast due to the low autofluorescence [4 ; 5].

The $\alpha_v\beta_3$ integrin $\alpha_v\beta_3$ displays increased expression levels on the surface of angiogenic endothelial cells compared with quiescent endothelial cells [6]. It is also expressed on the surface of several tumour cell types [7; 8]. The tripeptide RGD has been reported to be a specific recognition motif of the $\alpha_v\beta_3$ integrin, and such molecules as cRGD, a cyclic pentapeptide presenting the RGD sequence, which displays an increased affinity for this integrin, have been subsequently designed [9]. Several groups have synthesised multimeric cRGD-presenting compounds that display both enhanced binding affinity for $\alpha_v\beta_3$ and better tumour targeting efficacy (for review see [10]). We have developed a tetrameric cRGD-containing nano-probe, RAFT-(cRGDfK-)$_4$, by covalently linking four peptides (-cRGDfK-) to the cyclic decapeptide platform RAFT (Regioselectively Addressable Functionalised Template) [11]. This molecule is 5 nm on its larger face (formed by the ring of the 4 cRGD) and 1 nm at the level of the RAFT backbone. Thus, the molecule's shape ressembles that of cyclodextrins. The molecule is now commercially available under the name AngioLone™. A NIR 800 fluorescent dye was linked to the AngioLone™ platform, thus providing AngioStamp™. Alternatively, radioactive contrast agents have also been linked to AngioLone™ for radio-imaging [12; 13].

Using this targeted NIR probe, we previously demonstrated that optical guidance greatly improved the surgical quality by doubling the number of detected nodules and significantly reducing the duration of the surgery on mice bearing peritoneal carcinomatosis [14].

As an expectation of a clinical trial for humans we transferred this AngioStamp™ and Fluobeam™ technology into a clinical veterinary phase of surgery on spontaneous feline fibrosarcomas (fibroblastic sarcoma). The feline fibrosarcoma is a mesenchymal tumour that represents 40 to 50% of all skin tumours in cats. This neoplasm is one of the most common tumours in cats and shows an asymmetrical and infiltrating growth pattern. In general, the tumour can occur anywhere in the body; nevertheless, there is a preference for the interscapular region.

Long "tentacles" departing from the tumour mass and infiltrating the surrounding subcutaneous soft tissue and sometimes the underlying skeletal muscle are frequently observed. These characteristics account for the frequent local recurrence with rates ranging from 28% to 45% in different studies [15; 16]. Although a 'gold standard' treatment protocol for fibrosarcoma is not available, wide or radical surgical excision currently represents the main therapeutic option [17]. It is generally accepted that complete resection improves the disease-free interval while incomplete resection increases the probability of treatment failure [16; 17; 18]. Because the extension of fibrosarcoma to surgical margins is important in predicting local recurrence, it is clear that quality of the surgery is crucially involved in the management of fibrosarcoma. Post-surgical therapeutic decisions are based on the status of surgical margins.

Materials and Methods

Patient recruitment

Cats were addressed by veterinary practitioners. Twelve cats (3 males and 9 females; 9.8 ± 1.7 years old, weighing 4.7 ± 1.7 kg) were included in the study after obtaining the owners' information and consent. Diagnosis was based on clinical and morphological data (fine needle aspirations and biopsies), Extent of the disease as local staging of the tumour and metastatic spreading were evaluated by contrast enhanced CT (computed Tomography) (Figure 1A).

CT scanning was performed by a series of transverse 2 mm slices of the thorax, once without contrast agent and once after an intravenous iodide injection containing a contrast agent (iohexol). The contrast agent identified the tumour tissue as a homogenous mass.

This three-dimensional CT provided essential information for proper planning of aggressive surgical approach.

Fluorescent tumour-targeting probe

AngioStamp^{TM} (Fluoptics, Grenoble, France) is a NIR dye-labelled molecular probe targeting the $\alpha_v\beta_3$ integrin derived from the previously published RAFT(c[-RGDfK-])$_4$ [19; 20; 21; 22; 23].

The toxicity of increasing doses of the probe, which is eliminated by the kidneys, was tested in laboratory cats prior to this study (supplementary data) and validated by the veterinary faculty of Lyon (AgroSup Lyon, France).

The probe was injected in the cephalic vein of the animals at 0.6, 0.3 and 0.15 mg/kg. Surgical intervention was performed at 16, 24 and 36 h post-injection.

Portable clinical fluorescence imaging device

Real time fluorescence imaging was performed using a Fluobeam^{TM} NIR imaging system (Fluoptics, Grenoble, France). The system is compact and portable. . It consists of two parts: a control unit with a laser source emitting at 785 nm and a power supply for light-emitting diodes (LEDs), next to an optical head with a highly sensitive charge-coupled device camera and white LEDs for the illumination of the field of view. The laser beam is fiber-guided from the control unit to the optical head. The laser beam was spread to reach a 6-cm spot diameter at the working distance of 17 cm. The power density of the laser irradiation was 96 $\mu W/mm^2$. The NIR fluorescence image was 696×512 pixels and provided a resolution of two line pairs per millimeter allowing visualization of sub-millimeter structures [23; 24].

The Fluobeam™ system has been used with a dedicated single use CE marked sterile cover bearing an optical window compatible with NIR fluorescence measurements.

[23; 24].

Surgical fibrosarcoma resection

After preparation of the operation field and before incision of the skin, initial fluorescent images of the tumour were taken. After the beginning of the tumour resection, fluorescence imaging was performed at several steps of the surgery (tumour tissue, tumour margins and surrounding healthy tissues). Afterward, surgical specimens were cut and imaged, and the samples for histopathological analysis were resected under fluorescent guidance. Fluorescence imaging was performed after the removal of the tumour in order to check that no residual fluorescence remained.

After the surgery and recovery phases were completed, the cats returned home, and the owners were asked to bring them back regularly for long-term clinical follow-up.

Histo-pathological analyses and immunohistology

Surgical specimens were sampled into two pieces for the histo-pathological and immuno-histological analyses of the $\alpha_v\beta_3$ integrin expression level. A portion of samples were fixed in formaldehyde, embedded in paraffin and cut in 4-µm slices before Haematoxylin-Eosin standard staining, and other samples were frozen by placing them in isopentane and shock freezing them in liquid nitrogen. They were cut into 6 µm slices (microcryotome) and conserved at -80°C until fixation and staining. After warming up the frozen slices by leaving them at room temperature, they were fixed 10minutes in methanol at room temperature. After 5 minutes of rinsing in water, the slices were loaded in the staining automate "BENCHMARK" (protocol N° 781) and labelled with the mouse anti-human-integrin $\alpha_v\beta_3$ antibody (5µg/ml; 1/200 in Ventana diluent; clone LM609, Chemicon, USA) for 32 minutes at room temperature (antibody 5µg/ml; 1/200). After an automatic rinsing, the slices were incubated with the secondary antibody (Mouse IgG1-peroxidase), which was also used as negative control.

Analysis of NIR fluorescence data

The fluorescent data collected using Fluobeam™ was quantified with the image analysing programme WASABI (Hamamatsu Photonics GmbH, Germany) and Microsoft Excel. The intensity value of the different tissues was defined as the mean fluorescence intensity of the region of interest (ROI) minus the mean fluorescence intensity of the background divided by the exposure time in milliseconds, resulting in the relative light unit per pixel per millisecond (RLU/pixel/ms). For the fluorescence data three to 10 points were measured concerning the tumour and the healthy tissue each per animal. This was depending on the data collected and thus their exploitation possibilities (e.g. tumour sample not covered by tissues like thick muscle layers or skin; sharp images).

6

Results

AngioStamp™ labels feline fibrosarcoma

Surgery was performed in 12 cats bearing fibrosarcomas. Three of the cats had already undergone surgery once, and two others demonstrated lung metastases after tomography imaging. The fibrosarcomas were located in the thoracic / shoulder region, particular the interscapular region. (Figure 1). The exact location of the neoplasm and a table with examples of fluorescence imaging during surgery and *ex vivo* for each case is presented in the supplementary data.

In the first group, the injected dose of AngioStamp™ (0.6 mg/kg) was calculated as an extrapolation of the injected doses we optimised and routinely used in mice and rats ([19;20;25;26] and unpublished data). This dose was also validated in the preliminary toxicity assays performed in cats (Supplementary data). In addition, our experience in mice dictated that an injection 16 h before imaging provided an optimal tumour/noise ratio. Thus, we used this time point to perform a dose evaluation study. The results demonstrated that all of the animal tumours included in the study were labelled with AngioStamp™. Tumour tissue fluorescence was observed in 12/12 cats, and all of the tumours had fibrosarcoma histo-pathological diagnosis. The tumours were always more fluorescent compared with the surrounding healthy tissues including muscle, connective tissues, bones, skin and lymph nodes (Figure 2 and image in supplementary data).

However, to reach a tumour/tissue ratio that would allow the optimal delineation of tumours, we optimized the dose and timing of the surgery after injection of the tracer.

Optimisation of the signal/noise ratio

We progressively lowered the dose of injected AngioStamp™ from 0.6 down to 0.15 mg/kg. In addition, we increased the time period between injection and surgery to increase the signal/noise ratio. It is important to note that it is not convenient to inject the molecule more than 36 h before surgery for practical and financial reasons associated with housing the cats within the veterinarian facility. Altogether, we evaluated 5 different conditions in five groups of animals (Table 1).

The results presented in Figure 3A demonstrate the strong labelling of the tumour tissues, which can be distinguished from the surrounding healthy tissues.

In cats treated with 0.6 mg/kg AngioStamp™ 16 hours before surgery, we observed a strong fluorescent signal (148 ± 26 RLU/pixel/ms) in the tumour tissues and a mean of 34 ± 23 RLU/pixel/ms in the surrounding healthy tissues (*(significant difference between tumor and healthy tissue values) *p = 0.02*). When decreasing the dose to 0.3 mg/kg for a surgery 16 h later, the fluorescence signals remained as high as in the tumours (159 ± 67 RLU/pixel/ms) but started to decrease in the healthy tissues (21 ± 14 RLU/pixel/ms) (***p=0.001*). If AngioStamp™ is injected 24 or 36 h instead of 16 h

before surgery, the positive signal in the tumour remains constant (Figure 3), while the non-specific fluorescence in the surrounding tissues continues to decrease to 10 ± 4 RLU/pixel/ms in group 4 (***$p=0.001$). In the last tested condition *i.e.,* surgery at 36 h after injection of 0.15 mg/kg, the mean fluorescent signal of the tumour tissue is reduced (58 ± 19 RLU/pixel/ms) but is easily distinguishable from the corresponding background levels (8 ± 3 RLU/pixel/ms) (***$p=0.001$).

This is also reflected in the significant difference between the fluorescence signal in the tumour of group 1,2,3 and 4 compared to group 5 (*$p < 0.05$) and between the healthy tissue signal of group 2 compared to group 3,4 and 5 (**$p < 0.01$).

The *in vivo* tumour/healthy tissue ratio (Figure 3A-inclusion) increases from 4 in the first group (AngioStamp^{TM} 0.6 mg/kg 16 h before surgery; n = 1), 7.2 +/- 1.7 in the second group (0.3 mg/kg 16 h before surgery) to 14 in groups 3 and 4 (group 3 = 13.5 +/- 4.9; group 4 = 14 +/- 2.6). This ratio was lower in group 5 in which the lower dose was injected 36 h before surgery. However, this ratio is still very good (= 7 +/- 1.4), confirming that it is possible to distinguish the tumour from healthy tissues with this injection protocol.

In conclusion, lowering the doses from 0.6 to 0.3 mg/kg did not reduce the staining intensity in the tumours (± 150 RLU/pixel/ms; p non significative). In addition, it was preferable to increase the delay between injection and surgery because it reduced the background (from 34 RLU/pixel/ms to 8 RLU/pixel/ms) without affecting the positive signal. Thus, the best condition was obtained in group 4.

Similar results were obtained when the portions of the tumour were analysed *ex vivo* after surgery (Figure 3B). As they are more exposed to the excitation light, extracted tissues are usually brighter than during surgery. The average tumour signal varied between 240 and 95 RLU/pixel/ms in groups 1 and 4, while the background measured in the corresponding healthy samples ranged from 38 to 7 RLU/pixel/ms. As expected, the pattern of fluorescence in the different groups was similar to that obtained *in vivo*. The injection of 0.3 mg/kg 36 h before appeared the best condition in this case, as well.

Based on the values of the fluorescent signal during surgery in the different tissues treated with 0.3 mg/kg, we assumed that a signal higher than 30 RLU/pixel/ms designated tumour tissue, while a fluorescent signal lower than 20 RLU/pixel/ms was healthy tissue. Signals ranging between 20 and 30 RLU/pixel/ms were considered "doubtful" and sent for further histopathological analysis.

The imaging device helps to check complete excision

For instance checking the operation field after tumour excision and discriminating doubtful structures by consulting the Fluobeam™ was helpful in sense of reassuring the surgeon of complete removal of malignant tissue.

The fluorescent intensity correlates with the tumour cell quantity

The fluorescent intensities measured with Fluobeam™ are directly related to the percentage of tumour cells detected in parallel and double-blind histological examination of the samples by the pathologist. The fluorescent intensity linearly increases with the number of tumour cells per sample (Figure 4). Regarding the tissues with 0% tumour cells the non-specific fluorescent signal was no more than 20 RLU/pixel/ms for group 2 and 10 RLU/pixel/ms for group 4. Group 4 has a lower non-specific signal than the other two groups while rising in fluorescent intensity rapidly to be at the same level as group 2 for tissues with 60% and 80% tumour tissue.

Feline Fibrosarcoma does express the integrin $\alpha_v\beta_3$

Using immunohistological staining with an anti-human integrin antibody, we found that the tumour samples were positive for the presence of the $\alpha_v\beta_3$ integrin, the receptor targeted by AngioStamp™. The integrin was mainly present on the surface of endothelial cells (Figures 5A & D) but also in the vicinity of blood vessels on the surface of tumour cells (Figure 5B & E).

We also demonstrated a correlation between $\alpha_v\beta_3$ expression and AngioStamp™-mediated fluorescence labelling (Figure 6). The frozen slices were observed by the pathologist who evaluated the amount of tumour cells present per sample according to cytology (X axis). We then evaluated the percentage of anti-integrin $\alpha_v\beta_3$ positive cells present in each sample (left Y axis) and correlated these results with the amount of fluorescence provided by AngioStamp™ /Fluobeam™ (right Y axis). A correlative tendency among these three parameters was generally obtained as expected. Of interest, a portion of "negative" tissues (i.e., 0% tumour cells) were found positive for $\alpha_v\beta_3$ integrin expression but not for AngioStamp™ labelling. This may be explained by a certain cross reactivity of the antibody with other integrins overexpressed in the inflamed peritumoural tissues present in the cat that

9

are not recognised by the RGD motif present in AngioStamp™. Indeed, the cross reactivity of this antibody in the cat is not known.

In these negative samples, a weak 16 RLU/pixel/ms basal fluorescence signal was measured. As soon as 20% of the tumour cells are present in the sample, the mean fluorescent signal increases and reaches 79 RLU/pixel/ms, and it will peak at 248 RLU/pixel/ms when 90% of the samples are made of tumour tissue.

Long-term follow-up

Among the 12 cats, all but one undergoing the AngioStamp™ treatment recovered from surgery and were sent back to their owners. One cat died for unknown reasons after surgery, but the death was not related to the presence of the molecule that had been injected 36 h before at the lowest dose without providing any suspicious reactivity. The 11 other cats returned home, and the owners or the local veterinarians are contacted regularly for evaluation of the patients' progress. At present, the first cases of clinical follow-up now reaching 1 year, and there was one loss, which was caused by recurrence of the primary tumour and the appearance of metastases 6 months after surgery. All other patients present, according to case, with a good health status without any apparent side effects caused by the tracer or the imaging procedure.

Discussion

The major obstacle toward better outcome for patients with infiltrative tumours is the difficulty in delineating preoperative tumour margins.

Preoperative contrast CT, MRI and intraoperative ultrasonography are currently used for diagnosis and resection guidance in human patients. Several imaging devices are currently being tested for their medical application [14; 23; 24; 27; 28].

In this feasibility study, we evaluated how preoperative fluorescence imaging could help to better visualise and delineate highly infiltrative feline fibrosarcomas in cats. Using optical guidance, it is assumed that it is easier for a surgeon to excise malignant tissues exhaustively without harming healthy ones. Accordingly, a surgeon would eventually be able to save functional tissues, such as whole muscle complexes, nerves, vessels and articulations [2]. This approach may also shorten the surgery duration [14]. There are currently only two clinical NIR fluorescent probes available: ICG and methylene blue. While ICG is a promising probe in certain cases for cancer detection, it also has its limits as it is a non-specific marker with non-modifiable properties [3]. Alternatively, 5-aminolevulinic acid (ALA) may also be administered to patients with glioblastoma, and it was found to lead to the accumulation of fluorescent porphyrins in malignant glioma tissue by a non-specific way [29; 30]. Recently, folate conjugated to fluorescein isothiocyanate (folate-FITC) was also used in a clinical trial for the intraoperative imaging in ovarian cancer [31]. However, the use of FITC, which emits in the visible range, does not provide sufficient sensibility *in vivo* because of light absorption [32; 33].

We have developed an RGD-based tumour-targeting peptide, RAFT-c(RGDfK)4, which was labelled with a NIR fluorophore (AngioStamp^{TM}) and targets the $\alpha_v\beta_3$ transmembrane integrin with high selectivity [22]. Integrins play a role in a wide variety of biological processes, including inflammation, innate and antigen specific immunity, haemostasis, wound healing, tissue morphogenesis, and the regulation of cell growth and differentiation. Accordingly, specific integrin dysregulation phenomena have been linked to the pathogenesis of many disease states and are incessantly offering new druggable opportunities for a number of diseases, including asthma, cancer, epilepsy, hypercholesterolemia, inflammatory bowel disease, osteoarthritis, osteoporosis, schizophrenia, thrombosis, and vascular diseases. The $\alpha_v\beta_3$ integrin is overexpressed in neoendothelial cells that form tumour blood vessels, and it is also frequently overexpressed on tumour cells in lung cancers [34; 35], melanomas [36; 37], brain tumours [38], breast cancers [39] and sarcomas (unpublished data). However, its tumours overexpression may largely vary for several reasons. This variation can happen because the polyclonal expansion of a tumour cell can be either positive or negative for the presence of integrin, which will thus delineate the various domains within the tumours with variable levels of integrin $\alpha_v\beta_3$ expression. The level may also vary according to the location of the tumour cell i.e., at

the periphery or in the centre of a cell colony. Usually, the expansion front of a tumour is also more strongly positive, which may be an asset in our case for the better definition of tumour margins. It is interesting to note that we have a good correlation between the fluorescence intensity and the presence of tumour cells. However, the samples that were considered "inflammation positive" without containing tumour cells (0% in the graphs of Figures 3 and 5) presented between 20 and 30 RLU/pixel/ms (21, 25 and 39 RLU/pixel/ms for the three cats in group 4) and thus were considered "doubtful". It has often been reported that peripheral inflammatory infiltrates consisting of lymphocytes and macrophages can be observed in feline fibsosarcoma [40]. Inflammation is also known to precede the development of other types of cancers in cats and other species [41]. Thus, it is preferable to also remove this portion of the "doubtful" inflamed and weakly fluorescent peritumoural tissue, as it may potentially be irreversibly engaged in the transformation process.

Our results demonstrated that in all of the cases (i.e., 12 out of 12 cats), the fibrosarcoma was labelled with AngioStamp^{TM} after the intravenous administration. We could also establish a relative range for the classification of the tissues imaged, due to the fluorescent signal obtained. When a 0.3 mg/kg or lesser dose is used, a 30 RLU/pixel/ms or greater value may be indicative of tumour tissue, while tissues with less than 20 RLU/pixel/ms are considered healthy tissue. While the signal in the tissue decreases with injected doses lower than 0.3 mg/kg, it is not significantly augmented at higher doses. This observation suggests that the number of accessible targets is the limiting factor. Moreover, it is important to leave at least 36 h between the time of injection and surgery to favour the "washing out" of unbound molecules and augment the signal/noise ratio.

The fluorescent signal emitted from the malignant tissue can even be visualised through the skin. Nevertheless, its intensity also depends on the colour of the skin as a dark pigmented skin absorbs fluorescence, whereas clear skin reflects it, causing signal artefacts.

All but one patient supported the surgical intervention without any complications. The death of one cat was not attributable to this procedure. Another cat died 6 months after surgery, due to relapse. These results, plus additional information concerning acute toxicity in cats (supplementary data), demonstrates that the entire procedure seems to be safe, particularly the fact that the injected doses of AngioStamp™ used in this study can be injected without any sign of toxicity.

Altogether, this system is a promising tool for the accurate, safe and complete resection of feline fibrosarcomas under real surgical conditions. These characteristics, added to the fact that this spontaneous soft tissue sarcoma mimics its human counterpart [42], sustain the possibility of easily transferring the system into human clinical studies for further evaluation in oncological surgery. Nevertheless, it still needs to be established whether optical guided surgery using such a system truly improves the survival and minimises the risk of relapse.

Acknowledgments

Table 1

Group	AngioStamp™ (mg/kg)	Time of surgery after injection (hours)	Number of animals per group (n)
1	0.6	16	1
2	0.3	16	4
3	0.3	24	2
4	0.3	36	3
5	0.15	36	2

Figure 1: Clinical presentation of the feline fibrosarcoma. (A) Visualisation of thoracic fibrosarcoma in two different cats as observed using CT scanning. The examination consists of a series of transverse 2-mm slices of the thorax after intravenous injection of an iodide containing contrast agent (iohexol). The tumour tissue can be observed as a homogeneous mass. This procedure is important for the diagnosis and approximate evaluation of the degree of infiltration and metastasis and will thus serve to establish the surgical procedure. **(B)** After anaesthesia and the surgical preparation of the cat patients (a), the solid tumour is excised following the standard surgical protocol. In case (b), a portion of the spina scapulae had to be excised, as well. Afterward, fluorescent imaging of the excised tumour sample (c) is performed, and the sample is analysed by the pathologist.

Figure 2: Detection of tumours using fluorescence imaging. (A) Fluorescent imaging *in vivo* (group 4; 0.3 mg/kg at 36 h). During surgery, fluorescent images of different zones of the surgical field are taken. The fluorescent signal in the tumour (a) is more intense compared to the healthy tissues (b = soft tissue; c = bone). **(B)** Fluorescent imaging *ex vivo*. After resection, fluorescent images of different samples for histological analyses of the excised portion are taken. The fluorescent signal in the tumour (a) demonstrates a higher intensity compared with the healthy tissues (b = soft tissue; c = bone). The grey levels of the different images in (b) and (c) are normalised and represented by the scale on the right side. The dotted line represents the form of the samples.

Figure 3: Fluorescence intensity of the tumours and healthy tissues *in vivo* during surgery (A) or *ex vivo* on the extracted samples (B). The fluorescence level of each sample (each dot represents one sample) is measured in the different groups (groups 1 to 5). For each group, the tumours are on the left and the healthy tissues are on the right. The means and standard deviations are indicated by the box-blots. **(C) Tumour/healthy ratios are represented.** Strong fluorescence intensities are observed in the tumours *in vivo* and *ex vivo*, while healthy tissues remain poorly fluorescent, thereby providing an excellent ratio with the best ratio being obtained in group 4 (injected with 0.3 mg/kg of AngioStamp[TM], 36 h before surgery).

Figure 4: Correlation between fluorescence intensity and presence of tumour cells. We compared the fluorescence intensity of each sample with the percentage of tumour cells estimated after histopathological analysis of the paraffin embedded slices of each sample. This observation indicates a good correlation, *i.e.,* augmenting the quantity of tumour tissue is associated with an augmented fluorescent intensity due to the AngioStamp[TM] labelling.

Figure 5: Analysis of the $\alpha_v\beta_3$ integrin status of the tissue samples.

Representative images of the immunohistological staining (Peroxidase) of excised samples with the $\alpha_v\beta_3$ anti-integrin antibody. (A & D) represent positive staining of the vasculature at two different magnifications (20× and 40×), while (B & E) represent an example of positive labelling that is primarily of the tumour cells. (C & F) is representative of the negative controls (healthy tissues) that do not demonstrate labelling. The scale bars represent 200 μm.

Figure 6: Correlation between fluorescence labelling, tumour cell presence and the detection of the $\alpha_v\beta_3$ integrin

We compared the percentage of cells labelled by the LM609 antibody, which recognises human $\alpha_v\beta_3$ integrin (left axis), with the presence of tumour tissue being analysed by the pathologist (X axis), and we correlated these results with the average fluorescent signal obtained by AngioStamp™ labelling, which is expressed in RLU/pixel/ms (right axis). A good correlation is obtained between the presence of tumour cells and the intensity of fluorescence, while the detection of the integrin does not always correlate. This may be due to the poor specificity/affinity of the anti-human antibody for cat integrin and/or may also indicate that a positive integrin signal obtained in inflammatory tissues (qualified as "0%") may react with the LM609 antibody but not with AngioStamp™.

References

[1] O.P. Gautschi, K. van Leyen, D. Cadosch, G. Hildebrandt, J.Y. Fournier, [Fluorescence guided resection of malignant brain tumors - breakthrough in the surgery of brain tumors]. Praxis (Bern 1994) 98 (2009) 643-647.

[2] S.L. Gibbs-Strauss, M. Rosenberg, B.L. Clough, S.L. Troyan, J.V. Frangioni, First-in-human clinical trials of imaging devices: an example from optical imaging. Conference proceedings : ... Annual International Conference of the IEEE Engineering in Medicine and Biology Society. IEEE Engineering in Medicine and Biology Society. Conference 2009 (2009) 2001-2004.

[3] B.E. Schaafsma, J.S. Mieog, M. Hutteman, J.R. van der Vorst, P.J. Kuppen, C.W. Lowik, J.V. Frangioni, C.J. van de Velde, A.L. Vahrmeijer, The clinical use of indocyanine green as a near-infrared fluorescent contrast agent for image-guided oncologic surgery. J Surg Oncol 104 (2011) 323-332.

[4] B.W. Xie, I.M. Mol, S. Keereweer, E.R. van Beek, I. Que, T.J. Snoeks, A. Chan, E.L. Kaijzel, C.W. Lowik, Dual-wavelength imaging of tumor progression by activatable and targeting near-infrared fluorescent probes in a bioluminescent breast cancer model. PloS one 7 (2012) e31875.

[5] S. Gioux, H.S. Choi, J.V. Frangioni, Image-guided surgery using invisible near-infrared light: fundamentals of clinical translation. Molecular imaging 9 (2010) 237-255.

[6] S. Stromblad, D.A. Cheresh, Integrins, angiogenesis and vascular cell survival. Chem Biol 3 (1996) 881-885.

[7] J.S. Desgrosellier, D.A. Cheresh, Integrins in cancer: biological implications and therapeutic opportunities. Nature reviews. Cancer 10 (2010) 9-22.

[8] H. Jin, J. Varner, Integrins: roles in cancer development and as treatment targets. British journal of cancer 90 (2004) 561-565.

[9] M. Aumailley, M. Gurrath, G. Muller, J. Calvete, R. Timpl, H. Kessler, Arg-Gly-Asp constrained within cyclic pentapeptides. Strong and selective inhibitors of cell adhesion to vitronectin and laminin fragment P1. FEBS letters 291 (1991) 50-54.

[10] L. Auzzas, F. Zanardi, L. Battistini, P. Burreddu, P. Carta, G. Rassu, C. Curti, G. Casiraghi, Targeting alphavbeta3 integrin: design and applications of mono- and multifunctional RGD-based peptides and semipeptides. Curr Med Chem 17 (2010) 1255-1299.

[11] D. Boturyn, J.L. Coll, E. Garanger, M.C. Favrot, P. Dumy, Template assembled cyclopeptides as multimeric system for integrin targeting and endocytosis. J Am Chem Soc 126 (2004) 5730-5739.

[12] Z.H. Jin, T. Furukawa, M. Galibert, D. Boturyn, J.L. Coll, T. Fukumura, T. Saga, P. Dumy, Y. Fujibayashi, Noninvasive visualization and quantification of tumor alphaVbeta3 integrin expression using a novel positron emission tomography probe, 64Cu-cyclam-RAFT-c(-RGDfK-)4. Nuclear medicine and biology 38 (2011) 529-540.

[13] Z.H. Jin, T. Furukawa, M. Claron, D. Boturyn, J.L. Coll, T. Fukumura, Y. Fujibayashi, P. Dumy, T. Saga, Positron emission tomography imaging of tumor angiogenesis and monitoring of antiangiogenic efficacy using the novel tetrameric peptide probe (64)Cu-cyclam-RAFT-c(-RGDfK-) (4). Angiogenesis (2012).

[14] M. Kéramidas, V. Josserand, C.A. Righini, C. Wenk, C. Faure, J.L. Coll, Intraoperative near-infrared image-guided surgery of peritoneal carcinomatosis in a preclinical mouse model. British Journal of Surgery 97 (2010) 737–743.

[15] V.S. Bregazzi, S. M. LaRue, E. McNiel, D. W. Macy, W. S. Dernell, B. E. Powers, and S. J.

Withrow. Treatment with a Combination of Doxorubicin, Surgery, and Radiation Versus Surgery and Radiation Alone for Cats with Vaccine-associated Sarcomas: 25 Cases (1995-2000). Journal of the American Veterinary Medical Association 218, no. 4 (2001) 547–550.

[16] Kobayashi T, Hauck ML, Dodge R, et al. Preoperative radiotherapy for vaccine associated sarcoma in 92 cats. *Vet Radiol Ultrasound* 2002;43:473-479.

[17] A. E.Hershey, K. U. Sorenmo, M. J. Hendrick, F. S. Shofer, and D. M. Vail. Prognosis for Presumed Feline Vaccine-associated Sarcoma After Excision: 61 Cases (1986-1996). Journal of the American Veterinary Medical Association 216, no. 1 (January 1, 2000) 58–61.

[18] K. Cronin, R. L. Page, G. Spodnick, R. Dodge, E. N. Hardie, G. S. Price, D. Ruslander, and D. E. Thrall. Radiation Therapy and Surgery for Fibrosarcoma in 33 Cats. Veterinary Radiology & Ultrasound: The Official Journal of the American College of Veterinary Radiology and the International Veterinary Radiology Association 39, no. 1 (February 1998) 51–56.

[19] E. Garanger, D. Boturyn, Z. Jin, P. Dumy, M.C. Favrot, J.L. Coll, New multifunctional molecular conjugate vector for targeting, imaging, and therapy of tumors. Mol Ther 12 (2005) 1168-1175.

[20] Z.H. Jin, V. Josserand, S. Foillard, D. Boturyn, P. Dumy, M.C. Favrot, J.L. Coll, In vivo optical imaging of integrin alphaV-beta3 in mice using multivalent or monovalent cRGD targeting vectors. Mol Cancer 6 (2007) 41.

[21] L. Sancey, S. Dufort, V. Josserand, M. Keramidas, C.A. Righini, C. Rome, A.C. Faure, S. Foillard, S. Roux, D. Boturyn, O. Tillement, A. Koenig, J. Boutet, P. Rizo, P. Dumy, J.L. Coll, Drug development in oncology assisted by noninvasive optical imaging. Int. J. Pharm. 379 (2009) 309-316.

[22] L. Sancey, E. Garanger, S. Foillard, G. schoen, A. Hurbin, C. Albiges-Rizo, D. Boturyn, C. Souchier, A. Grichine, P. Dumy, J.L. Coll, Clustering and Internalization of Integrin alphavbeta3 With a Tetrameric RGD-synthetic Peptide. Mol Ther 17 (2009) 837-843.

[23] E. Mery, E. Jouve, S. Guillermet, M. Bourgognon, M. Castells, M. Golzio, P. Rizo, J.P. Delord, D. Querleu, B. Couderc, Intraoperative fluorescence imaging of peritoneal dissemination of ovarian carcinomas. A preclinical study. Gynecologic oncology 122 (2011) 155-162.

[24] D.A. Heuveling, G.W. Visser, M. de Groot, J.F. de Boer, M. Baclayon, W.H. Roos, G.J. Wuite, C.R. Leemans, R. de Bree, G.A. van Dongen, Nanocolloidal albumin-IRDye 800CW: a near-infrared fluorescent tracer with optimal retention in the sentinel lymph node. European journal of nuclear medicine and molecular imaging 39 (2012) 1161-1168.

[25] Z.H. Jin, V. Josserand, J. Razkin, E. Garanger, D. Boturyn, M.C. Favrot, P. Dumy, J.L. Coll, Noninvasive optical imaging of ovarian metastases using Cy5-labeled RAFT-c(-RGDfK-)4. Mol Imaging 5 (2006) 188-197.

[26] Z.H. Jin, J. Razkin, V. Josserand, D. Boturyn, A. Grichine, I. Texier, M.C. Favrot, P. Dumy, J.L. Coll, In vivo noninvasive optical imaging of receptor-mediated RGD internalization using self-quenched Cy5-labeled RAFT-c(-RGDfK-)(4). Mol Imaging 6 (2007) 43-55.

[27] S.L. Troyan, V. Kianzad, S.L. Gibbs-Strauss, S. Gioux, A. Matsui, R. Oketokoun, L. Ngo, A. Khamene, F. Azar, J.V. Frangioni, The FLARE() Intraoperative Near-Infrared Fluorescence Imaging System: A First-in-Human Clinical Trial in Breast Cancer Sentinel Lymph Node Mapping. Ann Surg Oncol (2009).

[28] G. Themelis, J.S. Yoo, K.S. Soh, R. Schulz, V. Ntziachristos, Real-time intraoperative fluorescence imaging system using light-absorption correction. Journal of biomedical optics 14 (2009) 064012.

[29] D. Wachter, K. Kallenberg, A. Wrede, W. Schulz-Schaeffer, T. Behm, V. Rohde, Fluorescence-Guided Operation in Recurrent Glioblastoma Multiforme Treated with Bevacizumab-Fluorescence of the Noncontrast Enhancing Tumor Tissue? J Neurol Surg A Cent Eur Neurosurg (2012).

[30] T. Tykocki, R. Michalik, W. Bonicki, P. Nauman, Fluorescence-guided resection of primary and recurrent malignant gliomas with 5-aminolevulinic acid. Preliminary results. Neurol Neurochir Pol 46 (2012) 47-51.

[31]G.M. van Dam, G. Themelis, L.M. Crane, N.J. Harlaar, R.G. Pleijhuis, W. Kelder, A. Sarantopoulos, J.S. de Jong, H.J. Arts, A.G. van der Zee, J. Bart, P.S. Low, V. Ntziachristos, Intraoperative tumor-specific fluorescence imaging in ovarian cancer by folate receptor-alpha targeting: first in-human results. Nature medicine 17 (2011) 1315-1319.

[32]D.A. Benaron, W.F. Cheong, D.K. Stevenson, Tissue optics. Science 276 (1997) 2002-2003.

[33]R. Weissleder, C.H. Tung, U. Mahmood, A. Bogdanov, Jr., In vivo imaging of tumors with protease-activated near-infrared fluorescent probes. Nat Biotechnol 17 (1999) 375-378.

[34]X. Chen, E. Sievers, Y. Hou, R. Park, M. Tohme, R. Bart, R. Bremner, J.R. Bading, P.S. Conti, Integrin alpha v beta 3-targeted imaging of lung cancer. Neoplasia 7 (2005) 271-279.

[35]T. Sato, K. Konishi, H. Kimura, K. Maeda, K. Yabushita, M. Tsuji, A. Miwa, Vascular integrin beta 3 and its relation to pulmonary metastasis of colorectal carcinoma. Anticancer Res 21 (2001) 643-647.

[36]K.R. Gehlsen, G.E. Davis, P. Sriramarao, Integrin expression in human melanoma cells with differing invasive and metastatic properties. Clin Exp Metastasis 10 (1992) 111-120.

[37]R.E. Seftor, E.A. Seftor, K.R. Gehlsen, W.G. Stetler-Stevenson, P.D. Brown, E. Ruoslahti, M.J. Hendrix, Role of the alpha v beta 3 integrin in human melanoma cell invasion. Proc Natl Acad Sci U S A 89 (1992) 1557-1561.

[38]C.L. Gladson, D.A. Cheresh, Glioblastoma expression of vitronectin and the alpha v beta 3 integrin. Adhesion mechanism for transformed glial cells. J Clin Invest 88 (1991) 1924-1932.

[39]M. Rolli, E. Fransvea, J. Pilch, A. Saven, B. Felding-Habermann, Activated integrin alphavbeta3 cooperates with metalloproteinase MMP-9 in regulating migration of metastatic breast cancer cells. Proc Natl Acad Sci U S A 100 (2003) 9482-9487.

[40]W.B. Morrison, R.M. Starr, Vaccine-associated feline sarcomas. J Am Vet Med Assoc 218 (2001) 697-702.

[41]W.B. Morrison, Environmental Causes of Naturally Occurring Cancers in Dogs and Cats., in: T.W.W. Co., (Ed.), Cancer in Dogs and Cats: Medical and Surgical Management, Philadelphia: , 1998, pp. 31 - 41.

[42]E.P. Spugnini, A. Baldi, B. Vincenzi, F. Bongiorni, C. Bellelli, G. Citro, A. Porrello, Intraoperative versus postoperative electrochemotherapy in high grade soft tissue sarcomas: a preliminary study in a spontaneous feline model. Cancer chemotherapy and pharmacology 59 (2007) 375-381.

Figures

Figure 1

Figure 2

A

In vivo

Group 1: 0.6 mg/kg; 16h
Group 2: 0.3 mg/kg; 16h
Group 3: 0.3 mg/kg; 24h
Group 4: 0.3 mg/kg; 36h
Group 5: 0.15 mg/kg; 36h
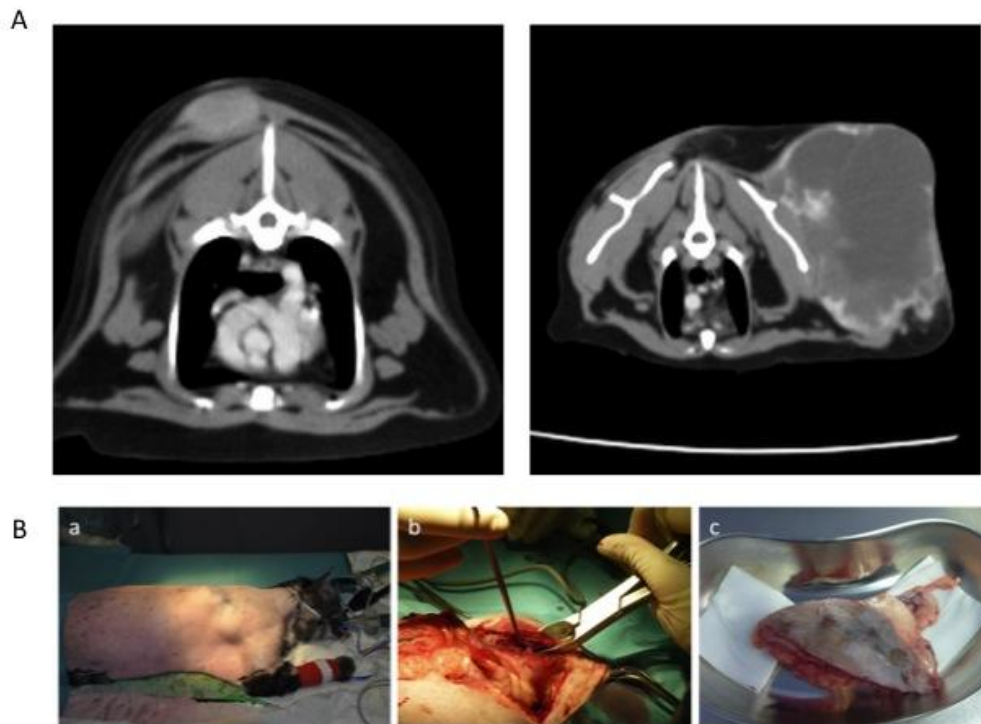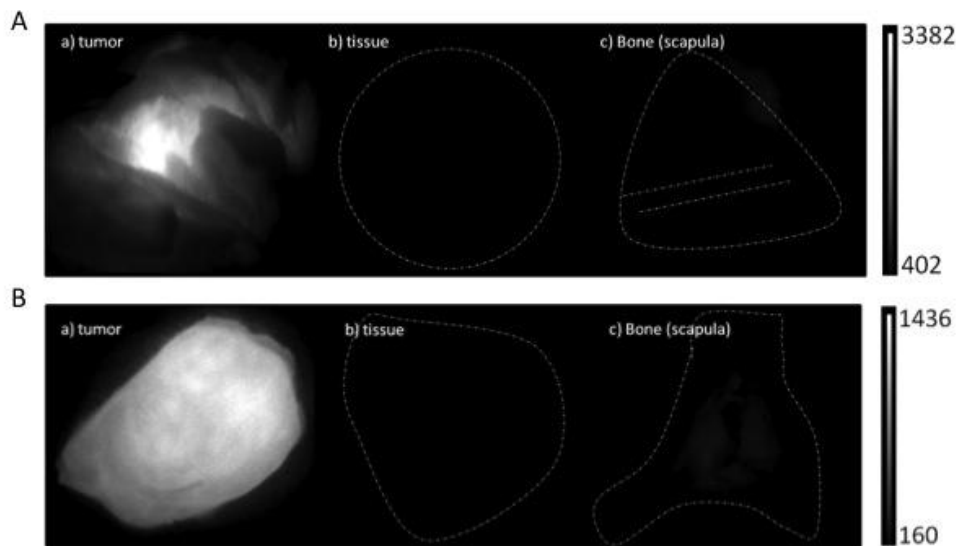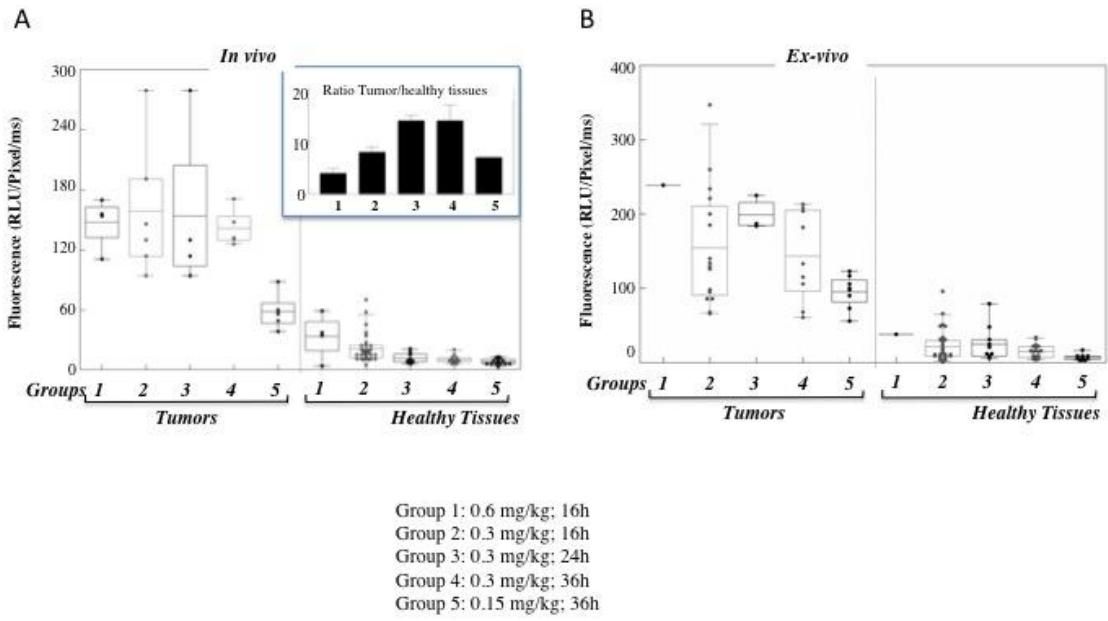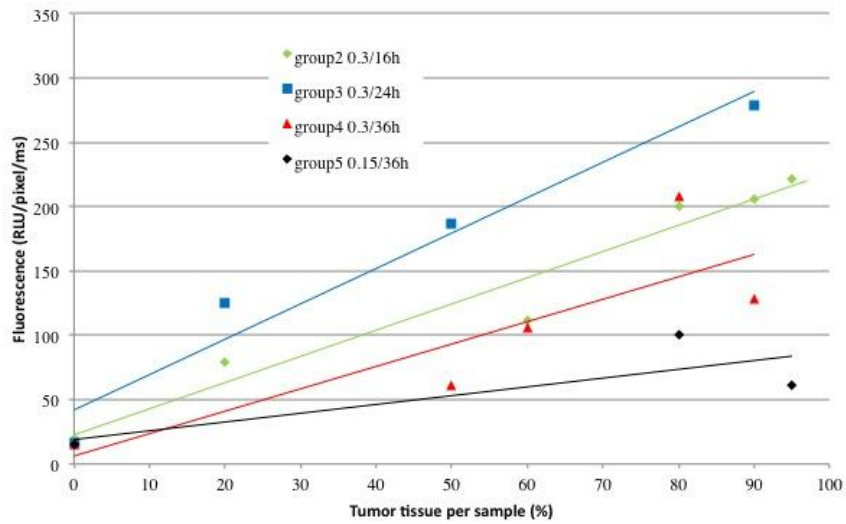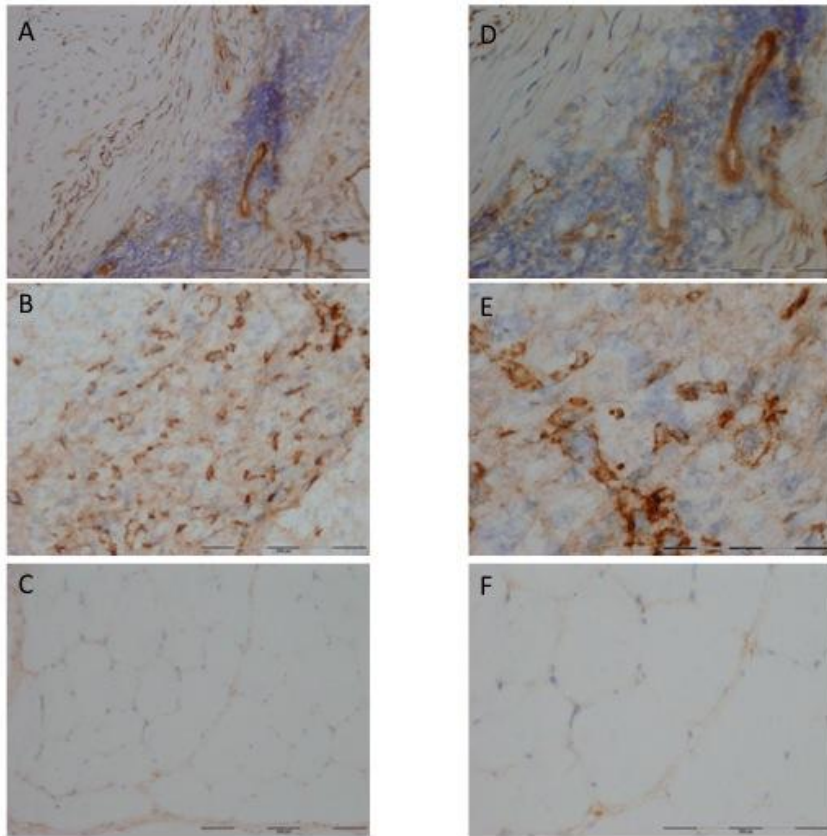
Figure 3

Figure 4

Figure 5
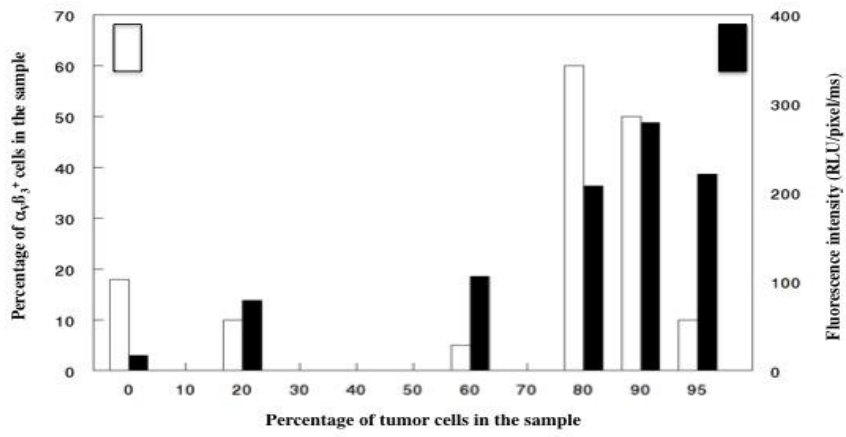
Figure 6

Supplementary data

Preliminary toxicological study in cats

The aim of this preliminary toxicological cat study was the evaluation of potential acute effects caused by the administration of a single intravenous dose of AngioStamp™.

Therefore, three cats were tested with increasing doses, i.e., 0.9, 2.4 and 4.5 mg/kg, which correspond to 1X, 3X and 5X imaging doses to estimate the doses used for imaging mice and rats.

Before and after injection, the cats were under medical control and were surveyed by haematological parameters including total blood cell count, WBC fractions, the RBC fraction, MCH, MCV, MCHC, Urea, Creatinine, ALT and PAL, a blood ionogram (Cl, K, Na) and the evaluation of the RPCU of the urine (urinary protein/creatinine ratio). These parameters were chosen as a control for the direct toxicological response and the control of kidney clearance, as the trace is eliminated via the renal pathway.

At the same time, a follow-up of the physiological status of the animal was performed by auscultation, checking of the pulse, examination of the cornea reflex, capillary refill and the general comportment of the cat.

These parameters were determined from the time of injection (T0) to 7 days post-injection.

After placing a catheter in the right jugular vein, blood samples were directly withdrawn before administration of AngioStamp™ (T0) and subsequently at 5 min, 15 min, 30 min, 1 h, 2 h, 4 h, 5 h 30, 24 h and 7 days after injection. The urine samples of approximately 5 mL were obtained via a steady urine catheter at the same time as the blood withdrawal took place.

Biochemical analyses of the blood and urine took place at T0, 5 h 30, 24 h and 7 days (except urine).

Results/ Conclusion:

We could not observe any adverse effects due to the administration of the intravenous application of AngioStamp™ at the 0.9, 2.4 and 4.5 mg/kg doses, which corresponds to the estimated single dose and three times and five times this dose.

Physical examination did not reveal any aberrations, and the biochemical parameters measured in the blood and the urine confirmed that a single AngioStamp™ administration at the tested doses does not lead to visible toxic effects in the cats, as there were no observed changes in the physiological parameters.
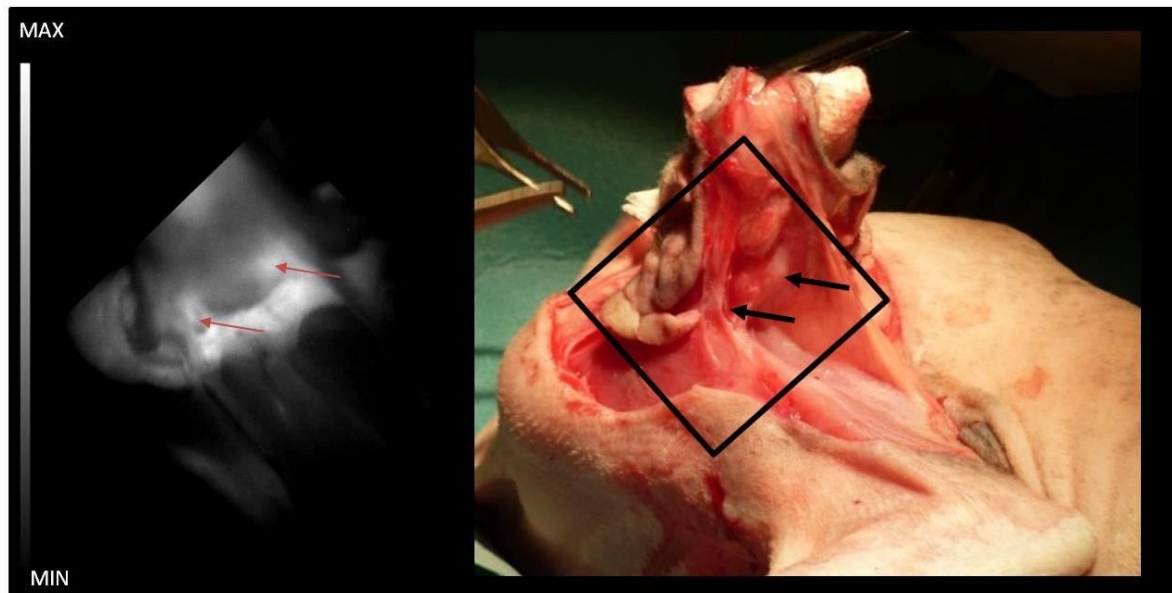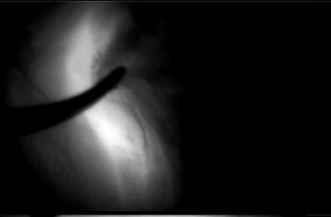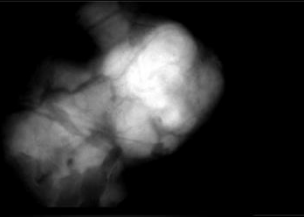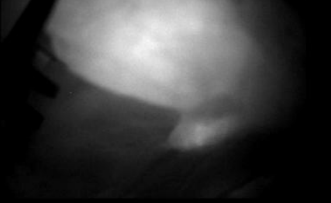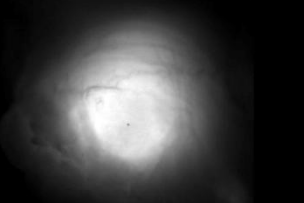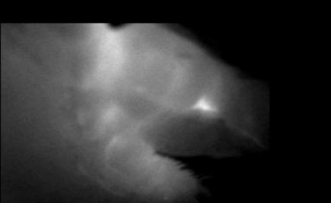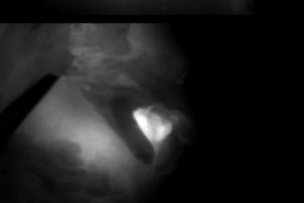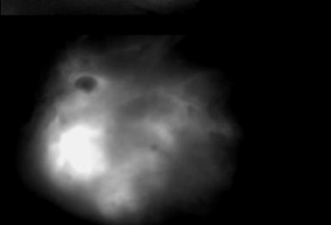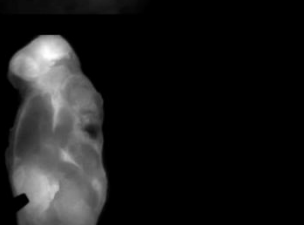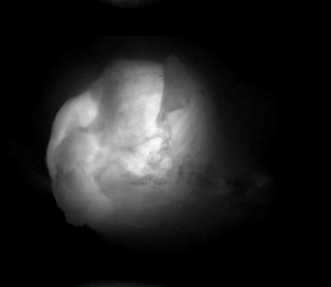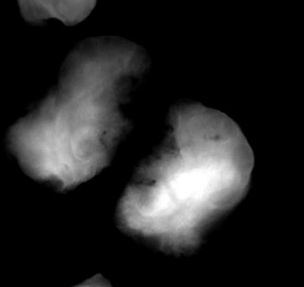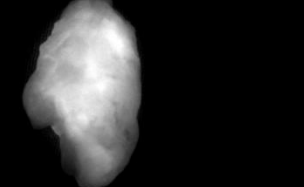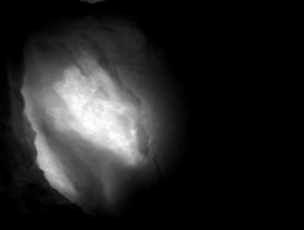
Image of the surgical field: on the left the fluorescent image during tumour resection (group 4; 0.3 mg/kg; surgery at 36 hours after injection of AngioStamp™) with its corresponding site on the photography on the right. The arrows are orientation points.

Patient & date of surgery	AngioStamp®800 (mg/kg)	Surgery (h p.i.)	Tumor location & health status (before surgery)	Weight (kg)	age (years) & sex	Color/ race	Remarks follow-up
1)" Sally " June 2011	0.6	16	Right shoulder & axillar region, anaemic	3.9	10; ♀	Tri-color/ ESH	n.r. until June 2012
2) "Sunny" June 2011	0.3	16	Left shoulder; n.r.*	2.8	11 ; ♀	Grey striped / ESH	n.r. until June 2012
3) "Mousse " 21/09/2011	0.3	16	right side of thorax; n.r.*	4.4	12; ♀ castrated	Tri-color/ ESH	n.r. until June 2012
4) " Lilou " October 2011	0.3	16	Left shoulder & axillar region until height of diaphragm;n.r. *	6.5	7; ♀	white/ ESH	n.r. until June 2012
5) "Comette" October 2011	0.3	24	Right shoulder incl. scapula; Tumor necrotic; lung-metastases	3.6	13; ♀	black / ESH	n.r. until June 2012
6) "Toundra " Oktober 2011	0.3	16	right side of thorax; n.r.*	3.2	9 ; ♀	Tri-color / ESH	n.r. until June 2012
7) " Pepper " November 2011	0.3	24	Dorsal (column vertebral, thoracal) n.r. *	5.7	9; ♀	Tri-color / ESH	n.r. until June 2012
8) "Chouchou" February 2012	0.3	36	Dorso-lateral dexter (scapula & column vertebral); 3rd surgery (= 2nd relaps)	8.2	8; ♂ castrated	Light-coloured grey-striped / ESH	† (relaps & metastases) ?
9) "Aragorn" February 2012	0.3	36	Dorsal (column vertebral, thoracal) n.r. *	5.8	8; ♂	gray- black striped / ESH	n.r. until June 2012
10) " Kochka " March 2012	0.15	36	Left shoulder; Amputation of left front leg; n.r.*	4.9	11.5; ♀ castrated	Black / ESH	n.r. until June 2012
11) "Nickdouille La Fripouille" March 2012	0.15	36	1) Left shoulder, necrotic; 2) right shoulder; n.r.*	3.8	10; ♂	Red-black striped / ESH	n.r. until June 2012
12) "Isis" March 2012	0.3	36	Rezidive, tumor left shoulder;	6.4	9; ♀	Red-black striped / ESH	† (not awakened after surgery, cause not known) ????
			n.r. *= no remarks			ESH = european short hair	

Group	Patient	Fluorescence *in vivo* (surgery) Auto-LUT	Fluorescenec *ex vivo* (sample) Auto-LUT
Group 1 (0.6mg/kg; surgery 16 hours after injection)			
Group 2 (0.3mg/kg; surgery 16 hours after injection)			
Group 3 (0.3mg/kg; surgery 24 hours after injection)			
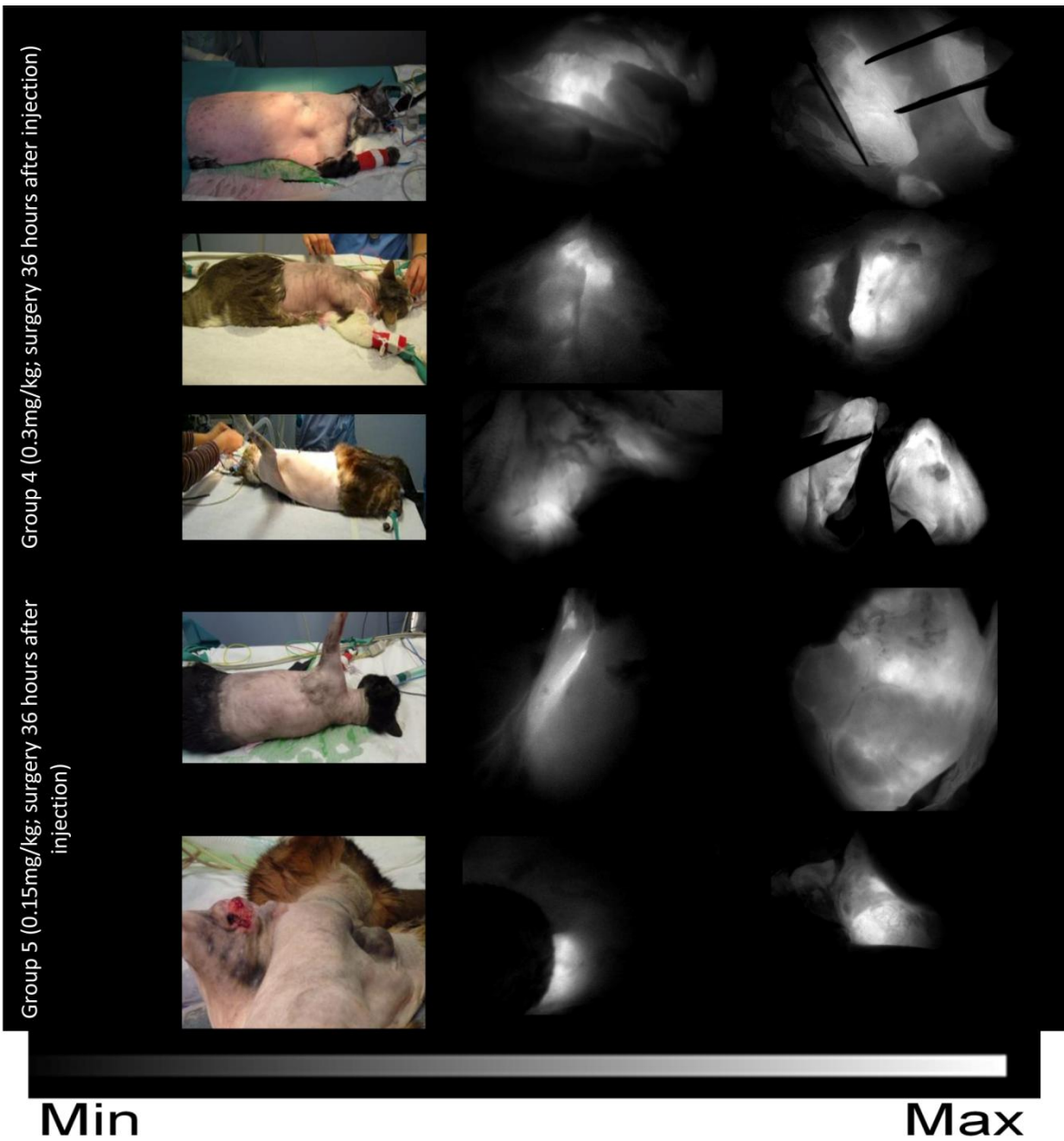
Figure : Photographies of the patients and fluorescence images during surgery and of the excised tumor sample. The LUT is not adapted but left on auto-adjust (auto-LUT).

I.4.1.   Surgery of group 6

The tumor-to-muscle ratio of the sixth group (0.15 mg/kg at 24 h) confirmed the results presented in the publication, since:

➢ The tumor signal was as elevated as in group 5, receiving the same dose but at 36 h before surgery;

➢ The signal in healthy tissues was slightly more elevated than in group 5 (Figure I-11);

➢ Finally the tumor-to-background (healthy tissue) ratio was not significantly improved (ratio of 10) (Figure I-12).

Group	AngioStamp™ (mg / kg)	Time of surgery post injection (hours)	Number of animals (n)
1	0.6	16	1
2	0.3	16	4
3	0.3	24	2
4	0.3	36	3
5	0.15	36	2
6	0.15	24	2
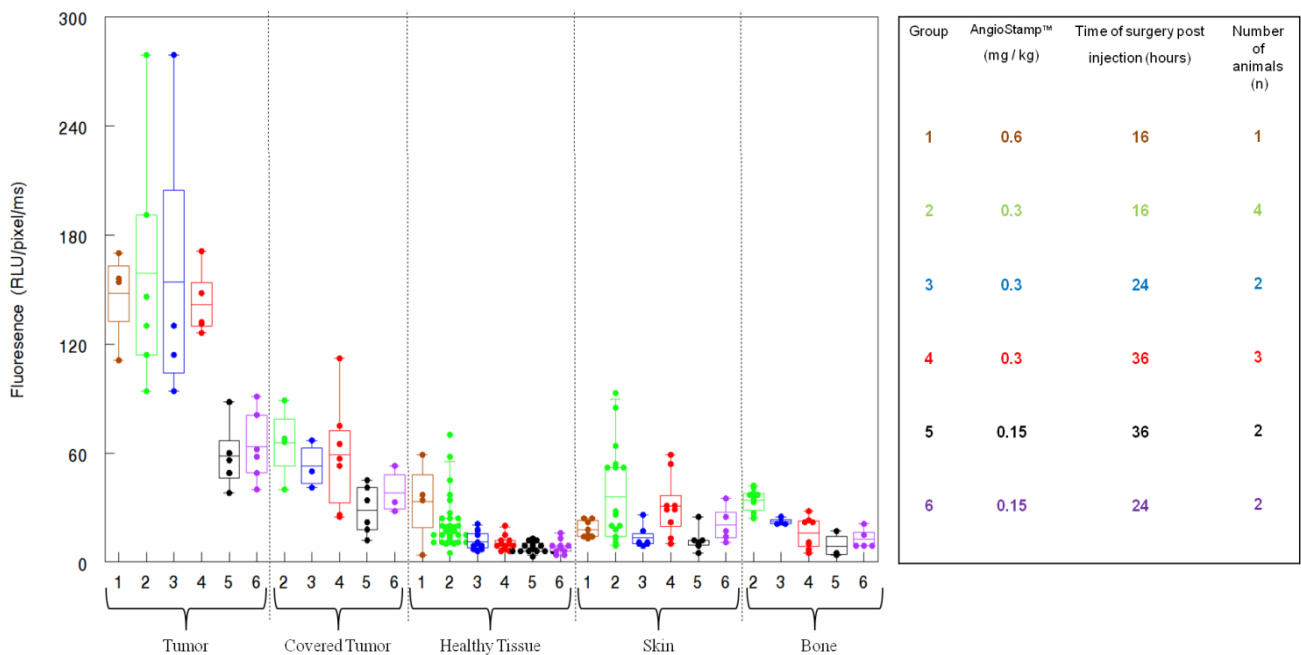
Figure I-11: Fluorescence intensity compared during surgery of all 6.
Each point corresponds to a specific measurement. The Box-Whisker represents the mean of each group, their maximum and minimum value and the interquartile range.

Ratio Tumor / Healthy Tissue
in vivo
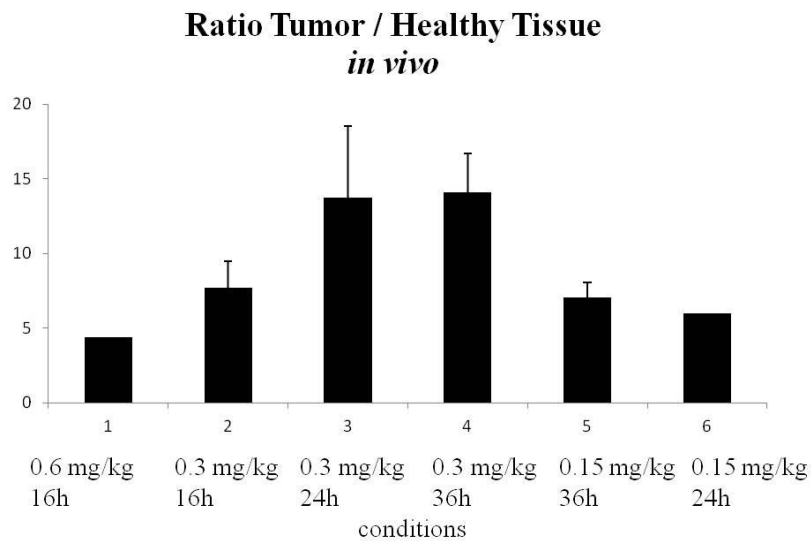
Figure I-12: Tumor-to-healthy tissue ratio of all 6 groups during surgery.

Thus, the results obtained with the two additional cats studied in group 6 did not change our global conclusion that the best dose of AngioStamp™ was at 0.3 mg/kg injected 36 h before surgery.

I.4.2.   *Dealing with the autofluorescence and "auto-LUT" during surgery*

Normally, The Fluobeam™ functions with enabled "auto-LUT". The LUT (Lookup table) is used to improve the visual presentation of an image on the screen. The 16-bit camera provides 65,536 gray level images. If the LUT signal is adjusted automatically, the sample will always appear "fluorescent" on the screen, even if it is negative. In contrast, if the LUT is fixed in order to provide the best visualization of the brightest areas, then negative signal will not be "visible" on the screen anymore. In the example of Figure I-13, the LUT is fixed on [0 – 3893], which corresponded to its best adjustment to the positive tumor sample. We can see that in these conditions, normal tissues are negative. This is not true on the bottom panel, in which the auto-LUT was turned enabled. In this case, it presents a confusing signal on normal tissues.
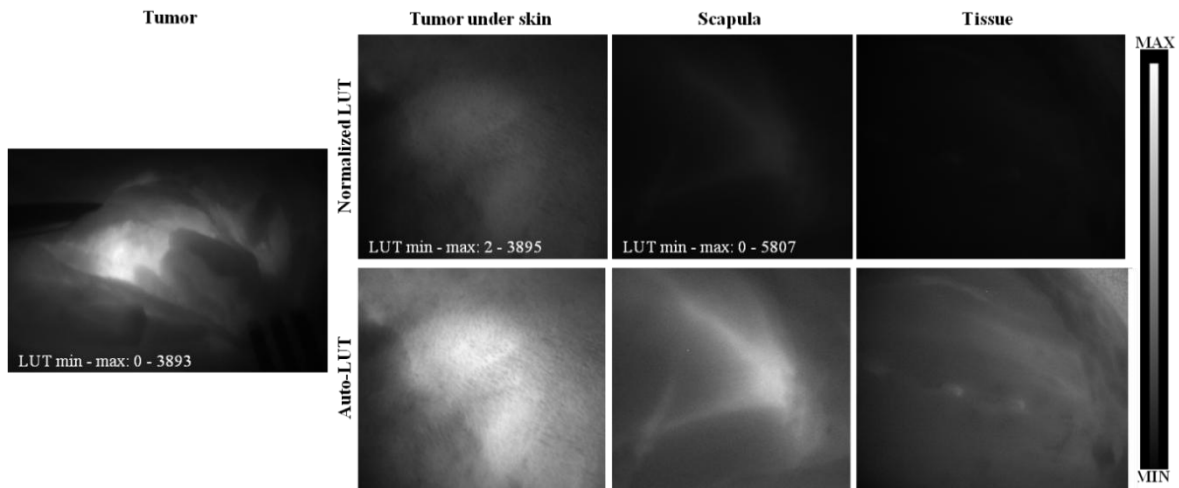
Figure I-13: Tumor-signal normalized LUT of different tissues compared to their Auto-LUT images.

I.4.3.   *Good positioning of the camera during surgery*

As expected, the vertical positioning of the Fluobeam™ on a given spot can dramatically change the quality of the recorded signal. The laser beam must be centered on the sample, as demonstrated in Figure I-14, if semi quantification is the issue.
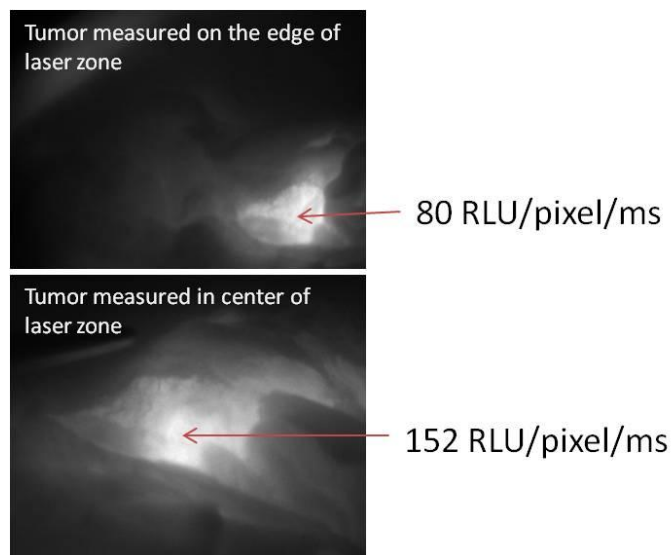
Figure I-14: Difference in measured fluorescence intensity dependent on the placement towards the central laser beam.

I.5.   *General conclusion*

As demonstrated, the fluorescent tracer AngioStamp™ does neither show any visible toxicological effect, nor side-effects until one year after injection.

In the clinical set-up, we found that the best tumor-to-healthy tissue ratio is at 0.3 mg/kg and surgery 36 h after injection. By lowering the dose, not all receptors are saturated, as we observed when using 0.15 mg/kg. Leaving less time between injection and surgery, not all non-specifically bound or circulating molecules are evacuated by the organism. This reduces the tumor-to-healthy tissue ratio as seen in the first three groups tested.

At the same time we demonstrated that training is important for appropriate handling of the Fluobeam™ imaging system as well as for correct image analysis and interpretation. The Fluobeam™ works with an auto adaptation of the LUT, which leads to the impression of false positive signal. Another result showed that the signal obtained was not reliable also when either the image was not correctly focused or if the measurement was made on the edge of the laser light cone.

As a general conclusion, we found that this system present enough interest to be used in surgery. Indeed, the intensity of the fluorescent signal can help the surgeon to detect low levels of tumor infiltration in normal tissues. However, this signal may not always be associated with the reactivity of the LM609 anti-human integrin in cats.

These results are extremely promising and justify the translation of this method in the clinics.

II. GELOFUSIN STUDY

As demonstrated in mice and cats, the RAFT-RGD peptide (and its fluorescent derivative AngioStamp™) is eliminated *via* the kidneys where it is strongly accumulated. This has several consequences that may limit its application in humans:

➢ Elevated risk of renal toxicity when RAFT-RGD is labeled with a radionuclide, or a drug.

➢ When fluorescent RAFT-RGD accumulates in kidneys, this will mask a possible signal within or beside this organ and thus limit its interest for the surgery of the peritoneal cavity.

Therefore, we decided to test different possibilities in order to decrease the RAFT-RGD accumulation in kidneys. This was performed in collaboration with the team of Pr C Ghezzi. We used RAFT-RGD-A700 (AlexaFluor®700) in parallel with radiolabeled ^{111}In-DOTA-RAFT-RGD to study the impact of Gelofusin pre-/treatment of mice.

In normal kidneys, reabsorption of filtered proteins occurs almost exclusively by receptor-mediated endocytosis in the proximal tubules. The efficient reabsorption of proteins in the primary urine is mediated by megalin-driven reabsorption of nearly all filtered plasma proteins in cooperation with the receptor protein cubilin, leading to receptor-mediated endocytosis in the proximal tubule[225]. As the megalin system was shown to be essential for kidney uptake of radiolabeled somatostatin analogs, interventions at the megalin level presented interesting potential targets for renal protection during peptide receptor radionuclide therapy[226].

Gelofusin is a gelatin-based plasma expander, playing a role in the Megalin/Cubilin system. Gelofusin is known to inhibit proximal tubular reabsorption[227].

---

[225]Christensen, Erik I, Henrik Birn, Tina Storm, Kathrin Weyer, und Rikke Nielsen. „Endocytic receptors in the renal proximal tubule". *Physiology (Bethesda, Md.)* 27, Nr. 4 (August 2012): 223–236.

[226]Rolleman, Edgar J, Marion de Jong, RoelfValkema, DikKwekkeboom, BoenKam, und Eric P Krenning. „Inhibition of kidney uptake of radiolabeled somatostatin analogs: amino acids or gelofusine?" *Journal of nuclear medicine: official publication, Society of Nuclear Medicine* 47, Nr. 10 (Oktober 2006): 1730–1731; author reply 1731.

[227]Gerritsen, Karin G., Hilde P. Peters, Tri Q. Nguyen, Maarten P. Koeners, Jack F. Wetzels, Jaap A. Joles, Erik I. Christensen, u. a. „Renal Proximal Tubular Dysfunction Is a Major Determinant of Urinary Connective Tissue Growth Factor Excretion". *American Journal of Physiology - Renal Physiology* 298, Nr. 6 (Januar 6, 2010): F1457–F1464.

Thus, regarding its importance in the tubular reabsorption of peptides and the fact that preinjection of Gelofusin was described to efficiently reduce renal retention of peptides, we tested its capacity of reducing the renal retention of RAFT-RGD-based molecules.

The study showed that indeed Gelofusin pretreatment of tumor-bearing mice was associated with a reduction of RAFT-RGD-A700 (AlexaFluor®700) as well as radiolabelled ^{111}In-DOTA-RAFT-RGD capture in the kidneys.

Reduction of renal uptake of ^{111}In-DOTA-labeled and A700-labeled RAFT-RGD during integrin αvβ3 targeting using single photon emission computed tomography and optical imaging

Arnaud Briat,[1,2,8] Christiane H. F. Wenk,[2,3,4,8] Mitra Ahmadi,[1,2] Michael Claron,[2,5] Didier Boturyn,[2,5] Véronique Josserand,[2,3,4] Pascal Dumy,[2,5] Daniel Fagret,[1,2,6] Jean-Luc Coll,[2,3] Catherine Ghezzi,[1,2] Lucie Sancey[2,3,7] and Jean-Philippe Vuillez[1,2,6]

[1]INSERM U877, Radiopharmaceutiques Biocliniques, Grenoble; [2]Université Joseph Fourier, Grenoble; [3]INSERM U823, Institut Albert Bonniot, Grenoble; [4]OPTIMAL, Small Animal Optical Imaging Platform, Grenoble; [5]UMR CRNS/UJF 5250, Grenoble; [6]CHU de Grenoble, La Tronche, France

Integrin αvβ3 expression is upregulated during tumor growth and invasion in newly formed endothelial cells in tumor neovasculature and in some tumor cells. A tetrameric RGD-based peptide, regioselectively addressable functionalized template-(cyclo-[RGDfK])4 (RAFT-RGD), specifically targets integrin αvβ3 *in vitro* and *in vivo*. When labeled with indium-111, the RAFT-RGD is partially reabsorbed and trapped in the kidneys, limiting its use for further internal targeted radiotherapy and imaging investigations. We studied the effect of Gelofusine on RAFT-RGD renal retention in tumor-bearing mice. Mice were imaged using single photon emission computed tomography and optical imaging 1 and 24 h following tracer injection. Distribution of RAFT-RGD was further investigated by tissue removal and direct counting of the tracer. Kidney sections were analyzed by confocal microscopy. Gelofusine significantly induced a >50% reduction of the renal reabsorption of ^{111}In-DOTA-RAFT-RGD and A700-RAFT-RGD, without affecting tumor uptake. Injection of Gelofusine significantly reduced the renal retention of labeled RAFT-RGD, while increasing the tumor over healthy tissue ratio. These results will lead to the development of future therapeutic approaches. (*Cancer Sci* 2012; 103: 1105–1110)

I t has been proposed that RGD-based peptides selectively target tumor neovasculature through αvβ3 integrin recognition.[1–4] In previous studies, we highlighted the specific targeting of tumors expressing αvβ3 in mice by a tetrameric RGD-peptide named RAFT-c[-RGDfK-]4, or regioselectively addressable functionalized template-(cyclo-[RGDfK])4 (RAFT-RGD).[5,6] This hydrophilic peptide-based compound (approximately 5 kDa) is highly specific, can be labeled with radionuclide[7–10] or fluorescence,[11–13] and is mainly eliminated by the kidneys. We therefore proposed RAFT-RGD as a potent tumor targeting agent for cancer diagnosis and therapy (internal targeted radiotherapy (ITRT) or drug-based therapy). However, we reported that approximately 30–50% of the total dose of RAFT-RGD labeled with technetium (^{99m}Tc) or indium-111 (^{111}In) remained trapped in the kidneys 24 h after injection (see Ahmadi *et al.* for biodistribution at 1, 4, 24, and 48 h).[7,10] Other studies also reported that the tetramerisation of RGD-tracers enhanced renal uptake, compared with monomers.[14] Such pharmacokinetic behavior could impair the optimal therapeutic dosing of the compound in patients.

Following glomerular filtration, peptides are reabsorbed and endocytosed by the tubular proximal cells into lysosomes for proteolytic digestion. Metabolized peptides are released into the bloodstream, whereas in the case of radiolabeled peptides,

radiometal chelated amino acids might been retained in the tubular cells, leading to high delivered dose, radiation-induced toxicity, and subsequent side-effects (nausea, hyperkalemia).[15] In the present case, part of the native and metabolized forms of radiolabeled ^{111}In-DOTA-RAFT-RGD, as well as fluorescent RAFT-RGD, is reabsorbed by the proximal tubules and retained in tubular cells, for at least 4 days postinjection. Such a long retention in patients under ITRT would leave the kidneys exposed to high energy radiations (90-Yttrium or 177-Lutetium), and might also generate a weak imaging contrast for tumors surrounding the kidneys.

To reduce the renal reabsorption of radiolabeled peptides or small molecules, a possible approach consists of interfering with the receptor-mediated endocytosis pathway at the membrane of the proximal tubule cells. The megalin/cubilin system has been described to play an important role among the different receptors involved in the tubular reabsorption of peptides.[16,17] Megalin is a multiligand receptor belonging to the low density lipoprotein (LDL)-receptor family. It is expressed on the apical border of renal proximal tubules as well as in the glomeruli. This receptor is a high-capacity transport system implicated in the reabsorption of vitamin D binding protein, albumin, β2- and α1-microglobulin, and several hormones.[16,18] Among the gelatin-based plasma expenders, that is, Voluven (hydroxyethylamidon; Fresenius Kabi, Paris, France), Heamaccel (Behring, Marburg, Germany), and Gelofusine (B. Braun Medical, Boulogne Billancourt, France), the latter consists of succinylated bovine gelatine molecules, a mixture of collagen-derived peptides, and is used in clinical emergency units. Infusion of Gelofusine has been reported to increase the renal excretion of megalin ligands.[19,20] For example, pre-injection of Gelofusine was described to efficiently reduce renal retention of somatostatin analogues by approximately 40%.[21] Similarly, Gelofusine infusions also lead to a decrease in the retention of radiolabeled compounds in the cortical proximal tubules. Thus, the total radiation delivered in the kidneys is reduced, through the increased urine elimination of the radioactive compound.

In the present study, we evaluated the effect of Gelofusine on renal reabsorption of fluorescent RAFT-RGD or radiolabeled ^{111}In-DOTA-RAFT-RGD in tumor-bearing mice using single

---

photon emission computed tomography (SPECT) and fluorescence imaging, to maximize tumor-to-background ratio during diagnostic imaging and to minimize radiation-induced nephrotoxicity during future ITRT settings with ^{90}Y-DOTA-RAFT-RGD. In this study, the effect of Gelofusine injection with radiolabeled or fluorescent RAFT-RGD on renal reabsorption and tumor uptake was investigated in $\alpha_v\beta_3$-positive tumor-bearing mice.

Materials and Methods

RGD-peptide synthesis and radioactive/fluorescent labeling. The different compounds were synthesized according to previously reported procedures.[5,22] Four copies of the c[-RGDfK-] peptide were grafted onto the upper face of the cyclic decapeptide RAFT backbone. On the opposite side, the radiolabeling with ^{111}In was possible due to the presence of a DOTA group. The radiolabeling was carried out as previously described.[7] For optical imaging experiments, the fluorescent AlexaFluor700 (A700) mono N-hydroxysuccinimide ester (Amersham Biosciences, Uppsala, Sweden) was grafted at a lysine side-chain, as previously described.[22]

Cell lines and culture conditions. Murine mammary carcinoma TS/A-pc cells were cultured in RPMI medium supplemented with 10% FCS. The cell line HEK293(β_3) is a stable human embryonic kidney cell line (HEK293) stably transfected with the human β_3 integrin that was cultured as described in Jin et al.[12] in DMEM supplemented with 1% glutamine, 10% FBS, and 700 μg/mL Geneticin (G418 sulfate; Gibco, Paisley, UK). All cell lines were cultured at 37°C in a humidified 95% air/5% CO$_2$ atmosphere. Cells described here are integrin $\alpha_v\beta_3$ positive.

In vivo imaging. Five- to six-week-old female NMRI nude mice were obtained from Janvier (Laval Le Genest, France). The animals were housed for 1 week prior to tumor cell administration with free access to water and standard or weakly fluorescent rodent food. All the experiments described in this study were approved by the Animal Care and Use Committee of the ComEth38 (Grenoble, France) (authorization #2010_57_IAB-U823-SL-05), and the experiments were carried out under the supervision of authorized individuals (L. Sancey, DDPP authorization #38 05 32 and A. Briat, DDPP authorization #38 74 23). Briefly, 10^6 TS/A-pc or 10^7 HEK293(β_3) cells (in 100 μL PBS) were injected s.c. in the right flank of mice. Once tumors reached approximately 200 mm^3, the animals were anesthetized by isoflurane (CSP, Cournon, France) 4% for induction and 2% thereafter.

Nuclear imaging. Twenty-four tumor-bearing mice were distributed in four groups (n = 6/group). Each received a tail vein injection of 4 μg ^{111}In-DOTA-RAFT-RGD (12 MBq). Gelofusine 4% or PBS was either pre- or co-injected with the tracer as follows: Group 1, co-injection (120 μL mix) of 4 mg Gelofusine (100 μL) and 12 MBq ^{111}In-DOTA-RAFT-RGD (20 μL); Group 2, co-injection (120 μL mix) of 12 MBq ^{111}In-DOTA-RAFT-RGD (20 μL) and PBS (100 μL); Group 3, pre-injection of 4 mg of Gelofusine (100 μL) 3 min prior to 12 MBq ^{111}In-DOTA-RAFT-RGD (100 μL); and Group 4, pre-injection of PBS (100 μL) 3 min prior to 12 MBq ^{111}In-DOTA-RAFT-RGD (100 μL).

At 1 and 24 h following tracer injection, animals were imaged using a small animal SPECT imaging camera (Nano-SPECT/CT; Bioscan, Washington, DC, USA) and whole-body SPECT/CT tomographic images were acquired (four detectors, nine-pinhole settings). Briefly, mice under general anesthesia were placed into an imaging cassette allowing full control of gas anesthesia and temperature (Minerve Anaesthesia; Minerve, Esternay, France). The CT and SPECT images were acquired sequentially using Nucline software (Mediso, http://www.mediso.hu/). The CT parameters were: 240 projections;

500 ms per projection; and 55 kV. The SPECT parameters were: 24 projections; and 80–100 s per projection. Reconstruction of SPECT images was carried out using HiSPECT NG (Bioscan). Reconstruction of CT images (Exact Cone Beam algorithm and Shepp Logan filter) and SPECT/CT image co-registration were carried out using InVivoScope 1.42 software (Bioscan). Animals were euthanized following the 24 h time point acquisition, and tissues were collected and weighed. Radioactivity was directly counted using a gamma counter (Berthold, Thoiry, France).

Optical imaging. Two hundred microliters of A700-RAFT-RGD (i.e. 10 nmol dye/mouse) was injected i.v. as described in the previous section, 2–5 min after i.v. injection of 100 μL Gelofusine 4% (n = 3/group, pre-injection). One to 24 h after injection, anesthetized animals were imaged by the Fluobeam-700 device (Fluoptics, Grenoble, France) as previously described.[23] Twenty-four hours after injection, mice were euthanized and organs were collected for ex vivo fluorescence imaging. Organs were illuminated by 660-nm light-emitting diodes equipped with interference filters. Fluorescence images as well as black and white pictures were acquired by a back-thinned CCD camera at −80°C (ORCAII-BT-512G; Hamamatsu, Massy, France) fitted with a colored glass high-pass RG 9 filter (Schott, Clichy, France).

Kidney section analysis. Confocal microscopy of thin kidney sections (7 μm) was carried out on an LSM710 LNO confocal microscope (Carl Zeiss, Jena, Germany) using a 40× oil immersion objective of 1.0 N.A. The 633-nm laser intensity was set up at 3% of its maximum intensity.

Statistical analysis. Statistical analysis was carried out using Statview software (SAS Institute, San Francisco, CA, USA). Tissue uptakes and ratios were compared using an unpaired t-test. A P-value ≤ 0.05 was considered as significant.

Results

Influence of Gelofusine on RAFT-RGD distribution: ex vivo biodistribution by direct gamma counting. Radiolabeled RAFT-RGD has been used to specifically target integrin $\alpha_v\beta_3$ in vitro and in vivo. In tumor-bearing mice, ^{111}In-DOTA-RAFT-RGD was mainly and rapidly cleared through the renal route. The amount of ^{111}In-DOTA-RAFT-RGD was <1% of injected dose per gram (%ID/g) in most of the organs, 1 h after injection, except in the tumor expressing integrin $\alpha_v\beta_3$ and in the kidneys. As shown in Figure 1, pre- and co-injection of Gelofusine strongly reduced the uptake of RAFT-RGD in the kidneys, as well as in urine; as described in other published reports, the amount of radiotracer in the kidneys was reduced, through the increased renal elimination of the radioactive compound. As the urine was collected at the end of the experiment (i.e. 24 h after injection), the remaining %ID/g of urine was very low in both conditions, with a significant difference in favor of Gelofusine, as expected. Pre-injection and co-injection of Gelofusine strongly reduced the activity in the kidney by 49.2% and 47.9%, respectively (P = 0.002 and P < 0.0001) (Fig. 1A). The presence of radioligand in the blood was comparable in the presence or absence of the plasma expender. Muscle uptake of ^{111}In-DOTA-RAFT-RGD was decreased by 10% in the presence of Gelofusine, whereas tumor uptake was not significantly affected (4.4% decrease with Gelofusine pre-injection, 16.4% increase with Gelofusine co-injection; P > 0.05, not significant [NS]). Similar results were obtained with the fluorescent A700-RAFT-RGD (Fig. 1B). Pre-injection of Gelofusine reduced A700-RAFT-RGD kidney uptake by 63% (P < 0.01) and tumor uptake was not significantly affected (P > 0.05, NS).

Influence of Gelofusine on RATF-RGD distribution: Non-invasive in vivo imaging. Non-invasive SPECT-CT imaging was used
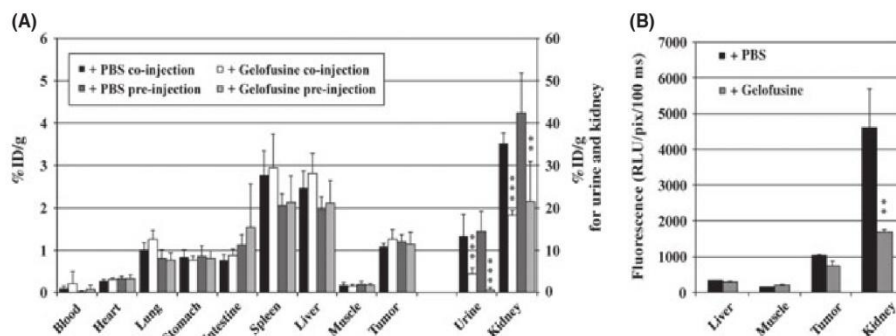
Fig. 1. Influence of Gelofusine on RAFT-RGD labeled with 111-indium (A) or A700 (B) biodistribution. (A) Mice were euthanized 24 h after i.v. injection of labeled RAFT-RGD, with preliminary injection of PBS or Gelofusine. Gelofusine significantly reduced renal and urine activities of ^{111}In-DOTA-RAFT-RGD. The results are expressed as the percentage of injected dose per gram of organ (%ID/g). (B) Similar results were obtained with pre-injection of Gelofusine (gray) before A700-RAFT-RGD. The results are expressed as the mean of the relative light unit (RLU) per pixel. **$P < 0.01$, ***$P < 0.001$, Gelofusine versus PBS.

to quantify the reduction of renal uptake and the effect of Gelofusine on the tumor imaging contrast, that is, tumor-to-contralateral muscle (T/M) and tumor-to-kidney (T/K) ratios (Fig. 2). In the kidneys, ^{111}In-DOTA-RAFT-RGD was mainly localized in the renal cortex, as shown in Figure 2(A). In the presence of Gelofusine, this renal capture was also localized in the cortex but was highly reduced (Fig. 2B). Optical imaging confirmed the reduction of fluorescent RAFT-RGD into kidney after Gelofusine injection, as shown in Figure 3. In both experimental conditions, tumors expressing integrin $\alpha_v\beta_3$ were seen (Fig. 2, bottom right panels). Quantitative values were obtained from the imaging experiments (Table 1). One hour after RAFT-RGD injection, the T/K ratio was significantly reduced in nuclear (0.06 ± 0.01 for PBS vs 0.16 ± 0.02 for Gelofusine; $P < 0.05$) and optical imaging (0.66 ± 0.13 for PBS vs 1.24 ± 0.26 for Gelofusine; $P < 0.05$, *). Similarly and in both imaging modalities, the quantifications on dissected organs confirmed that the T/K ratio was doubled 24 h after injection of Gelofusine ($P < 0.05$, *). Of note, the T/M ratio was usually not significantly different after PBS and Gelofusine injections.

Localization of labeled RAFT-RGD in kidneys. Labeled with single photon emitter [111]In (Fig. 4A) or with fluorescent A700 (Fig. 4B), RAFT-RGD was mainly trapped in the renal cortex 24 h after injection. Table 2 summarizes the quantifications of the tracer in the kidney, from the nuclear and the optical imaging as well as on isolated organs. Twenty-four hours after injection of Gelofusine, the presence of the tracer was reduced by 49% and 63% into the dissected kidneys compared with PBS, in nuclear and optical imaging, respectively. From the non-invasive imaging, the renal amount of tracer in the kidney was decreased by 31% in optical imaging in the Gelofusine injected mice, and decreased to 66% in nuclear imaging. The transversal sections of mice injected with ^{111}In-DOTA-RAFT-RGD clearly illustrated the efficient decrease of the accumulated RAFT-RGD trapped into the kidneys after pre-injection of Gelofusine (Fig. 4A). Thin kidney sections analyzed with the confocal microscope revealed no effect of Gelofusine on RAFT-RGD localization into the kidney or into a particular cell type. However, these analyses confirmed that Gelofusine reduced the amount of labeled peptide in the cortical region of the kidney.

Discussion

Targeting tumors expressing integrin $\alpha_v\beta_3$ is an intensive field of experimental and clinical research. Currently, RGD-based
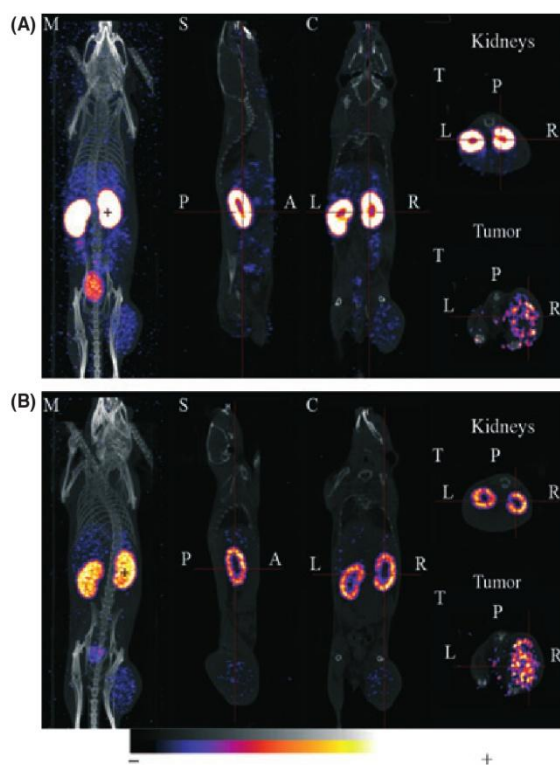
Fig. 2. Representative single photon emission computed tomography (SPECT)/CT imaging of tumor-bearing mice after injection of ^{111}In-DOTA-RAFT-RGD and PBS (A) or Gelofusine (B). The SPECT/CT images were acquired 24 h after i.v. injection of PBS + ^{111}In-DOTA-RAFT-RGD (A) or Gelofusine + ^{111}In-DOTA-RAFT-RGD (B). Gelofusine or PBS were injected 2–5 min prior to RAFT-RGD. Gelofusine strongly reduced renal uptake without affecting tumor uptake. From left to right, SPECT was merged with CT (M, maximum intensity projection or MIP), or representative sections, sagittal (S), coronal (C) or transversal (T), are shown. Scale bar for ^{111}In is 7–70% for MIP and kidney slices and 3–12% for tumor slices (minimum/maximum 0–20 Bq). Scale bar for CT is 1–70% (color set: exp; intensity 90%). A, anterior view; L, left; P, posterior view; R, right. [Correction added on 21 May 2012, after first online publication: 'single positron emission' in the first sentence is corrected to 'single photon emission'.]
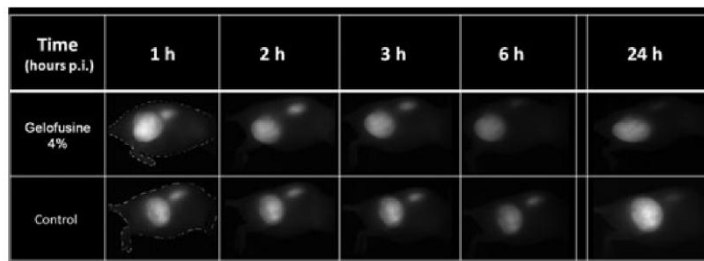
Fig. 3. Fluorescence imaging of tumor-bearing mice after injection of A700-RAFT-RGD with PBS or Gelofusine. (A) Representative images of tumor-bearing mice 1–24 h post-injection (p.i.) of A700-RAFT-RGD with PBS or Gelofusine 4%. (B) Organs were imaged at 24 h. Gelofusine strongly reduced renal uptake, as shown in whole body and organ imaging.

Table 1. Quantification of RAFT-RGD after PBS or Gelofusine pre-injection 5 min prior to labeled tracer

	PBS			Gelofusine		
	1 h	24 h	Dissected organs	1 h	24 h	Dissected organs
^{111}In						
T/M	4.24 ± 0.44	4.50 ± 0.90	6.42 ± 2.30	3.63 ± 0.66^{NS}	5.21 ± 0.76^{NS}	7.03 ± 1.62^{NS}
T/K	0.06 ± 0.01	0.05 ± 0.01	0.03 ± 0.01	0.16 ± 0.02*	0.16 ± 0.01*	0.06 ± 0.01*
A700						
T/M	2.02 ± 0.09	2.18 ± 0.33	6.87 ± 0.34	1.95 ± 0.43^{NS}	2.03 ± 0.64^{NS}	3.80 ± 0.04*
T/K	0.66 ± 0.13	1.33 ± 0.01	0.35 ± 0.12	1.24 ± 0.26*	1.68 ± 0.37^{NS}	0.73 ± 0.41*

Quantifications were obtained from analysis of non-invasive imaging at 1 and 24 h after injection or from analysis of dissected organs at 24 h after injection. Results are expressed as the mean ± SEM. ^{111}In, ^{111}In-DOTA-RAFT-RGD; A700, A700-RAFT-RGD; T/K, tumor-to-kidney ratio; T/M, tumor-to-contralateral muscle ratio. NS, $P > 0.05$, *$P < 0.05$, Gelofusine versus PBS.
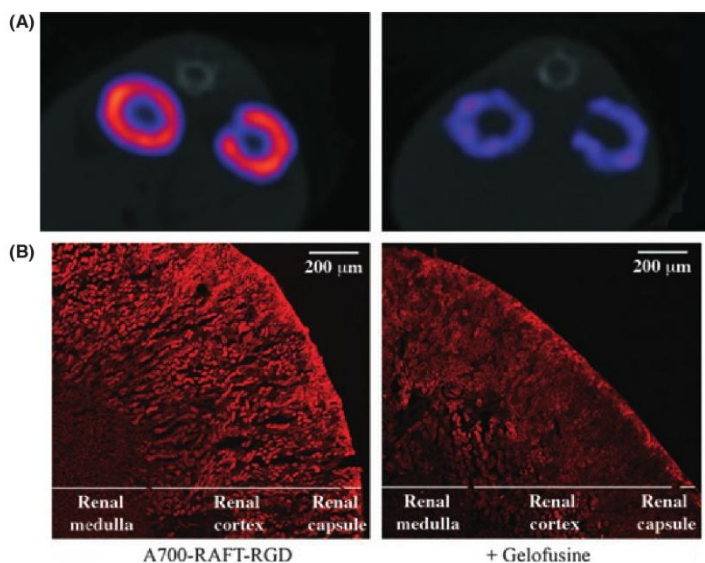
Fig. 4. Influence of Gelofusine on renal distribution of RAFT-RGD. (A) Transversal sections of mice crossing the two kidneys with pre-injection of PBS (left) or Gelofusine (right) before ^{111}In-DOTA-RAFT-RGD injection. (B) Zoom on a transversal section of kidney with pre-injection of PBS (left) or Gelofusine (right) before A700-RAFT-RGD. Gelofusine strongly reduced renal uptake of RAFT-RGD, without affecting its local distribution. Scale bar, 200 µm.

tracers are used in nuclear medicine units, where they provide information about tumor characterization and constitute a major tool for the assessment of anti-angiogenic treatment efficacy. RAFT-RGD was developed to efficiently target tumors expressing integrin $\alpha_v\beta_3$, as a contrast agent for nuclear medicine and optical imaging,[7,9,10,12] as well as an anticancer agent for ITRT and drug delivery.[22,24] During ITRT, the delivered dose is mainly determined by toxicity induced in fragile and vital tissues such as kidneys or bone marrow. Peptides and low-molecular-weight proteins are easily filtered and subsequently reabsorbed in the proximal tubule of kidney: this

reabsorption leads to the accumulation of those radiolabeled peptides in the kidney and thus might contribute to renal toxicity.

A decrease in RAFT-RGD renal retention is thus crucial to minimize nephrotoxicity during treatment with β-emitters such as ^{90}Y-labeled or ^{177}Lu-labeled RAFT-RGD. The partial reabsorption of RAFT-RGD was efficiently reduced through pre-injection or co-injection of Gelofusine, but still too high to prevent any renal damage during ITRT. Several studies, mainly focused on peptide-receptor radionuclide therapy, reported the use of Gelofusine, alone or in combination with

Table 2. Quantification of RAFT-RGD in mouse kidney after PBS or Gelofusine pre-injection 5 min prior to labeled tracer

	PBS			Gelofusine		
	1 h	24 h	Dissected organs	1 h	24 h	Dissected organs
^{111}In	13.35 ± 1.55	5.83 ± 0.52	42.30 ± 9.30	4.95 ± 0.95***	1.97 ± 0.23***	21.50 ± 9.30**
A700	10457 ± 1470	985 ± 213	4601 ± 1086	5040 ± 580**	682 ± 167*	1698 ± 61**

Quantifications were obtained from analysis of non-invasive imaging at 1 and 24 h after injection or from analysis of dissected organs 24 h after injection. Results are expressed as the mean ± SEM. ^{111}In, ^{111}In-DOTA-RAFT-RGD (% injected dose [ID]/500 mm³ or%ID/g); A700, A700-RAFT-RGD (mean of relative light unit [RLU]/pixel/100 ms). *P < 0.05, **P < 0.01, ***P < 0.001, Gelofusine versus PBS.

positively charged amino acids, to reduce renal uptake and/or enhance the amount of the therapeutic radionuclide to increase its effect.[21,25–27] Charges of ligands may play a crucial role in the binding to megalin; some ligands bind to megalin through their cationic sites and their reabsorption can be reduced by co-administration of cationic compounds such as lysine or a mixture of positively charged amino acids.[15] Therefore, co-injection of lysine and arginine has become a standard procedure during peptide receptor radionuclide therapy with ^{177}Lu-labeled or ^{90}Y-labeled somatostatin analogues,[28] and similarly reduced renal retention of the radio compound such as [^{111}In-DTPA°]-octreotide by approximately 40%.[28,29] Using Gelofusine alone, renal uptake of octreotate and octreotite were reduced by 42%[30] and 46%,[21] respectively, in kidneys of rats, whereas a combination of the two, positively charged amino acids plus Gelofusine, might be additive.[31] Surprisingly, tumor uptake was not affected by the combination of Gelofusine plus lysine in a study carried out on rats bearing sst2-receptor-expressing tumors.[25] We previously showed that 24 h after injection, approximately 6% of the RAFT-RGD metabolites are positively charged in mice kidneys.[7] In our case, pre-injection of positively charged amino acids did not affected RAFT-RGD renal retention (Arnaud Briat, unpublished data, 2010). Other plasma expenders, such as Voluven, or the lipid solution Medialipid (B. Braun Medical) were also pre-injected prior to labeled RAFT-RGD but failed to reduce renal retention (data not shown). If the renal accumulation of labeled RAFT-RGD was significantly reduced and would facilitate tumor imaging, further investigations are required into reducing renal accumulation more efficiently for ITRT.

The labeling of the tracer by radioactive ^{111}In or fluorescent A700 influenced the biodistribution of the tracer in a similar fashion; the tracer's biodistributions were similar when comparing both imaging methods. The differences observed for the dark-red organs, that is, spleen and liver, might be explained in part by the limits of optical imaging.[32] The fluorescence in these red-colored organs is always underestimated compared to the other "white" organs.

As described in Figure 4, the partial reabsorption of RAFT-RGD was mainly observed at the renal cortex. Gelofusine reduced the total amount of RAFT-RGD in the kidney, therefore contributing to lower the radiation dose delivered to this fragile organ. Several approaches have been developed to interfere with renal retention of radiolabeled peptides. When

other compounds are reabsorbed by endocytosis or transporters, co-injection of succinylated gelatin and/or positively charged amino acids (lysine/arginine) helps to saturate the kidney with competitive inhibitors.[29] Few anaphylactoid reactions were reported using gelatin derivatives and concerned approximately 0.033% of patients.[33] Other strategies have been suggested to decrease endocytosis, such as the use of colchicine, which interferes with the microtubule function preventing the megalin receptor to return to the cell membrane after endocytosis; unfortunately, its use in clinical investigations was not suitable because of potential toxicity.[34] Chemical modifications of the compound itself are also an attractive way to facilitate elimination. We previously added a glucose moiety on the RAFT scaffold of RAFT-RGD to increase its elimination.[35] The affinity for integrin $\alpha_v\beta_3$ was unaffected by this modification as well as tumor uptake, but it failed to reduce renal reabsorption. When reducing renal uptake is not efficient, alternative strategies might be useful, such as the use of radioprotectors that minimize oxidative stress (i.e., aminofostine),[36] dose fractionation that increases time to repair sublethal damages,[37] or the use of ^{177}Lu instead of ^{90}Y, which lowers the radiation dose delivered to the radiosensitive glomeruli.[38]

In complement to the optimisation of the delivered dose in radionuclide therapy, reduction of renal uptake would also be useful during tumor imaging, increasing information during imaging due to a better T/K ratio. Small targeted tumors next to the kidneys could be disguised by a high concentration of radiolabeled or fluorescent tracer in the kidney; by enhancing tracer elimination through the urine, imaging information would be gained.

Limiting the total dose delivered to patients, as well as reducing specific renal radiation, are major clinical points during ITRT. Similarly, reduction of background (i.e., non-specific organ uptake) is crucial during diagnostic imaging, for tumor localization and characterization. RAFT-RGD is a promising agent, for both $\alpha_v\beta_3$-positive tumor imaging and vectorization of radionuclides or therapeutic drugs for tumor therapy. Injection of the plasma expander Gelofusine efficiently reduced renal reabsorption of RAFT-RGD, therefore supporting its use for further preclinical and clinical investigations.

Disclosure Statement

The authors have no conflicts of interest.

References

1 Anderson CR, Hu X, Zhang H et al. Ultrasound molecular imaging of tumor angiogenesis with an integrin targeted microbubble contrast agent. *Invest Radiol* 2011; **46**: 215–24.
2 Beer AJ, Kessler H, Wester HJ, Schwaiger M. PET imaging of integrin alphaVbeta3 expression. *Theranostics* 2011; **1**: 48–57.
3 Pool SE, Krenning EP, Koning GA et al. Preclinical and clinical studies of peptide receptor radionuclide therapy. *Semin Nucl Med* 2010; **40**: 209–18.
4 Schnell O, Krebs B, Carlsen J et al. Imaging of integrin alpha(v)beta(3) expression in patients with malignant glioma by [18F] Galacto-RGD positron emission tomography. *Neuro Oncol* 2009; **11**: 861–70.
5 Boturyn D, Coll JL, Garanger E, Favrot MC, Dumy P. Template assembled cyclopeptides as multimeric system for integrin targeting and endocytosis. *J Am Chem Soc* 2004; **126**: 5730–9.
6 Garanger E, Boturyn D, Jin Z, Dumy P, Favrot MC, Coll JL. New multi-functional molecular conjugate vector for targeting, imaging, and therapy of tumors. *Mol Ther* 2005; **12**: 1168–75.

7 Ahmadi M, Sancey L, Briat A *et al.* Chemical and biological evaluations of an (111)in-labeled RGD-peptide targeting integrin alpha(V) beta(3) in a preclinical tumor model. *Cancer Biother Radiopharm* 2008; **23**: 691–700.

8 Dimastromatteo J, Riou LM, Ahmadi M *et al.* In vivo molecular imaging of myocardial angiogenesis using the alpha(v)beta3 integrin-targeted tracer 99mTc-RAFT-RGD. *J Nucl Cardiol* 2010; **17**: 435–43.

9 Jin ZH, Furukawa T, Galibert M *et al.* Noninvasive visualization and quantification of tumor alphaVbeta3 integrin expression using a novel positron emission tomography probe, 64Cu-cyclam-RAFT-c(-RGDfK-)4. *Nucl Med Biol* 2011; **38**: 529–40.

10 Sancey L, Ardisson V, Riou LM *et al.* In vivo imaging of tumour angiogenesis in mice with the alpha(v)beta (3) integrin-targeted tracer 99mTc-RAFT-RGD. *Eur J Nucl Med Mol Imaging* 2007; **34**: 2037–47.

11 Garanger E, Boturyn D, Dumy P. Tumor targeting with RGD peptide ligands-design of new molecular conjugates for imaging and therapy of cancers. *Anticancer Agents Med Chem* 2007; **7**: 552–8.

12 Jin ZH, Josserand V, Foillard S *et al.* In vivo optical imaging of integrin alphaV-beta3 in mice using multivalent or monovalent cRGD targeting vectors. *Mol Cancer* 2007; **6**: 41.

13 Jin ZH, Josserand V, Razkin J *et al.* Noninvasive optical imaging of ovarian metastases using Cy5-labeled RAFT-c(-RGDfK-)4. *Mol Imaging* 2006; **5**: 188–97.

14 Dijkgraaf I, Kruijtzer JA, Liu S *et al.* Improved targeting of the alpha(v)beta (3) integrin by multimerisation of RGD peptides. *Eur J Nucl Med Mol Imaging* 2007; **34**: 267–73.

15 Rolleman EJ, Valkema R, de Jong M, Kooij PP, Krenning EP. Safe and effective inhibition of renal uptake of radiolabelled octreotide by a combination of lysine and arginine. *Eur J Nucl Med Mol Imaging* 2003; **30**: 9–15.

16 Christensen EI, Birn H. Megalin and cubilin: synergistic endocytic receptors in renal proximal tubule. *Am J Physiol Renal Physiol* 2001; **280**: F562–73.

17 Baines RJ, Brunskill NJ. The molecular interactions between filtered proteins and proximal tubular cells in proteinuria. *Nephron Exp Nephrol* 2008; **110**: e67–71.

18 Christensen EI, Verroust PJ. Megalin and cubilin, role in proximal tubule function and during development. *Pediatr Nephrol* 2002; **17**: 993–9.

19 ten Dam MA, Branten AJ, Klasen IS, Wetzels JF. The gelatin-derived plasma substitute Gelofusine causes low-molecular-weight proteinuria by decreasing tubular protein reabsorption. *J Crit Care* 2001; **16**: 115–20.

20 Veldman BA, Schepkens HL, Vervoort G, Klasen I, Wetzels JF. Low concentrations of intravenous polygelines promote low-molecular weight proteinuria. *Eur J Clin Invest* 2003; **33**: 962–8.

21 van Eerd JE, Vegt E, Wetzels JF *et al.* Gelatin-based plasma expander effectively reduces renal uptake of 111In-octreotide in mice and rats. *J Nucl Med* 2006; **47**: 528–33.

22 Foillard S, Sancey L, Coll JL, Boturyn D, Dumy P. Targeted delivery of activatable fluorescent pro-apoptotic peptide into live cells. *Org Biomol Chem* 2009; **7**: 221–4.

23 Keramidas M, Josserand V, Righini CA, Wenk C, Faure C, Coll JL. Intraoperative near-infrared image-guided surgery for peritoneal carcinomatosis in a preclinical experimental model. *Br J Surg* 2010; **97**: 737–43.

24 Dufort S, Sancey L, Hurbin A *et al.* Targeted delivery of a proapoptotic peptide to tumors in vivo. *J Drug Target* 2011; **19**: 582–8.

25 Melis M, Bijster M, de Visser M *et al.* Dose-response effect of Gelofusine on renal uptake and retention of radiolabelled octreotate in rats with CA20948 tumours. *Eur J Nucl Med Mol Imaging* 2009; **36**: 1968–76.

26 Rolleman EJ, Melis M, Valkema R, Boerman OC, Krenning EP, de Jong M. Kidney protection during peptide receptor radionuclide therapy with somatostatin analogues. *Eur J Nucl Med Mol Imaging* 2010; **37**: 1018–31.

27 Vegt E, Eek A, Oyen WJ, de Jong M, Gotthardt M, Boerman OC. Albumin-derived peptides efficiently reduce renal uptake of radiolabelled peptides. *Eur J Nucl Med Mol Imaging* 2010; **37**: 226–34.

28 Valkema R, Pauwels SA, Kvols LK *et al.* Long-term follow-up of renal function after peptide receptor radiation therapy with (90)Y-DOTA(0),Tyr (3)-octreotide and (177)Lu-DOTA(0), Tyr(3)-octreotate. *J Nucl Med* 2005; **46**(Suppl 1): 83S–91S.

29 Vegt E, Wetzels JF, Russel FG *et al.* Renal uptake of radiolabeled octreotide in human subjects is efficiently inhibited by succinylated gelatin. *J Nucl Med* 2006; **47**: 432–6.

30 Rolleman EJ, Bernard BF, Breeman WA *et al.* Molecular imaging of reduced renal uptake of radiolabelled [DOTA0,Tyr3]octreotate by the combination of lysine and Gelofusine in rats. *Nuklearmedizin* 2008; **47**: 110–5.

31 Gotthardt M, van Eerd-Vismale J, Oyen WJ *et al.* Indication for different mechanisms of kidney uptake of radiolabeled peptides. *J Nucl Med* 2007; **48**: 596–601.

32 Josserand V, Texier-Nogues I, Huber P, Favrot MC, Coll JL. Non-invasive in vivo optical imaging of the lacZ and luc gene expression in mice. *Gene Ther* 2007; **14**: 1587–93.

33 Ring J, Messmer K. Incidence and severity of anaphylactoid reactions to colloid volume substitutes. *Lancet* 1977; **1**: 466–9.

34 Rolleman EJ, Krenning EP, Van Gameren A, Bernard BF, De Jong M. Uptake of [111In-DTPA0]octreotide in the rat kidney is inhibited by colchicine and not by fructose. *J Nucl Med* 2004; **45**: 709–13.

35 Galibert M, Sancey L, Renaudet O, Coll JL, Dumy P, Boturyn D. Application of click-click chemistry to the synthesis of new multivalent RGD conjugates. *Org Biomol Chem* 2010; **8**: 5133–8.

36 Vegt E, de Jong M, Wetzels JF *et al.* Renal toxicity of radiolabeled peptides and antibody fragments: mechanisms, impact on radionuclide therapy, and strategies for prevention. *J Nucl Med* 2010; **51**: 1049–58.

37 Stewart FA, Lebesque JV, Hart AA. Progressive development of radiation damage in mouse kidneys and the consequences for reirradiation tolerance. *Int J Radiat Biol Relat Stud Phys Chem Med* 1988; **53**: 405–15.

38 Bodei L, Cremonesi M, Ferrari M *et al.* Long-term evaluation of renal toxicity after peptide receptor radionuclide therapy with 90Y-DOTATOC and 177Lu-DOTATATE: the role of associated risk factors. *Eur J Nucl Med Mol Imaging* 2008; **35**: 1847–56.

III. DESIGN & CHARACTERIZATION OF ACTIVATABLE PROBES FOR CANCER IMAGING & THERAPY

Introduction

Integrin $\alpha_v\beta_3$ is overexpressed in response to an outside signal that indicates to the cell that it has to move toward a chemo-attractive gradient. Since a moving cell needs to degrade the ECM (*e.g.* collagen, fibrils) for moving, this cell must produce enzymes for ECM degradation. These are the so called matrix metalloproteases (MMPs) among which MMP-2 and MMP-9.

MMPs are a family of proteases that catalyze the destruction of particular peptidic sequences. We can thus use these sequences and the catalytic activity of MMPs to generate activatable molecular probes.

In addition, these proteases can serve as potential co-targets for new bifunctional derivatives of RAFT-RGD molecules with improved specificity and biological activities. The introduction of a cleavable bond can serve for on-target specific delivery of a prodrug, but we can also use this controlled degradation for fluorescence imaging like we already demonstrated with the introduction of a disulfide bond[228, 229].

The second part of my thesis project was thus focused on the synthesis of a second generation of activatable probes (Figure III-1).

---

[228]Foillard, Stéphanie, Zhao-hui Jin, Elisabeth Garanger, Didier Boturyn, Marie-Christine Favrot, Jean-Luc Coll, und Pascal Dumy. „Synthesis and biological characterisation of targeted pro-apoptotic peptide". *Chembiochem: a European journal of chemical biology* 9, Nr. 14 (September 22, 2008): 2326–2332.

[229]Dufort, Sandrine, Lucie Sancey, Amandine Hurbin, StéphanieFoillard, Didier Boturyn, Pascal Dumy, und Jean-Luc Coll. „Targeted delivery of a proapoptotic peptide to tumors in vivo". *Journal of Drug Targeting* 19, Nr. 7 (August 2011): 582–588.
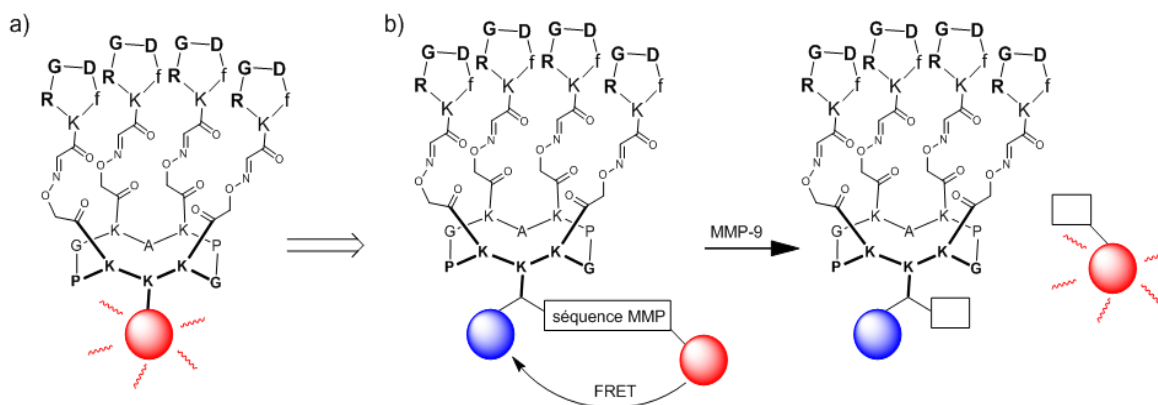
Figure III-1: Structure of the scaffold RAFT presenting the ligand « RGD ».
a) fluorescent compound, b) activatable compound.

At first we had to select appropriated MMP2/9 cleavable peptide sequences in order to combine them with the targeting molecule RAFT-c(RGD)$_4$, thus forming the afterwards called RAFT-RGD-MMP.

We chose a set of cleavable peptide sequences, based on the studies [230], [231] and the MEROPS peptide database. We tested their sensibility towards MMPs *in vitro* first. Afterwards, a cleavable sequence was chosen and synthesized with NIR-dyes to generate the self-quenched RAFT-RGD-MMP molecule which was then tested *in vitro* and *in vivo*.

As described in the experimental section linear peptides were synthesized by solid phase peptide synthesis (SPPS) using Fmoc/*t*Bu strategy. Functionalizations and molecular assemblies were carried out in solution.

III.1.   Results and discussion

III.1.1.   MMP-2 AND MMP-9 CLEAVAGE TEST – SEQUENCE SELECTION

The first step was the synthesis of peptide sequences cleaved by MMP-2 and/or MMP-9 (Figure III-2). Peptide **1** and peptide **2** were taken from Laure-Fields[230], whereas peptide **3** was designed after information of the peptide database "Merops" (http://merops.sanger.ac.uk/). Scramble peptide **4** was prepared to provide the negative control compound. All peptides were prepared by using a standard Fmoc/*t*Bu solid-phase chemistry on an acid-labile resin. Protective groups for Glutamine, Arginine and Tryptophan were respectively Trt, Pbf and Boc. The monitoring of MMP cleavage studies was performed thanks to the Dansyl labeling (λabs = 320 nm) at the N-terminal of all peptides (Figure III-3). Finally, peptides were released from the resin by treatments with acid solutions. Fluorescent peptides **1**-**4** were then characterized by RP-HPLC analysis and mass spectroscopy.
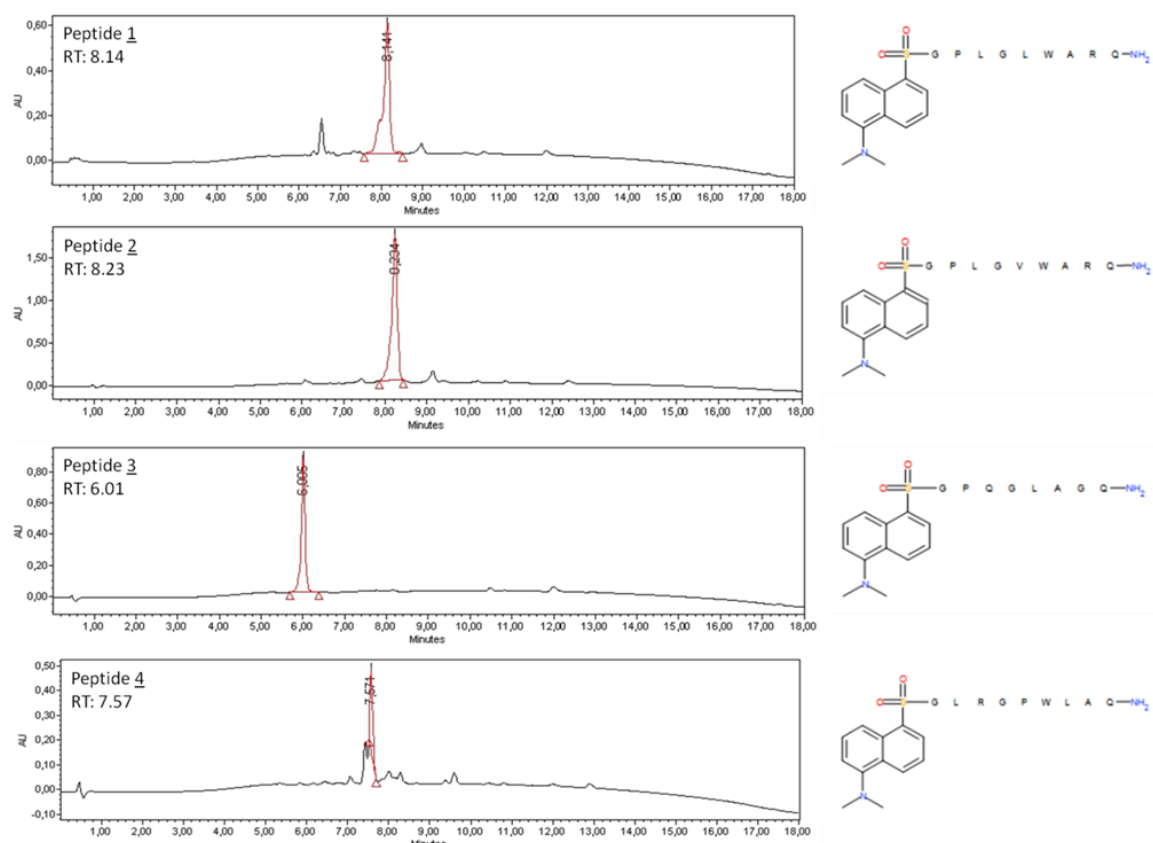
Figure III-2: Chromatograms of 1, 2, 3 and 4 at 214 nm and their structure.

[230]Lauer-Fields, Janelle L., ThilakaSritharan, M. Sharon Stack, Hideaki Nagase, und Gregg B. Fields. „Selective Hydrolysis of Triple-helical Substrates by Matrix Metalloproteinase-2 and -9". *Journal of Biological Chemistry* 278, Nr. 20 (Mai 16, 2003): 18140–18145.
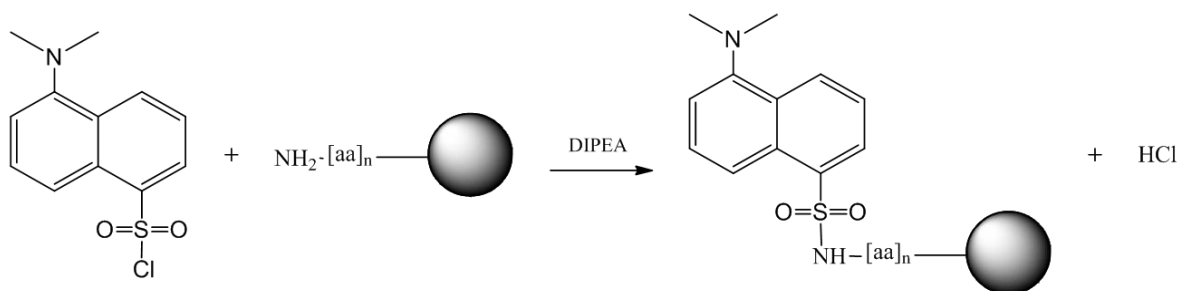
Figure III-3: Grafting of Dansyl fluorescent dye on resin.

As the MMP-9 and -2 cleavages occur at the Gly-Val bond or at the Gly-Leu bond (also by MMP-1;-8;-13; -14)[231,232] the following peptidic fragments were expected:

1: Dns- Gly-Pro-Leu-Gly   Leu-Trp-Ala-Arg-Gln-NH2
2: Dns- Gly-Pro-Leu-Gly   Val-Trp-Ala-Arg-Gln-NH$_2$
3: Dns- Gly-Pro-Gln-Gly   Leu-Ala-Gly-Gln-NH$_2$
4: Dns- Gly-Leu-Arg-Gly-Pro-Trp-Leu-Ala-Gln-NH$_2$ (none = control negative)

No full cleavage was observed for compounds **1** and **3** after incubation with MMP-2 or MMP-9. However, peptide **3** was totally cleaved by MMP-9 and partially by MMP-2 (Table III-1). Hence, we chose this compound for further *in vitro* and *in vivo* examinations.

peptide	Control (RT)	MMP-2 (RT)	MMP-9 (RT)
1	15.40	15.39 16.79	15.40 19.80
2	19.96	19.46	19.39 26.8
3	15.60	16.50 17.21 27.91	9.91
4	20.17	20.29	20.20 27.97

Table III-1: RT-HPLC measured retention times (RT) of compounds 1, 2, 3 and 4 of crude peptide (control) and of peptides after incubation with MMP-2 and MMP-9 (2 h, 37°C).
Green represents the uncleaved peptide, orange the products after peptide cleavage by MMP-2 and blue the products after peptide cleaved by MMP-9

[231]Lauer-Fields, Janelle L., ThilakaSritharan, M. Sharon Stack, Hideaki Nagase, und Gregg B. Fields. „Selective Hydrolysis of Triple-helical Substrates by Matrix Metalloproteinase-2 and -9". *Journal of Biological Chemistry* 278, Nr. 20 (Mai 16, 2003): 18140–18145.

[232]Kline, Toni, Michael Y Torgov, Brian A Mendelsohn, Charles G Cerveny, und Peter D Senter. „Novel antitumor prodrugs designed for activation by matrix metalloproteinases-2 and -9". *Molecular pharmaceutics* 1, Nr. 1 (Januar 12, 2004): 9–22.

Amongst others, we defined the percentage of compound **3** degradation by MMP-9. The test was done by means of reverse phase-HPLC (Figure III-4). We observed that 50 % of peptide was digested in 1 minute then digestion slowed down. After 2 h of incubation, 13 % of peptide **3** was present (Figure III-5).
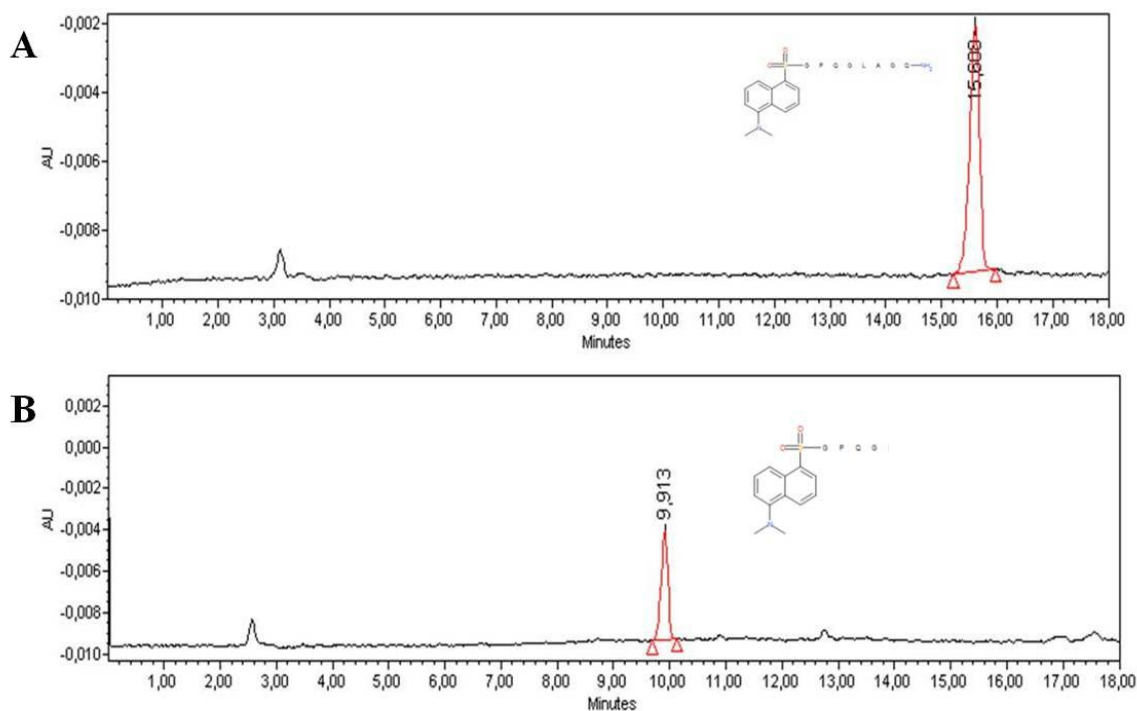
Figure III-4: RT-HPLC analysis at 633nm of the degradation of compound 3 by MMP-9, with structure of molecule.
Chromatogram **A** shows the HPLC profile of peptide **3**, Chromatogram **B** shows the HPLC profile of the molecule after 2 h of incubation with MMP-9 at 37°C.
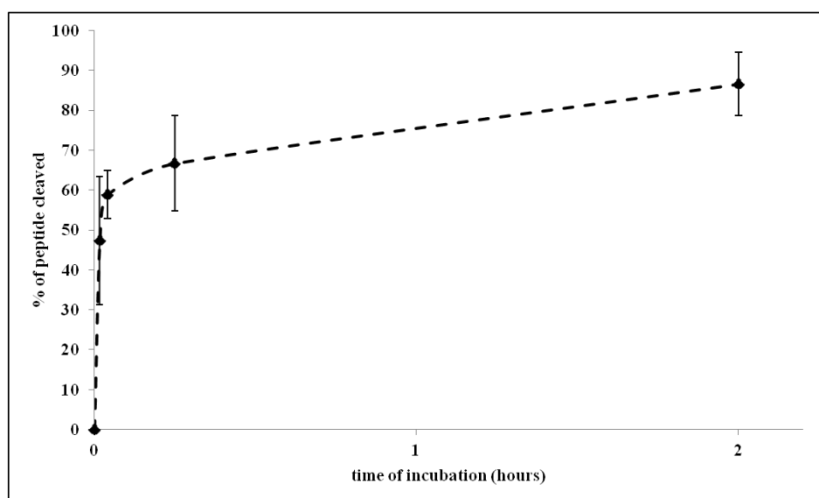
Figure III-5: Percentage of compound 3 cleavage after incubation with MMP-9.
Measurements *via* RT-HPLC at T0, 1 min, 2.5 min, 5 min, 15 min and 2 h after incubation with activated MMP-9 at 37°C.

III.1.2. *Synthesis of activatable probes*

Our macromolecular activatable fluorescent compound comprises a targeted drug delivery system based on the RAFT-RGD peptide and a quenched cyanine 5 (Cy5) dye-containing MMP peptidic sequence (Figure III-1). We decided to exploit a combination of Cy 5 fluorescent dye and QSY quencher that were successfully used for drug monitoring *in vivo*[233] recently. To graft these chromophores to the peptidic sequence **3**, we introduced functionalized lysines at the C-terminal and N-terminal, protected respectively by Alloc and Dde groups. For the assembly of RAFT-RGD molecules and activatable fluorescent MMP, we used oxime ligation. For this purpose, we added protected aminooxy function at the N-terminal of MMP fragment.

The linear peptide **5** Gly(boc)-Lys(Dde)-Gly-Pro-Gln(Trt)-Gly-Leu-Ala-Gly-Gln(Trt)-Lys(Alloc)-OH was prepared using acid sensitive chlorotrityl resin. The use of an acetic acid solution was essential to keep protective groups at the glutamine side chain and at the N-terminal (Figure III-6). Deprotection was then carried out by using hydrazine and subsequent coupling of succinimide ester of Cy 5 provided the fluorescent peptide **6a** Gly(boc)-Lys(Cy5)-Gly-Pro-Gln(Trt)-Gly-Leu-Ala-Gly-Gln(Trt)-Lys(Alloc)-OH.

Purification of peptide **6a** was carried out by using a microcolumn C18 (Chromafix®). The expected compound was obtained (Figure III-7) and we found the deconvoluted mass in total agreement with the calculated mass (Figure III-8).
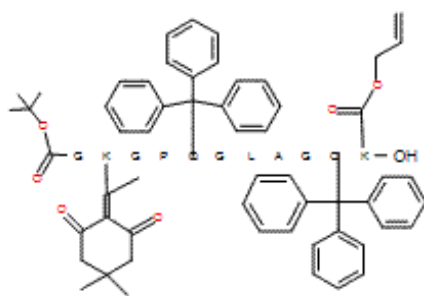
Figure III-6: Molecule structure of compound 5 showing orthogonal and N-terminal protection groups.

[233]Foillard, Stéphanie, Zhao-hui Jin, Elisabeth Garanger, Didier Boturyn, Marie-Christine Favrot, Jean-Luc Coll, und Pascal Dumy. „Synthesis and biological characterisation of targeted pro-apoptotic peptide". *Chembiochem: a European journal of chemical biology* 9, Nr. 14 (September 22, 2008): 2326–2332.
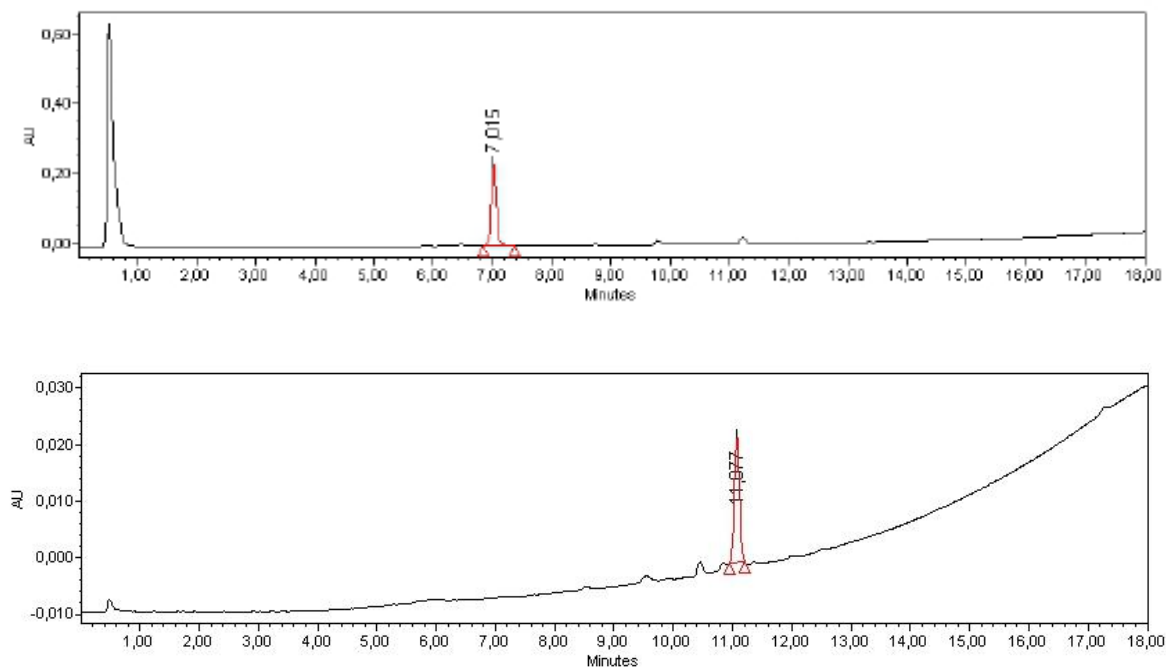
Figure III-7: RP-HPLC analysis of <u>5</u> (top) and <u>6a</u> (bottom).
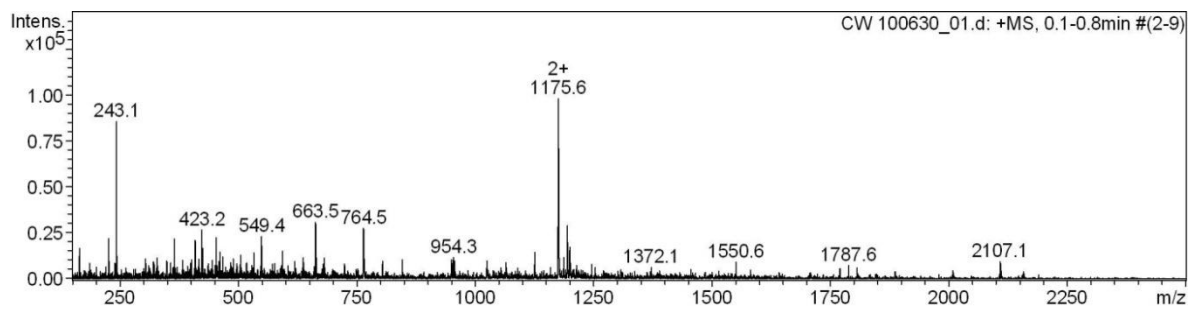
Figure III-8: Mass spectrometry analysis of <u>6a</u>.
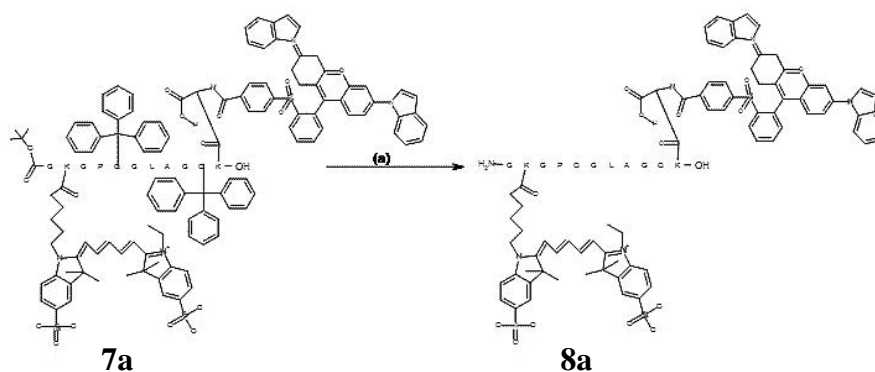
Figure III-9: Total deprotection of compound <u>7a</u>; (a) TFA 95%, H2O 2.5%, TIS 2.5%.

Thereafter Alloc deprotection was obtained by means of Tetrakis-Palladium and phenylsilane. The following grafting of succinimide ester of quencher QSY21 was then carried out. After two days reaction, the expected compound was not obtained in sufficient amounts to prepare the desired activatable peptide **<u>7a</u>** boc-Gly-Lys(Cy5)-Gly-Pro-Gln(Trt)-Gly-Leu-Ala-Gly-Gln(Trt)-Lys(QSY21) (compounds 7a and 8a are not listed in the Materials and Methods chapter). We suggest that steric hindrance of protected group such trityl prevents QSY21 from the coupling. We then decided to exploit an activatable fluorescent system based on the self-quenching of two cyanine 5 fluorescent dyes[234].

III.1.3. *Synthesis of final compound (RAFT-RGD-MMP)*

The final molecule (compound **<u>10</u>**) was synthesized as described in the submitted article presented afterwards (Wenk *et al*. "Integrin and Matrix Metalloprotease Dual-Targeting with MMP substrate-RGD conjugate").

---
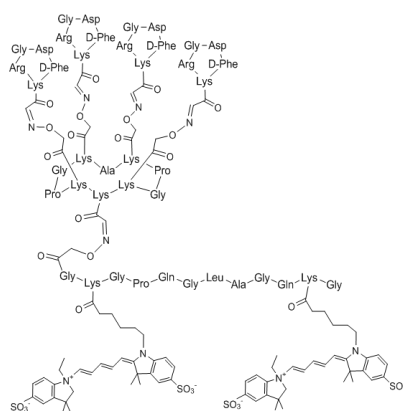
[234] Razkin, Jesus, Véronique Josserand, Didier Boturyn, Zhao-hui Jin, Pascal Dumy, Marie Favrot, Jean-Luc Coll, und Isabelle Texier. „Activatable fluorescent probes for tumour-targeting imaging in live mice". *ChemMedChem* 1, Nr. 10 (Oktober 2006): 1069–1072.

III.2.   *Fluorescent characteristics and cleavage properties of the RAFT-RGD-MMP*

After synthesis of the RAFT-RGD-MMP, the molecule properties were analyzed by means of fluorescence reflectance 2D imaging (FRI; Figure III-10) and Fluorescence Spectrometry and Absorbance measurements in order to define their quenching level and the level of dequenching by MMP-9.
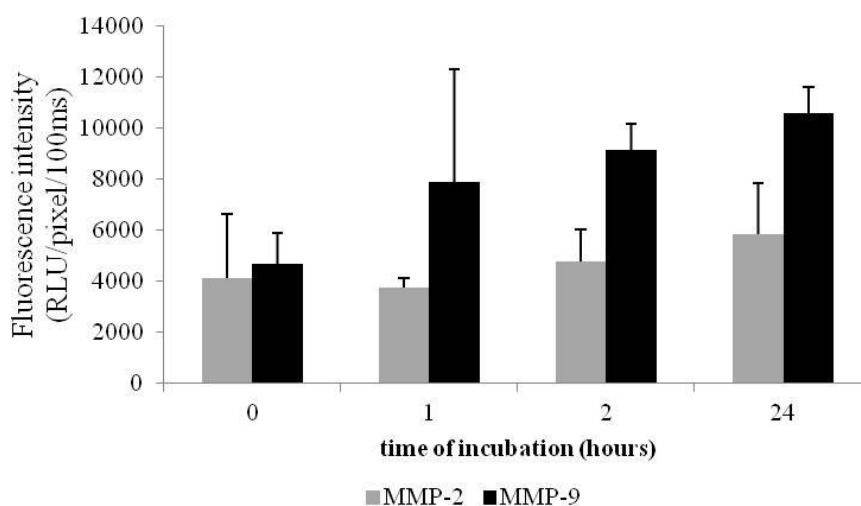
Figure III-10: Fluorescence imaging of RAFT-RGD-MMP drops before and after incubation with MMP-9 and MMP-2.

The first study shows a steady increase in the fluorescence intensity during the first two hours, then slowing down to be 2.3-times more intense after 24 h of incubation with active MMP-9. Incubated with active MMP-2, nearly no increase can be observed. The values of the sample MMP-2 show a slight 0.9-times increase in fluorescence at 24 h.

Afterwards the emission spectra of the RAFT-RGD-MMP compound were measured and compared to those of the RAFT-RGD-Cy5 control molecule. The spectra were normalized by their in parallel taken absorption spectra and machine errors as well as bleaching aberrances were minimized by using Cy5 controls (see Materials & Methods) (Figure III-11)
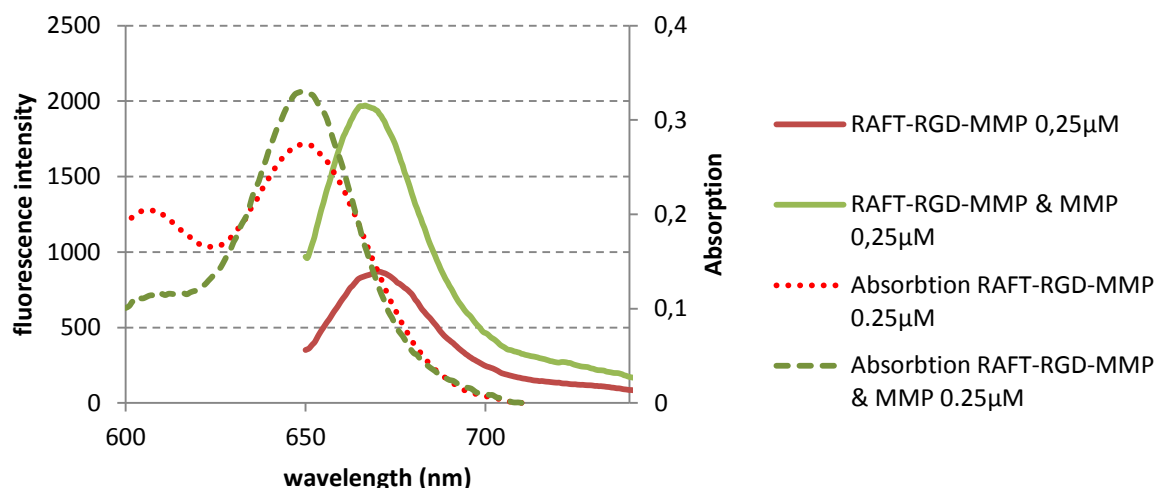
Figure III-11: Fluorescence emission spectra and corresponding absorption spectra of RAFT6RGD-MMP before and after incubation with MMP-9.

Comparing the emission spectra of the compound RAFT-RGD-MMP before and after incubation with MMP-9, a difference of the measured intensities could be observed. The initial molecule shows a peak of emission at 670 nm of 870 while after incubation with MMP-9 the maximum is at 666.5 nm with an intensity of 1972 (= 2.3 x the initial signal).

Regarding the absorption spectra the molecule initially shows a weak absorption peak at 650 nm compared to its spectra after MMP incubation. Furthermore a second peak at 610 nm before MMP incubation can be observed, which nearly disappeared after incubation with the enzyme.

Analyzing the fluorescence emission spectrum, it showed at 0.25 µM a quenching of 64 %, while after 48 h of incubation with active MMP-9, the molecule showed 21 % of quenching (Figure III-12).

The results are presented in the article *Wenk, C.H.F., Josserand, V., Coll, JL, Dumy, P and Boturyn, D, "Integrin and Matrix Metalloprotease Dual-Targeting with MMP substrate-RGD conjugate" (2012).*
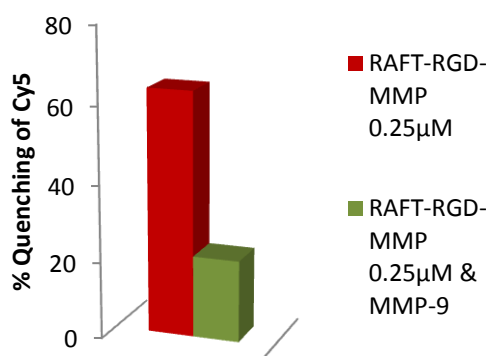
Figure III-12: Measured quenching of the compound RAFT-RGD-MMP before and after incubation with MMP-9.

In order to verify the differences in fluorescent intensity obtained, we analyzed the RAFT-RGD-MMP emission spectra while incubated with active MMP-9 and its competitive inhibitors CCT and SB3-CT and its stability in crude mouse plasma (Figure III-13).

The results obtained showed that the increase in fluorescence intensity is halved while incubated with the MMP inhibitors compared to the molecule incubated with MMP-9 only. Here it is worth noting that the inhibitors loose efficacy in the course of time and that activated MMPs do auto-degrade.

In plasma the fluorescence signal measured is staying at the same level for 24 h, rising after another 24 h of incubation at 37°C in plasma from 194 to 339 intensity units, which corresponds at 1.75 times of intensity increase, thus 0.55 times less than incubated with MMP-9.
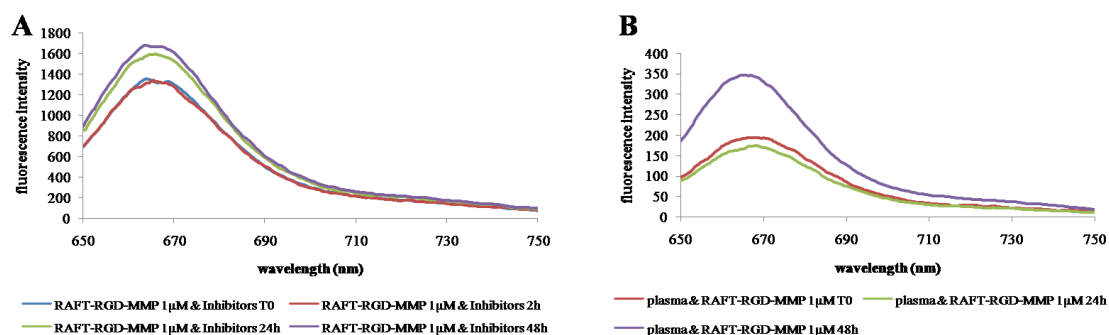
Figure III-13: Fluorescence emission spectra of RAFT-RGD-MMP: effect of A) MMP inhibition and B) Plasma stability.

"Integrin and Matrix Metalloprotease Dual-Targeting with MMP substrate-RGD conjugate" (Org. Biomol. Chem. **11**, 448–452 (2012)
Wenk, C.H.F., Josserand, V., Coll, JL, Dumy, P and Boturyn, D,

PAPER

Integrin and matrix metalloprotease dual-targeting with an MMP substrate–RGD conjugate†

Christiane H. F. Wenk,[a,b,c] Véronique Josserand,[b,c] Pascal Dumy,[a,c] Jean-Luc Coll*[b,c] and Didier Boturyn*[a,c]

A fluorescent clustered RGD-containing ligand encompassing an MMP substrate was designed and successfully used *in vivo* for the dual-targeting of $\alpha_V\beta_3$ integrin receptors and MMP-9 extracellular proteases in the tumor region.

Introduction

The identification of molecular markers that can differentiate a tumor from healthy tissue represents a major goal in cancer medicine. In this context, integrins, such as $\alpha_V\beta_3$, are attractive therapeutic targets.[1] These receptors are cell surface proteins that are highly expressed on tumor blood vessels during angiogenesis and on various tumor cells. A characteristic feature of the $\alpha_V\beta_3$ integrin is its high binding affinity for the ubiquitous triad sequence arginine-glycine-aspartic acid (RGD) of proteins such as vitronectin, fibronectin, osteopontin, which belong to the extracellular matrix. The design of numerous RGD-containing cyclopeptides has led to highly selective synthetic ligands with enhanced binding affinities.[2] Such peptides were further exploited for drug delivery and tumor imaging.[3] For instance, *in vivo* targeting of tumor vasculature using RGD conjugates opens up new perspectives for cancer detection and management[4,5] including imaging-guided surgery.[6]

We have shown that a clustered RGD-containing compound bearing a cytotoxic peptide offers an interesting outlook for tumor-targeted drug delivery.[7] Enzymatic reduction of a disulfide bond was used for the drug release within intracellular compartments.[8] To enhance the tumor selectivity, we describe in this report a dual targeting strategy exploiting the overexpression of $\alpha_V\beta_3$ integrin and active matrix metalloproteases (MMPs) in neovasculature that could be used for the drug delivery instead of enzymatic reduction of a disulfide bridge. Very recently, MMP was used for the activation of cell

penetrating peptide-bearing dendrimers for the *in vivo* fluorescence and magnetic resonance imaging (MRI) of proteases.[9] We then designed the peptidic macromolecule 1 (Fig. 1) comprising integrin-binding RGD motifs and an MMP-9 cleavable sequence as MMP-9 over-expression has been shown to be involved in cancer angiogenesis[10] and tumor cell invasion.[11] An imaging function was used to monitor the MMP activity. We decided to exploit an activatable fluorescent system based on the self-quenching of cyanine 5 fluorescent dyes.[12] A cyclodecapeptide scaffold allows a spatial separation between the targeting and the drug-delivery domains such that the individual properties of both motifs are not affected. With the molecule in hand, we focused our work on assessing biological activities to determine the potency of the MMP-activatable RGD-containing macromolecule.

Results and discussion

Chemical synthesis and characterization of fluorescent conjugate

The synthesis of activatable fluorescent conjugate 1 is reported in Scheme 1. Stable oxime bonds were utilized to append aldehyde-bearing RGD motifs to the cyclodecapeptide scaffold before grafting the MMP-9 peptidic sequence. All peptides were prepared *via* solid-phase peptide syntheses (SPPS) according to methods already developed by our group.[13] Aminooxy groups were directly incorporated during the SPPS by using 1-ethoxyethylidene containing building blocks.[14] The following head-to-tail cyclisation provided the fully protected cyclodecapeptide 4. Full deprotection of peptide 4 under acidic conditions allowed the grafting of glyoxylyl aldehyde containing RGD targeting elements (Scheme 1). The subsequent oxidative cleavage with sodium periodate of the amino-alcohol moiety of serine furnished the peptide intermediate 5 in satisfying 66% overall yield.

[a]Département de Chimie Moléculaire, CNRS: UMR 5250, ICMG FR 2607, Grenoble cedex 9, France. E-mail: didier.boturyn@ujf-grenoble.fr

[b]INSERM U823, Grenoble, France. E-mail: jean-luc.coll@ujf-grenoble.fr; Fax: +33 4 7654 9413; Tel: +33 4 7654 9553

[c]Université Joseph Fourier – Grenoble I, 570, rue de la chimie, BP53, 38041 Grenoble cedex 9, France. Fax: +33 4 5652 0803; Tel: +33 4 5652 0832

†Electronic supplementary information (ESI) available: Synthesis, RP-HPLC profile and ESI-MS of compounds 1, 4–6; fluospectroscopy, flow cytometry analysis and *in vivo* fluorescence imaging procedures. See DOI: 10.1039/c2ob26926k

Chemoselective addition of MMP peptide **6** on scaffold **5** was carried out in aqueous solution to obtain the peptide conjugate in 46% yield after purification. As expected,[13]

transoximation reaction did not occur during the second oxime ligation. Finally, the use of activated ester of cyanine 5 afforded activatable fluorescent conjugate **1**. Compound **1** was readily purified by reversed-phase HPLC methods and obtained in 31% yield. It was then characterized by electrospray ionization mass spectrometry (see the ESI†).

The fluorescence emission properties of compound **1** were then evaluated *in vitro*. When the cyanine 5 moieties are linked through the MMP sequence, an intramolecular quenching of Cy5 was observed at 665 nm (Φ/Φ (Cy5) $\sim$ 30%) as was previously observed for other linkers.[12,15] Treatment with active MMP-9 protease resulted in the expected recovery of the fluorescence intensity (Fig. 2). The spectrum after MMP cleavage matches that of control cyanine 5-containing peptide **7** prepared as described.[16] It is worth noting that compound **1** was found to be stable in buffer and plasma (see the ESI†). In parallel, the MMP-9 activity was carefully monitored by RP-HPLC (Fig. 3). Peptide fragment **2** was characterized by electrospray ionization mass spectroscopy without ambiguity since we found the deconvoluted mass to be in total agreement with the calculated mass ($M_{calc} = 5171.39$, $M_{found} = 5171.4$).
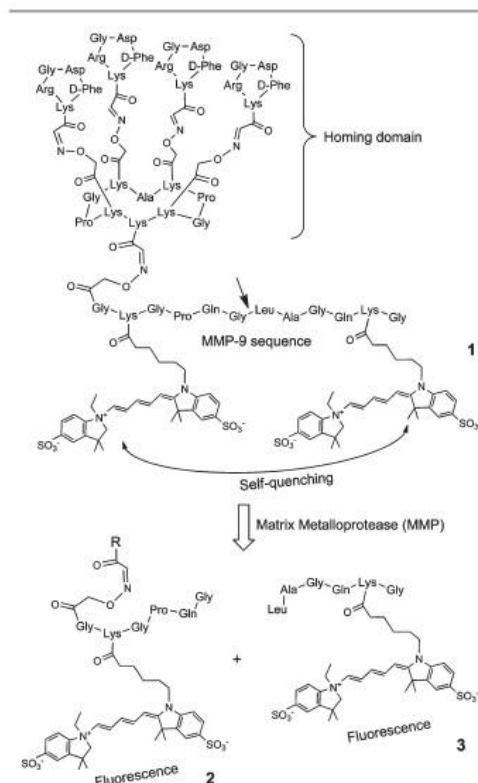
Fig. 1 Chemical structure of activatable fluorescent conjugate **1** (R = homing domain) bearing RGD ligands and MMP-9 cleavable sequence (the arrow shows the MMP-9 cleavage site).
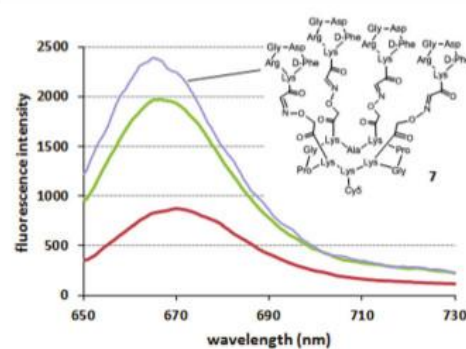
Fig. 2 Emission spectra for compound **1** (red), after addition of MMP-9 (green) at 24 h, and for control Cy5-containing peptide **7** (blue).
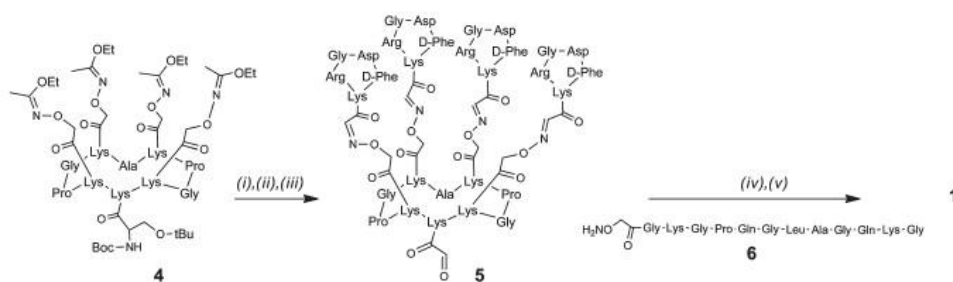
Scheme 1 Synthesis of **1**. (i) TFA–TIS–H$_2$O (95 : 2.5 : 2.5); (ii) 8.5 equiv. cyclo[-Arg-Gly-Asp-D-Phe-Lys(CO-CHO)-], H$_2$O; (iii) 10 equiv. NaIO$_4$, H$_2$O; (iv) 1.1 equiv. **6**, H$_2$O–CH$_3$CN (1 : 1); 2.6 equiv. Cy5-OSu, DMF, DIEA (pH 8.0).
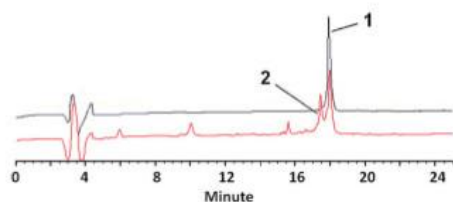
Fig. 3 HPLC profiles (214 nm) for compound **1** (black line) and after treatment with active MMP-9 protease (red line).

In vivo biological studies

We examined the behavior of compound **1** when injected into tumor-bearing mice. Several cell lines that differ in the expression of $\alpha_v\beta_3$ integrin and MMP-9 were selected. We decided to exploit the strongly $\alpha_v\beta_3$-positive HEK293(β3) human embryonic kidney cells, $\alpha_v\beta_3$-positive TS/A-pc mouse mammary carcinoma cells and A375 human melanoma cells, and $\alpha_v\beta_3$-negative HT1080 human fibrosarcoma cells. Integrin expression was monitored by flow cytometry using $\alpha_v\beta_3$ antibody (see the ESI†).

We then analyzed the capacity of activatable fluorescent compound **1** for the dual targeting of $\alpha_v\beta_3$ integrin and MMP-9. Nude mice bearing subcutaneous tumor xenografts received an intravenous injection of 2 nmol of **1**. To enable the MMP activity and the integrin expression, control mice were injected respectively with 2 nmol of commercially available MMPSense 680[17] or 2 nmol of fluorescent control peptide **7**. It is important to note that we routinely used a higher concentration of peptide **7** (10 nmol) for an optimal tumor imaging.[18] To establish the benefit of MMP, we decided to decrease the amount of the injected compound. Nude mice bearing tumor xenografts were then imaged at 24 h. As shown in Fig. 4, we found significantly lower MMP-9 activity in TS/A-pc than in other tumors. As expected, we observed a similar tumor uptake of cyanine 5-containing peptide **7** for control mice except for nude mice bearing tumor xenografts of HT1080. This result is in agreement with observed $\alpha_v\beta_3$ integrin expression by means of flow cytometry. When mice received activatable fluorescent compound **1**, a strong fluorescence signal showing the dequenching efficiency from MMP-9 was observed for mice bearing HEK(β3) while low emission was found in HT1080 tumor (dark grey bar, Fig. 4). These findings suggest that $\alpha_v\beta_3$ integrin expression is mandatory for the binding of compound **1** prior to the subsequent proteolytic cleavage from MMP-9, as HT1080 is a cell line known to highly express MMP-9.[19] Interestingly, more fluorescence was found in the TS/A-pc tumor than in the HT1080. This result confirms that activatable peptide **1** accumulates within the $\alpha_v\beta_3$-containing tumor, at best, as efficiently as control peptide **7**, then preventing its blood clearance. For tumors that expressed both $\alpha_v\beta_3$ integrin and MMP-9 (HEK-β3 and A375 tumors), the fluorescence signal is proportional to the observed integrin expression. Altogether, this study clearly shows the interest of
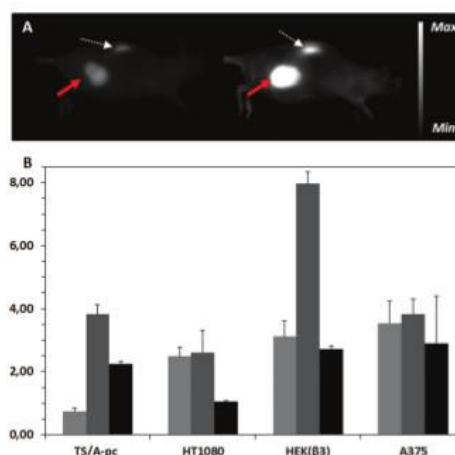
Fig. 4 (A) Fluorescence images of subcutaneous HEK(β3) tumor-bearing Swiss nude mice at 5 hours after intravenous injection of 2 nmol compound **1** (right) compared to 2 nmol compound **7** (left) (red arrow: tumor; white arrow: kidney; exposition time: 500 ms). (B) Tumor to muscle ratio of nude mice bearing tumor at 24 h after intravenous injection of 2 nmol MMPSense 680 (light grey bar), 2 nmol activatable fluorescent **1** (dark grey bar), or 2 nmol control Cy5-containing peptide **7** (dark bar).

introducing an MMP peptidic sequence for tumor detection as the dequenching from the MMP protease increases the tumor to muscle ratio.

Conclusion

In summary, a dual-specific MMP-activatable RGD compound was synthesized *via* iterative oxime ligations of peptide fragments. The ensuing compound was then evaluated through *in vitro* and *in vivo* experiments. Having established the principle of protease-activatable RGD targeting *in vivo*, we provide a strong molecular rationale for improving the design of targeted drug delivery vectors. An extension of the system combining a cytotoxic peptide and the MMP-activatable RGD compound is in progress and will be reported in due course.

Experimental section

RGD-containing peptide 5

Linear decapeptide was assembled on 2-chlorotritylchloride resin using building blocks and the subsequent head-to-tail cyclization was carried out as previously described affording peptide **4** that was used in the next step without further purification (see the ESI†).[14]

Full deprotection of peptide **4** (157.2 mg, 86 µmol) was carried out using 10 mL of a solution containing TFA–H$_2$O–TIS (95 : 2.5 : 2.5) at room temperature for 3 h. The product was

isolated after removal of solvents under reduced pressure and precipitation from diethyl ether to yield deprotected peptide as a white powder in quantitative yield (169 mg, 86 μmol). In parallel, cyclo[-Arg-Gly-Asp-D-Phe-Lys(-CO-CHO)-] was synthesized as previously described.[20]

To an aqueous solution (2 mL) containing the deprotected peptide (20 mg, 10.2 μmol) was added freshly prepared cyclo[-Arg-Gly-Asp-D-Phe-Lys(-CO-CHO)-] (67.5 mg, 87 μmol). The reaction mixture was stirred for 1 h at 25 °C. The RGD-containing conjugate was isolated after purification by RP-HPLC as a white powder (40.1 mg, 8.8 μmol, 86%). A serine oxidation of an RGD-containing conjugate (20 mg, 4.3 μmol) by an aqueous solution containing 10 equiv. of $NaIO_4$ (10.8 mg, 50.4 μmol) afforded the aldehyde component **5**. The product was directly purified by RP-HPLC to yield compound **5** as a white powder (14.6 mg, 3.3 μmol, 77%).

MMP peptide 6

Peptide synthesis was carried out as described in the general procedure (see the ESI†). Full deprotection of protected peptide $(Boc)_2NO-CH_2-CO$-Gly-Lys(Boc)-Gly-Pro-Gln(Trt)-Gly-Leu-Ala-Gly-Gln(Trt)-Lys(Boc)-Gly-OH (20 mg, 9.8 μmol) was done from a solution of $TFA-H_2O-TIS-EDT$ (90 : 5 : 2.5 : 2.5) for 2 h. The product was directly purified by RP-HPLC to yield compound **6** as a white powder (6 mg, 4 μmol, 41%).

Fluorescent conjugate 1

To a solution containing the derivative **5** (17 mg, 3.8 μmol) in 400 μL of H_2O-CH_3CN (1 : 1) was added the peptide **6** (6 mg, 4 μmol). The reaction mixture was stirred for 3 h at 25 °C. An MMP-containing conjugate was isolated after purification by RP-HPLC as a white powder (10 mg, 1.7 μmol, 46%). To a solution containing the MMP-containing conjugate (4 mg, 0.7 μmol) in 180 μL of DMF was added 3 μL DIPEA and cyanine 5-mono NHS ester (1.7 mg, 1.8 μmol). The reaction mixture was stirred overnight at room temperature. The product was directly purified by RP-HPLC to yield compound **1** as a blue powder (1.5 mg, 0.22 μmol, 31%).

Fluospectrometric analysis

Experiments were carried out by using 200 μL of 0.25 μM of compound **1** or control Cy-5 containing peptide in 50 mM Tris buffer (pH 7.5) with 150 mM NaCl, 5 mM $CaCl_2$ and 0.05% Brij-35 at 37 °C. Spectra were recorded from 650 to 750 nm. Samples were incubated at 37 °C and their spectra measured before incubation with the enzyme matrix metalloproteinase-9. Then, samples were incubated with 5 nM of MMP-9 at 37 °C for 24 hours (see also the ESI†).

In vivo fluorescence imaging

Nude mice (6–8 weeks old) received a sub-cutaneous xenograft of HEK293(β3) cells (20 × 10⁶ per mouse), HT1080 (10 × 10⁶ per mouse), A375 (10 × 10⁶ per mouse), or TS/A-pc cells (5 × 10⁶ per mouse). After tumor growth, mice (*n* = 3 for each group) were anesthetized (isoflurane/oxygen 4%/3.5% for induction and 2% thereafter) and were injected intravenously

into the tail vein with 200 μL of compound **1** or Cy5 control peptide (2 nmol) or 150 μL of MMPSense 680 (2 nmol), then they are illuminated by 633 nm (cyanine 5 compounds) or 660 nm (MMPSense) light-emitting diodes equipped with interference filters. Fluorescence images are acquired by a back-thinned CCD camera at −80 °C. After imaging at different time points after injection (30 minutes, 1 hour, 2 hours, 3 hours, 5 hours and 24 hours), the mice were sacrificed (at either 3 hours or 24 hours after injection) and dissected for imaging organs (see also the ESI†).

Acknowledgements

Notes and references

1 J. S. Desgrosellier and D. A. Cheresh, *Nat. Rev. Cancer*, 2010, **10**, 9.

2 (*a*) M. Pfaff, K. Tangemann, B. Müller, M. Gurrath, G. Müller, H. Kessler, R. Timpl and J. Engel, *J. Biol. Chem.*, 1994, **269**, 20233; (*b*) W. Arap, R. Pasqualini and E. Ruoslahti, *Science*, 1998, **279**, 377.

3 (*a*) K. Temming, R. M. Schiffelers, G. Molema and R. J. Kok, *Drug Resist. Updates*, 2005, **8**, 381; (*b*) E. Garanger, D. Boturyn and P. Dumy, *Anti-Cancer Agents Med. Chem.*, 2007, **7**, 552.

4 R. Haubner, W. A. Weber, A. J. Beer, E. Vabuliene, D. Reim, M. Sarbia, K.-F. Becker, M. Goebel, R. Hein, H.-J. Wester, H. Kessler and M. Schwaiger, *PLoS Med.*, 2005, **2**, e70.

5 W. Cai, D.-W. Shin, K. Chen, O. Gheysens, Q. Cao, S. X. Wang, S. S. Gambhir and X. Chen, *Nano Lett.*, 2006, **6**, 669.

6 M. Keramidas, V. Josserand, C. A. Righini, C. Wenk, C. Faure and J. L. Coll, *Br. J. Surg.*, 2010, **97**, 737.

7 S. Foillard, Z. Jin, E. Garanger, D. Boturyn, M.-C. Favrot, J.-L. Coll and P. Dumy, *ChemBioChem*, 2008, **9**, 2326.

8 S. Foillard, L. Sancey, J.-L. Coll, D. Boturyn and P. Dumy, *Org. Biomol. Chem.*, 2009, **7**, 221.

9 E. S. Olson, T. Jiang, T. A. Aguilera, Q. T. Nguyen, L. G. Ellies, M. Scadeng and R. Y. Tsien, *Proc. Natl. Acad. Sci. U. S. A.*, 2010, **107**, 4311.

10 G. Bergers, R. A. Brekken, G. McMahon, T. H. Vu, T. Itoh, K. Tamaki, K. Tanzawa, P. Thorpe, S. Itohara, Z. Werb and D. Hanahan, *Nat. Cell Biol.*, 2000, **2**, 737.

11 N. Ramos-DeSimone, E. Hahn-Dantona, J. Sipley, H. Nagase, D. L. French and J. P. Quigley, *J. Biol. Chem.*, 1999, **274**, 13066.

12 J. Razkin, V. Josserand, D. Boturyn, Z. Jin, P. Dumy, M. Favrot, J.-L. Coll and I. Texier, *ChemMedChem*, 2006, **1**, 1069.

13 E. Garanger, D. Boturyn, O. Renaudet, E. Defrancq and P. Dumy, *J. Org. Chem.*, 2006, **71**, 2402.

14 S. Foillard, M. Olsten Rasmussen, J. Razkin, D. Boturyn and P. Dumy, *J. Org. Chem.*, 2008, **73**, 983.

15 Φ/Φ (Cy5): relative fluorescence quantum yield of **1** in PBS (excitation at 649 nm, emission at 665 nm).

16 E. Garanger, D. Boturyn, Z. Jin, P. Dumy, M.-C. Favrot and J.-L. Coll, *Mol. Ther.*, 2005, **12**, 1168.

17 B. M. Wallis de Vries, J.-L. Hillebrands, G. M. van Dam, R. A. Tio, J. S. de Jong, R. H. J. A. Slart and C. J. Zeebregts, *Circulation*, 2009, **119**, e534.

18 Z. Jin, V. Josserand, J. Razkin, E. Garanger, D. Boturyn, M.-C. Favrot, P. Dumy and J.-L. Coll, *Mol. Imaging*, 2006, **5**, 188.

19 A. Faust, B. Waschkau, J. Waldeck, C. Höltke, H.-J. Breyholz, S. Wagner, K. Kopka, W. Heindel, M. Schäfers and C. Bremer, *Bioconjugate Chem.*, 2008, **19**, 1001.

20 D. Boturyn and P. Dumy, *Tetrahedron Lett.*, 2001, **42**, 2787.

III.2.1.   Conclusion

The RAFT-RGD-MMP compound is cleaved by active MMP-9, but not effectively by MMP-2.

Quenching can be observed, and dequenching due to the cleavage by MMP-9 can be measured by the increase in signal intensity and the RT-HPLC and mass analysis, which confirmed the cleavage site (see article). Another sign of the quenching – dequenching effect can be seen by observing the absorbance spectra and the shift in the emission spectra. The intact molecule has its emission peak in a slightly longer wavelength than the cleaved molecule. The absorption spectra shows a smaller principal absorption peak with a visible "pre-peak" at 610 nm due to the energy transfer of the two Cy5 next to each other. After cleavage of the Cy5 engrafted to the N-terminal extremity of the MMP-cleavable sequence the peak at 610 nm disappears and the principal peak augments, suggesting that digestion of the cleavage cassette occurred.

Reduced cleavage can be observed using MMP inhibitors. This confirms that the molecule is relatively stable and specifically cleaved by MMP-9 in the tested conditions. The slight increase in the fluorescence intensity observed is due to the loss of inhibitor efficacy in course of time as well as a certain non specific degradation of the molecule during incubation at 37°C for 48 h.

The molecule is stable in plasma for at least 24 h. After this time, it is slightly degraded due to plasma factors as well as the non specific decay due to incubation at 37°C for 48 h.

III.3. *In vitro characterization*

After studying the impact of MMP-9 on the cleavable cassette of the RAFT-RGD-MMP, the stability and its quenching / dequenching capacities, we studied the properties of RAFT-RGD-MMP in biological systems.

We firstly wanted to know, if the molecule reacted with the cell and if its specificity towards cancer cells was increased by the presence of the dual-recognition. Therefore we selected several cancer cell lines with different patterns of expression of integrin $\alpha_v\beta_3$ and MMP-9.

After testing the MMP expression *via* zymography (see supplementary information) and the integrin expression *via* flow cytometric analysis (FACS) using an immunolabeling with the LM609 antibody and RAFt-RGD-Cy5 (see supplementary information), the following cell lines were chosen:

Cell line	Integrin $\alpha_v\beta_3$ expression	MMP-9 expression
HEK293(β_3)	Very Strong (++++)	Strong (++++)
TS/A-pc	Medium (++/+)*	Medium (+++)
HT1080	Medium (++)/Weak (+)*	Strong (++++)
A375	Medium (++)/Weak (+)*	Medium(+++)
Colo829	Strong (+++)/Negative (-)*	Very weak (+)
PC-3	Negative (-)	Very weak (+)
HEK293(β_1)	Negative (-)	Weak (+)

Table III-2: Degree of integrin αvβ3 and MMP-9 expression of different cell lines.
*labeled by 0.2 μM RAFT-RGD-Cy5 at 30 min, 37°C

III.3.1. *Analysis of the RAFT-RGD-MMP binding on cells using flow cytometry*

The cells were incubated with either RAFT-RGD-MMP at 0.2μM or RAFT-RGD-Cy5 at 0.4μM at 37°C for 5 min, 15 min, 30 min, 1 h and 2 h. The control RAFT-RGD-Cy5 was used at twice the concentration of RAFT-RGD-MMP, in order to be at the same concentration of Cy5, since each RAFT-RGD-MMP was labeled with 2 Cy5 molecules.
For appropriate comparison of fluorescence intensity values within all conditions and cell lines, we calculated the percentage of augmentation of the MFI (mean fluorescence intensity) based on the control autofluorescence. The according unit is pa-MFI.

The human embryonic HEK 293 cell line is naturally expressing the α_v integrin but not the β_3 chain. For this reason it has been stably transfected with β_3 thus forming the HEK293(β_3) cell line that overexpresses a massive amount of β_3 and will serve as positive control for RGD binding. In addition, it is strongly positive also for MMP-9 expression.

As expected, this cell line is immediately and strongly labeled with both molecules (Figure III-14). Note that we always obtain two different populations of cells after labeling with RAFT-RGD, suggesting that this clone is not pure, with at least one "low" β_3 expressing and one "high" β_3 expressing population.

After 5 min of incubation, 86.2 % of the total cell population is already labeled by RAFT-RGD-MMP with a pa-MFI (Percentage of augmentation of the MFImean fluorescence intensity) of 1198. The cells treated with the control RAFT-RGD-Cy5, showed 80% of positive population, but a pa-MFI of 775 only. The RAFT-RGD-MMP over RAFT-RGD ratio is thus equal to1.56.
Both signals then regularly augment over time and finally the quasi totality of the cell population is labeled by each molecule, and the advantage is conserved for the RAFT-RGD-MMP (final ratio of 1.8 at 2h) (Figure III-15).

Figure III-14: Interaction of RAFT-RGD-MMP and RAFT-RGD-Cy5 (control) with HEK 293(β3) cells *in vitro*.
FACS analysis of cells incubated with RAFT-RGD-MMP (0.2μM) and RAFT-RGD-Cy5 (0.4μM) respectively at 37°C at T0, 5 min, 15 min, 30 min, 1 h and 2 h.
P2 indicates the auto-fluorescence, P3 the positively labeled cells. The percentage of the total population which is labeled positive is marked in the right upper corner.

Figure III-15: Evolution of pa- MFI (%) in HEK293(ß3) treated with either RAFT-RGD-MMP (0.2μM) or RAFT-RGD-Cy5 (0.4μM) at 37°C.

We then performed a competition assay in which the cells were firstly treated by unlabeled "cold" RAFT-RGD and later on with the fluorescent RAFT-RGD-MMP or RAFT-RGD-Cy5. The pretreatment with RAFT-RGD aimed at saturating the integrin $\alpha_v\beta_3$ receptors in order to better visualize the role of the enzyme (MMP) activity as well as the effect of non-specific interactions.

A very strong inhibition of the RAFT-RGD-MMP is observed in these conditions, with an almost 7-times reduced final MFI (2968 instead of 20 561 initially obtained without competition) (Figure III-16). This suggests that binding to the integrin is necessary before MMP-9 can function during the internalization process, since we can see here only the labeled cells and not the possible presence of unbound molecules in the medium.
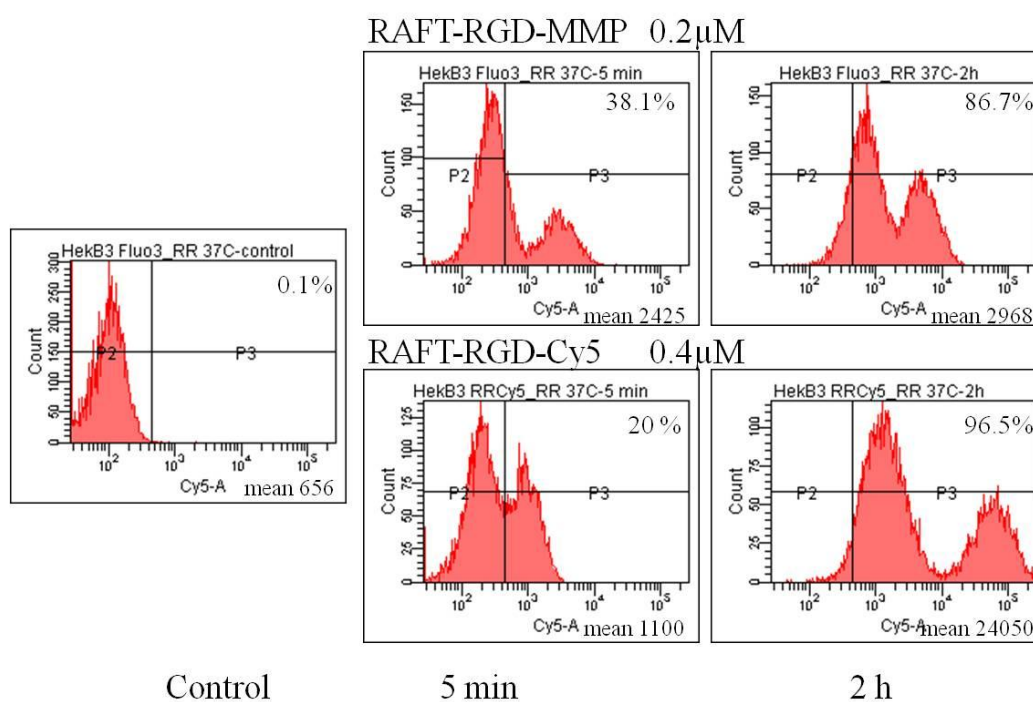
Figure III-16: FACS analysis of HEK 293(β3) pre-treated with RAFT-RGD and incubated with RAFT-RGD-MMP (0.2μM) and RAFT-RGD-Cy5 (0.4μM) respectively, at 37°C at T0, 5 min and 2 h.

The same tests were performed on the human a melanotic melanoma cell line A375 (Figure III-17). This cell line is expressing very low levels of RGD-interacting integrin as demonstrated by the labeling with RGD. Indeed, RAFT-RGD-Cy5 weakly labeled no more than 30 % of the cells after 2 h of incubation (pa-MFI = 116) (Figure III-18).

In contrast, nearly 100 % of these cells are fluorescent after 2 h of incubation with the RAFT-RGD-MMP at a pa-MFI of 298, thus providing a ratio of RAFT-RGD-MMP versus RAFT-RGD-Cy5 of 2.7.

Furthermore, the competition assay shows that the percentage of RAFT-RGD-MMP labeled cells drops from 100 down to 30% if the cells are concomitantly incubated with "cold" RAFT-RGD (Figure III-19).

This suggests that although the integrins are poorly expressed on the surface of these cells, the positive labeling obtained with RAFT-RGD-MMP requires its binding via RGD mainly.

Figure III-17: Interaction of RAFT-RGD-MMP and RAFT-RGD-Cy5 (control) with A375 cells *in vitro*.

FACS analysis of cells incubated with RAFT-RGD-MMP (0.2µM) and RAFT-RGD-Cy5 (0.4µM) respectively at 37°C at T0, 5 min, 15 min, 30 min, 1 h and 2 h.
P2 indicates the auto-fluorescence, P3 the positively labeled cells. The percentage of the total population which is labeled positive, is marked in the right upper corner.
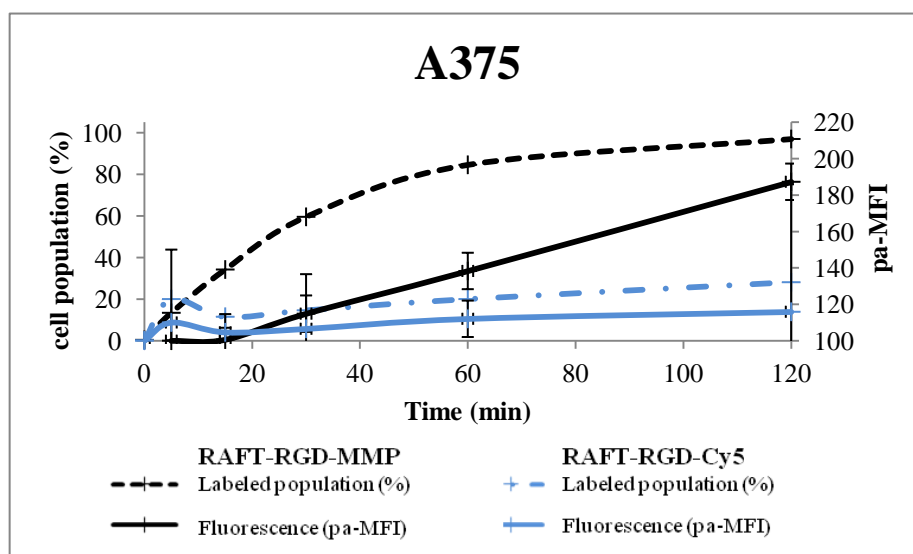
Figure III-18: Evolution of pa- MFI in A375 treated with either RAFT-RGD-MMP (0.2µM) or RAFT-RGD-Cy5 (0.4µM) at 37°C.
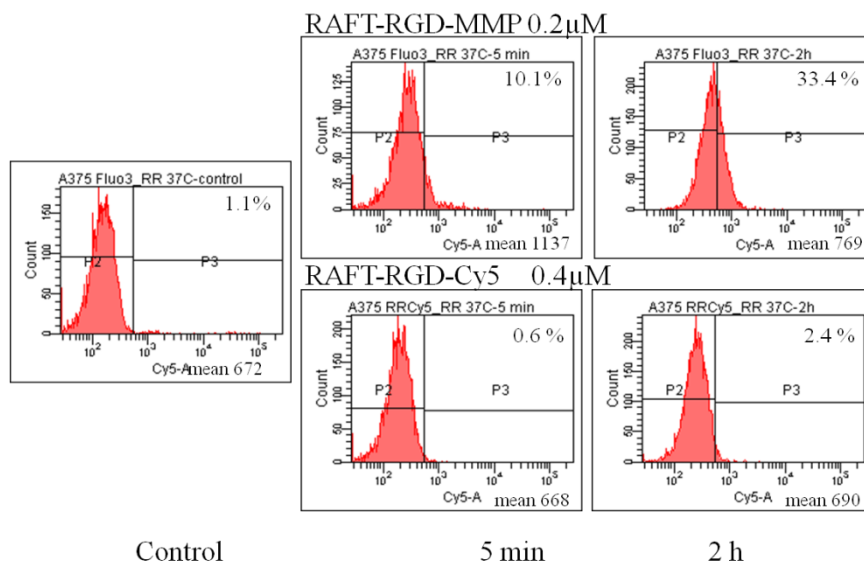
Figure III-19: FACS analysis of A375 pre-treated with RAFT-RGD and incubated with RAFT-RGD-MMP (0.2μM) and RAFT-RGD-Cy5 (0.4μM) respectively, at 37°C at T0, 5 min and 2 h.

When the same study was performed using the murine breast adenocarcinoma cell line TS/A-pc expressing moderately the integrin and MMP-9, the pattern of RAFT-RGD-MMP and RAFT-RGD-Cy5 labeling was quite similar to that of A375 (Figure III-20, Figure III-21). The ratio of both RAFT-RGD-MMP over RAFT-RGD-Cy5 reached a value of 3.2 after 2 h of incubation, confirming that MMP-9 was efficiently recruited by RAFT-RGD-MMP. This was further confirmed by repeating the experiment at 4°C instead of 37°C, thus strongly slowing down all enzymatic activities as well as internalization. In this case only 40% of the cells are labeled by RAFT-RGD-MMP after 2h, with a pa-MFI of 315 instead of 1127 at 37°C. Nonetheless, RAFT-RGD-MMP still performs better than RAFT-RGD at 4°C.
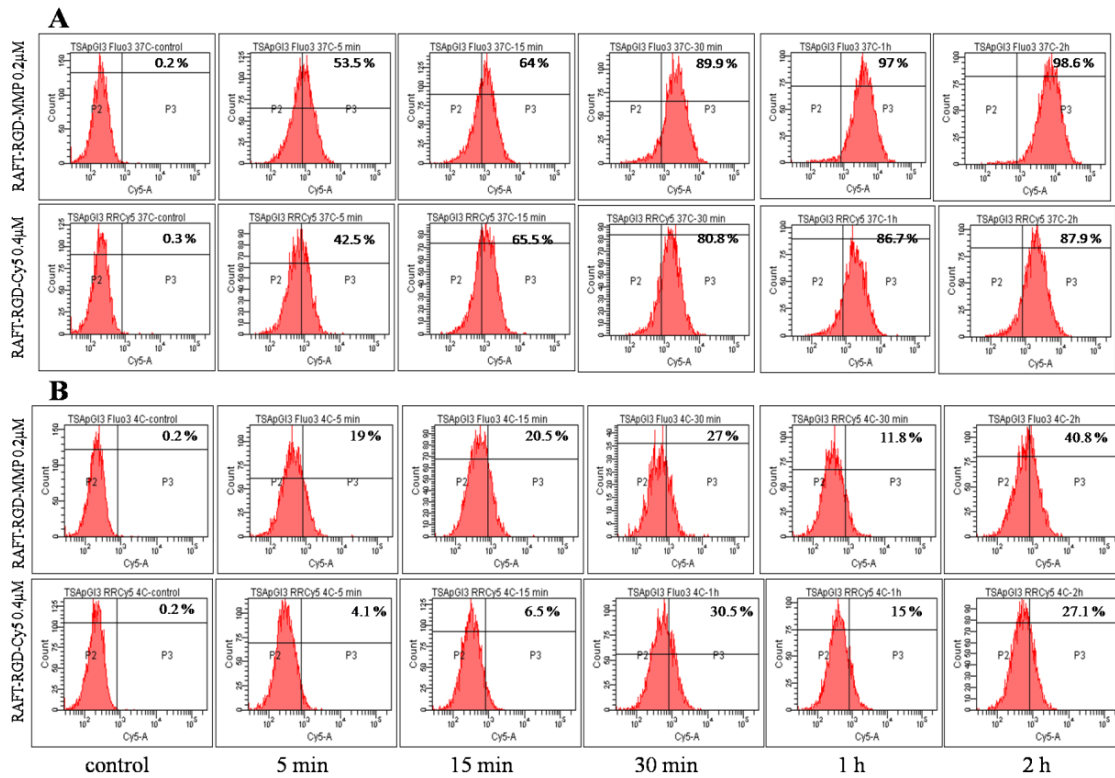
Figure III-20: Interaction of RAFT-RGD-MMP and RAFT-RGD-Cy5 (control) with TS/A-pc cells *in vitro*.

FACS analysis of cells incubated with RAFT-RGD-MMP (0.2μM) and RAFT-RGD-Cy5 (0.4μM) respectively at A) 37°C and B) 4°C at T0, 5 min, 15 min, 30 min, 1 h and 2 h.
P2 indicates the auto-fluorescence, P3 the positively labeled cells. The percentage of the total population which is labeled positive, is marked in the right upper corner.
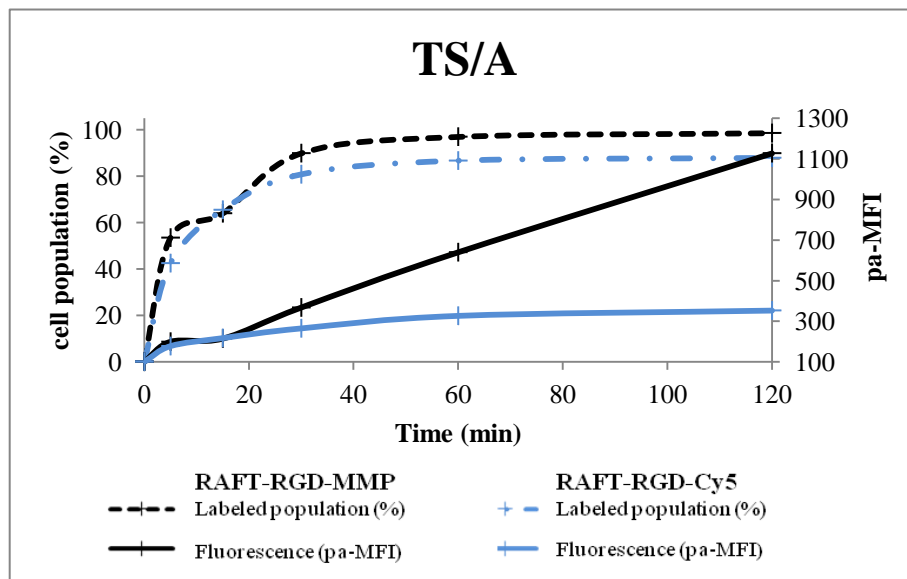
Figure III-21: Evolution of pa-MFI in TS/A treated with either RAFT-RGD-MMP (0.2μM) or RAFT-RGD-Cy5 (0.4μM) at 37°C.

The interest of using the bimodal RAFT-RGD-MMP molecule was even more obvious on the human sarcoma cell line HT1080 (Figure III-22 and Figure III-23). These weak integrin but high MMP-9 expressing cells are immediately labeled by RAFT-RGD-MMP (100 % of cells labeled at 5 min with a pa-MFI of 593). This signal steadily increased in intensity during the first 2h and reached a final pa- MFI value of 1856 as compared to 477, when they are incubated with RAFT-RGD-Cy5. The RAFT-RGD-MMP over RAFT-RGD-Cy5 ratio oscillated between 4 and 5 over time, suggesting a marked implication of the MMP-9. This was confirmed by repeating the same experiment at 4°C. In this case, only 50% of the cell population was labeled after 5 min and this level increased to nearly 80% after 2h but the max pa-MFI remained very low (194).

Once more, RAFT-RGD-MMP showed a stronger labeling also at 4°C as compared to the control RAFT-RGD-Cy5, thus confirming that the dual targeting is efficient.
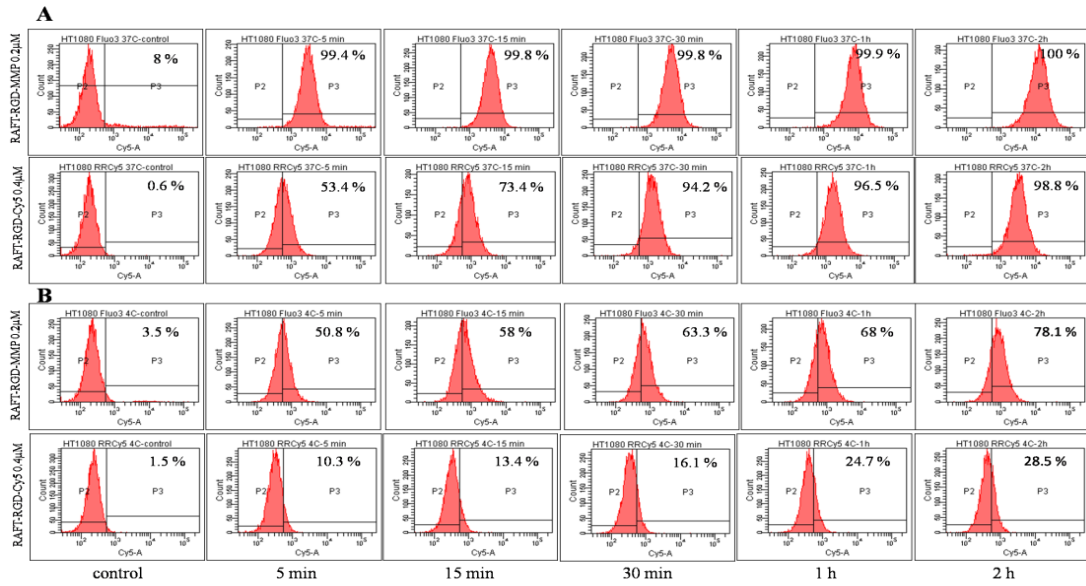
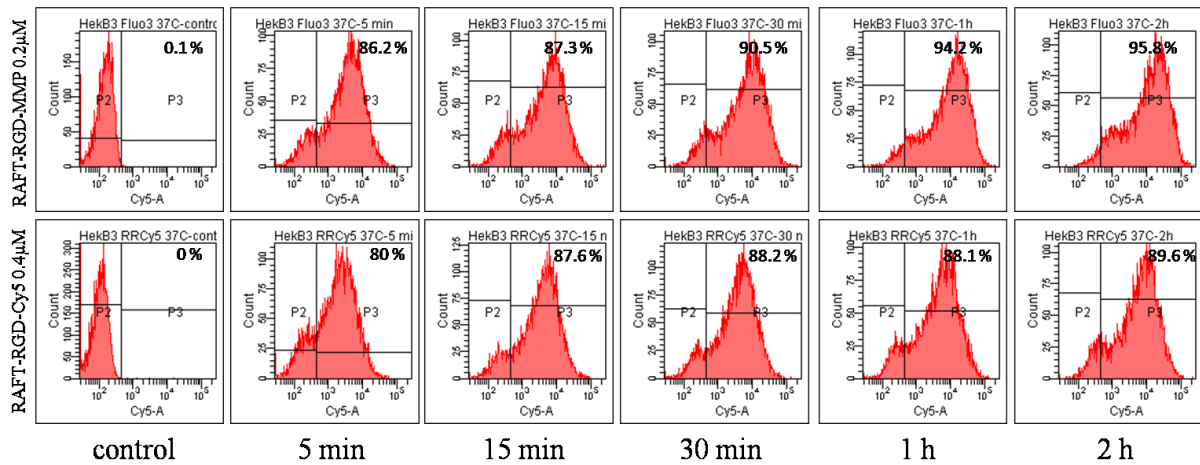**Figure III-22: Interaction of RAFT-RGD-MMP and RAFT-RGD-Cy5 (control) with HT1080 cells *in vitro*.**

FACS analysis of cells incubated with RAFT-RGD-MMP (0.2µM) and RAFT-RGD-Cy5 (0.4µM) respectively at A) 37°C and B) 4°C at T0, 5 min, 15 min, 30 min, 1 h and 2 h.
P2 indicates the auto-fluorescence, P3 the positively labeled cells. The percentage of the total population which is labeled positive, is marked in the right upper corner.
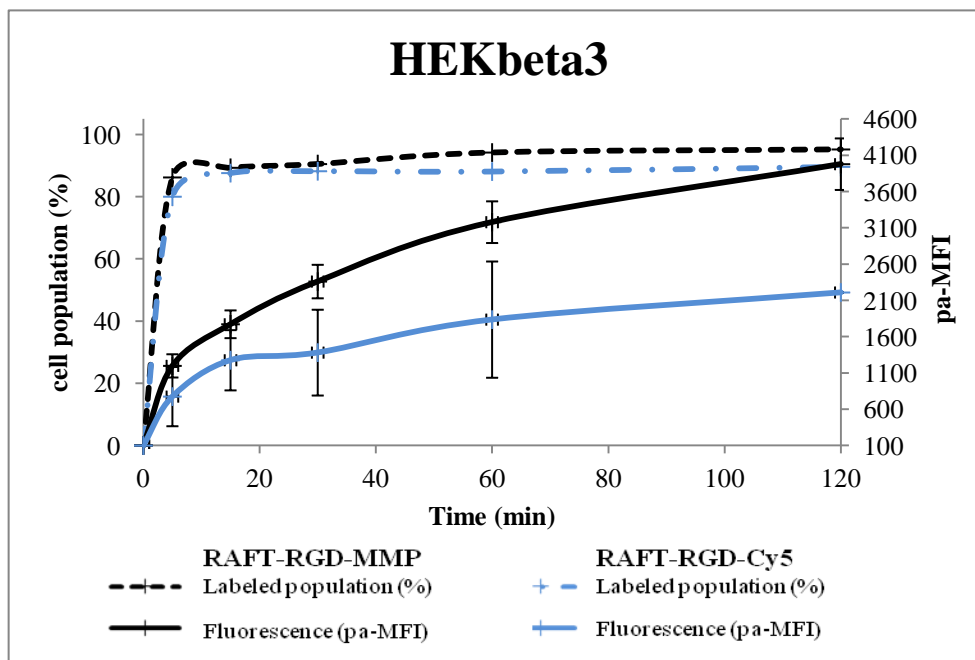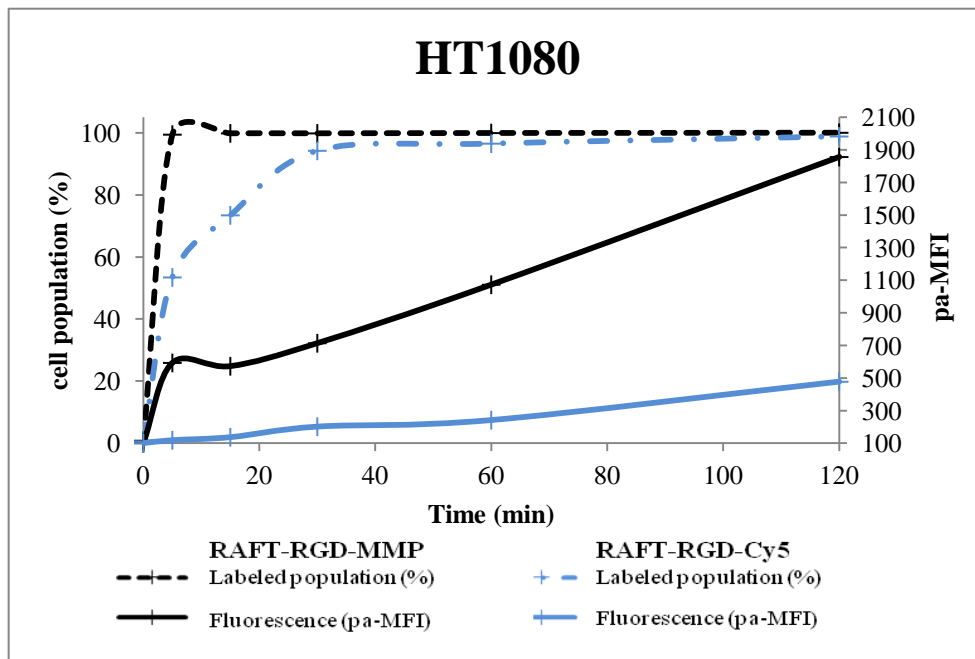

Figure III-23: Evolution of pa- MFI in HT1080 treated with either RAFT-RGD-MMP (0.2µM) or RAFT-RGD-Cy5 (0.4µM) at 37°C.

Observing the flow cytometry profiles at 37°C of Colo829 (Figure III-24 and

Figure III-25) and PC-3 (Figure III-26 and Figure III-27) cells, both with low RGD-binding and weak MMP-9 expression, a weak labeling of the cells can be observed.

In Colo829 the RAFT-RGD-MMP showed a weak binding, with a labeling at 2 h of 98.8 % of the population but only a pa-MFI of 220. The control RAFT-RGD-Cy5 showed fairly positive labeling of only 7.6 % of the population labeled at 2 h, with a pa-MFI of 121, thus nearly half the MFI compared to RAFT-RGD-MMP.

In PC-3 cells a similar effect can be observed. The RAFT-RGD-MMP interacted slowly with the cells, but labeled them completely after 2h of incubation whereas the RAFT-RGD-Cy5 shows only 30% labeling. These observations confirm the interest of a double targeting when dealing with cells expressing low levels of each target.
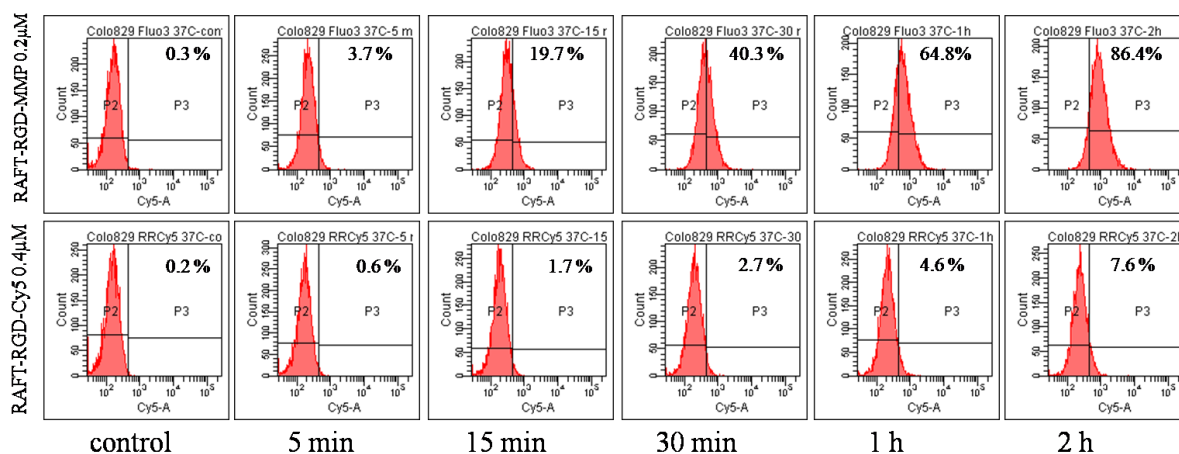
Figure III-24: Interaction of RAFT-RGD-MMP and RAFT-RGD-Cy5 (control) with Colo829 cells *in vitro*.

Flow cytometric analysis of cells incubated with RAFT-RGD-MMP (0.2μM) and RAFT-RGD-Cy5 (0.4μM) respectively at 37°C at T0, 5 minutes, 15 minutes, 30 minutes, 1 h and 2 h.
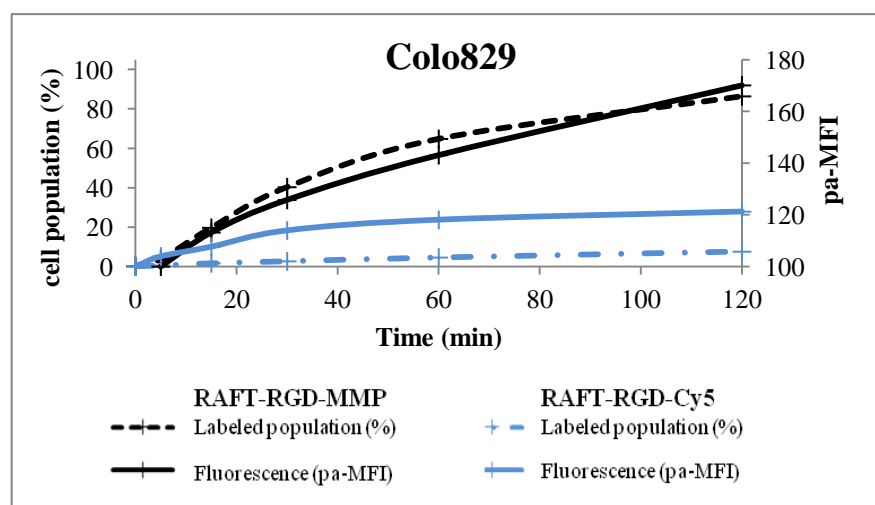
Figure III-25: Evolution of pa-MFI in Colo829 treated with either RAFT-RGD-MMP (0.2μM) or RAFT-RGD-Cy5 (0.4μM) at 37°C.
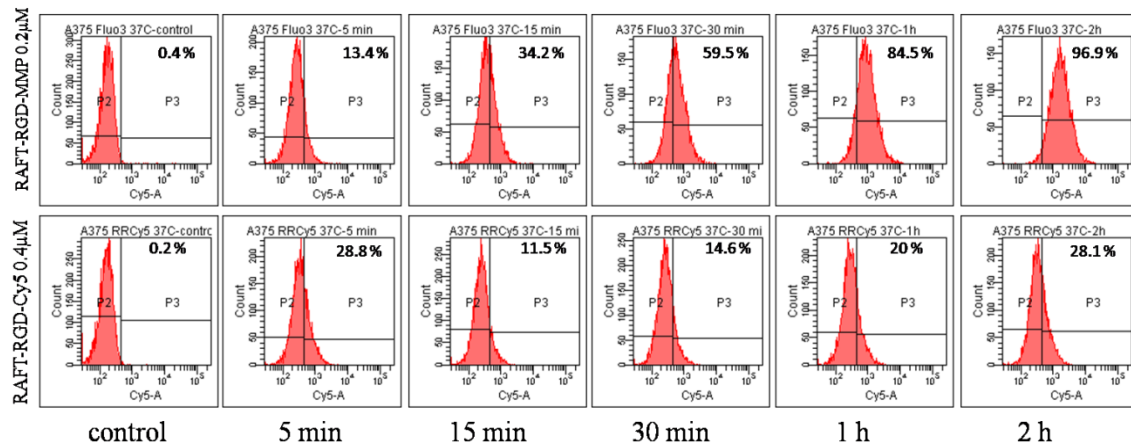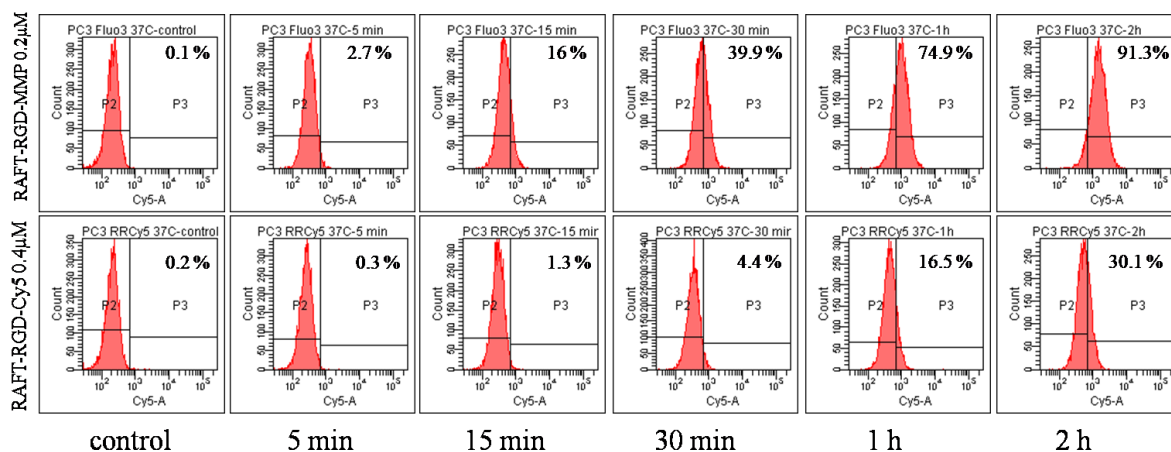

Figure III-26: Interaction of RAFT-RGD-MMP and RAFT-RGD-Cy5 (control) with PC-3 cells *in vitro*.

Flow cytometric analysis of cells incubated with RAFT-RGD-MMP (0.2μM) and RAFT-RGD-Cy5 (0.4μM) respectively at 37°C at T0, 5 minutes, 15 minutes, 30 minutes, 1 h and 2 h.
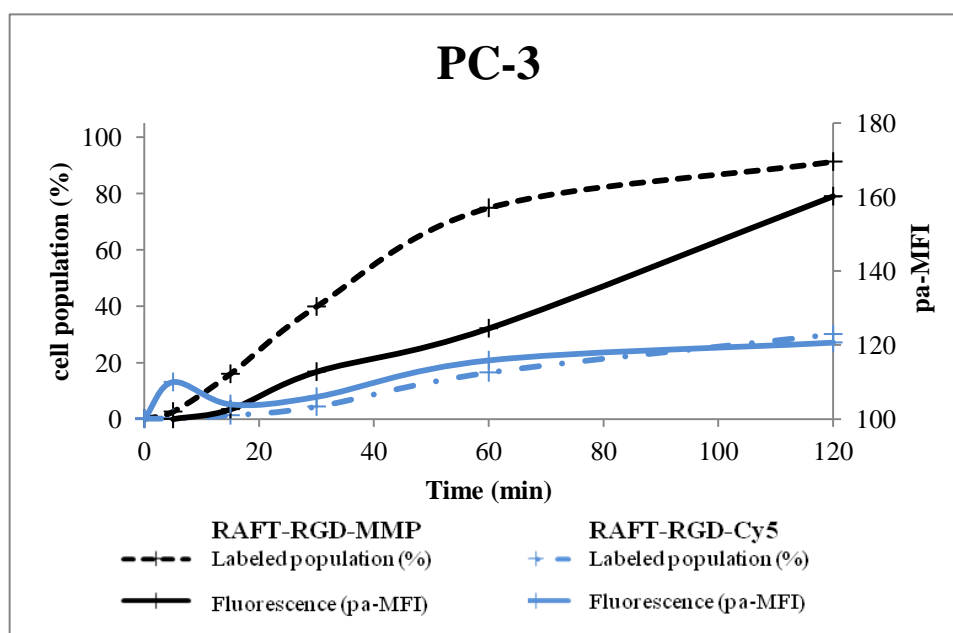
Figure III-27: Evolution of pa-MFI in PC-3 treated with either RAFT-RGD-MMP (0.2μM) or RAFT-RGD-Cy5 (0.4μM) at 37°C.

The RAFT-RGD-MMP in Hek293(β1) (Figure III-28) shows weak positive fluorescence when the incubation is performed at 37°C, while there is none at 4°C.

Hek293(β1) are $\alpha_v\beta_3$ integrin negative cells. At 37°C, 85 % of the cell population is labeled but only with very little intensity (pa-MFI of 186 at 2 h). Concerning RAFT-RGD-

Cy5 there is no labeling, thus the slight positive result has to be due to the MMP sequence added on the molecule

This confirms the increase in binding towards tumor cells, even if only few integrins are expressed. At 4°C no labeling can be observed in HEK293(β1) cells.
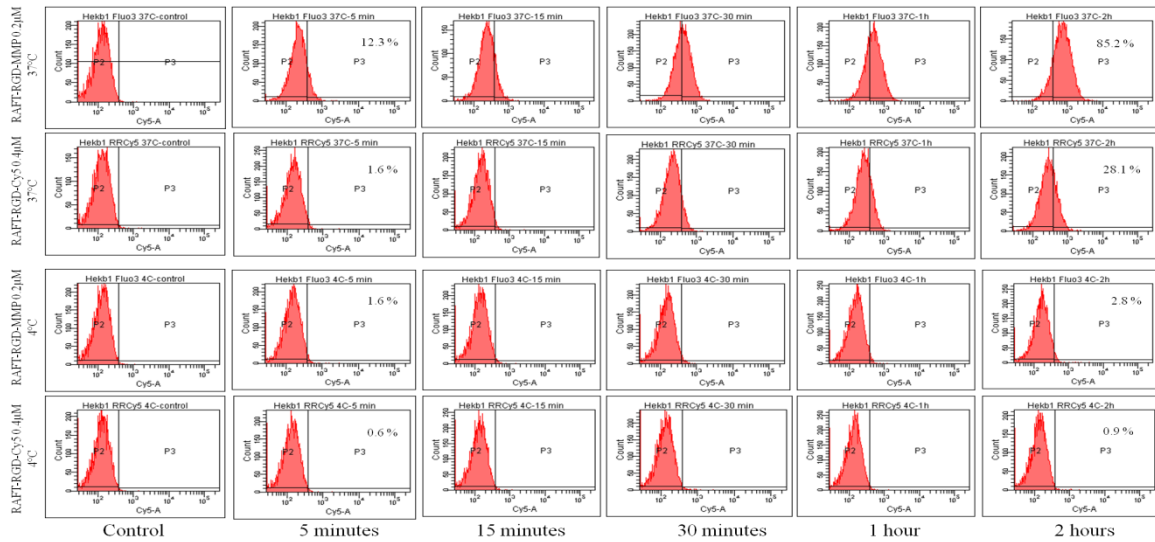
Figure III-28: Interaction of RAFT-RGD-MMP and RAFT-RGD-Cy5 (control) with Hek293(β1) cells
in vitro.

Flow cytometric analysis of cells incubated with RAFT-RGD-MMP (0.2μM) and RAFT-RGD-Cy5 (0.4μM) respectively at 37°C and 4°C at T0, 5 minutes, 15 minutes, 30 minutes, 1 h and 2 h.
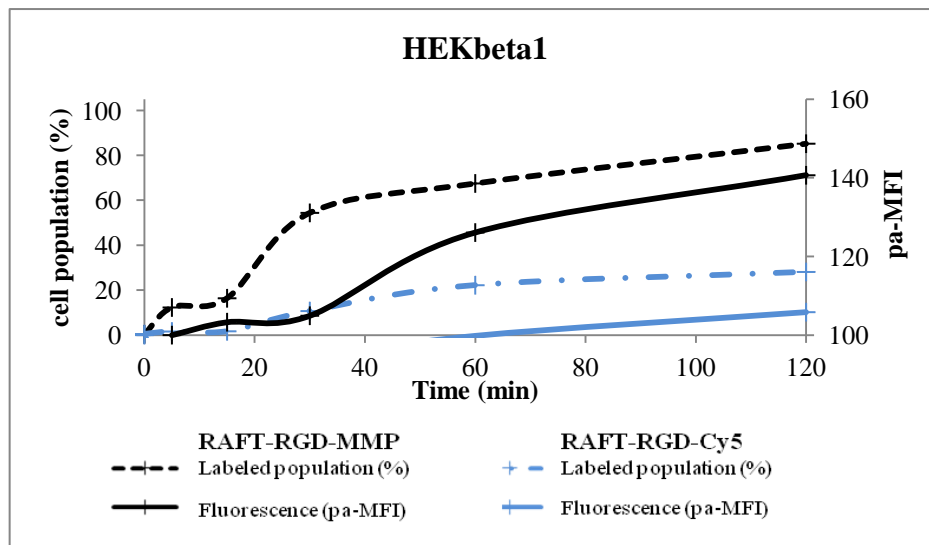
Figure III-29: Evolution of pa- MFI in HEK(β1) treated with either RAFT-RGD-MMP (0.2μM) or RAFT-RGD-Cy5 (0.4μM) at 37°C.

Comparing the data of all cell lines tested (Figure III-30), we can classify the different cell lines in 3 categories:

➢ HEKß3 is a particular case. Since it is expressing elevated levels of both targets, it is very strongly labeled by both molecules.

➢ HT1080, A375 and to a certain extend TS/A-pc cells are not perfectly labeled by the RAFT-RGD molecule but they are clearly better detected with the dual RAFT-MMP one.

➢ PC3, Colo829 and HEB293(ß1) are normally undetected by RAFT-RGD, but these tumors will certainly show up after 2h of labeling by the dual molecule.

This indicates that the dual RAFT-RGD-MMP will improve tumor labeling and detect some tumors that would have been left barely detectable by the initial RAFT-RGD tracer. However, this can also raise some concern about the specificity of the molecules toward other diseases that will express massively the MMP9 target.

Cell line	Integrin $\alpha_v\beta_3$ expression	MMP-9 expression
HEK293(β₃)	Very Strong (++++)	Strong (++++)
TS/A-pc	Medium (++/+)*	Medium (+++)
HT1080	Medium (++)/Weak (+)*	Strong (++++)
A375	Medium (++)/Weak (+)*	Medium(+++)
Colo829	Strong (+++)/Negative (-)*	Very weak (+)
PC-3	Negative (-)	Very weak (+)
HEK293(β₁)	Negative (-)	Weak (+)
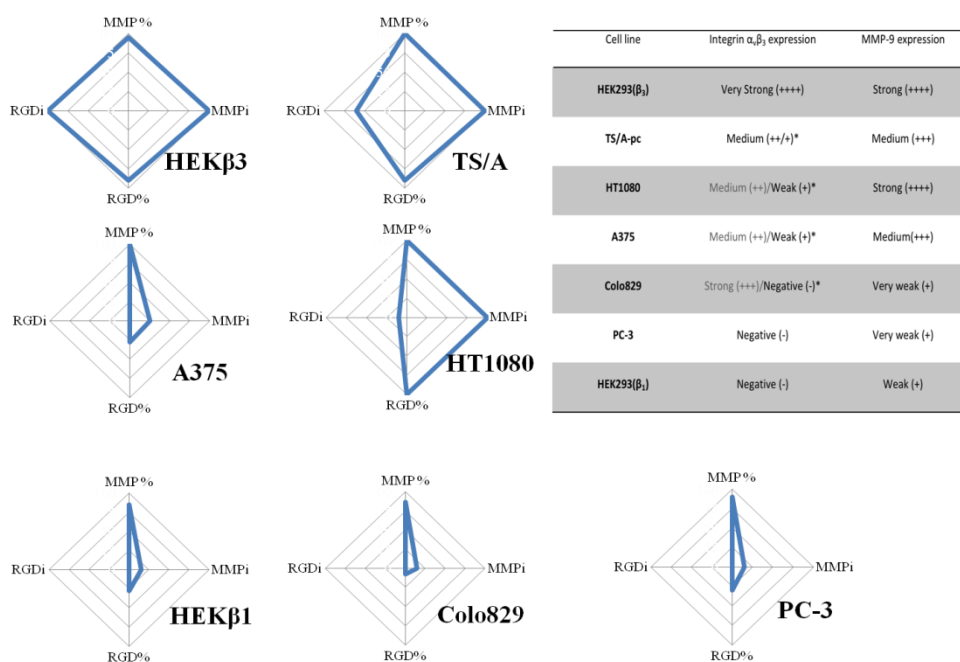
Figure III-30: FACS data of RAFT-RGD-Cy5 and RAFT-RGD-MMP compared.
Labeled population of RAFT-RGD-Cy5 (RGD%) and RAFT-RGD-MMP (MMP%) and pa-MFI of RAFT-RGD-Cy5 (RGDi) and RAFT-RGD-MMP (MMPi) at 2 h of incubation in the cell lines and HEK293(β3), A375, TS/A, HT1080 and HEK293(β1), Colo829 and PC-3 at 37°C.

III.3.2. Analysis of the RAFT-RGD-MMP binding on cells using confocal microscopy

In the next step, we studied the interaction between RAFT-RGD-MMP and the cells by confocal microscopy. We wanted to see in particular if the molecule was internalized and where its cleavage will take place. Living cells were observed during 15 min. The laser settings were adjusted before treatment with the molecule and kept at the same intensity throughout the whole acquisition in order to provide comparable information.

Using the integrin $\alpha_v\beta_3$ over-expressing HEK 293(β3) cells, a strong labeling of the cell membrane is seen at already 5 minutes, followed by a very powerful increase of fluorescence that saturates the camera at T=15 min (Figure III-31). In contrast, using the very weak integrin expressing cell line HT1080, no membrane labeling could be observed, neither at 5 nor at 15 min. However, the fluorescence intensity of the surrounding medium is positive after 15 min of incubation. This suggests that it is mainly the MMP-9 enzyme present in the extracellular medium that will act first. Note that the laser settings correctly adjusted for HEK 293(β3) cells at 5 min was not adapted to the visualization of low levels of labeling with HT1080.
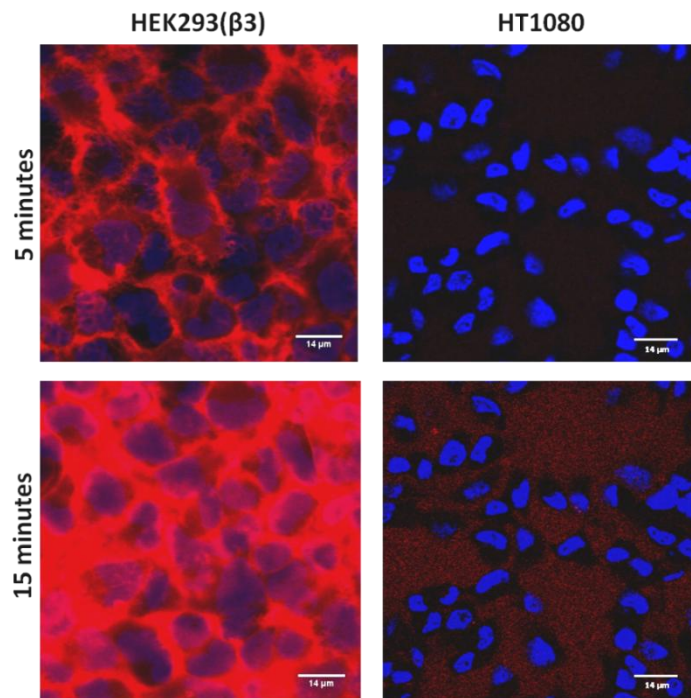
Figure III-31: Biphoton confocal microscopy of living cells.

HEK 293(β3) and HT1080 at 5 min and 15 min of incubation at 37°C with 0.6µM RAFT-RGD-MMP.

III.3.3.   Conclusion and discussion

These results suggest an important augmentation of the cell labeling when using RAFT-RGD-MMP instead of RAFT-RGD-Cy5, in particular for cell lines expressing moderate to low levels of integrin $\alpha_v\beta_3$.

The intensity of the labeling is always stronger when using RAFT-RGD-MMP in every cell line at 37°C. In addition, the blocking studies performed with HEK293(β3) or A375 cells confirmed the importance of the binding to the integrin that governs the final staining intensity. However, when using flow cytometry we followed the labeling of the cells but could not determine whether the labeling was present on the cell surface or within the intracellular compartments.

Nevertheless, the testing at 4°C compared to 37 °C lead to the conclusion that in cell lines with low levels of active integrin, like HT1080, PC-3 or Colo829 cells, the integrin binding is improved in the RAFT-RGD-MMP molecule, as seen in the higher MFI and percentage of labeled population, compared to the negative results obtained with RAFT-RGD-Cy5.

Here is to say, that an increase in non specific binding is not excluded, yet.
Using HT1080 we can see that although RAFT-RGD-MMP provides a stronger labeling of the cells as demonstrated by FACS, the predominant activity of MMP-9 over integrin binding is visible by confocal microscopy. This MMP-9 activity is present in the culture medium surrounding the cells. This indicates that this vector could release a pro-drug in the periphery of tumor cells in the cases where integrins are weak but MMP-9 is overexpressed and active.

The other tested cell lines over-expressed the integrin strongly (HEK 293(β3)), moderately (TS/A-pc) or weakly (A375) while MMP-9 activity was always present. Using these cell lines, we confirmed the impact and predominant importance of integrin interaction before MMP-9 can cleave the molecule. This was particularly obvious when RGD binding was prevented by a pre-incubation of the cells with "cold" RAFT-RGD and by incubation at 4°C.

III.4.   Double targeting effect in vivo

III.4.1.   Results

We then studied the interest of these molecules for *in vivo* tumor imaging. However, we were not able to run a lot of molecule-consuming experiments *in vivo*. This study is thus only preliminary.

Nude mice bearing subcutaneous HEK293(β3), TS/A-pc or A375 tumors, received an intravenous injection of 2 nmol RAFT-RGD-MMP (n = 3 mice per group) and were imaged several times during 24 h using 2D-FRI (fluorescence reflectance imaging).
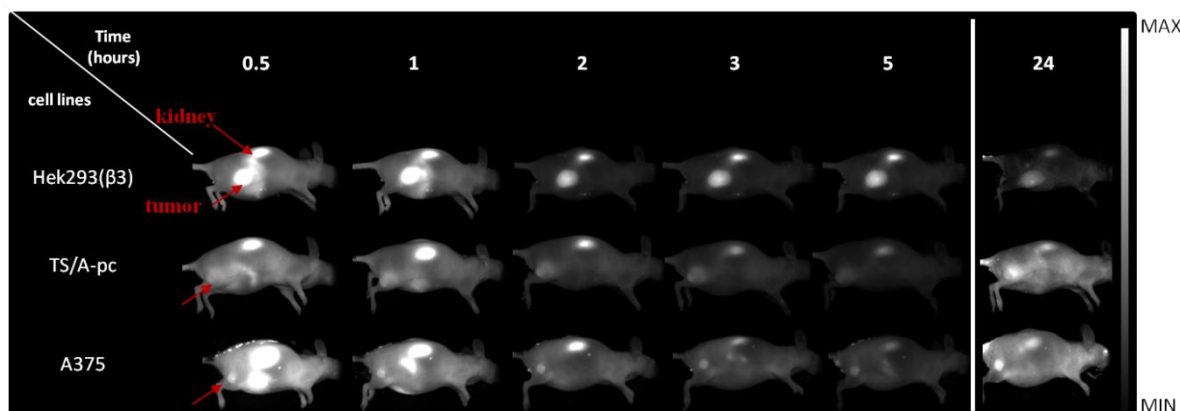
Figure III-32: Biodistribution of RAFT-RGD-MMP *in vivo*.
Subcutaneous tumor-bearing mice (HEK293(β3), TS/A-pc and A375) were imaged at different time, after intravenous injection of 2 nmol of RAFT-RGD-MMP.
Exposition time at 500ms; LUT min-max 2185-27743 for 0.5 to 5 h and 2185-4371 for 24 h.

As it can be observed, all the three types of tumors are positively labeled *in vivo*. A strong signal can also be observed in the kidneys as reported before when using RAFT-RGD derivatives, demonstrating the rapid and massive evacuation of these molecules by the renal elimination pathway. Accordingly, the non specific signal coming from unbound molecules and particularly visible in the skin, is rapidly decreasing, and reaches its background autofluorescence level after 2 h.

HEK293(β3) and A375 tumors are immediately labeled by the molecule, while the signal is building up more slowly in the TS/A-pc tumors. In each tumor, a positive signal can be detected during at least the first 24h.

We also compared the *in vivo* distribution with a quenched peptide sequence cleavable by MMPs (MMPSense™680, PerkinElmer, USA) and with RAFT-RGD-Cy5 in order to see the role of each of the two targets. Therefore, the same procedure was applied

as described before. Two nmol of each molecule was injected in subcutaneous tumor bearing mice (n = 3 mice per group) and the ratio of the fluorescence intensity over the measured intensity in the skin was calculated.

In the HEK293(β3) tumor bearing mice a quick and strong labeling of the tumor by RAFT-RDG-MMP is seen. It reaches a maximum at 5 h and decreases slowly afterwards (Figure III-33). The ratio at 5 h is 3-times more important compared to the control MMPSense and 1.5-fold higher compared to the RAFT-RGD-Cy5. In the weaker integrin A375 tumor, the ratio of tumor-to-skin is more rapidly increasing for the RAFT-RGD molecules compared to MMPSense680.

Compared to the profile in TS/A tumors, A375 show a softer increase until 5 h for RAFT-RGD molecules, demonstrating the importance of the initial integrin binding in TS/A and HEK293(β3).

In A375 tumors the ratio of the RAFT-RGD-MMP is decreasing very slowly compared to the integrin only targeting RAFT-RGD-Cy5. The ratio tumor-to-skin of MMPSense680 is rising very slowly, reaching the same level than RAFT-RGD-MMP but after 24 h.
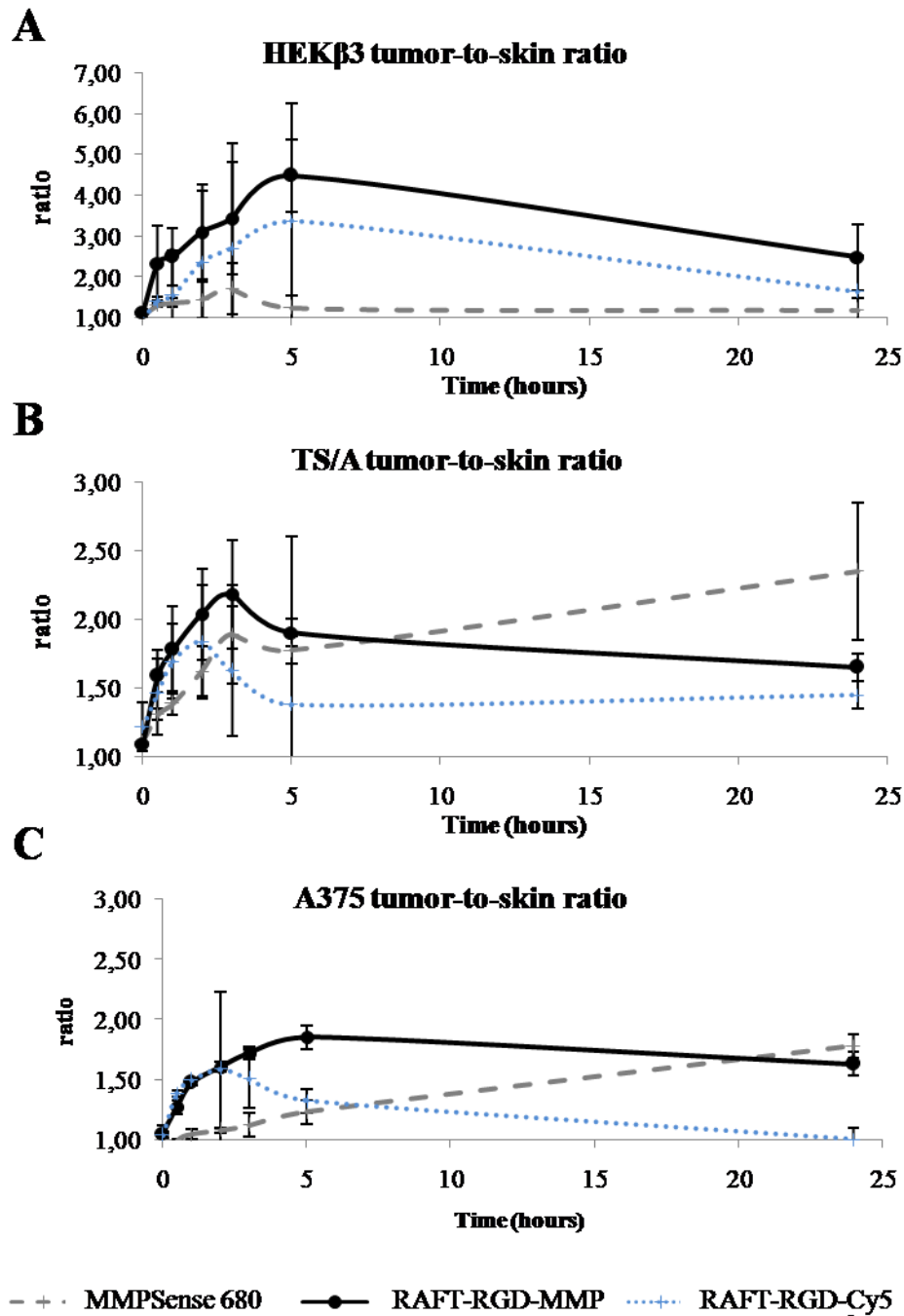
Figure III-33: Compared tumor-to-skin ratio during time *in vivo*.
Subcutaneous tumor-bearing mice (A) HEK293(β3), B) TS/A-pc and C) A375) were imaged at different times, after intravenous injection of 2 nmol of RAFT-RGD-MMP, MMPSense680 or RAFT-RGD-Cy5, respectively and their tumor-to-skin ratio compared.

Three h after injection of 2 nmol RAFT-RGD-MMP, an accumulation of fluorescence in the kidney and the tumor can be observed (Figure III-34).

The accumulation in the three tested tumors is particularly strong in HEK293(β3) and nearly even in TS/A and A375 at 3 h. The signal is barely detectable at 24 h except in the kidneys (Figure III-35). Interestingly, in terms of intensity, the tumor is coming in second position after the kidney while the other organs are not labeled, indicating the good targeting effect of our molecule. Accordingly a good tumor-to-muscle ratio is observed at 3 h (Figure III-36).
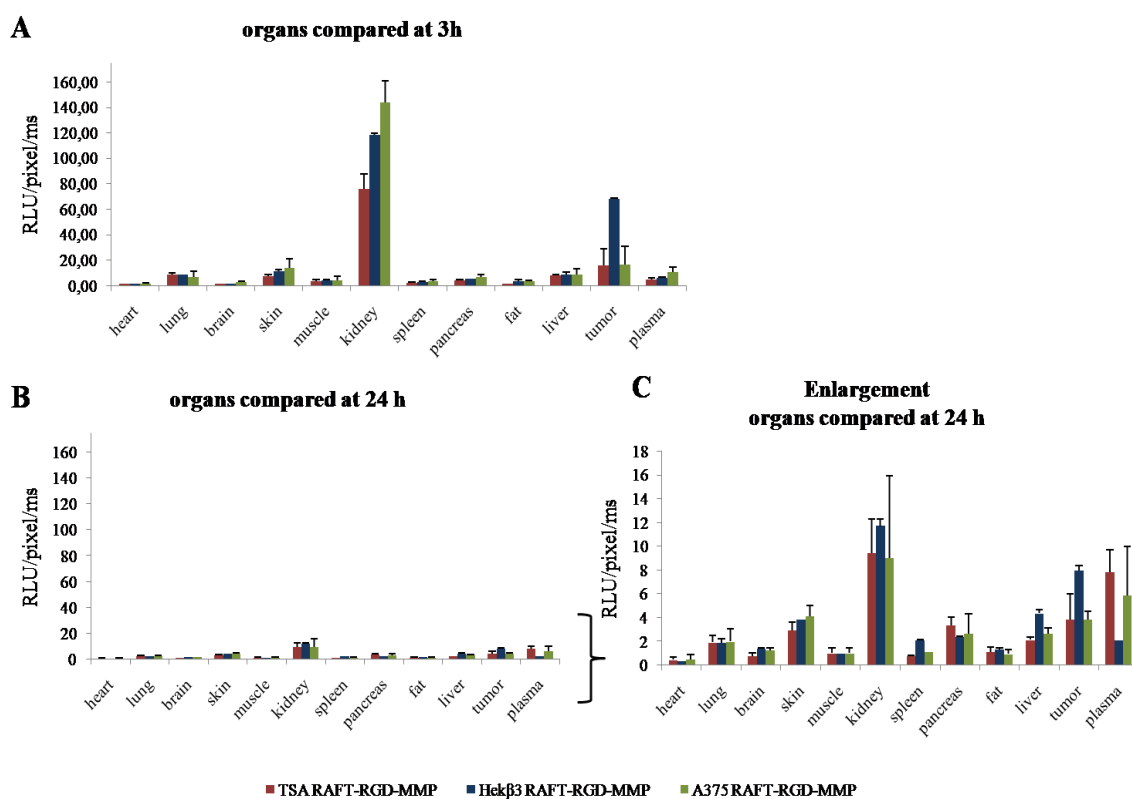
Figure III-34: Distribution of RAFT-RGD-MMP in different organs.
Fluorescence measured in different organs after sacrifice and dissection of mice at either A) 3 h (n = 3) or B)and C) 24 h (n = 3) post injection of 2nmol RAFT-RGD-MMP.
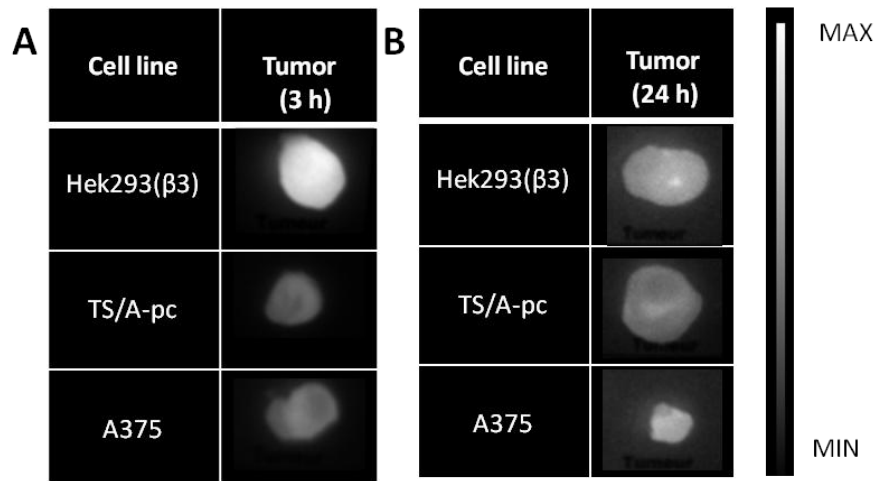
Figure III-35: Excised tumors (HEK293(β3), TS/A-pc and A375) of RAFT-RGD-MMP injected mice.
Fluorescence images of tumors *ex vivo* at either A) 3 h or B) 24 h post injection of 2 nmol RAFT-RGD-MMP.
Exposition time at 500 ms ; LUT min-max 1832-6779 (A) and 1832-41530 (B)
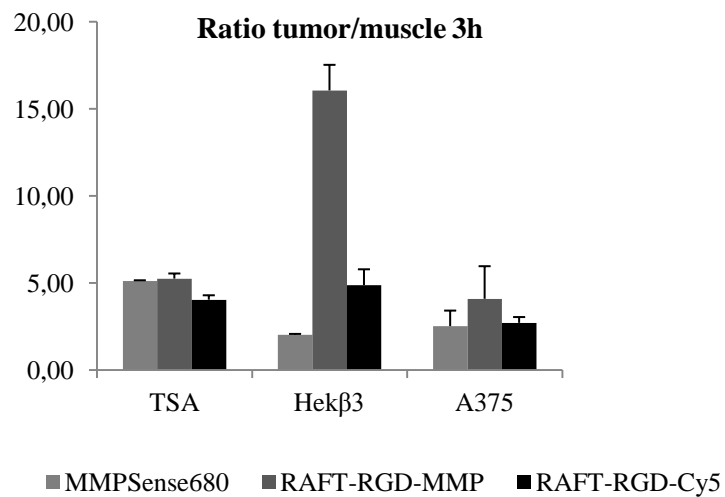
Figure III-36: Tumor-to-muscle ratio of subcutaneous tumor bearing mice at 3 h post injection of 2 nmol RAFT-RGD-MMP.

III.4.2. Conclusion

The RAFT-RGD-MMP labels the tumors *in vivo*, by reaching a best tumor-to-muscle ratio in HEK 293(β3) tumor bearing mice, followed by TS/A-pc and A375 tumor bearing mice. In TS/A-pc and A375, there is a final equal balance between integrin expression predominant in TS/A-pc cells and the MMP over-expression existing in A375 cells that can explain the similar patterns we observed. The molecule is obviously eliminated by the kidneys as RAFT-RGD-Cy5. Its excretion begins immediately after injection and is rapid and efficient since no or very little fluorescence can be detected at 24h. This is definitely an asset as far as imaging is concerned. Moreover it is also in favor of a low toxicity.

III.5.   *General conclusion*

RAFT-RGD-MMP is a peptide with a double-targeting function. Its cleavable cassette is sensitive to MMP-9 *in vitro*, which has been demonstrated by its measurable dequenching in the presence of this enzyme. At the same time the molecule is stable during 24 h in serum at 37°C, followed by a slow degradation.

It's interaction with cells *in vitro* is principally mediated by the RGD motif targeting integrin $\alpha_v\beta_3$ as confirmed by the blocking experiments. But the affinity of the molecule for the MMP-9 enzyme also contributes to its augmented binding on the cells, as shown by their improved fluorescent labeling (MFI) as compared to that obtained with RAFT-RGD-Cy5only. Indeed, all tested cell lines were more intensively stained by the dual molecule, leading to the conclusion, that a double targeting provides a stronger recognition of tumor cells.

Our preliminary tests *in vivo* indicates that the strongest interaction and additive effect can be observed as expected in HEK293(β3) cells, since these cells strongly over-express the two targets.

However, the gain provided by the presence of the MMP-specific sequence may eventually lead to a diminution of specificity. These molecules could be activated by other pathologies than cancer, like inflammation. However, if optical guided surgery is the issue this should not be a major problem since tumors are always inflammatory and should be more intensively labeled in their front of invasion, which is exactly, what we are looking for. Otherwise, removing inflammatory tissues that do not contain tumor cells would be augmented also, but this will need to be evaluated.

In addition, these dual molecules also have the advantage of being activatable as compared to the original RAFT-RGD and could thus be used for activatable drug release also. We did not optimized the gain provided by the presence of the cleavable cassette, since in our case the double labeling with Cy5 and expected quenching/dequenching is not fully functional. Additional experiments should be performed in order to generate better activatable optical probes.

III.6.   *Supplementary data RAFT-RGD-MMP*

III.6.1.   *Enzyme activity control and inhibitor test*
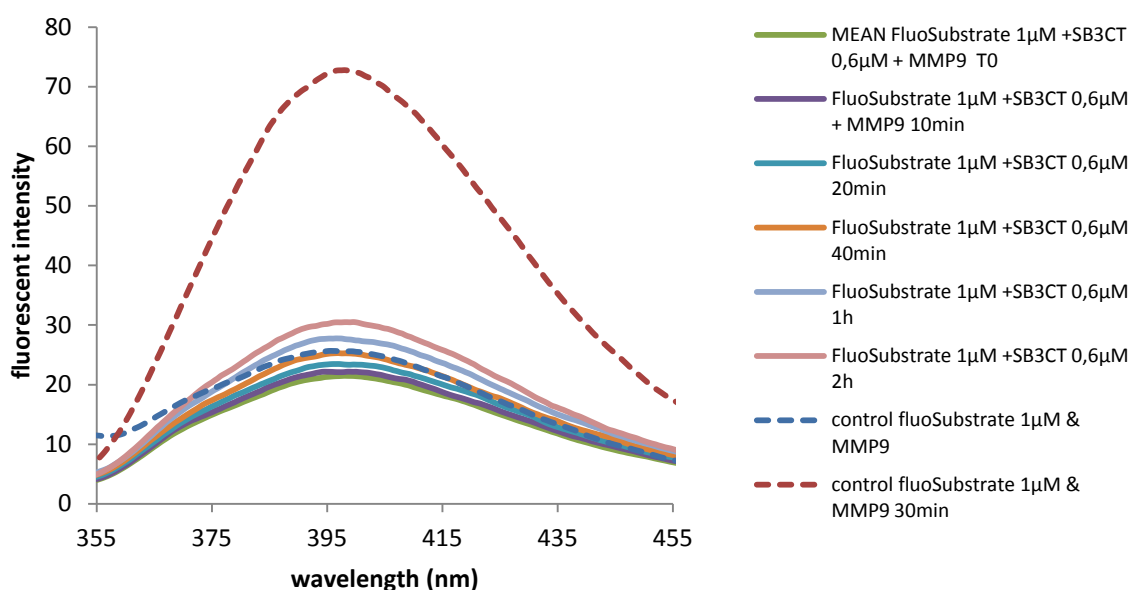
Figure III-37: Control of MMP-9 activity and inhibitor by means of Fluospectrometry.

1 µM of the MMP cleavable peptide fluorogenic substrate (EnzoLifescience) was incubated with MMP-9 and with the inhibitor SB3-CT and MMP-9 for 2 h.

The fluorogenic substrate was used to see whether the enzyme used was active or not and as control of the inhibition effect of SB3-CT, the inhibitor used.

In Figure III-37, we showed that the enzyme is degrading properly the molecule, seen by the increase in the fluorescence intensity measured by Fluospectrometry. The difference between the signals measured at time 0 and after 30 minutes is 3.75-times.

Concerning the inhibitor, the measurements show a slowing down of the enzyme activity, but not a complete inhibition. The SB3-CT efficacy decreases in course of time, visible by the slow increase of intensity during the first 40 minutes.

III.6.2.   MMP-2 and MMP-9 expression of different cell lines

Zymography is a method detecting the presence of active Gelatinases, such as MMP-2 (65 kDa) and MMP-9 (84 kDa). After electrophoretic separation, gelatinases are visible because they digest the gelatin substrate in the gel and are thus visible as clear bands after coomassie blue staining of the gelatin in the gel. MW: MMP-9 (zymogene/active) = 92/84 kDa; MMP-2 (zymogene/active) = 72/65 kDa

Using zymography we verified and/or confirmed the presence of MMP-9 and MMP-2 expressed by the different cell lines, and estimated their respective content as compared to the well known referenceHT1080cell line, over-expressing MMP-2 and MMP-9(Figure III-38; Figure III-39).

We measured that HEK293(β3) cells express nearly as much MMP9 (85%) as HT1080, while MMP-2 expression is even more elevated(138 %). TS/-A showed only 70% of MMP-9 expression and 25 % of MMP-2, followed by the cell line A375 with 40 % MMP-9 and 55 % MMP-2. Surprisingly HEK293(β1) cells only express 60 % of MMP-9 and 28 % of MMP-2. The lowest expression has been measured in PC-3 cells at 8 % MMP-9 and 20 % MMP-2 and the cell line Colo 829 with 19 % MMP-9 and 12 % MMP-2.
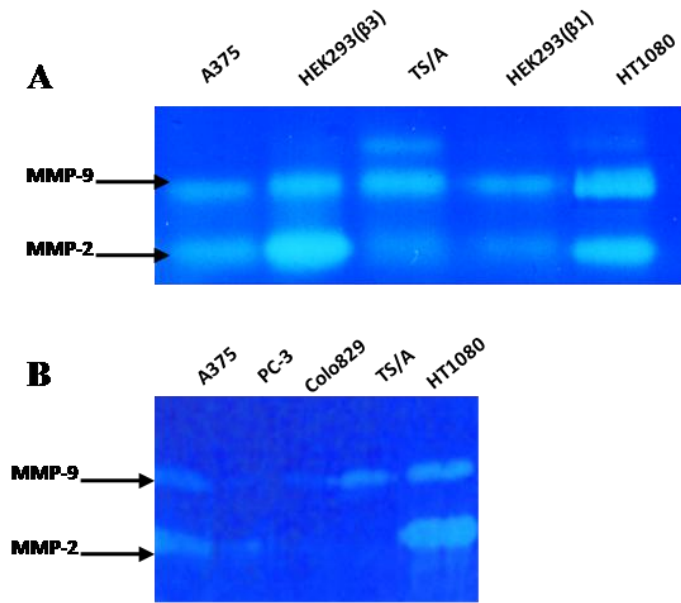
Figure III-38: Zymography of 10-times concentrated serum-free supernatant at 24 h of the cell lines A375, HEK293(β3), TS/A-pc, HEK293(β1) and HT1080 (A)and A375, PC-3, Colo829, TS/A-pc and HT1080 (B).
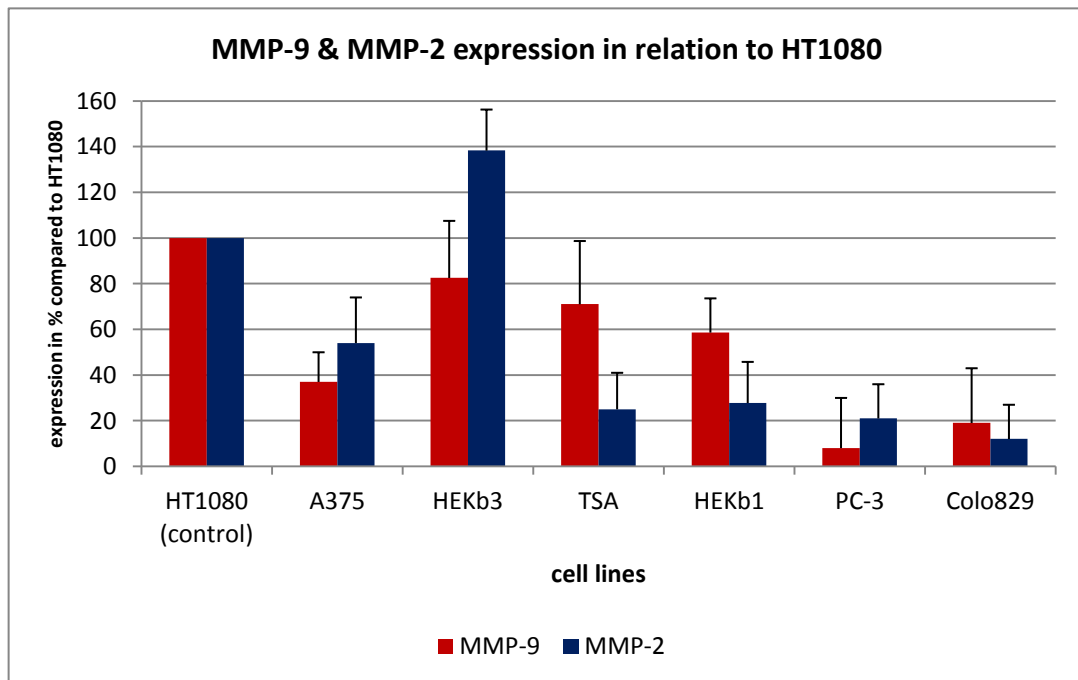
Figure III-39: Gelatinases expression of different cell lines used with HT1080 as reference.

(Quantification of Zymography gels showing the mean of MMP expression in relation to HT1080)

III.6.3.   *Flow cytometry analysis of the integrin $\alpha_v\beta_3$ expression*

The expression of the integrin has been tested by labeling *via* the antibody LM609 (anti-integrin αvβ3) indicated by "Integrin αvβ3" and RAFT-RGD-Cy5 in FACS analysis (Table III-3).

Integrin $\alpha_v\beta_3$		Integrin $\alpha_v\beta_3$	RAFT-RGD-Cy5
Literature	cell line	antibody	30 min; 37ºC; 0,2µM
		positive labeled population (%)	positive labeled population (%)
Positive	Hekβ3	99,9	99,4
Positive	M102	93,9	57,7
Positive	M288	98,3	6,5
Negative	M301	0,4	25,3
Positive (low)	FM29	97,6	94,6
Positive (low)	Gmel	97,4	37,5
Positive (low)	HT1080	76	45
Positive	A375	87.9	10 (but 30% after 2 h)
Negative	PC-3	1.4	2
?	Colo829	91.1	1
Positive	TS/A-pc		50

Table III-3: FACS analysis of integrin expression in different cell lines.

All cell lines except the human melanoma M301 and the human prostate carcinoma PC-3 are labeled by the antibody LM609 suggesting the presence of the integrin. However, the integrin may not always be functional and/or accessible and thus the labeling by RAFT-RGD–Cy5 can differ from that of the antibody. This is the case with the melanoma M288, the PC-3, Colo829 and the A375 cell lines.

III.6.4.   *Level of autofluorescence of mouse organs ex vivo*

The autofluorescence level at the same conditions used for *in vivo* and *ex vivo* imaging of the RAFT-RGD-MMP studies in mouse organs is presented in Figure III-40.

Here, we show that the level of the organs - except tumor and kidney − correspond to the *in vivo* studies of RAFT-RGD-MMP at 24 h.

Thus, no unspecific accumulation could be observed in the previous described study.
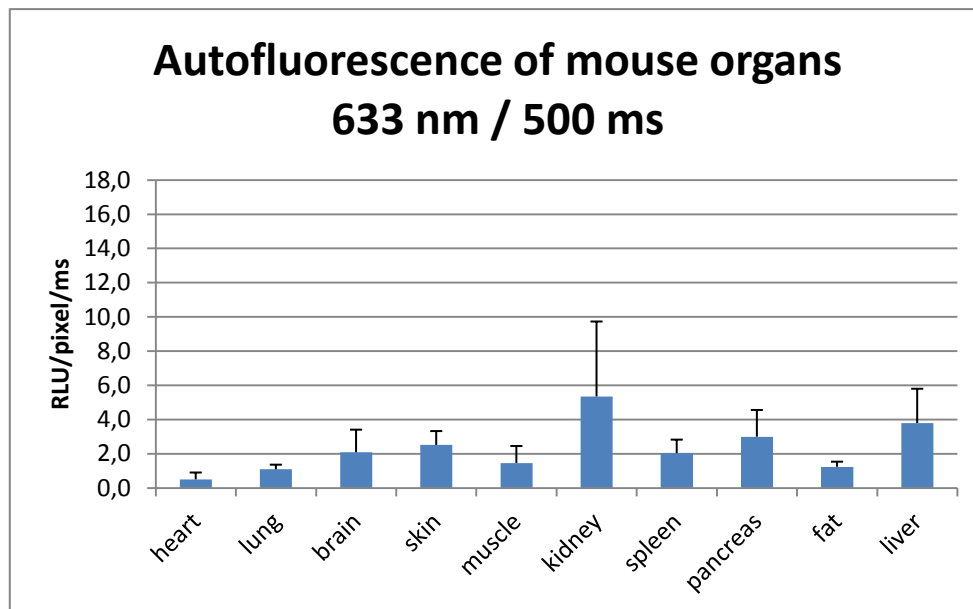
Figure III-40: Fluorescence intensity in non treated mouse organs *ex vivo*.

„Eine neue Idee ist ein Licht, welches Dinge beleuchtet, die, ehe das Licht darauf fiel, ohne Form für uns waren.“

Susanne K. Langer,1984

[A new idea is a light, illuminating a thing that, before the light touched it, was structureless for us.]

DISCUSSION AND PERSPECTIVES

I.   Near-infrared fluorescence guided surgery in the feline fibrosarcoma

The aim of my first project was the evaluation of an intra-operative near-infrared fluorescence (NIRF) imaging device in combination with a cancer targeting probe in clinical conditions. This clinical veterinary phase on spontaneous tumors is important for translating this technology towards clinical surgery in humans and was designed to provide information for the eventual adaption of the system.

The interest of this technology for cancer surgery is the based on several aspects. At first, tumor resection still represents the primary therapeutic indication before chemotherapy or radiotherapy in most cancers. Since survival strongly depends on the exhaustiveness of the tumor resection, innovative methods improving the quality of cancer surgery are needed to lower the risks of postoperative local recurrence. Second, up to now, no approved technology with high specificity and sensitivity, tracers included, are on the market for real-time image guided surgery of open surgical field.

I.1.   Feasibility of NIRF-guided surgery in veterinary clinic conditions

Our former results on mice bearing peritoneal carcinomatosis showed that NIRF optical guidance of surgery greatly improved the quality of the surgery by doubling the number of detected nodules and reducing two times the duration of the surgery.

In the present study on cats, my results show that the technology is adapted to intra-operative guided surgery, providing good tumor-to-healthy tissue delineation in clinical conditions.

AngioStamp™ has a high specificity towards the tumor and can provide elevated tumor-to-healthy tissue ratios (around 14 in 0.3 mg/kg at 36 h) as compared to other molecules like ICG[235].Moreover, a unique and relatively low dose of 0.3 mg/kg is sufficient.

No short-term toxicological effects in cats with high doses of AngioStamp™ have been observed. Fluorescence kinetics show that the tracer follows an efficient elimination of

---

[235]Crane, Lucia M.A., George Themelis, K. Tim Buddingh, Niels J. Harlaar, Rick G. Pleijhuis, Athanasios Sarantopoulos, Ate G.J. van der Zee, VasilisNtziachristos, und Gooitzen M. van Dam. „Multispectral Real-time Fluorescence Imaging for Intraoperative Detection of the Sentinel Lymph Node in Gynecologic Oncology". *Journal of Visualized Experiments : JoVE*, Nr. 44 (Oktober 20, 2010

first order, leaving a short F_{50} of minute range and the best labeling of the receptor after 36 h. This shows the suitability of AngioStamp™ for labeling cat tumors.

Thus my study provided important information about the absence of toxicity and adapted timing and dose of tracer required which are encouraging for its use in human afterwards.

Nevertheless, it still needs to be established whether optical guided surgery using such a system truly improves the survival and minimizes the risk of relapse, since in the present study, surgery was performed without optical-guidance.

I.2.   Continuation of the work

Further steps will imply that surgery is really guided by the system. This would allow to establish statistical values and to evaluate more precisely the therapeutic gain provided by this method.

The excised parts should be examined by histopathological means and compared to macroscopic analysis of thick tissue slices. This would give an idea of the real improvement concerning tumor-margin delineation.

At the same time, a real survival rate could be established if the instrument was really used for guided surgery. Even though the animals used in the present study are followed-up medically, the instrument wasn't used for resection itself and thus no direct information concerning the impact of NIRF guided surgery using the Fluobeam™ and AngioStamp® is determined.

Performing this study on pets with natural cancer is advantageous, since on the one hand the pathology is relevant to the human one and, on the other hand, it is faster and less expensive to generate enough data. Indeed, due to their shorter life expectation, it is much faster to compare the survival or life expectation rate of domestic animals than those of humans. Furthermore, while humans usually receive several types of treatments, the survival rate in pets is more directly related to the efficiency of a unique and initial treatment.

It would also be interesting to test other type of tumors in domestic animals with probable high recruiting rate, like the mastocytoma, lymphoma, or osteosarcoma of dogs or mammary adenocarcinoma and lymphoma of cats[236].

---

[236] See : Colloque INSERM, "modèles carnivores de tumeursspontanées", 2009

I.3.   RGD-motif, integrin and the study

This study demonstrates, that the feline fibrosarcoma is responding to RGD-based probes, leading to the conclusion that they express an integrin that share similar structures than the human isoform[237].

Regarding the patter of expression of the integrin within tumor masses, the front of expansion is usually richer in integrins than the center. This is logic, regarding the role of integrins during invasion and spreading and might be an advantage in our case for the better definition of tumor margins. At the same time some analyzed tumor-free margins were "doubtfully" labeled by AngioStamp™. These samples turned out to be inflammatory tissue. As inflammation, like here peripheral inflammatory infiltrates, are associated with tumor progression[238], it is preferable to remove also this part of "doubtful" inflamed and weakly fluorescent peritumoral tissue, as it may potentially be irreversibly engaged in the transformation process. However, this will apply only if no vital structures are present within these pseudo-sane margins.

The expression of integrin $\alpha_v\beta_3$ was analyzed by immuno-labeling of frozen slices of the samples taken during and after surgery. In parallel, other frozen slices were counterstained for histo-pathology (H&E staining) in order to evaluate the percentage of tumor cells present in the corresponding sample. We then compared the fluorescence staining by AngioStamp™ with the percentage of tumor tissue per sample and the presence of integrins. We showed that the fluorescence intensity was correlated with the quantity of tumor tissue but not or poorly with the expression of the integrin. This might be due to the limited-cross reactivity of the human anti-integrin antibody used. Up to now no specific cat-$\alpha_v\beta_3$-integrin antibody is available. Another possibility is that even if they are present and detected *in vitro* by the antibody on a thin section, these integrins may not easily be accessible for the AngioStamp™ *in vivo* because they can be already engaged with natural ligands such as vitronectin or fibronectin. As well the integrin can be present but in an inactive form. In addition, even if the integrin is active and not engaged, its accessibility may be limited because of the thickness of the glycocalyx[239]. Thus, one must keep in mind the extraordinary versatility of the cell-matrix

---

[237]Muzylak, M, A M Flanagan, K Ingham, N Gunn, J Price, und M A Horton. „A feline assay using osteoclasts generated in vitro from peripheral blood for screening anti-resorptive agents". *Research in veterinary science* 73, Nr. 3 (Dezember 2002): 283–290.

[238]Hanahan, Douglas, und Robert A. Weinberg. „Hallmarks of Cancer: The Next Generation". *Cell* 144, Nr. 5 (März 4, 2011): 646–674.

[239]Boettiger, David. „Mechanical control of integrin-mediated adhesion and signaling". *Current opinion in cell biology* (August 1, 2012).

interactions in 3D living tissues, and not only the presence of a molecule at a given location on a fixed tissue. When a RAFT-RGD-molecule is injected *in vivo* it circulates for a certain period of time in the organism, before it interacts with the receptor and can be internalized, as shown by Sancey *et al*[240]. Consequently the tracer has time to accumulate in the cells, even in those with low levels of integrin. On the contrary, depending on the microenvironment of the tumor cell, and thus the kind of natural ligands the integrin will encounter, active and/or numerous integrins may be "occupied" and the RAFT-RGD-tracer will have difficulties to label them.

In addition, the -RGD- motif we use is highly specific for integrin $\alpha_v\beta_3$ but it can also interact, with lower affinities, with integrins $\alpha_v\beta_5$[241], $\alpha_5\beta_1$ and $\alpha_{IIb}\beta_3$[242,243]. This could lead to a positive labeling of integrin $\alpha_v\beta_3$ negative areas (as determined with the LM609 antibody). Knowing that the $\alpha_v\beta_3$ integrin is especially and almost always overexpressed by neoangiogenic endothelial cells, the vast majority of solid tumors are always labeled, as demonstrated by numerous pre-clinical and clinical studies. Of interest, this angiogenesis as well as the infiltration of tumor stroma by immune cells, such as macrophages which are also $\alpha_v\beta_3$ positive, should clearly help to the delineation of tumor margins by AngioStamp™.

Finally, it should be pointed out that the use of multifunctional RGD derivatives carrying short half-live radio-nuclides in addition to the fluorescent tracer could be interesting because they could be evaluated first using approved medical imaging methods such as PET or SPECT. Furthermore, they would combine pre-operative whole body imaging with augmented, optical-guided surgery[244].

I.4.   Clinical set-up of instrumentation

During this study we observed that several artifacts could generate erroneous interpretation.

---

[240]Sancey, L., E. Garanger, S. Foillard, G. Schoehn, A. Hurbin, C. Albiges-Rizo, D. Boturyn, u. a. „Clustering and internalization of integrin alphavbeta3 with a tetrameric RGD-synthetic peptide". *Molecular Therapy*. 17(5), Mai 2009.

[241]Desgrosellier, Jay S, und David A Cheresh. „Integrins in cancer: biological implications and therapeutic opportunities". *Nature reviews. Cancer* 10, Nr. 1 (Januar 2010): 9–22.

[242] Humphries, Jonathan D., Adam Byron, und Martin J. Humphries. „Integrin Ligands at a Glance". *Journal of Cell Science* 119, Nr. 19 (Januar 10, 2006): 3901–3903.

[243] Chen, Kai, und Xiaoyuan Chen. „Integrin targeted delivery of chemotherapeutics". *Theranostics* 1 (2011): 189–200.

[244]Bunschoten, Anton, Tessa Buckle, Nils L Visser, JoeriKuil, Hushan Yuan, Lee Josephson, Alexander L Vahrmeijer, and Fijs W B van Leeuwen. „Multimodal interventional molecular imaging of tumor margins and distant metastases by targeting αvβ3 integrin". *Chembiochem: a European journal of chemical biology* 13, Nr. 7 (Mai 7, 2012): 1039–1045.

The level of autofluorescence varies between individuals. This is due to several phenomenons, but one of the most important one is the skin color. Bright skin reflect light while dark skin absorb it. The amount of fat can also generate elevated inter- as well as intra-individual variations.

The geometry of the system (distance and angles between the camera and the object) will also influence the quality and relevance of a signal. It is of great importance that the image is sharp, *i.e.* taken with an adequate focus. If not, light scattering and sometimes weakened or intensified information may lead to false interpretation. With respect to the experience during surgery we recommended the introduction of an autofocus in order to overcome this problem and to avoid wrong data interpretation. At the same time it facilitates the use of the system, being more comfortable to manipulate. The introduction of an autofocus is currently in progress.

The auto-LUT of the Fluobeam™ adapts the image on the screen to the highest signal obtained and adjusts the whole grayscale on this signal, lightning up even autofluorescence if no stronger signal is present. This might be confusing for the interpretation as well, and a real measurement of the intensity should be performed in order to avoid false interpretation. Therefore it might be of advantage to fix the LUT by using a defined "threshold". In our study, we defined such a correct threshold, but this could be an important problem for un-experienced users who would like to begin a new protocol without validation first.

Introduction of a threshold should be an option though, as different tumor models might lead to different thresholds, due to different levels of target expression or different access for the molecule towards the tumor site. Also legal recommendation would not recommend the definition of a threshold. Indeed, introduction of a threshold classifies the instrument no longer as guiding device but as diagnostic device and thus demands proof of accuracy of diagnostics with all additional tests demanded by legal authorities. This would slowdown the process of permission for clinic use of such technology and demands greater expenses.

Other difficulties are faced when starting a clinical investigation.
One of them concerns the sterilization process of the imaging device, before it can enter the operating room. It is not possible to drown the device in sterilization baths, specially the imaging head. Therefore we cover it with a sterile cover. The properties of different covers, concerning their shape and how to design them for easy and smooth handling in the clinical

environment, were tested and one was finally selected. The study showed the unproblematic use of the sterile cover, in handling as well as for imaging. Nevertheless the cover has to be improved, that is to say seamless in the distal section in order to be more resistant during exertions while wrapping up the imaging head. Another possibility would be the development of a shell around the imaging head allowing dip sterilization and thus making wrapping in sterile covers unnecessary. In the long-term this would also reduce the current expenses for the use of this device.

As already mentioned sharp images are crucial for correct interpretation of the images. This is difficult to do when the Fluobeam™ is manipulated at arm length and hand held. Therefore the idea of using a fixed holder emerged. Again, this is not a simple work, since everything should be sterilized.

Also the white light emerging from the LED should cover a very large radius in order to enable a bright, clear and full view of the operation field for the surgeon without changing the colors of the tissues. The conventional surgical light might even be replaced by the filtered white light of the imaging head. This has to be evaluated during real NIRF-guided surgery.

Another version of the device itself is the FluoSTIC, which is currently studied[245]. The FluoSTIC has 22 mm in diameter, 200 mm in height and weights less than 200g. It is a low-cost near-infrared imaging fluorescence system optimized for clinical use during oncologic surgeries that combines both white light and NIR excitation. FluoSTIC is lighter and thus should be easier to keep in hand. It is also smaller and thus appropriate for reaching deep or difficult zones of the operation field, whereas the Fluobeam™ is needed to cover a large surface.

I.5. Surgeon's impression

Apart from the technical aspects, the surgeon himself declared the interest of such a technology for surgery improvement. Although the system was not used in image-guided resection, the information mediated by the images after tumor resection and of *ex-vivo* pieces was of great interest for him.

---

[245] Gioux, Sylvain, Jean-Guillaume Coutard, Michel Berger, Henri Grateau, Véronique Josserand, Michelle Keramidas, Christian Righini, Jean-Luc Coll, und Jean-Marc Dinten. „FluoSTIC: miniaturized fluorescence image-guided surgery system". *Journal of biomedical optics* 17, Nr. 10 (Oktober 1, 2012): 106014.

In the study, zones which seemed doubtful for the experienced surgeon's eye were detected as "tumor negative" by the system. This was afterwards confirmed by histological analysis of these samples and showed the good specificity of this technology. In real conditions, that is to say operating while relying on the fluorescence information, several structures like vessels or nerves could be spared.

Finally, the next step is the translation into human clinics. This can be taken in consideration as soon as the tracer has the allowance of the authorities to be used in humans. Here I'd like to mention that AngioStamp™ is currently in a toxicological study according to regulations.

I precise also, that all the studies we have done are based on the follow-up of the fluorescence of the tracer. If the fluorophore is intact we can detect fluorescence even if the molecule itself is degraded. Hence we speak of fluorescence kinetics or implemented the term F_{50} and did not speak of pharmacokinetics and $T_{1/2}$ as this could lead to confusion with conventional pharmacological studies.

II. Reduction of renal retention of RAFT-RGD by pre-injection of gelofusin

Small peptidic molecules are known to be retained in the kidneys because of tubular reabsorption.

Knowing that AngioStamp™ is eliminated *via* the kidneys we thought about decreasing the accumulation in these organs. A rapid excretion of these compounds would be preferable to minimize toxicity but also to obtain high-quality images with low background signal and consequently allow improved detection a delineation of even tiny tumors in the vicinity of kidneys. This would be particularly important to lower the risk of toxicity when radio-nuclides are used instead of fluorescence.

Therefore we decided to study possibilities of reducing the accumulation of the RAFT-RGD compounds in the kidneys in collaboration with the group of C. Ghezzi.

In a fist attempt we have been working on the chemical composition of the RAFT-RGD. Glucose was engrafted on the RAFT-RGD-molecule[246] in order to obtain a molecule of higher hydrophilic property which could facilitate excretion. The affinity for integrin $\alpha_v\beta_3$ was shown to be unaffected by this modification as well as tumor uptake, but it failed to reduce renal reabsorption. Another attempt was to enhance the renal excretion and dilution by administration of a diuretic like Furosemid or co- and post-administration of PBS. None of these assays were successful (unpublished data).

Other approaches for reduction of renal retention described in the literature consisted in the pre- or co-administration of Lysine, Arginin or albumin[247]. This was aiming at targeting the megalin receptor in tubular cells, since it has been shown that some ligands bind to megalin *via* their cationic sites and that co-administration of basic compounds can inhibit their renal reabsorption. But none of these inhibit renal reabsorption completely. Therefore we tried to reduce retention in these cells by a pre-injection of gelofusin. Our results show that there is a significant reduction in the kidneys when using gelofusin, even without total inhibition of reabsorption.

---

[246]Galibert, Mathieu, Lucie Sancey, Olivier Renaudet, Jean-Luc Coll, Pascal Dumy, und Didier Boturyn. „Application of click-click chemistry to the synthesis of new multivalent RGD conjugates". *Organic &biomolecular chemistry* 8, Nr. 22 (November 21, 2010): 5133–5138.

[247]Vegt, Erik, Julliëtte E M van Eerd, Annemarie Eek, Wim J G Oyen, Jack F M Wetzels, Marion de Jong, Frans G M Russel, RosalindeMasereeuw, Martin Gotthardt, und Otto C Boerman. „Reducing renal uptake of radiolabeled peptides using albumin fragments". *Journal of nuclear medicine: official publication, Society of Nuclear Medicine* 49, Nr. 9 (September 2008): 1506–1511.

Therefore a combination of the plasma expander and gelofusin and a renal uptake reducing amino acid like Arginine or Lysine or even a combination with albumin might be additive[248].

---

[248]Gotthardt M, van Eerd-Vismale J, Oyen WJ et al. Indication for differentmechanisms of kidney uptake of radiolabeled peptides. J Nucl Med 2007; 48: 596–601.

III. Introduction of a bi-functional RAFT-RGD derivative: the RAFT-RGD-MMP

The aim of my work consisted in the development and evaluation of an innovative molecule for optical imaging of cancer and cancer therapy, capable of releasing a drug in the tumor with a high specificity.

We already demonstrated the interest of RAFT-RGD for tumor imaging, as well as its capacity to deliver a toxic KLAKLAK peptide specifically in the cytoplasm of the targeted tumor cells[249]. In the present work, we wanted to improve its capacity to detect tumor cells with low levels of integrins, and also to introduce an activatable function specific of an enzyme that would be overexpressed in tumors, rather than the non-specific disulfide bridge we initially used. Targeting two tumor-specific receptors by a single dualmolecule was expected to augment its specificity but also eventually to generate original biological activities due to the physical interaction it could promote between the 2 targets.

This approach has also been employed by the group of Chen, who combined MMP-2 and -9 cleavable sequences with an integrin $\alpha_v\beta_3$ ligand[250]. Like us, they tried to combine the double targeting by addressing a molecule to the αvβ3 integrin and the MMP. The rationale for a MMP-2/MMP-9-cleavable linker was that MMP-2 and MMP-9 bind to integrin $\alpha_v\beta_3$ and both are overexpressed in tumor vasculature. Their compound MMP-P-RGD (c(RGDyK)) serves as integrin ligand, while Gly-Pro-Leu-Gly-Val-Arg-Gly-Lys-Gly-Gly represents the MMP cleavable sequence (between Gly and Val), Cy5.5 and BHQ-3 as fluorophore – quencher pair (ex / em; 675 / 695 nm; abs. 650 nm). After conjugation of the RGD-part to NHS ester activated C-terminal carboxyl group in fully protected MMP substrate, the labeling NHS ester of the NIR dye followed. Then the NHS ester of the quencher was conjugated. Their molecule showed the interest of this principle as there was less non-specific accumulation without visible impact on the target affinity.

---

[249]Dufort, Sandrine, Lucie Sancey, Amandine Hurbin, StéphanieFoillard, Didier Boturyn, Pascal Dumy, und Jean-Luc Coll. „Targeted delivery of a proapoptotic peptide to tumors in vivo". *Journal of Drug Targeting* 19, Nr. 7 (August 2011): 582–588.

[250] Zhu, Lei, Jin Xie, Magdalena Swierczewska, Fan Zhang, Xin Lin, Xuexun Fang, Gang Niu, Seulki Lee, und Xiaoyuan Chen. „Dual-functional, receptor-targeted fluorogenic probe for in vivo imaging of extracellular protease expressions". *Bioconjugate chemistry* 22, Nr. 6 (Juni 15, 2011): 1001–1005.

Our molecule is based on the previously described RAFT-(cRGD)$_4$, a scaffold with 4 integrin $\alpha_v\beta_3$binding-domains, known to present a stronger Kd to the integrin as compared to the monomeric RGD. In addition its multivalency also allows integrin clustering and an efficient internalization[251]. By grafting an MMP-activatable and optically active cassette on the RAFT-RGD, we wanted to obtain a molecule for functional imaging of cancer presenting an improved signal-to-background ratio *in vivo*, which could also serve as template for a next generation of tumor specific pro-drugs.

III.1.   *Additional properties of the activatable dual-molecule*

The results show that the tumor-to-muscle ratio *in vivo* was higher than that of the control molecules. It is also worth noting that these satisfactory results were obtained after injection of only 2 µM per mouse, instead of the usual dose of 10 µM normally required for RAFT-RGD. This activatable probe accumulates with high specificity in tumors and dequenching after cleavage of RAFT-RGD-MMP can be correlated to the level of integrin expression.

Integrin $\alpha_v\beta_3$ is co-overexpressed, particularly during the angiogenic switch and during metastasis, with MMP-9. Furthermore, the integrin and MMP-2 or-9 are known to interact physically, as a result of the action of mechanisms like SIBLINGs. The binding of the dual molecule on the integrin can thus induce MMP-2 and consequently activate MMP-9. Hence, it is possible that a cooperative and cumulative binding of this dual molecule can take place, but this will need further investigation *in vivo*. This phenomenon would give the molecule an advantage to address tumors with not enough integrins to generate a positive signal with the original RAFT-RGD, as we already noticed *in vitro* on the different cell lines. As an example, Gelatinase expression is surprisingly low in HEK293(β1) as compared to HEK293(β3) cells. This could be a simple consequence of clonal variations between these 2 stable transfectants of the original HEK293 parental cell. However, another possible explication would be related to this integrin-MMP-interaction since integrin $\alpha_v\beta_3$ can influence gelatinase activity and *vice versa*. Presuming, in a highly simplified manner as demonstrated in Figure III-1, that integrin $\alpha_v\beta_3$ leads to activation of MMP-9 and MMP-2, which for its part activates MMP-9, the two enzymes degrade substrates, like collagen of the ECM. Degradation of these substrates leads to an easier recognition of their RGD-motif for the integrin, which up-regulates MMP-9 on

---

[251]Sancey, L., E. Garanger, S. Foillard, G. Schoehn, A. Hurbin, C. Albiges-Rizo, D. Boturyn, u. a. „Clustering and internalization of integrin alphavbeta3 with a tetrameric RGD-synthetic peptide". *Molecular Therapy*. 17(5), Mai 2009.

the transcription level due to substrate interaction and cell signaling[252]. This "positive feed-back loop" might thus cause a higher expression of MMP-9 in integrin $\alpha_v\beta_3$ positive cells compared to the same cell line but expressing the$\beta_1$variant.
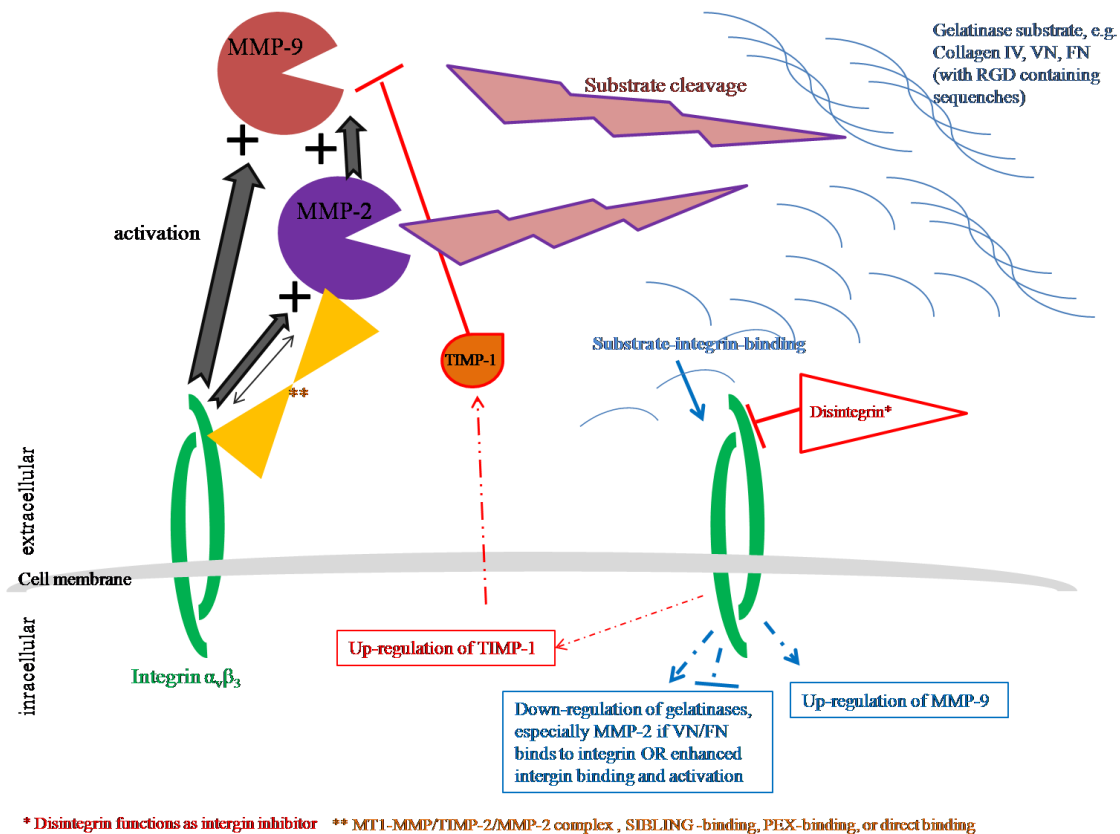
Figure III-1: Highly simplified diagram of integrin-gelatinases interaction.

III.2. In vivo studies

The profile of MMPSense *in vivo* shows a tumor-to-skin ratio in HEK293(β3) and TS/-A cells which does not correspond to the level of gelatinase expression, though the molecule is MMP-sensitive. This might be due to the so called enhanced permeability and retention (EPR) effect as the molecule is not captured by a fixed receptor. The slowly growing HEK293(β3) tumors present a well-structured, neo-angiogenic vasculature with tight endothelial junctions compared to TS/-A, where the tumor vasculature is totally disorganized and leaky. Thus, we previously classified HEK293(β3) tumors as EPR⁻ while in contrastTS/-

[252]Jin, Young-June, Iha Park, In-Kee Hong, Hee-Jung Byun, Jeongsuk Choi, Young-Myeong Kim, und Hansoo Lee. „Fibronectin and vitronectin induce AP-1-mediated matrix metalloproteinase-9 expression through integrin α(5)β(1)/α(v)β(3)-dependent Akt, ERK and JNK signaling pathways in human umbilical vein endothelial cells". *Cellular signalling* 23, Nr. 1 (Januar 2011): 125–134.

A tumors are strongly EPR[+253]. Accordingly, not-targeted and bio-available MMPSense molecules would accumulate more efficiently by passive EPR effect in TS/A tumors than in HEK293(β3). This could explain the enhanced cleavage of MMPSense in TS/-A tumors compared to HEK293(β3) tumors, although the later express gelatinases at a higher concentration. This is not happening with our RAFT-RGD-MMP molecule, which provides a fluorescence profile directly related to the cumulative index of integrin and MMP in these tumors.

It is very encouraging to observe the stability of the molecule in plasma, because it is a prerequisite for *in vivo* application. Indeed, the molecule is slowly degraded after 24 h in plasma. This is more than enough for imaging purposes, but additionally suggests, that the molecule will be slowly degraded and evacuated of the body, thus potentially less toxic. Like the parental RAFT-RGD, the RAFT-RGD-MMP is eliminated by renal excretion, eventually leading to possible damages in the kidneys. The already discussed gelofusin could thus be useful in this case.

III.3.   *Possible complementary studies*

It would be necessary to further demonstrate the role of MMP-9 in our double-targeting approach. This would have to be carried out by a siRNA approach, in order to inhibit this enzyme. That is of particular importance since we showed that the signal provided by the dual probe is always more important than the one obtained with the parental RAFT-RGD on all the tumor cell line tested. Thus it is possible that this probe is not that specific and could generate false positive signal. Therefore, in addition and/or in parallel with the siRNA studies, we should test the molecule with normal cells.

The molecule we used was "self-quenched" by the close vicinity of two Cy5 molecules. However, it is not possible to distinguish the fluorescence emitted of these two Cy5, while following molecule cleavage. Additionally, we cannot determine the percentage of degraded molecule when fluorescence is appearing, since the initial intact molecule theoretically should not be visible. In order to study in more details how efficiently, at what time and where exactly the cleavage of the MMP cassette occurs, it would be interesting to

---

[253]Hirsjärvi, Samuli, Sandrine Dufort, JulienGravier, Isabelle Texier, Qiao Yan, JéromeBibette, Lucie Sancey, u. a. „Influence of size, surface coating and fine chemical composition on the in vitro reactivity and in vivo biodistribution of lipid nanocapsules versus lipid nanoemulsions in cancer models". *Nanomedicine: nanotechnology, biology, and medicine* (September 6, 2012).

replace the two Cy5 by a FRET pair like Cy3 on one side and Cy5 on the other (Figure III-2). In FRET, we excite the donor. The emitted fluorescence of the donor then serves to excite the acceptor, which in turn will produce light at its emission wavelength. If molecule cleavage occurs, the two fluorophores have a greater distance between them and will recover their independent original emission spectra. Consequently, each part of the molecule can be traced separately, and, furthermore, we can evaluate the percentage of the probe that has been cleaved. Alternatively, a "dark" quencher at the place of one of the two initial Cy5 (Figure III-3), could also be used. In this case no light is emitted from the intact quenched molecule, but quenching would disappear as a direct function of the MMP activity.

Thus, on the one hand, using FRET would let us determine, which part of the molecule is internalized, the kinetic of cleavage, where this degradation takes place in the cell or organism. On the other hand, using a dark quencher would render the initial molecule completely invisible, and thus augment the tumor-to-noise signal. Additionally, each photon emitted can be correlated to an enzymatic degradation of one molecule. This approach is easier to follow *in vivo*, and gives simple and reliable interpretation. In contrast, FRET imaging *in vivo* is much more complicated in terms of data analysis since at least three different measurements should be done at each time. Finally, FRET needs also a good calibration of the system and quite an extensive knowledge of photochemistry.

Concerning our self-quenched molecule, the quenching is present but definitely not complete, leaving a lot of un-quenched signal (output-fluorescence). In our case we did not have a real "ON-OFF" quenching. Part of this could be due to the steric conformation of the molecule, and thus the donor-acceptor orientation in space. Since the molecule is always trying to get a stable conformation with the lowest energy input, the engrafted Cy5 fluorophores are orientated differently within a certain area in space and might show torsions in different directions, leading to changes in the distance of the two fluorophores of one molecule. This could influence the quenching efficiency since the transfer of energy decreases, when distance increases. Efficient quenching requires proximity between the donor and acceptor molecule of approximately 10 to 100 Å[254]. Nevertheless, the efficiency of quenching increases with decreasing distance of the two fluorophores. It has been described that a very good quenching can be achieved with a donor-acceptor distance of 10 to 30 Å[255].

[254]Marras, Salvatore A. E., Fred Russell Kramer, und Sanjay Tyagi. „Efficiencies of Fluorescence Resonance Energy Transfer and Contact-mediated Quenching in Oligonucleotide Probes". *NucleicAcidsResearch* 30, Nr. 21 (Januar 11, 2002): e122–e122.
[255] Zhu, Peizhi, Jean-Pierre Clamme, undAshok A. Deniz. „Fluorescence Quenching by TEMPO: A Sub-30 Å Single-Molecule Ruler". *Biophysical Journal* 89, Nr. 5 (November 2005): L37–L39.

Spectral overlap of the absorption spectrum of the acceptor with the emission spectrum of the donor is necessary.

When regarding the RAFT-RGD-MMP, we do have a distance of 30 Å between the two orthogonal Lys side chains of the MMP-sequence, on which the Cy5 is engrafted. This shows, that the distance between the Cy5 makes quenching feasible, but won't be in a perfect distance, which would be < 30 Å. As already mentioned, it is an autoquenching and thus the spectra of absorption and emission only partially overlapping. This results also in a decrease of the quenching efficacy.
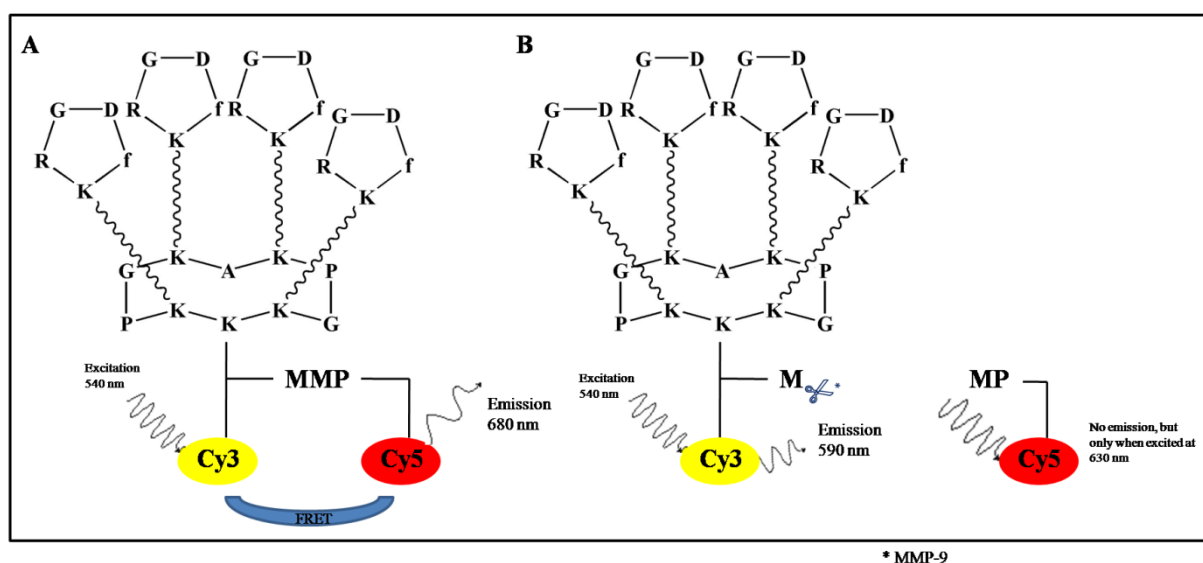
Figure III-2: Illustration of RAFT-RGD-MMP and FRET via Cy3 & Cy5 engraftment.
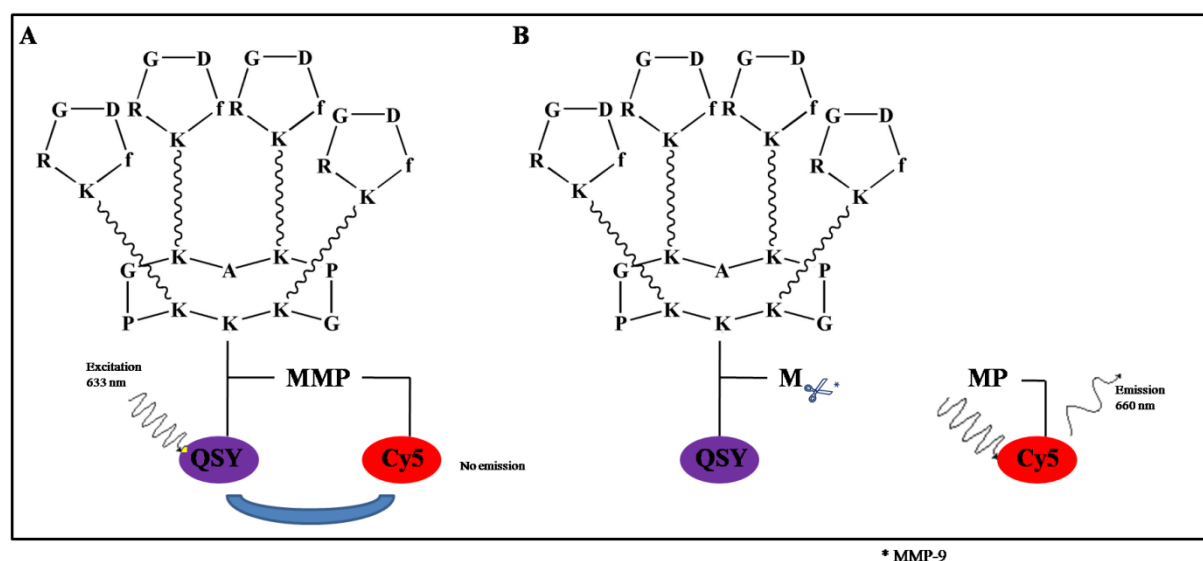
Figure III-3: Illustration of RAFT-RGD-MMP and Quenching via QSY & Cy5 engraftment.

III.4.   Double-targeting approach with other enzymes

It would be interesting to employ other enzymes, for example like Weissleder et al. targeting cathepsins[256]. Other enzymes like ADAMTs[257], MMPs - like MT1-MMP - or Human tissue kallikreins - which play a role in tumor development and angiogenesis[258]- and type II transmembrane serine proteases[259] are also of interest. In the case of caspases it has to be taken in consideration, that these enzymes are intracellular and thus need specific delivery mechanism, like cell-penetrating peptides (CPPs), consisting of a Lysine rich sequence or Arginine residues contain positively charged guanidinium groups. Their efficacy has already been tested by Maxwell et al. for imaging Apoptosis[260].

III.5.   SMARgeting molecule as prodrug and theranostic

Up to now, toxicity of chemotherapeutics towards normal cells and non-diseased tissues, especially fast growing cells - like blood, bone marrow and mucous membrane cells - cause serious side-effects that impose an administration of chemotherapeutic agents at sub-optimal doses[261]. Maximizing the therapeutic index of a chemotherapeutic agent could be achieved by strictly localizing its pharmacological activity to the site or tissue of action. This is the hallmark of so called prodrugs, which are transformed after administration, either by metabolism or spontaneous chemical breakdown, to pharmacologically active species.

Theranostics, that is to say the combination of a therapeutic agent and diagnostic agent in one, have the advantage, that one can follow the drug, evaluate the dose or accumulation of the molecule in the area of interest and measure the efficacy of the treatment at the same time.

---

[256]Quillard, T, K Croce, F A Jaffer, R Weissleder, und P Libby. „Molecular imaging of macrophage protease activity in cardiovascular inflammation in vivo". *Thrombosis and haemostasis* 105, Nr. 5 (Mai 2011): 828–836.

[257] Bridges, Lance C, und Ron D Bowditch. „ADAM-Integrin Interactions: potential integrin regulated ectodomain shedding activity". *Current pharmaceutical design* 11, Nr. 7 (2005): 837–847.
& Moss, Marcia L, und Jörg W Bartsch. „Therapeutic benefits from targeting of ADAM family members". *Biochemistry* 43, Nr. 23 (Juni 15, 2004): 7227–7235.

[258]Borgoño, Carla A, und Eleftherios P Diamandis. „The emerging roles of human tissue kallikreins in cancer". *Nature reviews. Cancer* 4, Nr. 11 (November 2004): 876–890.

[259]Szabo, Roman, und Thomas H Bugge. „Type II transmembrane serine proteases in development and disease". *The international journal of biochemistry & cell biology* 40, Nr. 6–7 (2008): 1297–1316.

[260] Maxwell, Dustin, Qing Chang, Xu Zhang, Edward M Barnett, und David Piwnica-Worms. „An improved cell-penetrating, caspase-activatable, near-infrared fluorescent peptide for apoptosis imaging". *Bioconjugate chemistry* 20, Nr. 4 (April 2009): 702–709.

[261]Garanger, Elisabeth, Didier Boturyn, und Pascal Dumy. „Tumor targeting with RGD peptide ligands-design of new molecular conjugates for imaging and therapy of cancers". *Anti-cancer agents in medicinal chemistry* 7, Nr. 5 (September 2007): 552–558.

As suggested by Shapira *et al.*, a theranostic nanomedicine must be multifunctional, and combine several components: (1) a selective targeting moiety, (2) a diagnostic imaging aid for the localization of the malignant tumor and its micro- or macrometastases, (3) a cytotoxic, small molecule drug(s) or novel biological therapeutic(s), and (4) a chemosensitizing agent, aimed at neutralizing a resistance mechanism, or exploiting a molecular "Achilles hill" of drug resistant cells[262].

Overcoming their non-specific signal due to the EPR effect, specification by engrafting activatable sequences resulting in dequenching and drug-release is an interesting point. This would allow simultaneous monitoring of not only targeting, but also possibly efficacy of therapy.

Kratz *et al*. used a divalent peptide cRGDfK with an introduced octapeptide, cleaved by MMP-2 and -9, to deliver Doxorubicin, a commonly used anti-cancer drug. They showed a tumor inhibition capacity of 6- to 10-fold higher compared to the unformulated control molecule[263]. In our case, the enzymatic cleavage takes place in the extracellular space, surrounding the cells. This is seen especially with the HT1080 cell line, overexpressing soluble MMP-9, but also during the internalization of the molecule. Therefore, such a drug delivery system will be particularly adapted to the drug release in the vicinity of the target cells. Accordingly, we must chose and attach drugs, which will be capable of entering the target cells on their own, after their release in the pericellular space. The presence of a tracer will help to follow the nanovector accumulation in the tumors (Figure III-4, A). Thus in its intact pro-drug form this molecule would be non-toxic, and its therapeutic activity will concentrate mainly within the tumor mass as well as directly into the target cells. This should eventually reduce the amount of molecule we need to administer, and reduce the apparition of side-effects.

The molecule could also be used to deliver two complementary therapeutic agents at the same time (Figure III-4, B), in order to increase the toxicological impact on the tumor cells and the neo-vasculature.

However, increasing the complexity of the nanovectors will also augment its non-specific binding, as already discussed in the results section, since the presence of the MMP cassette on

---

[262]Shapira, Alina, Yoav D Livney, Henk J Broxterman, und Yehuda G Assaraf. „Nanomedicine for targeted cancer therapy: towards the overcoming of drug resistance". *Drug resistance updates: reviews and commentaries in antimicrobial and anticancer chemotherapy* 14, Nr. 3 (Juni 2011): 150–163.

[263]Ryppa, Claudia, Hagit Mann-Steinberg, Iduna Fichtner, Holger Weber, RonitSatchi-Fainaro, Martin L Biniossek, und Felix Kratz. „In vitro and in vivo evaluation of doxorubicin conjugates with the divalent peptide E-[c(RGDfK)2] that targets integrin alphavbeta3". *Bioconjugate chemistry* 19, Nr. 7 (Juli 2008): 1414–1422.

the RAFT-RGD augmented the labeling of all the tested cell lines. However, this was not observed *in vivo*, since no non-specific accumulation of fluorescence was detected.

Indeed, only the tumor and kidneys, which are eliminating the probe, were positively labeled by the molecule. The molecule efficiency was such that we were able to reduce 5-times the amount of RAFT-RGD-MMP *in vivo* (2 nmol/mouse), compared to the conventional RAFT-RGD-Cy5. Therefore, it would have been very surprising to detect a sign of toxicity at such a low concentration. Thus we can anticipate that, if this is also true when the final molecule will deliver a pro-drug, we can really expect to generate active molecules with reduced side effects.
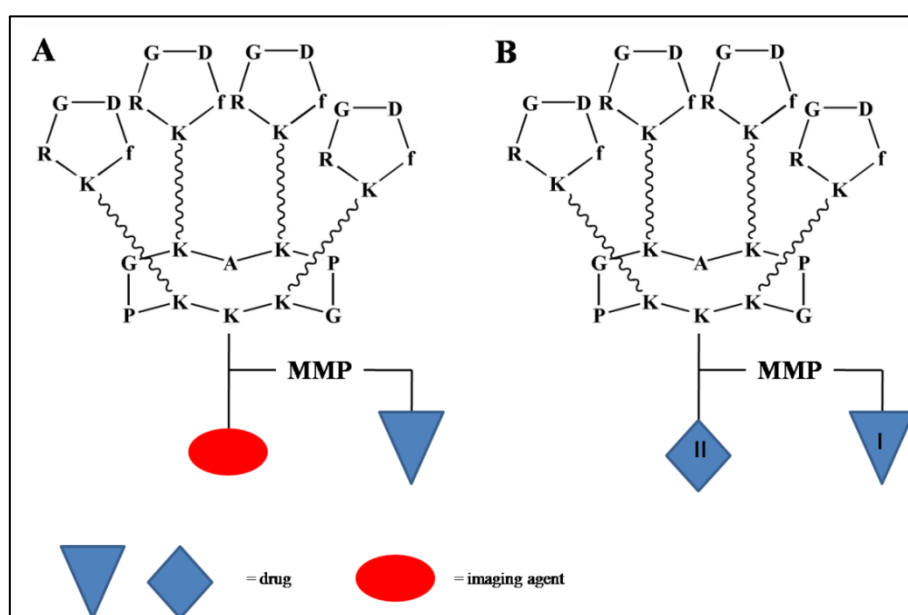
Figure III-4: Example of prodrug design based on the RAFT-RGD-MMP.
A) Theranostic approach with release of a drug, e.g. small molecules.
B) Prodrug approach with two different kinds of drugs: drug I for delivery in the tumor environment and drug II for activation in the cells due to internalization of the RAFT-RGD moiety.

The double targeting concept could also be used for imaging other diseases overexpressing proteases and receptors, like inflammatory diseases such as arthritis[264] or asthma[265], as well as for imaging of atherosclerotic lesions. In atherosclerosis plaques MMPs, especially MMP-2 and MMP-9, as well as the integrin $\alpha_v\beta_3$ are two current targets used and

---

[264]Wunder A, Tung CH, Muller-Ladner U, et al. In vivo imaging of protease activity in arthritis: anovel approach for monitoring treatment response. Arthritis Rheum. 2004 Aug; 50(8):2459–2465.

[265] Cortez-Retamozo V, Swirski FK, Waterman P, et al. Real-time assessment of inflammation and treatment response in a mouse model of allergic airway inflammation. J Clin Invest. 2008 Dec;118(12):4058–4066.

studied for molecular imaging[266]. MMPs are mostly secreted by lipid-engorged macrophages (foam cells) and proof-of-concept studies in imaging gelatinase activity in mice have already been done by the team of Weissleder. The integrin is expressed by neoformed blood vessels in advanced lesions. A theranostic approach using gadolinium-based paramagnetic nanoparticles, encapsulating the antiangiogenic agent fumagillin, yielded an increase in MRI signal as well as it showed a therapeutic effect[266].

The RAFT-RGD-MMP represents thus a potential functional molecule for theranostic purpose in cancer but also in several other diseases.

---

[266]Quillard, Thibaut, und Peter Libby. „Molecular Imaging of Atherosclerosis for Improving Diagnostic and Therapeutic Development". *Circulation Research* 111, Nr. 2 (Juni 7, 2012): 231–244.

« Ne crains pas d'avancer lentement, crains seulement de t'arrêter. »

<u>Chinese wisdom</u>

[Don't worry about progressing slowly, but only about standing still.]

MATERIALS AND METHODS

I.   Preliminary safety observation studies

I.1.   Animals

Three healthy laboratory cats of the veterinary university were included in the preliminary toxicological study.

I.2.   Fluorescent tumor-targeting probe

AngioStamp^{TM} (Fluoptics, Grenoble, France) is a NIR dye-labelled molecular probe targeting the $\alpha_v\beta_3$ integrin derived from the previously published RAFT(c[-RGDfK-])$_4$. AngioStamp™ was injected in the jugular vein at a concentration of either 0.9 mg/kg, 2.4 mg/kg or 4.5 mg/kg.

I.3.   General examination of the cats

General examination of the animal was done by checking the pulse, the heartbeat/noise, capillary refill, reflex (interdigital claw reflex, papillary and eyelid closure reflex) and observation of the animal's comportment.

I.4.   Physical and biochemical parameters

A urinary catheter as well as a catheter in the cephalic vein was placed under short anesthesia with Domitor$^®$ (medetomidine; 0.05 ml/kg) and Ketamin (0.05 ml/kg). The anesthesia was reversed by i.v. injection of Antisedan$^®$ (atipamezole; 0.02 ml/kg).

After awaken of the animal, the tracer AngioStamp™ was injected in the jugular vein. Medical control of the animals was done by survey of the hematological parameters including total blood cell count, white blood cell (WBC) fractions, including lymphocytes (LYM), monocytes (MON) and granulocytes (GRA) with their sub-class eosinophiles (EOS), red blood cell (RBC) fraction, hematocrit (HCT), platelets (PLT), the mean platelet volume (MPV), MCH (mean corpuscular hemoglobin), MCV (mean cell volume), MCHC (mean

corpuscular hemoglobin concentration), Urea[267], Creatinine, activities of enzymatic markers of liver dysfunction (ALT (liver transaminase) and PAL (phosphatase alkaline) activities, as well as the bilirubin rate[268], and a blood ionogram (Cl, K, Na) as well as the evaluation of the RPCU of urine (urinary protein/creatinine ratio). These parameters were chosen as control of direct toxicological response and control of kidney nuisance as the AngioStamp[TM] is eliminated via the renal pathway. Physical parameters (body weight, food and water intake) were studied 6 hours after of injection.

These parameters were determined just before injection of the tracer (T0) and until 7 days post injection.

Blood was withdrawn at the jugular vein with one-way catheters. Blood samples were taken directly before administration of AngioStamp™ (T0), then 5 min, 15min, 30 min, 1 h, 2 h, 4 h, 5 h 30, 24h and 7 days after injection. The urine samples of about 5mL were obtained via a steady urine catheter at the same time as the blood withdrawal took place.

I.5.   *Calculation for the dose 1X for cats*

The dose for cats was estimated from the optimal dose used for tumor imaging in mice[269] and rats (unpublished data). In mice the dose, providing the best tumor/healthy tissue ratio, is 10 nmol for a mouse of 25 g. In rats 20, 50, 70 and 100 nmol were evaluated and the best tumor/healthy tissue ratio was obtained with the dose 50 nmol for a rat of 250 g.
Drawing a linear correlation line between dose and body weight, we obtained the formula $y = 0.177x + 5.555$ (Figure I-1). This leads to an estimated dose of 895 nmol for cats (average weight of 5 kg) and 1784 nmol for dogs (average weight of 10 kg). Thus we chose the dose of 0.9 mg/kg for cats (Table I-1).

---

[267] Tamta, Anupama, Manu Chaudhary, und Rajesh Sehgal. „A 28-Days Sub-Acute Toxicity Study in Swiss Albino Mice to Evaluate Toxicity Profile of Neurotol Plus (Mannitol and Glycerol Combination)". *International Journal of Biomedical Science* 5, Nr. 4 (Dezember 15, 2009): 428–433.

[268] Hamden, Khaled, Serge Carrea U, Fatma Ayadi Marki, Hatem Masmoudi, and Abdelfattah El Feki. „Positive effects of Green Tea on hepatic dysfunction, lipid peroxidation and antioxidant defence depletion induced by cadmium". *Biological Research* 41, Nr. 3 (Januar 2008): 331–339.

[269] Garanger, E., D. Boturyn, P. Dumy, MC Favrot, und JL Coll. „New multifunctional molecular conjugate vector for targeting, imaging, and therapy of tumors". *Molecular Therapy*. 12(6), Dezember 2005.
Jin, Z.H., J. Razkin, V. Josserand, und et al. „In vivo noninvasive optical imaging of receptor-mediated RGD internalization using self-quenched Cy5-labeled RAFT-c(-RGDfK-)(4)". *Mol Imaging*. 6, 2007.
Jin, ZH, V. Josserand, S. Foillard, D. Boturyn, P. Dumy, MC Favrot, und JL Coll. „In vivo optical imaging of integrin alphaV-beta3 in mice using multivalent or monovalent cRGD targeting vectors". *Molecular Cancer*. 6, Juni 2007.
Sancey, L., E. Garanger, S. Foillard, G. Schoehn, A. Hurbin, C. Albiges-Rizo, D. Boturyn, u. a. „Clustering and internalization of integrin alphavbeta3 with a tetrameric RGD-synthetic peptide". *Molecular Therapy*. 17(5), Mai 2009.
Keramidas, M., V. Josserand, CA Righini, C Wenk, C Faure, und JL Coll. „Intraoperative near-infrared image-guided surgery for peritoneal carcinomatosis in a preclinical experimental model". *British Journal of Surgery*. 97(5), 2010.
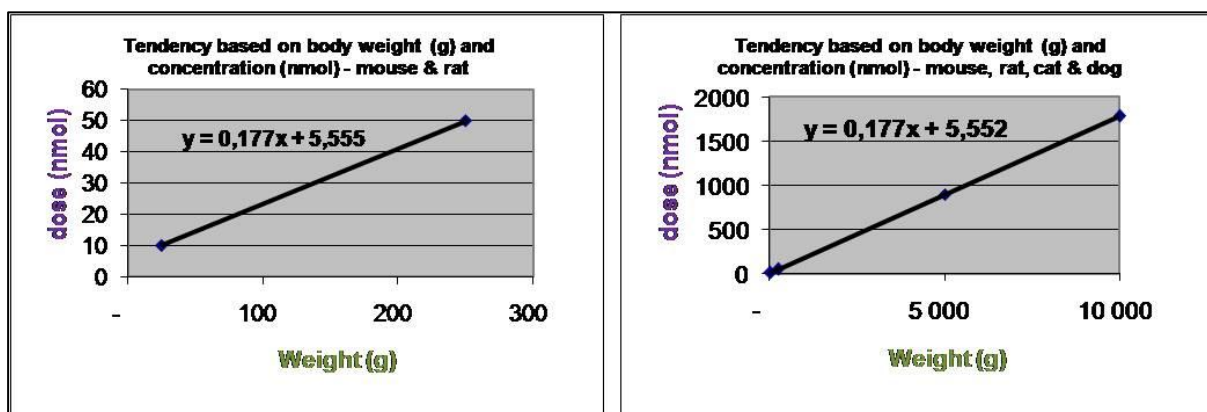
Figure I-1: Estimation of AngioStamp™ dose for cats.

Species	AngioStamp™ Molecular weight (g/mol)	Average body weight (g)	Dose (nmol)	Dose (mg/kg)
Mouse	4864.4	25	10	1.95
Rat	4864.4	250	50	0.97
Cat	4864.4	5000	895	0.87
Dog	4864.4	10000	1784	0.87

Table I-1: Species specific dose of AngioStamp™.

I.6. *Image analysis and unit definition*

Fluorescence data were analyzed by means of the software WASABI (Hamamatsu, Germany). The initial autofluorescence of the samples (blood, plasma, urine and body regions) was measured before administration of AngioStamp™ and was subtracted from the signal measured afterwards. Thus the values obtained were comparable each other.

The fluorescence is calculated using the semi-quantitative data obtained by drawing regions of interest (ROIs) on the spots ought to be studied. The fluorescence quantifications are expressed as a procedure defined unit (**p.d.u.**). This corresponds to the number of relative light units per pixel per millisecond (RLU/pix/ms) in the case of tissues and RLU per microliters per millisecond (RLU/µL/ms) in the case of liquids, with regard to the autofluorescent level.

I.7.   *Portable clinical fluorescence imaging device*

Real time in vivo fluorescence imaging was performed using the Fluobeam™ NIR imaging system (Fluoptics, Grenoble, France). This hand-held system is compact (7 cm in diameter and 20 cm in length, with a weight of 600 g) and consists of two parts: a control unit with a laser source emitting at the excitation wavelength 780 nm and a power supply for light-emitting diodes (LEDs), next to an optical head with a highly sensitive charge-coupled device camera and white LEDs for the illumination of the field of view at 5 kLux of high quality light (Color Rendering Index about 90%). The laser beam is fiber-guided from the control unit to the optical head. The detection of the emitted fluorescence is under 800 nm. The laser beam was spread to reach a 6-cm spot diameter at the working distance of 17 cm. The power density of the laser irradiation was 96 μW/mm^2. The NIR fluorescence image was 696×512 pixels and provided a resolution of two line pairs per millimeter (spatial resolution of 110 μm/pixel) allowing visualization of sub-millimeter structure[270]. The exposure time can be adjusted from 1 ms to 1 sec. The Sensitivity of the system is 1 picomol of fluorophore. The Fluobeam™ system has been used with a dedicated single use CE marked sterile cover bearing an optical window compatible with NIR fluorescence measurements[271].

II. Intra-operative surgery

II.1.   *Patient recruitment*

Cats were addressed by veterinary practitioners. Twelve cats (3 males and 9 females; 9.8 ± 1.7 years old, weighing 4.7 ± 1.7 kg) were included in the study after obtaining the owners' information and consent. Diagnosis was based on clinical and morphological data (fine needle aspirations and biopsies), Extent of the disease as local staging of the tumour and metastatic spreading were evaluated by contrast enhanced CT (computed Tomography)

---

[270] Heuveling, DA, GW Visser, M. de Groot, JF de Boer, M. Baclayon, WH Roos, GJ Wuite, CR Leemans, R. de Bree, und GA van Dongen. „Nanocolloidal albumin-IRDye 800CW: a near-infrared fluorescent tracer with optimal retention in the sentinel lymph node". *Eur J Nucl Med Mol Imaging*. 39(7), Juli 2012. &

Mery, E., E. Jouve, S. Guillermet, M. Bourgognon, M. Castells, M. Golzio, P. Rizo, JP Delord, D. Querleu, und B. Couders. „Intraoperative fluorescence imaging of peritoneal dissemination of ovarian carcinomas. A preclinical study." *Gynecol Oncol.* 122(1), Juli 2011.

[271] D. Wachter, K. Kallenberg, A. Wrede, W. Schulz-Schaeffer, T. Behm, V. Rohde, Fluorescence-Guided Operation in Recurrent Glioblastoma Multiforme Treated with Bevacizumab-Fluorescence of the Noncontrast Enhancing Tumor Tissue? J Neurol Surg A Cent Eur Neurosurg (2012). &

T. Tykocki, R. Michalik, W. Bonicki, P. Nauman, Fluorescence-guided resection of primary and recurrent malignant gliomas with 5-aminolevulinic acid. Preliminary results. Neurol Neurochir Pol 46 (2012) 47-51.

(Figure 1A).CT scanning was performed by a series of transverse 2 mm slices of the thorax, once without contrast agent and once after an intravenous iodide injection containing a contrast agent (iohexol). The contrast agent identified the tumour tissue as a homogenous mass. This three-dimensional CT provided essential information for proper planning of aggressive surgical approach.

II.2.   *Fluorescent tumor-targeting probe*

AngioStamp^{TM} (Fluoptics, Grenoble, France) was injected in the cephalic vein of the animals at 0.6, 0.3 and 0.15 mg/kg. Surgical intervention was performed at 16, 24 and 36 h post-injection.

II.3.   *Surgical fibrosarcoma resection and imaging*

Tumour excision was carried out according to the conventional surgical procedure. Per operative imaging was conducted in parallel and was not used to influence the resection gesture.

After preparation of the operation field and before incision of the skin, initial fluorescent images of the tumour were taken. After the beginning of the tumour resection, fluorescence imaging was performed at several steps of the surgery (tumour tissue, tumour margins and surrounding healthy tissues).

After surgery was completed, the operation field and especially the margins or doubtful structures were imaged. Afterward, surgical specimens were dissected into samples for histopathological analysis under fluorescent guidance. After the recovery phase, the cats returned home and the owners were asked to bring them back regularly for long-term clinical follow-up.

II.4.   *Histo-pathological and immuno-histological analyses*

Surgical specimens were sampled into two pieces for the histo-pathological and immuno-histological analyses of the $\alpha_v\beta_3$ integrin expression level. A portion of samples were fixed in formaldehyde, embedded in paraffin and cut in 4-µm slices before Haematoxylin-Eosin standard staining, and other samples were frozen by placing them in isopentane and shock freezing them in liquid nitrogen. They were cut into 6 µm slices (microcryotome) and

conserved at -80°C until fixation and staining. After warming up the frozen slices by leaving them at room temperature, they were fixed during 10 min in methanol at room temperature. After 5 min of rinsing in water, the slices were loaded in an automated instrument (BenchMark, Ventana Medical Systems, Strasbourg, France) and labelled with the mouse anti-human-integrin $\alpha_v\beta_3$ antibody clone LM609 (Chemicon, USA) for 32 minutes at room temperature at 5µg/ml (1/200). After an automatic rinsing, the slices were incubated with the OptiView DAB detection kit (Ventana Medical Systems) according to the manufacturer's instructions. Incubation with control mouse IgG1 at 5µg/ml served as negative control.

II.5.   *Analysis of NIR fluorescence data*

The fluorescent data collected using Fluobeam™ was quantified with the image analysing program WASABI (Hamamatsu Photonics GmbH, Germany) and Microsoft Excel. The intensity value of the different tissues was defined as the mean fluorescence intensity of the region of interest (ROI) minus the mean fluorescence intensity of the background divided by the exposure time in milliseconds, resulting in the relative light unit per pixel per millisecond (RLU/pixel/ms). Three to ten different ROIs were measured for each animal. These ROIs were taken on the tumour and the healthy tissues. The number of chosen ROIs depended on the exploitation possibilities of the images taken (e.g. tumour sample not covered by thick muscle layers or skin; sloping or blurred images).

II.6.   *Statistical analysis*

Statistical analysis was carried out using Statview software (SAS Institute, San Francisco, CA, USA). Tumor and tissue values were compared after Mann-Whitney (pair) and Kruskal-Wallis. A *p*-value under 0.05 was considered as significant (*), under 0.01 very significant (**) and under 0.001 as extraordinary significant (***).

III. Protocols for peptide synthesis

III.1.   Material and Equipment

Rink-amide MBHA® was obtained from Calbiochem-Novabiochem, Fmoc-Gly-SASRIN® resin from Bachem Biochimie SARL (Voisin-LesBretonneux, France) and 2-chlorotritylchloride® resin from Advanced ChemTech Europe (Brussels, Belgium). The protected amino acids were purchased from Activo tec (Cambridge, UK), Bachem Biochemie SARL (Voisins-les-Bois, France) or Calbiochem-Novabiochem (Merck Biosciences-VWR, Limonest, France). PyBOP® was procured from Calbiochem-Novabiochem, whereas other reagents were obtained from Aldrich (Saint-Quentin Fallavier, France) and Acros (Noisy-le-Grand, France). Cyanine™5 Mono NHS ester was purchased from Amersham Biosciences (Orsay, France) and QSY®21 NHS from Invitrogen (Cergy Pontoise, France).

Waters equipment was used for analyses by means of RP-HPLC. This comprises a Waters 600 controller, a Waters 2487 Dual Absorbance Detector and a Waters In-Line Degasser. The column used was a Nucleosil 120 Å A3 μm C18 particles, 30 x 4 mm^2 operated at 1.3 mL min^{-1} with a linear gradient program in 15 minutes run time (classical program 5 to 100% B in 15 minutes). UV monitoring was realized at 214 nm and 250 nm, respectively 320 nm with Dansyl group and 650 nm with Cy5/QSY dyes. Solvent A consisted of H_2O containing 0.1% TFA and solvent B of CH_3CN containing 9.9% H_2O and 0.1% TFA.

Electron spray ionization (ESI-MS) mass spectra were obtained on an Esquire 3000 (Bruker).

III.2.   General Peptide synthesis procedures

All linear protected peptides were synthesized manually or automatically by means of solid-phase peptide synthesis (SPPS) using the standard Fmoc/*t*Bu protection strategy[272,273].
For manual production a glass reaction vessel fitted with a sintered glass frit was used as device as it allows the removal of reagent excess and solvents under compressed air. To

---

[272] P. Lloyed-Williams, F. Albericio, and E. Giralt. "Chemical Approaches to the Synthesis of Peptides and Proteins". Ed. by Ed. C.W. Rees. CRC Press, NY, 1997, p. 278.

[273] R.B. Merrield. "Solid-Phase Peptide Synthesis. 3. An Improved Synthesis of Bradykinin." In: Biochemistry 3 (1964). SPPS, pp. 1385-1390.

prevent resin beads from sticking at the inside of the vessel, it is treated at least 12 hours before use with $(CH_3)_2SiCl_2$ for lubrication.

Washings with DCM (10 mL/g resin) were carried out until the complete clearance of acid traces. Resin was then swollen with DCM (10 mL/g resin) once for 30 min and twice for one minute, washed three times with DMF (10 mL/g resin) for 1 minute. Coupling reactions were performed using, relative to the resin loading, 2 equiv. of N^{α}-Fmoc-protected amino acid, 2 equiv. PyBOP and 3-4 equiv. of DIPEA, in order to obtain pH 8, DMF (10 mL/g resin) for 30 minutes. Then the resin was washed five times with DMF (10 mL/g resin) and once with DCM (10 mL/g resin) for one minute. The completeness of amino acid coupling reaction was checked by the TNBS test.

N^{α}-Fmoc-protection groups were then removed by treatment with a solution of 20% piperidine in DMF (10 mL/g resin) for 5 minutes twice and then once for 10 minutes (Figure III-1).
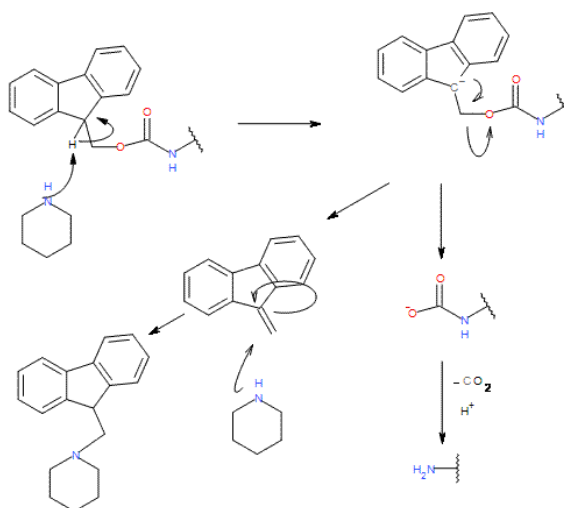
Figure III-1: Scheme of the removal of Fmoc with Piperidine

The resin beads were washed five times with DMF (10 mL/g resin).

Fmoc removal can be monitored spectrophotometrically because of the formation of dibenzofulvene or fulvene-piperidine adducts (λ = 299 nm). Thus cleavage and washing solutions were collected in a Vial and the volume adjusted to a known value (V) with MeOH. The absorbance at 299 nm gave the amount of Fmoc protecting groups released from the cleavage according to the Beer-Lamber relation:

$$nFmoc = (OD_{299nm} \times V)/(\varepsilon_{299v\mu} \times l)$$

$$A_{\lambda} = A_{lu} \times 30 \text{ (3fold dilution)}, A = \varepsilon \times l \times c$$

with l = length of optical path; $\varepsilon = 7800$ M^{-1} cm^{-1} and $l = 1$

This method was commonly used to determine the loading and thus indirectly allows the monitoring of the synthesis. Automated syntheses were performed on the "AB433A" Peptide Synthesizer (Applied Biosystems) with an UV/VIS Detector using standard solid-phase methods.

Finally, linear peptides were recovered from the resin beads under acidic conditions (Table III-1).

Resin	Cleavage solution	Procedure
2-chlorotritylchloride	TFE/AcOH/DCM (20/20/60)	(10 mL/g resin) 2 hrs
Rink-amide MBHA	TFA/Tis/H$_2$O (90/5/5)	(10 mL/g resin) 2 hrs
SASRIN	TFA/DCM (1/99)	(10 mL/g resin) 1 min 10 times

Table III-1: Procedures for cleavage from the resin

Cyclization reactions of peptides in solution were performed using protected linear peptides. They were dissolved in DMF (0.5 mM) at pH adjusted to 8-9 by addition of DIPEA. PyBOP (~1.1 equiv.) was added and the solution was stirred at room temperature for 30 minutes. The solvent was removed under reduced pressure and the residue dissolved in a minimum of DCM. Ether precipitation and washing afforded crude peptide that was used without further purification.

❖ TNBS test

Four drops of a solution containing 1% trinitrobenzene sulfonic acid in DMF and a solution containing 10% DIPEA in DMF were added to a small amount of resin beads. The mixture was left at room temperature for 1 minute. Remaining free amino functions resulted in a red coloration of the beads (positive TNBS test). Consequently the coupling reaction with

the protected amino acid should be repeated until the beads remain colorless (negative TNBS test).

> ❖ The cleavage of side-chain protecting groups in solution phase

• Deprotection of Boc, Pbf, Trt

The removal of protecting groups was carried out in a solution containing 95 % TFA, 2.5% Tis and 2.5% H_2O for 1 hour at room temperature. The solution was concentrated, and the crude peptide was triturated and washed with ether.

• Deprotection of Dde
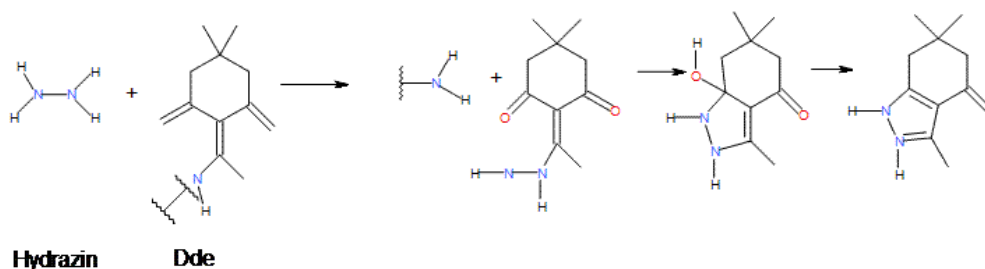
Figure III-2 Scheme of the removal of Dde

Deprotection of Dde at the lysine side-chain was performed using a solution containing Hydrazine (4%) and allyl alcohol (6%). To remove the Hydrazine, we used a C_{18} micro colomn (Chromafix). Afterwards, peptide was characterized by using HPLC analysis and mass spectroscopy.

• Deprotection of Alloc

The deprotection of Alloc at the lysine side-chain was performed by means of Tetrakis-Palladium [Pd(PPh$_3$)] under inert atmosphere. Therefore the peptide was dissolved in anhydrous DCM under argon and phenylsilane (25 eq.) was added. The solution was stirred 3 minutes before adding 0.2 equiv. of Pd(PPh$_3$)$_4$ and stirring for 1 hour at room temperature. The mixture was treated with Methanol for 15 minutes before evaporation of the solvents under reduced pressure. Finally the product was triturated and washed with ether. The peptide was then characterized by using HPLC analysis and mass spectroscopy.
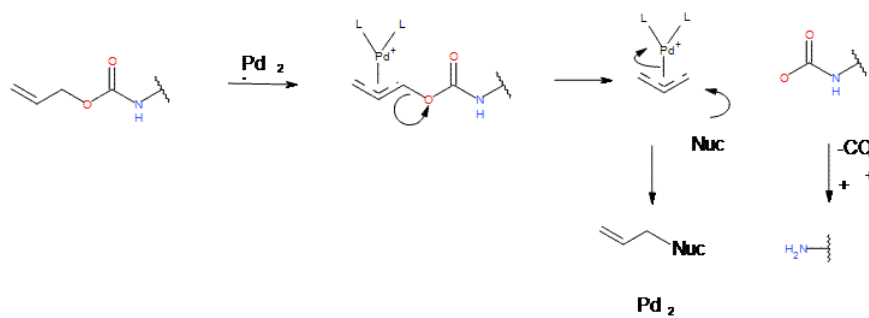
Figure III-3: Scheme of the Palladium assisted removal of Alloc

❖ Fluorescent dye coupling

The peptide was dissolved in DMF extra dry ($10\text{x}10^{-6}$ moles). One equiv. Cy5 was added and the solution was adjusted to pH 8 by adding 4 equiv. DIPEA and stirred for 1 hour. The reaction was checked by RP-HPLC. Then, peptide was obtained after an ether precipitation.

The same procedure was applied to graft QSY21 dye.

III.3. Compounds

1: Dansyl-Gly-Pro-Leu-Gly-Leu-Trp-Ala-Arg-Gln-NH₂

The peptide was assembled on RINK amide resin (110 mg, loading of 0.7 mmol/g) as described in the General Peptide synthesis procedures. Dansyl-containing peptide was obtained as a yellow fluffy powder (100 mg). Peptide **1** was then characterized by using RP-HPLC and mass spectrometry. HPLC purification of 10 mg gave pure peptide (1.4 mg).
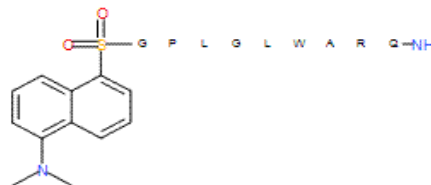
RP-HPLC peak: RT = 7.8 min
(C$_{18}$, 214 nm /320 nm, 5-10% B in 15 min)
Found mass: 1229 g mol^{-1}
Calculated mass = 1229 g mol^{-1}
Yield: 16 %

2: Dansyl-Gly-Pro-Leu-Gly-Val-Trp-Ala-Arg-Gln-NH₂

The peptide was synthesized on RINK amide resin (357 mg, 0.7 mmol/g) by using the peptide synthesizer "AB433". Dansyl-containing peptide was obtained as a yellow fluffy powder (500 mg). Peptide **2** was then characterized by using RP-HPLC and mass spectrometry. HPLC purification of 10 mg gave pure peptide (3.8 mg).
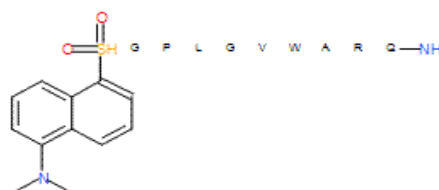
RP-HPLC peak: RT = 8.23 min
(C$_{18}$, 214 nm/320 nm, 5-10% B in 15 min)
Found mass: 1215 g mol^{-1}
Calculated mass = 1215 g mol^{-1}L
Yield: 24 %

3: Dansyl-Gly-Pro-Gln-Gly-Leu-Ala-Gly-Gln-NH₂

The peptide was synthesized on RINK amide resin (250mg, 0.7 mmol/g) by using the peptide synthesizer "AB433". Dansyl-containing peptide was obtained as a yellow fluffy powder (100 mg). Peptide **3** was then characterized by using RP-HPLC and mass spectrometry. HPLC purification of 10 mg gave pure peptide (4.1 mg).
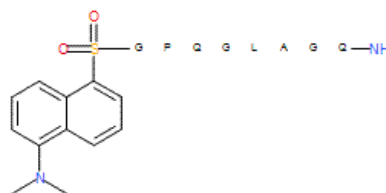
RP- RP-HPLC peak: RT = 5.98 min
(C_{18}, 214 nm/320 nm, 5-10% B in 15 min)
Found mass: 959 g mol^{-1}
Calculated mass = 959 g mol^{-1}
Yield: 6 %

4: Dansyl-Gly-Leu-Arg-Gly-Pro-Trp-Leu-Ala-Gln-NH₂

The peptide was synthesized on RINK amide resin (110 mg, 0.7 mmol/g) by using the peptide synthesizer "AB433". Dansyl-containing peptide was obtained as a yellow fluffy powder (100 mg). Peptide **4** was then characterized by using RP-HPLC and mass spectrometry. HPLC purification of 10 mg gave pure peptide (9 mg).
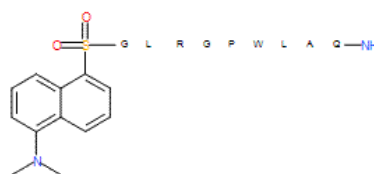
RP-HPLC peak: RT = 7.57 min
(C_{18}, 214nm/320nm, 5-10% B in 15 min)
Found mass: 1229 g mol^{-1}
Calculated mass = 1229 g mol^{-1}
Yield: 16 %

5:Gly(boc)-Lys(Dde)-Gly-Pro-Gln(Trt)-Gly-Leu-Ala-Gly-Gln(Trt)-Lys(Alloc)-OH

The peptide was synthesized manually on Chlorotrityl resin (450 mg, 0.4 mmol/g). Peptide **5** was obtained as a white powder (50 mg) and used for the next step without purification.
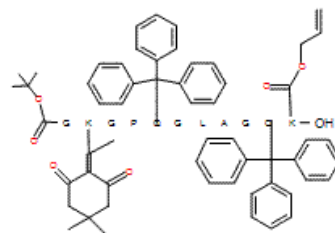
RP-HPLC peak: RT = 7.01 min

(C_{18}, 214 nm/250 nm, 5-10% B in 15 min)

Found mass: 1874 g mol^{-1}

Calculated mass = 1875 g mol^{-1}

Yield: 4 %

6a:Gly(boc)-Lys(Cy5)-Gly-Pro-Gln(Trt)-Gly-Leu-Ala-Gly-Gln(Trt)-Lys(Alloc)-OH

Starting from compound **5** (50 mg), Dde removal and Cy5 coupling afforded the cyanine 5-containing peptide **6a** as a blue powder (26 mg). Compound **6a** was then characterized by using RP-HPLC and mass spectrometry. The compound was used to engraft QSY21, which was abandoned due to low affinity of the reaction.
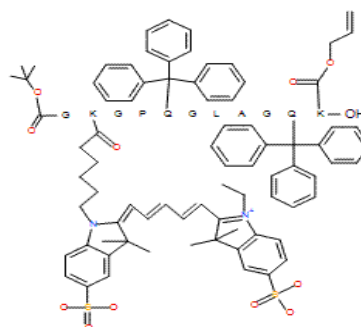
RP-HPLC peak: RT = 11.07 min

(C18, 214nm/250nm, 5-10% B in 15 min)

Found mass: 2347 g mol^{-1}

Calculated mass = 2346 g mol^{-1}

Yield: 52 %

6b: H_2NO-CH_2-CO-Gly-Lys-Gly-Pro-Gln-Gly-Leu-Ala-Gly-Gln-Lys-Gly-OH

Peptide synthesis was carried out as described in the general procedure. Full deprotection of protected peptide **5** ((Boc)$_2$NO-CH$_2$-CO-Gly-Lys(Boc)-Gly-Pro-Gln(Trt)-Gly-Leu-Ala-Gly-Gln(Trt)-Lys(Boc)-Gly-OH (20 mg, 9.8 μmol)) was done from a solution of TFA/H$_2$O/TIS/EDT (90:5:2.5:2.5) during 2 h. The product was directly purified by RP-HPLC to yield compound **6b** as a white powder (6 mg, 4 μmol).
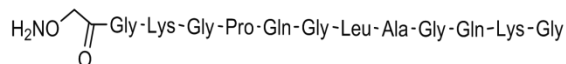
RP-HPLC peak: RT = 11.4 min
(C18, 214nm/250nm, 5-100% B in 20 min; 1 mL/min)

Found mass: 1170 g mol^{-1}

Calculated mass = 1169 g mol^{-1}

Yield: 41 %

7: cyclo[-Arg-Gly-Asp-DPhe-Lys(-CO-CHO)-]

In parallel, the synthesis of cyclo(RGDfK) ligand was carried out as described[274].

The linear peptide D(tBu)-f-K[BocS(tBu)]-R(Pmc)-G was produced *via* the SPPS method by using Fmoc-Gly-SASRIN resin (310 mg 0,8 mmol/g). Peptide cyclo[-Arg-Gly-Asp-DPhe-Lys(-CO-CHO)-] was obtained in three steps: (1) head-to-tail cyclization, (2) acid deprotection by using a solution of TFA/TIS/H$_2$O (95:2.5:2.5) and (3) a following periodate oxidation by using 10 equiv. NaIO$_4$ for 15 min in H$_2$O furnished the aldehyde-containing cyclopeptide cyclo[-Arg-Gly-Asp-DPhe-Lys(-CO-CHO)-]from HPLC purification (160 mg).
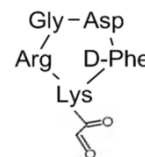
RP-HPLC peak: RT = 5.8 min
(C18, 214nm/250nm, 5-100% B in 20 min; 1 mL/min)

Found mass: 695 g mol^{-1}

Calculated mass = 695 g mol^{-1}

Yield: 84 %

---

[274] Boturyn, Didier, und Pascal Dumy. „A convenient access to αVβ3/αVβ5 integrin ligand conjugates: regioselective solid-phase functionalisation of an RGD based peptide". *Tetrahedron Letters* 42, Nr. 15 (April 9, 2001): 2787–2790.

8: RAFT =

c[-Lys(-CO-CH2ON=C(CH3)OEt)-Lys(-CO-CH(NH(Boc))-CH₂-O(tBu))-Lys(-CO-CH2ON=C(CH3)OEt)-Pro-Gly-Lys(-CO-CH2ON=C(CH3)OEt)-Ala-Lys(-CO-CH2ON=C(CH3)OEt)-Pro-Gly-]
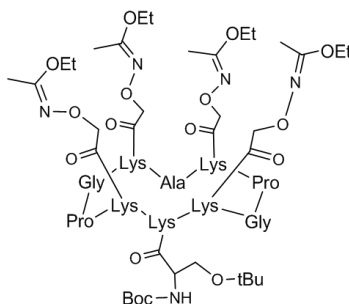
Linear peptide was prepared using building blocks as previously described.[275] linear peptide (0.5 mM) was dissolved in DMF and the pH values were adjusted to 8-9 by addition of DIPEA. PyBOP (1 equiv) was added and the solution stirred at room temperature for 1 h. Solvent was removed under reduced pressure and the residue dissolved in the minimum of methylene chloride. Diethyl ether was added to precipitate peptide. Then it was triturated and washed three times with diethyl ether to obtain crude material that was used in the next step without further purification. Yield: 31%

9: HC₂O₂-RAFT-(c[-RGDfK-])₄
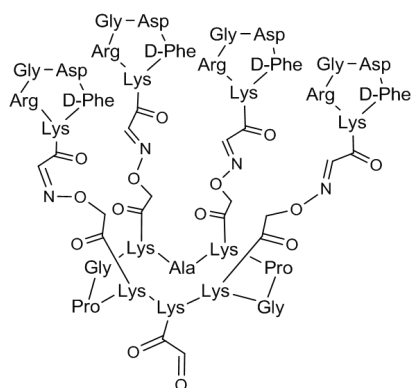
RP-HPLC peak: RT = 17.9 min
(C18, 214nm/250nm, 5-100% B in 30 min; 2 mL/min)
Found mass: 3935 g mol⁻¹
Calculated mass = 3934 g mol⁻¹
Yield: 77 %

Full deprotection of compound **8** (157.2 mg, 86 µmol) was carried out using 10 mL of a solution containing TFA/H₂O/TIS (95:2.5:2.5) at room temperature during 3 h. The product was isolated after removal of solvents under reduced pressure and precipitation from diethyl ether to yield deprotected peptide as a white powder in quantitative yield (169 mg, 86 µmol). In parallel, cyclo[-Arg-Gly-Asp-

---

[275] Foillard, Stéphanie, Martin Ohsten Rasmussen, Jesus Razkin, Didier Boturyn, und Pascal Dumy. "1-Ethoxyethylidene, a new group for the stepwise SPPS of aminooxyacetic acid containing peptides". *The Journal of organic chemistry* 73, Nr. 3 (February 1, 2008): 983–991.

DPhe-Lys(-CO-CHO)-] was synthesized as previously described.[276]

To an aqueous solution (2 mL) containing the deprotected peptide (20 mg, 10.2 μmol) was added freshly prepared cyclo[-Arg-Gly-Asp-D Phe-Lys(-CO-CHO)-] (67.5 mg, 87 μmol). The reaction was stirred for 1 h at 25°C. The RGD-containing conjugate was isolated after purification by RP-HPLC as a white powder (40.1 mg, 8.8 μmol, 86%). A serine oxidation of RGD-containing conjugate (20 mg, 4.3 μmol) by an aqueous solution containing 10 equiv. of $NaIO_4$ (10.8 mg, 50.4 μmol) afforded the aldehyde component **9**. The product was directly purified by RP-HPLC to yield compound **9** as a white powder (14.6 mg, 3.3 μmol).

10: RAFT-RGD-MMP =

[RAFT-c(RGDfK)4]-Gly-Lys(Cy5)-Gly-Pro-Gln-Gly-Leu-Ala-Gly-Gln-Lys(Cy5)-Gly-OH
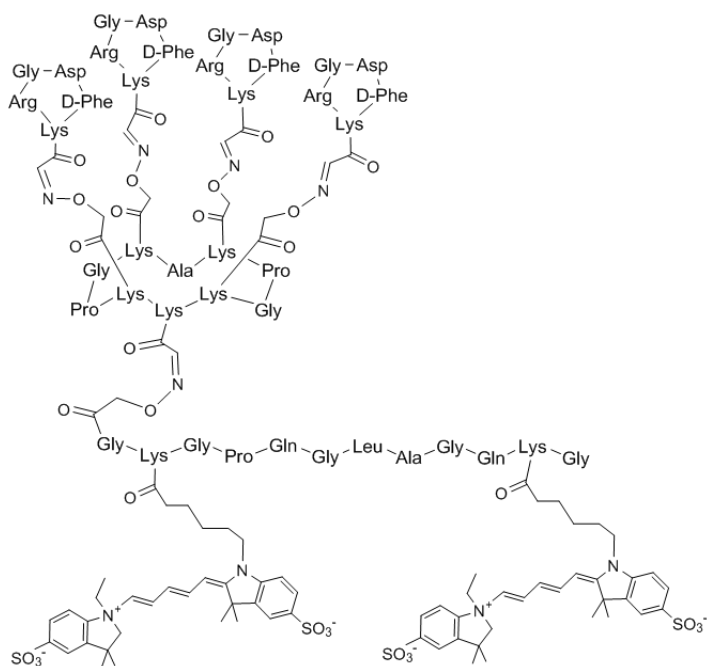
RP-HPLC peak: RT = 17.9 min (C18, 214nm/250nm, 5-100% B in 30 min; 2 mL/min)

Found mass: 6364 g mol^{-1}

Calculated mass = 6364 g mol^{-1}

Yield: 31%

To a solution containing the derivative 9 (17 mg, 3.8 μmol) in 400 μL of H_20/CH_3CN (1:1) was added the peptide 6b (6 mg, 4 μmol). The reaction was stirred for 3 h at 25 °C. MMP-containing conjugate was isolated after purification by RP-HPLC as a white powder (10 mg, 1.7 μmol, 46%). To a solution containing the MMP-containing conjugate (4 mg, 0.7 μmol) in 180 μL of DMF was added 3 μL DIPEA and Cyanine 5-mono NHS ester (1.7 mg, 1.8 μmol). The reaction was stirred overnight at room temperature. The product was directly purified by RP-HPLC to yield compound 10 as a blue powder (1.5 mg, 0.22 μmol).

---

[276] Boturyn, Didier, und Pascal Dumy. „A convenient access to αVβ3/αVβ5 integrin ligand conjugates: regioselective solid-phase functionalisation of an RGD based peptide". *Tetrahedron Letters* 42, Nr. 15 (April 9, 2001): 2787–2790.

❖ **RP-HPLC profile and ESI-MS analysis of 9**

RP-HPLC profile of **9** monitored at 214 nm.

Nucleosil column (300Å 6 µm C18 particles, 125 x 3 mm); linear gradient (5 to 100% B in 20 min; flow rate: 1mL/min).
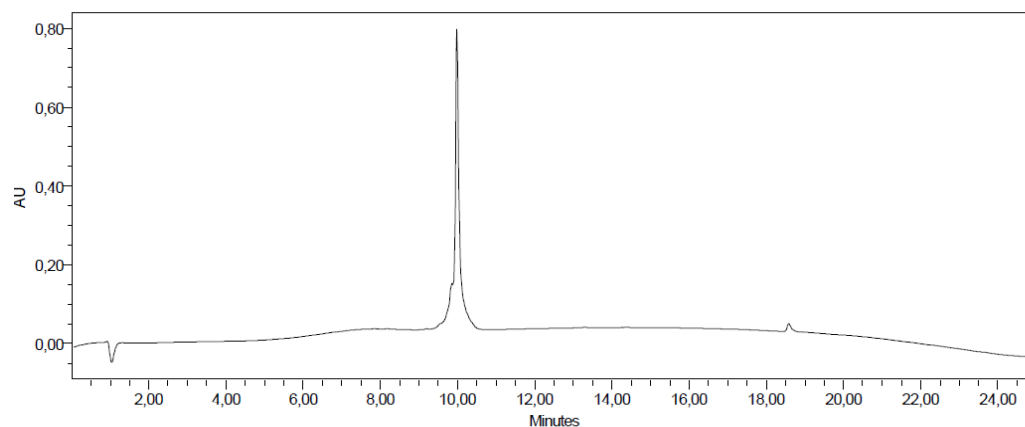
RT = 9.9 min

ESI-MS analysis of compound **9**
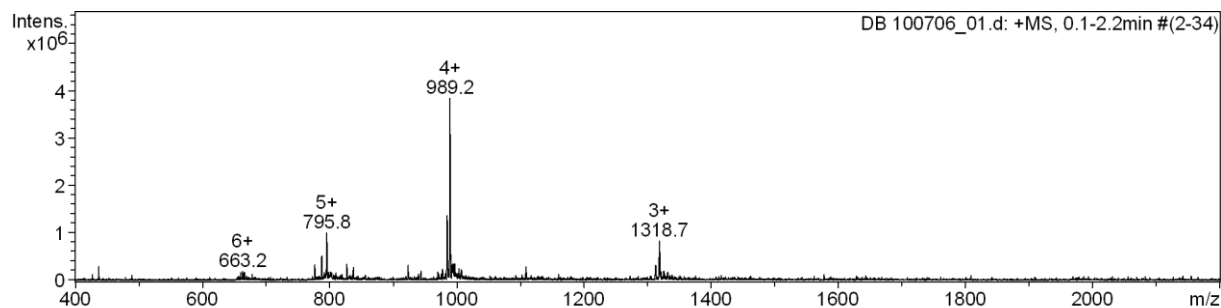
❖ *Deconvoluted mass: M_{found} = 3935.2; M_{calc} = 3934.9*

❖ **RP-HPLC profile and ESI-MS analysis of 6b**

RP-HPLC profile of **6b** monitored at 214 nm.

Nucleosil column (300Å 6 μm C18 particles, 125 x 3 mm); linear gradient (5 to 100% B in 20 min; flow rate: 1mL/min).
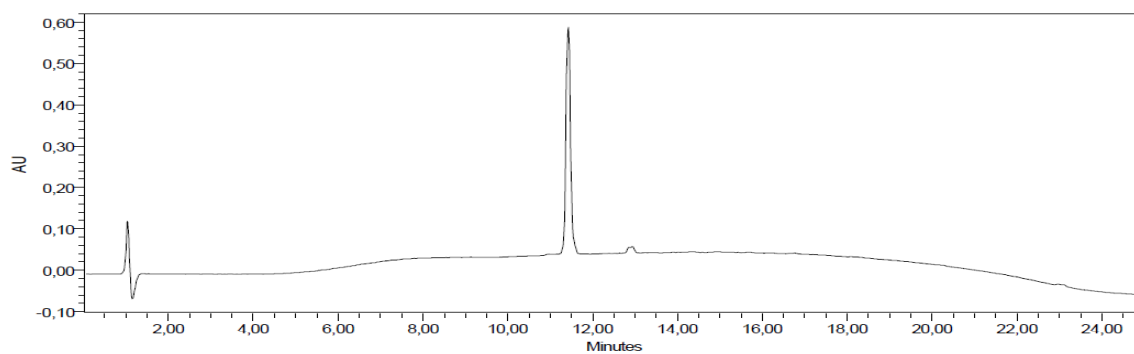
RT = 11.4 min

ESI-MS analysis of compound **6b**
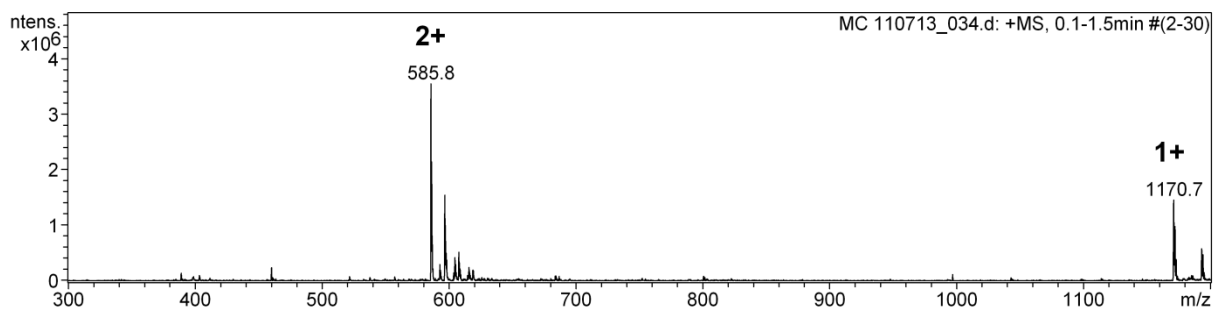
Deconvoluted mass: M_{found} = 1170.6; Mcalc = 1169.6

❖ **RP-HPLC profile and ESI-MS analysis of <u>10</u>**

RP-HPLC profile of <u>10</u> monitored at 214 nm.

Nucleosil column (100Å 5 μm C18 particles, 250 x 4.6 mm); linear gradient (5 to 100% B in 30 min; flow rate: 2 mL/min).
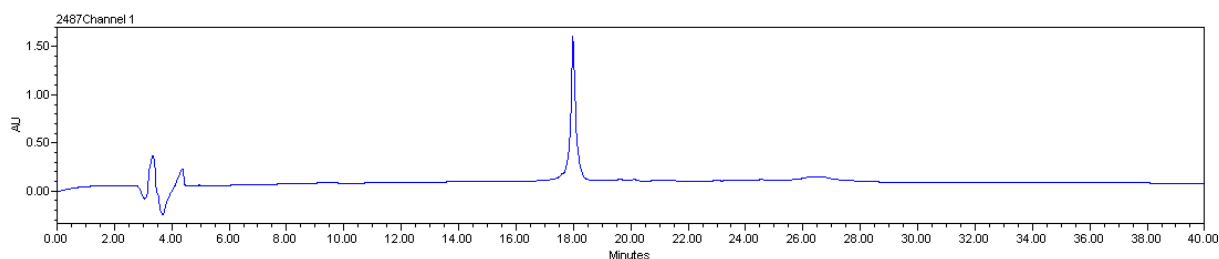
RT = 17.9 min

ESI-MS analysis of compound <u>10</u>
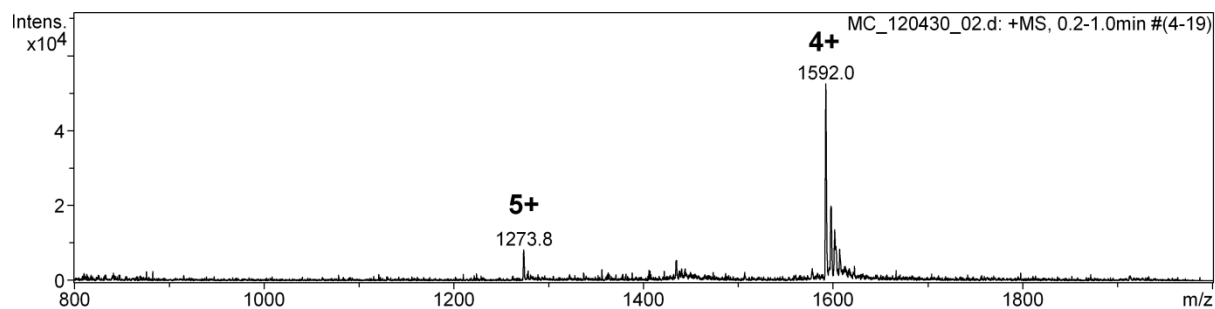
Deconvoluted mass: $M_{found} = 6364.9$; $M_{calc} = 6364.9$

❖ **RP-HPLC profile and ESI-MS analysis of cleavage product 11**

RP-HPLC profile of MMP cleavage affording peptide fragment **11** monitored at 214 nm. Nucleosil column (100Å 5 μm C18 particles, 250 x 4.6 mm); linear gradient (5 to 100% B in 30 min; flow rate: 2 mL/min).

2 μM of compound **10** in Tris Buffer (pH 7.8) was incubated with 5 nM of MMP-9 at 37°C for 24 hours, and analyzed by using RP-HPLC. The products observed were afterwards characterized using mass spectrometry.
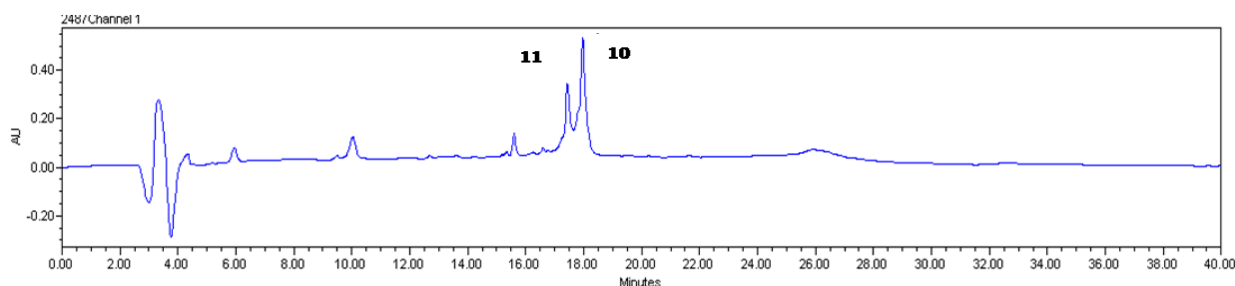
*RT (**10**) = 17.9 min; RT (**11**) =17.4 min*

ESI-MS analysis of compound **11**
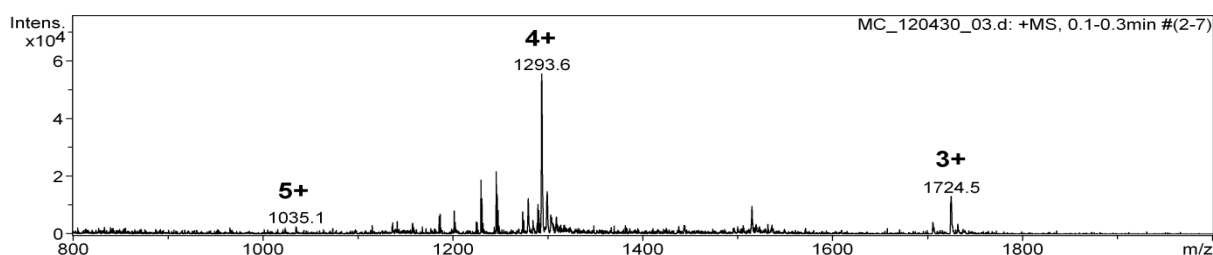
Deconvoluted mass: M_{found} = 5171.4; M_{calc} = 5171.4

IV. Cleavage studies of linear peptide sequences

Therefore human purified pro-MMP-2 and pro-MMP-9 were used (EnzoLifeScience). After activation of the enzymes using aminophenyl mercuric acetate (APMA, 20 mM), the enzymes were diluted in Tris buffer (50 nM, pH 7.5) to 0.2 ng/μL MMP-2 and 0.4 ng/μL MMP-9. Thereafter the incubation with 20 μM of substrate was followed (2 hrs, 37°C). The cleavage study was monitored by using RP-HPLC (C_{18}, Nucleosil column, CC250/4.6; 30 min linear program).

V. Cell culture

The cell lines **HEK293(β3)** and **HEK293(β1)** are sub-clones of the human embryonic kidney cells HEK293, stably transfected by means of human Integrin β3 and β1 coding plasmid (cell line from J-F. Gourvest, Aventis, France). These cell lines are cultivated in the cell culture medium DMEM (Gibco), with 4.5 g/l glucose, 10 % fetal calf serum, which was treated 30 minutes at 56°C for decomplemenation, and G418 (700 µg/ml) (Gibco).

The cell line **TS/A-pc** derives of a mouse breast cancer carcinoma model. The cells are cultivated in RPMI medium (Gibco), containing 10 % fetal calf serum decomplemented, 1 % glutamine and 25µM beta-mercaptoethanol.

The cell line **HT1080** is a human fibrosarcoma cell line. The cells are cultivated in DMEM medium (Gibco), containing 10 % fetal calf serum decomplemented and 1 % glutamine.

The cell line **A375** is a human melanoma cell line. These cell lines are cultivated in the cell culture medium DMEM (Gibco), with 4.5 g/l glucose and 10 % fetal calf serum.

The cell line **PC3** is a human prostate adenocarcinoma (cell line of G. Divita, UMR-5237 CNRS, Centre de Recherches de Biochimie Macromoléculaire, Montpellier, France). The cells are cultivated in RPMI medium (Gibco), containing 10 % fetal calf serum decomplemented and 1 % glutamine.

Colo829 are cells derived from human melanoma. The cells are cultivated in RPMI medium (Gibco), containing 10 % fetal calf serum decomplemented and 1 % glutamine.

The cells are cultivated at 37°C in humid atmosphere enriched with 5% CO_2. Cell-passage is done twice each week by dissociating the cell bed with trypsin/EDTA (Gibco).

The cell lines **HEK293(β3), TS/A-pc** are strongly Integrin αvβ3 positive and **A375** as well as **HT1080** and **Colo829** are weakly Integrin αvβ3 positive. The cell lines **HEK293(β1)** and **PC3** are Integrin αvβ3 neagtive.

Concerning the expression of MMP-9, HT1080 is used as control cell line as it is known to overexpress the active form of MMP-9[277].

Cell viability is estimated by the exclusion technique Trypan blue.

---

[277] Faust, A. *et al.* Synthesis and evaluation of a novel fluorescent photoprobe for imaging matrix metalloproteinases. *Bioconjug. Chem.* **19**, 1001–1008 (2008).

VI. Fluospectrometry

For the fluospectrometric analysis 200 µL of 0.25 µM of RAFT-RGD-MMP (compound **10**) and 0.5 µM of RAFT-RGD-Cy5 (provided by Didier Boturyn) were analyzed in 50mM Tris Buffer at pH 7.5 with 150 mM NaCl, 5mM $CaCl_2$ and 0.05% Brij-35 at 37°C. Fluorescence Emission spectra from 650 to 750 nm were recorded on a Perkin-Elmer LS 55 Fluorescence Spectrometer with PTP – 1 Fluorescence Peltier System equipped with a thermo-stated compartment (37°C) using a 120 V pulsed xenon lamp (excitation wavelength: 640 nm). In parallel the absorption spectra were recorded of each sample using the UV-visible Spectrophotometer Evolution 201 of ThermoScientific.

The Φ_F values were determined by the equation[278]:

$$\Phi = \Phi_{ref} * (F_{sample} / A_{sample})*(A_{ref}/F_{ref})$$
$$F=k*A*\Phi \quad => F= (A* \Phi)/(A_{ref}* \Phi_{ref}) * F_{ref}$$

where F and A are the measured fluorescence (area under the emission peak) normalized by its absorption spectrum and the absorbance at the excitation wavelength (640 nm). Cyanin 5 at 0.5 µM in Tris Buffer 7.5 was used as reference [$\Phi_{F(ref)}= 0.28$]

The Quenching was then calculated by using the following equation:

$$Quenching = (\Phi_{ref}- \Phi_{sample})/ \Phi_{ref}$$

The samples were incubated at 37°C and their spectra measured before incubation with the enzyme MatrixMetalloproteinase-9 (human recombinant MMP-9 catalytic domain, EnzoLifescience, Villeurbanne, France). Then the samples were incubated with 5nM of MMP-9 at 37°C, for 2 h, 24 h, and 48 h respectively (all spectra: T0 & T48h).

For the plasma test 1 µM of the molecule was incubated with 100 µL of fresh mouse plasma. The spectra were then analyses by the same procedure.

For MMP-Inhibition, the MMP-9 was pre-incubated with 600nM SB-3CT and 50µMCTT (specific competitive MMP inhibitors, EnzoLifescience, Villeurbanne, France) before incubated with 1 µM of RAFT-RGD-MMP.

The activity of the MMP and the inhibitors was controlled by using the fluorogenic substrate Mca-RPPGFSAFK(Dnp) (EnzoLifescience, Villeurbanne, France) which is cleaved by MMP-2 and -9.

---

[278]Gravier, Julien, Raphaël Schneider, Céline Frochot, Thierry Bastogne, Frédéric Schmitt, Jacques Didelon, François Guillemin, und Muriel Barberi-Heyob. „Improvement of meta-tetra(hydroxyphenyl)chlorin-like photosensitizer selectivity with folate-based targeted delivery. synthesis and in vivo delivery studies". *Journal of medicinal chemistry* 51, Nr. 13 (Juli 10, 2008): 3867–3877.

VII.   MMP -2 and -9 expression study

❖ Zymography

For the detection of active enzymes we used the electrophoretic technique called zymography. The substrates are co-polymerized with the polyacrylamid gel and the enzymes are separated by gel electrophoresis. Negative staining of the substrate gel reveals enzymatic activity because the protease has degraded the substrate in the gel[279] (white bands on blue gel). This method gives relative information about the quantity of active enzyme of the tested sample.

For gelatin zymography the supernatant of the different cell lines (24 to 48h in FCS-free medium) was collected and stored at -20°C like done by the team of Faust[280]. Thereafter the samples were diluted in non reducing sample buffer pH 6.8 (Tris 0.5M, SDS 10%, 20 % saccharose, bromphenol blue). Then the samples are deposed on an SDS-PAGE 10% which contains 0.1% gelatin. As control of the molecular weight human purified MMP-2 and MMP-9 with haemopexin domain were used (0.1 ng/µL; EnzoLifescience). After migration at 4°C for 30 minutes at 90V and another 2h30 at 140 V, the gel is washed twice for 30 minutes in Triton X-100 2.5%. Incubation at 37°C for 20 hours in incubation buffer at pH 7.2 (Tris 52mM, NaCl 200 mM, CaCl$_2$ 5mM, Triton X-100 0.01%) follows. The next step consists in staining of the gel, which takes place at room temperature for 30 minutes in staining buffer (Comassie brilliant blue G-250 in diluted methanol and acetic acid). The same buffer, but without Comassie blue is used to decolorize the gel for 1 hour at room temperature.

Afterwards the gel is scanned and dried via a gel drying pad on non laminated Whatman paper with under-pressure. Images are analyzed *via* ImageJ gel analyzing blot.

---

[279] Overall, C. M. & Kleifeld, O. Validating matrix metalloproteinases as drug targets and anti-targets for cancer therapy. *Nat Rev Cancer* **6**, 227–239 (2006).

[280] Faust, A. *et al.* Synthesis and evaluation of a novel fluorescent photoprobe for imaging matrix metalloproteinases. *Bioconjug. Chem.* **19**, 1001–1008 (2008).

VIII.   Flow cytometry analysis of integrin $\alpha_v\beta_3$ expression

For expression analysis, adherent cells are suspended with trypsin, washed once with cold PBS, and another time with PBS containing 1 mM $CaCl_2$ and 1 mM $MgCl_2$ (Ca^{2+}/Mg^{2+}). One million cells in a final volume of 200 mL are fixed with 2% PFA for 15 minutes, washed with PBS Ca^{2+}/Mg^{2+} twice and suspended in 500µl PBS containing 20 µL of the antibody CD51/CD61 R-Phycoerythrin clone 23C6 mouse anti-human (Pharmingen, BD Bioscience). After 1 hour of incubation at 4°C the volume was adjusted to 5 mL and the samples were centrifuged for 15 min at 4 °C. The solutions are removed and pellets carefully rinsed twice with PBS Ca^{2+}/Mg^{2+} (1 mM) at 4 °C. Cells are then rapidly analyzed by flow cytometry (FACS LSRII, BD bioscience, France). The results are reported as mean fluorescence intensity (MFI of Cy5) histogram counts.

Percentage of augmentation in MFI (mean fluorescence intensity) is calculated on the autofluorescence level. The results are expressed thus in pa-MFI (percentage of augmentation in MFI).

IX. Cell – molecule-interaction

The analysis of the molecule RAFT-RGD-MMP and cells is realized by means of flow cytometric and fluorescence microscopic analysis.

IX.1.   *Flow cytometry analysis (FACS) of the molecule – cell interaction*

One day before the actual trial 6 well dishes were prepared with 500 000 cells per well. The cells are incubated in 2mL of the corresponding Medium without FCS. 4 hours before FACS the cells are rinsed with 2 mL PBS (1mM $CaCl_2$ + 1mM $MgCl_2$). Then 800µL of FCS free medium (DMEM colorless, 10% GlutaMax, ITSpremix™ (BD, USA) 1mL/1L) is added. Three hours before analysis 200µL of RAFT-RGD-MMP (0.2µM final) or 200µL of RAFT-RGD-Cy5 (0.4µM final) as control is added and gently swiveled. This corresponds at 2 hours of incubation. The incubation is either at 37°C in a standard cell incubator or at 4°C (all

ingredients and plates placed on ice 10 minutes before). Incubation for 1 hour, 30 minutes, 15 minutes and 5 minutes followed. The liquid is removed gently and the cells rinsed once with cold PBS. After that the adherent cells are quickly suspended by trypsination (1-2mL) and diluted in excess of PBS (10mL) to be rapidly centrifugated by 4°C for 10 minutes at 1500rpm. Then a second centrifugation in 5 mL cold PBS follows. The liquid is removed and pellets carefully resuspended in 200µL PBS and the tubes are kept on ice and away from light. Cells are then rapidly analyzed by FACS (FACS LSRII, BD bioscience, France). The results are reported as MFI (Cy5) histogram counts.

For the Integrin inhibition study, the cell lines are incubated 5 minutes before each treatment with 20X RAFT-RGD (= 8µM).

IX.2. *Fluorescence microscopy analysis of the molecule – cell interaction*

For the analysis by means of confocal microscopy 4-well Lab-Tek™ chamber (ultra thin, borosilicate; ThermoFisher) are used. After coating with fibronectin, 50 000 cells are seed in 48 hours before the trial and incubated in the corresponding medium. The day before the trial, the medium is removed before the cells were gently rinsed and incubated in FCS-free medium over night. One hour before microscopic analysis, the medium was removed, the cells are gently washed with PBS and 300 µL Dulbecco's modified Eagle's medium w/o red phenol was added. After two hours 1µL Hoechst is added (for cell nucleus detection) and analysis of living cells with 0.6µL of RAFT-RGD-MMP occurred. During acquisition the cell containing Lab-Tek™ chamber is kept in a heated chamber at 37°C and 4% CO_2.

Confocal microscopy was performed on the Axiovert 200 LSM510 LNO Meta microscope (Carl Zeiss, Germany) using a 63× oil immersion objective of 1.4 N.A. A pinhole adjustment resulted in a 1 µm optical slice at scan zoom 1.5 and an image resolution of 516 x 516 pixel. The laser gain was fixed at 800. The 633 nm helium-neon laser (5mW) intensity was set up at 20% of its maximum intensity, which was set on the autofluorescence of the non treated cells. For imaging the Hoechst-labeled nucleus we used the laser Tsunami 1,5W sapphire-titan. The operating program was LSM software.

X. In vivo fluorescence imaging

All the animal experiments are performed in agreement with the EEC guidelines and the ''Principles of Laboratory Animal Care'' (NIH Publication No. 86-23, revised 1985).

Female NMRI Nude mice (6–8 weeks old, JANVIER, Le Genest Saint Isle, France) receive a sub-cutaneous xenograft of HEK293(b3) cells (20 x 10^6 per mouse), HT1080 (10 x 10^6 per mouse), A375 (10 x 10^6 per mouse), or TS/A-pc cells (5 x 10^6 per mouse). Once tumors reached approximately 200 mm^3, mice[281] are anesthetized (isoflurane/oxygen 4%/3.5% for induction and 2% thereafter) and are injected intravenously via the tail vein with 200 µL of RAFT-RGD-MMP or RAFT-RGD-Cy5 control peptide (2 nmol) (Cy5 Ex/Em: 633 nm/660 nm) or 150 µL of MMPSense680 (2 nmol; PerkinElmer's, Boston, USA) (Ex/Em: 680 nm/700 nm).

In vivo fluorescence imaging is realized with the Aequoria Hamamatsu system (Hamamatsu, Massy, France). Mice are illuminated by 633 nm (RAFT-RGD's) or 660 nm (MMPSense680) light-emitting diodes equipped with interference filters. Fluorescence images as well as black and white pictures are acquired by a back-thinned CCD camera at -80 °C (ORCAII-BT-512G) fitted with a high pass RG665 (Schott, Jena, Germany) for the 633 nm excitation or a high pass filter RG 9 (Schott, Jena, Germany) for the 660 nm excitation. All acquisitions are made with a medium gain and a binning 1x1 with an exposition time of 30 ms to 1s (depending on fluorescence level).After imaging at different time points after injection (30 min, 1 h, 2 h, 3 h, 5 h and 24 h), the mice are sacrificed (at either 3 h or 24 h after injection) and dissected for the imaging of organs ex vivo. The tumors are frozen in OCT and liquid nitrogen for storage at -80°C. Image display and analysis are performed using the Wasabi software (Hamamatsu, Massy, France).Semi-quantitative data of tumor and skin are obtained by drawing ROIs on the subcutaneous tumors and on the skin (shoulder region with no tumor; images *in vivo*). The tumor/skin ratio is then calculated using the semi-quantitative data obtained. The organ fluorescence quantifications are expressed as a number of relative light units per pixel per milliseconds (RLU/pix/ms) and the tumor/muscle ratio is calculated from these values. For all measurements the background noise is subtracted. All the data are expressed as mean ± standard deviation (SD) of three independent measurements.

---

[281] n = 3 for each group (per cell line; each cell line with sacrifice of one group at 3 h and one at 24 h, thus a total of n = 6 per cell line

« Ne me dites pas que ce problème est difficile. S'il n'était pas difficile, ce ne serait pas un problème. »

 Maréchal Ferdinand Foch (1851-1929)

[Don't tell me that this problem is difficult. If it wouldn't be difficult, it wouldn't be a problem.]

APPENDICES

Cat 2	T0	T0+2h	T0+5h30	T0+24h	T0+7jours	Physiologic parameters
WBC	4,4 .10^3/mm3	7,1	6,7	8,5	9,4	5,5-19,5.10^3/mm3
LYM	2,0.10^3/mm3	1,7	1,6	3,7	4,7	1,5-7,0 10^3/mm3
MON	0,0 .10^3/mm3	0	0	0,1	0,2	0,0-0,85.10^3/mm3
GRA	2,4 .10^3/mm3	5,4	5,1	4,7	4,5	2,5-14 10^3/mm3
EOS	0,3310^3/mm3	0,48	0,19	0,69	0,56	0,0-1,5 10^3/mm3
RBC	15,3.10^6/mm3	13,61	14,34	12,56	13,32	5,0-10,0 10^6/mm3
HGB	17,5 g/dL	15,2	15,8	14,2	14,7	8,0-15,0g/dL
HCT	61,8%	55,6	58,4	50,7	54,2	24,0-45,0%
MCV	40 µm^3	41	41	40	41	(3955µm^3)
MCH	11,4pg	11,2	11,0	11,3	11,0	(12,5-17,5pg)
MCHC	28,3 g/dL	27,4	27,1	28,1	27,1	(30,0-36,0 g/dL)
RDW	13,6%	15,0	14,3	14,5	14,8	(17,0-22,0%)
PLT	1045.10^3/mm3	952	1190	1036	1127	(300-800 10^3/mm3)
MPV	18,0 µm^3	17,4	17,0	17,1	17,2	(6,5-15,0µm^3)
Urée	7,4 mmol/L	/	5,8	9,8	8,6	(2-8mmol/L)
Creat	81 µmol/L	/	74	85	78	(20-135 µmol/L)
PAL	69 UI/L	/	60	42	46	(5-200 UI/L)
ALT	74 UI/L	/	76	92	56	(5-80)
PROT	72 g/L	/	68	61	64	(55-75)
CL	123 mmol/L	/	123	120	152	140-158 mmol/L
K	4,7 mmol/L	/	3,7	3,9	3,7	3,6-5,6 mmol/L
Na	155 mmol/L	/	157	152	117	105-122 mmol/L
RPCU	0,8	/	0,9	0,6	0,4	<0,5

Cat 3	T0	T0+5h30	T0+24h	T0+7jours	Physiologic parameters
WBC	22,8 10^3/mm3	29,7	12,2	10,7	5,5-19,5 10^3/mm3
LYM	8,9 10^3/mm3	5,9	2,7	3,7	1,5-7,0 10^3/mm3
MON	1,6 10^3/mm3	0,4	0,3	0,2	0,0-0,85 10^3/mm3
GRA	12,3.10^3/mm3	23,3	9,1	6,9	2,5-14 10^3/mm3
EOS	4,4 10^3/mm3	1,9	1,3	1,1	0,0-1,5 10^3/mm3
RBC	9,30 10^6/mm3	9,85	7,42	7,14	5,0-10,0 10^6/mm3
HGB	12,3 g/dL	13,3	10,2	9,7	8,0-15,0g/dL
HCT	45 %	48	35,7	34,9	24,0-45,0%
MCV	48 µm^3	49	48	49	(3955µm^3)
MCH	13,3 pg	13,4	13,8	13,6	(12,5-17,5pg)
MCHC	27,4 g/dL	27,6	28,6	27,8	(30,0-36,0 g/dL)
RDW	14,8%	14,8	14,9	15,0	(17,0-22,0%)
PLT	235 10^3/mm3	126	254	234	(300-800 10^3/mm3)
Urée	9,2 mmol/L	7,8	7,1	8,3	(2-8mmol/L)
Creat	98 µmol/L	109	84	80	(20-135 µmol/L)
PAL	37 UI/L	32	46	68	(5-200 UI/L)
ALT	65 UI/L	78	71	68	(5-80)
PROT	0,69 g/L	0,39	1,21	0,68	
CL	115 mmol/L	118	114	117	140-158 mmol/L
K	4,6 mmol/L	4,5	4,4	4,2	36-5,6 mmol/L
Na	146 mmol/L	152	147	149	105-122 mmol/L
RPCU	0,3	0,4	0,4	0,4	<0,5

The data show no strong parameters aberrations, which would indicate acute toxicity. The renal elimination of AngioStamp™ does not lead to measurable damage in the organ.

II. Table Of Amino Acids
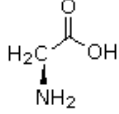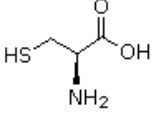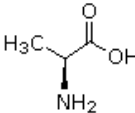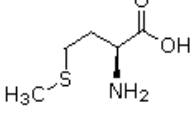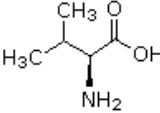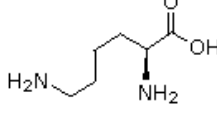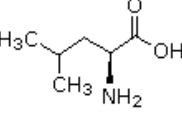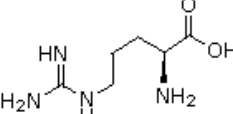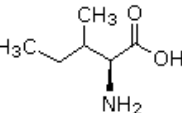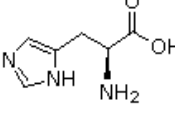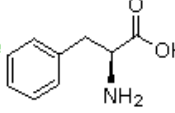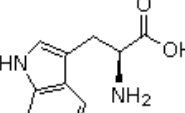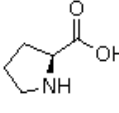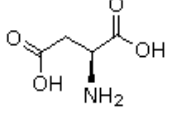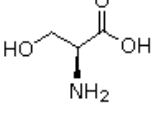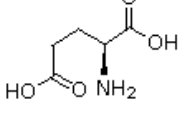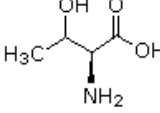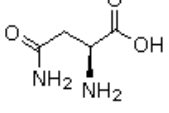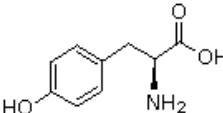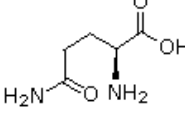
Name	Formula	Abbreviations		Name	Formula	Abbreviations	
Glycine		Gly	G	Cysteine		Cys	C
Alanine		Ala	A	Methionine		Met	M
Valine		Val	V	Lysine		Lys	K
Leucine		Leu	L	Arginine		Arg	R
Isoleucine		Ile	I	Histidine		His	H
Phenylalanine		Phe	F	Tryptophan		Trp	W
Proline		Pro	P	Aspartic Acid		Asp	D
Serine		Ser	S	Glutamic Acid		Glu	E
Threonine		Thr	T	Asparagine		Asn	N
Tyrosine		Tyr	Y	Glutamine		Gln	Q

Table II-1: The 20 natural amino acids.

III.Supplementary - Articles

❖ *Intraperoperative near-infrared image-guided surgery for peritoneal carcinomatosis in a preclinical experimental model*
Keramidas, M; Josserand, V.; Righini, C.; Wenk, C.H.F.; Faure, C; Coll, J.L. 2010.
British Journal of Surgery , Vol 97; ISSUE 5; pages 737-743.

❖ *Optical Small Animal Imaging in the Drug Discovery Process*
Dufort, S.; Sancey, L.; Wenk, C.; Josserand, V., Coll, J.L**.** 2010   Biochim. Biophys.
Acta Biomembrans **, 8**.

❖ *Des molécules fluorescentes au service de la chirurgie*
Pascal Dumy, Christiane Wenk, Michael Claron, Jean-Luc Coll, Bénédicte Allard,
Didier Boturyn 2012. L'Actualité Chimique , N°366 Pagination : 23-28

Intraoperative near-infrared image-guided surgery for peritoneal carcinomatosis in a preclinical experimental model

M. Keramidas[1,2], V. Josserand[1,2], C. A. Righini[1,2,3], C. Wenk[1,2], C. Faure[2,3] and J. L. Coll[1,2]

[1]Institut National de la Santé et de la Recherche Médicale U823, Institute Albert Bonniot, [2]University Joseph Fourier and [3]University Hospital of Grenoble, Grenoble, France
Correspondence to: Dr J. L. Coll, Institut National de la Santé et de la Recherche Médicale U823, Equipe 5, Institut Albert Bonniot, BP 170, 38 042 Grenoble cedex 9, France (e-mail: Jean-Luc.Coll@ujf-grenoble.fr)

Background: This study compared the quality of surgery performed under conventional light with near-infrared (NIR) image-guided surgery using a tumour-targeting probe and a portable clinical grade imaging device in a mouse model of peritoneal carcinomatosis.

Methods: Peritoneal carcinomatosis was induced by injection of luciferase-positive tumour cells, leading to the formation of small nodules in the peritoneal cavity. One day after intravenous injection of RAFT-c(RGDfK)$_4$-Alexa Fluor® 700, a fluorescent tumour-targeting probe, the surgeon operated using the Fluobeam®, a portable device that illuminated the mouse with NIR light and allowed NIR vision. The quality of the surgery was evaluated using bioluminescence, a highly sensitive method that detected the remaining tumour cells, and operating time was measured.

Results: Under normal light, the surgeon detected and removed a mean(s.d.) of only 50·6(2·3) per cent of the nodules that were visible under NIR light. The duration of surgery was reduced from 19·5(3·3) min under normal light to 14·0(2·6) min when NIR light was used ($P = 0.025$). The sensitivity of the NIR system allowed the detection of nodules containing as few as 227 tumour cells.

Conclusion: NIR image-guided surgery improved the quality of surgery for peritoneal carcinomatosis by doubling the number of nodules detected and significantly reducing the duration of surgery.

Introduction

Surgical removal of a tumour is often the best method of cure for cancer, but the likelihood of surgical cure depends on the size, location and stage of disease. Advances in surgical technique and practice have allowed surgeons to perform minimally invasive procedures while maintaining good safety margins. Nevertheless, improved vision is important for complete removal of tumours that are not fully discernible and small nodules that are barely detectable under normal light or by palpation. The generation of tumour-specific contrast agents and intraoperative fluorescent imaging devices is expected to improve the quality of tumour surgery[1].

Two-dimensional fluorescence–reflectance optical imaging (2D-FRI) is a non-invasive method that works in real time at good spatial (nanometre to millimetre range) and temporal (microseconds to a few minutes) resolution,

with high sensitivity (femtomolar to picomolar range) from the whole-body to the subcellular scale[2]. However, although fluorochromes emitting in the near-infrared (NIR) window (650–900 nm) are used, this method is limited in depth by the poor transmission of light through biological tissues[3]. A newly developed, handheld laser containing a FRI system was used in the present study, which has been adapted for clinical use; it is able to detect NIR photons even with the commonly used white surgical light illuminating the operative field.

The authors have developed a tumour-targeting peptide, RAFT-c(RGDfK)$_4$-Alexa Fluor® 700 (RAFT-RGD: Anglioney®; Fluoptics, Grenoble, France), which targets the transmembrane integrin $\alpha_v\beta_3$. This protein is overexpressed on neoendothelial cells that form tumour blood vessels but is also frequently overexpressed on tumour cells themselves in lung cancers[4,5], melanomas[6,7],

brain tumours[8] and breast cancers[9]. When combined with an optical or nuclear imaging agent, RAFT-RGD can detect metastatic tumours engrafted in mice[10–14].

The purpose of the present study was to evaluate the advantage to the surgeon of operating on peritoneal carcinomatosis using the NIR dual system comprising the Fluobeam® (Fluoptics) imaging device and the RAFT-RGD fluorescent tumour-targeting tracer.

Methods

Cell line and culture conditions

TSA-pGL3 is a cell line derived from the original TS/Apc mouse adenocarcinoma cell line stably transfected with the pGL3-luciferase reporter gene (Promega, Charbonnières, France). Cells were cultured at 37°C in a humidified 95 per cent air/5 per cent carbon dioxide atmosphere in RPMI 1640 supplemented with 1 per cent glutamine, 10 per cent fetal bovine serum, 50 units/ml penicillin, 50 μg/ml streptomycin and 700 μg/ml Geneticin® (G418 sulphate; Gibco, Paisley, UK). These cells express low levels of integrin $\alpha_v\beta_3$[13].

Animal and tumour models

All animal experiments were conducted in agreement with the Principles of Laboratory Animal Care (National Institutes of Health publication no. 86-23, revised 1985) and approved by the regional ethics committee. Female athymic Swiss nude mice (Janvier, Le Genest-Isle, France) were used in this study and maintained under specific pathogen-free conditions. A total of 500 000 TSA-pGL3 cells in 500 μl phosphate-buffered saline were injected intraperitoneally. These formed small nodules scattered in the peritoneal cavity, resembling peritoneal carcinomatosis, which could be detected by bioluminescence imaging or by fluorescence after intravenous injection of RAFT-RGD.

Bioluminescence imaging

Mice received an intraperitoneal injection of luciferin (150 mg/kg) 5 min before bioluminescence imaging, as described previously[12]. This allowed localization, quantitation and evaluation of the number of luciferase-positive nodules before, during and after surgery. Semiquantitative data were obtained from the bioluminescence images by drawing regions of interest on the area to be quantified. Results were expressed as the number of relative light units (RLU) per pixel per second.

Luciferase enzymatic activity was also assayed *in vitro* using a Luciferase Assay System (Promega). Tissues were mixed in 1 ml lysis buffer in order to extract the proteins. Ten microlitres of extract was mixed with 100 μl luciferase substrate and luciferase activity was measured for 10 s on a photoluminometer (Berthold, Illkirch, France). Luciferase activity was calculated as the number of RLU per 10 s per milligram of protein. This method was also used to determine the number of RLU per 10 s per TSA-pGL3 cell, by means of serial dilution of a known number of cells.

Fluorescent tumour-targeting probe and fluorescence–reflectance optical imaging system

The tumour-targeting peptide RAFT-RGD is illustrated in *Fig. 1a*. On the upper side, four copies of the c(RGDfK) peptide were grafted for recognition of integrin $\alpha_v\beta_3$. The bottom side was used to link the fluorescent agent used for *in vivo* molecular imaging, Alexa Fluor® 700 carboxylic acid with succinimidyl ester (Invitrogen, Cergy Pontoise, France), as described previously[15]. Alexa Fluor® 700 has an excitation maximum at 702 nm, and its maximum emission at 723 nm is well adapted to deep (±5 mm) and sensitive imaging. After systemic administration into the tail vein, RAFT-RGD recognizes integrin $\alpha_v\beta_3$ on the surface of the target cells[16,17], putting a fluorescent tag on the primary tumour[11] or metastasis[10,12].

Fluobeam® is a 2D-FRI system composed of two optical-fibre 690-nm emitting lasers (100 mW each) providing NIR excitation and a charged couple device (CCD) camera to detect fluorescence emitted by RAFT-RGD-labelled tumours (*Fig. 1b*). This system provides continuous NIR excitation of the whole body of the mouse because of the presence of a holographic lens that produces a homogeneous lightened field (6–8 cm in diameter) with an illumination power of 5 mW/cm². The fluorescence signal is collected through a high-pass filter (more than 720 nm) by a digital 12-bit CCD camera that records time-lapse sequences of images similar to a video rate (image size, 1392 × 1024; pixel size, 6·45 × 6·45 μm²). The fluorescent image (acquisition time adjustable between 5 μs and 65 s) is superimposed automatically on a visible light image obtained using an infrared-filtered white-light illuminator (7 × 10³ lux). Examples of real-time imaging can be seen in the supplementary data file (supporting information). The surgeon can therefore work as usual but will benefit from the deported screen that shows the location of fluorescent tumours continuously and in real time. The Fluobeam® is highly sensitive. A standard curve was prepared from serial RAFT-RGD dilutions and a signal-to-noise ratio of 1·5 or greater was considered the positive signal threshold. Under these conditions, a

a RAFT-RGD

b Fluobeam® system

Day 0	Day 7	Day 8 $t = 0$ min	Day 8 $t = 5$ min	Day 8 $t = 15–30$ min	Day 8 $t = 30$ min
Injection of 500 000 Luc+ tumour cells i.p.	Injection of 10 nmol RAFT-RGD i.v.	Injection of luciferin i.p.	Bioluminescence imaging Death	Surgery ± NIR imaging	NIR and bioluminescence imaging of nodules and carcass

c Experimental protocol
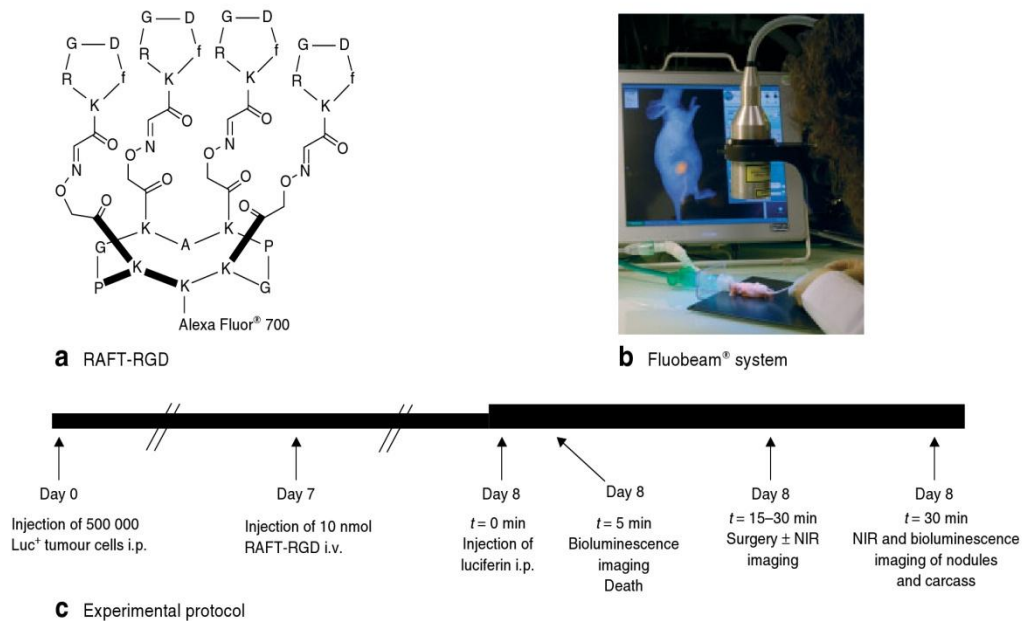
Fig. 1 **a** Structure of RAFT-c(RGDfK)$_4$-Alexa Fluor® 700 (RAFT-RGD). **b** Fluobeam® fluorescent intraoperative system. **c** Study protocol. Luc+, luciferase positive; i.p., intraperitoneally; i.v., intravenously; NIR, near-infrared

positive signal could be detected on a 10-μl drop containing 0·5 nmol/l of probe (0·5 femtomol/μl) with a 100-ms exposure. A longer exposure time enabled detection of as little as 0·35 nmol of probe in 500 ms (data not shown).

Experimental protocol

The protocol is summarized in *Fig. 1c*. TSA-pGL3 cells were engrafted at low density by intraperitoneal injection in a total of 15 nude mice. Seven days after tumour implantation the mice received an intravenous injection of 10 nmol RAFT-RGD. On day 8, they were anaesthetized just before surgery (isoflurane/oxygen 3·5 per cent for induction and 1·5 per cent thereafter) and the operation was performed under the field of view of the Fluobeam®. An intraperitoneal injection of luciferin was given and bioluminescence imaging was carried out 5 min later, after which the animals were killed immediately. In the first set of experiments (seven mice in three independent sets; $n = 2$, $n = 2$ and $n = 3$), to investigate whether the NIR imaging system would improve the detection and removal of nodules, complete removal of the visible nodules was performed under normal light. When the surgeon was satisfied with the conventional operation, the NIR system was turned on and the operation continued. The number

of extracted nodules and the operating time were recorded. In the second set of experiments (four sets of $n = 2$), the animals were treated according to the same protocol, except that surgery was performed under NIR light only and the number of excised nodes was counted. The carcass was evaluated by bioluminescence imaging to determine whether any tumour cells had been missed by NIR image-guided surgery. The number of luciferase-positive (Luc+) tumour cells in nodules was calculated after measurement of the luciferase enzymatic activities present in the proteins extracted from each nodule.

Results

Improved surgery using near-infrared image-guided surgery

Bioluminescence imaging indicated that multiple nodules were disseminated in the peritoneal cavity by day 8 after injection of TSA-pGL3 cells (*Fig. 2a*). As these mice received an injection of RAFT-RGD the day before, tumours were also visible using NIR imaging (*Fig. 2a*). There was a good correlation between the fluorescent and bioluminescent patterns, demonstrating the good targeting capacity of RAFT-RGD[12]. Immediately after bioluminescence imaging, the seven mice were killed and

a Before operation   **b** During operation

c Extracted nodules and carcass
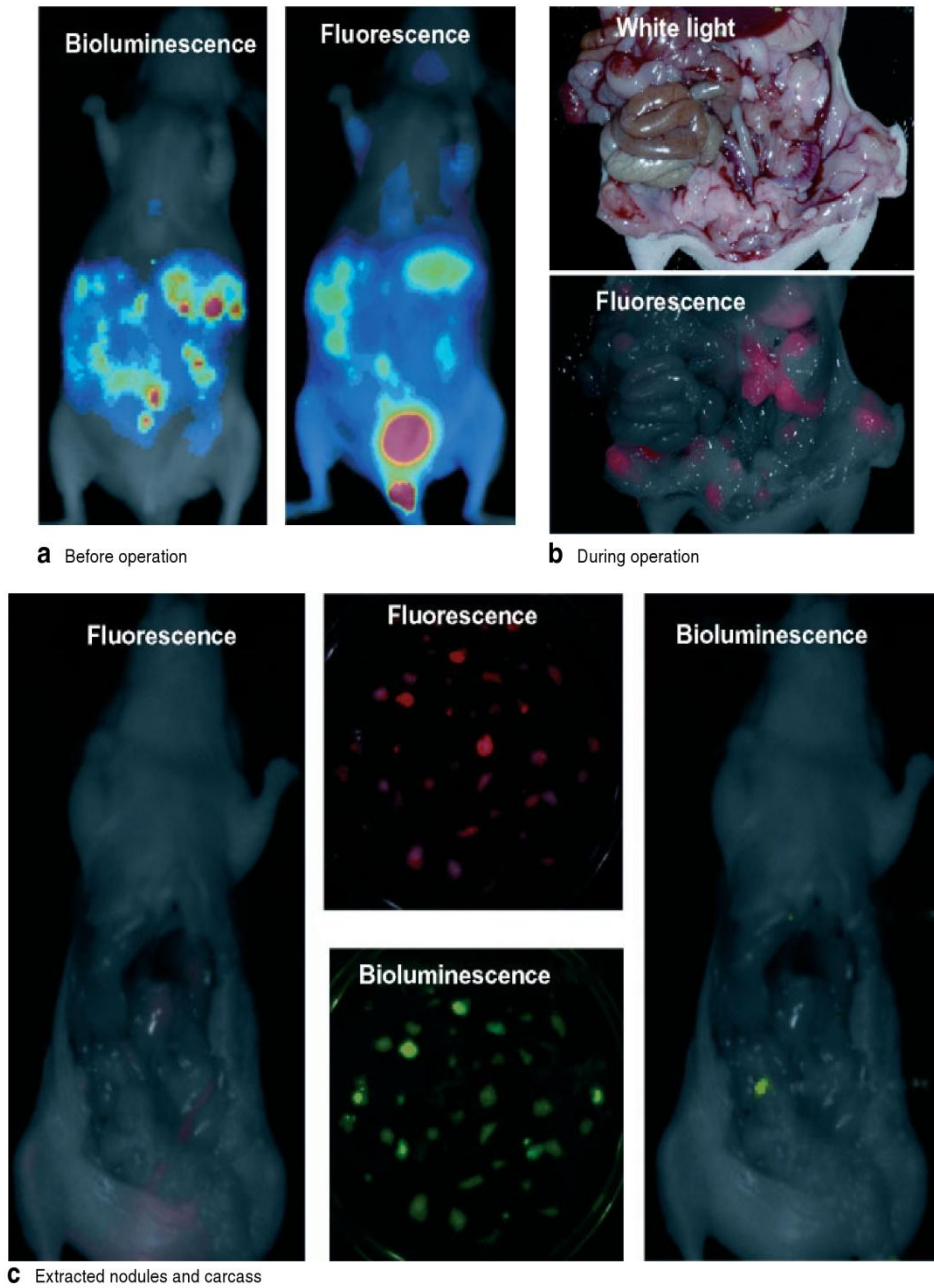
Fig. 2 Representative bioluminescence and fluorescence–reflectance optical images of a mouse with intraperitoneal nodules at different stages of surgery. **a** Bioluminescence (left) and fluorescence (right) images before operation. **b** Surgery performed under white light (upper panel) and with the near-infrared (NIR) image-guided system (lower panel). **c** The extracted nodules and carcass were examined with the NIR system and also exposed to bioluminescence imaging to detect the presence of false-negative nodules (luciferase positive/fluorescence negative)

a Proportion of nodules excised   **b** Cells per nodule
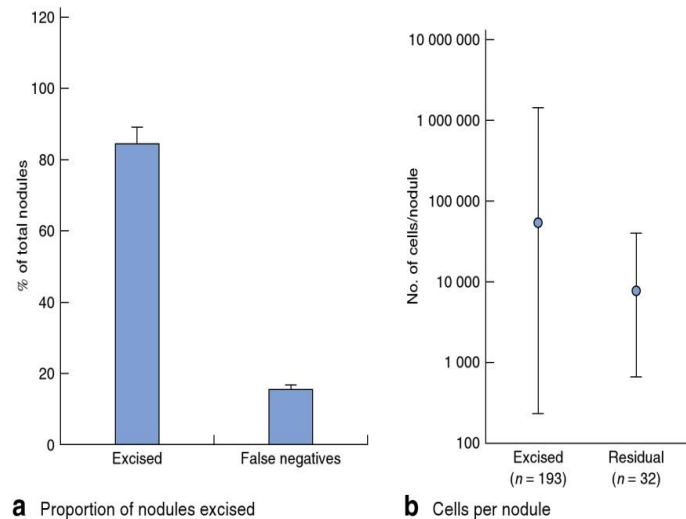
Fig. 3 a Proportion of luciferase-positive (Luc$^+$) nodules excised under near-infrared light and false negatives remaining in the carcass (luciferase positive/fluorescence negative). **b** Mean (range) number of Luc$^+$ tumour cells in excised and residual nodules

Table 1 Number of tumour nodules extracted with or without the aid of the near-infrared image-guided system

Mouse	No. of nodules detected		Fold increase
	Normal light	Near-infrared light	
1	10	20	2·0
2	23	37	1·6
3	20	38	1·9
4	16	28	1·8
5	23	42	1·8
6	14	26	1·9
7	11	40	3·6

complete removal of the visible nodules was performed under normal light (*Fig. 2b*). The number of nodules detected under normal light and with the NIR system is shown in *Table 1*. The surgeon detected and removed a mean(s.d.) of only 50·6(2·3) per cent of the nodules that were visible under NIR light in these seven mice. The mean(s.d.) duration of surgery was reduced from 19·5(3·3) min to 14·0(2·6) min with use of the NIR system ($P = 0.025$; $n = 6$).

Specificity of near-infrared image-guided surgery

Despite the clear increase in the quality of surgery, small tumours might have been left behind. This was investigated in mice that had surgery under NIR light only. The presence of remaining Luc$^+$ nodules in the carcass was evaluated by bioluminescence. Some false-negative nodules were detected (Fluor$^-$/Luc$^+$) (*Figs 2c* and *3a*) and it was estimated that, even with the help of NIR image guidance, 14 per cent of the Luc$^+$ nodules had still been missed. Examination of the extracted nodules confirmed that no false-positive nodules (fluorescence positive (Fluor$^+$)/Luc$^-$) had been extracted (*Fig. 2c*).

By comparing the level of luciferase enzymatic activity present in these nodules with a standard curve obtained with a known number of tumour cells (data not shown), the number of Luc$^+$ cells in each sample was calculated (*Fig. 3b*). Among the 193 nodules extracted, tumours containing as few as 227 cells were detected. The 32 false-negative nodules were very small (maximum 38 379 cells). Half of these nodules (7·1 per cent of the total) were located very close to the kidneys or bladder. These two organs emit NIR light as the probe is evacuated. The remaining false-negative nodules were located randomly and were considered to be genuine false negatives (6·5 per cent of the total). The surgeon also removed six 'suspicious' tissues that resembled nodules but were Fluor$^-$/Luc$^-$. Histopathological examination confirmed that none of them contained tumour cells.

Discussion

Cytoreductive surgery is often a critical treatment for patients with peritoneal carcinomatosis from colorectal cancer or other tumours that have spread to the peritoneal

surfaces. The factor most frequently associated with long-term survival is the completeness of cytoreduction or the removal of all visible tumours[18]. Cytoreductive surgery is often prolonged (12 h or more), requires large incisions and is associated with a high rate of postoperative complications. It is therefore important to develop new technologies that will help achieve precise delineation of tumour margins, improved visibility of small tumours or lesions that are difficult to distinguish from normal tissues, and reduced operating time.

Image-guided tumour resection is a promising emerging technology that should satisfy these three criteria. This preclinical study has shown the value of a novel handheld NIR device, based on the use of a laser and CCD camera to detect a tumour-specific NIR tracer, in improving the completeness of cytoreductive surgery and decreasing the duration of operation. NIR imaging provides immediate additional information about the malignant quality of a suspicious tissue as an RGD-based probe is used. Such imaging should help the surgeon but is not expected to replace current therapeutic protocols.

The Fluobeam® is a lightweight and portable system. It can function even under the powerful white light of the operating room. A more sophisticated intraoperative system has already been used in clinical trials[19] and in several animal experiments[20,21]. However, the FLARE™ system (http://www.frangionilab.org) is larger and cannot be handled as easily as the Fluobeam®.

The present study focused on the detection of small (submillimetre) tumours. Approximately 50 per cent of tiny nodules could not be seen under white light and were only visible using the NIR system. With this system, the duration of surgery was significantly reduced whereas the number of nodules removed was doubled. However, the cytoreduction was not complete. Using the highly bioluminescence-sensitive method it was demonstrated that a few very small Luc+ nodules were not removed. Half of these false-negative nodules (7·1 per cent) were not seen using NIR light because they were positioned very close to an organ that was strongly stained by the probe (kidneys, bladder).

The RAFT-RGD probe, which binds to the $\alpha_v\beta_3$ integrin expressed during neoangiogenesis, did not stain the other genuine false negatives (6·5 per cent) because these nodules were too small and were not angiogenic. However, the presence of these undetected nodules may also be a function of the sensitivity of the method (optics) and the choice of fluorophore (quantum yield, brightness). Switching to longer wavelengths (over 750 nm) or exchanging the organic fluorescent molecule (Alexa Fluor® 700) for

brighter fluorophores (quantum dots) may increase the sensitivity *in vivo*. The Fluobeam® fluence rate is 5 mW/cm^2. This does not produce any detectable photobleaching and so could also be increased to augment the sensitivity. However, it must remain[19] below 50 mW/cm^2.

This method has limitations in terms of depth of detection (a few millimetres depending on the tissue) and signal quantification. However, this may not be an issue for surgical applications and the system may actually have an advantage over γ probes. The signal-to-noise ratio of the γ probe is affected by the non-specific accumulation of the tracer in surrounding tissues, whereas 2D-FRI is highly surface weighted and will not be contaminated by far-travelling 'non-specific' photons. Overall, the quality of the surgery will rely on the specificity, brightness and pharmacokinetic properties of the NIR probe. The excellent properties of RAFT-RGD for tumour detection under NIR light have been demonstrated previously[11]. Because of its specificity, RAFT-RGD, in combination with the optical properties of the Fluobeam®, can be considered a promising dual tool to improve surgery.

Acknowledgements

References

1 Gutowski M, Carcenac M, Pourquier D, Larroque C, Saint-Aubert B, Rouanet P *et al*. Intraoperative immunophotodetection for radical resection of cancers: evaluation in an experimental model. *Clin Cancer Res* 2001; **7**: 1142–1148.

2 Kumar S, Richards-Kortum R. Optical molecular imaging agents for cancer diagnostics and therapeutics. *Nanomed* 2006; **1**: 23–30.

3 Ntziachristos V, Ripoll J, Wang LV, Weissleder R. Looking and listening to light: the evolution of whole-body photonic imaging. *Nat Biotechnol* 2005; **23**: 313–320.

4 Chen X, Sievers E, Hou Y, Park R, Tohme M, Bart R *et al.* Integrin alpha v beta 3-targeted imaging of lung cancer. *Neoplasia* 2005; **7**: 271–279.

5 Sato T, Konishi K, Kimura H, Maeda K, Yabushita K, Tsuji M *et al.* Vascular integrin beta 3 and its relation to pulmonary metastasis of colorectal carcinoma. *Anticancer Res* 2001; **21**: 643–647.

6 Gehlsen KR, Davis GE, Sriramarao P. Integrin expression in human melanoma cells with differing invasive and metastatic properties. *Clin Exp Metastasis* 1992; **10**: 111–120.

7 Seftor RE, Seftor EA, Gehlsen KR, Stetler-Stevenson WG, Brown PD, Ruoslahti E *et al.* Role of the alpha v beta 3 integrin in human melanoma cell invasion. *Proc Natl Acad Sci U S A* 1992; **89**: 1557–1561.

8 Gladson CL, Cheresh DA. Glioblastoma expression of vitronectin and the alpha v beta 3 integrin. Adhesion mechanism for transformed glial cells. *J Clin Invest* 1991; **88**: 1924–1932.

9 Rolli M, Fransvea E, Pilch J, Saven A, Felding-Habermann B. Activated integrin alphavbeta3 cooperates with metalloproteinase MMP-9 in regulating migration of metastatic breast cancer cells. *Proc Natl Acad Sci U S A* 2003; **100**: 9482–9487.

10 Garanger E, Boturyn D, Jin Z, Dumy P, Favrot MC, Coll JL. New multifunctional molecular conjugate vector for targeting, imaging, and therapy of tumors. *Mol Ther* 2005; **12**: 1168–1175.

11 Jin ZH, Josserand V, Foillard S, Boturyn D, Dumy P, Favrot MC *et al. In vivo* optical imaging of integrin alphaV-beta3 in mice using multivalent or monovalent cRGD targeting vectors. *Mol Cancer* 2007; **6**: 41.

12 Jin ZH, Josserand V, Razkin J, Garanger E, Boturyn D, Favrot MC *et al.* Noninvasive optical imaging of ovarian metastases using Cy5-labeled RAFT-c(-RGDfK-)4. *Mol Imaging* 2006; **5**: 188–197.

13 Sancey L, Ardisson V, Riou LM, Ahmadi M, Marti-Batlle D, Boturyn D *et al. In vivo* imaging of tumour angiogenesis in

mice with the alpha(v)beta (3) integrin-targeted tracer 99mTc-RAFT-RGD. *Eur J Nucl Med Mol Imaging* 2007; **34**: 2037–2047.

14 Foillard S, Jin ZH, Garanger E, Boturyn D, Favrot MC, Coll JL *et al.* Synthesis and biological characterisation of targeted pro-apoptotic peptide. *Chembiochem* 2008; **9**: 2326–2332.

15 Garanger E, Boturyn D, Coll JL, Favrot MC, Dumy P. Multivalent RGD synthetic peptides as potent alphaVbeta3 integrin ligands. *Org Biomol Chem* 2006; **4**: 1958–1965.

16 Boturyn D, Coll JL, Garanger E, Favrot MC, Dumy P. Template assembled cyclopeptides as multimeric system for integrin targeting and endocytosis. *J Am Chem Soc* 2004; **126**: 5730–5739.

17 Sancey L, Garanger E, Foillard S, Schoen G, Hurbin A, Albiges-Rizo C *et al.* Clustering and internalization of integrin alphavbeta3 with a tetrameric RGD-synthetic peptide. *Mol Ther* 2009; **17**: 837–843.

18 Glehen O, Kwiatkowski F, Sugarbaker PH, Elias D, Levine EA, De Simone M *et al.* Cytoreductive surgery combined with perioperative intraperitoneal chemotherapy for the management of peritoneal carcinomatosis from colorectal cancer: a multi-institutional study. *J Clin Oncol* 2004; **22**: 3284–3292.

19 Troyan SL, Kianzad V, Gibbs-Strauss SL, Gioux S, Matsui A, Oketokoun R *et al.* The FLARE intraoperative near-infrared fluorescence imaging system: a first-in-human clinical trial in breast cancer sentinel lymph node mapping. *Ann Surg Oncol* 2009; **16**: 2943–2952.

20 Nakayama A, del Monte F, Hajjar RJ, Frangioni JV. Functional near-infrared fluorescence imaging for cardiac surgery and targeted gene therapy. *Mol Imaging* 2002; **1**: 365–377.

21 Frangioni JV. New technologies for human cancer imaging. *J Clin Oncol* 2008; **26**: 4012–4021.

Optical Small Animal Imaging in the Drug Discovery Process
Dufort, S.; Sancey, L.; Wenk, C.; Josserand, V., Coll, J.L. 2010   Biochim. Biophys. Acta Biomembrans , 8.

Review

Optical small animal imaging in the drug discovery process

S. Dufort [a,b,c,1], L. Sancey [a,b,1], C. Wenk [a,b], V. Josserand [a,b], J.L. Coll [a,b,*]

[a] CRI-INSERM U823, Cibles diagnostiques ou thérapeutiques et vectorisation de drogues dans les cellules tumorales, Institut Albert Bonniot, BP 170, 38 042 Grenoble cedex 9, France
[b] Université Joseph Fourier, BP 53, 38 041 Grenoble cedex 9, France
[c] UF Cancérologie Biologique et Biothérapie, pôle de biologie et pathologie, CHU de Grenoble, BP 217, 38 043 Grenoble cedex 9, France

ARTICLE INFO

ABSTRACT

Molecular imaging of tumors in preclinical models is of the utmost importance for developing innovative cancer treatments. This field is moving extremely rapidly, with recent advances in optical imaging technologies and sophisticated molecular probes for *in vivo* imaging. The aim of this review is to provide a succinct overview of the imaging modalities available for rodents and with focus on describing optical probes for cancer imaging.

© 2010 Elsevier B.V. All rights reserved.

Contents

1. Introduction

Molecular imaging can be used as a non-invasive means to evaluate pathophysiological processes, such as cancer, in rodents. Indeed, these techniques provide real-time information for early diagnosis, allow longitudinal follow-up of tumor development, and facilitate studies of therapeutic activity and antitumor efficacy of new anti-cancer drugs. Because drug development is an expensive and complicated process with an extremely slim chance of success for any given molecule, molecular imaging can play an important role in drug discovery in the laboratory, during the translation phase from *in vitro* assays to preclinical systems, and eventually in evaluating the biodistribution, pharmacokinetics and biological activity of potentially therapeutics molecules [1].

These applications necessitate the generation of suitable imaging devices and imaging probes. This review presents the most commonly used methods for small animal imaging. We will focus mainly on optical imaging techniques and probes that are actively being developed for their sensitivity, inherent biological safely, and relative ease of use (see Table 1). In addition, we will present the translation of novel optical devices, methods and techniques into the clinic, which are areas of increased interest.

2. Commonly used small animal imaging technologies

2.1. X-ray computed tomography (CT)

CT is very commonly used on human patients, but until recently its application in rodents has been limited by its spatial resolution. X-rays are absorbed to varying degrees by different biological tissues. Recently, micro-CT devices have been developed to image rodents with a spatial resolution ranging from 10 to 100 μm [2]. Micro-CT is a powerful and cost-effective method for imaging soft-tissue structures, skeletal abnormalities and tumors. Micro-CT systems provide excellent sensitivity for skeletal tissue (Table 1).

2.2. Magnetic resonance imaging (MRI)

MRI is another standard method of clinical imaging, and recent improvements and adaptations have expanded its use to specialized animal facilities. ^{1}H-MRI is based on the fact that when a sample lying within a magnetic field is subjected to a radio-frequency pulse its protons absorb energy and generate a detectable signal during the relaxation phase. The strength of the signal is a function of the number of protons. The relaxation process can be described by two fundamental rate constants: T1 (longitudinal relaxation) and T2 (transverse relaxation) [3]. The sensitivity of this method is low (mM concentrations) but its spatial resolution is extremely good (μm). MRI is very useful for detecting tumors and measuring morphologic parameters. Because there is no damaging radiation, multiple imaging sessions can be performed safely, allowing longitudinal follow-up of tumor growth. Finally, contrast agents influencing either the T1 or T2 relaxation time constants are being developed to allow functional imaging [4–7].

2.3. PET and SPECT

Positron emission tomography (PET) requires the use of radioactive isotopes that emit positrons, such as ^{18}F, ^{15}O, ^{13}N, and ^{11}C [8], while SPECT (single photon emission computed tomography) uses tracers that emit gamma ray or high-energy X-ray photons, such as ^{123}I, ^{125}I, and ^{99}mTc. Positrons move a short distance through tissues, losing energy as they collide with other molecules, and eventually combine with electrons ("annihilation"), producing two high-energy gamma rays or photons traveling outward and in opposite directions. In SPECT, a single photon per event is directly emitted, and this photon interacts with electrons and nuclei of nearby atoms within the tissue. Unlike positrons, these energetic photons do not "slow down"

but are attenuated. Because there is only one photon per event, electronic collimation is not possible, and a physical collimator must be added. Sensitivities are on the order of 10^{-14}–10^{-15} M for PET and 10^{-14} M for SPECT, and spatial resolution can reach 1.3 mm for PET and is sub-millimetric for SPECT [9]. PET and SPECT give information about physiological functions at the molecular level and are thus well suited to monitoring many vital processes, such as glucose metabolism, blood flow and perfusion, receptor-ligand binding rates, and oxygen utilization.

2.4. Optical imaging

Optical imaging is based on the detection of light passing through the tissues. Several major obstacles must be resolved for optical imaging, including surface reflectance, absorption, scattering (deviation of the photon from its original path) and autofluorescence. Absorption and autofluorescence are important factors in fluorescence imaging in the visible wavelengths (400–650 nm) but are less problematic in the near-infrared (NIR) (650–900 nm). Above 900 nm, however, water absorption is an issue because it prevents deep penetration of the light. Absorption is affected by the thickness and optical properties of the tissues. The body heterogeneity will compromise the linearity of measurements. *In vivo*, scattering of far-red photons affects the spatial resolution, which is dependent on the depth of observation. Spatial resolution is mainly affected by an animal's skin, which reflects light, but intravital microscopy greatly improves the resolution [1].

Light can be produced in live animals by two main types of reaction: bioluminescence (BLI) and fluorescence (for reviews see [10,11]). BLI is based on the self-emission of green to yellow light due to the oxidation of luciferin in the presence of luciferase enzymes (Firefly, Renilla, Aequoria…). BLI has minimal background signal and an excellent signal-to-noise ratio (SNR). Acquisition times range from seconds to minutes.

Two-dimensional fluorescence reflectance imaging (FRI) uses fluorescent probes to produce detectable signals (Fig. 1). In FRI, the sample is submitted to an NIR light (excitation) that can be absorbed by the fluorescent probe, which then emits light (fluoresces) at a longer wavelength as it returns from an excited electronic state to its ground level. The probe could be a protein (e.g., green fluorescent protein (GFP) or DsRed) present in genetically modified animals or cells or an exogenous fluorophore. Because these fluorescent proteins are not excitable in the far-red or NIR spectrum, but only in the 450–650 nm window, they are not well adapted to whole-body small animal imaging, and their detection is limited by depth (typically 1–2 mm). In contrast, some other fluorophores (such as cyanines, quantum dots, and lanthanides) can be exited in the far-red window, allowing deeper detection (typically 1–2 cm). Sensitivity is very good (10^{-12} M), spatial resolution varies from 100 μm *in vitro* to 2 mm *in vivo* and temporal resolution is in the range of milliseconds to seconds. However, 2D-FRI is highly surface-weighted, and quantification is at best semi-quantitative.

Recent development of 2D-FRI may allow its application in the clinic for improving cancer surgery. The Fluobeam® system (Fluoptics, Grenoble, France) uses a laser and small charge-coupled device (CCD) camera within a portable 2D-FRI system. It can function under the normal light of an operating room [12]. Another intraoperative device, the FLARE system (fluorescence-assisted resection and exploration), has already been used in preclinical trials [13–15].

Because of problems with absorption and autofluorescence, deep and absorbing tissues like lung, spleen or liver cannot be investigated non-invasively using 2D-FRI. Imaging these tissues requires the use of fluorescence molecular tomography (FMT) [16]. FMT provides 3D volumetric imaging, true quantification independent of depth, tissue optical properties and heterogeneity, and augmentation of the contrast by reducing the autofluorescence. Detecting deep events

Table 1
Characteristics of the different imaging devices.

Technique	Resolution	Depth	Time	Quantitative	Clinical use
CT	20 μm	No limit	Minutes	Yes	Yes
MRI	10 μm	No limit	Minutes to hours	Yes	Yes
PET	1–2 mm	No limit	Minutes to hours	Yes	Yes
SPECT	1 mm	No limit	Minutes to hours	Yes	Yes
FRI	μm to mm	<1 cm	Seconds	No	Yes
FMT	1 mm	<5 cm	Minutes to hours	Yes	Soon
BLI	1 mm	<1.5 cm	Minutes	No	No

A

2D-FRI
(Fluorescence Reflectance Imaging)

B

3D imaging
(Fluorescence Molecular Tomography)

C

Image guided surgery
(Fluobeam imaging device)
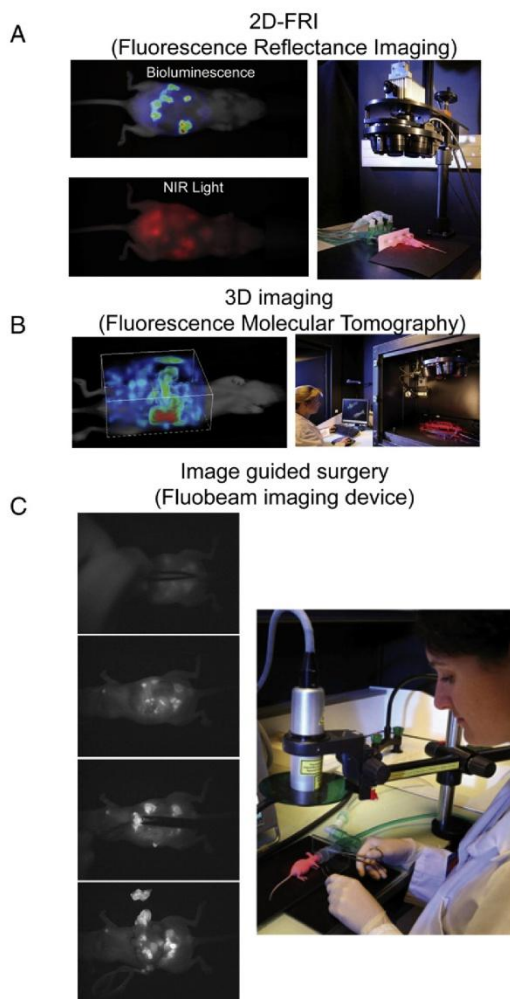
Fig. 1. Optical imaging of peritoneal carcinomatosis. (A) Tumor cells stably transfected with a luciferase reporter gene are injected into the peritoneal cavity of the mouse (top left image). The presence of small nodules is detected 12 days later using bioluminescence. The same nodules are also detected using 2D near-infrared fluorescence (bottom left image) due to the intravenous injection of 10 nmol Angiostamp (multimeric RGD compound described in [34–39,63–65]) the day before imaging using the 2D-FRI imaging system presented on the right. (B) Angiostamp-labeled nodules of the same animal can also be visualized in 3D using the tomographic system. (C) Optic-guided surgery can then be performed under near-infrared excitation using the Fluobeam device even when the surgical white light is illuminating the field of operation, allowing the surgeon to detect easily and remove all the labeled tumors as presented in the 4 consecutive images on the left.

requires transillumination to avoid autofluorescence [17]. Transillumination can be done using a simple optical bench adapted to continuous wave acquisitions [18–20]. The mouse is scanned with an NIR laser light, and the transmitted and emitted fluorescence are recorded allowing construction of a 3-D fluorescence map. Deeper imaging can be obtained using time-resolved imaging. Deeper imaging necessitates the use of expensive femtosecond pulsed lasers

and must be used in the time-resolved FDOT mode. Briefly, this process calculates and analyzes the time that each photon travels, whereas the photons are "simply" captured by the CCD as they arrive in continuous acquisition. This method will soon be transferred to the clinic for imaging deep events [21]. Recent work suggests that a fluorescent signal can be obtained in samples 2 to 5-cm thick, which could be sufficient, for example, for prostate imaging.

3. Fluorescent optical probes

As mentioned above, optical imaging of small animals requires the use of imaging devices and of fluorescent probes adapted to functional imaging. Several types of probes can be classified into three different categories, as summarized by R Weilssleider [22]. The simplest probes are usually large molecules that remain in circulation in the blood and can provide information about physiological processes, such as changes in blood volume, perfusion and angiogenesis. The second probe category targets a specific molecule, including receptors for somatostatin, epidermal growth factor (EGF), integrins, folate, or antigen-targeted antibodies, and can be used to visualize pathological tissues and/or monitor the expression level of a target. The third group of probes is composed of "smart probes" that undergo a change in optical properties when in contact with their targets (Fig. 2). These activatable probes are well adapted for detecting thioreductases, proteases, such as matrix metalloproteinases (MMPs), cathepsins, caspases, or other enzymes and physicochemical parameters. In this chapter, we will focus on "targeted" and "activatable" probes; finally, we will describe the use of nanoparticles as optical imaging tools.

3.1. Receptor-targeted probes

Early diagnostics and image-guided tumor surgery are two key objectives of optical imaging. Kobayashi and colleagues developed several activatable probes and multicolor and multimodality imaging systems to enhance surgical outcomes. They demonstrated the feasibility of simultaneous visualization of two fluorophores using either a transfected cell line and an anti-HER2 antibody coupled with rhodamine G, or two antibodies labeled with two different fluorophores [23–25]. The next stage of development for this technique will concern the fluorophores themselves, as only one compound, indocyanin green (ICG), is currently approved for medical use.

Probes containing the Arg-Gly-Asp motif (RGD) have been intensively developed to follow expression of integrin $\alpha_v\beta_3$ [26], a protein that is expressed by the neo-endothelial cells that form tumor blood vessels and is also frequently overexpressed on tumor cells themselves, such as in lung cancers [27,28], melanomas [29,30], brain tumors [31] or breast cancers [32]. Because of the extraordinary potential of RGD derivatives as tumor targeting ligands, several teams have developed probes with improved receptor specificity and affinity. The first example, c(-RGDf[NMe]V), known as cilengitide, was developed through extensive work by Kessler et al. and has entered phase II trials for patients with glioblastoma. More recently, this group designed new molecules that could be even more specific and are capable of recognizing the $\alpha_v\beta_3$ or $\alpha_5\beta_1$ integrins [33]. RGD utility has also been greatly improved with the construction of scaffolds or polymers that allow multimeric presentation of the RGD triad. For example, our group developed a scaffold containing four copies of c(-RGDfK-) and compared its specificity *in vitro* and *in vivo* as well as its accumulation in tumors in $\alpha_v\beta_3$-positive tumor-bearing mice. The tetrameric RGD-probe showed a better affinity toward $\alpha_v\beta_3$, improved active internalization into the target cells and an augmented SNR *in vivo* compared to the monomeric molecule [34–39]. Because of their specific targeting properties, RGD probes can be used to monitor the efficacy of an anti-integrin or anti-angiogenic
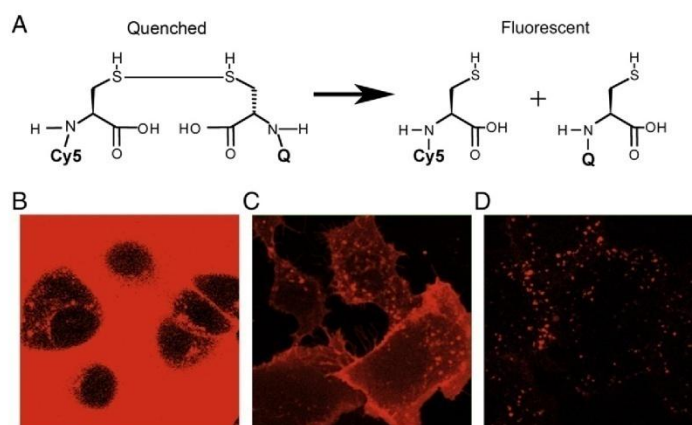
Fig. 2. Use of a quenched probe. (A) Schematic representation of the quenching system, containing a disulfide bridge to separate the quencher from the fluorescent cyanine 5 (Cy5) molecule. When the distance between the quencher and the Cy5 increases, the molecule becomes visible. (B) When the RAFT-RGD-Cy5 [35,37,39] probe is present in the culture medium without the quenching system, the cells are barely visible under the confocal microscope due to the surrounding fluorescence. (C) After removing the excess of RAFT-RGD-Cy5 from the medium, the cells are visible because the probes are attached to and internalized within the cell. (D) However, when a quenched probe is used, only the signal coming from the probe that is reduced during its internalization is visible, and the live cells can be observed even with a large excess of invisible quenched probe in the culture medium.

treatment non-invasively and in real time, as demonstrated in an orthotopic glioblastoma model [40]. In our laboratory, we also showed the utility of visualizing the multimeric RAFT-cRGD molecule using the portable intraoperative Fluobeam® imaging device to improved the quality and outcome of tumor surgery (Fig. 1) [12].

Monitoring the efficacy of recently developed anti-EGF receptor (EGFR) cancer treatments is of the utmost importance. To assess EGF binding/anti-EGF treatments efficacy and cell viability, anti-EGFR coupled with IRDye® 800 CW (LI-COR, NIR800) and annexin-V coupled with IRDye® 700DX (LI-COR, NIR700) were used to follow EGFR expression in colorectal tumors-bearing mice [41]. This study showed that anti-EGF-NIR800 accumulated more actively in tumors expressing high levels of EGFR and, annexin-V-NIR700 staining intensity was elevated in sensitive tumors treated with cetuximab compared to control groups. These imaging approaches may prove useful for serial, non-invasive monitoring of the biological effects of EGFR inhibition in preclinical studies and may also be adapted for clinical use. As described for cRGD, cyanine 5.5-labeled cetuximab has also been used to improve tumor resection and margin prevention in head and neck carcinomas [42].

3.2. Activatable molecules for fluorescent imaging

Optical imaging is the method of choice for functional, real-time, *in vivo* monitoring because it provides an "easy" approach for measuring enzymatic activities, thus enabling researchers to follow, for example, the activation of signal transduction pathways, target gene expression and drug–target interactions [43]. It also allows the *in vivo* analysis of drug efficacy and pharmacodynamic properties.

Several proteases are overexpressed or activated during cancer progression and are thus attractive targets for the so-called "smart" probes, also known as activatable molecules (Fig. 2). Activatable means that a change in signal intensity or wavelength can be detected in response to the interaction of the probe with its target [19,44]. Activatable molecules have several advantages, including minimal non-specific background and improved contrast in the targeted organ [43,45,46]. Proteases were the first enzymes to be targeted in this way, as described for cathepsins (cathepsin B and cathepsin D for cancer progression and cathepsin K for the detection of osteoclasts), caspases-1 and -3 (indicators of apoptosis) and MMPs 2, -7, -9, and

-14 (inflammation and cancer) [22,47–49]. Because the signals produced by these probes are a direct function of their biological activity, smart probes can be used to measure the activity of a drug on its target [50–54].

One of the first NIR activatable probes, described by Weissleder et al., is a polymer of poly-L-lysine and methoxypolyethylene glycol succinate [55]. This probe has a long circulation time, and its fluorescence is quenched in the presence of a high concentration of fluorescent molecules. A detectable NIR signal is (re)-generated when these self-quenched molecules are digested by lysosomal proteases after internalization in the target tumor cells, allowing the detection of sub-millimeter-sized nodules. A similar strategy was used to detect cathepsins B, K, L, and S in cardiac pathologies [56] and image cancer in mouse model of adenoma of the gastrointestinal track [57], or rhabdomyosarcoma [58].

In vivo monitoring of apoptosis is also of great interest. Using a self-quenched caspase-activatable peptide (TcapQ647), Bullok et al. measured *in vivo* apoptosis that was induced by bacterial infection. Activation of the probe was confirmed by *ex-vivo* TUNEL analysis of the tissues and by detection of activated caspase-3 [59]. However, good enzymatic specificity is still an issue facing this technique. For example, it is difficult to design a caspase-specific probe that has low cross-reactivity for cathepsins or legumain. To circumvent this problem, Edgington et al. developed NIR activity-based molecules that form permanent covalent bonds with target proteases, based on acyloxymethyl ketone (AOMK) probes. These probes can be used to monitor early stages of apoptosis using whole-body, non-invasive optical imaging, as demonstrated in human colorectal tumor-bearing mice [60].

The search for new drugs capable of inhibiting receptor tyrosine kinases (RTK) such as EGFR is currently a major issue for cancer treatment. To assess drug efficiency against EGFR, a novel biolumi-nescent-based approach using a bifragment luciferase reconstitution system was recently reported [61]. EGFR and its interacting partner proteins were fused to the NH2- and COOH-terminal fragments of firefly luciferase. This method allowed the identification and quanti-fication of EGFR activation in mice before and after anti-EGFR treatments, such as gefitinib or radiotherapy. This technique is a promising tool that could enhance the preclinical evaluation of novel RTK-targeted therapeutics.

Other activatable compounds have been developed to target viable cancer cells. Urano et al. made a pH-activatable probe coupled to the anti-HER-2 monoclonal antibody trastuzumab. In mice bearing subcutaneous tumors, the probe was highly specific for HER-2-positive tumors with a minimal background signal. Because the energy-consuming proton pumps maintain an acidic pH in lysosomes, only viable HER-2-positive cancer cells showed a high signal [62]. The intracellular redox environments of viable cells can also be used to design probes in which fluorescence will be released after rupture of a disulfide bridge during following internalization. Our group used this method to design RGD-based targeted probes that allow the tracking of a pro-apoptotic toxic peptide released within the target cells [63–66].

3.3. Nanoparticles developed for in vivo applications

During the last few years, a wide variety of nanoparticles were developed as contrast agents for *in vivo* fluorescence imaging applications. Due to their size, these particles offer new structural and optical properties. They have better signal intensity than organic fluorophores, enabling detection of weakly expressed targeted biomarkers. In addition, because of their relatively large surface area, nanoparticles can accommodate multiple probes, enabling multivalent targeting of several biomarkers and thus increasing the affinity of each individual probe. All of these properties make nanoparticles good candidates for biomedical imaging, therapeutic applications or a combination of both (theranostics).

Quantum dots (QDs) are the most extensively described and studied nanoparticles [67–76]. These small nanocrystals are made of semiconductive material and have an emission color that can be precisely tuned by adjusting their composition and size [77]. They can thus be used across a wide spectrum, from the ultraviolet to the NIR and are also photostable and extremely bright [78]. Recently, QDs were also encapsulated in phospholipid micelles to image tumors [79,80]. The encapsulation of QDs enhanced their biodistribution and their passive accumulation in tumors. Various nanoparticles have also been developed for *in vivo* fluorescence imaging applications: these nanoparticles include gold nanoparticles [81,82], hybrid nanoparticles [83–86], C dots [87], lipid nanoparticles [88], liposomes [89], polymeric nanoparticles [90,91], and biodegradable luminescent porous silicon nanoparticles [92].

Several applications have been developed using these new contrast agents. In 2004, Kim et al. demonstrated that QDs translocated to sentinel lymph nodes after intra-dermal injection, likely due to a combination of passive flow in lymphatic vessels and active migration of dendritic cells that had engulfed the nanoparticles [70]. This application could have a great clinical impact, enabling surgeons to rapidly identify and excise draining lymph nodes from tumors for staging cancer using optical guided surgery [93]. The major limitation of QDs is their possible toxicity, which thus far precludes their use in humans. A recent study found no appreciable toxicity of QD, even after their breakdown *in vivo* [94]; however, because of their different chemical formulations and nanoparticle structures, the absence of toxicity of each type of QD, as well as that of each of its byproducts, must be very carefully investigated. Currently, this technique has been used to localize various cancers in animal models, including subcutaneous tumors [95], lungs [71,72], esophagus [73], and head and neck [76].

The key challenge for *in vivo* imaging applications is to develop nanoparticles with an optimized biodistribution. Several studies have shown the particular importance of particle size, PEGylation and surface coating. These properties affect the mean of accumulation in and elimination from tumors through the enhanced permeability and retention (EPR) effect (Fig. 3) [83,95,96]. Indeed, during tumor-induced angiogenesis, blood vessels are abnormal and present large pores, allowing the extravasation of macromolecules up to 400 nm in

Fig. 3. The EPR effect allows passive targeting of a nanoparticle into a subcutaneous tumor. Intravenous injection of a solid PEG2000-coated particle in a *nude* mouse bearing a subcutaneous tumor. Fluorescence image obtained 24 h after injection shows the accumulation of the nanoparticle in the tumor, due to the enhanced permeability and retention (EPR) effect.

size, that can accumulate in the tumor microenvironment [97]. This EPR effect has inspired the development of a variety of nanoparticles to treat and image tumors. Several groups have studied the biodistribution of hydrophobically modified glycol chitosan nanoparticles loaded with cisplatin, camptothecin or paclitaxel by *in vivo* NIR imaging [98–100]. These groups have found a passive but specific accumulation in subcutaneous tumors due to the EPR effect, as well as increased effectiveness of encapsulated drugs compared to free drugs.

To improve the tumor targeting selectivity, specific ligands can be grafted onto the surface of nanoparticles. Again, one of the most commonly described ligands for tumor targeting is the RGD peptide [69,75,101], though several specific other tumor ligands have also been investigated. *In vivo* targeted imaging was demonstrated in a mouse model, using a copolymer functionalized QD conjugated to an antibody that targets a prostate-specific membrane antigen [68]. Gold nanoparticles labeled with anti-EGFR monoclonal antibodies also have a large range of potential applications, from the cellular to the animal levels [81]. Lee et al. [102] recently developed a multifunctional gold nanoprobe for sensitive detection of reactive oxygen species (ROS) and hyaluronidase, which could be used for localized detection of hyaluronic acid degradation due to the diseases such as rheumatoid arthritis and metastatic tumors. Yang et al. described iron oxide nanoparticles that target urokinase plasminogen activator (uPA) receptor and demonstrated their usefulness in detecting breast and pancreatic cancer [91,103].

Finally, nanoprobes can also be powerful tools for evaluating the efficiency of targeted cancer therapies. Medarova et al. [104] described a tumor-specific contrast agent (iron oxide nanoparticles labeled with Cy5.5 dye) targeting underglycolated mucin 1 (uMUC-1), a tumor antigen present on more than 90% of breast cancers and predictive of chemotherapeutic response. After doxorubicin treatment, nanoparticle probes were present at a lower level in the treated tumors compared to untreated tumors, reflecting the reduced expression of uMUC-1. To confirm these findings, similar results were obtained using *in vivo* fluorescence imaging and MRI. The same kind of nanoparticle was also used to deliver small interfering RNA (siRNA) *in vivo* and track their successful delivery by non-invasive imaging [105].

In conclusion, nano-sized contrast agents offer several advantages over conventional agents because they can be passively targeted to the tumors via the EPR effect or actively targeted by specific ligands. Most importantly, nanoparticles offer multifunctionality, such as combining imaging and drug (or siRNA) delivery or, providing dual-modality imaging that combines NIR and either MRI or PET [106]. Thus, these nanoparticles promise great versatility in the detection and treatment of diseases.

4. Conclusion

Optical imaging is an inexpensive, easy-to-use, and non-radiative tool that can provide rapid semi-qualitative (2D), quantitative (3D), and functional information from the cellular to the several centimeter scale. Fluorescence molecular tomography is the preferred method for quantifying protein levels and enzymatic activities. 2D-fluorescent reflectance optical imaging is poised to be the premier approach in molecular imaging, especially for researchers who are not specialists in medical imaging or who do not have access to a nuclear medicine facility or very expensive magnets. However, the future of cancer imaging in mice will rely on the development of a large collection of highly specific tracers or smart contrasting agents. Coupling high-resolution methods like micro-CT or MRI with highly sensitive techniques adapted to functional imaging, such as PET, SPECT or optical imaging, will soon open new frontiers in the study of cancer in small animals and will provide efficient tools for evaluating new treatments. Importantly, a major bottleneck that inhibits the widespread application and generation of these probes concerns the use of NIR fluorophores in human clinical trials by legal agencies. In response to this issue, the FDA recently established the Process Analytical Technologies initiative, which will certainly facilitate the manufacture and use of NIR probes.

References

[1] M. Baker, Whole-animal imaging: the whole picture, Nature 463 (2010) 977–980.
[2] D.W. Holdsworth, M.M. Thornton, Micro-CT in small animal and specimen imaging, Trends Biotechnol. 20 (2002) s34–s39.
[3] P.J. Cassidy, G.K. Radda, Molecular imaging perspectives, J. R. Soc. Interface 2 (2005) 133–144.
[4] A. Louie, Design and characterization of magnetic resonance imaging gene reporters, Methods Mol. Med. 124 (2006) 401–417.
[5] T. Barrett, H. Kobayashi, M. Brechbiel, P.L. Choyke, Macromolecular MRI contrast agents for imaging tumor angiogenesis, Eur. J. Radiol. 60 (2006) 353–366.
[6] M. Beaumont, B. Lemasson, R. Farion, C. Segebarth, C. Remy, E.L. Barbier, Characterization of tumor angiogenesis in rat brain using iron-based vessel size index MRI in combination with gadolinium-based dynamic contrast-enhanced MRI, J. Cereb. Blood Flow Metab. 29 (2009) 1714–1726.
[7] C.A. Cuenod, L. Fournier, D. Balvay, J.M. Guinebretiere, Tumor angiogenesis: pathophysiology and implications for contrast-enhanced MRI and CT assessment, Abdom. Imaging 31 (2006) 188–193.
[8] C.S. Levin, Primer on molecular imaging technology, Eur. J. Nucl. Med. Mol. Imaging 32 (Suppl 2) (2005) S325–S345.
[9] A.F. Chatziioannou, S.R. Cherry, Y. Shao, R.W. Silverman, K. Meadors, T.H. Farquhar, M. Pedarsani, M.E. Phelps, Performance evaluation of microPET: a high-resolution lutetium oxyorthosilicate PET scanner for animal imaging, J. Nucl. Med. 40 (1999) 1164–1175.
[10] D.K. Welsh, S.A. Kay, Bioluminescence imaging in living organisms, Curr. Opin. Biotechnol. 16 (2005) 73–78.
[11] C. Bremer, V. Ntziachristos, R. Weissleder, Optical-based molecular imaging: contrast agents and potential medical applications, Eur. Radiol. 13 (2003) 231–243.
[12] M. Kéramidas, V. Josserand, C.A. Righini, C. Wenk, C. Coll, J.L. Faure, Intraoperative near-infrared image-guided surgery of peritoneal carcinomatosis in a preclinical mouse model, British Journal of Surgery (2010) (Mar. 22, Electronic publication ahead of print), doi:10.1002/bjs.6986.
[13] S.L. Troyan, V. Kianzad, S.L. Gibbs-Strauss, S. Gioux, A. Matsui, R. Oketokoun, L. Ngo, A. Khamene, F. Azar, J.V. Frangioni, The FLARE intraoperative near-infrared fluorescence imaging system: a first-in-human clinical trial in breast cancer sentinel lymph node mapping, Ann. Surg. Oncol. 16 (10) (2009) 2943–2952.
[14] A. Nakayama, F. del Monte, R.J. Hajjar, J.V. Frangioni, Functional near-infrared fluorescence imaging for cardiac surgery and targeted gene therapy, Mol. Imaging 1 (2002) 365–377.
[15] J.V. Frangioni, New technologies for human cancer imaging, J. Clin. Oncol. 26 (2008) 4012–4021.
[16] V. Ntziachristos, C. Bremer, E.E. Graves, J. Ripoll, R. Weissleder, In vivo tomographic imaging of near-infrared fluorescent probes, Mol. Imaging 1 (2002) 82–88.
[17] A. Koenig, L. Herve, V. Josserand, M. Berger, J. Boutet, A. Da Silva, J.M. Dinten, P. Peltie, J.L. Coll, P. Rizo, In vivo mice lung tumor follow-up with fluorescence diffuse optical tomography, J. Biomed. Opt. 13 (2008) 011008.
[18] A. Da Silva, J.M. Dinten, J.L. Coll, P. Rizo, From bench-top small animal diffuse optical tomography towards clinical imaging, Conf. Proc. IEEE Eng. Med. Biol. Soc. (2007) 526–529.
[19] V. Ntziachristos, C.H. Tung, C. Bremer, R. Weissleder, Fluorescence molecular tomography resolves protease activity in vivo, Nat. Med. 8 (2002) 757–760.

[20] X. Montet, V. Ntziachristos, J. Grimm, R. Weissleder, Tomographic fluorescence mapping of tumor targets, Cancer Res. 65 (2005) 6330–6336.
[21] J. Boutet, L. Herve, M. Debourdeau, L. Guyon, P. Peltie, J.M. Dinten, L. Saroul, F. Duboeuf, D. Vray, Bimodal ultrasound and fluorescence approach for prostate cancer diagnosis, J. Biomed. Opt. 14 (2009) 064001.
[22] R. Weissleder, V. Ntziachristos, Shedding light onto live molecular targets, Nat. Med. 9 (2003) 123–128.
[23] M. Longmire, N. Kosaka, M. Ogawa, P.L. Choyke, H. Kobayashi, Multicolor in vivo targeted imaging to guide real-time surgery of HER2-positive micrometastases in a two-tumor coincident model of ovarian cancer, Cancer Sci. 100 (2009) 1099–1104.
[24] M. Ogawa, C.A. Regino, P.L. Choyke, H. Kobayashi, In vivo target-specific activatable near-infrared optical labeling of humanized monoclonal antibodies, Mol. Cancer Ther. 8 (2009) 232–239.
[25] M. Ogawa, N. Kosaka, P.L. Choyke, H. Kobayashi, In vivo molecular imaging of cancer with a quenching near-infrared fluorescent probe using conjugates of monoclonal antibodies and indocyanine green, Cancer Res. 69 (2009) 1268–1272.
[26] X. Chen, P.S. Conti, R.A. Moats, In vivo near-infrared fluorescence imaging of integrin alphavbeta3 in brain tumor xenografts, Cancer Res. 64 (2004) 8009–8014.
[27] X. Chen, E. Sievers, Y. Hou, R. Park, M. Tohme, R. Bart, R. Bremner, J.R. Bading, P.S. Conti, Integrin alpha v beta 3-targeted imaging of lung cancer, Neoplasia 7 (2005) 271–279.
[28] T. Sato, K. Konishi, H. Kimura, K. Maeda, K. Yabushita, M. Tsuji, A. Miwa, Vascular integrin beta 3 and its relation to pulmonary metastasis of colorectal carcinoma, Anticancer Res. 21 (2001) 643–647.
[29] K.R. Gehlsen, G.E. Davis, P. Sriramarao, Integrin expression in human melanoma cells with differing invasive and metastatic properties, Clin. Exp. Metastasis 10 (1992) 111–120.
[30] R.E. Seftor, E.A. Seftor, K.R. Gehlsen, W.G. Stetler-Stevenson, P.D. Brown, E. Ruoslahti, M.J. Hendrix, Role of the alpha v beta 3 integrin in human melanoma cell invasion, Proc. Natl. Acad. Sci. U. S. A. 89 (1992) 1557–1561.
[31] C.L. Gladson, D.A. Cheresh, Glioblastoma expression of vitronectin and the alpha v beta 3 integrin. Adhesion mechanism for transformed glial cells, J. Clin. Invest. 88 (1991) 1924–1932.
[32] M. Rolli, E. Fransvea, J. Pilch, A. Saven, B. Felding-Habermann, Activated integrin alphavbeta3 cooperates with metalloproteinase MMP-9 in regulating migration of metastatic breast cancer cells, Proc. Natl. Acad. Sci. U. S. A. 100 (2003) 9482–9487.
[33] D. Heckmann, A. Meyer, L. Marinelli, G. Zahn, R. Stragies, H. Kessler, Probing integrin selectivity: rational design of highly active and selective ligands for the alpha5beta1 and alphavbeta3 integrin receptor, Angew. Chem. Int. Ed. Engl. 46 (2007) 3571–3574.
[34] D. Boturyn, J.L. Coll, E. Garanger, M.C. Favrot, P. Dumy, Template assembled cyclopeptides as multimeric system for integrin targeting and endocytosis, J. Am. Chem. Soc. 126 (2004) 5730–5739.
[35] L. Sancey, E. Garanger, S. Foillard, G. Schoehn, A. Hurbin, C. Albiges-Rizo, D. Boturyn, C. Souchier, A. Grichine, P. Dumy, J.L. Coll, Clustering and internalization of integrin alphavbeta3 with a tetrameric RGD-synthetic peptide, Mol. Ther. 17 (2009) 837–843.
[36] Z.H. Jin, V. Josserand, S. Foillard, D. Boturyn, P. Dumy, M.C. Favrot, J.L. Coll, In vivo optical imaging of integrin alphaV-beta3 in mice using multivalent or monovalent cRGD targeting vectors, Mol. Cancer 6 (2007) 41.
[37] Z.H. Jin, V. Josserand, J. Razkin, E. Garanger, D. Boturyn, M.C. Favrot, P. Dumy, J.L. Coll, Noninvasive optical imaging of ovarian metastases using Cy5-labeled RAFT-c(-RGDfK-)4, Mol. Imaging 5 (2006) 188–197.
[38] L. Sancey, V. Ardisson, L.M. Riou, M. Ahmadi, D. Marti-Batlle, D. Boturyn, P. Dumy, D. Fagret, C. Ghezzi, J.P. Vuillez, In vivo imaging of tumour angiogenesis in mice with the alpha(v)beta (3) integrin-targeted tracer 99mTc-RAFT-RGD, Eur. J. Nucl. Med. Mol. Imaging 34 (2007) 2037–2047.
[39] L. Sancey, S. Dufort, V. Josserand, M. Keramidas, C.A. Righini, C. Rome, A.C. Faure, S. Foillard, S. Roux, D. Boturyn, O. Tillement, A. Koenig, J. Boutet, P. Rizo, P. Dumy, J.L. Coll, Drug development in oncology assisted by noninvasive optical imaging, Int. J. Pharm. 379 (2009) 309–316.
[40] A.R. Hsu, L.C. Hou, A. Veeravagu, J.M. Greve, H. Vogel, V. Tse, X. Chen, In vivo near-infrared fluorescence imaging of integrin alphavbeta3 in an orthotopic glioblastoma model, Mol. Imaging Biol. 8 (2006) 315–323.
[41] H.C. Manning, N.B. Merchant, A.C. Foutch, J.M. Virostko, S.K. Wyatt, C. Shah, E. T. McKinley, J. Xie, N.J. Mutic, M.K. Washington, B. LaFleur, M.N. Tantawy, T.E. Peterson, M.S. Ansari, R.M. Baldwin, M.L. Rothenberg, D.J. Bornhop, J.C. Gore, R. J. Coffey, Molecular imaging of therapeutic response to epidermal growth factor receptor blockade in colorectal cancer, Clin. Cancer Res. 14 (2008) 7413–7422.
[42] E.L. Rosenthal, B.D. Kulbersh, T. King, T.R. Chaudhuri, K.R. Zinn, Use of fluorescent labeled anti-epidermal growth factor receptor antibody to image head and neck squamous cell carcinoma xenografts, Mol. Cancer Ther. 6 (2007) 1230–1238.
[43] S.B. Raymond, J. Skoch, I.D. Hills, E.E. Nesterov, T.M. Swager, B.J. Bacskai, Smart optical probes for near-infrared fluorescence imaging of Alzheimer's disease pathology, Eur. J. Nucl. Med. Mol. Imaging 35 (Suppl 1) (2008) S93–S98.
[44] M.C. Pierce, D.J. Javier, R. Richards-Kortum, Optical contrast agents and imaging systems for detection and diagnosis of cancer, Int. J. Cancer 123 (2008) 1979–1990.
[45] M. Ogawa, C.A. Regino, J. Seidel, M.V. Green, W. Xi, M. Williams, N. Kosaka, P.L. Choyke, H. Kobayashi, Dual-modality molecular imaging using antibodies

labeled with activatable fluorescence and a radionuclide for specific and quantitative targeted cancer detection, Bioconjug. Chem. 20 (2009) 2177–2184.

[46] D.R. Elias, D.L. Thorek, A.K. Chen, J. Czupryna, A. Tsourkas, In vivo imaging of cancer biomarkers using activatable molecular probes, Cancer Biomark. 4 (2008) 287–305.

[47] C. Bremer, V. Ntziachristos, R. Weissleder, Optical-based molecular imaging: contrast agents and potential medical applications, Eur. Radiol. 13 (2003) 231–243.

[48] J.L. Figueiredo, H. Alencar, R. Weissleder, U. Mahmood, Near infrared thoracoscopy of tumoral protease activity for improved detection of peripheral lung cancer, Int. J. Cancer 118 (2006) 2672–2677.

[49] G. Blum, G. von Degenfeld, M.J. Merchant, H.M. Blau, M. Bogyo, Noninvasive optical imaging of cysteine protease activity using fluorescently quenched activity-based probes, Nat. Chem. Biol. 3 (2007) 668–677.

[50] F. Zhou, D. Xing, S. Wu, W.R. Chen, Intravital imaging of tumor apoptosis with FRET probes during tumor therapy, Mol. Imaging Biol. 12 (1) (2010) 63–70.

[51] A. Sierra, Animal models of breast cancer for the study of pathogenesis and therapeutic insights, Clin. Transl. Oncol. 11 (2009) 721–727.

[52] J. Ripoll, V. Ntziachristos, C. Cannet, A.L. Babin, R. Kneuer, H.U. Gremlich, N. Beckmann, Investigating pharmacology in vivo using magnetic resonance and optical imaging, Drugs R D 9 (2008) 277–306.

[53] D.A. Torigian, S.S. Huang, M. Houseni, A. Alavi, Functional imaging of cancer with emphasis on molecular techniques, CA Cancer J. Clin. 57 (2007) 206–224.

[54] R.L. Scherer, M.N. VanSaun, J.O. McIntyre, L.M. Matrisian, Optical imaging of matrix metalloproteinase-7 activity in vivo using a proteolytic nanobeacon, Mol. Imaging 7 (2008) 118–131.

[55] R. Weissleder, C.H. Tung, U. Mahmood, A. Bogdanov Jr., In vivo imaging of tumors with protease-activated near-infrared fluorescent probes, Nat. Biotechnol. 17 (1999) 375–378.

[56] M. Nahrendorf, D.E. Sosnovik, P. Waterman, F.K. Swirski, A.N. Pande, E. Aikawa, J. L. Figueiredo, M.J. Pittet, R. Weissleder, Dual channel optical tomographic imaging of leukocyte recruitment and protease activity in the healing myocardial infarct, Circ. Res. 100 (2007) 1218–1225.

[57] H. Zhang, D. Morgan, G. Cecil, A. Burkholder, N. Ramocki, B. Scull, P.K. Lund, Biochromoendoscopy: molecular imaging with capsule endoscopy for detection of adenomas of the GI tract, Gastrointest. Endosc. 68 (2008) 520–527.

[58] S. Kossodo, M. Pickarski, S.A. Lin, A. Gleason, R. Gaspar, C. Buono, G. Ho, A. Blusztajn, G. Cuneo, J. Zhang, J. Jensen, R. Hargreaves, P. Coleman, G. Hartman, M. Rajopadhye, L.T. Duong, C. Sur, W. Yared, J. Peterson, B. Bednar, Dual in vivo quantification of integrin-targeted and protease-activated agents in cancer using fluorescence molecular tomography (FMT), Mol. Imaging Biol. (2009) (Dec. 4, Electronic publication ahead of print), doi:10.1007/s11307-009-0279-z.

[59] K.E. Bullok, D. Maxwell, A.H. Kesarwala, S. Gammon, J.L. Prior, M. Snow, S. Stanley, D. Piwnica-Worms, Biochemical and in vivo characterization of a small, membrane-permeant, caspase-activatable far-red fluorescent peptide for imaging apoptosis, Biochemistry 46 (2007) 4055–4065.

[60] L.E. Edgington, A.B. Berger, G. Blum, V.E. Albrow, M.G. Paulick, N. Lineberry, M. Bogyo, Noninvasive optical imaging of apoptosis by caspase-targeted activity-based probes, Nat. Med. 15 (2009) 967–973.

[61] W. Li, F. Li, Q. Huang, B. Frederick, S. Bao, C.Y. Li, Noninvasive imaging and quantification of epidermal growth factor receptor kinase activation in vivo, Cancer Res. 68 (2008) 4990–4997.

[62] Y. Urano, D. Asanuma, Y. Hama, Y. Koyama, T. Barrett, M. Kamiya, T. Nagano, T. Watanabe, A. Hasegawa, P.L. Choyke, H. Kobayashi, Selective molecular imaging of viable cancer cells with pH-activatable fluorescence probes, Nat. Med. 15 (2009) 104–109.

[63] S. Foillard, L. Sancey, J.L. Coll, D. Boturyn, P. Dumy, Targeted delivery of activatable fluorescent pro-apoptotic peptide into live cells, Org. Biomol. Chem. 7 (2009) 221–224.

[64] Z.H. Jin, J. Razkin, V. Josserand, D. Boturyn, A. Grichine, I. Texier, M.C. Favrot, P. Dumy, J.L. Coll, In vivo noninvasive optical imaging of receptor-mediated RGD internalization using self-quenched Cy5-labeled RAFT-c(-RGDfK-)(4), Mol. Imaging 6 (2007) 43–55.

[65] J. Razkin, V. Josserand, D. Boturyn, Z.H. Jin, P. Dumy, M. Favrot, J.L. Coll, I. Texier, Activatable fluorescent probes for tumour-targeting imaging in live mice, ChemMedChem 1 (2006) 1069–1072.

[66] I. Texier-Nogues, J. Razkin, V. Josserand, D. Boturyn, P. Dumy, J.L. Coll, P. Rizo, Activatable probes for non-invasive small animal fluorescence imaging, Nucl. Instrum. Methods Phys. Res. A (2007) 165–168.

[67] B. Dubertret, P. Skourides, D.J. Norris, V. Noireaux, A.H. Brivanlou, A. Libchaber, In vivo imaging of quantum dots encapsulated in phospholipid micelles, Science 298 (2002) 1759–1762.

[68] X. Gao, Y. Cui, R.M. Levenson, L.W. Chung, S. Nie, In vivo cancer targeting and imaging with semiconductor quantum dots, Nat. Biotechnol. 22 (2004) 969–976.

[69] W. Cai, D.W. Shin, K. Chen, O. Gheysens, Q. Cao, S.X. Wang, S.S. Gambhir, X. Chen, Peptide-labeled near-infrared quantum dots for imaging tumor vasculature in living subjects, Nano Lett. 6 (2006) 669–676.

[70] S. Kim, Y.T. Lim, E.G. Soltesz, A.M. De Grand, J. Lee, A. Nakayama, J.A. Parker, T. Mihaljevic, R.G. Laurence, D.M. Dor, L.H. Cohn, M.G. Bawendi, J.V. Frangioni, Near-infrared fluorescent type II quantum dots for sentinel lymph node mapping, Nat. Biotechnol. 22 (2004) 93–97.

[71] E.G. Soltesz, S. Kim, R.G. Laurence, A.M. DeGrand, C.P. Parungo, D.M. Dor, L.H. Cohn, M.G. Bawendi, J.V. Frangioni, T. Mihaljevic, Intraoperative sentinel lymph node mapping of the lung using near-infrared fluorescent quantum dots, Ann. Thorac. Surg. 79 (2005) 269–277 discussion 269–277.

[72] C.P. Parungo, Y.L. Colson, S.W. Kim, S. Kim, L.H. Cohn, M.G. Bawendi, J.V. Frangioni, Sentinel lymph node mapping of the pleural space, Chest 127 (2005) 1799–1804.

[73] C.P. Parungo, S. Ohnishi, S.W. Kim, S. Kim, R.G. Laurence, E.G. Soltesz, F.Y. Chen, Y. L. Colson, L.H. Cohn, M.G. Bawendi, J.V. Frangioni, Intraoperative identification of esophageal sentinel lymph nodes with near-infrared fluorescence imaging, J. Thorac. Cardiovasc. Surg. 129 (2005) 844–850.

[74] B. Ballou, L.A. Ernst, S. Andreko, T. Harper, J.A. Fitzpatrick, A.S. Waggoner, M.P. Bruchez, Sentinel lymph node imaging using quantum dots in mouse tumor models, Bioconjug. Chem. 18 (2007) 389–396.

[75] W. Cai, X. Chen, Preparation of peptide-conjugated quantum dots for tumor vasculature-targeted imaging, Nat. Protoc. 3 (2008) 89–96.

[76] H. Kobayashi, M. Ogawa, N. Kosaka, P.L. Choyke, Y. Urano, Multicolor imaging of lymphatic function with two nanomaterials: quantum dot-labeled cancer cells and dendrimer-based optical agents, Nanomed 4 (2009) 411–419.

[77] L.A. Bentolila, Y. Ebensteinn, S. Weiss, Quantum dots for in vivo small-animal imaging, J. Nucl. Med. 50 (2009) 493–496.

[78] B. Mahler, P. Spinicelli, S. Buil, X. Quelin, J.P. Hermier, B. Dubertret, Towards non-blinking colloidal quantum dots, Nat. Mater. 7 (2008) 659–664.

[79] O. Carion, B. Mahler, T. Pons, B. Dubertret, Synthesis, encapsulation, purification and coupling of single quantum dots in phospholipid micelles for their use in cellular and in vivo imaging, Nat. Protoc. 2 (2007) 2383–2390.

[80] A. Papagiannaros, T. Levchenko, W. Hartner, D. Mongayt, V. Torchilin, Quantum dots encapsulated in phospholipid micelles for imaging and quantification of tumors in the near-infrared region, Nanomedicine 5 (2009) 216–224.

[81] J. Aaron, N. Nitin, K. Travis, S. Kumar, T. Collier, S.Y. Park, M. Jose-Yacaman, L. Coghlan, M. Follen, R. Richards-Kortum, K. Sokolov, Plasmon resonance coupling of metal nanoparticles for molecular imaging of carcinogenesis in vivo, J. Biomed. Opt. 12 (2007) 034007.

[82] P. Puvanakrishnan, J. Park, P. Diagaradjane, J.A. Schwartz, C.L. Coleman, K.L. Gill-Sharp, K.L. Sang, J.D. Payne, S. Krishnan, J.W. Tunnell, Near-infrared narrow-band imaging of gold/silica nanoshells in tumors, J. Biomed. Opt. 14 (2009) 024044.

[83] A.C. Faure, S. Dufort, V. Josserand, P. Perriat, J.L. Coll, S. Roux, O. Tillement, Control of the in vivo biodistribution of hybrid nanoparticles with different poly (ethylene glycol) coatings, Small 5 (2009) 2565–2575.

[84] C. Chen, J. Peng, H.S. Xia, G.F. Yang, Q.S. Wu, L.D. Chen, L.B. Zeng, Z.L. Zhang, D.W. Pang, Y. Li, Quantum dots-based immunofluorescence technology for the quantitative determination of HER2 expression in breast cancer, Biomaterials 30 (2009) 2912–2918.

[85] C. Yang, N. Ding, Y. Xu, X. Qu, J. Zhang, C. Zhao, L. Hong, Y. Lu, G. Xiang, Folate receptor-targeted quantum dot liposomes as fluorescence probes, J. Drug Target. 17 (2009) 502–511.

[86] C.H. Yang, S.H. Yang, C.S. Hsu, Solution-processable phosphorescent to organic light-emitting diodes based on chromophoric amphiphile/silica nanocomposite, Nanotechnology 20 (2009) 315601.

[87] A.A. Burns, J. Vider, H. Ow, E. Herz, O. Penate-Medina, M. Baumgart, S.M. Larson, U. Wiesner, M. Bradbury, Fluorescent silica nanoparticles with efficient urinary excretion for nanomedicine, Nano Lett. 9 (2009) 442–448.

[88] I. Texier, M. Goutayer, A. Da Silva, L. Guyon, N. Djaker, V. Josserand, E. Neumann, J. Bibette, F. Vinet, Cyanine-loaded lipid nanoparticles for improved in vivo fluorescence imaging, J. Biomed. Opt. 14 (2009) 054005.

[89] K.C. Weng, C.O. Noble, B. Papahadjopoulos-Sternberg, F.F. Chen, D.C. Drummond, D. B. Kirpotin, D. Wang, Y.K. Hom, B. Hann, J.W. Park, Targeted tumor cell internalization and imaging of multifunctional quantum dot-conjugated immunoliposomes in vitro and in vivo, Nano Lett. 8 (2008) 2851–2857.

[90] A. Almutairi, R. Rossin, M. Shokeen, A. Hagooly, A. Ananth, B. Capoccia, S. Guillaudeu, D. Abendschein, C.J. Anderson, M.J. Welch, J.M. Frechet, Biodegradable dendritic positron-emitting nanoprobes for the noninvasive imaging of angiogenesis, Proc. Natl. Acad. Sci. U. S. A. 106 (2009) 685–690.

[91] L. Yang, H. Mao, Z. Cao, Y.A. Wang, X. Peng, X. Wang, H.K. Sajja, L. Wang, H. Duan, C. Ni, C.A. Staley, W.C. Wood, X. Gao, S. Nie, Molecular imaging of pancreatic cancer in an animal model using targeted multifunctional nanoparticles, Gastroenterology 136 (2009) 1514–1525 e1512.

[92] J.H. Park, L. Gu, G. von Maltzahn, E. Ruoslahti, S.N. Bhatia, M.J. Sailor, Biodegradable luminescent porous silicon nanoparticles for in vivo applications, Nat. Mater. 8 (2009) 331–336.

[93] E. Pic, T. Pons, L. Bezdetnaya, A. Leroux, F. Guillemin, B. Dubertret, F. Marchal, Fluorescence imaging and whole-body biodistribution of near-infrared-emitting quantum dots after subcutaneous injection for regional lymph node mapping in mice, Mol. Imaging Biol. (2009) (Nov. 21, Electronic publication ahead of print), doi:10.1007/s11307-009-0288-y.

[94] T.S. Hauck, R.E. Anderson, H.C. Fischer, S. Newbigging, W. Chan, In vivo quantum-dot toxicity assessment, Small 6 (2010) 138–144.

[95] B. Ballou, B.C. Lagerholm, L.A. Ernst, M.P. Bruchez, A.S. Waggoner, Noninvasive imaging of quantum dots in mice, Bioconjug. Chem. 15 (2004) 79–86.

[96] M.L. Schipper, G. Iyer, A.L. Koh, Z. Cheng, Y. Ebenstein, A. Aharoni, S. Keren, L.A. Bentolila, J. Li, J. Rao, X. Chen, U. Banin, A.M. Wu, R. Sinclair, S. Weiss, S.S. Gambhir, Particle size, surface coating, and PEGylation influence the biodistribution of quantum dots in living mice, Small 5 (2009) 126–134.

[97] H. Maeda, J. Wu, T. Sawa, Y. Matsumura, K. Hori, Tumor vascular permeability and the EPR effect in macromolecular therapeutics: a review, J. Control. Release 65 (2000) 271–284.

[98] J.H. Kim, Y.S. Kim, K. Park, S. Lee, H.Y. Nam, K.H. Min, H.G. Jo, J.H. Park, K. Choi, S.Y. Jeong, R.W. Park, I.S. Kim, K. Kim, I.C. Kwon, Antitumor efficacy of cisplatin-loaded glycol chitosan nanoparticles in tumor-bearing mice, J. Control. Release 127 (2008) 41–49.

[99] K.H. Min, K. Park, Y.S. Kim, S.M. Bae, S. Lee, H.G. Jo, R.W. Park, I.S. Kim, S.Y. Jeong, K. Kim, I.C. Kwon, Hydrophobically modified glycol chitosan nanoparticles-encapsulated camptothecin enhance the drug stability and tumor targeting in cancer therapy, J. Control. Release 127 (2008) 208–218.

[100] G. Saravanakumar, K.H. Min, D.S. Min, A.Y. Kim, C.M. Lee, Y.W. Cho, S.C. Lee, K. Kim, S.Y. Jeong, K. Park, J.H. Park, I.C. Kwon, Hydrotropic oligomer-conjugated glycol chitosan as a carrier of paclitaxel: synthesis, characterization, and in vivo biodistribution, J. Control. Release 140 (2009) 210–217.

[101] K. Chen, J. Xie, H. Xu, D. Behera, M.H. Michalski, S. Biswal, A. Wang, X. Chen, Triblock copolymer coated iron oxide nanoparticle conjugate for tumor integrin targeting, Biomaterials 30 (2009) 6912–6919.

[102] H. Lee, K. Lee, I.K. Kim, T.G. Park, Synthesis, characterization, and in vivo diagnostic applications of hyaluronic acid immobilized gold nanoprobes, Biomaterials 29 (2008) 4709–4718.

[103] L. Yang, X.H. Peng, Y.A. Wang, X. Wang, Z. Cao, C. Ni, P. Karna, X. Zhang, W.C. Wood, X. Gao, S. Nie, H. Mao, Receptor-targeted nanoparticles for in vivo imaging of breast cancer, Clin. Cancer Res. 15 (2009) 4722–4732.

[104] Z. Medarova, L. Rashkovetsky, P. Pantazopoulos, A. Moore, Multiparametric monitoring of tumor response to chemotherapy by noninvasive imaging, Cancer Res. 69 (2009) 1182–1189.

[105] Z. Medarova, M. Kumar, S.W. Ng, A. Moore, Development and application of a dual-purpose nanoparticle platform for delivery and imaging of siRNA in tumors, Methods Mol. Biol. 555 (2009) 1–13.

[106] F. Duconge, T. Pons, C. Pestourie, L. Herin, B. Theze, K. Gombert, B. Mahler, F. Hinnen, B. Kuhnast, F. Dolle, B. Dubertret, B. Tavitian, Fluorine-18-labeled phospholipid quantum dot micelles for in vivo multimodal imaging from whole body to cellular scales, Bioconjug. Chem. 19 (2008) 1921–1926.

Des molécules fluorescentes au service de la chirurgie

Pascal Dumy, Christiane Wenk, Michael Claron, Jean-Luc Coll,
Odile Allard et Didier Boturyn

Résumé   L'assemblage chimique de fonctions de reconnaissance cellulaire et de détection sur châssis moléculaire permet d'obtenir des systèmes de guidage tumoral sélectifs et modulables qui ouvrent des applications inédites dans le domaine de la détection et de la thérapie. En particulier, la validation chez l'animal de systèmes fluorescents de guidage vers les tumeurs avec le développement de caméras de détection proche infrarouge a pu être valorisée pour le développement de technologies telles que l'aide au geste chirurgical par imagerie de fluorescence en temps réel.

Mots-clés   **Peptides RGD, ligations chimiosélectives, sondes fluorescentes, chirurgie guidée par imagerie proche IR, innovation.**

Abstract   **Fluorescent molecules for surgery**
The chemical assembly of functions such cellular recognition and detection on molecular frame allows to obtain selective and flexible tumour guidance systems which open new applications in the field of the detection and therapy. In particular, the validation in animal of fluorescent guidance systems for tumour with the development of near infrared cameras is able to be valued for the development of technologies such as the assistance to the surgical gesture by real-time fluorescence imaging.

Keywords   **RGD peptides, chemoselective ligations, fluorescent probes, NIR image-guided surgery, innovation.**

À la mémoire de Gérard Déleris.

L'avenir des traitements contre le cancer ainsi que des stratégies de prévention et de dépistage va être fortement influencé par l'utilisation de biomarqueurs tumoraux qui permettent de concevoir de nouvelles molécules pour des thérapies ciblées (« targeted therapy »). Ces produits, véritables missiles à tête chercheuse, visent précisément les caractéristiques spécifiques de la cellule cancéreuse ou de son environnement, sans léser les tissus sains, et avec des effets secondaires moins sévères et différents de ceux de la chimiothérapie. Avec les avancées de la génomique, de la protéomique et de la pharmacogénomique, il est possible d'identifier des biomarqueurs propres à chaque patient qui permettraient d'établir diagnostic et traitement associé ainsi qu'un suivi du traitement adaptés à la bonne personne plutôt qu'à un groupe d'individus. Des exemples de thérapie ciblée, basés notamment sur les biotechnologies et l'utilisation d'anticorps spécifiques dirigés contre un ligand ou un récepteur impliqué dans le cancer, ouvrent la voie vers une médecine personnalisable et appropriée à l'individu. Dans cet article, nous décrirons une des contributions de notre groupe de recherche dans le domaine de la chimie des biomolécules avec une approche de recherche « translationnelle » pour le ciblage tumoral et sa valorisation pour l'aide au geste chirurgical, notamment pour la résection[(1)] tumorale. La chirurgie du cancer reste aujourd'hui l'un des traitements les plus efficaces contre la maladie : cinq millions de personnes souffrant d'un cancer sont opérées chaque année dans le monde, dont près de 370 000 en France, soit une toutes les 90 secondes.

Parmi les cibles potentielles se trouvant dans l'environnement tumoral, un récepteur transmembranaire, l'intégrine $\alpha_V\beta_3$ [1], a particulièrement attiré l'attention de certains groupes de recherche. Cette protéine est surexprimée à la surface des cellules endothéliales constituant les néovaisseaux tumoraux lors de l'angiogenèse tumorale et sur certaines lignées cancéreuses métastasiques. Plusieurs équipes ont démontré que des peptides contenant la séquence « RGD » (-Arg-Gly-Asp-) permettent de cibler cette intégrine avec une très bonne efficacité et spécificité [2]. Un cyclopentapeptide, le cilengitide (Merck KGaA, Darmstadt) découvert dans le laboratoire du professeur Horst Kessler [3], est utilisé comme inhibiteur de l'angiogenèse dans plusieurs phases cliniques. Actuellement, de nombreux travaux sont menés pour développer de nouveaux composés ciblant la néoangiogenèse tumorale pour des applications thérapeutiques et diagnostiques ou leur combinaison théragnostique[(2)].

Le ciblage tumoral *via* un cluster de ligands « RGD »

De nombreux systèmes biologiques contrôlent les interactions ligand-récepteur par des effets de multivalence. C'est devenu un nouveau centre d'intérêt dans la recherche et la conception de nouveaux composés plus affins pour leur cible. L'utilisation d'interactions multivalentes peut aussi engendrer des propriétés biologiques fondamentalement différentes de celles trouvées lors des interactions moléculaires monovalentes [4]. Dans ce contexte, nous avons été parmi les pionniers à concevoir des ligands multivalents ciblant l'intégrine $\alpha_V\beta_3$ grâce à l'utilisation d'un châssis moléculaire de présentation multivalente nommé RAFT et au développement de méthodes chimiques

permettant leur fonctionnalisation par des biomolécules polyfonctionnelles.

Un châssis moléculaire nommé RAFT

Les molécules RAFT (« regioselectively addressable functionalized template »), développées au début des années 1990 dans le domaine du « protein de novo design » [5] sont des décapeptides cycliques comportant deux coudes β de type II dus à l'enchaînement proline-glycine qui leur confère une mobilité conformationnelle réduite, conduisant à une orientation des chaînes latérales des six autres acides aminés du cycle de part et d'autre du plan moyen du cycle (*figure 1*). L'originalité de ce système est qu'il permet de définir deux faces fonctionnalisables grâce aux chaînes latérales qui peuvent être ainsi adressables chimiquement de manière indépendante. Nous utilisons ces RAFT pour combiner une fonction de reconnaissance (ligands) et des fonctions conférant à la molécule des propriétés de détection ou de destruction (molécules fluorescentes, cytotoxiques...). Le ciblage tumoral *via* l'intégrine $\alpha_V\beta_3$ a été mis en évidence en utilisant un édifice RAFT portant un cluster de quatre ligands cyclopentapeptidiques, RAFTc(-RGDfK)$_4$ (dénoté « RGD »), et un fluorophore permettant l'étude de ses propriétés [6] (*figure 2*).

Les RAFT ont aussi été utilisés pour d'autres applications comme la conception de mimes de surface (4-helix-bundle) [7-8], de canaux ioniques [9], la stabilisation de G-quadruplexe[(3)] [10] ou la formation de mimes de fibres amyloïdes [11].
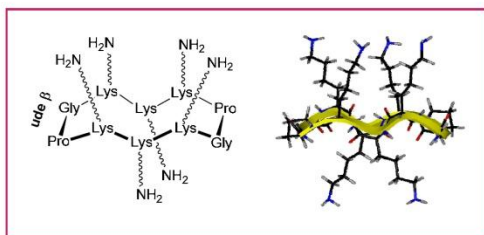
Construction chimique de type « LEGO® moléculaires »

Pour réaliser des structures complexes, de haut poids moléculaire et qui combinent différentes biomolécules, le chimiste a besoin de réactions performantes et compatibles avec les différentes classes de biomolécules (peptides, sucres, acides nucléiques). Parmi les nombreuses réactions couramment utilisées par les chimistes pour modifier une biomolécule, un intérêt particulier a été accordé aux réactions chimiosélectives [12]. Depuis une quinzaine d'années, nous avons été parmi les premiers à utiliser le lien éther d'oxime qui est obtenu par l'addition d'une fonction oxyamine sur un dérivé carbonylé du type cétone ou aldéhyde. L'utilisation de ce lien chimique permet ainsi l'ingénierie contrôlée de biomolécules à la manière d'un LEGO® en codant l'assemblage par réaction chimiosélective entre oxyamine et carbonyle en milieu aqueux, sans besoin de réactif de couplage et de groupes protecteurs.

Nous avons montré que la formation successive de liens éther d'oxime permet de synthétiser des macromolécules peptidiques composées d'un cluster de cyclopeptide « RGD » conjugué à des acides nucléiques [13] ou à des résidus carbohydrates [14], combinant ainsi leurs propriétés intrinsèques de reconnaissance, de toxicité intracellulaire ou de solubilisation. Pour accéder à ce type de composés, la stratégie de synthèse consiste à (i) former un premier lien éther d'oxime pour greffer sur le cyclodécapeptide une première molécule d'intérêt (ligand « RGD »), (ii) oxyder une sérine (aldéhyde masqué), puis (iii) coupler une deuxième molécule d'intérêt (acides nucléiques, sucres) (*figure 3a*).

Figure 1 - Structure d'un cyclodécapeptide RAFT contenant six lysines [5].

Figure 2 - Structure d'un composé fluorescent ciblant l'intégrine $\alpha_V\beta_3$ [6].
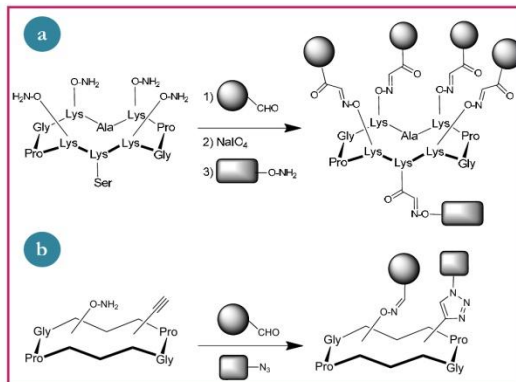
Figure 3 - Stratégie de synthèse (a) itérative oxime-oxime [13] ; (b) « one-pot » oxime-cycloaddition [15].

Bien qu'efficace et conduisant à des structures hautement complexes, cette stratégie nécessite plusieurs étapes successives qui limitent les rendements. Ceci nous a conduits à développer un procédé de synthèse convergeant « one-pot » : nous avons choisi d'associer à la réaction de formation d'éther d'oxime, la cycloaddition 1,3-dipolaire catalysée par le cuivre(I) entre un azoture et un alcyne (CuAAC) (*figure 3b*) [15].

Au cours de cette étude, nous avons validé la compatibilité des deux réactions chimiosélectives. En d'autres termes, il est ainsi possible de coder le site de réaction sur chacun des partenaires pour que, lorsqu'ils

sont mélangés, ils puissent réagir chimiosélectivement et régiosélectivement et être assemblés sur le RAFT. À ce jour, ces différentes méthodes de synthèse permettent d'obtenir des composés combinant un cluster de ligand « RGD » et diverses fonctions utilisées pour améliorer sa biodistribution, pour des applications diagnostiques et/ou thérapeutiques.

Évaluation des composés comportant un cluster de ligand « RGD »

Les propriétés résultant du cluster de quatre ligands « RGD » porté par le RAFT ont été étudiées au travers d'expériences réalisées *in vitro* à partir de lignées cellulaires surexprimant la protéine transmembranaire $\alpha_V\beta_3$. Nous avons estimé l'efficacité des composés « RGD » dans un essai de compétition contre la vitronectine, ligand naturel de l'intégrine $\alpha_V\beta_3$, en utilisant des cellules HEK293 (« human embryonic kidney »). La capacité de chaque composé à inhiber l'adhésion des cellules à une plaque recouverte de vitronectine a été exprimée comme sa valeur d'IC50[4]. Les résultats sont illustrés dans la *figure 4*. Le composé « contrôle négatif » RAFTc(-RADfK)$_4$ n'inhibe pas l'adhésion cellulaire, tandis que le composé RAFTc(-RGDfK)$_4$ empêche fortement l'attachement cellulaire avec un IC50 de 3 µM contre 30 µM pour le composé monovalent c(-RGDfK) [16-17]. Ces résultats ont été corroborés par des expériences de compétition contre un anticorps monoclonal (mAb) spécifique de $\alpha_V\beta_3$ [18]. Finalement, des expériences de spectroscopie de corrélation de fluorescence (FCS) ont permis de mesurer des constantes cinétiques pour l'intégrine : le composé tétramérique RAFTc(-RGDfK)$_4$ est douze fois plus affin ($K_D = 3,8$ nM) que le composé monovalent [19].
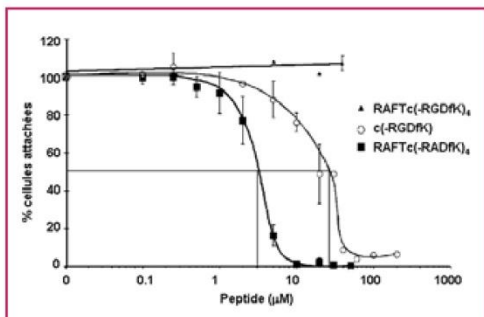
Figure 4 - Inhibition de l'adhésion de cellules HEK à la vitronectine par des ligands « RGD ».

Études du « trafficking » cellulaire[5] à partir de composés fluorescents

Avant d'utiliser les composés « RGD » pour des applications anticancéreuses, nous avons étudié leur comportement vis-à-vis de cellules cibles par microscopie de fluorescence qui permet la visualisation d'éléments ou molécules à l'aide de fluorochromes. L'acquisition d'images est réalisée sur des échantillons très fins (monocouches cellulaires) afin d'observer la transmission de la lumière visible et d'obtenir un bon contraste. Les résultats montrent que le composé contenant un cluster de « RGD » muni d'une

fluorescéine (*figure 2*) est internalisé à 37 °C avec une meilleure efficacité que le peptide contrôle monovalent c(-RGDfK)-Fluo (*figure 5*) [6]. Récemment, il a été mis en évidence que les composés RAFTc(-RGDfK) sont internalisés avec l'intégrine $\alpha_V\beta_3$ par une endocytose[6] médiée par la clathrine[7] [19].
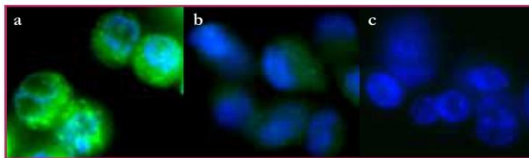
Figure 5 - Imagerie de fluorescence de cellules CHO-3a à 15 min traitées par 10 µM (a) RAFTc(-RGDfK)$_4$-Fluo à 37 °C, (b) RAFTc(-RGDfK)$_4$-Fluo à 4 °C, et (c) c(-RGDfK)-Fluo à 37 °C.

Ces résultats montrent que le RAFTc(-RGDfK)$_4$ est non seulement sélectif de la cible, mais permet de plus de pénétrer dans la cellule par endocytose à la manière des protéines, ce qui ouvre des perspectives pour ces composés pour la vectorisation ciblée de drogues et/ou de fluorophores pour des applications anticancéreuses. La multivalence permet ici non seulement d'augmenter l'affinité pour la cible, mais également d'internaliser la molécule de manière active.

Le ciblage et l'imagerie *in vivo* : applications anticancéreuses

Imagerie non invasive chez le petit animal

Les expériences réalisées chez le petit animal ont permis de valider la sélectivité de nos composés *in vivo*. En exploitant la capacité de la lumière proche infrarouge à pénétrer les tissus, l'imagerie et la spectroscopie optiques peuvent être utilisées pour détecter des tissus cancéreux de façon non invasive. Dans ce contexte, une série de molécules fluorescentes a été préparée en incorporant sur le RAFT un chromophore proche IR du type cyanine 5 ($\lambda_{abs} = 649$ nm ; $\lambda_{em} = 670$ nm). L'injection des différents composés par voie intraveineuse a été effectuée sur des souris nude[8] porteuses de modèles de tumeurs sous-cutanées surexprimant ou pas l'intégrine $\alpha_V\beta_3$, respectivement HEK293(β3) et HEK293(β1) [20]. Comme on peut le voir sur la *figure 6*, quatre heures après l'injection, un signal beaucoup plus intense est observé pour la souris recevant le composé « RAFTc(-RGDfK)$_4$-Cy5 » par rapport à la souris recevant le ligand monovalent c(-RGDfK)-Cy5. La tumeur HEK293(β1), ne captant pas le ligand fluorescent « RGD », démontre la sélectivité de notre système pour l'intégrine $\alpha_V\beta_3$. Nous avons cependant noté une faible rétention du composé « RAFTc(-RGDfK)$_4$-Cy5 » au niveau des reins. Les études de ces différents systèmes de fluorescence proche infrarouge ciblants ont également permis le développement de nouveaux systèmes de caméras

Figure 6 - Imagerie non invasive à 4 h de souris nude traitées par 10 nmol de composés.
Les animaux portent des tumeurs sous-cutanées HEK293(β3) (a-b) ou HEK293(β1) (c).

portables pour le petit animal et de méthodes de tomographie de fluorescence pour le suivi en fluorescence et reconstruction 3D de métastases sur des modèles animal.

L'utilisation d'une fonction de détection (sonde fluorescente) permet ainsi d'étudier la biodistribution, de détecter *in vivo* l'intégrine $\alpha_V\beta_3$, et donc de localiser la tumeur. Nous avons préparé une nouvelle génération de composés comportant une fonction activable dès que la cible est atteinte. Le but ici est d'obtenir un signal de fluorescence uniquement après ciblage de $\alpha_V\beta_3$. Pour cela, un quencheur de fluorescence[9] (QSY : λ_{abs} = 660 nm) est rattaché à notre vecteur portant le fluorophore cyanine 5 par un pont disulfure (*figure 7*). Ce composé, appelé « Smart Probe », est fluorescent (activation) dès lors que le pont disulfure est réduit dans la cellule, soit dans le cytosol par la thioredoxine, soit dans les endosomes[10] tardifs par la réductase GILT (« gamma-interferon-inducible lysosomal thiol reductase ») [21]. L'observation de fluorescence *in vivo* démontre ainsi non seulement que le vecteur a atteint sa cible, mais qu'il y a pénétré, puis a relargué le quencheur dans la cellule [22].
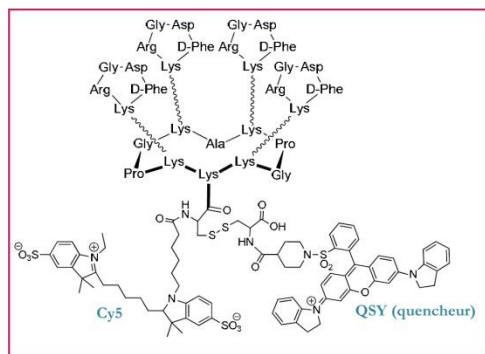
Figure 7 - Structure d'un composé « Smart Probe ».

Système fluorescent activable pour étudier la vectorisation de médicaments

Nous avons exploité le système fluorescent activable « Smart Probe » précédent pour étudier le suivi intracellulaire d'un peptide « KLA » qui induit l'apoptose[11] dans des cellules vivantes. Ce type de composé nous a permis de visualiser la libération du peptide « KLA » dans l'endosome et sa migration vers les mitochondries (*figure 8*) [23]. Ce résultat corrobore ceux de la littérature où il est montré que le peptide « KLA » peut adopter une structure en hélice amphiphile capable de s'ancrer dans la membrane mitochondriale et déclencher la mort cellulaire par apoptose. L'étude *in vivo* chez la souris a permis également de valider le relargage du peptide « KLA » après ciblage et internalisation, ce qui fait de cette « Smart Probe » un outil intéressant pour le développement de thérapies ciblées.

Application clinique d'un traceur fluorescent : l'aide à la chirurgie

L'aide à la chirurgie en clinique vétérinaire

Fort de l'expérience acquise en imagerie du petit animal par fluorescence, associant chimistes, biologistes,
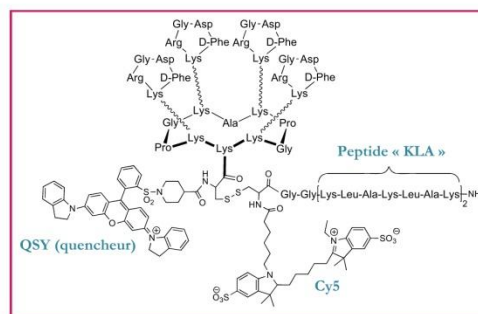
Figure 8 - Structure du conjugué drogue-« Smart Probe ».

physiciens et médecins depuis une dizaine d'années à Grenoble, nous nous sommes dirigés vers le guidage du geste chirurgical par fluorescence. Cette approche est en cours de validation sur des animaux domestiques (chats, chiens) atteints de fibrosarcome nécessitant une intervention chirurgicale (*figure 9*). À ce jour, tous les essais vétérinaires ont été réalisés avec succès.

Figure 9 - Chirurgie en salle opératoire en clinique vétérinaire.

Fluoptics : valorisation et commercialisation du système AngioStamp™-Fluobeam™

La molécule développée par le Département de Chimie moléculaire (Grenoble) associé à l'Institut Albert Bonniot (Grenoble) a été licenciée à la société grenobloise Fluoptics qui l'industrialise sous le nom commercial d'AngioStamp™. Fluoptics est une start-up issue du CEA dont l'objectif est de développer et de commercialiser des traceurs et des
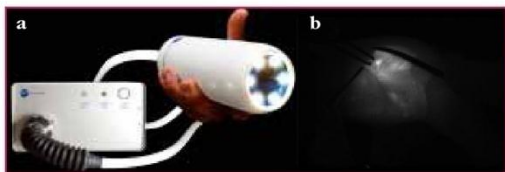
Figure 10 - (a) Présentation de la sonde : l'instrument est constitué d'un boîtier de contrôle et d'une tête (caméra et éclairage) reliés au boîtier par un câble pouvant être déconnecté. Le système est relié à un ordinateur par une connexion USB2. (b) Exemple de nodule de petite taille détecté par le couple AngioStamp™-Fluobeam™.

instruments pour guider le geste chirurgical par imagerie de fluorescence dans le proche infrarouge.

L'un des domaines les plus prometteurs étudiés aujourd'hui par la société est l'aide à la chirurgie du cancer. Fluoptics a développé dans ce champ une technologie destinée à aider le chirurgien lors de l'ablation de tumeurs cancéreuses. Cette technologie repose sur la combinaison d'un système d'imagerie optique en temps réel et de traceurs fluorescents qui ciblent spécifiquement les cellules tumorales (*figure 10*). Une fois injecté, le traceur émet un signal infrarouge permettant « d'illuminer » les cellules cancéreuses qui deviennent alors visibles à l'écran. Ce procédé autorise une chirurgie de précision pour enlever des métastases non visibles à l'œil nu (jusqu'à 300 microns), permettant de préserver les tissus sains.

L'imagerie de fluorescence est une innovation technologique majeure qui devrait bouleverser d'ici quelques années la façon dont on traite de nombreuses maladies, et en premier lieu les cancers. En particulier avec les traceurs ciblants tels qu'AngioStamp™, elle va permettre au chirurgien de voir au plus près et en temps réel l'exacte localisation des tumeurs et des cellules cancéreuses, et ce avec une précision inégalée à ce jour.

AngioStamp™ est le premier traceur de Fluoptics ; il est en cours de développement avec pour objectif la réalisation d'un essai clinique chez l'homme en 2013. Il est utilisé actuellement en routine dans de nombreuses applications précliniques [24-25] et dans la validation vétérinaire listée précédemment.

Le traceur est injecté la veille de l'opération, ce qui laisse le temps à AngioStamp™ de se fixer sur les zones cibles et permet à l'organisme d'évacuer le traceur qui n'est pas fixé de manière spécifique.

Le principe de l'instrument Fluobeam™ développé par Fluoptics est le suivant : un système d'éclairage filtré pour supprimer les longueurs d'onde du proche infrarouge correspondant aux longueurs d'ondes d'émission du traceur éclaire la zone d'intérêt. Un laser ayant une longueur d'onde proche du maximum d'absorption des fluorophores utilisés est diffusé sur cette même zone et permet d'exciter la fluorescence du traceur. La zone d'intérêt est vue par une caméra CCD filtrée qui ne détecte que les longueurs d'ondes correspondant à cette fluorescence. Fluobeam™ permet

d'acquérir les images de fluorescence en temps réel et de les projeter sur un écran face au chirurgien (*figure 11*).

La technologie mise au point par la start-up grenobloise est susceptible de nombreuses autres applications, par exemple en chirurgie cardiovasculaire et chirurgie reconstructrice, ou encore pour détecter les ganglions sentinelles dans le cadre de l'ablation d'une tumeur cancéreuse.

Conclusion

Le développement d'approches chimiques permettant l'assemblage multimérique de biomolécules ciblant l'intégrine $\alpha_V\beta_3$ sur un châssis cyclopeptidique et les combinaisons avec des fonctions de détection ont permis d'obtenir des systèmes ciblant l'angiogenèse tumorale *in vivo*. La flexibilité et la grande efficacité de cette approche ont permis d'effectuer une recherche translationnelle impliquant chimistes, biologistes et technologues, qui a abouti à la valorisation d'un agent fluorescent de ciblage tumoral et de caméras proche infrarouge pour les mesures en temps réel. Ces développements sont exploités par la start-up Fluoptics pour développer et commercialiser des traceurs et des instruments pour guider le geste chirurgical et améliorer les berges de résection, sans modifier les conditions opératoires actuelles.

Figure 11 - Sonde en situation lors de chirurgie sur gros animaux.

Notes et références

(1) *Résection* : retrait chirurgical d'une partie d'organe ou d'un tissu pathologique comme une tumeur.
(2) *Théragnostique* : association d'un test diagnostic à une thérapie.
(3) *G-quadruplexes* : structures secondaires à quatre brins que peuvent adopter les acides nucléiques (ADN et ARN) riches en guanines.
(4) *IC50* : concentration d'un composé inhibant 50 % de l'effet observé.
(5) *« Trafficking » cellulaire* : signalisation cellulaire.
(6) *Endocytose* : mécanisme de transport de molécules voire de particules (virales, bactériennes, etc.) vers l'intérieur de la cellule.
(7) *Clathrine* : protéine structurelle constituant l'enveloppe (ou manteau) de certaines vésicules.
(8) *Souris nude* : souche mutante de souris dépourvues de poils et de thymus, affectées d'un déficit immunitaire important.
(9) *Quencheur de fluorescence* : composé chimique ou atome conduisant à la perte de fluorescence du fluorophore concerné.
(10) *Endosomes* : sous-compartiments de la cellule, ou organites (organelles), sur lesquels les vésicules d'endocytose s'accrochent et fusionnent pour relarguer leur contenu.
(11) *Apoptose* (ou mort cellulaire programmée) : processus par lequel des cellules déclenchent leur autodestruction en réponse à un signal.

[1] Jin H., Varner J., Integrins: roles in cancer development and as treatment targets, *Br. J. Surg.*, **2004**, *90*, p. 561.
[2] Temming K., Schiffelers R.M., Molema G., Kok R.J., RGD-based strategies for selective delivery of therapeutics and imaging agents to the tumour vasculature, *Drug Resist. Update*, **2005**, *8*, p. 381.
[3] Goodman S.L., Hoelzemann G., Sulyok G.A.G., Kessler H, *N*-methylated cyclic RGD peptides as highly active and selective $\alpha_V\beta_3$ integrin antagonists, *J. Med. Chem.*, **1999**, *42*, p. 3033.
[4] Mammen M., Choi S.-K., Whitesides G.M., Polyvalent interactions in biological systems: implications for design and use of multivalent ligands and inhibitors, *Angew. Chem. Int. Ed.*, **1998**, *37*, p. 2754.
[5] Dumy P., Eggleston I.M., Cervigni S., Sila U., Sun X., Mutter M., A convenient synthesis of cyclic peptides as regioselectively addressable functionalized templates (RAFT), *Tetrahedron Lett.*, **1995**, *36*, p. 1255.
[6] Boturyn D., Coll J.-L., Garanger E., Favrot M.C., Dumy P., Template assembled cyclopeptides as multimeric system for integrin targeting and endocytosis, *J. Am. Chem. Soc.*, **2004**, *126*, p. 5730.

[7] Mutter M., Tuchscherer G.G., Miller C., Altmann K.H., Carey R.I., Wyss D.F., Labhardt A.M., Rivier J.E., Template-assembled synthetic proteins with 4-helix-bundle topology: Total chemical synthesis and conformational studies, *J. Am. Chem. Soc.*, **1992**, *114*, p. 1463.

[8] Rau H.K., Haehnel W., Design, synthesis, and properties of a novel cytochrome b model, *J. Am. Chem. Soc.*, **1998**, *120*, p. 468.

[9] Futaki S., Peptide ion channels: Design and creation of function, *Biopolymers*, **1998**, *47*, p. 75.

[10] Murat P., Cressend D., Spinelli N., Van der Heyden A., Labbe P., Dumy P., Defrancq E., A novel conformationally constrained parallel g quadruplex, *ChemBioChem*, **2008**, *9*, p. 2588.

[11] Dolphin G.T., Dumy P., Garcia J., Control of amyloid beta-peptide protoribril formation by a designed template assembly, *Angew. Chem. Int. Ed.*, **2006**, *45*, p. 2699.

[12] Hackenberger C.P.R., Schwarzer D., Chemoselective ligation and modification strategies for peptides and proteins, *Angew. Chem. Int. Ed.*, **2008**, *47*, p. 10030.

[13] Garanger E., Boturyn D., Renaudet O., Defrancq E., Dumy P., Chemoselectively addressable template: A valuable tool for the engineering of molecular conjugates, *J. Org. Chem.*, **2006**, *71*, p. 2402.

[14] Renaudet O., Boturyn D., Dumy P., Biomolecular assembly by iterative oxime ligations, *Bioorg. Med. Chem. Lett.*, **2009**, *19*, p. 3880.

[15] Galibert M., Dumy P., Boturyn D., One-pot approach to well-defined biomolecular assemblies *via* orthogonal chemoselective ligations, *Angew. Chem. Int. Ed.*, **2009**, *48*, p. 2576.

[16] Garanger E., Boturyn D., Jin Z., Dumy P., Favrot M.-C., Coll J.-L., New multifunctional molecular conjugate vector for targeting, imaging, and therapy of tumors, *Mol. Ther.*, **2005**, *12*, p. 1168.

[17] Galibert M., Sancey L., Renaudet O., Coll J.-L., Dumy P., Boturyn D., Application of click-click chemistry to the synthesis of new multivalent RGD conjugates, *Org. Biomol. Chem.*, **2010**, *8*, p. 5133.

[18] Garanger E., Boturyn D., Coll J.-L., Favrot M.-C., Dumy P., Multivalent RGD synthetic peptides as potent $\alpha_V\beta_3$ integrin ligands, *Org. Biomol. Chem.*, **2006**, *4*, p. 1958.

[19] Sancey L., Garanger E., Foillard S., Schoehn G., Hurbin A., Albiges-Rizo C., Boturyn D., Souchier C., Grichine A., Dumy P., Coll J.-L., Clustering and internalization of integrin $\alpha_V\beta_3$ with a tetrameric RGD-synthetic peptide, *Mol. Ther.*, **2009**, *17*, p. 837.

[20] Jin Z., Josserand V., Foillard S., Boturyn D., Dumy P., Favrot M.-C., Coll J.-L., *In vivo* optical imaging of integrin $\alpha_V\beta_3$ in mice using multivalent or monovalent cRGD targeting vectors, *Mol. Cancer*, **2007**, *6*, p. 41.

[21] Arunachalam B., Phan U.T., Geuze H.J., Cresswell P., Enzymatic reduction of disulfide bonds in lysosomes: Characterization of a gamma-interferon-inducible lysosomal thiol reductase (GILT), *Proc. Natl. Acad. Sci. USA*, **2000**, *97*, p. 745.

[22] Razkin J., Josserand V., Boturyn D., Jin Z., Dumy P., Favrot M.-C., Coll J.-L., Texier I., Activatable fluorescent probes for tumour-targeting imaging in live mice, *ChemMedChem*, **2006**, *1*, p. 1069.

[23] Foillard S., Sancey L., Coll J.-L., Boturyn D., Dumy P, Targeted Delivery of activatable fluorescent pro-apoptotic peptide into live cells, *Org. Biomol. Chem.*, **2009**, *7*, p. 221.

[24] Keramidas M., Josserand V., Righini C.A., Wenk C., Faure C., Coll J.L., Intraoperative near-infrared image-guided surgery for peritoneal carcinomatosis in a preclinical experimental model, *Br. J. Surg.*, **2010**, *97*, p. 737.

[25] Mery E., Jouve E., Guillermet S., Bourgognon M., Castells M., Golzio M., Rizo P., Delord J.P., Querleu D., Couderc B., Intraoperative fluorescence imaging of peritoneal dissemination of ovarian carcinomas: A preclinical study, *Gynecol. Oncol.*, **2011**, *122*, p. 155.

P. Dumy **C. Wenk** **M. Claron**

J.-L. Coll **O. Allard** **D. Boturyn**

Pascal Dumy (*auteur correspondant*)
est professeur à l'Université Grenoble 1 et responsable de l'équipe « Ingénierie et interaction biomoléculaires »[1]. Il est directeur de l'École Nationale Supérieure de Chimie de Montpellier depuis février 2012.

Christiane Wenk
est doctorante en cotutelle de thèse avec les équipes « Ingénierie et interaction biomoléculaires »[1] et « Thérapie ciblée, diagnostic précoce et imagerie du cancer »[2].

Michaël Claron
est doctorant dans l'équipe « Ingénierie et interaction biomoléculaires »[1].

Jean-Luc Coll
est directeur de recherche de l'Inserm et dirige l'équipe « Thérapie ciblée, diagnostic précoce et imagerie du cancer » à l'Institut Albert Bonniot[2]. Il est responsable de la plate-forme « Imagerie optique du petit animal *in vivo* ».

Odile Allard
est la PDG de Fluoptics[3], entreprise qui développe des solutions pour le guidage du geste chirurgical par fluorescence.

Didier Boturyn
est directeur de recherche au CNRS et dirige le groupe de recherche « Ingénierie de peptide et reconnaissance moléculaire »[1].

[1] Équipe « Ingénierie et interaction biomoléculaires », UMR 5250 CNRS/UJF, BP 53, F-38041 Grenoble Cedex 9.
Courriel : pascal.dumy@ujf-grenoble.fr

[2] Équipe « Thérapie ciblée, diagnostic précoce et imagerie du cancer », Institut Albert Bonniot, CRI Inserm/UJF U823, Rond point de la Chantourne, F-38706 La Tronche Cedex.

[3] Fluoptics, Minatec-BHT, Bât. 52, 7 parvis Louis Néel, BP 50, F-38040 Grenoble Cedex 9.
www.fluoptics.com

BIBLIOGRAPHY

BIBLIOGRAPHY

A

Abboud, Bassam, und Jenny Tannoury. „Surgical treatment of papillary thyroid carcinoma". *Le Journal médical libanais. The Lebanese medical journal* 59, Nr. 4 (Dezember 2011): 206–212.

Abernethy, L J, S Avula, G M Hughes, E J Wright, und C L Mallucci. „Intra-operative 3-T MRI for paediatric brain tumours: challenges and perspectives". *Pediatric radiology* 42, Nr. 2 (February 2012): 147–157.

Akers, Walter J, Baogang Xu, Hyeran Lee, Gail P Sudlow, Gregg B Fields, Samuel Achilefu, and W Barry Edwards. "Detection of MMP-2 and MMP-9 Activity in Vivo with a Triple-helical Peptide Optical Probe." *Bioconjugate Chemistry* 23, no. 3 (March 21, 2012): 656–663.

Alencar H, Funovics MA, Figueiredo J, Sawaya H, Weissleder R, Mahmood U. Colonic adenocarcinomas: Near-infrared microcatheter imaging of smart probes for early detection – Study in mice. Radiology. 2007; 244:232–238.

Aoki, T., D. Yasuda, Y. Shimizu, et al. "Image-guided Liver Mapping Using Fluorescence Navigation System with Indocyanine Green for Anatomical Hepatic Resection." *World J Surg*. 32, n.d., sec. 2008.1763-1767.

Arap, W, R Pasqualini, und E Ruoslahti. „Cancer treatment by targeted drug delivery to tumor vasculature in a mouse model". *Science (New York, N.Y.)* 279, Nr. 5349 (Januar 16, 1998): 377–380.

Atkinson, J M, C S Siller, und J H Gill. „Tumour endoproteases: the cutting edge of cancer drug delivery?" *British journal of pharmacology* 153, Nr. 7 (April 2008): 1344–1352.

Auzzas, L, F Zanardi, L Battistini, P Burreddu, P Carta, G Rassu, C Curti, and G Casiraghi. "Targeting Alphavbeta3 Integrin: Design and Applications of Mono- and Multifunctional RGD-based Peptides and Semipeptides." *Current Medicinal Chemistry* 17, no. 13 (2010): 1255–1299.

B

Baba, Alecsandru Ioan A I, und Cornel C Câtoi. *Comparative Oncology*. Bucharest: The Publishing House of the Romanian Academy, 2007.

Barrett, Tristan, Hisataka Kobayashi, Martin Brechbiel, and Peter L Choyke. "Macromolecular MRI Contrast Agents for Imaging Tumor Angiogenesis." *European Journal of Radiology* 60, no. 3 (December 2006): 353–366.

Beaumont, Marine, Benjamin Lemasson, Régine Farion, Christoph Segebarth, Chantal Rémy, and Emmanuel L Barbier. "Characterization of Tumor Angiogenesis in Rat Brain Using Iron-based Vessel Size Index MRI in Combination with Gadolinium-based Dynamic Contrast-enhanced MRI." *Journal of Cerebral Blood Flow and Metabolism: Official Journal of the International Society of Cerebral Blood Flow and Metabolism* 29, no. 10 (October 2009): 1714–1726.

Bergers, G, R Brekken, G McMahon, T H Vu, T Itoh, K Tamaki, K Tanzawa, u. a. „Matrix metalloproteinase-9 triggers the angiogenic switch during carcinogenesis". *Nature cell biology* 2, Nr. 10 (Oktober 2000): 737–744.

Bilimoria, Karl Y., David J. Bentrem, Clifford Y. Ko, Andrew K. Stewart, David P. Winchester, Mark S. Talamonti, und Cord Sturgeon. „Extent of Surgery Affects Survival for Papillary Thyroid Cancer". *Annals of Surgery* 246, Nr. 3 (September 2007): 375–384.

Boettiger, David. „Mechanical control of integrin-mediated adhesion and signaling". *Current opinion in cell biology* (August 1, 2012).

Borgoño, Carla A, und Eleftherios P Diamandis. „The emerging roles of human tissue kallikreins in cancer". *Nature reviews. Cancer* 4, Nr. 11 (November 2004): 876–890.

Boturyn, Didier, und Pascal Dumy. „A convenient access to αVβ3/αVβ5 integrin ligand conjugates: regioselective solid-phase functionalisation of an RGD based peptide". *Tetrahedron Letters* 42, Nr. 15 (April 9, 2001): 2787–2790.

Brand, L and Johnson, M.L., Eds., *Fluorescence Spectroscopy (Methods in Enzymology, Volume 450)*, Academic Press (2008).

Bregazzi V.S., S. M. LaRue, E. McNiel, D. W. Macy, W. S. Dernell, B. E. Powers, and S. J. Withrow. Treatment with a Combination of Doxorubicin, Surgery, and Radiation Versus Surgery and Radiation Alone for Cats with Vaccine-associated Sarcomas: 25 Cases (1995-2000). Journal of the American Veterinary Medical Association 218, no. 4 (2001) 547–550.; Kobayashi T, Hauck ML, Dodge R, et al. Preoperative radiotherapy for vaccine associated sarcoma in 92 cats. *Vet Radiol Ultrasound* 2002;43:473-479.

Bremer, C., Tung, C. H., and Weissleder, R. (2001) In vivo molecular target assessment of matrix metalloproteinase inhibition. Nat. Med. 7, 743–748.

Brennan, M.F. "80 - Total Gastrectomy for Carcinoma." In *Mastery of Surgery*, 1:916–928. 5th ed. Boston, Massachusetts: Fischer, Josef E., 2007.

Bridges, Lance C, und Ron D Bowditch. „ADAM-Integrin Interactions: potential integrin regulated ectodomain shedding activity". *Current pharmaceutical design* 11, Nr. 7 (2005): 837–847.

Bridgewater, Rebecca E, Jim C Norman, und Patrick T Caswell. „Integrin trafficking at a glance". *Journal of cell science* 125, Nr. Pt 16 (August 15, 2012): 3695–3701.

Brooks P.C., S. Silletti, T.L. von Schalscha, M. Friedlander, D.A. Cheresh, Disruption of angiogenesis by PEX, a noncatalytic metalloproteinase fragment with integrin binding activity, Cell 92 (1998) 391–400.

Brooks P.C., S. Strömblad, L.C. Sanders, T.L. von Schalscha, R.T. Aimes, W.G. Stetler Stevenson, et al., Localization of matrix metalloproteinase MMP-2 to the surface of invasive cells by interaction with integrin alpha v beta 3, Cell 85 (1996) 683–693.

Buchs, Nicolas C, Monika E Hagen, François Pugin, Francesco Volonte, Pascal Bucher, Eduardo Schiffer, und Philippe Morel. „Intra-operative fluorescent cholangiography using indocyanin green during robotic single site cholecystectomy". *The international journal of medical robotics + computer assisted surgery: MRCAS* (Mai 31, 2012).

Bunschoten, Anton, Tessa Buckle, Nils L Visser, JoeriKuil, Hushan Yuan, Lee Josephson, Alexander L Vahrmeijer, and Fijs W B van Leeuwen. „Multimodal interventional molecular imaging of tumor margins and distant metastases by targeting αvβ3 integrin". *Chembiochem: a European journal of chemical biology* 13, Nr. 7 (Mai 7, 2012): 1039–1045.

Burgess, K, D Lim, und S A Mousa. „Synthesis and solution conformation of cyclo[RGDRGD]: a cyclic peptide with selectivity for the alpha V beta 3 receptor". *Journal of medicinal chemistry* 39, Nr. 22 (Oktober 25, 1996): 4520–4526.

C

Carey, R I, K H Altmann, und M Mutter. „Protein design: template-assembled synthetic proteins". *Ciba Foundation symposium* 158 (1991): 187–199; discussion 199–203, 204–212.

Carmeliet, P, und R K Jain. „Angiogenesis in cancer and other diseases". *Nature* 407, Nr. 6801 (September 14, 2000): 249–257.

Carmeliet, Peter. „Angiogenesis in health and disease". *Nature medicine* 9, Nr. 6 (Juni 2003): 653–660.

Cassidy, Paul J, and George K Radda. "Molecular Imaging Perspectives." *Journal of the Royal Society, Interface / the Royal Society* 2, no. 3 (June 22, 2005): 133–144.

Chatziioannou, A F, S R Cherry, Y Shao, R W Silverman, K Meadors, T H Farquhar, M Pedarsani, and M E Phelps. "Performance Evaluation of microPET: a High-resolution Lutetium Oxyorthosilicate PET Scanner for Animal Imaging." *Journal of Nuclear Medicine: Official Publication, Society of Nuclear Medicine* 40, no. 7 (July 1999): 1164–1175.

Chau, Ying, Frederick E Tan, und Robert Langer. „Synthesis and characterization of dextran-peptide-methotrexate conjugates for tumor targeting via mediation by matrix metalloproteinase II and matrix metalloproteinase IX". *Bioconjugate chemistry* 15, Nr. 4 (August 2004): 931–941.

Chen, K., J. Xie, and X. Chen. "RGD-human Serum Albumin Conjugates as Efficient Tumor Targeting Probes." *Mol Imaging*. 8, 2009.65-73.

Chen, Kai, und Xiaoyuan Chen. „Integrin targeted delivery of chemotherapeutics". *Theranostics* 1 (2011): 189–200.

Chen, Ying-Ju, Ying-Ying Wei, Hsien-Te Chen, Yi-Chin Fong, Chin-Jung Hsu, Chun-Hao Tsai, Horng-Chaung Hsu, Shing-Hwa Liu, und Chih-Hsin Tang. „Osteopontin increases migration and MMP-9 up-regulation via alphavbeta3 integrin, FAK, ERK, and NF-kappaB-dependent pathway in human chondrosarcoma cells". *Journal of cellular physiology* 221, Nr. 1 (Oktober 2009): 98–108.

Choe, R., S.D. Konecky, A. Corlu et al. "Differentiation of Benign and Malignant Breast Tumors by in Vivo Three-dimensional Parallel-plate Diffuse Optical Tomography." *J Biomed Opt*. 14, 024020

Choi, J., A.A. Burns, R.M. Williams, et al. "Core-shell Silica Nanoparticles as Fluorescent Labels for Nanomedicine." *J Biomed Opt*. 12, 2007.064007.

Choi, Naeun, Sung-Min Kim, Kwan Soo Hong, Gyunggoo Cho, Jee-Hyun Cho, Chulhyun Lee, und Eun Kyoung Ryu. „The use of the fusion protein RGD-HSA-TIMP2 as a tumor targeting imaging probe for SPECT and PET". *Biomaterials* 32, Nr. 29 (Oktober 2011): 7151–7158.

Christensen, Erik I, Henrik Birn, Tina Storm, Kathrin Weyer, und Rikke Nielsen. „Endocytic receptors in the renal proximal tubule". *Physiology (Bethesda, Md.)* 27, Nr. 4 (August 2012): 223–236.

Cirocchi, Roberto, Stefano Trastulli, Carlo Boselli, Alessandro Montedori, Davide Cavaliere, Amilcare Parisi, Giuseppe Noya, und Iosief Abraha. „Radiofrequency ablation in the treatment of liver metastases from colorectal cancer". *Cochrane database of systematic reviews (Online)* 6 (2012): CD006317.

Cortez-Retamozo V, Swirski FK, Waterman P, et al. Real-time assessment of inflammation and treatment response in a mouse model of allergic airway inflammation. J Clin Invest. 2008 Dec;118(12):4058–4066.

Cortnum, Søren, und René Johannes Laursen. „Fluorescence-guided resection of gliomas". *Danish medical journal* 59, Nr. 8 (August 2012): A4460.

Coulouarn, Cédric, Anne Corlu, Denise Glaise, Isabelle Guénon, Snorri S Thorgeirsson, und Bruno Clément. „Hepatocyte-stellate cell cross-talk in the liver engenders a permissive inflammatory microenvironment that drives progression in hepatocellular carcinoma". *Cancer research* 72, Nr. 10 (Mai 15, 2012): 2533–2542.

Crane, Lucia M.A., George Themelis, K. Tim Buddingh, Niels J. Harlaar, Rick G. Pleijhuis, Athanasios Sarantopoulos, Ate G.J. van der Zee, Vasilis Ntziachristos, und Gooitzen M. van Dam. „Multispectral Real-time Fluorescence Imaging for Intraoperative Detection of the Sentinel Lymph Node in Gynecologic Oncology". *Journal of Visualized Experiments : JoVE*, Nr. 44 (Oktober 20, 2010). http://www.ncbi.nlm.nih.gov/pmc/articles/PMC3185642/.

Cronin K., R. L. Page, G. Spodnick, R. Dodge, E. N. Hardie, G. S. Price, D. Ruslander, and D. E. Thrall. Radiation Therapy and Surgery for Fibrosarcoma in 33 Cats. Veterinary Radiology & Ultrasound: The Official Journal of the American College of Veterinary Radiology and the International Veterinary Radiology Association 39, no. 1 (February 1998) 51–56.

Cudic, Mare, und Gregg B Fields. „Extracellular proteases as targets for drug development". *Current protein & peptide science* 10, Nr. 4 (August 2009): 297–307.

Cuenod, C A, L Fournier, D Balvay, and J-M Guinebretière. "Tumor Angiogenesis: Pathophysiology and Implications for Contrast-enhanced MRI and CT Assessment." *Abdominal Imaging* 31, no. 2 (April 2006): 188–193.

Curley, S.A., and J.S. Zager. "Cancer Radiofrequency Ablation and Other Tissue Ablative Techniques - Chapter 13." In *Mastery of Surgery*, 1:181–185. 5th ed. Boston, Massachusetts: Fischer, Josef E., 2007.

D

Dam, Gooitzen M. van, George Themelis, Lucia M. A. Crane, Niels J. Harlaar, Rick G. Pleijhuis, Wendy Kelder, Athanasios Sarantopoulos, et al. "Intraoperative Tumor-specific Fluorescence Imaging in Ovarian Cancer by Folate Receptor-α Targeting: First In-human Results". *Nature Medicine* 17, Nr. 10 (2011): 1315–1319.

Danhier, Fabienne, Aude Le Breton, und Veronique Preat. „RGD -based strategies to target alpha(v) beta(3) integrin in cancer therapy and diagnosis". *Molecular pharmaceutics* (September 11, 2012). http://www.ncbi.nlm.nih.gov/pubmed/22967287.

De Grand, A.M., und JV Frangioni. „An operational near-infrared fluorescence imaging system proyotype for large animal surgery". *Technol Cancer Res Treat*. 2, 2003.

Desgrosellier, Jay S, und David A Cheresh. „Integrins in cancer: biological implications and therapeutic opportunities". *Nature reviews. Cancer* 10, Nr. 1 (Januar 2010): 9–22.

Dong Seok, Ok-Hee Jeon, Hee Doo Lee, Kyung Ho Yoo, und Doo-Sik Kim. „Integrin alphavbeta3-mediated transcriptional regulation of TIMP-1 in a human ovarian cancer cell line". *Biochemical and biophysical research communications* 377, Nr. 2 (Dezember 12, 2008): 479–483.

Drag, Marcin, und Guy S Salvesen. „Emerging principles in protease-based drug discovery". *Nature reviews. Drug discovery* 9, Nr. 9 (September 2010): 690–701.

Dufort, S, L Sancey, C Wenk, V Josserand, und J L Coll. „Optical small animal imaging in the drug discovery process". *Biochimica et biophysica acta* 1798, Nr. 12 (Dezember 2010): 2266–2273.

Dufort, Sandrine, Lucie Sancey, Amandine Hurbin, StéphanieFoillard, Didier Boturyn, Pascal Dumy, und Jean-Luc Coll. „Targeted delivery of a proapoptotic peptide to tumors in vivo". *Journal of Drug Targeting* 19, Nr. 7 (August 2011): 582–588.

Dufour, Antoine, Stanley Zucker, Nicole S Sampson, Cem Kuscu, und Jian Cao. „Role of matrix metalloproteinase-9 dimers in cell migration: design of inhibitory peptides". *The Journal of biological chemistry* 285, Nr. 46 (November 12, 2010): 35944–35956.

Dufour, Antoine, Stanley Zucker, Nicole S Sampson, Cem Kuscu, und Jian Cao. „Role of matrix metalloproteinase-9 dimers in cell migration: design of inhibitory peptides". *The Journal of biological chemistry* 285, Nr. 46 (November 12, 2010): 35944–35956.

Dumy, P.; Eggleston, I. M.; Cervigni, S.; Sila, U.; Sun, X.; Mutter, M. A convenient synthesis of cyclic peptides as regioselectively addressable functionalized templates (RAFT). *Tetrahedron Lett* **1995**, *36*, 1255- 1258.

Dumy, P.; Favrot, M.-C.; Boturyn, D.; Coll, J.-L. Synthesis and characterization of novel systems for guidance and vectorization of compounds having a therapeutic activity. Brevet PCT/FR2003/002773 WO 2004/02894, 19 Septembre 2003.

E

Eliceiri, B P, und D A Cheresh. „Adhesion events in angiogenesis". *Current opinion in cell biology* 13, Nr. 5 (Oktober 2001): 563–568.

F

Faust, A. *et al.* Synthesis and evaluation of a novel fluorescent photoprobe for imaging matrix metalloproteinases. *Bioconjug. Chem.* **19**, 1001–1008 (2008).

Faust, Andreas, Bianca Waschkau, Jens Waldeck, Carsten Höltke, Hans-Jörg Breyholz, Stefan Wagner, Klaus Kopka, u. a. „Synthesis and evaluation of a novel hydroxamate based fluorescent photoprobe for imaging of matrix metalloproteinases". *Bioconjugate chemistry* 20, Nr. 5 (Mai 20, 2009): 904–912.

Faust, Andreas, Bianca Waschkau, Jens Waldeck, Carsten Höltke, Hans-Jörg Breyholz, Stefan Wagner, Klaus Kopka, Walter Heindel, Michael Schäfers, und Christoph Bremer. „Synthesis and evaluation of a novel fluorescent photoprobe for imaging matrix metalloproteinases". *Bioconjugate chemistry* 19, Nr. 5 (Mai 2008): 1001–1008.

Fedarko, Neal S, Alka Jain, Abdullah Karadag, und Larry W Fisher. „Three small integrin binding ligand N-linked glycoproteins (SIBLINGs) bind and activate specific matrix metalloproteinases". *FASEB journal: official publication of the Federation of American Societies for Experimental Biology* 18, Nr. 6 (April 2004): 734–736.

Fleming, et al. "Surgery in the Management of Gastric Lymphoma." *Cancer Vol 49*, March 1982.*;* Caroll, W.R. "25 - Surgery for Cancer of the Oral Cavity." In *Mastery of Surgery*, 1:305–318. 5th ed. Boston, Massachusetts: Fischer, Josef E., 2007.

Foillard, Stéphanie, Martin Ohsten Rasmussen, Jesus Razkin, Didier Boturyn, und Pascal Dumy. "1-Ethoxyethylidene, a   new group for the stepwise SPPS of aminooxyacetic acid containing peptides". *The Journal of organic chemistry*   73, Nr. 3 (February 1, 2008): 983–991.

Foillard, Stéphanie, Zhao-hui Jin, Elisabeth Garanger, Didier Boturyn, Marie-Christine Favrot, Jean-Luc Coll, und Pascal Dumy. „Synthesis and biological characterisation of targeted pro-apoptotic peptide". *Chembiochem: a European journal of chemical biology* 9, Nr. 14 (September 22, 2008): 2326–2332.

Folkman, J, und D Hanahan. „Switch to the angiogenic phenotype during tumorigenesis". *Princess Takamatsu symposia* 22 (1991): 339–347.

G

Galibert, Mathieu, Lucie Sancey, Olivier Renaudet, Jean-Luc Coll, Pascal Dumy, und Didier Boturyn. „Application of click-click chemistry to the synthesis of new multivalent RGD conjugates". *Organic &biomolecular chemistry* 8, Nr. 22 (November 21, 2010): 5133–5138.

Garanger, E., D. Boturyn, P. Dumy, MC Favrot, und JL Coll. „New multifunctional molecular conjugate vector for targeting, imaging, and therapy of tumors". *Molecular Therapy*. 12(6), Dezember 2005.

Garanger, Elisabeth, Didier Boturyn, und Pascal Dumy. „Tumor targeting with RGD peptide ligands-design of new molecular conjugates for imaging and therapy of cancers". *Anti-cancer agents in medicinal chemistry* 7, Nr. 5 (September 2007): 552–558.

Gautschi, O.P., K. van Leyen, D. Cadosch, G. Hildebrandt, und J.-Y. Fournier. „Fluorescence Guided Resection ofMalignant Brain Tumors – Breakthrough in the Surgery of Brain Tumors". *Praxis* 98 (o. J.): 643–647.

Gerritsen, Karin G., Hilde P. Peters, Tri Q. Nguyen, Maarten P. Koeners, Jack F. Wetzels, Jaap A. Joles, Erik I. Christensen, u. a. „Renal Proximal Tubular Dysfunction Is a Major Determinant of Urinary Connective Tissue Growth Factor Excretion". *American Journal of Physiology - Renal Physiology* 298, Nr. 6 (Januar 6, 2010): F1457–F1464.

Gimbrone, M A, Jr, S B Leapman, R S Cotran, und J Folkman. „Tumor dormancy in vivo by prevention of neovascularization". *The Journal of experimental medicine* 136, Nr. 2 (August 1, 1972): 261–276.

Gioux, Sylvain, Jean-Guillaume Coutard, Michel Berger, Henri Grateau, Véronique Josserand, Michelle Keramidas, Christian Righini, Jean-Luc Coll, und Jean-Marc Dinten. „FluoSTIC: miniaturized fluorescence image-guided surgery system". *Journal of biomedical optics* 17, Nr. 10 (Oktober 1, 2012): 106014.

Gleysteen, J.P., R.D. Duncan, J.S. Magnuson, J.B. Skipper, K.R. Zinn, and E. Rosenthal. "Fluorescently Labeled Cetuximab to Evaluate Head and Neck Cancer Response to Treatment." *Cancer Biol Ther.* 6, 2007.1181-1185.

Gotthardt M, van Eerd-Vismale J, Oyen WJ et al. Indication for differentmechanisms of kidney uptake of radiolabeled peptides. J Nucl Med 2007; 48: 596–601.

Gravier, Julien, Raphaël Schneider, Céline Frochot, Thierry Bastogne, Frédéric Schmitt, Jacques Didelon, François Guillemin, und Muriel Barberi-Heyob. „Improvement of meta-tetra(hydroxyphenyl)chlorin-like photosensitizer selectivity with folate-based targeted delivery. synthesis and in vivo delivery studies". *Journal of medicinal chemistry* 51, Nr. 13 (Juli 10, 2008): 3867–3877.

Gurrath, M, G Müller, H Kessler, M Aumailley, und R Timpl. „Conformation/activity studies of rationally designed potent anti-adhesive RGD peptides". *European journal of biochemistry / FEBS* 210, Nr. 3 (Dezember 15, 1992): 911–921.

H

Hamden, Khaled, Serge Carrea U, Fatma Ayadi Marki, Hatem Masmoudi, and Abdelfattah El Feki. „Positive effects of Green Tea on hepatic dysfunction, lipid peroxidation and antioxidant defence depletion induced by cadmium". *Biological Research* 41, Nr. 3 (Januar 2008): 331–339.

Hanahan, D., und R. A. Weinberg. „The hallmarks of cancer". *Cell* 100 (2000): 57–70.

Hanahan, Douglas, und Robert A. Weinberg. „Hallmarks of Cancer: The Next Generation". *Cell* 144, Nr. 5 (March 4, 2011): 646–674.

Hershey A. E., K. U. Sorenmo, M. J. Hendrick, F. S. Shofer, and D. M. Vail. Prognosis for Presumed Feline Vaccine-associated Sarcoma After Excision: 61 Cases (1986-1996). Journal of the American Veterinary Medical Association 216, no. 1 (January 1, 2000) 58–61.

Hershey E., K. U. Sorenmo, M. J. Hendrick, F. S. Shofer, and D. M. Vail. Prognosis for Presumed Feline Vaccine-associated Sarcoma After Excision: 61 Cases (1986-1996). Journal of the American Veterinary Medical Association 216, no. 1 (January 1, 2000) 58–61.

Heuveling D.A., G.W. Visser, M. de Groot, J.F. de Boer, M. Baclayon, W.H. Roos, G.J. Wuite, C.R. Leemans, R. de Bree, G.A. van Dongen, Nanocolloidal albumin-IRDye 800CW: a near-infrared fluorescent tracer with optimal retention in the sentinel lymph node. European journal of nuclear medicine and molecular imaging 39 (2012) 1161-1168.

Heuveling, DA, GW Visser, M. de Groot, JF de Boer, M. Baclayon, WH Roos, GJ Wuite, CR Leemans, R. de Bree, und GA van Dongen. „Nanocolloidal albumin-IRDye 800CW: a near-infrared fluorescent tracer with optimal retention in the sentinel lymph node". *Eur J Nucl Med Mol Imaging*. 39(7), Juli 2012.

Hirsjärvi, Samuli, Sandrine Dufort, JulienGravier, Isabelle Texier, Qiao Yan, JérômeBibette, Lucie Sancey, u. a. „Influence of size, surface coating and fine chemical composition on the in vitro reactivity and in vivo biodistribution of lipid nanocapsules versus lipid nanoemulsions in cancer models". *Nanomedicine: nanotechnology, biology, and medicine* (September 6, 2012).

Hofmann, Uta B., Roland Houben, Eva-B. Bröcker, and Jürgen C. Becker. "Role of Matrix Metalloproteinases in Melanoma Cell Invasion." *Biochimie* 87, no. 3–4 (March 2005): 307–314.

Humphries, Jonathan D., Adam Byron, und Martin J. Humphries. „Integrin Ligands at a Glance". *Journal of Cell Science* 119, Nr. 19 (Januar 10, 2006): 3901–3903.

Humphries, M.J. (2000) "Integrin structure" Biochem Soc Trans 28(4): 311-39

Hynes R.O., Integrins: versatility, modulation, and signaling in cell adhesion, Cell 69 (1992) 11–25.

I

Intes X (2005) Time-domain optical mammography SoftScan: initial results. Acad Radiol 12: 934-947.

Ishizawa, T., N. Fukushima, J. Shibahara, et al. "Real-time Identification of Liver Cancers by Using Indocyanine Green Fluorescent Imaging." *Cancer*. 115, 2009.2491-2504.

J

Jarnagin, W R, A M Bach, C B Winston, L E Hann, N Heffernan, T Loumeau, R P DeMatteo, Y Fong, und L H Blumgart. „What is the yield of intraoperative ultrasonography during partial hepatectomy for malignant disease?" *Journal of the American College of Surgeons* 192, Nr. 5 (Mai 2001): 577–583.

Jiang, T., E.S. Olson, Q.T. Nguyen, M. Roy, P.A. Jennings, and R.Y. Tsien. "Tumor Imaging by Means of Proteolytic Activation of Cell-penetrating Peptides." *Proc Natl Acad Sci USA*. 101, 2004.17867-17872.

Jiao, Yang, Xue Feng, Yinpeng Zhan, Ruifei Wang, Sheng Zheng, Wenguang Liu, und Xianlu Zeng. „Matrix metalloproteinase-2 promotes αvβ3 integrin-mediated adhesion and migration of human melanoma cells by cleaving fibronectin". *PloS one* 7, Nr. 7 (2012): e41591.

Jin, Young-June, Iha Park, In-Kee Hong, Hee-Jung Byun, Jeongsuk Choi, Young-Myeong Kim, und Hansoo Lee. „Fibronectin and vitronectin induce AP-1-mediated matrix metalloproteinase-9 expression through integrin α(5)β(1)/α(v)β(3)-dependent Akt, ERK and JNK signaling pathways in human umbilical vein endothelial cells". *Cellular signalling* 23, Nr. 1 (Januar 2011): 125–134.

Jin, Z.H., J. Razkin, V. Josserand, et al. "In Vivo Noninvasive Optical Imaging of Receptor-mediated RGD Internalization Using Self-quenched Cy5-labeled RAFT-c(-RGDfK-)(4)." *Mol Imaging*. 6, 2007.43-55.

Jin, ZH, V. Josserand, S. Foillard, D. Boturyn, P. Dumy, MC Favrot, und JL Coll. „In vivo optical imaging of integrin alphaV-beta3 in mice using multivalent or monovalent cRGD targeting vectors". *Molecular Cancer*. 6, Juni 2007.

Jin, Zhao-Hui, Veronique Josserand, Jesus Razkin, Elisabeth Garanger, Didier Boturyn, Marie-Christine Favrot, Pascal Dumy, und Jean-Luc Coll. „Noninvasive optical imaging of ovarian metastases using Cy5-labeled RAFT-c(-RGDfK-)4". *Molecular imaging* 5, Nr. 3 (Juli 2006): 188–197.

K

Kazuki, N. et al; tissue-penetrating delivery of compounds and nanoparticles into tumors, *Cancer Cell* 2009

Kedar, Uttam, PrasannaPhutane, SupriyaShidhaye, und VilasraoKadam. „Advances in polymeric micelles for drug delivery and tumor targeting". *Nanomedicine: nanotechnology, biology, and medicine* 6, Nr. 6 (Dezember 2010): 714–729.

Keereweer, S., et al. "NIR Spectroscopic Detection of Breast Cancer". Montreal, Canada, 2011

Keereweer, S., J.D.F. Kerrebijn, P.B.A.A. van Driel, B. Xie, E.L. Kaijzel, T.J.A. Snoeks, I. Que, et al. "Optical Image-guided Surgery - Where Do We Stand?" *Mol Imaging Biol*. 13, 2011. 199-207.

Keereweer, Stijn, Jeroen D. F. Kerrebijn, Isabel M. Mol, J. Sven D. Mieog, Pieter B. A. A. Van Driel, Robert J. Baatenburg de Jong, Alexander L. Vahrmeijer, und Clemens W. G. M. Löwik. „Optical Imaging of Oral Squamous Cell Carcinoma and Cervical Lymph Node Metastasis". *Head & Neck* 34, Nr. 7 (2012): 1002–1008.

Keramidas, M, V Josserand, C A Righini, C Wenk, C Faure, and J L Coll. "Intraoperative Near-infrared Image-guided Surgery for Peritoneal Carcinomatosis in a Preclinical Experimental Model." *The British Journal of Surgery* 97, no. 5 (May 2010): 737–743.

Kim, Dong Seok, Ok-Hee Jeon, Hee Doo Lee, Kyung Ho Yoo, und Doo-Sik Kim. „Integrin alphavbeta3-mediated transcriptional regulation of TIMP-1 in a human ovarian cancer cell line". *Biochemical and biophysical research communications* 377, Nr. 2 (Dezember 12, 2008): 479–483.

Kirchner, C., T. Liedl, S. Kudera, et al. "Cytotxicity of Colloidal CdSe and CdSe/ZnS Nanoparticles." *Nano Lett*. 5, 2005.331-338; Lewinski, N., V. Colvin, and R. Drezek. "Cytotoxicity of Nanoparticles." *Small*. 4, 2008.26-49.

Klar, M, M Bossart, E Stickeler, I Brink, M Orlowska-Volk, und D Denschlag. „Sentinel lymph node detection in patients with vulvar carcinoma; Feasibility of intra-operative mapping with technetium-99m-labeled nanocolloid". *European journal of surgical oncology: the journal of the European Society of Surgical Oncology and the British Association of Surgical Oncology* 37, Nr. 9 (September 2011): 818–823.

Kline, Toni, Michael Y Torgov, Brian A Mendelsohn, Charles G Cerveny, und Peter D Senter. „Novel antitumor prodrugs designed for activation by matrix metalloproteinases-2 and -9". *Molecular pharmaceutics* 1, Nr. 1 (Januar 12, 2004): 9–22.

Klohs, J., N. Baeva, J. Steinbrink, et al. "In Vivo Near-infrared Fluorescence Imaging of Matrix Metalloproteinase Activity After Cerebral Ischemia." *J Cereb Blood Flow Metab*, 2009.1284-1292.

Knight, C G, F Willenbrock, und G Murphy. „A novel coumarin-labelled peptide for sensitive continuous assays of the matrix metalloproteinases". *FEBS letters* 296, Nr. 3 (Januar 27, 1992): 263–266.

Kobayashi T, Hauck ML, Dodge R, et al. Preoperative radiotherapy for vaccine associated sarcoma in 92 cats. *Vet Radiol Ultrasound* 2002;43:473-479.

Kobayashi, H., Ogawa, M., Alford, R., Choyke, P.L and Urano, Y., "New strategies for fluorescent probe design in medical diagnostic imaging," Chem Rev (2010) 110:2620–2640.

Kossodo, S., M. Pickarski, S.A. Lin, et al. "Dual in Vivo Quantification of Integrin-targeted and Protease-activated Agents in Cancer Using Fluorescence Molecular Tomography (FMT)." *Mol Imaging Biol.*, 2009.

Krüger, R. Soeltl, I. Sopov, C. Kopitz, M. Arlt,V. Magdolen, et al., Hydroxamate-type matrix metalloproteinase inhibitor batimastat promotes liver metastasis, Cancer Res. 61 (2001) 1272–1275.

L

Lakowicz, J.R., *Principles of Fluorescence Spectroscopy, Third Edition*, Springer (2006).

Larkin, Deirdre, Achim Treumann, Derek Murphy, Ciaran DeChaumont, Aoife Kiernan, und Niamh Moran. „Compartmentalization regulates the interaction between the platelet integrin alpha IIb beta 3 and ICln". *British journal of haematology* 144, Nr. 4 (Februar 2009): 580–590.

Lauer-Fields Janelle et al. "Selective Modulation of Matrix Metalloproteinase 9 Functions via Exosite Inhibition", Journal of Biological Chemistry, Jluy 18,2008, Vol. 283, No. 29, PP. 20087-20095.

Lauer-Fields, Janelle L, Thilaka Sritharan, M Sharon Stack, Hideaki Nagase, und Gregg B Fields. „Selective hydrolysis of triple-helical substrates by matrix metalloproteinase-2 and -9". *The Journal of biological chemistry* 278, Nr. 20 (Mai 16, 2003): 18140–18145.

Lee, Bernard T, Merlijn Hutteman, Sylvain Gioux, Alan Stockdale, Samuel J Lin, Long H Ngo, und John V Frangioni. „The FLARE intraoperative near-infrared fluorescence imaging system: a first-in-human clinical trial in perforator flap breast reconstruction". *Plastic and reconstructive surgery* 126, Nr. 5 (November 2010): 1472–1481.

Lee, S., Cha, E. J., Park, K., Lee, S. Y., Hong, J. K., Sun, I. C., Kim, S. Y., Choi, K., Kwon, I. C., Kim, K., and Ahn, C. H. (2008) A nearinfrared-fluorescence-quenched gold-nanoparticle imaging probe for in vivo drug screening and protease activity determination. Angew. Chem., Int. Ed. Engl. 47, 2804–2807.

Lee, S.B., M. Hassan, R. Fisher, et al. "Affibody Molecules for in Vivo Characterization Oh HER2-positive Tumors by Near-infrared Imaging." *Clin Cancer Res*. 14, 2008.3840-3849.

Levin, Craig S. "Primer on Molecular Imaging Technology." *European Journal of Nuclear Medicine and Molecular Imaging* 32 Suppl 2 (December 2005): S325–345.

Li, Zhi-Wei, und William S Dalton. „Tumor microenvironment and drug resistance in hematologic malignancies". *Blood reviews* 20, Nr. 6 (November 2006): 333–342.

Lloyed-Williams P., Albericio F., and Giralt E. ,"Chemical Approaches to the Synthesis of Peptides and Proteins". Ed. by Ed. C.W. Rees. CRC Press, NY, 1997, p. 278.

Lombard, Carine, Joëlle Saulnier, and Jean Wallach. "Assays of Matrix Metalloproteinases (MMPs) Activities: a Review." *Biochimie* 87, no. 3–4 (March 2005): 265–272.

López-Otín, Carlos, und Lynn M. Matrisian. „Emerging Roles of Proteases in Tumour Suppression". *Nature Reviews Cancer* 7, Nr. 10 (Oktober 1, 2007): 800–808.

Louie, Angelique. "Design and Characterization of Magnetic Resonance Imaging Gene Reporters." *Methods in Molecular Medicine* 124 (2006): 401–417.

Lu-Emerson, Christine, und April F Eichler. „Brain metastases". *Continuum (Minneapolis, Minn.)* 18, Nr. 2 (April 2012): 295–311.

Lyden, D, K Hattori, S Dias, C Costa, P Blaikie, L Butros, A Chadburn, u. a. „Impaired recruitment of bone-marrow-derived endothelial and hematopoietic precursor cells blocks tumor angiogenesis and growth". *Nature medicine* 7, Nr. 11 (November 2001): 1194–1201.

M

Mahmood, U., and R. Weissleder. "Near-infrared Optical Imaging of Proteases in Cancer." *Mol Cancer Ther*. 2, 2003.489-496.

Malinin, Nikolay, Elzbieta Pluskota, and Tatiana Byzova. "Integrin Signaling in Vascular Function." *Current Opinion in Hematology May 2012* 19, no. 3 (2012): 206–211.

Marras, Salvatore A. E., Fred Russell Kramer, und Sanjay Tyagi. „Efficiencies of Fluorescence Resonance Energy Transfer and Contact-mediated Quenching in Oligonucleotide Probes". *NucleicAcidsResearch* 30, Nr. 21 (Januar 11, 2002): e122–e122.

Matsui, Aya, Eiichi Tanaka, Hak Soo Choi, Vida Kianzad, Sylvain Gioux, Stephen J Lomnes, und John V Frangioni. „Real-time, near-infrared, fluorescence-guided identification of the ureters using methylene blue". *Surgery* 148, Nr. 1 (Juli 2010): 78–86.

Maxwell, Dustin, Qing Chang, Xu Zhang, Edward M Barnett, und David Piwnica-Worms. „An improved cell-penetrating, caspase-activatable, near-infrared fluorescent peptide for apoptosis imaging". *Bioconjugate chemistry* 20, Nr. 4 (April 2009): 702–709.

McDonald, G A, G Zhu, Y Li, I Kovesdi, T J Wickham, und V P Sukhatme. „Efficient adenoviral gene transfer to kidney cortical vasculature utilizing a fiber modified vector". *The journal of gene medicine* 1, Nr. 2 (April 1999): 103–110.

Merrield. R.B. "Solid-Phase Peptide Synthesis. 3. An Improved Synthesis of Bradykinin." In: Biochemistry 3 (1964). SPPS, pp. 1385-1390.

Mery, E., E. Jouve, S. Guillermet, M. Bourgognon, M. Castells, M. Golzio, P. Rizo, JP Delord, D. Querleu, und B. Couders. „Intraoperative fluorescence imaging of peritoneal dissemination of ovarian carcinomas. A preclinical study." *Gynecol Oncol*. 122(1), Juli 2011, 155-162.

Mieog, J. Sven D., Susan L. Troyan, Merlijn Hutteman, Kevin J. Donohoe, Joost R. van der Vorst, Alan Stockdale, Gerrit-Jan Liefers, u. a. „Toward Optimization of Imaging System and Lymphatic Tracer for Near-Infrared Fluorescent Sentinel Lymph Node Mapping in Breast Cancer". *Ann Surg Oncol*. 18, 2011.

Mizejewski, G J. „Role of integrins in cancer: survey of expression patterns". *Proceedings of the Society for Experimental Biology and Medicine. Society for Experimental Biology and Medicine (New York, N.Y.)* 222, Nr. 2 (November 1999): 124–138.

Moss, Marcia L, und Jörg W Bartsch. „Therapeutic benefits from targeting of ADAM family members". *Biochemistry* 43, Nr. 23 (Juni 15, 2004): 7227–7235.

Moustoifa, El-Farouck, Mohamed-Anis Alouini, Arnaud Salaün, Thomas Berthelot, Aghleb Bartegi, Sandra Albenque-Rubio, und Gérard Déléris. „Novel cyclopeptides for the design of MMP directed delivery devices: a novel smart delivery paradigm". *Pharmaceutical research* 27, Nr. 8 (August 2010): 1713–1721.

Mulder, W.J., K. Castermans, J.R. van Beijnum, et al. "Molecular Imaging of Tumor Angiogenesis Using Alphavbeta3-integrin Targeted Multimodal Quantum Dots." *Angiogenesis*. 12, 2009.17-24.

Muzylak, M, A M Flanagan, K Ingham, N Gunn, J Price, und M A Horton. „A feline assay using osteoclasts generated in vitro from peripheral blood for screening anti-resorptive agents". *Research in veterinary science* 73, Nr. 3 (Dezember 2002): 283–290.

N

Nagase H., Activation mechanisms of matrix metalloproteinases, Biol. Chem. 378 (1997) 151–160.

Nioka, S, and B Chance. "NIR Spectroscopic Detection of Breast Cancer." *Technol Cancer Res Treat*. 4, 2005.497-512

Nisato, Riccardo E, Ghamartaj Hosseini, Christian Sirrenberg, Georgina S Butler, Thomas Crabbe, Andrew J P Docherty, Matthias Wiesner, u. a. „Dissecting the role of matrix metalloproteinases (MMP) and integrin alpha(v)beta3 in angiogenesis in vitro: absence of hemopexin C domain bioactivity, but membrane-Type 1-MMP and alpha(v)beta3 are critical". *Cancer research* 65, Nr. 20 (Oktober 15, 2005): 9377–9387.

Ntziachristos, Vasilis. „Fluorescence molecular imaging". *Annual review of biomedical engineering* 8 (2006): 1–33.

O

Oberdorster, G., E. Oberdorster, and J. Oberdorster. "Nanotoxicology: An Emerging Discipline Evolving from Studies of Ultrafine Particles." *Environ Health Perspect*. 113, 2005.823-839.

Ogawa, M., N. Kosaka, M.R. Longmire, Y. Urano, P.L. Choyke, and H. Kobayashi. "Fluorophore-quencher Based Activatable Targeted Optical Probes for Detecting in Vivo." *Mol Pharm*. 6(2), 2009.386-395.

Optical contrast agents and imaging systems for detection anddiagnosis of cancer; Mark C. Pierce, David J. Javier, and Rebecca Richards-Kortum Int J Cancer. 2008 November 1; 123(9): 1979–1990.

Overall, C. M. & Kleifeld, O. Validating matrix metalloproteinases as drug targets and anti-targets for cancer therapy. *Nat Rev Cancer* **6**, 227–239 (2006).

Overall, Christopher M, und Carl P Blobel. „In search of partners: linking extracellular proteases to substrates". *Nature reviews. Molecular cell biology* 8, Nr. 3 (März 2007): 245–257.

P

Pepper, M S. „Role of the matrix metalloproteinase and plasminogen activator-plasmin systems in angiogenesis". *Arteriosclerosis, thrombosis, and vascular biology* 21, Nr. 7 (Juli 2001): 1104–1117.

Pierce, M.C., D.J. Jvier, and R. Richards-Kortum. "Optical Contrast Agents and Imaging Systems for Detection and Diagnosis of Cancer." *Int J Cancer*. 123, 2008.1979-1990.

Pierschbacher, M D, und E Ruoslahti. „Variants of the cell recognition site of fibronectin that retain attachment-promoting activity". *Proceedings of the National Academy of Sciences of the United States of America* 81, Nr. 19 (Oktober 1984): 5985–5988.

Porter, J C, and N Hogg. "Integrins Take Partners: Cross-talk Between Integrins and Other Membrane Receptors." *Trends in Cell Biology* 8, no. 10 (October 1998): 390–396.

Q

Quillard, T, K Croce, F A Jaffer, R Weissleder, und P Libby. „Molecular imaging of macrophage protease activity in cardiovascular inflammation in vivo". *Thrombosis and haemostasis* 105, Nr. 5 (Mai 2011): 828–836.

Quillard, Thibaut, und Peter Libby. „Molecular Imaging of Atherosclerosis for Improving Diagnostic and Therapeutic Development". *Circulation Research* 111, Nr. 2 (Juni 7, 2012): 231–244.

R

Rawlings, Neil D, Alan J Barrett, und Alex Bateman. „MEROPS: the database of proteolytic enzymes, their substrates and inhibitors". *Nucleic acids research* 40, Nr. Database issue (January 2012): D343–350.

Rolleman, Edgar J, Marion de Jong, RoelfValkema, DikKwekkeboom, BoenKam, und Eric P Krenning. „Inhibition of kidney uptake of radiolabeled somatostatin analogs: amino acids or gelofusine?" *Journal of nuclear medicine: official publication, Society of Nuclear Medicine* 47, Nr. 10 (Oktober 2006): 1730–1731; author reply 1731.

Rolli, Melanie, Emilia Fransvea, Jan Pilch, Alan Saven, und Brunhilde Felding-Habermann. „Activated integrin alphavbeta3 cooperates with metalloproteinase MMP-9 in regulating migration of metastatic breast cancer cells". *Proceedings of the National Academy of Sciences of the United States of America* 100, Nr. 16 (August 5, 2003): 9482–9487.

Rooks, V, W D Beecken, I Iordanescu, and G A Taylor. "Sonographic Evaluation of Orthotopic Bladder Tumors in Mice Treated with TNP-470, an Angiogenic Inhibitor." *Academic Radiology* 8, no. 2 (February 2001): 121–127.

Royer, C.A., "Approaches to teaching fluorescence spectroscopy," Biophys J (1995) 68:1191–1195.

Rundhaug, Joyce E. „Matrix Metalloproteinases and Angiogenesis". *Journal of Cellular and Molecular Medicine* 9, Nr. 2 (2005): 267–285.

Ruoslahti, Erkki. „Antiangiogenics meet nanotechnology". *Cancer cell* 2, Nr. 2 (August 2002): 97–98.

Ryppa, Claudia, Hagit Mann-Steinberg, Iduna Fichtner, Holger Weber, Ronit Satchi-Fainaro, Martin L Biniossek, und Felix Kratz. „In vitro and in vivo evaluation of doxorubicin conjugates with the divalent peptide E-[c(RGDfK)2] that targets integrin alphavbeta3". *Bioconjugate chemistry* 19, Nr. 7 (July 2008): 1414–1422.

S

Sancey, L., E. Garanger, S. Foillard, G. Schoehn, A. Hurbin, C. Albiges-Rizo, D. Boturyn, u. a. „Clustering and internalization of integrin alphavbeta3 with a tetrameric RGD-synthetic peptide". *Molecular Therapy*. 17(5), Mai 2009.

Schaafsma, BE, JS Mieog, M. Hutteman, JR van der Vorst, PJ Kuppen, CW Löwik, JV Frangioni, CJ van de Velde, and A. L. Vahrmeijer. "The Clinical Use of Indocyanine Green as a Near-infrared Fluorescent Contrast Agent for Image-guided Oncologic Surgery." *J Surg Oncol.* 104(3), September 2011.

Schaafsma, Boudewijn E, Joost R van der Vorst, Katja N Gaarenstroom, Alexander A W Peters, Floris P R Verbeek, Cornelis D de Kroon, J Baptist M Z Trimbos, u. a. „Randomized comparison of near-infrared fluorescence lymphatic tracers for sentinel lymph node mapping of cervical cancer". *Gynecologic oncology* (July 10, 2012).

Seftor R.E., E.A. Seftor, M.J. Hendrix, Molecular role(s) for integrins in human melanoma invasion, Cancer Metastasis Rev. 18 (1999) 359–375.

Sevick-Muraca, E M. „Translation of near-infrared fluorescence imaging technologies: emerging clinical applications". *Annual review of medicine* 63 (2012): 217–231.

Shapira, Alina, Yoav D Livney, Henk J Broxterman, und Yehuda G Assaraf. „Nanomedicine for targeted cancer therapy: towards the overcoming of drug resistance". *Drug resistance updates: reviews and commentaries in antimicrobial and anticancer chemotherapy* 14, Nr. 3 (Juni 2011): 150–163.

Sipkins, D A, D A Cheresh, M R Kazemi, L M Nevin, M D Bednarski, und K C Li. „Detection of tumor angiogenesis in vivo by alphaVbeta3-targeted magnetic resonance imaging". *Nature medicine* 4, Nr. 5 (Mai 1998): 623–626.

Spugnini E.P., A. Baldi, B. Vincenzi, F. Bongiorni, C. Bellelli, G. Citro, A. Porrello, Intraoperative versus postoperative electrochemotherapy in high grade soft tissue sarcomas: a preliminary study in a spontaneous feline model. Cancer chemotherapy and pharmacology 59 (2007) 375-381.

Stockdale, A., R. Oketokoun, S. Gioux, and JV Frangioni. "Mini-FLARE: a Compact and Ergonomic Dual-channel Near-infrared Fluorescence Image-guided Surgery System." *Abstract*, 2010

Strong, V.E., J. Humm, P. Russo, et al. "A Novel Method to Localize Antibody-targeted Cancer Deposits Intraoperatively Using Handheld PET Beta and Gamma Probes." *Surg Endosc*. 22, 2008. 386-391.

Sutcliffe-Goulden, Julie L, Michael J O'Doherty, Paul K Marsden, Ian R Hart, John F Marshall, und Sukvinder S Bansal. „Rapid solid phase synthesis and biodistribution of 18F-labelled linear peptides". *European journal of nuclear medicine and molecular imaging* 29, Nr. 6 (Juni 2002): 754–759.

Szabo, Roman, und Thomas H Bugge. „Type II transmembrane serine proteases in development and disease". *The international journal of biochemistry & cell biology* 40, Nr. 6–7 (2008): 1297–1316.

T

Takagi, Junichi, and Timothy A Springer. "Integrin Activation and Structural Rearrangement." *Immunological Reviews* 186 (August 2002): 141–163.

Takeda, Ikuko, Shin-Ichiro Maruya, Takashi Shirasaki, Hiroki Mizukami, Takenori Takahata, Jeffrey N Myers, Seiji Kakehata, Soroku Yagihashi, and Hideichi Shinkawa. "Simvastatin Inactivates Beta1-integrin and Extracellular Signal-related Kinase Signaling and Inhibits Cell Proliferation in Head and Neck Squamous Cell Carcinoma Cells." *Cancer Science* 98, no. 6 (June 2007): 890–899.

Tamta, Anupama, Manu Chaudhary, und Rajesh Sehgal. „A 28-Days Sub-Acute Toxicity Study in Swiss Albino Mice to Evaluate Toxicity Profile of Neurotol Plus (Mannitol and Glycerol Combination)". *International Journal of Biomedical Science* 5, Nr. 4 (Dezember 15, 2009): 428–433.

Tanaka, Eiichi, Hak Soo Choi, Hirofumi Fujii, Moungi G Bawendi, und John V Frangioni. „Image-guided oncologic surgery using invisible light: completed pre-clinical development for sentinel lymph node mapping". *Annals of surgical oncology* 13, Nr. 12 (December 2006): 1671–1681.

Themelis, George, Jung Sun Yoo, Kwang-Sup Soh, Ralf Schulz, und Vasilis Ntziachristos. „Real-time intraoperative fluorescence imaging system using light-absorption correction". *Journal of Biomedical Optics* 14, Nr. 6 (November 1, 2009): 064012–064012.

Themelis, George, Niels J Harlaar, Wendy Kelder, Joost Bart, Athanasios Sarantopoulos, Gooitzen M van Dam, und Vasilis Ntziachristos. „Enhancing surgical vision by using real-time imaging of αvβ3-integrin targeted near-infrared fluorescent agent". *Annals of surgical oncology* 18, Nr. 12 (November 2011): 3506–3513.

Tobis, Scott, Joy K Knopf, Christopher R Silvers, Jonah Marshall, Allison Cardin, Ronald W Wood, Jay E Reeder, u. a. „Near infrared fluorescence imaging after intravenous indocyanine green: initial clinical experience with open partial nephrectomy for renal cortical tumors". *Urology* 79, Nr. 4 (April 2012): 958–964.

Troyan, Susan L, Vida Kianzad, Summer L Gibbs-Strauss, Sylvain Gioux, Aya Matsui, Rafiou Oketokoun, Long Ngo, Ali Khamene, Fred Azar, und John V Frangioni. „The FLARE intraoperative near-infrared fluorescence imaging system: a first-in-human clinical trial in breast cancer sentinel lymph node mapping". Annals of surgical oncology 16, Nr. 10 (Oktober 2009): 2943–2952.

Turk, Boris. „Targeting proteases: successes, failures and future prospects". *Nature reviews. Drug discovery* 5, Nr. 9 (September 2006): 785–799.

Turpeenniemi-Hujanen, T. „Gelatinases (MMP-2 and -9) and their natural inhibitors as prognostic indicators in solid cancers". *Biochimie* 87, Nr. 3–4 (März 2005): 287–297.

Tykocki T., R. Michalik, W. Bonicki, P. Nauman, Fluorescence-guided resection of primary and recurrent malignant gliomas with 5-aminolevulinic acid. Preliminary results. Neurol Neurochir Pol 46 (2012) 47-51.

V

van den Steen *et al.,* 2006, Journal of biol. Chem.. 281, 18626-18637.

van der Vorst, Joost R., Boudewijn E. Schaafsma, Floris P.R. Verbeek, Stijn Keereweer, Jeroen C. Jansen, Lilly-Ann van der Velden, Antonius P.M. Langeveld, u. a. „Near-infrared fluorescence sentinel lymph node mapping of the oral cavity in head and neck cancer patients". *Oral Oncology* (o. J.). http://www.sciencedirect.com/science/article/pii/S136883751200245X.

Vartak, Deepali G, und Richard A Gemeinhart. „Matrix metalloproteases: underutilized targets for drug delivery". *Journal of drug targeting* 15, Nr. 1 (Januar 2007): 1–20.

Vegt, Erik, Julliëtte E M van Eerd, Annemarie Eek, Wim J G Oyen, Jack F M Wetzels, Marion de Jong, Frans G M Russel, RosalindeMasereeuw, Martin Gotthardt, und Otto C Boerman. „Reducing renal uptake of radiolabeled peptides using albumin fragments". *Journal of nuclear medicine: official publication, Society of Nuclear Medicine* 49, Nr. 9 (September 2008): 1506–1511.

Verbeek, F. et al., WMIC, 2012: SS 168

W

Wachter D., K. Kallenberg, A. Wrede, W. Schulz-Schaeffer, T. Behm, V. Rohde, Fluorescence-Guided Operation in Recurrent Glioblastoma Multiforme Treated with Bevacizumab-Fluorescence of the Noncontrast Enhancing Tumor Tissue? J Neurol Surg A Cent Eur Neurosurg (2012).

Weis, Sara M, und David A Cheresh. „αv Integrins in Angiogenesis and Cancer". *Cold Spring Harbor perspectives in medicine* 1, Nr. 1 (September 2011): a006478.

Wells Jr., S.A. "35 - Total Thyroidectomy, Lymph Node Dissection for Cancer." In *Mastery of Surgery*, 1:411–433. 5th ed. Boston, Massachusetts: Fischer, Josef E., 2007.

Wenk, C.H.F., Josserand, V., Coll, JL, Dumy, P and Boturyn, D*, "Integrin and Matrix Metalloprotease Dual-Targeting with MMP substrate-RGD conjugate" (submitted).*

Withrow, K.P., J.R. Newman, J.B. Skipper, et al. "Assessment of Bevacizumab Conjugated to Cy5.5 for Detection of Head and Neck Cancer Xenografts." *Technol Cancer Res Treat*. 7, 2008.61-66.

Wunder A, Tung CH, Muller-Ladner U, et al. In vivo imaging of protease activity in arthritis: anovel approach for monitoring treatment response. Arthritis Rheum. 2004 Aug; 50(8):2459–2465.

Wunder, A., R.H. Straub, S. Gay, J. Funk, and U. Muller-Ladner. "Molecular Imaging: Novel Tools in Visualizing Rheumatoid Arthritis." *Rheumatology*. (Oxford) 44, 2009.1341-1349.

Wunderbaldinger, P., K. Turetschek, and C. Bremer. "Near-infrared Fluorescence Imaging of Lymph Nodes Using a New Enzyme Sensing Activatable Macromolecular Optical Probe." *Eur Radiol*. 13, 2003.2206-2211.

X

Xie, G., J. Sun, G. Zhong, L. Shi, and D. Zhang. "Biodistribution and Toxicity of Intravenously Administered Silica Nanoparticles in Mice." *Arch Toxicol*. 84(3), 2009.183-190.

Xiong, Jian-Ping, Thilo Stehle, Rongguang Zhang, Andrzej Joachimiak, Matthias Frech, Simon L Goodman, und M Amin Arnaout. „Crystal structure of the extracellular segment of integrin alpha Vbeta3 in complex with an Arg-Gly-Asp ligand". *Science (New York, N.Y.)* 296, Nr. 5565 (April 5, 2002): 151–155.

Y

Yang, Jie, Zhihong Zhang, Juqiang Lin, Jinling Lu, Bi-feng Liu, Shaoqun Zeng, und Qingming Luo. „Detection of MMP activity in living cells by a genetically encoded surface-displayed FRET sensor". *Biochimica et biophysica acta* 1773, Nr. 3 (März 2007): 400–407.

Z

Zhou, H., K. Luby-Phelps, B.E. Mickey, A.A. Habib, R.P. Mason, and D. Zhao. "Dynamic Near-infred Optical Imaging of 2-deoxyglucose Uptake by Intracranial Glioma of Athymic Mice." *PLoS ONE*. 4, 2009.e8051

Zhu, Lei, Jin Xie, Magdalena Swierczewska, Fan Zhang, Xin Lin, Xuexun Fang, Gang Niu, Seulki Lee, und Xiaoyuan Chen. „Dual-functional, receptor-targeted fluorogenic probe for in vivo imaging of extracellular protease expressions". *Bioconjugate chemistry* 22, Nr. 6 (Juni 15, 2011): 1001–1005.

Zhu, Peizhi, Jean-Pierre Clamme, undAshok A. Deniz. „Fluorescence Quenching by TEMPO: A Sub-30 Å Single-Molecule Ruler". *Biophysical Journal* 89, Nr. 5 (November 2005): L37–L39.

Zitzmann, Sabine, Volker Ehemann, und Manfred Schwab. „Arginine-glycine-aspartic acid (RGD)-peptide binds to both tumor and tumor-endothelial cells in vivo". *Cancer research* 62, Nr. 18 (September 15, 2002): 5139–5143.

Other:

„Longer Survival Rates After Surgery For Prostate Cancer Patients". *Medical News Today*, o. J. http://www.medicalnewstoday.com/articles/84936.php.)

„Pharmakokinetik". Institut für Biochemische Pharmakologie Universität Innsbruck, 2. Auflage 1994.

„Treatment of non-localised, non-metastatic rectal cancer". *Prescrire international* 21, Nr. 128 (June 2012): 158–162.

American Cancer Society, 2012 / American Cancer Society, Intramural Research 2012

Colloque INSERM, "modèles carnivores de tumeurs spontanées", 2009, Nantes

http://merops.sanger.ac.uk/

Molecular Imaging and Contrast Agent Database (MICAD). Bethesda (MD): National Center for Biotechnology Information (US), 2004. http://www.ncbi.nlm.nih.gov/pubmed/22649804.

Thèse soutenue par Christiane Hanna Frederike WENK

CHIRURGIE GUIDEE PAR FLUORESCENCE DU FIBROSARCOME FELIN ET DEVELOPPEMENT ET CARACTERISATION D'UN VECTEUR BI-FONCTIONNEL POUR LE CIBLAGE DU CANCER

Actuellement, la chirurgie représente la première indication pour la thérapie du cancer. Néanmoins, la résection complète du tissu tumoral, la détection des micrométastases et la préservation des tissus sains pendant l'intervention représentent un enjeu majeur et influencent fortement le pronostic du patient. Les récents développements technologiques en imagerie pour la chirurgie guidée des cancers ont conduit à des résultats précliniques prometteurs et les premiers essais cliniques utilisant des traceurs non-spécifiques confirment déjà le potentiel de ces systèmes pour l'amélioration de la chirurgie. De plus, le diagnostic précoce des tumeurs, ainsi que le développement de thérapies ciblées sont également des axes majeurs de recherche en cancérologie. Dans ce contexte notre équipe a précédemment développé un vecteur synthétique ciblant un récepteur cellulaire l'intégrine $\alpha_v\beta_3$. Ce vecteur est constitué d'un châssis décapeptidique cyclique RAFT (*Regioselectively Addressable Functionalized Template*) et présentant deux domaines indépendants permettant de séparer les deux fonctions du vecteur. Sur un domaine, la fonction de ciblage est assurée par la présentation multivalente de ligands -RGD- spécifiques du récepteur. L'autre domaine du vecteur porte les molécules d'intérêt à vectoriser, agents thérapeutiques ou de détection pour l'imagerie médicale.

Dans la première partie de ces travaux, nous avons évalué la combinaison de ce vecteur couplé à un fluorophore avec une sonde portative pour imager et guider le chirurgien pendant la chirurgie des fibrosarcomes spontanés chez le chat. Cette étude représente une preuve de concept pour la translation clinique chez l'homme. Les résultats ont montré que l'injection du traceur ne provoquait pas d'effets toxiques chez le chat et permettait un marquage spécifique de la tumeur avec un bon ratio tumeur/tissu sain, qui devrait améliorer la qualité de la résection tumorale en aidant le chirurgien à mieux délimiter les marges du tissu tumoral.

Dans la seconde partie de ces travaux nous avons développé un nouveau vecteur bi-fonctionnel dérivé du RAFT-RGD. Au composé d'origine a été ajoutée une séquence peptidique clivable par la matrixmetalloprotease-9, une enzyme surexprimée dans la tumorigénèse. Cette molécule à fluorescence activable a montré une amélioration du ciblage tumoral *in vitro* et *in vivo* comparée au RAFT-RGD suggérant un effet additionnel lié au double ciblage. Ces résultats préliminaires encouragent la poursuite de sa caractérisation pour son potentiel de « pro-drug » mais également pour l'étude des interactions entre l'intégrine et l'environnement tumoraux.

OPTICAL-GUIDED SURGERY OF THE FELINE FIBROSARCOMA AND DEVELOPMENT AND CHARACTERIZATION OF A BI-FUNCTIONAL VECTOR FOR CANCER TARGETING

Cancer surgery is still the gold standard therapy in most cancers. Nevertheless, total tumor resection and metastasis detection while preserving healthy tissues represent a crucial point for further prognosis. Development of imaging technologies for intra-operative guided surgery provided promising results and efficient application in preclinical studies and first clinical trials using non-specific tracers already confirmed the improved out-come in surgery. Moreover early and precise diagnosis and targeted therapies are major domains of cancer research. In this context our team previously developed a synthetic vector based on a cyclic decapeptide scaffold RAFT (*Regioselectively Addressable Functionalized Template*) which allows the independent functionalizing of two domains: a targeting domain with multivalent RGD-ligand targeting the cell receptor integrin $\alpha_v\beta_3$, and a vehicle domain grafted with a pro-drug or an imaging agent. One part of this work consisted in the evaluation of the combination of this molecule carrying a fluorophore with a portable fluorescent imaging device for image-guided surgery of natural occurring feline fibrosarcoma. This study represents a proof of concept for further translation into human clinics. No toxic effects in cats after administration of the tracer could be reported. Furthermore the tumors were specifically labeled showing a good tumor-to-healthy tissue ratio. This should improve tumor resection by helping the surgeon to delineate tumor margins. In parallel we developed a bi-functional derivative of the RAFT-RGD. Therefore we engrafted a peptide sequence flanked by two fluorophores, which is activatable by matrixmetalloprotease-9, an enzyme overexpressed in tumors. This molecule showed an improved tumor labeling *in vitro* and *in vivo* compared to the conventional RAFT-RGD, suggesting an additional effect of the double targeting. These preliminary results encourage further characterization for its potential as pro-drug vehicle, as well as for studying interactions between the integrin and the tumor environment.

Mots Clés : tumeur, peptides ciblés, imagerie de fluorescence *in vitro* et *in vivo*, imagerie per-opératoire, RAFT-RGD, chirurgie du cancer guidée par la fluorescence

Keywords: cancer, targeting peptides, *in vitro* and *in vivo* fluorescence imaging, inter-operative imaging, RAFT-RGD, fluorescent guided cancer surgery

---